ISSN 0370—8691

NATIONAL ACADEMY OF SCIENCES OF THE REPUBLIC OF ARMENIA

Communications of the Byurakan Astrophysical Observatory

2

Erevan 2023

Is the Andromeda galaxy approaching our galaxy Milky Way?

Harutyunian H.A. *[1], Grigoryan A.M.[1], Khasawneh A.[2], and Torosyan A.A.[3]

[1]Byurakan Astrophysical Observatory, Armenia
[2]Sharjah University, UAE
[3]Yerevan State University, Armenia

Abstract

No doubt that the dark energy carrier interacts with the baryonic matter. Due to this interaction some portions of energy are transferring gradually to all baryonic objects and their systems without any exception at all hierarchical levels of the baryonic world. The consequences of the energy transfer are quite dramatic for all objects. The most dramatic changes take place at the nuclear level. Objects of this particular level have the universal property of converting energy into mass, which ultimately affects the cosmic objects of all levels and the baryonic Universe as whole. Hear we consider the side effect of growing mass of nuclei. That is the inevitable blueshift of spectral lines of atoms possessing higher mass nuclei compared with the atoms having nuclei of lesser mass. We hypothesize here that the Andromeda galaxy spectral blueshift can be resulted by Doppler effect as accepted but due to the more advanced evolution compared with our galaxy but not by its approaching velocity.

Keywords: *dark energy, baryon matter, interaction, energy exchange: Andromeda galaxy, spectral blueshift*

1. Introduction

Measurements show that the galactocentric spectral shift of the Andromeda galaxy is about -0.00037. Its interpretation as a result of the Doppler effect gives an approach speed of 110 km/s. And therefore, it is believed by astronomers and physicists that in the distant future the Andromeda galaxy will collide with our Galaxy. The scenario of the huge merger of these two giant galaxies has been repeatedly discussed not only in scientific articles, but even more intensely in popular literature.

However, it is clear that there is only one indisputable issue, and that is the observed spectral shift of the neighboring galaxy. Doppler mechanism for its interpretation is chosen a priori as a granted one. Therefore, while discussing this observational fact no other spectral blueshift mechanisms have been even considered. On the other hand, the discovery of dark energy provides a new possible way for interpretation of the blueshift in spectra of cosmic objects without involving the Doppler effect and the corresponding velocity. In a series of papers, one of the authors of the present report explored the consequences of the interaction between the dark energy carrier and baryonic matter. The fact of such an interaction is obvious, since dark energy was discovered and brought into consideration solely due to the acceleration of the Universe expansion (Perlmutter et al., 1999, Riess et al., 1998). Indeed, no physical mechanism is known to accelerate galaxies expansion velocities without interaction with them. Therefore, we accept from the very beginning that if the phenomenon of the dark energy is real, we should inevitably arrive at a conclusion that its carrier interacts with the ordinary baryonic matter.

In this paper we are going to discuss the physical mechanism leading to formation of a blueshift effect not connected with velocity. Perhaps, we might call it an evolutionary effect since such a spectral shift arises due to energetic changes in atomic nuclei as a result of long lasting interaction with the dark energy carrier (DEC). It seems obvious that if the dark energy is added into the toolkit of the modern physics, one should consider all the consequences to which leads the usage of this newfound tool.

Although we do not know the real physical essence of the dark energy carrier, the scientific community has accepted that dark energy fills all the three-dimensional space absolutely homogeneously. Moreover, that

*hhayk@bao.sci.am, Corresponding author

doi: https://doi.org/10.52526/25792776-23.70.2-165

statement is correct for at all scales. Therefore, one should consider the physical picture self-consistently taking account at least mentioned two issues, namely, obvious interaction between the carrier of dark energy and baryonic matter, as well as, the existence of DEC at all scales from the microcosm up to the mega world. If one of these these features is not taken into account, the picture cannot be correct.

2. Does dark energy influence the baryonic matter?

We already have considered several physical consequences of interaction between the DEC and baryonic matter (Harutyunian & Grigoryan, 2018, Harutyunian et al., 2019). As it was shown in previous papers, at the level of the gravitationally configurated objects and systems, such an interaction affects baryonic objects and their systems injecting some portions of dark energy into them. Due to this process the baryonic world gains energy which inevitably should destabilize them. The energy transferred to the baryonic objects and their systems by DEC can be responsible for the variety of non-stable phenomena at all the levels of baryonic world hierarchical structure (Harutyunian, 2023).

However, this is not the only physical consequence of the interaction between mentioned two substances. This effect has different manifestations at various hierarchical levels. In the microworld where the objects' stability is provided by residual strong forces, the situation is absolutely different than in larger structures, where the electric or gravitational forces are responsible for integrity of baryonic objects. Only in the microcosm acts one of the most essential laws of baryonic matter – transformation between mass and energy.

Note also that almost all mass of baryonic matter is concentrated in the atomic nuclei, and atomic nuclei themselves exist as separate integrites exceptionally owing to the mass defect or energy lack in them. In atomic nuclei all baryons possess of mass which is lower than one they should have being outside of nuclei. Every physicist can easily recall the standard diagram showing the mass defect depending on the atomic number. All baryons loss some part of their mass for fitting themselves to the physical conditions inside the nuclei.

The nuclear feature, called mass defect, is very important for more comprehensive understanding of global properties of our baryonic world. This feature provides very essential fingerprints of how was originated the baryonic world. But much more essential conclusion one can make is the following. The such quantum objects as baryons, which are considered to be unchangeable, have smaller masses being parts of any atomic nucleus. Moreover, in different nuclei they have different masses. So, we can conclude that these baryons change their mass depending on the physical conditions they are involved and can show quite different mass-losses. An essential question is arising therefore: can this fitting conditions change in the course of time following to some evolutionary path? And also, what we can say about the free baryons which also have complex structure and exist because of the same strong forces?

Interaction of atomic nuclei with DEC decreases the absolute value of their (negative) nuclear binding energy. In other words, this interaction decreases the lack of energy which could decay the atomic nuclei and split it into the separated free baryons with their known masses. Since the nuclear binding energy simply is the lack of mass in energetic terms, its decreasing leads to the growth of nuclear mass.

These predicted phenomena have been considered in the previous papers of one of the authors. In more detail it is discussed in association with the, so called, "Hubble tension" (Harutyunian, 2021), the problem of the growth of the Astronomical Unit (Harutyunian & Grigoryan, 2018), and while considering the galaxy redshift dependence on the luminosity in the clusters of galaxies (Harutyunian et al., 2019). In all the mentioned papers the phenomenon of atomic nuclear mass increase is considered for interpretation of observational paradoxes. The nuclear mass growth has a particular manifestation which is evident when one uses the Rydberg relation for spectral lines frequencies, which has the following form for the hydrogen like atoms:

$$\frac{1}{\lambda_{ij}} = Ry\frac{1}{hc}\frac{M_n}{M_n + m_e}\left(\frac{1}{i^2} - \frac{1}{j^2}\right) \tag{1}$$

where

$$Ry = \frac{m_e e^4}{8\varepsilon_0^2 h^2} \tag{2}$$

is the Rydberg constant. We see that the wavelengths of spectral lines depend inversely on the reduced

doi: https://doi.org/10.52526/25792776-23.70.2-165

mass of nucleus and electron

$$m_r = \frac{M_n m_e}{M_n + m_e}. \tag{3}$$

Obviously, when the masses of the nucleus and electron increase, spectral lines get blueshifted.

It is clear that the spectrum of any object should be blue-shifted relative to another if it has been more influenced by dark energy. A greater influence is determined either by a longer duration of exposure or by a greater intensity of the process of this influence. Therefore, it is necessary to clearly determine which objects are easily susceptible to this influence and which are more stable.

For this purpose, we introduced into consideration a coefficient showing the ratio of the gravitational energy of a given object to the amount of dark energy in the volume of the same object. Gravitational or any other energy that is responsible for preserving a given object as an integrity, is the only tool for a given object preventing any changes caused by dark energy. Therefore, the coefficient introduced in this way can serve as a kind of "resistance index". The higher this index, the more difficult it is for dark energy to make changes in an object and, therefore, the slower evolutionary changes take place under the influence of dark energy.

It is known that the gravitational energy of any object is proportional to the second power of its mass and inversely proportional to the size (radius) of the object. Considering that the mass is proportional to the third power of the radius, we come to the conclusion that gravitational energy is proportional to the fifth power of the radius. On the other hand, with a uniform distribution of dark energy, its amount in the volume occupied by the object is proportional to the third order of magnitude. This means that the ratio of an object's gravitational energy to dark energy increases as the second power of the object's size.

This simple qualitative analysis shows that the more massive objects belonging to the same hierarchical class cosmic objects are more resistive against the evolutionary changes caused by dark energy. In other words, all the changes resulted from the interaction between baryonic matter and DEC easier exhibit the objects of lesser mass. All the changes predicted on the base of analysis of the interaction process, if any, take place easier and sooner, for example, in dwarf galaxies than in giant ones.

Taking into account the above conclusion we may say that evolutionary time for dwarf objects is shorter than for giants, provided that average density of matter is approximately the same. Density dependence makes considerable changes and, of course, should be studied in detail for any particular case. Hear, for the rough qualitative estimates, we consider a simpler situation when the density does not depend on the size of the object.

There are two main observable features very sensitive to the dark energy influence. One is the metallicity of the object. The longer is the evolutionary time the higher should be the metallicity, since it lasts longer to decrease the nuclear binding energy and decay the heavier nuclei through radioactivity. It means that the relative amount of light elements, including the hydrogen, grows more slowly and metallicity remains higher. This effect is known already for a half of century, namely, since the last quarter of the last century. Indeed, in a series of papers on the base of a huge observational data was approved the result stating that the metallicity of faint galaxies is lower comping with giant ones.

The second feature, which can also be easily detected during observations, in our opinion, should be a noticeable blue shift in the spectra of more evolved objects. Therefore, we statistically studied the dependence of the redshift of galaxies in clusters on their apparent magnitude. For the two closest clusters in Virgo and Fornax, we obtained a clear relationship with a very high correlation coefficient (Harutyunian et al., 2019). A fairly significant dependence was also obtained for the galaxies of the Coma cluster. In all the cases considered, with a decrease in the luminosity of galaxies, a decrease in redshift is observed, which can be explained by the faster evolution of objects with lower masses.

3. The blueshift of the Andromeda galaxy

The Andromeda Galaxy is located at the distance of about 770 kpc (2.5 million light years). This means that what all observable information we have today is obtained from the light, which was emitted by this galaxy about 2.5 million years ago. And the most intriguing question is the following: was really at that time the Andromeda Galaxy ahead of our Galaxy on the evolutionary path of baryonic matter. In the other words, was the evolution of the matter belonging to the Andromeda galaxy longer, was it more evolved than the matter of our galaxy today?

The question formulated above is very essential for the problem under consideration. Indeed, if the neighboring galaxy is ahead in evolutionary path, then according to our conclusion made on the base of the

doi: https://doi.org/10.52526/25792776-23.70.2-165

known physical laws, it should be blueshifted relative to us. Although we will never be able to check in any other way, the similar self-consistent argumentation and calculations, on the other hand, suggest that for an observer, living somewhere in the Andromeda nebula, our Galaxy should be redshifted. So, a spectral shift of any type exhibited by an object has a sense, if determined relative to some other system, which can be tied to some object. If the Doppler shift is symmetrical for two objects, the evolutionary shift is not. In one of the upcoming papers we will dwell on this issue in more detail.

Obviously, for a more solid argumentation of the proposed idea, and simultaneously as a necessary condition for maintaining this idea at the level of provable truth, one needs to find reliable observational facts showing that the Andromeda galaxy is really ahead of the Milky Way on its evolutionary path. It is obvious that in reality this is by no means an easy task. For such a conclusion one should analyse in detail many different physical features of both objects.

The modern astronomical data argues that Andromeda galaxy is approximately 2-2.5 times more massive than the Milky Way, which makes it more "resistant" to the changing influence of dark energy. The only possible way to achieve the necessary arguments for its longer evolutionary path can serve an unshakable proof that our neighboring giant galaxy is significantly older than ours. Therefore, the correct galaxy aging "fingerprints" should be used. The more such "fingerprints" there are, the more confidently we can talk about this issue.

However, the adopted by astronomers estimates give for the Andromeda galaxy a surprisingly small age. One should check the methods used for obtaining these estimates. If this estimates are correct, Andromeda galaxy appears to be much younger than our Milky Way. And if it is so, we should admit that there is incorrectness in our argumentation and search for an explanation of obvious inconsistency between observational data and physical conclusion made on their base. Therefore, we are going to compare as many as possible physical characteristics of these two giant inhabitants of the Local Group.

Within the paradigm we follow here, the main evolutionary processes occur in the microcosm, although their manifestation is better visible at cosmological scales. It is in the microcosm that the universal mechanism of converting portions of dark energy into mass operates, gradually reducing the nuclear binding energy in multi-baryon atomic nuclei and converting it into a mass of baryons without changing their total number. This process increases the mass of the atomic nuclei, and, as a result, growing the mass of all cosmic objects and the Universe itself.

Constructing this hypothesis on the base of observational data, we inevitably arrive at a conclusion that in the past all baryons should have been possessing of a much smaller masses. One can call them "baryonic embryos", which could join together and build atomic nuclei consisting of vast number of baryons. Moreover, such embryonic baryons and nuclei should exist at present in the cores of very massive objects (stars, galactic nuclei). These huge numbers of embryos, which continue to survive at present owing to the supporting physical conditions with a high high "resistant index", potentially contain masses able to originate new stars and even new galaxies.

On the other hand, a decrease of the nuclear binding energy and an increase of the mass of the nucleus gradually destabilize the nucleus itself, which at a certain moment of time moves from the class of stable nuclei into the class of radioactive ones and necessarily should eject the excessive mass and energy through decay. At present, we see some distribution of stable and unstable nuclei, which corresponds to the baryon/DEC going on interaction present situation in our galaxy. If the hypothesis is correct, in the future this distribution will change in favour of unstable and lighter nuclei.

The same process is observed at higher hierarchical levels as well, namely, gravitationally bound objects and their systems gradually increase their masses and energy, simultaneously exhibiting various phenomena of instability. It seems rather plausible that all instability phenomena are manifestations of the mentioned interaction and energy transfer into the baryonic world, The most obvious manifestation of this effect is observed in clusters of galaxies and in the Universe itself as a whole formation. As is known, under the dictates of the dominant Kant-Laplacian hypothesis, Zwicky introduced the concept of dark matter into astrophysical research (Zwicky, 1933, 1937), which is not revealed up to nowadays.

It is clear that the blueshift of the spectrum, due to a larger "evolutionary age," can only be detected in relatively closer galaxies. In the spectra of distant galaxies, the "evolutionary lag" adds its contribution to the value of the cosmological redshift and decreases it, but cannot make it negative and therefore is not noticeable without special research approach. We considered this issue in connection with the, so called, "Hubble tension" (Harutyunian, 2021), and it allowed explain the new-born paradox in a natural way. It was useful also for interpretation of lesser redshift of the fainter galaxies in the clusters of galaxies (Harutyunian et al., 2019). Therefore, we consider the Andromeda nebula with its blueshift as a good "laboratory" for

doi: https://doi.org/10.52526/25792776-23.70.2-165

testing the idea.

4. Concluding remarks.

The blueshift of the Andromeda galaxy provides an excellent opportunity to test the hypothesis of the evolution of atomic nuclei under the influence of dark energy. The self-consistent application of the laws of physics suggests that the interaction of atomic nuclei and free baryons with the dark energy carrier should lead to a gradual increase of their mass. The nuclear mass increase, in turn, shifts the spectral lines of these atoms to the blue end of the spectrum. The more an object is evolved under the influence of dark energy, the greater its blueshift for an observer who is in an environment where the evolution of matter lags behind.

It is on the basis of these considerations that we approach the question of the spectral blueshift of the Andromeda nebula, which is usually interpreted as a result of Doppler effect, suggesting that the neighboring galaxy is approaching to the Milky Way. By studying all relevant features of the neighboring galaxy and comparing with the same characteristics of our own galaxy, we are going to find out whether it is ahead of our Galaxy in the sense of the evolution of matter itself. First of all we need to find the physical features, which show clear dependence on the matter evolution and compare them for two galaxies.

For this purpose, at the first stage of research, we are going to compare the stellar content of two galaxies, various manifestations of activity, the metallicity dependence on the galactocentric distances for all components of galaxies, the content and distribution of globular clusters, the content of gas and dust etc. All these physical characteristics which somehow depend on the age of galaxy should provide the necessary keys for the comparison we need.

References

Harutyunian H. A., 2021, Astrophysics, 64, 435

Harutyunian H. A., 2022, Communications of the Byurakan Astrophysical Observatory, 69, 1

Harutyunian H. A., 2023, Communications of the Byurakan Astrophysical Observatory, 70, ?

Harutyunian H. A., Grigoryan A. M., 2018, Communications of the Byurakan Astrophysical Observatory, 65, 268

Harutyunian H. A., Grigoryan A. M., Khasawneh A., 2019, Communications of the Byurakan Astrophysical Observatory, 66, 25

Perlmutter S., et al., 1999, Astrophys. J. , 517, 565

Riess A. G., et al., 1998, Astron. J. , 116, 1009

Zwicky F., 1933, Helvetica Physica Acta, 6, 110

Zwicky F., 1937, Astrophys. J. , 86, 217

doi: https://doi.org/10.52526/25792776-23.70.2-165

Inertia I: The global MS_p-SUSY induced uniform motion

G.Ter-Kazarian*

Byurakan Astrophysical Observatory, Byurakan, Aragatsotn Province, Armenia

Abstract

In this communication our main emphasis is on the review of the foundations of standard Lorentz code (SLC) of a particle motion. To this aim, we develop the theory of global, so-called, \`double space´- or *master space* (MS_p)-supersymmetry, subject to certain rules, wherein the superspace is a 14D-extension of a direct sum of background spaces $M_4 \oplus \mathrm{MS}_p$ by the inclusion of additional 8D fermionic coordinates. The latter is induced by the spinors $\underline{\theta}$ and $\bar{\underline{\theta}}$ referred to MS_p. While all the particles are living on M_4, their superpartners can be viewed as living on MS_p. This is a main ground for introducing MS_p, which is *unmanifested* individual companion to the particle of interest. Supersymmetry transformation is defined as a translation in superspace, specified by the group element with corresponding anticommuting parameters. The multiplication of two successive transformations induce the motion. As a corollary, we derive SLC in a new perspective of global double MS_p-SUSY transformations in terms of Lorentz spinors $(\underline{\theta}, \bar{\underline{\theta}})$. This calls for a complete reconsideration of our ideas of Lorentz motion code, to be now referred to as the *individual code of a particle*, defined as its intrinsic property. In MS_p-SUSY theory, obviously as in standard unbroken SUSY theory, the vacuum zero point energy problem, standing before any quantum field theory in M_4, is solved. The particles in M_4 themselves can be considered as excited states above the underlying quantum vacuum of background double spaces $M_4 \oplus \mathrm{MS}_p$, where the zero point cancellation occurs at ground-state energy, provided that the natural frequencies are set equal ($q_0^2 \equiv \nu_b = \nu_f$), because the fermion field has a negative zero point energy while the boson field has a positive zero point energy. On these premises, we derive the two postulates on which the Special Relativity (SR) is based.

Keywords: *Special relativity–Lorentz and Poincaré invariance–Supersymmetry–Supersymmetric models*

1. Introduction

In the present article we study the first part of the phenomenon of inertia dedicated to the *inertial uniform motion*. This article is a more detailed exposition of the first part of work (Ter-Kazarian, 2024). Governing the motions of planets, both fundamental phenomena of nature the gravity and inertia reside at the very beginning of physics. Despite the advocated success of general relativity (GR) in explaining the gravity, which was a significant landmark in the development of the field, the problem of inertia stood open and it is still the most important incomprehensive problem that needs to be solved. Today there is no known feasible way to account for credible explanation of this problem, consisting of two parts: the *inertial uniform motion* of a body, and how this is affected by applied forces (the *accelerated motion and inertia effects*).

The beginning of the study of phenomenon of inertia can be attributed to the works of Galileo (Drake, 1978) and Newton (Newton, 1687). Certainly, more than four centuries passed since the famous far-reaching discovery of Galileo (in 1602-1604) that all bodies fall at the same rate (Drake, 1978), which led to an early empirical version of the suggestion that the gravity and inertia may somehow result from a single mechanism. Besides describing these early gravitational experiments, Newton in *Principia Mathematica* (Newton, 1687) has proposed a comprehensive approach to studying the relation between the gravitational and inertial masses of a body. Ever since, there is an ongoing quest to understand the reason for the universality of the gravity and inertia, attributing to the *weak* principle of equivalence (WPE), which establishes the independence of free-fall trajectories of the internal composition and structure of bodies. The variety of consequences of the precision experiments from astrophysical observations makes it possible to probe this fundamental issue more deeply by imposing the constraints of various analyzes. Currently, the observations

*gago_50@yahoo.com

doi: https://doi.org/10.52526/25792776-23.70.2-170

performed in the Earth-Moon-Sun system, or at galactic and cosmological scales, probe more deeply the WPE.

The inertia effects cannot be in full generality identified with gravity within GR as it was proposed by Einstein in 1907, because there are many experimental controversies to question the validity of such a description, for details see (Ter-Kazarian, 2012) and references therein. The universality of the gravity and inertia effects attribute to the geometry but as having a different natures. Unlike gravity, here a curvature has arisen entirely due to the inertial properties of the Lorentz-rotated frame of interest, i.e. a "fictitious gravity" which can be globally removed by appropriate coordinate transformations, refers to this coordinate system itself, without relation to other systems or matter fields. The key to our construction procedure of the toy model (Ter-Kazarian, 2012) is an assignment to each and every particle individually a new fundamental constituent of hypothetical 2D, so-called, *master-space* (MS_p), subject to certain rules. The MS_p, embedded in the background 4D-space, is an *unmanifested* indispensable individual companion to the particle of interest. This together with the idea that the inertia effects arise as a deformation/(distortion of local internal properties) of MS_p, are the highlights of the alternative *relativistic theory of inertia* (RTI). The crucial point is to observe that, in spite of totally different and independent physical sources of gravity and inertia, the RTI furnishes justification for the introduction of the WPE.

However, the RTI obviously is incomplete theory unless it has conceptual problems for further motivation and justification of introducing the fundamental concept of MS_p. The way we assigned such a property to the MS_p is completely *ad hoc* and there are some obscure aspects of this hypothesis. Moreover, this theory should certainly be incomplete without revealing the physical processes that underly the *inertial uniform motion* of a particle in flat space. Therefore, the present paper purports to develop a consistent solution of this problem, which is probably the most fascinating challenge for physical research.

From its historical development the principles of classical mechanics are constructed on the premises of our experience about relative locations and relative motions. In reducing the decision to that of whether a body is at rest or in *uniform motion* is disjunctive and, therefore, it is inherently indeterminate. This aspect of mechanics which deserves further investigation, unfortunately, has attracted little attention in subsequent developments. There is nothing in the basic postulates of physics to decide on the issue. The view that the problem of motion can be completely discussed in terms of observables implies that a kinematical description of all the relative motions in the universe completely specifies the system, so that kinematically equivalent motions must be dynamically equivalent. The notion of *uniform motion* of a particle, which is the mill-stone put into physics by hand, at first glance seemed to be classified as an empirical term rather than as a notion of pure reason and, thus, this is not a subject of perception. Although this question seems to be a purely philosophical problem, nevertheless, it has an outstanding physical significance for fundamentals of physics, and the SR in particular. Certainly, in recent years the violation of CPT and Lorentz invariance at huge energies has become a major preoccupation of physicists. This idea gathers support from a breakthrough made in recent observational and theoretical efforts in this field.

One of the achievements of present experimental high energy astrophysics is the testing of violation of SR for ultra-high energy cosmic rays (UHECRs) and TeV-γ photons observed (for a comprehensive review see (Batista & et al., 2019)). The Lorentz invariance violation (LIV) phenomenology for UHECRs has been intensely studied in the last few decades, even though the progress has been dramatic. A propagation in intergalactic space through the cosmic microwave background (CMB) radiation necessarily should reduce energy of UHECRs below the Greisen-Zatsepin-Kuzmin (GZK) limit, 5×10^{19} eV. The existence of this effect is uncertain owing to conflicting observational data and small number statistics. This is commonly referred as the GZK anomaly. Observed air showers experiment show an excess of muons compared to predictions of standard hadronic interaction models above $\simeq 10^{16}$ eV, which indicates a longer-than-expected muon attenuation length. If the muon excess cannot be explained by improved hadronic event generators with in the Standard Model, new physics could qualitatively play a role. Comparatively large increases of muon number over a small primary energy range would likely be a hint for Lorentz symmetry violation at very high Lorentz factors.

The TeV-γ paradox is another one related to the transparency of the CMB. The HEGRA has detected high-energy photons with a spectrum ranging up to 24 TeV (Aharonian & et al., 1999) from Mk 501, a BL Lac object at a redshift of 0.034 ($\sim$ 157 Mpc). The recent confirmation that at least some γ-ray bursts originate at cosmological distances (Metzger & et al., 1997, van Paradis & et al., 1997) suggests that the radiation from these sources could be used to probe some of the fundamental laws of physics.

Most ideas in phenomenology reflect the expectation that the characteristic scale of quantum spacetime effects, which will strongly affect the nature of spacetime, should be within a two or three orders of magnitude

doi: https://doi.org/10.52526/25792776-23.70.2-170

of the Planck scale, $E_P = M_P c^2$ ($\sim 1.22 \times 10^{19}$ GeV). Enormous efforts have been made over the past decade to test LIV as quantum spacetime effects in terms of expansions in powers of Planck energy scale in various scenarious of quantum gravity, see e.g. (Alfaro & Palma, 2003, Amelino-Camelia & Piran, 2001, Mattingly, 2005). But since the theory of quantum gravity based on noncommutative geometry is at earlier stage of development, and the possibility to preserve a Lorentz-invariant interpretation of noncommutative spacetime is still not excluded (Balachandran et al., 2008, Chaichian et al., 2004, Fiore & Wess, 2007), it is natural to tie the LIV to various alternatives for the yet nonexistent theory, see e.g. (Alfaro & Palma, 2002, 2003, Alfaro et al., 2002a,b). However, even thanks to the fruitful interplay between phenomenological analysis and high energy astronomical experiments, the scientific situation remains, in fact, more inconsistent to day. Moreover, a systematic analysis of these properties happens to be surprisingly difficult by conventional theoretical methods.

In the present paper we develop on so-called `double space´- or `MS$_p$-SUSY´ theory, subject to certain rules. The fundamental notion of the particle *motion* in full generality relies on the concept of locality which refers to the original continuous spacetime. The important reason to question the validity of such a description is the fact that we do not understand the nature of phenomenon of *motion*. It must suffice to expect some objections against the idealization of an arbitrarily precise localization in terms of points in spacetime. In the first step it proves necessary to introduce a constitutive ansatz of the simple, yet tentative, *unmanifested* intermediate *motion* state, as shown in Section 2. We derive SLC in a new perspective of global double MS$_p$-SUSY transformations in terms of Lorentz spinors $(\underline{\theta}, \bar{\underline{\theta}})$ referred to MS$_p$. This allows to introduce the physical finite *relative time* interval between two events as integer number of the *own atomic duration time* of double transition of a particle from M_4 to MS$_p$ and back. This is a main ground for introducing MS$_p$, which is *unmanifested* individual companion to the particle of interest. We place the emphasis on the fundamental difference between the standard SUSY theories and some rather unusual properties of MS$_p$-SUSY theory. While the standard SUSY theory can be realized only as a spontaneously broken symmetry since the experiments do not show elementary particles to be accompanied by superpartners with different spin but identical mass, the MS$_p$-SUSY, in contrary, is realized as an *exact* SUSY, where all particles are living on 4D Minkowski space, but their superpartners can be viewed as living on MS$_p$.

With this perspective in sight, we will proceed according to the following structure. To start with, Section 2 is devoted to probing SLC behind the `double space´- or MS$_p$-SUSY. Giving a first glance at MS$_p$ in Subsection 2.1, we motivate and justify its introduction, and outline the objectives of the proposed symmetry. In Section 3 we give a hard look at MS$_p$. The MS$_p$-SUSY is worked out as a guiding principle in Section 4. In Section 5, we turn to non-trivial linear representation of MS$_p$-SUSY algebra. In Section 6, we discuss the general superfields. On these premises, in Section 7, we derive the two postulates on which the theory of SR is based. In light of the absence of compelling experimental evidence for LIV, there does not appear to be any immediate motivation for the proposed theory. Therefore, as a physical outlook and concluding remarks, we list in Section 8 of what we think is the most important that distinguish this theory from phenomenological approaches of differing MAVs in the published literature. For brevity, whenever possible undotted and dotted spinor indices often can be ruthlessly suppressed without ambiguity. Unless indicated otherwise, we take natural units, $h = c = 1$.

2. Probing SLC behind the `double space´- or MS$_p$-SUSY

With regard to our original question as to the understanding of the physical processes underlying the *motion*, we tackle the problem in the framework of quantum field theory. In what follows, we should compare and contrast the particle quantum states defined on the two background spaces M_4 and MS$_p$, forming a basis in the Hilbert space. Let us consider functional integrals for a quantum-mechanical system with one degree of freedom. Denote by $x(t)$ the position operator in the Heisenberg picture, and by $|x, t>$ its eigenstates. The Schwinger transformation function, $F(x't'; xt)$, (Milton, 2000, 2015, Schwinger, 1960, 2000), is the probability amplitude that a particle which was at x at time t, on the path with no coinciding points, will be at point x' at time t'. To express the function $F(x't'; xt)$ as a path integral in M_4, we usually choose n intermediate points (x''_i, t''_i) on the path and divide the finite time interval into $n+1$ small intervals: $t = t_0, t_1, \ldots, t_{n+1} = t'$; $\quad t_i = t_0 + i\varepsilon$, where ε can be made arbitrarily small by increasing n. According to Trotter product formula (Hall, 2015), the noncommutativity of the kinetic and potential energy operators

doi: https://doi.org/10.52526/25792776-23.70.2-170

can be ignored. Then $F(x't';xt)$ can be computed as a product of ordinary integrals

$$F(x't';xt) = \int dx'' < x't'\,|x''t'' >< x''t''|xt > . \tag{1}$$

In the limit $n \to \infty$, the function $F(x't';xt)$ becomes an operational definition of the path integral.

2.1. Motivation of MS$_p$: In search of symmetry

We assume that a flat MS$_p$ is the 2D composite space MS$_p \equiv \underline{M}_2$ (see (3)). The elementary act of particle motion at each time step (t_i) through the infinitely small spatial interval $\triangle x_i = (x_{i+1} - x_i)$ during the time interval $\triangle t_i = (t_{i+1} - t_i) = \varepsilon$ is probably the most fascinating challenge for physical research. Since this is beyond our perception, it appears legitimate to consider extension to the infinitesimal Schwinger transformation function, $F_{ext}(x_{i+1}, t_{i+1}; x_i, t_i)$, in fundamentally different aspect.

We hypothesize that

in the limit $n \to \infty(\varepsilon \to 0)$, the elementary act of motion consists of an `annihilation´ of a particle at point $(x_i, t_i) \in M_4$, which can be thought of as the transition from initial state $|x_i, t_i >$ into unmanifested intermediate state, so-called, `motion´ state, $|\underline{x}_i, \underline{t}_i >$, and of subsequent `creation´ of a particle at infinitely close final point $(x_{i+1}, t_{i+1}) \in M_4$, which means the transition from `motion´ state, $|\underline{x}_i, \underline{t}_i >$, into final state, $|x_{i+1}, t_{i+1} >$. The motion state, $|\underline{x}_i, \underline{t}_i) >$, should be defined on unmanifested `master´ space, $\underline{M}_2$, which includes the points of all the atomic elements, $(\underline{x}_i, \underline{t}_i) \in \underline{M}_2$ $(i = 1, 2, ...)$.

This furnishes justification for an introduction of *unmanifested master space*, $\underline{M}_2$. A fundamental composition property of transformation functions (Schwinger, 2000), written in this limit for the extended Schwinger transformation function,

$$\lim_{n\to\infty} \left(F_{ext}(x_{i+1}, t_{i+1}; x_i, t_i) = \sum_{\underline{x}_i} < x_{i+1}, t_{i+1}|\underline{x}_i, \underline{t}_i >< \underline{x}_i, \underline{t}_i|x_i, t_i > \right), \tag{2}$$

would evidently imply that the number of intermediate points $(\underline{x}_i)$ should be set to one. The possibility of contemplating such a mechanism of motion is facilitated by the fact that although at first glance this is the only, not necessarily the most perfect, but rather clear way of setting the problem. To clarify the setup of the extended Schwinger transformation function, it should help a few noteworthy points of Fig. 1. The net result of each atomic double transition of a particle $M_4 \rightleftharpoons \underline{M}_2$ (from M_4 to $\underline{M}_2$ and back) is as if we had operated with a space-time *translation* on the original space M_4. So, the symmetry we are looking for must mix the particle quantum states during its propagation in order to reproduce the central relationship between the two successive transformations of this symmetry and the generators of space-time translations. Namely, the subsequent operation of two finite transformations will induce a translation in space and time of the states on which they operate. Such successive transformations will induce in M_4 the inhomogeneous Lorentz group, or Poincaré group, and that the unitary linear transformation $|x, t >\to U(\Lambda, a)|x, t >$ on vectors in the physical Hilbert space. Thus, the underlying algebraic structure of this symmetry generators closes with the algebra of *translations* on the original space M_4 in a way that it can then be summarized as a non-trivial extension of the Poincaré group algebra, including the generators of translations. Essentially the only truly appealing possibility of known symmetry possessing such manageable properties is the supersymmetry (SUSY), see e.g. (Aitchison, 2007, Baer & Tata, 2006, Dreiner et al., 2004, Fayet & Ferrara, 1977, Ferrara et al., 1974, Sohnius, 1985, Wess & Bagger, 1993, West, 1987). SUSY is accepted as a legitimate feature of nature, although the presence of specific `sparticle´ modes may be of some concern, since they have not (yet) been observed, except a few examples (Aharonov & Casher, 1979, Jackiw, 1984, Landau, 1930, Ravndal, 1980). SUSY-multiplets contain different spins but are always degenerate in mass and SUSY must be broken in nature where elementary particles do not come in mass-degenerate multiplets.

The successive atomic double transitions of a particle $M_4 \rightleftharpoons \underline{M}_2$ can necessarily be investigated coherently, at least conceptually, with SUSY-theory techniques, but certainly, we need to drastically change the scope of the standard SUSY to build up the `double space´- or `MS$_p$´-SUSY theory. As we will see, this is firstly related to the `superspace´ which is a direct sum extension of background double spaces $M_4 \oplus \underline{M}_2$, with an inclusion of additional fermionic coordinates induced by the spinors $(\underline{\theta}, \bar{\underline{\theta}})$, which refer to $\underline{M}_2$. Secondly, thanks to the embedding map (10), the spinors $(\underline{\theta}, \bar{\underline{\theta}})$, in turn, induce the spinors $\theta(\underline{\theta}, \bar{\underline{\theta}})$ and $\bar{\theta}(\underline{\theta}, \bar{\underline{\theta}})$ (see (93)), as to M_4. Consequently, the `symmetric´ superspace can be parameterized by

doi: https://doi.org/10.52526/25792776-23.70.2-170

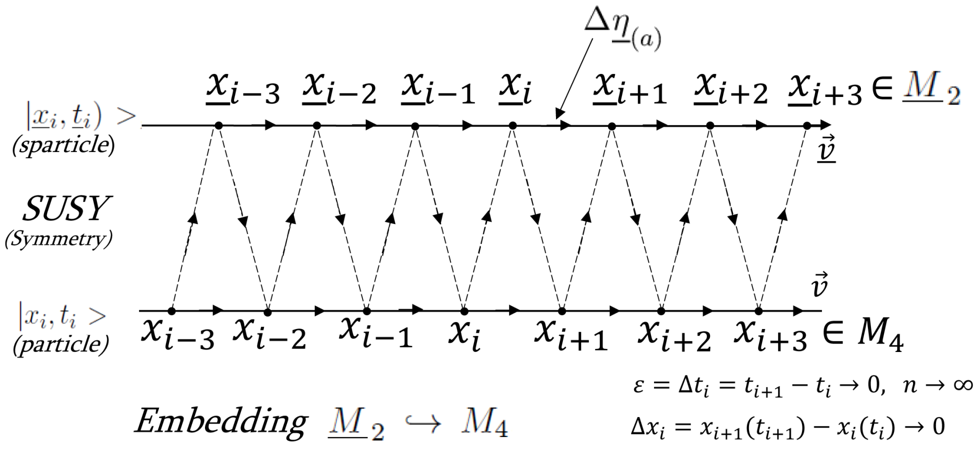

Figure 1. The extended Schwinger transformation function geometry. The `master´ space, MS$_p \equiv \underline{M}_2$, embedded in the background 4D-space M_4, is an unmanifested indispensable individual companion to the particle of interest, devoid of any external influence. A *creation* of a particle in $\underline{M}_2$ means its transition from initial state defined on M_4 into intermediate state defined on $\underline{M}_2$, while an *annihilation* of a particle in $\underline{M}_2$ means vice versa. The same interpretation holds for the *creation* and *annihilation* processes in M_4. The net result of each atomic double transition of a particle $M_4 \rightleftharpoons \underline{M}_2$ (from M_4 to $\underline{M}_2$ and back) is as if we had operated with a space-time *translation* on the original space M_4. The *atomic displacement*, $\Delta\underline{\eta}_{(a)}$, is caused in $\underline{M}_2$ by double transition of a particle, $\underline{M}_2 \rightleftharpoons M_4$. All the particles are living on M_4, while their superpartners can be viewed as living on $\underline{M}_2$.

$\Omega = \Omega_q(x^m,\ \theta(\underline{\theta},\bar{\underline{\theta}}),\ \bar{\theta}(\underline{\theta},\bar{\underline{\theta}})) \times \Omega_{\underline{q}}(\underline{\eta}^{\underline{m}},\ \underline{\theta},\ \bar{\underline{\theta}})$(*see* (66)). This is just enough to achieve the desired goal of deriving SLC in terms of spinors related to $\underline{M}_2$. This allows to introduce the physical finite *relative time* interval between two events, as integer number of the *own atomic duration time* of double transition of a particle $M_4 \rightleftharpoons \underline{M}_2$ (97). It is to be stressed that the ground state of MS$_p$-SUSY model has a vanishing energy value and is nondegenerate (SUSY unbroken). All the particles are living on M_4, and their superpartners can be viewed as living on $\underline{M}_2$. The particles in M_4 themselves can be considered as excited states above the underlying quantum vacuum of background double spaces $M_4 \oplus \underline{M}_2$, where the zero point cancellation occurs at ground-state energy, provided that the natural frequencies are set equal ($q_0^2 \equiv \nu_b = \nu_f$), because the fermion field has a negative zero point energy while the boson field has a positive zero point energy.

3. A hard look at MSp: Embedding $\underline{M}_2 \hookrightarrow M_4$

A notable conceptual element of our approach is the concept of, so-called, `master´ space (MS$_p$), which is indispensably tied to propagating particle of interest without relation to the other particles. The geometry of MS$_p$ is a new physical entity, with degrees of freedom and a dynamics of its own. We assume that a flat MS$_p$ is the 2D composite space,

$$\underline{M}_2 = \underline{R}^1_{(+)} \oplus \underline{R}^1_{(-)}. \tag{3}$$

The ingredient 1D-space $\underline{R}^1_{\underline{m}}$ is spanned by the coordinates $\underline{\eta}^{\underline{m}}$. The following notational conventions are used throughout this paper: all quantities related to the space $\underline{M}_2$ will be underlined. In particular, the underlined lower case Latin letters $\underline{m}, \underline{n}, ... = (\pm)$ denote the world indices related to $\underline{M}_2$. The Lorentz metric in $\underline{M}_2$ is

$$\underline{g} = \underline{g}(\underline{e}_{\underline{m}},\ \underline{e}_{\underline{n}})\,\underline{\vartheta}^{\underline{m}} \otimes \underline{\vartheta}^{\underline{n}}, \tag{4}$$

where $\underline{\vartheta}^{\underline{m}} = d\underline{\eta}^{\underline{m}}$ is the infinitesimal displacement. The basis $\underline{e}_{\underline{m}}$ at the point of interest in $\underline{M}_2$ is consisted of two real *null vectors*:

$$\underline{g}(\underline{e}_{\underline{m}},\ \underline{e}_{\underline{n}}) \equiv <\underline{e}_{\underline{m}},\ \underline{e}_{\underline{n}}> = {}^*o_{\underline{m}\underline{n}},\ ({}^*o_{\underline{m}\underline{n}}) = \begin{pmatrix} 0 & 1 \\ 1 & 0 \end{pmatrix}. \tag{5}$$

The norm, $i\underline{d} \equiv d\hat{\underline{\eta}}$, reads $i\underline{d} = \underline{e}\,\underline{\vartheta} = \underline{e}_{\underline{m}} \otimes \underline{\vartheta}^{\underline{m}}$, where $i\underline{d}$ is the tautological tensor field of type (1,1), $\underline{e}$ is a shorthand for the collection of the 2-tuplet $(\underline{e}_{(+)},\ \underline{e}_{(-)})$, and $\underline{\vartheta} = \begin{pmatrix} \underline{\vartheta}^{(+)} \\ \underline{\vartheta}^{(-)} \end{pmatrix}$. We may equivalently use a

doi: https://doi.org/10.52526/25792776-23.70.2-170

temporal $\underline{x}^{\underline{0}} \in \underline{T}^{\underline{1}}$ and a spatial $\underline{x}^{\underline{1}} \in \underline{R}^{\underline{1}}$ variables $\underline{x}^{\underline{r}}(\underline{x}^{\underline{0}},\, \underline{x}^{\underline{1}})(\underline{r}=\underline{0},\,\underline{1})$, such that

$$\underline{M}_2 = \underline{R}^{\underline{1}} \oplus \underline{T}^{\underline{1}}. \tag{6}$$

The norm, $i\underline{d}$, now can be rewritten in terms of displacement, $d\underline{x}^{\underline{r}}$, as

$$i\underline{d} = d\hat{\underline{x}} = \underline{e}_{\underline{0}} \otimes d\underline{x}^{\underline{0}} + \underline{e}_{\underline{1}} \otimes d\underline{x}^{\underline{1}}, \tag{7}$$

where $\underline{e}_{\underline{0}}$ and $\underline{e}_{\underline{1}}$ are, respectively, the temporal and spatial basis vectors:

$$\begin{array}{l} \underline{e}_{\underline{0}} = \frac{1}{\sqrt{2}}\left(\underline{e}_{(+)} + \underline{e}_{(-)}\right), \quad \underline{e}_{\underline{1}} = \frac{1}{\sqrt{2}}\left(\underline{e}_{(+)} - \underline{e}_{(-)}\right), \\ \underline{g}(\underline{e}_{\underline{r}},\, \underline{e}_{\underline{s}}) \equiv < \underline{e}_{\underline{r}},\, \underline{e}_{\underline{s}} >= diag(1,-1), \end{array} \tag{8}$$

and the corresponding coordinates are

$$\underline{x}^{\underline{0}} = \frac{1}{\sqrt{2}}\left(\underline{\eta}^{(+)} + \underline{\eta}^{(-)}\right), \quad \underline{x}^{\underline{1}} = \frac{1}{\sqrt{2}}\left(\underline{\eta}^{(+)} - \underline{\eta}^{(-)}\right). \tag{9}$$

Suppose the position of the particle is specified by the coordinates $x^m(s)$ $(x^0 = t)$ in the basis e_m (m=0,1,2,3) at given point in the background M_4 space. Consider a smooth (injective and continuous) embedding $\underline{M}_2 \hookrightarrow M_4$. That is, a smooth map $f:\ \underline{M}_2 \longrightarrow M_4$ is defined to be an immersion (the embedding which is a function that is a homeomorphism onto its image):

$$\underline{e}_{\underline{0}} = e_0, \quad \underline{x}^{\underline{0}} = x^0, \quad \underline{e}_{\underline{1}} = \vec{n}, \quad \underline{x}^{\underline{1}} = |\vec{x}|, \tag{10}$$

where $\vec{x} = e_i x^i = \vec{n}|\vec{x}|$ $(i = 1,2,3)$. Given the inertial frames $S_{(4)}, S'_{(4)}, S''_{(4)}, \ldots$ in unaccelerated uniform motion in M_4, we may define the corresponding inertial frames $\underline{S}_{(2)},\, \underline{S'}_{(2)},\, \underline{S''}_{(2)},\ldots$ in $\underline{M}_2$, which are used by the non-accelerated observers for the positions $\underline{x}^{\underline{r}}, \underline{x}'^{\underline{r}}, \underline{x}''^{\underline{r}}, \ldots$ of a free particle in flat $\underline{M}_2$. According to (10), the time axes of the two systems $\underline{S}_{(2)}$ and $S_{(4)}$ coincide in direction, and the time coordinates are taken the same. For the case at hand,

$$\underline{v}^{(\pm)} = \frac{d\underline{\eta}^{(\pm)}}{d\underline{x}^{\underline{0}}} = \frac{1}{\sqrt{2}}(\underline{v}^{\underline{0}} \pm \underline{v}^{\underline{1}}), \quad \underline{v}^{\underline{1}} = \frac{d\underline{x}^{\underline{1}}}{d\underline{x}^{\underline{0}}} = |\vec{v}| = |\frac{d\vec{x}}{dx^0}|, \tag{11}$$

and that

$$\underline{u} = \underline{e}_{\underline{m}}\underline{v}^{\underline{m}} = (\vec{\underline{v}}_{\underline{0}}, \vec{\underline{v}}_{\underline{1}}), \quad \vec{\underline{v}}_{\underline{0}} = \underline{e}_0\underline{v}^{\underline{0}}, \quad \vec{\underline{v}}_{\underline{1}} = \underline{e}_{\underline{1}}\underline{v}^{\underline{1}} = \vec{n}|\vec{v}| = \vec{v}, \tag{12}$$

therefore, $\underline{u} = u = (e_0, \vec{v})$. To explain why MS$_p$ is two dimensional, we note that only 2D real *null vectors* (8) are allowed as the basis at given point in MS$_p$, which is embedded in M_4. Literally speaking, the $\underline{M}_2$ can be viewed as 2D space living on the 4D world sheet.

Suppose the elements of the Hilbert space can be generated by the action of field-valued operators $\phi(x)\,(\chi(x),\, A(x))$ $(x \in M_4)$, where $\chi(x)$ is the Weyl fermion and $A(x)$ is the complex scalar bosonic field defined on M_4, and accordingly, of field-valued operators $\underline{\phi}(\underline{\eta})\,(\underline{\chi}(\underline{\eta})),\, \underline{A}(\underline{\eta}))$ $\quad \underline{\eta} \in \underline{M}_2)$, where $\underline{\chi}(\eta)$ is the Weyl fermion and $\underline{A}(\eta)$ is the complex scalar bosonic field defined on $\underline{M}_2$, on the translationally invariant vacuum:

$$\begin{array}{lll} |x>= \phi(x)|0>, & |x_1, x_2>= \phi(x_1)\phi(x_2)|0> & \text{(referring to } \ M_4), \\ |\underline{\eta}>= \underline{\phi}(\underline{\eta})|0>, & |\underline{\eta}_1, \underline{\eta}_2>= \underline{\phi}(\underline{\eta}_1)\underline{\phi}(\underline{\eta}_2)|0> & \text{(referring to } \ \underline{M}_2). \end{array} \tag{13}$$

The displacement of the field takes the form

$$\phi(x_1+x_2) = e^{ix_2^m p_m}\,\phi(x_1)\,e^{-ix_2^m p_m}, \quad \underline{\phi}(\underline{\eta}_1+\underline{\eta}_2) = e^{i\underline{\eta}_2^{\underline{m}}\underline{p}_{\underline{m}}}\,\underline{\phi}(\underline{\eta}_1)\,e^{-i\underline{\eta}_2^{\underline{m}}\underline{p}_{\underline{m}}}, \tag{14}$$

where $p_m = i\partial_m$ is the generator of translations on quantum fields $\phi(x)$, and $\underline{p}_{\underline{m}} = i\underline{\partial}_{\underline{m}}$ is the generator of translations on quantum fields $\underline{\phi}(\underline{\eta}) \equiv \underline{\phi}(\underline{x}^{\underline{0}}, \underline{x}^{\underline{1}})$:

$$[\phi, p_m] = i\partial_m\,\phi, \quad [\underline{\phi}, \underline{p}_{\underline{m}}] = i\underline{\partial}_{\underline{m}}\,\underline{\phi}, \tag{15}$$

where, according to embedding map (10), $(\underline{m} = (\pm)$ or $\underline{0}, \underline{1})$. The relation between the fields $\phi(x)$ and $\underline{\phi}(\underline{\eta})$ can be given by the proper orthochronous Lorentz transformation. For a field of spin-$\vec{S}$, the general transformation law reads

$$\phi'_\alpha(x') = M_\alpha{}^\beta\,\phi_\beta(x) = \exp\left(-\tfrac{1}{2}\vartheta^{mn}S_{mn}\right)_\alpha{}^\beta\,\phi_\beta(x) = \exp\left(-i\vec{\vartheta}\cdot\vec{S} - i\vec{\zeta}\cdot\vec{K}\right)_\alpha{}^\beta\,\phi_\beta(x), \tag{16}$$

doi: https://doi.org/10.52526/25792776-23.70.2-170

where the two-by-two matrix M ($M \in SL(2,C)$) of determinant one represents the action of the Lorentz group on two-component Weyl spinors, $\vec{\vartheta}$ is the rotation angle about an axis $\vec{k}$ ($\vec{\vartheta} \equiv \vartheta\vec{k}$), and $\vec{\zeta}$ is the boost vector $\vec{\zeta} \equiv \vec{e}_v \cdot \tan h^{-1} |\vec{v}|$, provided $\vec{e}_v \equiv \vec{v}/|\vec{v}|$, $\vartheta^i \equiv (1/2)\varepsilon^{ijk}\vartheta_k$ $(i,j,k = 1,2,3)$, and $\zeta^i \equiv \vartheta^{i0} = -\vartheta^{0i}$. The antisymmetric tensor $S_{mn} = -S_{nm}$, satisfying the commutation relations of the $SL(2.C)$, is the (finite-dimensional) irreducible matrix representations of the Lie algebra of the Lorentz group, and α and β label the components of the matrix representation space, the dimension of which is related to the spin $S^i \equiv (1/2)\varepsilon^{ijk} S_k$ of the particle. The spin $\vec{S}$ generates three-dimensional rotations in space and the $K^i \equiv S^{0i}$ generate the Lorentz-boosts. The fields of spin-zero ($\vec{S} = \vec{K} = 0$) scalar field $A(x)$ and spin-one $A^n(x)$, corresponding to the $(1/2,1/2)$ representation, transform under a general Lorentz transformation as folloqws:

$$\begin{array}{ll} \underline{A}(\underline{\eta}) \equiv A(x), & (\text{spin} \quad 0); \\ \underline{A}^{\underline{m}}(\underline{\eta}) = \Lambda^{\underline{m}}_{\ n} A^n(x), & (\text{spin} \quad 1). \end{array} \tag{17}$$

The map from $SL(2,C)$ to the Lorentz group is established through the $\vec{\sigma}$-Pauli spin matrices, $\sigma^m = (\sigma^0, \sigma^1, \sigma^2, \sigma^3) \equiv (I_2, \vec{\sigma})$, $\bar{\sigma}^m \equiv (I_2, -\vec{\sigma})$, where I_2 is the identity two-by-two matrix. Both hermitian matrices P and P' or $\underline{P}$ and $\underline{P'}$ have expansions, respectively, in σ or $\underline{\sigma}$:

$$(\sigma^m p'_m) = M(\sigma^m p_m)M^\dagger, \quad (\sigma^{\underline{m}} p'_{\underline{m}}) = M(\sigma^{\underline{m}} p_{\underline{m}})M^\dagger, \tag{18}$$

where $M(M \in SL(2,C))$ is unimodular two-by-two matrix. According to embedding map (10), the $\underline{\sigma}$-matrices are

$$\sigma^{\underline{m}} = \sigma^{(\pm)} = \frac{1}{\sqrt{2}}(\sigma^{\underline{0}} \pm \sigma^{\underline{1}}) = \frac{1}{\sqrt{2}}(\sigma^0 \pm \sigma^3). \tag{19}$$

The matrices $\sigma^{\underline{m}}$ form a basis for two-by-two complex matrices $\underline{P}$:

$$\underline{P} = (p_{\underline{m}}\sigma^{\underline{m}}) = (p_{(\pm)}\sigma^{(\pm)}) = (p_{\underline{0}}\sigma^{\underline{0}} + p_{\underline{1}}\sigma^{\underline{1}}), \tag{20}$$

provided $p_{(\pm)} = i\partial_{\underline{\eta}^{(\pm)}}$, $p_{\underline{0}} = i\partial_{\underline{x}^{\underline{0}}}$ and $p_{\underline{1}} = i\partial_{\underline{x}^{\underline{1}}}$. The real coefficients $p'_{\underline{m}}$ and $p_{\underline{m}}$, like p'_m and p_m, are related by a Lorentz transformation $p'_{\underline{m}} = \Lambda^{\underline{n}}_{\underline{m}} p_{\underline{n}}$, because the relations $det(\sigma^{\underline{m}} p_{\underline{m}}) = p^2_{\underline{0}} - p^2_{\underline{1}}$ and $det\, M = 1$ yield $p'^{\,2}_{\underline{0}} - p'^{\,2}_{\underline{1}} = p^2_{\underline{0}} - p^2_{\underline{1}}$. Correspondence of $p_{\underline{m}}$ and $\underline{P}$ is uniquely: $p_{\underline{m}} = \frac{1}{2}Tr(\sigma^{\underline{m}}\underline{P})$, which combined with (18) yields

$$\Lambda^{\underline{m}}_{\underline{n}}(M) = \frac{1}{2}\, Tr\left(\sigma^{\underline{m}} M \sigma^{\underline{n}} M^\dagger\right). \tag{21}$$

Meanwhile $(\underline{\chi}\, \sigma^{\underline{m}} \bar{\underline{\zeta}})\, \underline{A}_{\underline{m}}$ is a Lorentz scalar if the following condition is satisfied:

$$\Lambda^{\underline{m}}_{\underline{n}}(M)\sigma^{\underline{n}}_{\alpha\dot{\alpha}} = (M^{-1})_\alpha^{\ \beta}\sigma^{\underline{m}}_{\beta\dot{\beta}}(M^{-1})^{\dagger\dot{\beta}}{}_{\dot{\alpha}}. \tag{22}$$

A two-component $(1/2,0)$ Weyl fermion, $\chi_\beta(x)$, therefore, transforms under Lorentz transformation to yield $\underline{\chi}_\alpha(\underline{\eta})$:

$$\chi_\beta(x) \longrightarrow \underline{\chi}_\alpha(\underline{\eta}) = (M_R)_\alpha^{\ \beta} \chi_\beta(x), \quad \alpha, \beta = 1, 2, \tag{23}$$

where the orthochronous Lorentz transformation, corresponding to a rotation by the angles ϑ_3 and ϑ_2 about, respectively, the axes n_3 and n_2, is given by rotation matrix

$$M_R = e^{i\frac{1}{2}\sigma_2\vartheta_2} e^{i\frac{1}{2}\sigma_3\vartheta_3}. \tag{24}$$

There with the rotation of an hermitian matrix P is

$$p_{\underline{m}}\sigma^{\underline{m}} = M_R\, p_m \sigma^m\, M_R^\dagger, \tag{25}$$

where p_m and $p_{\underline{m}}$ denote the momenta $p_m \equiv m(ch\beta,\ sh\beta \sin\vartheta_2 \cos\vartheta_3,\ sh\beta \sin\vartheta_2 \sin\vartheta_3,$ $sh\beta \cos\vartheta_2)$, and $p_{\underline{m}} \equiv m(ch\underline{\beta},\ 0,\ 0,\ sh\underline{\beta})$.

A two-component $(0,1/2)$ Weyl spinor field is denoted by $\bar{\chi}^{\dot{\beta}}(x)$, and transforms as

$$\bar{\chi}^{\dot{\beta}}(x) \longrightarrow \underline{\bar{\chi}}^{\dot{\alpha}}(\underline{\eta}) = (M_R^{-1})^{\dagger\dot{\alpha}}{}_{\dot{\beta}}\, \bar{\chi}^{\dot{\beta}}(x), \quad \dot{\alpha}, \dot{\beta} = 1, 2. \tag{26}$$

The so-called `dotted´ indices have been introduced to distinguish the $(0,1/2)$ representation from the $(1/2,0)$ representation. The `bar´ over the spinor is a convention that this is the $(0,1/2)$-representation.

doi: https://doi.org/10.52526/25792776-23.70.2-170

We used the Van der Waerden notations for the Weyl two-component formalism: $(\bar{\underline{\chi}}_{\dot{\alpha}})^* = \underline{\chi}_\alpha$ and $\bar{\underline{\chi}}_{\dot{\alpha}} = (\underline{\chi}_\alpha)^*$. The infinitesimal Lorentz transformation matrices for the $(1/2, 0)$ and $(0, 1/2)$ representations,

$$\begin{array}{ll} M \simeq I_2 - \frac{i}{2}\vec{\vartheta}\cdot\vec{\sigma} - \frac{1}{2}\vec{\zeta}\cdot\vec{\sigma}, & \text{for } (\frac{1}{2}, 0); \\ (M^{-1})^\dagger \simeq I_2 - \frac{i}{2}\vec{\vartheta}\cdot\vec{\sigma} + \frac{1}{2}\vec{\zeta}\cdot\vec{\sigma}, & \text{for } \quad (0, \frac{1}{2}) \end{array} \tag{27}$$

give $S^{mn} = \sigma^{mn}$ for the $(1/2, 0)$ representation, and $S^{mn} = \bar{\sigma}^{mn}$ for the $(0, 1/2)$ representation, where the bilinear covariants that transform as a Lorentz second-rank tensor read

$$(\sigma^{mn})_\alpha{}^\beta \equiv \frac{i}{4}(\sigma^m_{\alpha\dot{\alpha}}\,\bar{\sigma}^{n\dot{\alpha}\beta} - \sigma^n_{\alpha\dot{\alpha}}\,\bar{\sigma}^{m\dot{\alpha}\beta}), \quad (\bar{\sigma}^{mn})^{\dot{\alpha}}{}_{\dot{\beta}} \equiv \frac{i}{4}(\bar{\sigma}^{m\dot{\alpha}\alpha}\,\sigma^n_{\alpha\dot{\beta}} - \bar{\sigma}^{n\dot{\alpha}\alpha}\,\sigma^m_{\alpha\dot{\beta}}), \tag{28}$$

provided $\bar{\sigma}^m \equiv (I_2; -\vec{\sigma})$, $(\sigma^{m*})_{\alpha\dot{\beta}} = \sigma^m_{\beta\dot{\alpha}}$ and $(\bar{\sigma}^{m*})^{\dot{\alpha}\beta} = \bar{\sigma}^{m\dot{\beta}\alpha}$.

4. The MS$_p$-SUSY

The theoretical significance resides in constructing the MS$_p$-SUSY as a guiding principle. If that is the case as above, a *creation* of a particle in $\underline{M}_2$ means its transition from initial state defined on M_4 into intermediate state defined on $\underline{M}_2$, while an *annihilation* of a particle in $\underline{M}_2$ means vice versa. The same interpretation holds for the *creation* and *annihilation* processes in M_4. All the fermionic and bosonic states taken together form a basis in the Hilbert space. The basis vectors in the Hilbert space composed of $H_B \otimes H_F$ is given by

$$\{|\underline{n}_b > \otimes |0>_f,\ |\underline{n}_b > \otimes f^\dagger\,|0>_f\},$$

or

$$\{|n_b > \otimes |\underline{0}>_f,\ |n_b > \otimes \underline{f}^\dagger\,|\underline{0}>_f\},$$

where we consider two pairs of creation and annihilation operators $(b^\dagger,\, b)$ and $(f^\dagger,\, f)$ for bosons and fermions, respectively, referred to the background space M_4, as well as $(\underline{b}^\dagger,\, \underline{b})$ and $(\underline{f}^\dagger,\, \underline{f})$ for bosons and fermions, respectively, as to background master space $\underline{M}_2$. The boson and fermion number operators are $N_b = b^\dagger b$ or $\underline{N}_b = \underline{b}^\dagger\underline{b}$, where $N_b|n_b >= n_b|n_b >$ and $\underline{N}_b|\underline{n}_b >= \underline{n}_b|\underline{n}_b >$ $(= 0, 1, ..., \infty)$, and $N_f = f^\dagger f$ or $\underline{N}_f = \underline{f}^\dagger\underline{f}$, provided $N_f|n_f >= n_f|n_f >$ and $\underline{N}_f|\underline{n}_f >= \underline{n}_f|\underline{n}_f >$ $(= 0, 1)$. Taking into account the action of $(b, b^\dagger)$ or $(\underline{b}, \underline{b}^\dagger)$ upon the eigenstates $|n_b >$ or $|\underline{n}_b >$, respectively:

$$\begin{array}{ll} b|n_b >= \sqrt{n_b}|n_b - 1>, & b^\dagger|n_b >= \sqrt{n_{b+1}}|n_b + 1>, \\ \underline{b}|\underline{n}_b >= \sqrt{\underline{n}_b}|\underline{n}_b - 1>, & \underline{b}^\dagger|\underline{n}_b >= \sqrt{\underline{n}_b + 1}|\underline{n}_b + 1>, \end{array} \tag{29}$$

we may construct the quantum operators, $(q^\dagger,\, \underline{q}^\dagger)$ and $(q,\, \underline{q})$, which replace bosons by fermions and vice versa:

$$\begin{array}{l} q\,|\underline{n}_b,\, n_f >= q_0\sqrt{\underline{n}_b}\,|\underline{n}_b - 1,\, n_f + 1>, \\ q^\dagger\,|\underline{n}_b,\, n_f >= q_0\sqrt{\underline{n}_b + 1}\,|\underline{n}_b + 1,\, n_f - 1>, \end{array} \tag{30}$$

and that

$$\begin{array}{l} \underline{q}\,|n_b,\, \underline{n}_f >= q_0\sqrt{n_b}\,|n_b - 1,\, \underline{n}_f + 1>, \\ \underline{q}^\dagger\,|n_b,\, \underline{n}_f > q_0\sqrt{n_b + 1}\,|n_b + 1,\, \underline{n}_f - 1>\,. \end{array} \tag{31}$$

This framework combines bosonic and fermionic states on the same footing, rotating them into each other under the action of operators q and $\underline{q}$. Putting two operators in one $B = (\underline{b}$ or $b)$ and $F = (f$ or $\underline{f})$, the canonical quantization rules can be written most elegantly as

$$\begin{array}{l} [B,\, B^\dagger] = 1; \quad \{F,\, F^\dagger\} = 1; \quad [B,\, B] = [B^\dagger,\, B^\dagger] = \{F,\, F\} = \{F^\dagger,\, F^\dagger\} \\ = [B,\, F] = [B,\, F^\dagger] = [B^\dagger,\, F] = [B^\dagger,\, F^\dagger] = 0, \end{array} \tag{32}$$

where we note that $\delta_{ij}\delta^3(\vec{p} - \vec{p}')$ and $\delta_{ij}\delta^3(\underline{\vec{p}} - \underline{\vec{p}}')$ are the unit element 1 of the convolution product *, while according to embedding map (10), we have $\underline{\vec{p}} = \vec{n}|\vec{p}| = \vec{p}$ and $\underline{\vec{p}}' = \vec{p}'$. The operators q and $\underline{q}$ can be constructed as

$$q = q_0,\underline{b}\,f^\dagger, \quad q^\dagger = q_0\,\underline{b}^\dagger\,f, \quad \underline{q} = q_0\,b\underline{f}^\dagger, \quad \underline{q}^\dagger = q_0\,b^\dagger\,\underline{f}. \tag{33}$$

So, we may refer the action of the supercharge operators q and $q^\dagger$ to the background space M_4, having applied in the chain transformations of fermion χ (accompanied with the auxiliary field F as it will be seen later on) to boson $\underline{A}$, defined on $\underline{M}_2$:

$$\longrightarrow \chi^{(F)} \longrightarrow \underline{A} \longrightarrow \chi^{(F)} \longrightarrow \underline{A} \longrightarrow \chi^{(F)} \longrightarrow . \tag{34}$$

doi: https://doi.org/10.52526/25792776-23.70.2-170

Respectively, we may refer the action of the supercharge operators $\underline{q}$ and $\underline{q}^\dagger$ to the $\underline{M}_2$, having applied in the chain transformations of fermion $\underline{\chi}$ (accompanied with the auxiliary field $\underline{F}$) to boson A, defined on the background space M_4:

$$\longrightarrow \underline{\chi}^{(\underline{F})} \longrightarrow A \longrightarrow \underline{\chi}^{(\underline{F})} \longrightarrow A \longrightarrow \underline{\chi}^{(\underline{F})} \longrightarrow . \tag{35}$$

Written in one notation, $Q = (q \text{ or } \underline{q})$, the operators (33) become

$$Q = q_0\, B^\dagger F = (q \text{ or } \underline{q}), \quad Q^\dagger = q_0\, BF^\dagger = (q^\dagger \text{ or } \underline{q}^\dagger). \tag{36}$$

Due to nilpotent fermionic operators $F^2 = (F^\dagger)^2 = 0$, the operators Q and $Q\dagger$ also are nilpotent: $Q^2 = (Q^\dagger)^2 = 0$. Hence, the quantum system can be described in one notation by the selfadjoint Hamiltonian $\mathcal{H} \equiv \{Q^\dagger, Q\} = (H_q \equiv \{q^\dagger, q\} \text{ or } H_{\underline{q}} \equiv \{\underline{q}^\dagger, \underline{q}\})$, and the generators Q and $Q^\dagger$, where the commutators as well as anticommutators appear in the algebra of symmetry generators. Such an algebra involving commutators and anticommutators is called a Lie algebra (GLA):

$$\mathcal{H} = \{Q^\dagger, Q\} \geq 0; \quad [\mathcal{H}, Q] = [\mathcal{H}, Q^\dagger] = 0. \tag{37}$$

This is a sum of Hamiltonian of bosonic and fermionic noninteracting oscillators, which decouples, for $Q = q$, into

$$H_q = q_0^2\, (\underline{b}^\dagger \underline{b} + f^\dagger f) = q_0^2\, (\underline{b}^\dagger \underline{b} + \tfrac{1}{2}) + q_0^2\, (f^\dagger f - \tfrac{1}{2}) \equiv H_{\underline{b}} + H_f, \tag{38}$$

or, for $Q = \underline{q}$, into

$$H_{\underline{q}} = q_0^2\, (b^\dagger b + \underline{f}^\dagger \underline{f}) = q_0^2\, (b^\dagger b + \tfrac{1}{2}) + q_0^2\, (\underline{f}^\dagger \underline{f} - \tfrac{1}{2}) \equiv H_b + H_{\underline{f}}, \tag{39}$$

with the corresponding energies:

$$E_q = q_0^2\, (\underline{n}_b + \tfrac{1}{2}) + q_0^2\, (n_f - \tfrac{1}{2}), \quad E_{\underline{q}} = q_0^2\, (n_b + \tfrac{1}{2}) + q_0^2\, (\underline{n}_f - \tfrac{1}{2}). \tag{40}$$

The proposed algebra (37) becomes more clear in a normalization $q_0 = \sqrt{m}$:

$$\{Q^\dagger, Q\} = 2m; \quad \{Q, Q\} = \{Q^\dagger, Q^\dagger\} = 0. \tag{41}$$

The latter has underlying algebraic structure of the superalgebra for massive *one-particle* states in the rest frame of $N = 1$ SUSY theory without central charges. This is rather technical topic, and it requires care to do correctly. In what follows we only give a brief sketch. The extension of the MS_p-SUSY superalgebra (41) in general case when $\vec{p} = i\vec{\partial} \neq 0$ in M_4 or $\vec{\underline{p}}_1 = i\vec{\underline{\partial}}_1 \neq 0$ in $\underline{M}_2$, and assuming that the resulting motion of a particle in M_4 is governed by the Lorentz symmetries, the MS_p-SUSY algebra can then be summarized as a non-trivial extension of the Poincaré group algebra those of the commutation relations of the bosonic generators of four momenta and six Lorentz generators referred to M_4. Moreover, if there are several spinor generators $Q_\alpha{}^i$ with $i = 1, ..., N$ - theory with $N-$extended supersymmetry, can be written as a GLA of SUSY field theories, with commuting and anticommuting generators:

$$\begin{aligned} &\{Q_\alpha{}^i, \bar{Q}^j{}_{\dot{\alpha}}\} = 2\delta^{ij}\, \sigma^{\hat{m}}_{\alpha\dot{\alpha}}\, p_{\hat{m}}; \\ &\{Q_\alpha{}^i, Q_\beta{}^j\} = \{\bar{Q}^i{}_{\dot{\alpha}}, \bar{Q}^j{}_{\dot{\beta}}\} = 0; \\ &[p_{\hat{m}}, Q_\alpha{}^i] = [p_{\hat{m}}, \bar{Q}^j{}_{\dot{\alpha}}] = 0, \quad [p_{\hat{m}}, p_{\hat{n}}] = 0. \end{aligned} \tag{42}$$

The odd part of the supersymmetry algebra is composed entirely of the spin-1/2 operators $Q_\alpha{}^i$, $Q_\beta{}^j$. In order to trace a maximal resemblance in outward appearance to the standard SUSY theories, here we set one notation $\hat{m} = (m \quad \text{if} \quad Q = q, \text{ or } \underline{m} \quad \text{if} \quad Q = \underline{q})$, and as before the indices α and $\dot{\alpha}$ run over 1 and 2.

The supersymmetry charges, $Q_\alpha{}^i$, can be obtained as usual Noether charges associated with a conserved fermionic Noether current, $J_\alpha{}^{i\,\hat{m}} = (j_\alpha{}^{i\,m} \text{ or } \underline{j}_\alpha{}^{i\,\underline{m}})$,

$$q_\alpha{}^i = \int d^3x\, j_\alpha{}^{i\,0}, \quad \text{or} \quad \underline{q}_\alpha{}^i = \int d\eta\, \underline{j}_\alpha{}^{i\,\underline{0}}. \tag{43}$$

The supercurrent $J_\alpha{}^{i\,\hat{m}}$ is an anticommuting six-vector, which also carries a spinor index, as befits the current associated with a symmetry with fermionic generators, where the supercurrent and its hermitian

doi: https://doi.org/10.52526/25792776-23.70.2-170

conjugate are separately conserved ($\partial_m j_\alpha{}^{im} = 0$ and $\partial_m \bar{j}_\alpha{}^{im} = 0$), and ($\partial_{\underline{m}} \underline{j}_\alpha{}^{i\underline{m}} = 0$ and $\partial_{\underline{m}} \bar{\underline{j}}_\alpha{}^{i\underline{m}} = 0$). So for both supercharges, q and $\underline{q}$, we get a supersymmetric models, respectively:

$$\begin{aligned} &\{q_\alpha{}^i,\, \bar{q}^j{}_{\dot\alpha}\} = 2\delta^{ij}\, \sigma^m_{\alpha\dot\alpha}\, p_m; \\ &\{q_\alpha{}^i,\, q_\beta{}^j\} = \{\bar{q}^i{}_{\dot\alpha},\, \bar{q}^j{}_{\dot\beta}\} = 0; \\ &[p_m,\, q_\alpha{}^i] = [p_m,\, \bar{q}^j{}_{\dot\alpha}] = 0, \quad [p_m,\, p_n] = 0. \end{aligned} \tag{44}$$

and

$$\begin{aligned} &\{\underline{q}_\alpha{}^i,\, \bar{\underline{q}}^j{}_{\dot\alpha}\} = 2\delta^{ij}\, \sigma^{\underline{m}}_{\alpha\dot\alpha}\, p_{\underline{m}}; \\ &\{\underline{q}_\alpha{}^i,\, \underline{q}_\beta{}^j\} = \{\bar{\underline{q}}^i{}_{\dot\alpha},\, \bar{\underline{q}}^j{}_{\dot\beta}\} = 0; \\ &[p_{\underline{m}},\, \underline{q}_\alpha{}^i] = [p_{\underline{m}},\, \bar{\underline{q}}^j{}_{\dot\alpha}] = 0, \quad [p_{\underline{m}},\, p_{\underline{n}}] = 0. \end{aligned} \tag{45}$$

Remark: In the standard theory, the Q's operate with fields defined in the single M_4 space. It is why the result of a Lorentz transformation in M_4 followed by a supersymmetry transformation is different from that when the order of the transformations is reversed (Sohnius, 1985). But, in the MS_p-SUSY theory, the Q's ((33), (36)) operate with fields defined on both M_4 and $\underline{M}_2$ spaces, fulfilling a transition of a particle between these spaces ($M_4 \rightleftharpoons \underline{M}_2$). The particle motion arises as a complex process of the global MS_p-SUSY double transformations, therefore we will obtain the same result if we reverse the order of the Lorentz and supersymmetry transformations.

We cut short further description of the unitary supersymmetry representations that give rise to the concept of supermultiplets, since they are so well known.

5. Non-trivial linear representation of the MS_p-SUSY algebra

With these guidelines to follow, we start by considering the simplest example of a supersymmetric theory in six dimensional background space $M_4 \oplus \underline{M}_2$ as the MS_p-generalization of free Wess-Zumino toy model (Wess & Zumino, 1974) of standard theory. To obtain a feeling for this model we may consider first example of non-trivial linear representation $(\psi, \mathcal{A}, \mathcal{F})$, of the MS_p-SUSY algebra. This has $N = 1$ and $s_0 = 0$, and contains two Weyl spinor states of a massive Majorana spinor $\psi(\chi,\, \underline{\chi})$, two complex scalar fields $\mathcal{A}(A,\, \underline{A})$, and two more real scalar degrees of freedom in the complex auxiliary fields $\mathcal{F}(F,\, \underline{F})$, which provide in supersymmetry theory the fermionic and bosonic degrees of freedom to be equal off-shell as well as on-shell, and are eliminated when one goes on-shell. The component multiplets, $(\psi, \mathcal{A}, \mathcal{F})$, are called the chiral or scalar multiplets. This model is instructive because it contains the essential elements of the MS_p-induced SUSY and, therefore, intended to be rather complementary to the superfield derivations given in next section.

The anticommuting (Grassmann) parameters $\epsilon^\alpha(\xi^\alpha,\, \underline{\xi}^\alpha)$ and $\bar\epsilon^\alpha(\bar\xi^\alpha,\, \bar{\underline{\xi}}^\alpha)$:

$$\begin{aligned} &\{\epsilon^\alpha,\, \epsilon^\beta\} = \{\bar\epsilon^\alpha,\, \bar\epsilon^\beta\} = \{\epsilon^\alpha,\, \bar\epsilon^\beta\} = 0, \\ &\{\epsilon^\alpha,\, Q_\beta\} = \cdots = [p_{\hat m},\, \epsilon^\alpha] = 0, \end{aligned} \tag{46}$$

allow us to write the algebra (42) for ($N = 1$) entirely in terms of commutators:

$$\begin{aligned} &[\epsilon Q,\, \bar Q\bar\epsilon] = 2\epsilon\sigma^{\hat m}\bar\epsilon p_{\hat m}, \\ &[\epsilon Q,\, \epsilon Q] = [\bar Q\bar\epsilon,\, \bar Q\bar\epsilon] = [p^{\hat m},\, \epsilon Q] = [p^{\hat m},\, \bar Q\bar\epsilon] = 0. \end{aligned} \tag{47}$$

For brevity, here the indices $\epsilon Q = \epsilon^\alpha Q_\alpha$ and $\bar\epsilon\bar Q = \bar\epsilon_{\dot\alpha}\bar Q^{\dot\alpha}$ will be suppressed unless indicated otherwise. This supersymmetry transformation maps tensor fields $\mathcal{A}(A,\, \underline{A})$ into spinor fields $\psi(\chi,\, \underline{\chi})$ and vice versa. From the algebra (47) we see that Q has mass dimension $1/2$. Therefore, as usual, fields of dimension ℓ transform into fields of dimension $\ell + 1/2$ or into derivatives of fields of lower dimension.

Starting with the scalar field $\underline{A}(\underline{\eta}) = A(x)$ (17), in the view of chain transformations (34), we should define the spinor χ as the field into which $\underline{A}(\underline{\eta})$ transforms:

$$\delta_\xi \underline{A} = (\xi q + \bar\xi\bar q) \times \underline{A} = \sqrt{2}\xi\chi. \tag{48}$$

The field χ transforms into a tensor field of higher dimension and into the derivative of $\underline{A}$ itself:

$$\delta_\xi \chi = (\xi q + \bar\xi\bar q) \times \chi = i\sqrt{2}\sigma^m\bar\xi(\delta^0_m\, \underline{\partial}_{\underline{0}} + \tfrac{1}{|\vec{x}|}x^i\delta_{im}\, \underline{\partial}_{\underline{1}})\underline{A} + \sqrt{2}\xi F, \tag{49}$$

doi: https://doi.org/10.52526/25792776-23.70.2-170

where $i = 1, 2, 3$. The coefficient of $(\delta^0_{\underline{m}}\,\underline{\partial_0} + \frac{1}{|\vec{x}|}x^i\delta_{im}\,\underline{\partial_1})\underline{A}$ is chosen to guarantee that the commutator of

$$\delta_{\xi_1}\delta_{\xi_2}\underline{A} = i2\xi_1\sigma^m\bar{\xi}_2(\delta^0_{\underline{m}}\,\underline{\partial_0} + \tfrac{1}{|\vec{x}|}x^i\delta_{im}\,\underline{\partial_1})\underline{A} + 2\xi_1\bar{\xi}_2 F \tag{50}$$

closes in the sense of

$$(\delta_{\xi_1}\delta_{\xi_2} - \delta_{\xi_2}\delta_{\xi_1})\underline{A} = -2i(\xi_1\sigma^m\bar{\xi}_2 - \xi_2\sigma^m\bar{\xi}_1) \times (\delta^0_{\underline{m}}\underline{\partial_0} + \tfrac{1}{|\vec{x}|}x^i\delta_{im}\underline{\partial_1})\underline{A}. \tag{51}$$

The same commutator acting on the field χ: $(\delta_{\xi_1}\delta_{\xi_2} - \delta_{\xi_2}\delta_{\xi_1})\chi$, closes if

$$\delta_\xi F = (\xi q + \bar{\xi}\bar{q}) \times F = i\sqrt{2}\bar{\xi}\bar{\sigma}^m\partial_m\chi. \tag{52}$$

In the same way, we should define the spinor $\underline{\chi}$ as the field into which $A(x)$ transforms. In this case, the infinitesimal supersymmetry transformations for $Q = \underline{q}$, by virtue of (35), read

$$\begin{aligned} &\delta_{\underline{\xi}} A = (\underline{\xi}\,\underline{q} + \bar{\underline{\xi}}\,\bar{\underline{q}}) \times A = \sqrt{2}\,\underline{\xi}\,\underline{\chi},\\ &\delta_{\underline{\xi}}\,\underline{\chi} = (\underline{\xi}\,\underline{q} + \bar{\underline{\xi}}\,\bar{\underline{q}}) \times \underline{\chi} = i\sqrt{2}\,\sigma^{\underline{m}}\,\bar{\underline{\xi}}\,(\delta^0_{\underline{m}}\,\partial_0 + \tfrac{|\vec{x}|}{x^i}\,\delta^1_{\underline{m}}\,\partial_i)A + \sqrt{2}\underline{\xi}\,\underline{F},\\ &\delta_{\underline{\xi}}\,\underline{F} = (\underline{\xi}\,\underline{q} + \bar{\underline{\xi}}\,\bar{\underline{q}}) \times \underline{F} = i\sqrt{2}\,\bar{\underline{\xi}}\,\bar{\sigma}^{\underline{m}}\,\partial_{\underline{m}}\,\underline{\chi}. \end{aligned} \tag{53}$$

If $\mathcal{A}$ has dimension 1, then ψ has dimension 3/2, while $\mathcal{F}$ has dimension 2 and must assume the role of auxiliary field. We see that the latter transforms into a space derivative under δ_ξ or $\delta_{\underline{\xi}}$. This will always be the case for the component of highest dimension in any given multiplet. The first relation in (47) means that there should be a particular way of going from one subspace (bosonic/fermionic) to the other and back, such that the net result is as if we had operator of translation $p_{\hat{m}}$ on the original subspace. Actually, in general, the supersymmetry transformations close supersymmetry algebra for $\mathcal{A}$, ψ and $\mathcal{F}$.

To construct an invariant action it is sufficient to find combinations of fields which transform into space derivatives. The supersymmetric kinetic energy defined in terms of superfields, $\underline{\phi}(\underline{z}^{(M_2)})$, constructed in the superspace $\underline{z}^{(M_2)} = (\underline{\eta}^{\underline{m}}, \underline{\theta}, \bar{\underline{\theta}})$, is

$$\int d^2\underline{\eta}\, d^4\underline{\theta}\,\underline{\phi}^\dagger\,\underline{\phi}, \tag{54}$$

where the superspace Lagrangian is written

$$\begin{aligned} &\underline{\phi}^\dagger\,\underline{\phi} = A^*A + \cdots + \underline{\theta}\,\underline{\theta}\,\bar{\underline{\theta}}\,\bar{\underline{\theta}}\left[\tfrac{1}{4}A^*\Box A + \tfrac{1}{4}\Box A^*A - \tfrac{1}{2}\partial_m A^*\,\partial^m A\right.\\ &\left.+\underline{F}^*\,\underline{F} + \tfrac{i}{2}\partial_{\underline{m}}\,\bar{\underline{\chi}}\,\bar{\sigma}^{\underline{m}}\,\underline{\chi} - \tfrac{i}{2}\,\bar{\underline{\chi}}\bar{\sigma}^{\underline{m}}\,\partial_{\underline{m}}\,\underline{\chi}\right]. \end{aligned} \tag{55}$$

In (54), as usual, we imply the measures in terms of four Grassmannian variables $\underline{\theta}_1, \underline{\theta}_2$ and $\bar{\underline{\theta}}^1, \bar{\underline{\theta}}^2$ as follows:

$$\begin{aligned} &d^4\underline{\theta} = d^2\underline{\theta}\,d^2\bar{\underline{\theta}}, \quad d^2\underline{\theta} = -\tfrac{1}{4}\varepsilon_{\alpha\beta}\,\underline{\theta}^\alpha\,\underline{\theta}^\beta,\\ &d^2\bar{\underline{\theta}} = -\tfrac{1}{4}\varepsilon^{\dot{\alpha}\dot{\beta}}\,\bar{\underline{\theta}}_{\dot{\alpha}}\,\bar{\underline{\theta}}_{\dot{\beta}}, \end{aligned} \tag{56}$$

where involving Berezin's integration in the superspace, we have

$$\int \underline{\theta}^2\,d^2\underline{\theta} = \int \bar{\underline{\theta}}^2\,d^2\bar{\underline{\theta}} = 1, \quad \int \underline{\theta}^2\bar{\underline{\theta}}^2\,d^4\underline{\theta} = 1. \tag{57}$$

All other integrations give zero. Similarly, consider the superspace $z^{(M_4)} = (x^m,\, \theta(\underline{\theta}, \bar{\underline{\theta}})),\, \bar{\theta}(\underline{\theta}, \bar{\underline{\theta}}))$, which is an extension of M_4 by the inclusion of additional spinors, induced by the spinors $\underline{\theta}$ and $\bar{\underline{\theta}}$ (see (93)). The supervolume integrals of products of superfields, $\phi(z^{(M_4)})$, constructed in the superspace $z^{(M_4)}$ will lead to the supersymmetric kinetic energy for the MS$_p$-Wess-Zumino model

$$\int d^4x\, d^4\theta\,\phi^\dagger\phi, \tag{58}$$

where the superspace Lagrangian reads

$$\begin{aligned} &\phi^\dagger\phi = \underline{A}^*\,\underline{A} + \cdots + \theta\theta\bar{\theta}\bar{\theta}\,\left[\tfrac{1}{4}\underline{A}^*\,\underline{\Box}\,\underline{A} + \tfrac{1}{4}\underline{\Box}\,\underline{A}^*\,\underline{A} - \tfrac{1}{2}\partial_{\underline{m}}\underline{A}^*\,\partial^{\underline{m}}\underline{A}\right.\\ &\left.+F^*F + \tfrac{i}{2}\partial_m\bar{\chi}\bar{\sigma}^m\chi - \tfrac{i}{2}\bar{\chi}\bar{\sigma}^m\partial_m\chi\right], \end{aligned} \tag{59}$$

and $\Box A = \underline{\Box}\,\underline{A}$, $\partial_{\underline{m}}\underline{A}^*\,\partial^{\underline{m}}\underline{A} = \partial_m A^*\,\partial^m A$.

Thus, the equations of motion for non-trivial linear representation model can be derived from the following Lagrangians:

$$\mathcal{L}_{Q=q} = \mathcal{L}_0 + m\mathcal{L}_m, \quad \mathcal{L}_{Q=\underline{q}} = \underline{\mathcal{L}}_0 + m\underline{\mathcal{L}}_m, \tag{60}$$

doi: https://doi.org/10.52526/25792776-23.70.2-170

provided,

$$\begin{array}{ll} \mathcal{L}_0 = i\partial_m\bar{\chi}\bar{\sigma}^m\chi + \underline{A}^*\underline{\Box}\,\underline{A} + F^*F, & \mathcal{L}_m = \underline{A}\,F + \underline{A}^*\,F^* - \frac{1}{2}\chi\chi - \frac{1}{2}\bar{\chi}\bar{\chi}, \\ \underline{\mathcal{L}}_0 = i\partial_{\underline{m}}\,\underline{\bar{\chi}}\bar{\sigma}^m\underline{\chi} + A^*\Box A + \underline{F}^*\underline{F}, & \underline{\mathcal{L}}_{\underline{m}} = A\,\underline{F} + A^*\,\underline{F}^* - \frac{1}{2}\underline{\chi}\,\underline{\chi} - \frac{1}{2}\underline{\bar{\chi}}\,\underline{\bar{\chi}}, \end{array} \tag{61}$$

and $\Box = \underline{\Box}$, $A \equiv \underline{A}$. Whereupon, the equations for the Weyl spinor ψ and complex scalar $\mathcal{A}$ of the same mass m, are

$$\begin{array}{lcl} i\bar{\sigma}^m\,\partial_m\,\chi + m\bar{\chi} = 0, & & i\bar{\sigma}^{\underline{m}}\,\partial_{\underline{m}}\,\underline{\chi} + m\underline{\bar{\chi}} = 0, \\ F + m\underline{A}^* = 0, & \text{and} & \underline{F} + mA^* = 0, \\ \underline{\Box}\,\underline{A} + mF^* = 0, & & \Box A + m\underline{F}^* = 0. \\ (a) & & (b) \end{array} \tag{62}$$

In accord to (34) and (35), respectively, (a) stands for $Q = q$ (referring to the motion of a fermion, χ, in M_4) and (b) stands for $Q = \underline{q}$ (so, of a boson, A, in M_4). Finally, the algebraic auxiliary field $\mathcal{F}$ can be eliminated to find

$$\begin{array}{l} \mathcal{L}_{Q=q} = i\partial_m\bar{\chi}\bar{\sigma}^m\chi - \frac{1}{2}(\chi\chi + \bar{\chi}\bar{\chi}) + \underline{A}^*\underline{\Box}\,\underline{A} - m^2\underline{A}^*\underline{A}, \\ \underline{\mathcal{L}}_{Q=\underline{q}} = i\partial_{\underline{m}}\,\underline{\bar{\chi}}\bar{\sigma}^m\underline{\chi} - \frac{1}{2}(\underline{\chi}\,\underline{\chi} + \underline{\bar{\chi}}\,\underline{\bar{\chi}}) + A^*\Box A - m^2A^*A. \end{array} \tag{63}$$

To complete the model, we also need superspace expressions for the masses and couplings, which can be easily found in analogy of the standard theory, namely: 1) fermion masses and Yukawa couplings, $(\partial^2\mathcal{P}/\partial\mathcal{A}^2)\psi\psi$; and 2) the scalar potential, $\mathcal{V}(\mathcal{A},\,\mathcal{A}^*) = |\partial\mathcal{P}/\partial\mathcal{A}|^2$; where $\mathcal{P} = (1/2)\,m\,\Phi^2 + (1/3)\,\lambda\,\Phi^3$ is the most general renormalizable interaction for a single chiral superfield. Thereby, the auxiliary field equation of motion reads $\mathcal{F}^* + (\partial\mathcal{P}/\partial\mathcal{A}) = 0$. Similarly, we can treat the vector superfields, etc. Here we shall forbear to write them out as the standard theory is so well known. Divergences in SUSY field theories are greatly reduced. Indeed all the quadratic divergences disappear in the renormalized supersymmetric Lagrangian and the number of independent renormalization constants is kept to a minimum.

6. Rigid superspace geometry, superfields

In the framework of standard generalization of the coset construction (Callan et al., 1969, Coleman et al., 1969, Salam & Strathdee, 1974, Weinberg, 1968), we will take $G = G_q \times G_{\underline{q}}$ to be the supergroup generated by the MS$_p$-SUSY algebra (42). Let the stability group $H = H_q \times H_{\underline{q}}$ be the Lorentz group (referred to M_4 and $\underline{M}_2$), and we choose to keep all of G unbroken. Given G and H, we can construct the coset, G/H, by an equivalence relation on the elements of G: $\Omega \sim \Omega h$, where $\Omega = \Omega_q \times \Omega_{\underline{q}} \in G$ and $h = h_q \times h_{\underline{q}} \in H$, so that the coset can be pictured as a section of a fiber bundle with total space, G, and fiber, H. So, the Maurer-Cartan form, $\Omega^{-1}d\Omega$, is valued in the Lie algebra of G, and transforms as follows under a global G transformation,

$$\begin{array}{l} \Omega \longrightarrow g\Omega h^{-1}, \\ \Omega^{-1}d\Omega \longrightarrow h(\Omega^{-1}d\Omega)h^{-1} - dh\,h^{-1}, \end{array} \tag{64}$$

with $g \in G$. We also consider a superspace which is a 14D-extension of a direct sum of background spaces $M_4 \oplus \underline{M}_2$ (spanned by the 6D-coordinates $X^{\hat{m}} = (x^m,\,\underline{\eta}^{\underline{m}})$ by the inclusion of additional 8D-fermionic coordinates $\Theta^\alpha = (\theta^\alpha,\,\underline{\theta}^\alpha)$ and $\bar{\Theta}_{\dot{\alpha}} = (\bar{\theta}_{\dot{\alpha}},\,\underline{\bar{\theta}}_{\dot{\alpha}})$, as to $(q,\,\underline{q})$, respectively. These spinors satisfy the following relations:

$$\begin{array}{l} \{\Theta^\alpha,\,\Theta^\beta\} = \{\bar{\Theta}_{\dot{\alpha}},\,\bar{\Theta}_{\dot{\beta}}\} = \{\Theta^\alpha,\,\bar{\Theta}_{\dot{\beta}}\} = 0, \\ [x^m,\,\theta^\alpha] = [x^m,\,\bar{\theta}_{\dot{\alpha}}] = 0, \\ [\underline{\eta}^{\underline{m}},\,\underline{\theta}^\alpha] = [\underline{\eta}^{\underline{m}},\,\underline{\bar{\theta}}_{\dot{\alpha}}] = 0. \end{array} \tag{65}$$

and $\Theta^{\alpha *} = \bar{\Theta}^{\dot{\alpha}}$. Points in superspace are identified by the generalized coordinates

$$z^{(M)} = (X^{\hat{m}},\,\Theta^\alpha,\,\bar{\Theta}_{\dot{\alpha}}) = (x^m,\,\theta^\alpha,\,\bar{\theta}_{\dot{\alpha}}) \oplus (\underline{\eta}^{\underline{m}},\underline{\theta}^\alpha,\,\underline{\bar{\theta}}_{\dot{\alpha}}).$$

We have then the one most commonly used `real´ or `symmetric´ superspace parametrized by

$$\Omega(X,\,\Theta,\,\bar{\Theta}) = e^{i(-X^{\hat{m}}p_{\hat{m}} + \Theta^\alpha Q_\alpha + \bar{\Theta}_{\dot{\alpha}}\bar{Q}^{\dot{\alpha}})} = \Omega_q(x,\,\theta,\,\bar{\theta}) \times \Omega_{\underline{q}}(\underline{\eta},\,\underline{\theta},\,\underline{\bar{\theta}}), \tag{66}$$

where we now imply a summation over $\hat{m}$, etc., such that

$$\Omega_q(x,\,\theta,\,\bar{\theta}) = e^{i(-x^m p_m + \theta^\alpha q_\alpha + \bar{\theta}_{\dot{\alpha}}\bar{q}^{\dot{\alpha}})}, \quad \Omega_{\underline{q}}(\underline{\eta},\,\underline{\theta},\,\underline{\bar{\theta}}) = e^{i(-\underline{\eta}^{\underline{m}}p_{\underline{m}} + \underline{\theta}^\alpha \underline{q}_\alpha + \underline{\bar{\theta}}_{\dot{\alpha}}\underline{\bar{q}}^{\dot{\alpha}})}. \tag{67}$$

Supersymmetry transformation will be defined as a translation in superspace, specified by the group element

$$g(0,\,\epsilon,\,\bar{\epsilon}) = e^{i(\epsilon^\alpha Q_\alpha + \bar{\epsilon}_{\dot{\alpha}}\bar{Q}^{\dot{\alpha}})} = g_q(0,\,\xi,\,\bar{\xi}) \times g_{\underline{q}}(0,\,\underline{\xi},\,\underline{\bar{\xi}}) = e^{i(\xi^\alpha q_\alpha + \bar{\xi}_{\dot{\alpha}}\bar{q}^{\dot{\alpha}})} \times e^{i(\underline{\xi}^\alpha \underline{q}_\alpha + \underline{\bar{\xi}}_{\dot{\alpha}}\underline{\bar{q}}^{\dot{\alpha}})}, \tag{68}$$

doi: https://doi.org/10.52526/25792776-23.70.2-170

with corresponding anticommuting parameters $\epsilon = (\xi \text{ or } \underline{\xi})$. To study the effect of supersymmetry transformations (64) and $h = 1$, we consider

$$g(0,\,\epsilon,\,\bar\epsilon)\,\Omega(X,\,\Theta,\,\bar\Theta) = e^{i(\epsilon^\alpha Q_\alpha + \bar\epsilon_{\dot\alpha}\bar Q^{\dot\alpha})}\,e^{i(-X^{\hat m}p_{\hat m} + \Theta^\alpha Q_\alpha + \bar\Theta_{\dot\alpha}\bar Q^{\dot\alpha})}. \tag{69}$$

The multiplication of two successive transformations can be computed with the help of the Baker-Campbell-Hausdorf formula $e^A e^B = e^{A+B+(1/2)[A,\,B]+\cdots}$. Hence the transformation (69) induces the motion as is evident from the first relation of (47):

$$g(0,\,\epsilon,\,\bar\epsilon)\,\Omega(X^{\hat m},\,\Theta,\,\bar\Theta)\;\to (X^{\hat m} + i\,\Theta\,\sigma^{\hat m}\,\bar\epsilon - i\,\epsilon\,\sigma^{\hat m}\,\bar\Theta,\;\Theta+\epsilon,\,\bar\Theta+\bar\epsilon), \tag{70}$$

namely,

$$\begin{aligned} g_q(0,\,\xi,\,\bar\xi)\,\Omega_q(x,\,\theta,\,\bar\theta)\;&\to (x^m + i\,\theta\,\sigma^m\,\bar\xi - i\,\xi\,\sigma^m\,\bar\theta,\;\theta+\xi,\,\bar\theta+\bar\xi),\\ g_{\underline{q}}(0,\,\underline{\xi},\,\underline{\bar\xi})\,\Omega_{\underline{q}}(\eta,\,\underline{\theta},\,\underline{\bar\theta})\;&\to (\underline{\eta^m} + i\,\underline{\theta}\,\sigma^{\underline{m}}\,\underline{\bar\xi} - i\,\underline{\xi}\,\sigma^{\underline{m}}\,\underline{\bar\theta},\;\underline{\theta}+\underline{\xi},\,\underline{\bar\theta}+\underline{\bar\xi}). \end{aligned} \tag{71}$$

The spinors $\theta(\underline{\theta},\underline{\bar\theta})$ and $\bar\theta(\underline{\theta},\underline{\bar\theta})$ satisfy the embedding map (10), namely $\Delta\underline{x}^0 = \Delta x^0$ and $\Delta\underline{x}^2 = (\Delta\vec x)^2$, so from (71) we obtain

$$\begin{aligned} &\underline{\theta}\,\sigma^0\,\underline{\bar\xi} - \underline{\xi}\,\sigma^0\,\underline{\bar\theta} = \theta\,\sigma^0\,\bar\xi - \xi\,\sigma^0\,\bar\theta,\\ &(\underline{\theta}\,\sigma^3\,\underline{\bar\xi} - \underline{\xi}\,\sigma^3\,\underline{\bar\theta})^2 = (\theta\,\vec\sigma\,\bar\xi - \xi\,\vec\sigma\,\bar\theta)^2. \end{aligned} \tag{72}$$

The superfield $\Phi(z^{(M)}) = \phi(z^{(M_4)})$ or $\underline{\phi}(\underline{z}^{(\underline{M}_2)})$, which has a finite number of terms in its expansion in terms of Θ and $\bar\Theta$ owing to their anticommuting property, can be considered as the generator of the various components of the supermultiplets. We will consider only a scalar superfield $\Phi'(z'^{(M)}) = \Phi(z^{(M)})$, an infinitesimal supersymmetry transformation of which is given as

$$\delta_\epsilon\,\Phi(z^{(M)}) = (\epsilon^\alpha Q_\alpha + \bar\epsilon_{\dot\alpha}\bar Q^{\dot\alpha}) \times \Phi(z^{(M)}). \tag{73}$$

Acting on this space of functions, the Q and $\bar Q$ can be represented as differential operators:

$$Q_\alpha = \tfrac{\partial}{\partial\Theta^\alpha} - i\sigma^{\hat m}_{\ \alpha\dot\alpha}\bar\Theta^{\dot\alpha}\partial_{\hat m}, \quad \bar Q^{\dot\alpha} = \tfrac{\partial}{\partial\bar\Theta_{\dot\alpha}} - i\Theta^\alpha\sigma^{\hat m}_{\ \alpha\dot\beta}\varepsilon^{\dot\beta\dot\alpha}\partial_{\hat m}, \tag{74}$$

where, as usual, the undotted/dotted spinor indices can be raised and lowered with a two dimensional undotted/dotted $\varepsilon-$tensors, and the anticommuting derivatives obey the relations

$$\tfrac{\partial}{\partial\Theta^\alpha}\,\Theta^\beta = \delta^\beta_\alpha, \quad \tfrac{\partial}{\partial\Theta^\alpha}\,\Theta^\beta\Theta^\gamma = \delta^\beta_\alpha\Theta^\gamma - \delta^\gamma_\alpha\Theta^\beta, \tag{75}$$

and similarly for $\bar\Theta$. In order to write the exterior product in terms of differential operators, one induces a new basis in rigid superspace of supervielbein 1-form

$$e^A(z) = dz^M\,e^A_M(z), \tag{76}$$

and that

$$D_A = e_A^{\ N}(z)\tfrac{\partial}{\partial z^N}, \tag{77}$$

where to be brief we left implicit the symbol $\wedge$ in writing of exterior product. The inverse vielbein $E_A^{\ M}(z)$ is defined by the relations $E^A_M(z)E_A^{\ N}(z) = \delta_M^{\ N}$, and $E_A^{\ M}(z)E_M^{\ B}(z) = \delta_A^{\ B}$. The covariant derivative operators

$$\begin{aligned} &D_{\hat m} = \partial_{\hat m}, \quad D_\alpha = \tfrac{\partial}{\partial\Theta^\alpha} + i\sigma^{\hat m}_{\ \alpha\dot\alpha}\bar\Theta^{\dot\alpha}\partial_{\hat m},\\ &\bar D^{\dot\alpha} = \tfrac{\partial}{\partial\bar\Theta_{\dot\alpha}} + i\Theta^\alpha\sigma^{\hat m}_{\ \alpha\dot\beta}\varepsilon^{\dot\beta\dot\alpha}\partial_{\hat m}, \end{aligned} \tag{78}$$

anticommute with the Q and $\bar Q$

$$\{Q_\alpha,\,D_\beta\} = \{\bar Q_{\dot\alpha},\,\bar D_{\dot\beta}\} = \{Q_\alpha,\,\bar D_{\dot\beta}\} = \{\bar Q_{\dot\alpha},\,D_\beta\} = 0, \tag{79}$$

and satisfy the following structure relations:

$$\begin{aligned} &\{D_\alpha,\,D_{\dot\alpha}\} = -2i\sigma^{\hat m}_{\ \alpha\dot\alpha}\partial_{\hat m},\\ &\{D_\alpha,\,D_\beta\} = \{\bar D_{\dot\alpha},\,\bar D_{\dot\beta}\} = 0. \end{aligned} \tag{80}$$

doi: https://doi.org/10.52526/25792776-23.70.2-170

From (78), we obtain

$$e_A{}^M = \begin{pmatrix} e_{\hat{a}}{}^{\hat{m}} = \delta_{\hat{a}}^{\hat{m}} & e_{\hat{a}}{}^{\mu} = 0 & e_{\hat{a}\,\dot{\mu}} = 0 \\ e_{\alpha}{}^{\hat{m}} = i\sigma^{\hat{m}}_{\alpha\dot{\alpha}}\bar{\Theta}^{\dot{\alpha}} & e_{\alpha}{}^{\mu} = \delta_{\alpha}^{\mu} & e_{\alpha\,\dot{\mu}} = 0 \\ e^{\dot{\alpha}\,\hat{m}} = i\Theta^{\alpha}\sigma^{\hat{m}}_{\alpha\dot{\beta}}\varepsilon^{\dot{\beta}\dot{\alpha}} & e^{\dot{\alpha}\,\mu} = 0 & e^{\dot{\alpha}}{}_{\dot{\mu}} = \delta^{\dot{\alpha}}_{\dot{\mu}} \end{pmatrix}, \tag{81}$$

where $\hat{a} = (a \text{ or } \underline{a})$, $\quad a = 0, 1, 2, 3;\quad \underline{a} = (+), (-)$. The supersymmetry transformations of the component fields can be found using the differential operators (78).

The covariant constraint

$$\bar{D}_{\dot{\alpha}}\Phi(z^{(M)}) = 0, \tag{82}$$

which does not impose equations of motion on the component fields, defines the chiral superfield, Φ. Under the supersymmetry transformation (70) the chiral field transforms as follows:

$$\delta_\xi\Phi = \begin{cases} (\xi q + \bar{\xi}\bar{q}) \times \phi = \delta_\xi\, \underline{A}(\eta) + \sqrt{2}\theta\delta_\xi\chi(x) + \theta\theta\delta_\xi F(x) + \cdots, & \text{at } Q = q, \\ (\underline{\xi}\underline{q} + \bar{\underline{\xi}}\,\bar{\underline{q}}) \times \underline{\phi} = \delta_{\underline{\xi}}\, A(x) + \sqrt{2}\underline{\theta}\delta_{\underline{\xi}}\,\underline{\chi}(\underline{\eta}) + \underline{\theta}\,\underline{\theta}\delta_{\underline{\xi}}\,\underline{F}(\underline{\eta}) + \cdots, & \text{at } Q = \underline{q}. \end{cases} \tag{83}$$

Equation (83) show that the chiral superfield contains the same component fields as the MS_p-Wess-Zumino toy model.

7. Two postulates of SR

In this section we derive two postulates on which the theory of SR is based. Let us focus on the simple case of a peculiar anticommuting spinors $(\underline{\xi}, \bar{\underline{\xi}})$ and $(\xi, \bar{\xi})$ defined as

$$\underline{\xi}^{\alpha} = i\,\tfrac{\tau}{2}\,\underline{\theta}^{\alpha}, \quad \bar{\underline{\xi}}_{\dot{\alpha}} = -i\,\tfrac{\tau^*}{2}\,\bar{\underline{\theta}}_{\dot{\alpha}}, \quad \xi^{\alpha} = i\tfrac{\tau}{2}\theta^{\alpha}, \quad \bar{\xi}_{\dot{\alpha}} = -i\tfrac{\tau^*}{2}\bar{\theta}_{\dot{\alpha}}. \tag{84}$$

The *atomic displacement* caused by double transition of a particle $M_4 \rightleftharpoons \underline{M}_2$, according to (12), reads

$$\Delta\underline{\eta}_{(a)} = \underline{e}_{\underline{m}}\Delta\underline{\eta}^{\underline{m}}_{(a)} = \underline{u}\tau, \tag{85}$$

where the components $\Delta\underline{\eta}^{\underline{m}}_{(a)}$, according to (71), are written

$$\Delta\underline{\eta}^{\underline{m}}_{(a)} = \underline{v}^{\underline{m}}\tau = i\underline{\theta}\,\sigma^{\underline{m}}\,\bar{\underline{\xi}} - i\underline{\xi}\,\sigma^{\underline{m}}\,\bar{\underline{\theta}}. \tag{86}$$

Here the real parameter $\tau\,(=\tau^*)$ can physically be interpreted as the *atomic duration time* of double transition. By virtue of (84), the (86) is reduced to

$$\Delta\underline{\eta}^{\underline{m}}_{(a)} = (\underline{\theta}\,\sigma^{\underline{m}}\,\bar{\underline{\theta}})\tau. \tag{87}$$

In Van der Warden notations for the Weyl two-component formalism $\bar{\underline{\theta}}_{\dot{\alpha}} = (\underline{\theta}_{\alpha})^*$ (App.A), the (85), gives

$$\Delta\underline{\eta}^2_{(a)} = \underline{u}^2\tau^2 = \underline{v}^{(+)}\underline{v}^{(-)}\tau^2 = 2(\underline{\theta}_1\,\bar{\underline{\theta}}_1\underline{\theta}_2\,\bar{\underline{\theta}}_2)\tau^2 = 2(\underline{\theta}_1^2\underline{\theta}_2^2)\tau^2 \geq 0, \tag{88}$$

provided, $\underline{v}^{(+)} = \sqrt{2}\,\underline{\theta}_1\,\bar{\underline{\theta}}_1 = \sqrt{2}\,\underline{\theta}_1^2$ and $\underline{v}^{(-)} = \sqrt{2}\,\underline{\theta}_2\,\bar{\underline{\theta}}_2 = \sqrt{2}\,\underline{\theta}_2^2$. The (88), combined with (10), (11) and (19), can be recast into the form

$$\Delta\underline{\eta}^2_{(a)} = \tfrac{1}{2}\left[(\Delta\underline{x}^0_{(a)})^2 - (\Delta\underline{x}^1_{(a)})^2\right], \tag{89}$$

where $\Delta\underline{x}^0_{(a)} = \underline{v}^0\tau$, $\Delta\underline{x}^1_{(a)} = \underline{v}^1\tau$, and $\underline{v}^{(\pm)} = \frac{1}{\sqrt{2}}(\underline{v}^0 \pm \underline{v}^1)$. Hence the velocities of light in vacuum, $\underline{v}^0 = c$, and of a particle ,$\underline{\vec{v}}_1 = \underline{e}_1\underline{v}^1 = \vec{n}|\vec{v}| = \vec{v}\ (|\vec{v}| \leq c)$, are

$$\begin{aligned} \underline{v}^0 &= \underline{\theta}\,\sigma^0\,\bar{\underline{\theta}} = (\underline{\theta}_1\,\bar{\underline{\theta}}_1 + \underline{\theta}_2\,\bar{\underline{\theta}}_2) = \underline{\theta}\,\bar{\underline{\theta}}, \\ \underline{v}^1 &= \underline{\theta}\,\sigma^1\,\bar{\underline{\theta}} = (\underline{\theta}_1\,\bar{\underline{\theta}}_1 - \underline{\theta}_2\,\bar{\underline{\theta}}_2). \end{aligned} \tag{90}$$

Both map relationship in (72) are reduced by (84) to

$$\theta\bar{\theta} = \underline{v}^0, \quad \theta\theta\bar{\theta}\bar{\theta} = \tfrac{2}{3}(\underline{v}^1)^2. \tag{91}$$

doi: https://doi.org/10.52526/25792776-23.70.2-170

Here we have used the following spinor algebra relations:

$$(\theta\sigma^m\bar{\theta})(\theta\sigma^n\bar{\theta}) = \tfrac{1}{2}\,\theta\theta\bar{\theta}\bar{\theta}\,g^{mn}. \tag{92}$$

By virtue of relations $\theta_\alpha\theta_\beta = \frac{1}{2}\varepsilon_{\alpha\beta}\theta\theta$ and $\bar{\theta}_{\dot\alpha}\bar{\theta}_{\dot\beta} = -\frac{1}{2}\varepsilon_{\dot\alpha\dot\beta}\bar{\theta}\bar{\theta}$, where the antisymmetric tensors $\varepsilon_{\alpha\beta}$ and $\varepsilon^{\alpha\beta}$ ($\varepsilon_{21} = \varepsilon^{12} = 1, \varepsilon_{12} = \varepsilon^{21} = -1, \varepsilon_{11} = \varepsilon_{22} = 0$), and that of bilinear combinations $\theta\theta$ and $\bar{\theta}\bar{\theta}$, are invariant under Lorentz transformations, we obtain from (91): $\theta_1^2 + \theta_2^2 = \underline{v}^0$, and $\theta_1\theta_2 = \frac{1}{\sqrt{6}}\underline{v}^1$, which yield

$$\begin{aligned} \theta_1(\underline{\theta},\,\bar{\underline{\theta}}) &= \tfrac{1}{2}\left[\left(\underline{v}^0 + \sqrt{\tfrac{2}{3}}\underline{v}^1\right)^{1/2} + \left(\underline{v}^0 - \sqrt{\tfrac{2}{3}}\underline{v}^1\right)^{1/2}\right], \\ \theta_2(\underline{\theta},\,\bar{\underline{\theta}}) &= \tfrac{1}{2}\left[\left(\underline{v}^0 + \sqrt{\tfrac{2}{3}}\underline{v}^1\right)^{1/2} - \left(\underline{v}^0 - \sqrt{\tfrac{2}{3}}\underline{v}^1\right)^{1/2}\right]. \end{aligned} \tag{93}$$

We conclude that the *motion of a particle in M_4 is encoded in the spinors $\underline{\theta}$ and $\bar{\underline{\theta}}$ referred to the master space $\underline{M}_2$, which is indispensably tied to the propagating particle of interest.* The Lorentz invariance is a fundamental symmetry and refers to measurements of ideal inertial observers that move uniformly forever on rectilinear timelike worldlines. In view of relativity of all kinds of motion, we are of course not limited to any particular constant spinor $\underline{\theta}$ which yields the velocity $\vec{v}(\underline{\theta})$, but can choose at will any other constant spinors $\underline{\theta}'$, $\underline{\theta}''$, ... yielding respectively the velocities $\vec{v'}(\underline{\theta}'), \vec{v}\,''(\underline{\theta}''), \ldots$, whose transformational law on the original spinor $\underline{\theta}$ is known (16):

$$\underline{\theta}'_\alpha = M_\alpha^{\;\beta}\underline{\theta}_\beta, \quad \bar{\underline{\theta}}_{\dot\alpha} = (M^*)_{\dot\alpha}^{\;\dot\beta}\,\bar{\underline{\theta}}_{\dot\beta}, \quad \dot\alpha, \dot\beta = 1, 2, \tag{94}$$

where $M \in SL(2, C)$, the hermitian matrix M^* is related by a similarity transformation to $(M^{-1})^\dagger$, i.e. $(M^\dagger)^\beta{}_\alpha = (M^*)_\alpha{}^\beta$.

Aforesaid ensures to obtain some feeling about the origin of the two postulates of SR. Certainly, by virtue of (94) and (22), we derive the first founding property (i) that *the atomic displacement* $\Delta\underline{\eta}_{(a)}$, caused by double transition of a particle $M_4 \rightleftharpoons \underline{M}_2$, is an invariant:

$$\text{(i)} \quad \Delta\underline{\eta}_{(a)} = \Delta\underline{\eta}'_{(a)} = \cdots = inv. \tag{95}$$

The (94) also gives the second (ii) founding property that the bilinear combination $\underline{\theta}\,\bar{\underline{\theta}}$ is a constant:

$$\text{(ii)} \quad c = \underline{\theta}\,\bar{\underline{\theta}} = \underline{\theta}'\,\bar{\underline{\theta}}' = \cdots = const. \tag{96}$$

The latter yields a second postulate of SR (Einstein's postulate) - *the velocity of light, c, in free space appears the same to all observers regardless the relative motion of the source of light and the observer.* The c is the maximum attainable velocity (90) for uniform motion of a particle in Minkowski background space, M_4. Equally noteworthy is the fact that (95) and (96) combined yield *invariance of the element of interval between two events $\Delta x = k\Delta\underline{\eta}_{(a)}$ (for given integer number k) with respect to the Lorentz transformation*:

$$\begin{aligned} &k^2\Delta\underline{\eta}^2_{(a)} = (c^2 - \underline{v}_1^2)\Delta t^2 = (c^2 - \vec{v}^{\,2})\Delta t^2 = (\Delta x^0)^2 - (\Delta\vec{x})^2 \equiv (\Delta s)^2 = \\ &(\Delta x'^0)^2 - (\Delta\vec{x})'^2 \equiv (\Delta s')^2 = \cdots = inv., \end{aligned} \tag{97}$$

where $x^0 = ct, \quad x^{0'} = ct', \ldots$. We have here introduced a notion of physical relative finite *time intervals* between two events $\Delta t = k\tau/\sqrt{2}$, $\Delta t' = k\tau'/\sqrt{2}, \ldots$.

The motion, say, of spin-0 particle in $\underline{M}_2$ can be described by the chiral superfield $\underline{\Phi}(\underline{\eta}^m, \underline{\theta}, \bar{\underline{\theta}})$, while a similar motion of spin-1/2 particle in M_4 can be described by the chiral superfield $\Phi(x^m, \theta, \bar{\theta})$, etc. Therefore, what has been said above will require a complete revision of our ideas about the Lorentz code of motion, to be now referred to as the *individual code of a particle*, defined as its intrinsic property.

Having SLC to be equipped with the MS$_p$-SUSY mechanism, the spinors $\underline{\theta}$ encode all of the information necessary for the two founding properties (95) and (96) of SR. In subsequent paper (**?**), we will address the deformation of these spinors: $\underline{\theta} \to \tilde{\underline{\theta}} = \lambda^{1/2}\,\underline{\theta}$, etc., where λ appears as a deformation function of the Lorentz invariance (LIDF). This yields a consistent microscopic theory of Lorentz invariance violation (LIV) caused by the deformation of both the line element, $\tilde{ds} = \lambda ds$, and maximum attainable velocity, $\tilde{c} = \lambda c$, of a particle. We will discuss the corresponding deformed geometry at LIV, and complement this conceptual investigation with testing of various LIDFs in the UHECR- and TeV-γ threshold anomalies with in several instructive scenarios: the Coleman and Glashow-type perturbative extension of SLC, the LID extension of standard model, the LID in quantum gravity motivated space-time models and the LID in loop quantum gravity models. Consequently, in the third paper of this series, we will construct the framework of local MSp-SUSY (**?**), which will address the *accelerated motion* and inertia effects.

doi: https://doi.org/10.52526/25792776-23.70.2-170

8. The physical outlook and concluding remarks

Resuming the whole physical picture, in this Section 8 we expose the assertions made through a brief physical outlook of the key points of proposed theory. As concluding remarks, we also present what we think is the most important that distinguish this theory from phenomenological approaches of differing MAVs in the published literature.

Underlying physical processes. We identify the physical processes underlying the inertial uniform motion, which is probably the most fascinating challenge for physical research, and review the foundations of SLC.

MS_p. We motivate the subject by conceiving of double background spaces - 4D Minkowski space, M_4, and MS_p for each particle. The geometry of MS_p is a new physical entity, with degrees of freedom and a dynamics of its own. We assume that a flat MS_p is the 2D composite space $\underline{M}_2$. Then, a smooth embedding map $f: \ \underline{M}_2 \longrightarrow M_4$ is defined to be an immersion - an embedding which is a function that is a homeomorphism onto its image. So that the $MS_p \equiv \underline{M}_2$ is viewed as 2D space living on the 4D world sheet. Given the inertial frames $S_{(4)}, S'_{(4)}, S''_{(4)}, \ldots$ in M_4, we define the corresponding inertial frames $\underline{S}_{(2)}$, $\underline{S'}_{(2)}$, $\underline{S''}_{(2)}$,... in $\underline{M}_2$, which used by the non-accelerated observers for the positions $\underline{x}^r, \underline{x}'^r, \underline{x}''^r, \ldots$ of a free particle in flat $\underline{M}_2$. Thereby the time axes of the two systems $\underline{S}_{(2)}$ and $S_{(4)}$ coincide in direction and that the time coordinates are taken the same.

We hypothesize that the elementary act of motion consists of an \`annihilation´ of a particle at point $(x,t) \in M_4$, which can be understood as the transition from initial state $|x,t>$ to *unmanifested* intermediate state (\`motion´ state), $|\underline{x},\underline{t}>$, and of subsequent \`creation´ of a particle at infinitely close final point $(x',t') \in M_4$, which means the transition from \`motion´ state, $|\underline{x},\underline{t}>$, to final state, $|x',t'>$. The motion state, $|\underline{x},\underline{t})>$, is defined on *unmanifested* \`master´ space, $\underline{M}_2$, which includes the points of all the atomic elements, $(\underline{x},\underline{t}) \in \underline{M}_2$. This furnishes justification for an introduction of *master space*, $\underline{M}_2$. The $\underline{M}_2$ is indispensably tied to propagating particle, without relation to the other particles.

\`Double space´- or \`MS_p´-SUSY. The net result of each atomic double transition of a particle $M_4 \rightleftharpoons \underline{M}_2$ is as if we had operated with a space-time *translation* on the original space M_4. Such successive transformations will induce in M_4 the inhomogeneous Lorentz group, or Poincaré group, and that the unitary linear transformation $|x,t> \rightarrow U(\Lambda,a)|x,t>$ on vectors in the physical Hilbert space. We build up the \`double space´- or \`MS_p´-SUSY theory, wherein the superspace is a 14D-extension of a direct sum of background spaces $M_4 \oplus \underline{M}_2$ by the inclusion of additional 8D fermionic coordinates. The latter is induced by the spinors $\underline{\theta}$ and $\bar{\underline{\theta}}$ referred to $\underline{M}_2$. By virtue of embedding map (10), the spinors $\underline{\theta}$ and $\bar{\underline{\theta}}$, in turn, induce the respective spinors $\theta(\underline{\theta},\bar{\underline{\theta}})$ and $\bar{\theta}(\underline{\theta},\bar{\underline{\theta}})$ (see (93)), as to M_4. Consequently, the \`symmetric´ superspace is parameterized (see (66)) by $\Omega = \Omega_q(x^m,\, \theta(\underline{\theta},\bar{\underline{\theta}}),\, \bar{\theta}(\underline{\theta},\bar{\underline{\theta}})) \times \Omega_{\underline{q}}(\underline{\eta}^m,\, \underline{\theta},\, \bar{\underline{\theta}})$. Supersymmetry transformation is defined as a translation in superspace, specified by the group element with corresponding anticommuting parameters. The multiplication of two successive transformations induce the motion. Obviously the ground state of MS_p-SUSY has a vanishing energy value and is nondegenerate (SUSY unbroken). All the particles are living on M_4, their superpartners can be viewed as living on $\underline{M}_2$. We emphasize that in MS_p-SUSY theory, alike in standard exact SUSY theory, the vacuum zero point energy problem, standing before any quantum field theory in M_4, will be solved. The particles in M_4 themselves can be considered as excited states above the underlying quantum vacuum of background double space $M_4 \oplus \underline{M}_2$, where the zero point cancellation occurs at ground-state energy, provided that the natural frequencies are set equal ($q_0^2 \equiv \nu_b = \nu_f$), because the fermion field has a negative zero point energy while the boson field has a positive zero point energy.

Two founding properties. On the premises of previous paragraph, we derive the two founding properties that (i) the atomic displacement $\Delta\underline{\eta}_{(a)}$, caused by double transition of a particle $M_4 \rightleftharpoons \underline{M}_2$, is an invariant; and (ii) the bilinear combination $\underline{\theta}\,\bar{\underline{\theta}}$ is a constant. These properties underly the two postulates on which the theory of SR is based. Thus, we show that the motion of a particle in M_4 is encoded in the spinors $\underline{\theta}$ and $\bar{\underline{\theta}}$ referred to the master space $\underline{M}_2$. This calls for a complete reconsideration of our ideas of Lorentz motion code, to be now referred to as the *individual code of a particle*, defined as its intrinsic property.

doi: https://doi.org/10.52526/25792776-23.70.2-170

This framework allows to introduce the physical finite *relative time* interval between two events as integer number of the *own atomic duration time* of double transition of a particle $M_4 \rightleftharpoons \underline{M}_2$.

Intrinsic code. The predictions of proposed theory require a complete revision of our ideas about the Lorentz code, to be now referred to as the individual code of a particle, defined as its intrinsic property. The MS_p , embedded in the background 4D-space, is an unmanifested indispensable individual companion to the particle of interest, devoid of any external influence.

References

Aharonian F., et al. 1999, Astron. Astrophys., 349, 11

Aharonov Y., Casher A., 1979, Phys. Rev. Ser. A, 19, 2461

Aitchison I. R., 2007, Supersymmetry. Oxford: Oxford University Press

Alfaro J., Palma G., 2002, Phys. Rev. D, 65, 103516

Alfaro J., Palma G., 2003, Phys. Rev. D, 67, 083003

Alfaro J., Morales-Técotl H., Urrutia L., 2002a, Phys. Rev. D, 65, 103509

Alfaro J., Morales-Técotl H., Urrutia L., 2002b, Phys. Rev. D, 66, 124006

Amelino-Camelia G., Majid S., 2000, Int. J. Mod. Phys. A, 15, 4301

Amelino-Camelia G., Piran T., 2001, Phys. Rev. D, 64, 036005

Baer H., Tata X., 2006, Weak Scale Supersymmetry: From Superfields to Scattering Events. Cambridge: Cambridge University Press

Balachandran A., Pinzul A., Queiroz A., 2008, Phys. Lett. B, 668, 241

Batista R., et al. 2019, Frontiers in Astronomy and Space Sciences, 6, 1, Article 23

Callan C., Coleman S., Wess J., Zumino B., 1969, Phys. Rev., 177, 2247

Chaichian M., Kulish P., Nishijima K., Tureanu A., 2004, Phys. Lett. B, 604, 98

Coleman S., Wess J., Zumino B., 1969, Phys. Rev., 177, 2239

Drake S., 1978, Galileo at work. Chicago, University of Chicago Press

Dreiner H., Haber H., Martin S., 2004, Supersymmetry. CUP draft Sept.

Fayet P., Ferrara S., 1977, Physics Reports, 328, 249

Ferrara S., Wess J., Zumino B., 1974, Phys. Letters, 51, 239

Fiore G., Wess J., 2007, Phys. Rev. D, 751, 105022

Hall B. C., 2015, Lie Groups, Lie Algebras, and Representations: An Elementary Introduction. Graduate Texts in Mathematics, vol. 222 (2nd ed.), Springer, ISBN 978-0-387-40122-5

Jackiw R., 1984, Phys. Rev. Ser. D, 29, 2375

Landau L., 1930, Zeits. für Phys. (in German). Springer Science and Business Media LLC, 64, 629

Mattingly D., 2005, Living Rev. Relativity, 8, 5

Metzger M., et al. 1997, Nature, 87, 878

Milton K. E., 2000, Quantum Legacy, Seminal Papers of Julian Schwinger. World Scientific Publishing Co. Pte. Ltd.

Milton K., 2015, Schwinger's Quantum Action Principle. Springer Briefs in Physics

Newton I., 1687, Philosophiae Naturalis Principia Mathematica. http://plato.stanford.edu/entries/newton-principia

Ravndal F., 1980, Phys. Rev. Ser. D, 21, 2823

Salam A., Strathdee J., 1974, Nucl. Phys. B, 76, 477

Schutz B., 1982, Geometrical Methods of Mathematical Physics. Cambridge University Press

Schwinger J., 1960, Proc. Natl. Acad. Sci. U.S.A., 46, 1401

Schwinger J., 2000, Quantum Kinematics and Dynamics. (1st ed. (1991)), 2nd ed. (2000) by Westview Press, USA

Sohnius M., 1985, Physics Reports, 128, 39

doi: https://doi.org/10.52526/25792776-23.70.2-170

Ter-Kazarian G., 2011, Class. Quantum Grav., 28, 055003

Ter-Kazarian G., 2012, Advances in Mathematical Physics, 2012, Article ID 692030, 41 pages,doi:10.1155/2012/692030, Hindawi Publ. Corporation

Ter-Kazarian G., 2024, To appear in Grav. Cosmol., 30, No 1

Weinberg S., 1968, Phys. Rev., 166, 1568

Wess J., Bagger J., 1993, Supersymmetry and Supergravity. Princeton University Press, Princeton

Wess J., Zumino B., 1974, PhyPhys. Lett. B, 49, 52

West P., 1987, Introduction to Supersymmetry and Supergravity. World Scientific, Singapure

van Paradis J., et al. 1997, Nature, 386, 686

doi: https://doi.org/10.52526/25792776-23.70.2-170

Communications of BAO, Vol. 70, Issue 2, 2023, pp. 188-203

Deformation of Special Relativity in ultra-high energy astrophysics

G.Ter-Kazarian*

Byurakan Astrophysical Observatory, Byurakan, Aragatsotn Province, Armenia

Abstract

We review deformation of both postulates of Special Relativity (SR) theory, tested in experiments for ultra-high energy cosmic ray (UHECRs) and TeV-γ photons observed. To this aim, we utilize the theory of, so-called, *master space* (MS_p) induced supersymmetry (Ter-Kazarian, 2023, 2024), wherein the standard Lorentz code (SLC) is derived in a new perspective of double global MS_p-SUSY transformations in terms of Lorentz spinors $(\underline{\theta}, \bar{\underline{\theta}})$ referred to MS_p. This allows to introduce the physical finite *relative time* interval between two events as integer number of the *own atomic duration time* of double transition of a particle from M_4 to MS_p and back. While all the particles are living on M_4, their superpartners can be viewed as living on MS_p. This is a main ground for introducing MS_p, which is *unmanifested* individual companion to the particle of interest. Continuing along this line, in present communication we address the deformation of these spinors: $\underline{\theta} \to \tilde{\underline{\theta}} = \lambda^{1/2}\,\underline{\theta}$, etc., where λ appears as a scalar deformation function of the Lorentz invariance (LIDF). This yields both the DLE and DMAV, respectively, in the form $\tilde{ds} = \lambda ds$ and $\tilde{c} = \lambda c$, provided, the invariance of DLE, and the same value of DMAV in free space hold for all inertial systems. Thus, the LID-generalization of global MS_p-SUSY theory formulates the generalized relativity postulates in a way that preserve the relativity of inertial frames, in spite of the appearance of modified terms in the LID dispersion relations. We complement this conceptual investigation with testing of various LIDFs in the UHECR- and TeV-γ threshold anomalies by implications for several scenarios: the Coleman and Glashow-type perturbative extension of SLC, the LID extension of standard model, the LID in quantum gravity motivated space-time models, the LID in loop quantum gravity models, and the LIDF for the models preserving the relativity of inertial frames.

Keywords: *Deformation of Lorentz invariance–deformed geometry at LIV–cosmic rays–quantum spacetime–loop quantum gravity–spacetime noncommutativity*

1. Introduction

Numerous tests of Lorentz symmetry have been performed in recent years. The UHECR- and TeV-γ threshold anomalies found in high-energy experiments for UHECRs and TeV-γ photons observed provide a wealth of invaluable modern tests of the origin of LIV and has a strong potential in providing competitive constraints on suggested scenarios. The LIV phenomenology for UHECRs has been intensely studied in the last few decades, even the progress has been dramatic (for a comprehensive review see Batista & et al. (2019)). A propagation in intergalactic space through the cosmic microwave background (CMB) radiation necessarily should reduce energy of UHECRs below the Greisen-Zatsepin-Kuzmin (GZK) limit, 5×10^{19} eV. Stecker Stecker (1968) showed that for cosmic rays with energies above 1×10^{20} eV, an effective absorption mean-free-path should be less than 100 Mpc. More detailed approaches to the GZK cutoff feature have been made by e.g. Berezinsky & Grigorieva (1988), Scully & Stecker (2002). Hence, the GZK cutoff exists in the form of a suppression in the predicted flux of cosmic rays with energies above $\sim 8 \times 10^{19}$eV. The observations from the AGASA group found an abundant flux of incoming particles with energies above 1×10^{20}eV, violating the GZK cutoff Takeda & et al. (1998). Meantime, the observations from the HiRes Abbasi & et al. (2008) and Pierre Auger Observatory groups Abraham & et al. (2008), Abram & et al. (2010), Parizot (2007), with larger exposures, seem to be consistent with the presence of the GZK suppression effect. There are even some data Abram & et al. (2007, 2011), suggesting that some relatively close sources can be associated with observed cosmic rays with the highest energy. However, a reanalysis of the AGASA data

*gago_50@yahoo.com

doi: https://doi.org/10.52526/25792776-23.70.2-188

has resulted in cutting their originally reported number of trans-GZK events by half Scully & Stecker (2009). The existence of such cutoff effect is uncertain owing to conflicting observational data and small number statistics. This is commonly referred as the GZK anomaly. Observed air showers in the KASCADE-Grande experiment show an excess of muons compared to predictions of standard hadronic interaction models above $\simeq 10^{16}$ eV, which indicates a longer-than-expected muon attenuation length Apel & et al. (2017). The Pierre Auger Observatory group also sees a muon excess by a factor $\simeq 1.5$ Aab & et al. (2016). For a solution of the GZK paradox it would be sufficient to push the threshold energy upwards by a factor of 6. If the muon excess cannot be explained by improved hadronic event generators with in the Standard Model, new physics could qualitatively play a role Batista & et al. (2019), Anchordoqui et al. (2017), Farrar & Allen (2013a,b), Olinto (2001). Comparatively large increases of muon number over a small primary energy range, which is possible in the hadronic channel in UHERCs, would likely be a hint for Lorentz symmetry violation at very high Lorentz factors.

The TeV-γ paradox is another one related to the transparency of the CMB. The HEGRA has detected high-energy photons with a spectrum ranging up to 24 TeV Aharonian & et al. (1999) from Mk 501, a BL Lac object at a redshift of 0.034 ($\sim$ 157 Mpc). Unlike the GZK paradox only a few solutions have been proposed for the TeV-γ paradox. The recent confirmation that at least some γ-ray bursts originate at cosmological distances Metzger & et al. (1997), van Paradis & et al. (1997) suggests that the radiation from these sources could be used to probe some of the fundamental laws of physics.

The quantum-gravitational effects may be playing a decisive role for LIV in the propagation of UHECR-particles. Most ideas in phenomenology reflect the expectation that the characteristic scale of quantum spacetime effects should be within a two or three orders of magnitude of the Planck scale, $E_P = M_P c^2$ ($\sim 1.22 \times 10^{19}$ GeV), at which quantum effects are expected to strongly affect the nature of spacetime. So that it should be possible to analyze quantum spacetime effects in terms of expansions in powers of Planck energy scale. The opportunity that the cosmic-ray threshold anomaly could be a signal of LIV had already been emphasized in e.g. Aloisio et al. (2000), Amelino-Camelias et al. (1998), Bertolami & Carvalho (2000), Coleman & Glashow (1999), Gonzalez-Mestres (1997), Jackiw & Kostelecky (1999), Sato (Sato), Stecker & Scully (2005). Enormous efforts have been made over the past decade to test LIV in various scenarious of quantum gravity Scully & Stecker (2009), Alfaro & Palma (2003), Amelino-Camelia & Piran (2001), Jacobson et al. (2003), Kifune (1999), Kluzniak (Kluzniak, 1999), Mattingly (2005), Protheroe & Meyer (2000), Stecker (2003). All these assumptions usually converged on a common way of solving and explaining the threshold UHECR and TeV-γ- anomalies with the help of efficient models for describing the propagation of astroparticles.

Since the theory of quantum gravity based on noncommutative geometry is at earlier stage of development Alfaro et al. (2000a), Amelino-Camelia & Majid (2000), Douglas & Nekrasov (2001), Gambini & Pullin (1999), Lukierski et al. (1992, 1995), Madore et al. (2000), Smolin (1999), and the possibility to preserve a Lorentz-invariant interpretation of noncommutative space-time is still not excluded Balachandran et al. (2008), Chaichian et al. (2004), Fiore & Wess (2007), there are claims in the literature that it is natural to tie the LIV to various alternatives for the yet nonexistent theory, see e.g. Aloisio et al. (2000), Alfaro & Palma (2003), Jacobson et al. (2003), Mattingly (2005), Stecker (2003), Alfaro & Palma (2002), Jacobson et al. (2004), Smolin (Smolin). In Alfaro & Palma (2002), Alfaro et al. (2000b, 2002a,b) the authors utilize the loop quantum gravity approach, whereas the discrete nature of space at short distances is expected to induce violations of Lorentz invariance and CPT. The loop quantum gravity provides the kinematics of the `Minkowski limit´ of the LIV may well be reachable.

However, even thanks to the fruitful interplay between phenomenological analysis and high energy astronomical experiments, the scientific situation remains, in fact, more inconsistent to day. Moreover, a systematic analysis of these properties happens to be surprisingly difficult by conventional theoretical methods. It should be noticed that currently no single scenario will be able to address explicit deformation of both postulates of the SLC. Literally speaking, when testing LID ansatze relied on a phenomenological approach to experiments with ultrahigh-energy astroparticles, as natural for phenomenology, we are allowed to determine only LIDF - λ_2 (for deformed maximum attainable velocity $\tilde{c} = \lambda_2 c$), but λ_1 (for deformed line element $\widetilde{ds} = \lambda_1\, ds$) is left unknown (see (24)). Therefore, other scenarios and possibilities should not be completely ruled out. The perturbative LIV expansions that are often needed for the analysis of these experiments might require the development of new techniques for description of deformed geometry at LIV.

In present paper we analyze the deformed geometry at LIV, for which we determine both LIDF - functions explicitly in terms of microscopic approach. We develop on MS$_p$-SUSY theory (Ter-Kazarian, 2023) (which is first paper of this series). Therewith, the SCL is derived in terms of Lorentz spinors $(\underline{\theta}, \underline{\bar{\theta}})$ referred to

doi: https://doi.org/10.52526/25792776-23.70.2-188

MS_p. On these premises, we derive the two postulates on which the theory of SR is based. This calls for a complete reconsideration of our ideas of Lorentz motion code, to be now referred to as the *individual code of a particle*, defined as its intrinsic property. To place the emphasis on the fundamental difference between the standard SUSY theories and some rather unusual properties of MS_p-SUSY theory, note that while the standard SUSY theory can be realized only as a spontaneously broken symmetry since the experiments do not show elementary particles to be accompanied by superpartners with different spin but identical mass, the MS_p-SUSY, in contrary, is realized as an *exact* SUSY, where all particles are living on 4D Minkowski space, but their superpartners can be viewed as living on MS_p. In MS_p-SUSY theory, obviously as in standard unbroken SUSY theory, the vacuum zero point energy problem, standing before any quantum field theory in M_4, is solved. The particles in M_4 themselves can be considered as excited states above the underlying quantum vacuum of background double spaces $M_4 \oplus$ MS_p, where the zero point cancellation occurs at ground-state energy, provided that the natural frequencies are set equal ($q_0^2 \equiv \nu_b = \nu_f$), because the fermion field has a negative zero point energy while the boson field has a positive zero point energy.

Continuing along this line we now address the deformation of the Lorentz spinors: $\underline{\theta} \rightarrow \tilde{\underline{\theta}} = \lambda^{1/2}\, \underline{\theta}$, for given scalar LIDF, etc. This yields a deformed dispersion relation of a particle, which modifies the threshold condition for a reaction between a primary cosmic ray and a CMB radiation photon, leading to LIV effects at detectable levels. We relate LID to more general deformed smooth differential 4D-manifold $\mathcal{M}_4$. Since there are still issues of considerable interest, we finally complement this conceptual investigation with testing of various LIDFs in the UHECR- and TeV-γ- threshold anomalies with in several scenarios of the Coleman and Glashow-type perturbative extension of SLC developed in the context of conventional quantum field theory, the LID extension of standard model, the LID in quantum gravity motivated space-time models and the LID in loop quantum gravity models, and the LIDF for the models preserving the relativity of inertial frames.

Finally our main emphasis is on the important properties of the LID-generalization (see (27)) of global MS_p-SUSY theory. The quantum gravity theory implies that global Lorentz invariance is no more than an accidental symmetry of the ground state of the classical limit of the theory, therefore the corrections to Lorentz invariance appear as corrections to the laws of the relativity of inertial frames. The LID occurred at Planck scale energies leads to further predictions that there should be a preferred frame of reference in nature, or leads to prediction of an energy dependent speed of light. Such predictions are falsifiable in TeV energy gamma ray observations Amelino-Camelia (2002), Magueijo & Smolin (2003). In resolving this problems, Amelino-Camelia (2002) purports to shown that it is possible to formulate the relativity postulates in the new conceptual framework that does not lead to inconsistencies. The hypothesis that the Lorentz transformations may be modified at Planck scale is proposed by Magueijo & Smolin (2003), which preserve the relativity of inertial frames. In that respect, we stress that the proposed LID-generalization of global MS_p-SUSY theory strongly supports the major goal of works Amelino-Camelia (2002), Magueijo & Smolin (2003), because this theory formulates the LID-generalized relativity postulates in a way that preserve the relativity of inertial frames. (see subsect.5.5).

We will proceed according to the following structure. To start with, in Section 2 we necessarily recount some of the highlights behind of MS_p-SUSY. Section 3 deals with deformed geometry at LID in the framework of microscopic approach. In Section 4 we address possible deformation of two postulates of SR in the high-energy limit for the UHECRs and the TeV-γ photons observed. Various LIDFs allow us to test different LID ansatze yielding LIV in the UHECR- and TeV-γ- threshold anomalies with in several special scenarios: (Subsection 5.1) - The LIDF for Coleman and Glashow-type perturbative extension of SLC; (Subsection 5.2) - The LIDF for LIV extension of the standard model; (Subsection 5.3) - The LIDF for quantum gravity motivated space-time models; (Subsection 5.4) - The LIDF for the loop quantum gravity models; (Subsection 5.5) - The LIDF for the models preserving the relativity of inertial frames. A physical outlook and concluding remarks are presented in Section 6. For brevity, whenever possible undotted and dotted spinor indices often can be ruthlessly suppressed without ambiguity. Unless indicated otherwise, we take natural units, $h = c = 1$.

2. Probing SR behind the MS_p-SUSY, revisited

For a benefit of the reader, as a guiding principle to make the rest of paper understandable, in this section we necessarily recount some of the highlights behind of MS_p-SUSY (Ter-Kazarian, 2023, 2024), which are in use throughout the paper.

The flat MS_p is the 2D composite space $\mathrm{MS}_p \equiv \underline{M}_2 = \underline{R}^1_{(+)} \oplus \underline{R}^1_{(-)}$ with Lorentz metric. The ingredient

doi: https://doi.org/10.52526/25792776-23.70.2-188

1D-space $\underline{R}^1_m$ is spanned by the coordinates $\underline{\eta}^m$. The following notational conventions are used throughout this paper: all quantities related to the space $\underline{M}_2$ will be underlined. In particular, the underlined lower case Latin letters $\underline{m}, \underline{n}, ... = (\pm)$ denote the world indices related to $\underline{M}_2$. The MS$_p$ is smoothly (injective and continuous) embedded in 4D Minkowski space, $\underline{M}_2 \hookrightarrow M_4$. The elementary act of particle motion at each time step (t_i) through the infinitely small spatial interval $\triangle x_i = (x_{i+1} - x_i)$ in M_4 during the time interval $\triangle t_i = (t_{i+1} - t_i) = \varepsilon$ is probably the most fascinating challenge for physical research. Since this is beyond our perception, it appears legitimate to consider extension to the infinitesimal Schwinger transformation function, $F_{ext}(x_{i+1}, t_{i+1}; x_i, t_i)$, in fundamentally different aspect. We hypothesize that

in the limit $n \to \infty (\varepsilon \to 0)$, the elementary act of motion consists of an `annihilation´ of a particle at point $(x_i, t_i) \in M_4$, which can be thought of as the transition from initial state $|x_i, t_i >$ into unmanifested intermediate state, so-called, `motion´ state, $|\underline{x}_i, \underline{t}_i >$, and of subsequent `creation´ of a particle at infinitely close final point $(x_{i+1}, t_{i+1}) \in M_4$, which means the transition from `motion´ state, $|\underline{x}_i, \underline{t}_i >$, into final state, $|x_{i+1}, t_{i+1} >$. The motion state, $|\underline{x}_i, \underline{t}_i) >$, should be defined on unmanifested `master´ space, $\underline{M}_2$, which includes the points of all the atomic elements, $(\underline{x}_i, \underline{t}_i) \in \underline{M}_2$ $(i = 1, 2, ...)$.

This furnishes justification for an introduction of *unmanifested master space*, $\underline{M}_2$. If that is the case as above, a *creation* of a particle in $\underline{M}_2$ means its transition from initial state defined on M_4 into intermediate state defined on $\underline{M}_2$, while an *annihilation* of a particle in $\underline{M}_2$ means vice versa. The same interpretation holds for the *creation* and *annihilation* processes in M_4. All the fermionic and bosonic states taken together form a basis in the Hilbert space. The basis vectors in the Hilbert space composed of $H_B \otimes H_F$ is given by

$$\{|\underline{n}_b > \otimes |0>_f, \; |\underline{n}_b > \otimes f^\dagger \, |0>_f\},$$

or

$$\{|n_b > \otimes |\underline{0}>_f, \; |n_b > \otimes \underline{f}^\dagger \, |\underline{0}>_f\},$$

where we consider two pairs of creation and annihilation operators $(b^\dagger, \, b)$ and $(f^\dagger, \, f)$ for bosons and fermions, respectively, referred to the background space M_4, as well as $(\underline{b}^\dagger, \, \underline{b})$ and $(\underline{f}^\dagger, \, \underline{f})$ for bosons and fermions, respectively, as to background master space $\underline{M}_2$. Accordingly, we construct the quantum operators, $(q^\dagger, \, \underline{q}^\dagger)$ and $(q, \, \underline{q})$, which replace bosons by fermions and vice versa:

$$\begin{array}{l} q \, |\underline{n}_b, \, n_f >= q_0 \sqrt{\underline{n}_b} \, |\underline{n}_b - 1, \, n_f + 1 >, \\ q^\dagger \, |\underline{n}_b, \, n_f >= q_0 \sqrt{\underline{n}_b + 1} \, |\underline{n}_b + 1, \, n_f - 1 >, \end{array} \tag{1}$$

and that

$$\begin{array}{l} \underline{q} \, |n_b, \, \underline{n}_f >= q_0 \sqrt{n_b} \, |n_b - 1, \, \underline{n}_f + 1 >, \\ \underline{q}^\dagger \, |n_b, \, \underline{n}_f > q_0 \sqrt{n_b + 1} \, |n_b + 1, \, \underline{n}_f - 1 > . \end{array} \tag{2}$$

This framework combines bosonic and fermionic states on the same footing, rotating them into each other under the action of operators q and $\underline{q}$. So, we may refer the action of the supercharge operators q and $q^\dagger$ to the background space M_4, having applied in the chain transformations of fermion χ (accompanied with the auxiliary field F as it will be seen later on) to boson $\underline{A}$, defined on $\underline{M}_2$:

$$\longrightarrow \chi^{(F)} \longrightarrow \underline{A} \longrightarrow \chi^{(F)} \longrightarrow \underline{A} \longrightarrow \chi^{(F)} \longrightarrow . \tag{3}$$

Respectively, we may refer the action of the supercharge operators $\underline{q}$ and $\underline{q}^\dagger$ to the $\underline{M}_2$, having applied in the chain transformations of fermion $\underline{\chi}$ (accompanied with the auxiliary field $\underline{F}$) to boson A, defined on the background space M_4:

$$\longrightarrow \underline{\chi}^{(\underline{F})} \longrightarrow A \longrightarrow \underline{\chi}^{(\underline{F})} \longrightarrow A \longrightarrow \underline{\chi}^{(\underline{F})} \longrightarrow . \tag{4}$$

The successive atomic double transitions of a particle $M_4 \rightleftharpoons \underline{M}_2$ is investigated within MS$_p$-SUSY, wherein all the particles are living on M_4, their superpartners can be viewed as living on MS$_p$. The underlying algebraic structure of MS$_p$-SUSY generators closes with the algebra of *translations* on the original space M_4 in a way that it can then be summarized as a non-trivial extension of the Poincaré group algebra those of the commutation relations of the bosonic generators of four momenta and six Lorentz generators referred to M_4. Moreover, if there are several spinor generators ${Q_\alpha}^i$ with $i = 1, ..., N$ - theory with $N-$extended supersymmetry, can be written as a graded Lie algebra of SUSY field theories, with commuting and anticommuting generators:

$$\begin{array}{l} \{{Q_\alpha}^i, \, {\bar{Q}^j}_{\dot{\alpha}}\} = 2\delta^{ij} \, \sigma^{\hat{m}}_{\alpha\dot{\alpha}} \, p_{\hat{m}}; \\ \{{Q_\alpha}^i, \, {Q_\beta}^j\} = \{{\bar{Q}^i}_{\dot{\alpha}}, \, {\bar{Q}^j}_{\dot{\beta}}\} = 0; \quad [p_{\hat{m}}, \, {Q_\alpha}^i] = [p_{\hat{m}}, \, {\bar{Q}^j}_{\dot{\alpha}}] = 0, \quad [p_{\hat{m}}, \, p_{\hat{n}}] = 0. \end{array} \tag{5}$$

doi: https://doi.org/10.52526/25792776-23.70.2-188

The map from $SL(2,C)$ to the Lorentz group is established through the $\vec{\sigma}$-Pauli spin matrices, $\sigma^m = (\sigma^0, \sigma^1, \sigma^2, \sigma^3) \equiv (I_2, \vec{\sigma})$, $\bar{\sigma}^m \equiv (I_2, -\vec{\sigma})$, where I_2 is the identity two-by-two matrix. Both hermitian matrices P and P' or $\underline{P}$ and $\underline{P'}$ have expansions, respectively, in σ or $\underline{\sigma}$:

$$(\sigma^m p'_m) = M(\sigma^m p_m)M^\dagger, \quad (\sigma^{\underline{m}} p'_{\underline{m}}) = M(\sigma^{\underline{m}} p_{\underline{m}})M^\dagger, \tag{6}$$

where $M(M \in SL(2,C))$ is unimodular two-by-two matrix. The odd part of the supersymmetry algebra is composed entirely of the spin-1/2 operators $Q_\alpha^{\ i}$, $Q_{\beta}^{\ j}$. In order to trace a maximal resemblance in outward appearance to the standard SUSY theories, here we set one notation $\hat{m} = (m \quad \text{if} \quad Q = q$, or $\underline{m} \quad \text{if} \quad Q = \underline{q})$, and as before the indices α and $\dot{\alpha}$ run over 1 and 2.

The guiding principle of MS$_p$-SUSY resides in constructing the superspace which is a 14D-extension of a direct sum of background spaces $M_4 \oplus \underline{M}_2$ (spanned by the 6D-coordinates $X^{\hat{m}} = (x^m, \underline{\eta}^{\underline{m}})$ by the inclusion of additional 8D-fermionic coordinates $\Theta^\alpha = (\theta^\alpha, \underline{\theta}^\alpha)$ and $\bar{\Theta}_{\dot{\alpha}} = (\bar{\theta}_{\dot{\alpha}}, \bar{\underline{\theta}}_{\dot{\alpha}})$, as to $(q, \underline{q})$, respectively. Therewith thanks to the embedding $\underline{M}_2 \hookrightarrow M_4$, the spinors $(\underline{\theta}, \bar{\underline{\theta}})$, in turn, induce the spinors $\theta(\underline{\theta}, \bar{\underline{\theta}})$ and $\bar{\theta}(\underline{\theta}, \bar{\underline{\theta}})$, as to M_4. These spinors satisfy the following relations:

$$\begin{array}{l} \{\Theta^\alpha,\, \Theta^\beta\} = \{\bar{\Theta}_{\dot{\alpha}},\, \bar{\Theta}_{\dot{\beta}}\} = \{\Theta^\alpha,\, \bar{\Theta}_{\dot{\beta}}\} = 0, \\ {[x^m,\, \theta^\alpha]} = [x^m,\, \bar{\theta}_{\dot{\alpha}}] = 0, \quad [\underline{\eta}^{\underline{m}},\, \underline{\theta}^\alpha] = [\underline{\eta}^{\underline{m}},\, \bar{\underline{\theta}}_{\dot{\alpha}}] = 0. \end{array} \tag{7}$$

and $\Theta^{\alpha *} = \bar{\Theta}^{\dot{\alpha}}$. Points in superspace are then identified by the generalized coordinates $z^{(M)} = (X^{\hat{m}},\, \Theta^\alpha,\, \bar{\Theta}_{\dot{\alpha}})$. We have then the one most commonly used ˋrealˊ or ˋsymmetricˊ superspace parametrized by

$$\Omega(X,\, \Theta,\, \bar{\Theta}) = e^{i(-X^{\hat{m}} p_{\hat{m}} + \Theta^\alpha Q_\alpha + \bar{\Theta}_{\dot{\alpha}} \bar{Q}^{\dot{\alpha}})} = \Omega_q(x,\, \theta,\, \bar{\theta}) \times \Omega_{\underline{q}}(\underline{\eta},\, \underline{\theta},\, \bar{\underline{\theta}}), \tag{8}$$

where we now imply a summation over $\hat{m} = (m, \underline{m})$. To study the effect of supersymmetry transformations, we consider

$$g(0,\, \epsilon,\, \bar{\epsilon})\, \Omega(X,\, \Theta,\, \bar{\Theta}) = e^{i(\epsilon^\alpha Q_\alpha + \bar{\epsilon}_{\dot{\alpha}} \bar{Q}^{\dot{\alpha}})}\, e^{i(-X^{\hat{m}} p_{\hat{m}} + \Theta^\alpha Q_\alpha + \bar{\Theta}_{\dot{\alpha}} \bar{Q}^{\dot{\alpha}})}. \tag{9}$$

the transformation (9) induces the motion:

$$g(0,\, \epsilon,\, \bar{\epsilon})\, \Omega(X^{\hat{m}},\, \Theta,\, \bar{\Theta}) \;\to (X^{\hat{m}} + i\, \Theta\, \sigma^{\hat{m}}\, \bar{\epsilon} - i\, \epsilon\, \sigma^{\hat{m}}\, \bar{\Theta},\; \Theta + \epsilon,\; \bar{\Theta} + \bar{\epsilon}), \tag{10}$$

namely,

$$\begin{array}{l} g_q(0,\, \xi,\, \bar{\xi})\, \Omega_q(x,\, \theta,\, \bar{\theta}) \;\to (x^m + i\, \theta\, \sigma^m\, \bar{\xi} - i\, \xi\, \sigma^m\, \bar{\theta},\; \theta + \xi,\; \bar{\theta} + \bar{\xi}), \\ g_{\underline{q}}(0,\, \underline{\xi},\, \bar{\underline{\xi}})\, \Omega_{\underline{q}}(\underline{\eta},\, \underline{\theta},\, \bar{\underline{\theta}}) \;\to (\underline{\eta}^{\underline{m}} + i\, \underline{\theta}\, \sigma^{\underline{m}}\, \bar{\underline{\xi}} - i\, \underline{\xi}\, \sigma^{\underline{m}}\, \bar{\underline{\theta}},\; \underline{\theta} + \underline{\xi},\; \bar{\underline{\theta}} + \bar{\underline{\xi}}). \end{array} \tag{11}$$

The spinors $\theta(\underline{\theta}, \bar{\underline{\theta}})$ and $\bar{\theta}(\underline{\theta}, \bar{\underline{\theta}})$ satisfy the embedding relations $\Delta\underline{x}^0 = \Delta x^0$ and $\Delta\underline{x}^2 = (\Delta\vec{x})^2$, so from (11) we obtain

$$\underline{\theta}\, \sigma^0\, \bar{\underline{\xi}} - \underline{\xi}\, \sigma^0\, \bar{\underline{\theta}} = \theta\, \sigma^0\, \bar{\xi} - \xi\, \sigma^0\, \bar{\theta}, \quad (\underline{\theta}\, \sigma^3\, \bar{\underline{\xi}} - \underline{\xi}\, \sigma^3\, \bar{\underline{\theta}})^2 = (\theta\, \vec{\sigma}\, \bar{\xi} - \xi\, \vec{\sigma}\, \bar{\theta})^2. \tag{12}$$

The *atomic displacement* caused by double transition of a particle $M_4 \rightleftharpoons \underline{M}_2$ reads

$$\Delta\underline{\eta}_{(a)} = \underline{e}_{\underline{m}} \Delta\underline{\eta}^{\underline{m}}_{(a)} = \underline{u}\tau, \tag{13}$$

where the components $\Delta\underline{\eta}^{\underline{m}}_{(a)}$ are written

$$\Delta\underline{\eta}^{\underline{m}}_{(a)} = (\underline{\theta}\, \sigma^{\underline{m}}\, \bar{\underline{\theta}})\tau. \tag{14}$$

In Van der Warden notations for the Weyl two-component formalism $\bar{\underline{\theta}}_{\dot{\alpha}} = (\underline{\theta}_\alpha)^*$, the (13) can be recast into the form

$$\Delta\underline{\eta}^2_{(a)} = \tfrac{1}{2}\left[(\Delta\underline{x}^0_{(a)} q)^2 - (\Delta\underline{x}^1_{(a)})^2\right], \tag{15}$$

where $\Delta\underline{x}^0_{(a)} = \underline{v}^0\tau$, $\Delta\underline{x}^1_{(a)} = \underline{v}^1\tau$, and $\underline{v}^{(\pm)} = \frac{1}{\sqrt{2}}(\underline{v}^0 \pm \underline{v}^1)$. Hence the velocities of light in vacuum, $\underline{v}^0 = c$, and of a particle ,$\underline{\vec{v}}_1 = \underline{e}_1\underline{v}^1 = \vec{n}|\vec{v}| = \vec{v}$ $(|\vec{v}| \le c)$, are

$$\begin{array}{l} \underline{v}^0 = \underline{\theta}\, \sigma^0\, \bar{\underline{\theta}} = (\underline{\theta}_1\, \bar{\underline{\theta}}_1 + \underline{\theta}_2\, \bar{\underline{\theta}}_2) = \underline{\theta}\, \bar{\underline{\theta}}, \\ \underline{v}^1 = \underline{\theta}\, \sigma^1\, \bar{\underline{\theta}} = (\underline{\theta}_1\, \bar{\underline{\theta}}_1 - \underline{\theta}_2\, \bar{\underline{\theta}}_2), \end{array} \tag{16}$$

where

$$\begin{array}{l} \theta_1(\underline{\theta},\, \bar{\underline{\theta}}) = \frac{1}{2}\left[\left(\underline{v}^0 + \sqrt{\frac{2}{3}}\underline{v}^1\right)^{1/2} + \left(\underline{v}^0 - \sqrt{\frac{2}{3}}\underline{v}^1\right)^{1/2}\right], \\ \theta_2(\underline{\theta},\, \bar{\underline{\theta}}) = \frac{1}{2}\left[\left(\underline{v}^0 + \sqrt{\frac{2}{3}}\underline{v}^1\right)^{1/2} - \left(\underline{v}^0 - \sqrt{\frac{2}{3}}\underline{v}^1\right)^{1/2}\right]. \end{array} \tag{17}$$

doi: https://doi.org/10.52526/25792776-23.70.2-188

Thus we derive the first founding property (i) that *the atomic displacement* $\Delta\underline{\eta}_{(a)}$, caused by double transition of a particle $M_4 \rightleftharpoons \underline{M}_2$, is an invariant:

$$\text{(i)} \quad \Delta\underline{\eta}_{(a)} = \Delta\underline{\eta}'_{(a)} = \cdots = inv. \tag{18}$$

The (16) gives the second (ii) founding property that the bilinear combination $\underline{\theta}\,\bar{\underline{\theta}}$ is a constant:

$$\text{(ii)} \quad c = \underline{\theta}\,\bar{\underline{\theta}} = \underline{\theta}'\,\bar{\underline{\theta}}' = \cdots = const. \tag{19}$$

The latter yields a second postulate of SR (Einstein's postulate)- *the velocity of light, c, in free space appears the same to all observers regardless the relative motion of the source of light and the observer.* The c is the maximum attainable velocity (16) for uniform motion of a particle in Minkowski background space, M_4. Equally noteworthy is the fact that (18) and (19) combined yield *invariance of the element of interval between two events* $\Delta x = k\Delta\underline{\eta}_{(a)}$ *(for given integer number k) with respect to the Lorentz transformation*:

$$\begin{aligned} &k^2\Delta\underline{\eta}^2_{(a)} = (c^2 - \underline{v}_1^2)\Delta t^2 = (c^2 - \vec{v}^{\,2})\Delta t^2 = (\Delta x^0)^2 - (\Delta\vec{x})^2 \equiv (\Delta s)^2 = (\Delta x'^0)^2 - \\ &(\Delta\vec{x})'^2 \equiv (\Delta s')^2 = \cdots = inv., \end{aligned} \tag{20}$$

where $x^0 = ct, \quad x^{0'} = ct', \ldots.$ We have here introduced a notion of physical relative finite *time intervals* between two events $\Delta t = k\tau/\sqrt{2}$, $\Delta t' = k\tau'/\sqrt{2}, \ldots.$

3. Deformation of both postulates of SR

Having SLC to be equipped with the MS$_p$-SUSY mechanism, the spinors $\underline{\theta}$ encode all of the information necessary for the two founding properties (18) and (19) of SR. In what follows, we will address violation of these properties, and that of both postulates of SR, and discuss the deformed geometry at LID. The LID is caused by two deformations

$$\Delta\widetilde{\underline{\eta}}_{(a)} = \lambda_1\,\Delta\underline{\eta}_{(a)} \Rightarrow (\widetilde{ds} = \lambda_1\,ds), \quad \tilde{c} = \lambda_2\,c, \tag{21}$$

where $\widetilde{ds}$ and $\tilde{c}$ are, respectively, deformed line element and deformed maximum attainable velocity of a particle. The deformed action of a free particle is written

$$\tilde{S} = -m_0\tilde{c}\int_a^b \widetilde{ds} = (\lambda_1\lambda_2)S, \tag{22}$$

where m_0 is the mass at rest, S is the undeformed action of a free particle. The (22) defines the energy-momentum eigenstates of the particle by means of deformed dispersion relation as follows:

$$\tilde{p}^2_\mu = (\lambda_1\lambda_2)^2 p^2_\mu = (\lambda_1\lambda_2)^2 m_0^2 c^4, \tag{23}$$

which yields the following corrections to the energy-momentum on-shell relation or LID ansatz:

$$\begin{aligned} &\tilde{E}^2 - c^2\tilde{\vec{p}}^2 - m_0^2c^4 = f(\lambda_1, \lambda_2, \epsilon) \\ &\equiv m_0^2c^4\left[(\lambda_2^2 - 1)\epsilon^2 + (\lambda_1\lambda_2)^2 - 1\right], \end{aligned} \tag{24}$$

where $\tilde{E}$ and $\tilde{\vec{p}}$ denote respectively energy and (3-component) momentum of the particle, $\epsilon \equiv \tilde{E}/m_0c^2$, and we also set $c\tilde{\vec{p}} \simeq \tilde{E}$ at high-energy limit.

Remark: We emphasize that testing the $f(\lambda_1, \lambda_2, \epsilon)$ phenomenologically in the ultra-high energy astroparticle experiments, we are allowed to determine only λ_2 (for deformed maximum attainable velocity), but λ_1 (for deformed line element) is left unknown. To determine both coefficients, therefore, we consider a constitutive ansatz of simple, yet tentative, deformation of spinors $\underline{\theta}$ with given scalar LIDF, λ:

$$\underline{\theta} \to \tilde{\underline{\theta}} = \lambda^{1/2}\,\underline{\theta}. \tag{25}$$

doi: https://doi.org/10.52526/25792776-23.70.2-188

This, by virtue of (??), (16) and (25), leads to (21) for $\lambda = \lambda_1 = \lambda_2$. In this case

$$\begin{aligned} &\widetilde{ds} = \sqrt{2}(\underset{\sim}{\tilde{\theta}}_1 \,\underset{\sim}{\tilde{\tilde{\theta}}}_1 \,\underset{\sim}{\tilde{\theta}}_2 \underset{\sim}{\tilde{\tilde{\theta}}}_2)^{1/2}\, t = \lambda\, ds, \\ &\tilde{c} \equiv \underset{\sim}{\tilde{\theta}}\, \underset{\sim}{\tilde{\tilde{\theta}}} = \lambda c. \end{aligned} \tag{26}$$

To this end we note that the invariance of DLE, and the same value of DMAV in free space hold for all inertial frames

$$\begin{aligned} &\widetilde{ds}^{\,2} = \widetilde{ds'}^{\,2} = \widetilde{ds''}^{\,2} = \cdot = inv, \\ &\tilde{c} = \tilde{c'} = \tilde{c''} = \cdots . \end{aligned} \tag{27}$$

The relativity of inertial frames and validity of deformed Lorentz symmetry evidently is left unchanged, in spite of the appearance of modified terms in the LID dispersion relations. The LID ansatz (24) is reduced to

$$f(\lambda, \epsilon) = m_0^2 c^4 \left[(\lambda^2 - 1)\epsilon^2 + \lambda^4 - 1\right]. \tag{28}$$

According to (24) and (28), in the relativistic limit, the group velocity to first order in $m_0^2 c^4$ and $f(\lambda, \epsilon)$ reads

$$\frac{v_{gr}^{\pm}}{c} = \frac{\partial E}{c\partial p} \simeq \frac{1}{2} - \frac{\lambda^4}{2\epsilon^2} + \frac{\lambda^2}{2} + \lambda(\epsilon + \frac{2\lambda^2}{\epsilon})\frac{\partial \lambda}{\partial \epsilon}. \tag{29}$$

As we will see in next section, different choices of the LIDFs produce different LID ansatze yielding very different types of LIV behavior, which caused the UHECR- and TeV-γ threshold anomalies detected.

4. Deformed geometry at LID

A common conjecture for the behavior of spacetime in quantum gravity is that the algebra of spacetime coordinates is actually noncommutative (Douglas & Nekrasov, 2001, Mattingly, 2005), (Hinchliffe et al., 2004, Kowalski-Glikman & Nowak, 2003). The most familiar form of spacetime non-commutativity, "canonical" non-commutativity, where the spacetime coordinates acquire the non-commutativity relation, $[x_\alpha, x_\beta] = (i/\Lambda_{NC}^2)\Theta_{\alpha\beta}$, at the characteristic noncommutative energy scale Λ_{NC} (Mattingly, 2005). This scale is presumably near the Planck scale if the non-commutativity comes from quantum gravity. However, in large extra dimension scenarios Λ_{NC} could be as low as 1 TeV. The existence of Λ_{NC} manifestly breaks Lorentz invariance, the size of which is constrained by tests of Lorentz violation. All the approaches use an expansion in this scale to get some low energy effective field theory. For discussions of other types of non-commutativity, including those that preserve Lorentz invariance, see (Douglas & Nekrasov, 2001), (Hinchliffe et al., 2004, Kowalski-Glikman & Nowak, 2003).

In this section, therefore, we relate LIV to more general deformed smooth differential 4D-manifold $\mathcal{M}_4$. Meanwhile, there is a need to introduce the soldering tools, which are the linear frames and forms in tangent fiber-bundles to the external general smooth differential manifold, whose components are so-called tetrad (vierbein) fields. Consider a smooth deformation map (Ter-Kazarian, 2011)

$$\Omega : M_4 \to \mathcal{M}_4, \tag{30}$$

written in terms of the *world-deformation* tensor Ω, the flat Minkowski, M_4, and general, $\mathcal{M}_4$, smooth differential 4D-manifolds. Here we use Greek alphabet $(l, k, \rho, ... = 0, 1, 2, 3)$ to denote the holonomic world indices related to $\mathcal{M}_4$, and the second half of Latin alphabet $(l, m, k, ... = 0, 1, 2, 3)$ to stand for the world indices related to M_4. The M_4 has at each point a tangent space, $T_x M_4$, spanned by the holonomic orthonormal frame field, $\hat{e}_{(l)}$, as a shorthand for the collection of the 4-tuplet $(\hat{e}_{(0)}, \cdots, \hat{e}_{(3)})$. If the $\hat{e}_{(l)}$ are holonomic basis, their commutator will vanish $\left[\hat{e}_{(l)}, \hat{e}_{(k)}\right] = 0$, or converse, if the commutator vanishes one can find coordinates y^l such that $\hat{e}_{(l)} = \partial/\partial y^l$, which is known as Frobenius's Theorem (Schutz, 1982). Then any abstract vector $V \in M_4$ can be written as a linear combination of basis vectors, $V = V^l \hat{e}_{(l)}$. The real vector is an abstract geometrical entity, while the components are just the coefficients of the basis vectors in some convenient basis. Consider the tangent vector $V(u)$ with components $V^l(u) = dx^l/du$ to a parameterized curve $x^l(u)$, where u is the affine parameter. Under a Lorentz transformation the coordinates x^l change $x^{k\prime} = \Lambda_l^{k'} x^l$, while the parameterization u is unaltered. We can therefore deduce that the Lorentz transformation rule for basis vectors is $\hat{e}_{(k')} = \Lambda_{k'}^{l}\, \hat{e}_{(l)}$. The frame field, $\hat{e}$, then defines a dual vector, $\hat{\vartheta} \in {}^*T_x M_4$ (${}^*T_x M_4$ is the cotangent space), of differential forms, $\hat{\vartheta} = \begin{pmatrix} \hat{\vartheta}^{(0)} \\ \vdots \\ \hat{\vartheta}^{(3)} \end{pmatrix}$, as a shorthand for the

doi: https://doi.org/10.52526/25792776-23.70.2-188

collection of the $\hat{\vartheta}^{(k)} = e^k{}_l\, dx^l$, whose values at every point form the dual basis, such that $\hat{e}_{(l)} \rfloor \hat{\vartheta}^{(k)} = \delta^k_l$. Here $\rfloor$ denotes the interior product, namely, this is a C^∞-bilinear map $\rfloor : \Omega^1 \to \Omega^0$ with Ω^p denotes the C^∞-modulo of differential p-forms on M_4. In components $e_\sigma{}^k\, e^\sigma{}_l = \delta^k_l$.

Every dual vector $\omega \in M_4$ can be written in terms of its components labeled with lower indices: $\omega = \omega_l \hat{\vartheta}^{(l)}$. Whereas the dual space to the dual vector space is the original vector space itself: $V(\omega) = \omega(V) = \omega_l V^l$. The Lorentz transformation rule for dual basis vectors is $\hat{\vartheta}^{(k')} = \Lambda^{k'}_l\, \hat{\vartheta}^{(l)}$. To this end we could define the components of arbitrary tensor as $T^{l_1 \cdots l_k}_{k_1 \cdots k_l} = T(\hat{\vartheta}^{(l_1)}, \ldots, \hat{\vartheta}^{(l_k)}, \hat{e}_{(k_1)}, \ldots, \hat{e}_{(k_l)})$. The action of the tensors on a set of vectors and dual vectors is $T(\omega^{(1)}, \ldots, \omega^{(k)}, V^{(1)}, \ldots, V^{(l)}) = T^{l_1 \cdots l_k}_{k_1 \cdots k_l} \omega^{(1)}_{l_1}, \ldots, \omega^{(k)}_{l_k} V^{(1)k_1}, \ldots, V^{(l)k_l}$.

On the manifold, M_4, the tautological tensor field, id, of type (1,1) is defined which assigns to each tangent space the identity linear transformation. Thus for any point $x \in M_4$, and any vector $\xi \in T_x M_4$, one has $id(\xi) = \xi$. In terms of the frame field, the $\hat{\vartheta}^{(l)}$ give the expression for id as $id = \hat{e}\hat{\vartheta} = \hat{e}_{(0)} \otimes \hat{\vartheta}^{(0)} + \cdots \hat{e}_{(3)} \otimes \hat{\vartheta}^{(3)}$, in the sense that both sides yield ξ when applied to any tangent vector ξ in the domain of definition of the frame field. One can also consider general transformations of the linear group, $GL(4, R)$, taking any basis into any other set of four linearly independent fields. The notation, $\{\hat{e}_{(l)}, \hat{\vartheta}^{(k)}\}$, will be used below for general linear frames. The holonomic metric on the space M_4 can be recast in the form $\eta = \eta_{lk}\, \hat{\vartheta}^{(l)} \otimes \hat{\vartheta}^{(k)} = \eta(\hat{e}_{(l)}, \hat{e}_{(k)})\, \hat{\vartheta}^{(l)} \otimes \hat{\vartheta}^{(k)}$ with the components $\eta_{lk} = \eta(\hat{e}_{(l)}, \hat{e}_{(k)})$ in dual holonomic basis. We may define a p-form A to be closed if $dA = 0$, and exact if $A = dB$ for some $(p-1)$-form B. The pth de Rham cohomology vector space $H^p(M) = Z^p(M)/B^p(M)$, defined on the arbitrary manifold M, depends only on the topology of the manifold M, where $Z^p(M)$ is the vector space of closed p-forms. Minkowski space M_4 is topologically equivalent to $\mathbf{R^4}$, so that all of the $H^p(M)$ vanish for $p > 0$; for $p = 0$ we have $H^0(M) = \mathbf{R}$. Therefore in Minkowski space all closed forms are exact except for zero-forms; zero-forms can't be exact since there are no -1-forms for them to be the exterior derivative.

In turn, the general manifold $\mathcal{M}_4$ in (30) has at each point a tangent space, $T_x\mathcal{M}_4$, spanned by the anholonomic orthonormal frame field, e, as a shorthand for the collection of the 4-tuplet $(e_0, \cdots, e_3)$, where $e_a = e_a{}^\mu\, \partial_\mu$. We use the first half of Latin alphabet $(a, b, c, ... = 0, 1, 2, 3)$ to denote the anholonomic indices related to the tangent space. The frame field, e, then defines a dual vector, $\vartheta \in {}^*T_x\mathcal{M}_4$, of differential forms, $\vartheta = \begin{pmatrix} \vartheta^0 \\ \vdots \\ \vartheta^3 \end{pmatrix}$, as a shorthand for the collection of the $\vartheta^b = e^b{}_\mu\, dx^\mu$, whose values at every point form the dual basis, such that $e_a \rfloor \vartheta^b = \delta^b_a$. In components $e_a{}^\mu\, e^b{}_\mu = \delta^b_a$.

Constructing a smooth deformation map (30), let introduce so-called the *first deformation matrices*, $\pi_a{}^l$ and $\pi^a{}_k\, (\in GL(4, \mathcal{M})\, \forall\, x^\mu)$, which yield local tetrad deformations

$$e_a = \pi_a{}^l\, \hat{e}_{(l)}, \quad \vartheta^a = \pi^a{}_k\, \hat{\vartheta}^{(k)}, \tag{31}$$

provided,

$$\pi_a{}^l = \lambda^{1/2} e_a{}^l, \quad \pi^a{}_k = \lambda^{1/2} e^a{}_k, \tag{32}$$

so that

$$e_\mu = \pi_\mu{}^l\, \hat{e}_{(l)}, \quad \vartheta^\mu = \pi^\mu{}_k\, \hat{\vartheta}^{(k)}, \quad \pi_\mu{}^l = e_\mu{}^a \pi_a{}^l, \quad \pi^\mu{}_k = e^\mu{}_a \pi^a{}_k. \tag{33}$$

With this provision, we build up a *world-deformation* tensor,

$$\Omega^k{}_l = \pi^k{}_\mu\, \pi^\mu{}_l = \pi^k{}_a\, \pi^a{}_l = e^a{}_l e_b{}^l \Omega^b{}_a = \lambda\, (e^k{}_\mu\, e^\mu{}_l) = \lambda\, (e^k{}_a\, e^a{}_l) = \lambda\, \delta^k_l. \tag{34}$$

Thus, according to (26), the tautological tensor field $\tilde{id} \in \mathcal{M}_4$ of type (1,1), assigned to each tangent space $T_x\mathcal{M}_4$ the identity linear transformation:

$$\tilde{ds} = \tilde{id} = e_a \otimes \vartheta^a = \lambda\, \hat{e}_{(l)} \otimes \hat{\vartheta}^{(l)} = \lambda\, id = \lambda\, ds, \tag{35}$$

where $ds = id \in M_4$. The *first deformation matrices* π, in general, give rise to the right cosets of the Lorentz group, i.e. they are the elements of the quotient group $GL(4, \mathcal{M})/SO(3, 1)$. If we deform the co-tetrad according to (31), we have two choices to recast metric as follows: either writing the deformation of the metric in the space of tetrads or deforming the tetrad field:

$$g = o_{ab}\, \vartheta^a \otimes \vartheta^b = o_{ab}\, \pi^a{}_l\, \pi^b{}_k\, \hat{\vartheta}^{(l)} \otimes \hat{\vartheta}^{(k)} = \gamma_{lk}\, \hat{\vartheta}^{(l)} \otimes \hat{\vartheta}^{(k)}, \tag{36}$$

doi: https://doi.org/10.52526/25792776-23.70.2-188

where γ_{lk} is, so-called, *second deformation matrix*:

$$\gamma_{lk} = o_{ab}\,\pi^a{}_l\,\pi^b{}_k = \lambda\, o_{ab}\, e^a{}_l\, e^b{}_k. \tag{37}$$

The deformed metric splits as

$$g_{\mu\nu} = \Upsilon^2\,\eta_{\mu\nu} + \gamma_{\mu\nu}, \tag{38}$$

provided,

$$\gamma_{\mu\nu} = (\gamma_{al} - \Upsilon^2\, o_{al})\, e^a{}_\mu\, \pi^l{}_\nu = (\gamma_{ks} - \Upsilon^2\,\eta_{ks})\,\pi^k{}_\mu\,\pi^s{}_\nu, \tag{39}$$

where $\Upsilon = \pi^a{}_a = \pi^k{}_k$, and $\gamma_{al} = \gamma_{kl}\pi_a{}^k$. The anholonomic orthonormal frame field, e, relates g to the tangent space metric, $o_{ab} = diag(+---)$, by $o_{ab} = g(e_a, e_b) = g_{\mu\nu}\, e_a{}^\mu\, e_b{}^\nu$, which has the converse $g_{\mu\nu} = o_{ab}\, e^a{}_\mu\, e^b{}_\nu$ because $e_a{}^\mu\, e^a{}_\nu = \delta^\mu_\nu$. The γ_{lm} can be decomposed in terms of symmetric, $\pi_{(al)}$, and antisymmetric, $\pi_{[al]}$, parts of the matrix $\pi_{al} = o_{ac}\pi^c{}_l$ (or respectively in terms of $\pi_{(kl)}$ and $\pi_{[kl]}$, where $\pi_{kl} = \eta_{ks}\,\pi^s{}_l$) as

$$\gamma_{al} = \Upsilon^2\, o_{al} + 2\Upsilon\,\Theta_{al} + o_{cd}\,\Theta^c{}_a\,\Theta^d{}_l + o_{cd}\,(\Theta^c{}_a\,\varphi^d{}_l + \varphi^c{}_a\,\Theta^d{}_l) + o_{cd}\,\varphi^c{}_a\,\varphi^d{}_l, \tag{40}$$

where

$$\pi_{al} = \Upsilon o_{al} + \Theta_{al} + \varphi_{al}, \tag{41}$$

provided Θ_{al} is the traceless symmetric part and φ_{al} is the skew symmetric part of the first deformation matrix. The anholonomy objects defined on the tangent space, $T_x\mathcal{M}_4$, read

$$C^a: \quad = d\,\vartheta^a = \tfrac{1}{2}\, C^a{}_{bc}\,\vartheta^b \wedge \vartheta^c, \tag{42}$$

where the anholonomy coefficients, $C^a{}_{bc}$, which represent the curls of the basis members, are

$$\begin{aligned} C^c{}_{ab} &= -\vartheta^c([e_a, e_b]) = e_a{}^\mu e_b{}^\nu(\partial_\mu e^c{}_\nu - \partial_\nu e^c{}_\mu) - e^c{}_\mu[e_a(e_b{}^\mu) - e_b(e_a{}^\mu)] \\ &= 2\,\pi^c{}_l\,\pi^\mu_m\,\left(\pi^{-1m}{}_{[a}\partial_\mu\,\pi^{-1l}{}_{b]}\right). \end{aligned} \tag{43}$$

In particular case of constant metric in the tetradic space, the deformed connection can be written as

$$\Gamma^a{}_{bc} = \tfrac{1}{2}\left(C^a{}_{bc} - o^{aa'}\,o_{bb'}\,C^{b'}{}_{a'c} - o^{aa'}\,o_{cc'}\,C^{c'}{}_{a'b}\right). \tag{44}$$

A deformed general spin connection defined on the tangent space $T_x\mathcal{M}_4$ then is

$$\omega^a{}_{b\mu} = \pi_c{}^a\hat{\omega}^c{}_{d\mu}\pi^d{}_b + \pi_c{}^a\,\partial_\mu\,\pi^c{}_b = \pi_c{}^a\,\partial_\mu\,\pi^c{}_b, \tag{45}$$

because the spin connection, $\hat{\omega}^c{}_{d\mu}$, defined on the tangent space T_xM_4 is zero. As far as

$$\pi_c{}^a = \pi_\mu{}^a e_c{}^\mu = \lambda^{1/2}\, e_\mu{}^a e_c{}^\mu = \lambda^{1/2}\,\delta^a_c, \tag{46}$$

the spin connection (45) becomes

$$\omega^a{}_{b\mu} = \tfrac{1}{2}\delta^a_b\,\partial_\mu\,\lambda. \tag{47}$$

To have a complete picture of deformed geometry, there is a need for testing different LIDFs in several scenarios of LIV.

5. Testing LIDFs in the UHECR- and TeV-γ threshold anomalies

Having given some examples of the ways in which LIV arises, in this section let us turn to the complementary type of issues that are in focus when one studies the UHECRs and TeV-γ photons observed. We give a brief sketch of testing different LIDFs in several scenarios of the Coleman and Glashow-type perturbative extension of SLC, the LID extension of standard model, the LID in quantum gravity motivated space-time models and the LID in loop quantum gravity models.

doi: https://doi.org/10.52526/25792776-23.70.2-188

5.1. The LIDF for Coleman and Glashow-type perturbative extension of SLC

Let us consider a particular LIDF

$$\lambda_a = 1 + \delta_a, \quad 0 < |\delta_a| \ll 1, \tag{48}$$

with constant δ_a. Then a particle of specie (a) has, in addition to its own mass m_a, its own maximum attainable velocity $c_a = c\lambda_a$ (its own velocity of light c_a) as measured in the preferred frame:

$$\tilde{E}_a^2 = c_a^2 \tilde{\vec{p}}_a^2 + m_a^2 c_a^4, \tag{49}$$

where $\tilde{E}_a$ and $\tilde{\vec{p}}_a$ denote the energy and the (3-component) momentum of a-th particle. In this case, according to (28), the LID ansatz is

$$f_a = m_a^2 c^4 \left[\epsilon_a^2 \left(1 - \lambda_a^2\right) + 1 - \lambda_a^4\right], \tag{50}$$

where $\epsilon_a = \tilde{E}_a / m_a c^2$. This ansatz yields the CG Coleman & Glashow (1999)-type perturbative extension of SLC. Coleman and Glashow have developed a perturbative framework of LIV, by introducing noninvariant terms in the context of conventional quantum field theory. These terms assumed to be renormalizable in dimension no greater than four, gauge invariant under $SU(3)\otimes SU(2)\otimes U(1)$ local group, and the Lagrangian is rotationally and translationally invariant in a preferred frame which is presumed to be the rest frame of the CMB. The threshold condition for a reaction to take place can be substantially modified if the difference $\lambda_a - \lambda_b$ is nonzero (a and b are two particles involved in the reaction). This leads to new effects and predictions such as an abundant flux of cosmic rays well beyond the GZK cutoff energy. The reaction $(p + \gamma \rightarrow p + \pi)$ happens through several channels, for example, the baryonic $\triangle$ and N and mesonic ρ and ω resonance channels, and is the main reason for the appearance of the GZK cutoff. Following Stecker & Scully (2005), the CBR photopion production $(p + \gamma \rightarrow N + \pi' s)$, on CBR photons of energy E' and temperature $T_{CBR} = 2.73$ K, is turned off if in terms of LIDF $\lambda_\pi - \lambda_p > 5 \times 10^{-24} (E'/2.73K)^2/c$. In this case, the description of the UHECR threshold anomaly requires together with conditions on $\lambda_\triangle - \lambda_\pi$ that $\lambda_\pi - \lambda_p > 10^{-24}/c$, where λ_π and λ_p are the λ_a for $a \equiv$ pions and $a \equiv$ protons, respectively. A resolution of the TeV-γ threshold anomaly with in this scheme Amelino-Camelia & Piran (2001) requires the additional condition $\lambda_e - \lambda_\gamma > 5 \times 10^{-16}/c$. This combines with the absence of vacuum Cherenkov radiation by electrons with energies up to 500 GeV in such a way that the allowed values for $\lambda_e - \lambda_\gamma$ lying in a relatively narrow range of $5 \times 10^{-16}/c < \lambda_e - \lambda_\gamma < 5 \times 10^{-13}/c$.

5.2. The LIDF for LIV extension of the standard model

The development of air showers can be influenced both by Lorentz invariant new physics acting on primaries or secondaries with energy $E \gtrsim 2 \times 10^{17}$eV, and also by LIV involving large Lorentz boosts. Therefore we now address LIDF for LIV extension of the minimal $SU(3) \otimes SU(2) \otimes U(1)$ standard model, including CPT-even and CPT-odd terms. This can be viewed as the low-energy limit of a physically relevant fundamental theory with Lorentz-covariant dynamics in which spontaneous Lorentz violation occurs Colladay & Kostelecky (1997, 1998), Kostelecky & Mewes (2008). The LIV is induced by non-renormalizable operators that conserve gauge invariance but break parts of the Poincaré group. One possible effect is vacuum birefringence, which could be bounded from cosmological observations. The LIDF for left- and right-handed photons or fermions can be written

$$\lambda_\pm(\epsilon/\epsilon_P, \eta_\pm, n) = \frac{\epsilon}{\sqrt{2}} \left\{-1 + \sqrt{1 + \frac{4}{\epsilon^4}\left[1 + \epsilon^2 (1 + f_\pm(\epsilon/\epsilon_P, \eta_\pm, n))\right]}\right\}^{1/2}, \tag{51}$$

provided the LID ansatz, following Amelino-Camelia et al. (2005), Christian (2005), Diaz (2014), is

$$f_\pm(\epsilon/\epsilon_P, \eta_\pm, n) = \eta_\pm \epsilon^2 \left(\frac{\epsilon}{\epsilon_P}\right)^n, \tag{52}$$

where dimensionless numbers $\eta_\pm$ refer to positive and negative helicity states, and $n = d - 4$ for a d-dimensional operator. On the right-hand side we highlighted the fact that this correction would come in suppressed with respect to the standard leading term by a factor of given by the degree of ratio ϵ/ϵ_P of the

doi: https://doi.org/10.52526/25792776-23.70.2-188

energy and Planck energy scale. In general, in effective field theory one has $\eta_+ = (-1)^n\eta_-$. In (51), $d \leq 4$ for renormalizable LIV terms, and n is negative. A tiny deformation

$$\underset{\sim}{\tilde{\theta}} \simeq \left[1 + \frac{\eta_\pm}{2}(n+1)\left(\frac{\epsilon}{\epsilon_P}\right)^n\right]^{1/2} \underset{\sim}{\theta}, \tag{53}$$

where the corresponding parameter $\eta_\pm$ should be of order 1, yields variation in photon speed, which, when accumulated over cosmological light-travel times, may be revealed by observing LIV effects. For the LID ansatz (52), the group velocity (29) can be recast into the form

$$\frac{v_{gr}^\pm}{c} \simeq 1 - \frac{1}{2\epsilon^2} + \frac{\eta_\pm}{2}(n+1)\left(\frac{\epsilon}{\epsilon_P}\right)^n. \tag{54}$$

This leads to energy-dependent delays in the propagation time from the sources to Earth. However, the interplay between LIV and violations of CPT symmetry is still the subject of a lively debate, see e.g. Chaichian et al. (2011).

5.3. The LIDF for quantum gravity motivated space-time models

In models for quantum gravity involving large extra dimensions, the energy scale at which gravity becomes strong can occur at a scale, $E_{QG} << E_P$, even approaching a TeV. In the most commonly considered case, the phenomenological approach is motivated by the role that the deformed dispersion relation might have in quantum gravity, the energy scale E_{QG} of which is expected to be somewhere between $E_{GUT} < E_{QG} < E_P$, where E_{GUT} is the energy scale of grand unified theory (GUT). The quantum-gravity effects inducing some level of nonlocality or noncommutativity would affect even the most basic flat-space continuous symmetries, such as Lorentz invariance. This intuition would be seen as a way to develop the LIV. The expectations of the quantum gravity motivated space-time models known to support such violations of Lorentz invariance: an integer value of the dimensionless parameter and a characteristic energy scale constrained to a narrow interval in the neighborhood of the Planck scale Amelino-Camelia & Piran (2001), Amelino-Camelias et al. (1998). In this case, the LIDF should be the scalar function, $\lambda(\epsilon,\, \epsilon_P)$ of the energy and Planck energy scale, which yields $\tilde{c}(\epsilon,\, \epsilon_P) = \underset{\sim}{\tilde{\theta}}(\epsilon,\, \epsilon_P)\,\underset{\sim}{\tilde{\tilde{\theta}}}(\epsilon,\, \epsilon_P)$ - a deformed velocity. Within the phenomenological approach, the UHECR and TeV-γ threshold anomalies are due to a class of deformed dispersion relations, which are invariant under the subgroup of rotations $SO(3)$, but is not locally Lorentz invariant. In this scenario, the LIDF can be written as

$$\lambda(\epsilon,\, \epsilon_P, \eta, \alpha) = \frac{\epsilon}{\sqrt{2}}\left\{-1 + \sqrt{1 + \frac{4}{\epsilon^4}\left[1 + \epsilon^2(1 + f(\epsilon,\, \epsilon_P, \eta, \alpha))\right]}\right\}^{1/2}, \tag{55}$$

where the LID ansatz, following Amelino-Camelia & Piran (2001), Amelino-Camelias et al. (1998) for $\alpha = 1$, and Amelino-Camelia (1997, 2000, 2013) for a general α, takes the form

$$f(\epsilon,\, \epsilon_P, \eta, \alpha) \equiv \epsilon^2\eta\left(\frac{\epsilon}{\epsilon_P}\right)^\alpha. \tag{56}$$

The free parameters α and η are characterizing the deviation from standard Lorentz invariance. The η is a dimensionless parameter of order 1. The α specifies how strongly the magnitude of the violation is suppressed by E_P. Using the UHECR and TeV-γ data, as well as upper bounds on time-of-flight differences between photons of different energies, the LID parameter space is constrain. Concerning the consistency of the interpretation of the threshold anomalies as manifestations of LID it is also important to observe that the modified dispersion relation (56), in spite of affecting so significantly the GZK and TeV-γ thresholds, does not affect significantly the processes used for the detection of the relevant high-energy particles. The quantum-gravity intuition would then be seen as a way to develop a theoretical prejudice for plausible values of η and α . In particular, corrections going as ϵ/ϵ_P a typically emerge in quantum gravity as leading order pieces of some more complicated analytic structures Amelino-Camelias et al. (1998), Amelino-Camelia & Majid (2000), Lukierski et al. (1992, 1995), Amelino-Camelia (1997). This provides, of course, a special motivation for the study of the cases $\alpha = 1$ and $\alpha = 2$ $[f(\epsilon/\epsilon_P) \approx 1 + \alpha_1(\epsilon/\epsilon_P)^{n_1} + \cdots]$. Moreover, the fact that $E_{GUT} < E_{QG} < E_P$ corresponds to the expectation that η should not be far from the range $1 \leq \eta \leq 10^{3\alpha}$. At $f(\epsilon,\, \epsilon_P, \eta, \alpha) \ll 1$, in the first order over f, (55) gives a deformation

$$\underset{\sim}{\tilde{\theta}} \simeq \left[1 + \epsilon^2\eta\left(\frac{\epsilon}{\epsilon_P}\right)^{\alpha(\sim 1,2)}\right]^{1/2} \underset{\sim}{\theta}, \tag{57}$$

doi: https://doi.org/10.52526/25792776-23.70.2-188

which will cause a significant upward shift above the GZK cutoff determined by the threshold equation Amelino-Camelia & Piran (2001)

$$E_{p,th} = \frac{c^4[(m_p+m_\pi)^2-m_p^2]}{4E_\gamma} + \eta\frac{E_{p,th}^{2+\alpha}}{4E_\gamma E_P^\alpha}\left(\frac{m_p^{1+\alpha}+m_\pi^{1+\alpha}}{(m_p+m_\pi)^{1+\alpha}} - 1\right), \tag{58}$$

where $E_{p,th}$ is the threshold energy of the proton and E_γ is the energy of the photon, in the head-on collision between a soft photon and a high-energy proton of photoproduction process $p+\gamma \to p+\pi$.

5.4. The LIDF for the loop quantum gravity models

Alternatively, loop quantum gravity is a canonical approach to the problem of gravity quantization. It is based on the construction of a spin network basis, labeled by graphs embedded in a three-dimensional insertion Σ in spacetime. In Alfaro & Palma (2002, 2003), Alfaro et al. (2000b, 2002a,b) the authors present some techniques to establish and analyze new constraints on the loop quantum gravity parameters. The effects of the loop structure of space at the Planck level are treated semiclassically through a coarse-grained approximation. An interesting feature of these methods is the explicit appearance of the two length scales: Planck scale $\ell_P \approx 1.62 \times 10^{-33}$cm and, so-called , `weave´ scale $\mathcal{L} \gg \ell_P$. It is possible, however, to introduce a loop state which approximates a flat three-metric on Σ at length scales greater than the length scale $\mathcal{L} \gg \ell_P$. There with for distances $d \ll \mathcal{L}$ the quantum loop structure of space is manifest, while for distances $d \geq \mathcal{L}$ the continuous flat geometry is regained. Such effective theories introduce LID's to the dispersion relations. The dispersion relation for fermions can be obtained through the development of a Klein-Gordon-like equation. The lower contributions in both scales ℓ_P and $\mathcal{L}$ yield the following LIDF:

$$\lambda_\pm(\epsilon,\ell_P,\mathcal{L}) = \frac{\epsilon}{\sqrt{2}}\left\{-1+\sqrt{1+\frac{4}{\epsilon^4}\left[1+\epsilon^2(1+f_\pm(\epsilon,\ell_P,\mathcal{L}))\right]}\right\}^{1/2}. \tag{59}$$

Provided the LID ansatz is given Alfaro & Palma (2002, 2003)

$$f_\pm(\epsilon,\ell_P,\mathcal{L}) = 2\alpha\epsilon^2 + \eta\epsilon^4 \pm 2\lambda\epsilon, \tag{60}$$

where the $\pm$ signs correspond to the helicity state of the described particle, and the parameters (α,η,λ) are functions of these two scales as

$$\alpha = k_\alpha(\ell_P/\mathcal{L})^2, \quad \eta = k_\eta \ell_P^2, \quad \lambda = k_\lambda \ell_P/2\mathcal{L}^2, \tag{61}$$

and the dimensionless parameters $k_\alpha, k_\eta, k_\lambda$ are of order 1. For the electromagnetic sector of the theory, the LIDF for the photon is written

$$\lambda_\pm(\epsilon,\ell_P,\mathcal{L}) = \frac{\epsilon}{\sqrt{2}}\left\{-1+\sqrt{1+\frac{4}{\epsilon^4}\left[1+\epsilon^2(1+2\alpha_\gamma k^2 \pm 2\theta_\gamma \ell_P k^3\right]}\right\}^{1/2}. \tag{62}$$

where $\alpha_\gamma = k_\gamma$. There with the condition for significantly increasing the threshold for electron-positron pair production interactions $(p+\gamma \to p+e^+ + e^-)$ is obtained $\lambda_e - \lambda_p > (m_p+m_e)m_p c^3/E_f^2$, which is $O(10^{-22}/c)$ for a fiducial energy $E_f = 100$ EeV. Thus, given even a very small amount of deformation,

$$\underset{\sim}{\tilde{\theta}} \simeq \left[1+2\alpha\epsilon^2+\eta\epsilon^4 \pm 2\lambda\epsilon\right]^{1/2}\underset{\sim}{\theta}, \tag{63}$$

both photopion and pair-production interactions of UHECR with the CBR can be turned off, and it could explain the UHECR spectrum which shows an excess of UHECRs at energies above GZK limit. Since a detailed knowledge of the deviation parameters figured in (63) is absent, the different corrections are studied independently in Alfaro & Palma (2003), with hope that there will always exist the possibility of having an adequate combination of these parameter values that could affect the threshold conditions simultaneously. This threshold analysis gives the following constraints for a significant increase or decrease in the threshold energy for pair production: $|\alpha_p - \alpha_e| < 9.8 \times 10^{-22}$; $\quad 2.6 \times 10^{-18}\text{eV}^{-1} \lesssim \mathcal{L} \lesssim 1.6 \times 10^{-17}\text{eV}^{-1}$. If no GZK anomaly is confirmed in future experimental observations, then one should state a stronger bound $|\alpha_\pi - \alpha_p| < 2.3 \times 10^{-23}$, or $\lesssim \mathcal{L} \gtrsim 1.7 \times 10^{-17}\text{eV}^{-1}$. For η- and λ-corrections are respectively obtained: $|\eta| < 1.6 \times 10^{-60}\text{eV}^{-2}$ and $|\lambda_e| < 1.6 \times 10^{-5}$eV. However, the present stage of UHECR observations requires that one proceeds with caution, as far as each one of these parameters will be significant at different energy ranges.

doi: https://doi.org/10.52526/25792776-23.70.2-188

5.5. The LIDF for the models preserving the relativity of inertial frames

Einstein's Relativity postulates provide an example in which the Relativity Principle coexists with an observer-independent (velocity) scale. In Amelino-Camelia (2002) it is assumed that Relativity can also be "doubly special", in the sense that the Relativity Principle can coexist with observer-independent scales of both velocity and length. As a corollary, the Relativity Principle can be formulated in a way that does not lead to inconsistencies in the case of space-times whose short-distance structure is governed by an observer-independent length scale. In the proposed a new conceptual framework, it is shown by Amelino-Camelia (2002) that the relativistic treatment of the known in literature dispersion relation, $E^2 = c^4m^2 + c^2p^2 - \widetilde{\ell}_P cp^2E$, leads to threshold anomalies. This, by virtue of (28), yields following LIDF:

$$\lambda_\pm(\epsilon,\ell_P,\mathcal{L}) = \frac{\epsilon}{\sqrt{2}}\Big\{-1+ \sqrt{1+\frac{4}{\epsilon^4}\left[1+\epsilon^2(1+\widetilde{\ell}_P cp^2E)\right]}\Big\}^{1/2}. \tag{64}$$

The interesting hypothesis that the Lorentz transformations may be modified at Planck scale is proposed by Magueijo & Smolin (2003), which preserve the relativity of inertial frames with a non-linear action of the Lorentz transformations on momentum space.In contrast to other definitions, this leads to a commutative spacetime geometry. But the commutation relations between position and momentum become energy dependent, leading to a new energy dependent modification of the uncertainty relations. The most general invariant associated with the new group action is $||p||^2 \equiv \eta^{ab}U(p_a)U(p_b)$, where the modified boost generators can be written in the form $K^i = U^{-1}[p_0]L^i_0U[p_0]$. This, incorporating with (28), yield

$$\lambda_\pm(\epsilon,\ell_P,\mathcal{L}) = \frac{\epsilon}{\sqrt{2}}\Big\{-1+ \sqrt{1+\frac{4}{\epsilon^4}\left[1+\epsilon^2(\frac{\eta^{ab}U(p_a)U(p_b)}{m^2c^2})\right]}\Big\}^{1/2}, \tag{65}$$

where L_{ab} are the standard Lorentz generators. For the particular boosts, one has $U[p_0] \equiv \exp(\varsigma p_0 D)$ (ς may have either sign, and that it is expected to be proportional to plus or minus the Planck length), where $D = p_a\frac{\partial}{\partial p_a}$ is a dilatation, or more specifically: $U[p_0](p_a) = p_a/(1-\varsigma p_0)$ (for a more detailed analysis see Magueijo & Smolin (2003)). In that respect, we stress that the proposed LID-generalization of global MS$_p$-SUSY theory strongly supports the major goal of works Amelino-Camelia (2002) and Magueijo & Smolin (2003), because this theory formulates the LID-generalized relativity postulates in a way that preserve the relativity of inertial frames.

6. The physical outlook and concluding remarks

In this paper we have presented a general overview of the effects of deviations from exact Lorentz invariance in the context of double space- or MS$_p$-SUSY.

Deformation of the spinors: $\underline{\theta} \to \underline{\tilde{\theta}} = \lambda^{1/2}\,\underline{\theta}$, etc., where λ is figured as the scalar LIDF, yields both the DLE and DMAV, respectively, in the form $\tilde{ds} = \lambda ds$ and $\tilde{c} = \lambda c$, provided, the invariance of DLE, and the same value of DMAV in free space hold for all inertial systems. This evidently maintains the relativity of inertial frames and validity of deformed Lorentz symmetry, in spite of the appearance of modified terms in the LID dispersion relations.

Deformed geometry at LIV. We relate LID to more general deformed smooth differential 4D-manifold $\mathcal{M}_4$. Whereas, a smooth deformation map $\Omega : M_4 \to \mathcal{M}_4$, is written in terms of the *world-deformation* tensor Ω, the flat Minkowski, M_4, and general, $\mathcal{M}_4$, smooth differential 4D-manifolds. The general manifold $\mathcal{M}_4$ in (30) has at each point a tangent space, $T_x\mathcal{M}_4$, spanned by the anholonomic orthonormal frame field. Building up the *world-dqeformation* tensor, we introduce the *first deformation matrices*, which, in general, give rise to the right cosets of the Lorentz group, i.e. they are the elements of the quotient group $GL(4,\mathcal{M})/SO(3,1)$. If we deform the co-tetrad, we have two choices to recast metric either writing the deformation of the metric in the space of tetrads or deforming the tetrad field.

We complement this investigation with testing of various LIDFs in the UHECR- and TeV-γ- threshold anomalies with in several scenarios of the Coleman and Glashow-type perturbative extension of SLC developed in the context of conventional quantum field theory, the LID extension of standard model, the LID in quantum gravity motivated space-time models and the LID in loop quantum gravity models.

doi: https://doi.org/10.52526/25792776-23.70.2-188

LIDF in CG-type LIV. In the case of CG-type perturbative extension of SLC ($\lambda_a = 1+\delta_a, \quad 0 < |\delta_a| \ll 1$), the CBR photopion production ($p + \gamma \to N + \pi' s$), on CBR photons of energy E' and temperature $T_{CBR} = 2.73$ K, is turned off if in terms of LIDF $\lambda_\pi - \lambda_p > 5 \times 10^{-24}(E'/2.73K)^2/c$. The description of the UHECR threshold anomaly requires together with conditions on $\lambda_\triangle - \lambda_\pi$ that $\lambda_\pi - \lambda_p > 10^{-24}/c$. A resolution of the TeV-γ threshold anomaly with in this scheme requires the additional condition $\lambda_e - \lambda_\gamma > 5 \times 10^{-16}/c$. This combines with the absence of vacuum Cherenkov radiation by electrons with energies up to 500 GeV in such a way that the allowed values for $\lambda_e - \lambda_\gamma$ lying in a relatively narrow range of $5 \times 10^{-16}/c < \lambda_e - \lambda_\gamma < 5 \times 10^{-13}/c$.

LIDF in LIV extension of standard model. The LIV extension of the minimal standard model, including CPT-even and CPT-odd terms, shows that a tiny deformation $\underline{\tilde{\theta}} \simeq \left[1 + \frac{\eta_\pm}{2}(n+1)\left(\frac{\epsilon}{\epsilon_P}\right)^n\right]^{1/2} \underline{\theta}$, where the corresponding parameter $\eta_\pm$ should be of order 1, yields variation in photon speed, which, when accumulated over cosmological light-travel times, may be revealed by observing LIV effects.

LIDF in quantum gravity models. The corrections going as E/E_P in quantum gravity motivate a deformation $\underline{\tilde{\theta}} = \left[E^2\eta\left(\frac{E}{E_P}\right)^{\alpha(\sim 1,2)}\right]^{1/2} \underline{\theta}$, which causes a significant upward shift above the GZK cutoff determined by the threshold equation.

LIDF in loop quantum gravity models. In the coarse-grained approximation of the loop quantum gravity models, the condition for significantly increasing the threshold for electron-positron pair production interactions ($p+\gamma \to p+e^+ + e^-$) is obtained $\lambda_e - \lambda_p > (m_p + m_e)m_p c^3/E_f^2$, which is $O(10^{-22}/c)$ for a fiducial energy $E_f = 100$ EeV. Thus, for a very small amount of deformation, $\underline{\tilde{\theta}} \simeq \left[1 + 2\alpha\epsilon^2 + \eta\epsilon^4 \pm 2\lambda\epsilon\right]^{1/2} \underline{\theta}$, both photopion and pair-production interactions of UHECR with the CBR can be turned off, and it could explain the UHECR spectrum which shows an excess of UHECRs at energies above GZK limit.

LIDF for the models preserving the relativity of inertial frames. We stress that the proposed LID-generalization of global MS_p-SUSY theory strongly supports the major goal of works Amelino-Camelia (2002), Magueijo & Smolin (2003), because this theory formulates the LID-generalized relativity postulates in a way that preserve the relativity of inertial frames.

References

Aab A., et al. 2016, Phys. Rev. Lett., 117, 192001

Abbasi R., et al. 2008, Phys. Rev. Lett., 100, 101101

Abraham J., et al. 2008, Phys. Rev. Lett., 101, 061101

Abram J., et al. 2007, Science, 318, 938

Abram J., et al. 2010, Phys. Lett. B, 685, 239

Abram A., et al. 2011, Astropart. Phys., 34, 738

Aharonian F., et al. 1999, Astron. Astrophys., 349, 11

Alfaro J., Palma G., 2002, Phys. Rev. D, 65, 103516

Alfaro J., Palma G., 2003, Phys. Rev. D, 67, 083003

Alfaro J., Morales-Técotl H., Urrutia L., 2000a, Phys. Rev. Lett., 84, 2318

Alfaro J., Morales-Técotl H., Urrutia L., 2000b, Phys. Rev. Lett., 84, 2318

Alfaro J., Morales-Técotl H., Urrutia L., 2002a, Phys. Rev. D, 65, 103509

Alfaro J., Morales-Técotl H., Urrutia L., 2002b, Phys. Rev. D, 66, 124006

Aloisio R., Blasi P., Ghia P., Grillo A., 2000, Phys. Rev. D, 62, 053010

Amelino-Camelia G., 1997, Phys. Lett. B, 392, 283

Amelino-Camelia G., 2000, Are we at the dawn of quantum-gravity phenomenology? in Towards Quantum Gravity. edited J. Kowalski-Glikman Springer-Verlag, Heidelberg

doi: https://doi.org/10.52526/25792776-23.70.2-188

Amelino-Camelia G., 2002, Int. J. Mod. Phys. D, 11, 35

Amelino-Camelia G., 2013, Living Reviews in Relativity, 16, 5

Amelino-Camelia G., Majid S., 2000, Int. J. Mod. Phys. A, 15, 4301

Amelino-Camelia G., Piran T., 2001, Phys. Rev. D, 64, 036005

Amelino-Camelia G., Mandanici G., Procaccini A., 2005, Int. J. Mod. Phys. A, 20, 6007

Amelino-Camelias G., Ellis J., Mavromatos N., Nanopoulos D., Sarkar S., 1998, Nature, 393, 763

Anchordoqui L., Goldberg H., Weiler T., 2017, Phys. Rev. D, 95, 063005

Apel W., et al. 2017, Astropart. Phys., 95, 25

Balachandran A., Pinzul A., Queiroz A., 2008, Phys. Lett. B, 668, 241

Batista R., et al. 2019, Frontiers in Astronomy and Space Sciences, 6, 1, Article 23

Berezinsky V., Grigorieva S., 1988, Astron. Astrophys., 199, 1

Bertolami O., Carvalho C., 2000, Phys. Rev. D, 61, 103002

Chaichian M., Kulish P., Nishijima K., Tureanu A., 2004, Phys. Lett. B, 604, 98

Chaichian M., Dolgov A., Novikov V., Tureanu A., 2011, Phys. Lett. B, 699, 177

Christian J., 2005, Phys. Rev. D, 71, 024012

Coleman S., Glashow S., 1999, Phys. Rev. D, 59, 116008

Colladay D., Kostelecky V., 1997, Phys. Rev. D, 55, 6760

Colladay D., Kostelecky V., 1998, Phys. Rev. D, 58, 116002

Diaz J., 2014, Adv. High Energy Phys., 2014, 962410

Douglas N., Nekrasov N., 2001, Rev. Mod. Phys., 73, 977

Farrar G., Allen J., 2013a, EPJ Web Conf., 52, 07005

Farrar G., Allen J., 2013b, EPJ Web Conf., 53, 07007

Fiore G., Wess J., 2007, Phys. Rev. D, 751, 105022

Gambini R., Pullin J., 1999, Phys. Rev. D, 59, 124021

Gonzalez-Mestres L., 1997, Proc. 25th Intl. Cosmic Ray Conf., 1997, 6, 113

Hall B. C., 2015, Lie Groups, Lie Algebras, and Representations: An Elementary Introduction. Graduate Texts in Mathematics, vol. 222 (2nd ed.), Springer, ISBN 978-0-387-40122-5

Hinchliffe I., Kersting N., Ma Y., 2004, Int. J. Mod. Phys. A, 19, 179

Jackiw R., Kostelecky V., 1999, Phys. Rev. Lett., 82, 3572

Jacobson T., Liberati S., Mattingly D., 2003, Nature, 424, 1019

Jacobson T., Liberati S., Mattingly D., Stecker F., 2004, Phys. Rev. Lett., 93, 021101

Kifune T., 1999, Astrophys. J. Lett., 8518, L21

Kluzniak W., , astro-ph/9905308

Kluzniak W., 1999, Astropart. Phys., 11, 117

Kostelecky V., Mewes M., 2008, Astrophys. J., 689, L1

Kowalski-Glikman J., Nowak S., 2003, Int. J. Mod. Phys. D, 12, 299

Lukierski J., Nowicki A., Ruegg H., 1992, Phys. Lett. B, 293, 344

Lukierski J., Ruegg H., Zakrzewski W., 1995, Ann. Phys., 243, 90

Madore J., Schraml S., Schupp P., Wess J., 2000, Eur. Phys. J. C, 16, 1611

Magueijo J., Smolin L., 2003, Phys.Rev. D, 67, 044017

Mattingly D., 2005, Living Rev. Relativity, 8, 5

Metzger M., et al. 1997, Nature, 87, 878

doi: https://doi.org/10.52526/25792776-23.70.2-188

Milton K. E., 2000, Quantum Legacy, Seminal Papers of Julian Schwinger. World Scientific Publishing Co. Pte. Ltd.

Milton K., 2015, Schwinger's Quantum Action Principle. Springer Briefs in Physics

Olinto A., 2001, Nuclear Physics B - Proc. Suppl., 97, 66

Parizot E., 2007, [arXiv:0709.2500 [astro-ph]]

Protheroe R. J., Meyer H., 2000, Phys. Lett. B, 493, 1

Sato H., , astro-ph/0005218

Schutz B., 1982, Geometrical Methods of Mathematical Physics. Cambridge University Press

Schwinger J., 1960, Proc. Natl. Acad. Sci. U.S.A., 46, 1401

Schwinger J., 2000, Quantum Kinematics and Dynamics. (1st ed. (1991)), 2nd ed. (2000) by Westview Press, USA

Scully S., Stecker F., 2002, Astropart. Phys., 16, 271

Scully S., Stecker F., 2009, Astropart. Phys., 31, 220

Smolin L., , e-print arxiv:0808.3765

Smolin L., 1999, Physics World, 12, 79

Stecker F., 1968, Phys. Rev. Lett., 21, 1016

Stecker F., 2003, Astropart. Phys., 20, 85

Stecker F., Scully S., 2005, Astropart. Phys., 23, 203

Takeda M., et al. 1998, Phys. Rev. Lett., 81, 1163

Ter-Kazarian G., 2011, Class. Quantum Grav., 28, 055003

Ter-Kazarian G., 2023, Communications of BAO, 70, ??

Ter-Kazarian G., 2024, To appear in Grav. Cosmol., 30, No 1

van Paradis J., et al. 1997, Nature, 386, 686

doi: https://doi.org/10.52526/25792776-23.70.2-188

Separation of Frequency Variables in the Problem of Diffuse Reflection from a Semi-Infinite Medium under Isotropic Scattering with a General Law of Radiation Redistribution by Frequencies

H. V. Pikichyan

Byurakan Astrophysical Observatory, 378433, Aragatsotn Region, Armenia

Abstract

In the presented work, with the help of a new approach previously proposed by the author, the problem of diffuse reflection of radiation from a plane-parallel semi-infinite medium under isotropic scattering in the case of the general law of radiation redistribution by frequencies is solved. Resulting solution implements the possibility of separating a pair of independent variables (namely, the frequency and direction of the quantum) of entering the medium quanta from the same pair of exiting quanta. The advantage of this approach in relation to the known methods is that the separation of the explanatory variables is achieved without the need to solve the additional problem of separation or any special representation of the characteristics of a single act of scattering. Here, in an expanded form is sought namely the solution of the modified initial problem, instead of a preliminary decomposition of the characteristics of a single act of scattering. As a result, the unknown function of the four explanatory variables is expressed explicitly through a system of auxiliary functions that depend on only two variables. For this purpose, a problem for eigenvalues and eigenfunctions is formulated for a specially selected and previously unknown kernel. Bilateral relationships between the solutions of the new and traditionally used methods are obtained, which makes it possible to directly compare their accuracy and efficiency. The general scheme of the organization of calculations is also discussed.

Keywords: *radiative transfer, diffuse reflection problem, separation of variables, nonlinear Ambartsumian's functional equation, eigenfunctions and eigenvalues problem*

1. Introduction and purpose of the work

The problem of diffuse reflection of radiation (or particles) from a semi-infinite plane-parallel medium is one of the classical problems of theoretical astrophysics. It is widely used to interpret the brightness and spectra of space objects and cosmic media where there is multiple interactions between radiation and matter. For example, planetary and stellar atmospheres, the interstellar medium, various kinds of space gas and dust complexes, as well as the optics of the Earth's atmosphere and ocean, the engineering problems of nuclear reactors, as well as radiation protection from ionizing radiation, etc. The solution of the diffuse reflection problem depends on many independent variables that describe the parameters of diffusing photons (or particles) as they enter the medium and then when they exit it after multiple scatterings. Therefore, when solving such problems, they traditionally try to separate independent variables from each other, as a result, reducing the problem to the construction of auxiliary functions of a smaller number of independent variables. The introduction of the so-called "Ambartsumian's principle of invariance" (Ambartsumian, 1942, 1943a,b, 1944a,b,c)made it possible to obtain a functional equation for the direct finding of the diffuse reflection function. In contrast to the traditional way of solving the integro differential or integral transfer equations, there was no need to consider the intensity of the radiation coming out of the medium together with the field inside the medium, i.e., it was possible to limit oneself to the analysis of the processes of absorption and re-emission of quanta only at the boundary of the medium. In solving the problem of diffuse reflection in the case of monochromatic and isotropic scattering, the exact separation of angular variables in this way was achieved in the work Ambartsumian (1942) and see also Sobolev (1963), i.e., the desired diffuse reflection function $\rho(\mu, \mu')$, which depends on two angular variables, was clearly expressed through

doi: https://doi.org/10.52526/25792776-23.70.2-204

an auxiliary function, $\varphi(\mu)$ of only one angular variable:

$$\rho(\mu,\mu') = \frac{\lambda}{2\mu'} \frac{\varphi(\mu)\,\varphi(\mu')}{\frac{1}{\mu}+\frac{1}{\mu'}}, \qquad \varphi(\mu) = 1 + \int_0^1 \rho(\mu,\mu')\,d\mu', \tag{1}$$

$$\varphi(\mu) = 1 + \frac{\lambda}{2}\mu\varphi(\mu)\int_0^1 \frac{\varphi(\mu')}{\mu+\mu'}d\mu'. \tag{2}$$

Here: $\rho(\mu,\mu')$ is the probability density that the quantum falling on the boundary of the medium from the direction μ', inside the solid angle $2\pi d\mu'$ after arbitrary wanderings in the medium will leave it in the direction of μ, inside the solid angle $2\pi d\mu$ (μ' and μ are cosines of the angles of incidence and diffuse reflection at the boundary of the medium in relation to the normal to its boundary, respectively), λ is the probability of the quantum surviving in the elementary act of scattering.

A generalization of the problem in the case of anisotropic scattering was carried out in the paper (Ambartsumian, 1943a, 1944a). In order to achieve separation of angular variables in the problem of diffuse reflection in the case of anisotropic scattering, an additional problem of separation of angular variables in a single act of scattering was posed and solved. This was done by means of a special representation of the scattering indicatrix in the form of a series over Legendre polynomials (Ambartsumian, 1941, § 8-9). In the case of incoherent scattering, it was necessary to separate the frequency variables. Such a property is naturally manifested in the case of so-called "complete redistribution of radiation by frequencies" or "completely incoherent scattering" takes place during an elementary act of scattering (see for example: Ivanov, 1973, Sobolev, 1963). In the case of the general law of redistribution of radiation by frequencies or the so-called "partially incoherent scattering", the separation of frequency variables in the diffuse reflection problem is achieved by representing the redistribution function in a unit act of scattering as a bilinear series over a pre-selected system of eigenfunctions (Engibaryan, 1971, Engibaryan & Nikogosyan, 1972). Further, it was noted that in the case of the general law of redistribution of radiation by frequencies, in particular case of isotropic scattering, the property of separation of angular variables naturally already follows from the isotropy of a single act of scattering (Pikichian, 1978, 1980). At the same time, since the frequency variables are not separated in the unit act of scattering, they are not separated also in multiple scatterings, i.e. in the diffuse reflection function. Namely, the diffuse reflection function $\rho(x,\mu;x',\mu')$ which depends on four independent variables is expressed by the auxiliary function $\varphi(x';x,\mu)$ depending on three independent variables (two frequency variables (x',x) and one angular variable μ). Here, the value of x' denotes the dimensionless frequency of the quantum incident on the medium, and x is the corresponding frequency of the quantum diffusely reflected from the medium. The values μ' and μ represent the cosines of the corresponding angles of incidence and diffuse reflection in relation to the boundary normal of the medium. Thus, a direct generalization of the classical solution of Ambartsumian (1)-(2) in the case of the general law $r(x'',x''')$ of redistribution of radiation by frequencies was obtained in Pikichian (1978, 1980) in the form of

$$\rho(x,\mu;x',\mu') = \frac{\lambda}{2\mu'} \frac{\int_{-\infty}^{+\infty}\int_{-\infty}^{+\infty}\varphi(x'';x,\mu)\,r(x'',x''')\,\varphi(x''';x',\mu')\,dx''dx'''}{\frac{\alpha(x)}{\mu}+\frac{\alpha(x')}{\mu'}}, \tag{3}$$

where a "non-coherent" analogue of Ambartsumian's auxiliary function is introduced by means of

$$\varphi(x',x;\mu) = \delta(x'-x) + \int_0^1 \rho(x,\mu;x',\mu')\,d\mu'. \tag{4}$$

From (3) and (4) followed the corresponding Ambartsumian's functional equation

$$\varphi(x',x;\mu) = \delta(x'-x) + \frac{\lambda}{2\mu'}\int_{-\infty}^{+\infty}\varphi(x'';x,\mu)\,dx''\int_{-\infty}^{+\infty} r(x'',x''')\,dx'''\int_0^1 \frac{\varphi(x''';x',\mu')}{\frac{\alpha(x)}{\mu}+\frac{\alpha(x')}{\mu'}}d\mu'. \tag{5}$$

Here value $\alpha(x)$ is the absorption profile. The ratios (3)-(5) in particular naturally turn to the above-mentioned well-known solution of the complete redistribution of radiation by frequencies, or to the results obtained by using a bilinear representation of the general law of radiation redistribution by frequency. To do this, it is enough to directly use the substitutions $r(x,x') = \alpha(x)\,\delta(x-x')$ or $r(x,x') = \sum_j A_j\alpha_j(x)\alpha_j(x')$, respectively.

Thus, to achieve the separation of variables in both anisotropic and incoherent scattering problems, traditionally used the representation of the characteristics of the elementary act of scattering through a

doi: https://doi.org/10.52526/25792776-23.70.2-204

bilinear series of some specially selected eigenfunctions system. In Pikichyan (2023) for the solving the same problems a new approach was proposed, where there is no need of decomposition or any special representation of the characteristics of a single act of scattering. In this paper, the advantages of the proposed approach in relation to the traditional method of decomposition of the characteristics of a single act of scattering were discussed using two examples: a one-dimensional problem of incoherent scattering and a monochromatic problem of anisotropic scattering. Analytically, the bilateral relationship between the results of both approaches was also shown. In the proposed new approach, in contrast to the well-known one, instead of the characteristics of a single act of scattering, in the form of decomposition according to a certain system of eigenfunctions, the slightly modified resulting characteristics of the radiation field (i. e., field of multiple interaction of radiation with matter) are sought. The physical basis for the expediency of such an approach is the obvious fact that during the process of multiple scattering of radiation in the medium, in each subsequent act of scattering, due to the presence of mathematical procedures of integration, the radiation field in the medium becomes more and more smooth. As a convergent series, with the same required accuracy of calculation, its description will obviously be simpler (i.e., it will include a smaller number of series members) than through a preliminary decomposition of the initial "unsmoothed" characteristics of a single act of scattering.

In problem (3)-(5), as noted above, the separation of angular variables has already been achieved naturally due to the isotropy of scattering. At the same time, it can be seen that the frequency variables in the case of the general law of radiation redistribution are not separated, since the single act of scattering itself does not possess this property.

The purpose of this work is to further simplify the solution of the problem of diffuse reflection (3)-(5) by achieving the separation of frequency variables without decomposition or any special representation of the general law - $r(x, x')$ of radiation redistribution by frequencies. This is achieved by applying the approach proposed in Pikichyan (2023).

2. Mathematical formulation of the problem

Let's introduce a new value by means of the

$$K\left(x,\mu;x',\mu'\right) \equiv \mu'\left[\frac{\alpha(x)}{\mu}+\frac{\alpha(x')}{\mu'}\right]\rho\left(x,\mu;x',\mu'\right). \tag{6}$$

It is well known that the symmetry of the elementary act of scattering also implies the symmetry of the resulting field of multiple scattering, i.e., the function of diffuse reflection (see, for example, Pikichian, 1980):

$$r\left(x'',x'''\right)=r\left(x''',x''\right)\Rightarrow \rho\left(x,\mu;x',\mu'\right)\mu'=\rho\left(x',\mu';x,\mu\right)\mu, \tag{7}$$

but from the ratios (7) and (6), in turn, follows the symmetry of the introduced function

$$K\left(x,\mu;x',\mu'\right)=K\left(x',\mu';x,\mu\right). \tag{8}$$

Let the kernel $K(x,\mu;x',\mu')$ will be the function you are looking for. Its knowledge unambiguously determines the solution of the problem of diffuse reflection $\rho(x,\mu;x',\mu')$.

For the integral operator $\mathrm{A}\equiv\int_{-\infty}^{+\infty}\int_0^1 K(x,\mu;x',\mu')\ldots d\mu' dx'$ let's formulate the eigenvalues $\Lambda\equiv(\nu_1,\ldots,\nu_N)$ and the eigenvector $\overrightarrow{\beta}\equiv(\beta_1(x,\mu),\ldots,\beta_N(x,\mu))$ problem in the form $\mathrm{A}\overrightarrow{\beta}=\Lambda\overrightarrow{\beta}$, with $N{=}\infty$:

$$\nu_j\beta_j(x,\mu)=\int_{-\infty}^{+\infty}\int_0^1 K\left(x,\mu;x',\mu'\right)\beta_j\left(x',\mu'\right)d\mu' dx', \tag{9}$$

see, e.g., Vasilyeva & Tikhonov (1989), there is also the condition of orthonormality

$$\int_{-\infty}^{+\infty}\int_0^1 \beta_i(x,\mu)\,\beta_j(x,\mu)\,d\mu dx=\delta_{ij}. \tag{10}$$

Continuous, positive, and symmetric kernel $K(x,\mu;x',\mu')$ let's roughly replace with a bilinear series the partial sum of eigenfunctions $\beta_j(x,\mu)$ with a finite number of terms - N :

$$K\left(x,\mu;x',\mu'\right)\sim K_N\left(x,\mu;x',\mu'\right)=\sum_{j=1}^{N}\nu_j\beta_j(x,\mu)\,\beta_j\left(x',\mu'\right). \tag{11}$$

doi: https://doi.org/10.52526/25792776-23.70.2-204

In (11), obviously, there is already a joint separation of frequency and angular variables in relation to the parameters of the quantum entering and exiting the medium, but neither the kernel itself - $K\left(x,\mu;x',\mu'\right)$, neither its proper functions - $\beta_j\left(x,\mu\right)$ nor its eigenvalues - ν_j are yet known. The challenge is to find them.

3. Analytical solution of the problem

First, we get an analogue of the Ambartsumian's functional equation for the desired kernel $K\left(x,\mu;x',\mu'\right)$. From the ratios (3)-(4) and (6) it follows:

$$\frac{2}{\lambda}K\left(x,\mu;x',\mu'\right)=\int_{-\infty}^{+\infty}\int_{-\infty}^{+\infty}\varphi\left(x'';x,\mu\right)r\left(x'',x'''\right)\varphi\left(x''';x',\mu'\right)dx''dx''', \tag{12}$$

$$\varphi\left(x';x,\mu\right)=\delta\left(x'-x\right)+\int_0^1\frac{K\left(x,\mu;x',\mu'\right)}{\frac{\alpha(x)}{\mu}+\frac{\alpha(x')}{\mu'}}\frac{d\mu'}{\mu'}, \tag{13}$$

and by setting (12) to (13) we arrive at the equation

$$\frac{2}{\lambda}K\left(x,\mu;x',\mu'\right)=\int_{-\infty}^{+\infty}\int_{-\infty}^{+\infty}\left[\delta\left(x''-x\right)+\int_0^1\frac{K\left(x,\mu;x'',\mu''\right)}{\frac{\alpha(x)}{\mu}+\frac{\alpha(x'')}{\mu''}}\frac{d\mu''}{\mu''}\right]r\left(x'',x'''\right)$$

$$\left[\delta\left(x'''-x'\right)+\int_0^1\frac{K\left(x',\mu';x''',\mu'''\right)}{\frac{\alpha(x')}{\mu'}+\frac{\alpha(x''')}{\mu'''}}\frac{d\mu'''}{\mu'''}\right]dx''dx''', \tag{14}$$

which, when the square brackets are opened, will take the form

$$\frac{2}{\lambda}K\left(x,\mu;x',\mu'\right)=r\left(x,x'\right)+\int_{-\infty}^{+\infty}r\left(x,x''\right)dx''\int_0^1\frac{K\left(x',\mu';x'',\mu''\right)}{\frac{\alpha(x')}{\mu'}+\frac{\alpha(x'')}{\mu''}}\frac{d\mu''}{\mu''}$$

$$+\int_{-\infty}^{+\infty}r\left(x'',x'\right)dx''\int_0^1\frac{K\left(x,\mu;x'',\mu''\right)}{\frac{\alpha(x)}{\mu}+\frac{\alpha(x'')}{\mu''}}\frac{d\mu''}{\mu''}+$$

$$+\int_{-\infty}^{+\infty}\int_{-\infty}^{+\infty}\left[\int_0^1\frac{K\left(x,\mu;x'',\mu''\right)}{\frac{\alpha(x)}{\mu}+\frac{\alpha(x'')}{\mu''}}\frac{d\mu''}{\mu''}r\left(x'',x'''\right)\int_0^1\frac{K\left(x',\mu';x''',\mu'''\right)}{\frac{\alpha(x')}{\mu'}+\frac{\alpha(x''')}{\mu'''}}\frac{d\mu'''}{\mu'''}\right]dx''dx'''. \tag{15}$$

Thus, the eigenfunctions problem (9) needs to be solved for a previously unknown kernel that satisfies the nonlinear "Ambartsumian's functional equation" (15).

By introducing an auxiliary function,

$$w(x'';x',\mu')\equiv\int_0^1\frac{K\left(x',\mu';x'',\mu''\right)}{\frac{\alpha(x')}{\mu'}+\frac{\alpha(x'')}{\mu''}}\frac{d\mu''}{\mu''}, \tag{16}$$

equation (15) is rewritten as

$$\frac{2}{\lambda}K\left(x,\mu;x',\mu'\right)=r\left(x,x'\right)+\int_{-\infty}^{+\infty}r\left(x,x''\right)w(x'';x',\mu')dx''$$

$$+\int_{-\infty}^{+\infty}r\left(x',x''\right)w(x'';x,\mu)dx''+\int_{-\infty}^{+\infty}\int_{-\infty}^{+\infty}w(x'';x,\mu)r\left(x'',x'''\right)w(x''';x',\mu')dx''dx'''. \tag{17}$$

From (17) and (9) it is not difficult to derive a system of equations for finding eigenfunctions $\beta_j\left(x,\mu\right)$

$$\frac{2}{\lambda}\nu_j\beta_j\left(x,\mu\right)=Z_j\left(x\right)+\int_{-\infty}^{+\infty}r\left(x,x''\right)\overline{w}_j\left(x''\right)dx''$$

$$+\int_{-\infty}^{+\infty}Z_j\left(x''\right)w(x'';x,\mu)dx''+\int_{-\infty}^{+\infty}\int_{-\infty}^{+\infty}w(x'';x,\mu)r\left(x'',x'''\right)\overline{w}_j\left(x'''\right)dx''dx''', \tag{18}$$

doi: https://doi.org/10.52526/25792776-23.70.2-204

where are:

$$Z_j(x) \equiv \int_{-\infty}^{+\infty} r(x,x')\,\overline{\beta}_j(x')\,dx', \quad \overline{\beta}_j(x') \equiv \int_0^1 \beta_j(x',\mu')\,d\mu', \tag{19}$$

$$\overline{w}_j(x'') \equiv \int_{-\infty}^{+\infty}\int_0^1 w(x'';x',\mu')\beta_j(x',\mu')\,d\mu' dx'. \tag{20}$$

Taking into account in the ratio (16) of the desired bilinear form (11) of the kernel $K(x,\mu;x',\mu')$, gives the value $w(x'';x',\mu')$:

$$w(x'';x',\mu') = \sum_{k=1}^{n} \nu_k w_k(x'',x',\mu'), \;\; w_k(x'',x',\mu') = \beta_k(x',\mu') \int_0^1 \frac{\beta_k(x'',\mu'')}{\frac{\alpha(x')}{\mu'} + \frac{\alpha(x'')}{\mu''}} \frac{d\mu''}{\mu''}. \tag{21}$$

By accounting (20)-(21), the value $\overline{w}_j(x'')$ is rewritten as:

$$\overline{w}_j(x'') = \sum_{k=1}^{n} \nu_k w_{kj}(x''), \quad w_{kj}(x'') \equiv \int_{-\infty}^{+\infty}\int_0^1 w_k(x'',x',\mu')\,\beta_j(x',\mu')\,d\mu' dx'. \tag{22}$$

Substituting (21) and (22) in (18) we finally get the expression

$$\frac{2}{\lambda}\nu_j\beta_j(x,\mu) = Z_j(x) + \sum_{k=1}^{n}\nu_k D_{kj}(x,\mu) + \sum_{k=1}^{n}\sum_{l=1}^{n}\nu_k\nu_l V_{klj}(x,\mu), \tag{23}$$

where the following symbols are entered:

$$D_{kj}(x,\mu) \equiv \int_{-\infty}^{+\infty} r(x,x'')\,w_{kj}(x'')\,dx'' + \int_{-\infty}^{+\infty}\int_{-\infty}^{+\infty} w_k(x'',x,\mu)\,r(x'',x')\,\overline{\beta}_j(x')\,dx'dx'', \tag{24}$$

$$V_{klj}(x,\mu) \equiv \int_{-\infty}^{+\infty}\int_{-\infty}^{+\infty} w_k(x'',x,\mu)\,r(x'',x''')\,w_{lj}(x''')\,dx''dx'''. \tag{25}$$

The relation (23) is a system of nonlinear integral equations for determining eigenfunctions - $\beta_j(x',\mu')$, where the eigenvalues of ν_j are not yet known. To determine the latter, it is enough to use the operator $\int_{-\infty}^{+\infty}\int_0^1 \ldots \beta_i(x,\mu)\,d\mu dx$ act on (23), taking into account the orthonormalization condition (10), a system of nonlinear algebraic equations is obtained

$$\frac{2}{\lambda}\nu_i = b_i + \sum_{k=1}^{n}\nu_k c_{ki} + \sum_{k=1}^{n}\sum_{l=1}^{n}\nu_k\nu_l f_{kli}, \tag{26}$$

where it is indicated:

$$b_i \equiv \int_{-\infty}^{+\infty}\int_0^1 Z_i(x)\,\beta_i(x,\mu)\,d\mu dx, \quad c_{ki} \equiv \int_{-\infty}^{+\infty}\int_0^1 D_{ki}(x,\mu)\,\beta_i(x,\mu)\,d\mu dx, \tag{27}$$

$$f_{kli} \equiv \int_{-\infty}^{+\infty}\int_0^1 V_{kli}(x,\mu)\,\beta_i(x,\mu)\,d\mu dx. \tag{28}$$

Accounting in (27) -(28) ratios (19), (24) -(25), (22) finally leads them to forms

$$b_i = \int_{-\infty}^{+\infty}\int_{-\infty}^{+\infty} \overline{\beta}_i(x)\,r(x,x')\,\overline{\beta}_i(x')\,dx'dx, \tag{29}$$

$$c_{ki} = 2\int_{-\infty}^{+\infty}\int_{-\infty}^{+\infty} w_{ki}(x'')\,r(x'',x')\,\overline{\beta}_i(x')\,dx'dx'', \tag{30}$$

$$f_{kli} = \int_{-\infty}^{+\infty}\int_{-\infty}^{+\infty} w_{ki}(x'')\,r(x'',x''')\,w_{li}(x''')\,dx''dx'''. \tag{31}$$

The system of functional nonlinear integral equations (23) taking into account (24)-(25) and (19), (21)-(22) together with the system of algebraic equations (26) taking into account (29)-(31) and (19), (22) are a closed system of equations for self-consistent finding of eigenvalues ν_k and eigenfunctions $\beta_k(x',\mu')$. After determining ν_k and $\beta_k(x',\mu')$, the solution of the initial problem, according to (6) and (11), is constructed by an explicit expression

$$\rho(x,\mu;x',\mu') = \frac{1}{\mu'}\frac{\sum_{i=1}^{N}\nu_i\beta_i(x,\mu)\,\beta_i(x',\mu')}{\frac{\alpha(x)}{\mu} + \frac{\alpha(x')}{\mu'}}. \tag{32}$$

doi: https://doi.org/10.52526/25792776-23.70.2-204

4. To the joint calculation of systems

For the combined calculation of systems (23) and (26), it seems easiest to first use a suitably chosen system of some orthonormalized functions as a zero approximation of $\beta_i^{(0)}(x,\mu)$, and then the values $b_i^{(0)}$, $c_{ki}^{(0)}$, $f_{kli}^{(0)}$ are calculated using (29)-(31). Then, taking $\nu_i^{(0)} \equiv b_i^{(0)}$ as the zero approximation of eigenvalues, the first approximation of eigenvalues $\nu_i^{(1)}$ is computed using the right-hand side (26). Then, from these zero approximations $\beta_i^{(0)}(x,\mu)$ and $\nu_i^{(1)}$, compute the first approximation for eigenfunctions $\beta_i^{(1)}(x,\mu)$ using the right-hand side (23). Then, again, according to (26), calculate the next (in this case, the second) approximation of eigenvalues $\nu_i^{(2)}$, and with their help, through the right side (23), obtain the values of $\beta_i^{(2)}(x,\mu)$ of the second approximation of eigenfunctions, and so on. Sequential approximations

$$\begin{bmatrix} \beta_i^{(m)}(x,\mu) \\ \nu_i^{(m)} \end{bmatrix} \to \begin{bmatrix} \nu_i^{(m+1)} \\ \beta_i^{(m)}(x,\mu) \end{bmatrix} \to \begin{bmatrix} \beta_i^{(m+1)}(x,\mu) \\ \nu_i^{(m+1)} \end{bmatrix} \to \cdots \to \begin{bmatrix} \nu_i^{(M)} \\ \beta_i^{(M-1)}(x,\mu) \end{bmatrix} \to \beta_i^{(M)}(x,\mu)$$

are constructed as specified for $m = 0,\ 1, 2, \dots M$. At the same time, at each next step of the calculation, the accuracy of the convergence of iterations according to some suitable criterion is evaluated until a satisfactory calculation accuracy is achieved at a certain number M.

5. Relationship between the results of the method proposed here and the traditional one

In order to compare the accuracy and efficiency of the methods proposed here and the traditionally known methods, it is very expedient to derive analytic expressions of bilateral relationship of the solutions built with their help. Let us write down the traditional solution of the problem of diffuse reflection by substituting in (3) the bilinear decomposition of the frequencies redistribution function of radiation for an elementary act of scattering $r(x,x') = \sum_{i=1}^N A_i\alpha_i(x)\alpha_i(x')$, then we get:

$$\rho(x,\mu;x',\mu') = \frac{\lambda}{2\mu'} \frac{\sum_{i=1}^N A_i\varphi_i(x,\mu)\varphi_i(x',\mu')}{\frac{\alpha(x)}{\mu}+\frac{\alpha(x')}{\mu'}}, \quad \varphi_i(x,\mu) \equiv \int_{-\infty}^{+\infty} \alpha_i(x')\varphi(x';x,\mu)\,dx', \tag{33}$$

$$\varphi_i(x,\mu) = \alpha_i(x) + \frac{\lambda}{2}\sum_{i=1}^N A_i\varphi_i(x,\mu)\int_{-\infty}^{+\infty}\alpha_i(x')\,dx'\int_0^1 \frac{\varphi_i\left(x',\mu'\right)}{\frac{\alpha(x)}{\mu}+\frac{\alpha(x')}{\mu'}}\frac{d\mu'}{\mu'}. \tag{34}$$

5.1. Suppose $\varphi_i(x,\mu)$ are known, the definition of $\beta_j(x,\mu)$ and ν_j is required

$$\sum_{j=1}^N \nu_j\beta_j(x,\mu)\beta_j\left(x',\mu'\right) = \frac{\lambda}{2}\sum_{i=1}^N A_i\varphi_i(x,\mu)\varphi_i\left(x',\mu'\right). \tag{35}$$

Use the operator $\int_{-\infty}^{+\infty}\int_0^1 \dots \beta_j(x',\mu')\,d\mu' dx'$ to (35), taking into account (10) we get

$$\nu_j\beta_j(x,\mu) = \frac{\lambda}{2}\sum_{i=1}^N A_i\varphi_i(x,\mu)\,q_{ij}, \quad q_{ij} \equiv \int_{-\infty}^{+\infty}\int_0^1 \varphi_i\left(x',\mu'\right)\beta_j\left(x',\mu'\right)d\mu' dx'. \tag{36}$$

By influencing the first relation of (36) with the same operator, we arrive at the expression

$$\nu_j = \frac{\lambda}{2}\sum_{i=1}^N A_i q_{ij}^2. \tag{37}$$

Expressions (36) and (37) define eigenfunctions $\beta_j(x,\mu)$ and eigenvalues ν_j by means of the values of pre-known auxiliary functions $\varphi_i(x,\mu)$, if q_{ij} values are available.

doi: https://doi.org/10.52526/25792776-23.70.2-204

To find the latter, it is enough to use the operator $\int_{-\infty}^{+\infty}\int_0^1 \ldots \varphi_k(x',\mu')\,d\mu' dx'$ to affect the first of the formulas (36), then we get:

$$\nu_j q_{kj} = \frac{\lambda}{2}\sum_{i=1}^{N} A_i a_{ik} q_{ij}, \quad a_{ik} \equiv \int_{-\infty}^{+\infty}\int_0^1 \varphi_i(x,\mu)\,\varphi_k(x,\mu)\,d\mu dx, \tag{38}$$

and with the help of (37) and the first of the ratios (38) we finally arrive at the system

$$q_{kj} = \frac{\sum_{i=1}^{N} A_i a_{ik} q_{ij}}{\sum_{i=1}^{N} A_i q_{ij}^2}. \tag{39}$$

The ratios (36) and (37) together express $\beta_j(x,\mu)$ by means of $\varphi_i(x,\mu)$

$$\beta_j(x,\mu) = \frac{\sum_{i=1}^{N} A_i \varphi_i(x,\mu)\, q_{ij}}{\sum_{i=1}^{N} A_i q_{ij}^2}, \tag{40}$$

where the values of q_{ij} are of (39). The corresponding eigenvalues of ν_j are expressed in terms of previously known A_i and q_{ij} in terms of the relation (37). Now let's get the feedback ratio.

5.2. Suppose $\beta_j(x,\mu)$, are known, and $\varphi_i(x,\mu)$ is to be found through them

From the ratios (4) and the second of (33) it follows

$$\varphi_i(x,\mu) = \int_{-\infty}^{+\infty} \alpha_i(x')\left[\delta(x'-x) + \int_0^1 \rho(x,\mu;x',\mu')\,d\mu'\right]dx', \tag{41}$$

and by opening in (41) square brackets, we get the expression

$$\varphi_i(x,\mu) = \alpha_i(x) + \int_{-\infty}^{+\infty} \alpha_i(x')\,dx' \int_0^1 \rho(x,\mu;x',\mu')\,d\mu', \tag{42}$$

then, substituting (32) into (42), we arrive at the relation

$$\varphi_i(x,\mu) = \alpha_i(x) + \sum_{j=1}^{N} \nu_j \beta_j(x,\mu)\, Q_{ij}(x,\mu), \tag{43}$$

where it is indicated

$$Q_{ij}(x,\mu) \equiv \int_{-\infty}^{+\infty} \alpha_i(x')\,dx' \int_0^1 \frac{\beta_j(x',\mu')}{\frac{\alpha(x)}{\mu} + \frac{\alpha(x')}{\mu'}} \frac{d\mu'}{\mu'}. \tag{44}$$

Thus, the relations (37), (39), (40) make it possible to proceed explicitly to the solution of the same problem (i. e, the problem of determining the values of ν_j and $\beta_j(x,\mu)$), which would be obtained by finding a solution by directly decomposing the characteristics of the initial problem of multiple scattering, through a known solution (i. e, through the known auxiliary functions of $\varphi_i(x,\mu)$). And the relations (43)-(44), on the contrary, make it possible to express the solution of the problem of diffuse reflection (i. e, the problem of determining the auxiliary functions of $\varphi_i(x,\mu)$) with the decomposed characteristics of a single act of scattering (here the values of A_i and $\alpha_i(x)$ are considered known) through the solution (i. e, through the values ν_j and $\beta_j(x,\mu)$) obtained by direct decomposition of the final characteristics of multiple scattering. With the help of these explicit expressions of bilateral relationship, it is not difficult to make a comparative analysis of the accuracy and efficiency of the above two methods of solving the diffuse reflection problem. For example, suppose the auxiliary functions $\widetilde{\varphi}_j(x,\mu)$ are obtained by some predetermined precision for a given number of terms of the expansion $\widetilde{N}$, then $\widetilde{\nu}_j$ and $\widetilde{\beta}_j(x,\mu)$ are computed according to (37), (39)-(40). The same values $\widetilde{\nu}_j$ and $\widetilde{\beta}_j(x,\mu)$ are then calculated by means of the system (23), (26) and, by comparing these results with each other, it is determined at what number $N < \widetilde{N}$ the second method provides the same accuracy. When $N = \widetilde{N}$, it is also possible to estimate (using some specially selected metric) how far the values of the quantities ($\widetilde{\nu}_j$, $\widetilde{\beta}_j(x,\mu)$) and (ν_j $\beta_j(x,\mu)$) are from each other.

doi: https://doi.org/10.52526/25792776-23.70.2-204

6. Conclusion

In the presented work, using the new approach previously proposed by the author (Pikichyan, 2023), the problem of diffuse reflection of radiation from a plane-parallel semi-infinite medium under isotropic scattering in the case of the general law of radiation redistribution by frequencies is solved. In the resulting solution, it is possible to separate the pair (namely, the dimensionless frequency and direction of the quantum) of independent variables when entering the medium from the same pair when exiting it. The advantage of this approach over the known ones is that this separation of the independent variables is achieved without the need to first solve an additional problem of decomposition or any special representation of the characteristics of a single act of scattering. Here, the solution of the modified initial problem itself is sought directly in a decomposed form, instead of a preliminary decomposition of the characteristics of a single act of scattering. As a result, the function to be found, which depends on four independent variables explicitly, is expressed in terms of a system of auxiliary functions that depend on only two variables. For this purpose, a problem for eigenvalues and eigenfunctions is formulated for a specially selected and previously unknown kernel. There is also a bilateral relationship between the solutions of the traditionally known and the new methods, which makes it possible to directly compare their accuracy and efficiency. The presented paper also discusses the general scheme of the organization of calculations.

References

Ambartsumian V. A., 1941, Uchyoniye Zapiski LGU (in Russian), No. 82, Seriya Math. Nauk (Astronomiya), Vipusk 11, Trudi Astron. Observ. LGU,, 12, 64

Ambartsumian V. A., 1942, Astron. Zhour. (in Russian), (Engl. transl., V. A. Ambartsumian: Selected papers, Part I., Ed. Meylan, pp.159-180, CSP, 2010), 19, 30

Ambartsumian V. A., 1943a, Zhour. Theor. Exp. Phys. (in Russian), (Engl. transl., V. A. Ambartsumian: Selected papers, Part I., Ed. Meylan, pp.187-208, CSP, 2010), 13, 323

Ambartsumian V. A., 1943b, Dokl. AN SSSR (in Russian), (Engl. transl., V. A. Ambartsumian: Selected papers, Part I., Ed. Meylan, pp.181-185, CSP, 2010), 38, 257

Ambartsumian V. A., 1944a, J. Phys., 8, 65

Ambartsumian V. A., 1944b, Dokl. AN SSSR (in Russian), (Engl. transl., V. A. Ambartsumian: Selected papers, Part I., Ed. Meylan, pp.203-208, CSP, 2010.), 43, 106

Ambartsumian V. A., 1944c, Izvestiya AN Arm. SSR, Natural Sci. (in Russian), No.1-2, 31, (Engl.transl., V. A. Ambartsumian: Selected papers, Part I., Ed. Meylan, pp.209-214, CSP, 2010), 1-2, 31

Engibaryan N. B., 1971, Astrophysics, 7, 340

Engibaryan N. B., Nikogosyan A. G., 1972, Astrophysics, 8, 128

Ivanov V. V., 1973, Transfer of radiation in spectral lines

Pikichian O. V., 1978, Akademiya Nauk Armianskoy SSR Doklady, 67, 151

Pikichian O. V., 1980, Soobshcheniya Byurakanskoy Observatorii (in Russian), 52, 148

Pikichyan H. V., 2023, Communications of the Byurakan Astrophysical Observatory, 70, 143

Sobolev V. V., 1963, A treatise on radiative transfer, D. Van Nostrand

Vasilyeva A. B., Tikhonov N. A., 1989, Integralniye Uravneniya, Izd, Moskovskogo Universiteta (in Russian)

doi: https://doi.org/10.52526/25792776-23.70.2-204

Communications of BAO, Vol. 70, Issue 2, 2023, pp. 212-234

Inertia II: The local $\widetilde{MS}_p$-SUSY induced inertia effects

G.Ter-Kazarian*

Byurakan Astrophysical Observatory, Byurakan, Aragatsotn Province, Armenia

Abstract

In the framework of *local* $\widetilde{MS}_p$-SUSY theory, which is extension of *global*, so called, *master space* (MS_p)-SUSY theory (Ter-Kazarian, 2023, 2024), we address the *accelerated motion and inertia effects*. The superspace is a direct sum of curved background double spaces $\widetilde{M}_4 \oplus \widetilde{MS}_p$, with an inclusion of additional fermionic coordinates $(\Theta, \bar{\Theta})$ induced by the spinors $(\underline{\theta}, \bar{\underline{\theta}})$, which refer to $\widetilde{MS}_p$. We take the Lorentz group as our structure group in order to recover rigid superspace as a limiting solution to our dynamical theory. The local $\widetilde{MS}_p$-SUSY is conceived as a quantum field theory whose action includes the *fictitious gravitation field term*, where the graviton coexists with a fermionic field of, so-called, gravitino (sparticle) described by the Rarita-Scwinger kinetic term. A significant difference between standard theories of supergravity and the local $\widetilde{MS}_p$-SUSY theory is that a coupling of supergravity with matter superfields no longer holds. We argue that a deformation/(distortion of local internal properties) of MS_p, is the origin of the *absolute acceleration* ($\vec{a}_{abs} \neq 0$) and inertia effects (*fictitious graviton*). These gravitational fields had no sources and were generated by coordinate transformations. A curvature of $\widetilde{MS}_p$ arises entirely due to the inertial properties of the Lorentz-rotated frame of interest. This refers to the particle of interest itself, without relation to other matter fields, so that this can be globally removed by appropriate coordinate transformations. The supervielbein $E^A(z)$, being an alogue of Cartan's local frame, is the dynamical variable of superspace formulation, which identifies the tetrad field $e_{\hat{m}}{}^{\hat{a}}(X)$ and the Rarita-Schwinger fields. The connection is the second dynamical variable in this theory. The field $e_{\hat{m}}{}^{\hat{a}}(X)$ plays the role of a gauge field associated with local transformations (*fictitious graviton*). The *fictitious gravitino* is the gauge field related to local supersymmetry. The two fields differ in their spin: 2 for the graviton, 3/2 for the gravitino. These two particles are the two bosonic and fermionic states of a gauge particle in the curved background spaces $\widetilde{M}_4$ and $\widetilde{MS}_p$, respectively, or vice versa. Following (Ter-Kazarian, 2012), in the framework of classical physics, we discuss the inertia effects by going beyond the hypothesis of locality, and derive the explicit form of the vierbien $e_{\hat{m}}{}^{\hat{a}}(\varrho) \equiv (e_m{}^a(\varrho),\, e_{\underline{m}}{}^{\underline{a}}(\varrho))$. This theory furnishes justification for the introduction of the *weak principle of equivalence* (WPE). We derive a general expression of the relativistic inertial force exerted on the extended spinning body moving in the Rieman-Cartan space.

Keywords: *Supersymmetry–Supergravity–Inertia effects*

1. Introduction

The phenomenon of inertia may be the most profound mystery in physics. Its solution could shed light on or be central to unraveling other important puzzles. In (Ter-Kazarian, 2023, 2024) we have studied the first part of phenomenon of inertia, which governs the *inertial uniform motion* of a particle in 4D flat Minkowski space, M_4. This is probably the most fascinating challenge for physical research. We have developed the theory of global, so-called, `double space´- or *master space* (MS_p)- supersymmetry, subject to certain rules, wherein the superspace is a 14D-extension of a direct sum of background spaces $M_4 \oplus$ MS_p by the inclusion of additional 8D fermionic coordinates. The latter is induced by the spinors $\underline{\theta}$ and $\bar{\underline{\theta}}$ referred to MS_p. While all the particles are living on M_4, their superpartners can be viewed as living on MS_p. This is a main ground for introducing MS_p, which is *unmanifested* individual companion to the particle of interest. Supersymmetry transformation is defined as a translation in superspace, specified by the group element with corresponding anticommuting parameters. The multiplication of two successive transformations induce the motion. As a corollary, we have derived SLC in a new perspective of global double MS_p-SUSY transformations in terms of Lorentz spinors $(\underline{\theta}, \bar{\underline{\theta}})$. This calls for a complete reconsideration of our ideas of Lorentz motion code,

*gago_50@yahoo.com

doi: https://doi.org/10.52526/25792776-23.70.2-212

to be now referred to as the *individual code of a particle*, defined as its intrinsic property. In MS_p-SUSY theory, obviously as in standard unbroken SUSY theory, the vacuum zero point energy problem, standing before any quantum field theory in M_4, is solved. The particles in M_4 themselves can be considered as excited states above the underlying quantum vacuum of background double spaces $M_4\oplus$ MS_p, where the zero point cancellation occurs at ground-state energy, provided that the natural frequencies are set equal ($q_0^2 \equiv \nu_b = \nu_f$), because the fermion field has a negative zero point energy while the boson field has a positive zero point energy. On these premises, we have derived the two postulates on which the theory of Special Relativity (SR) is based.

The second part of phenomenon of inertia describes how the *inertial uniform motion* of a particle is affected by applied forces (*the accelerated motion and inertia effects*). A puzzling underlying reality of inertia effects stood open more than four centuries, and that this physics is still an unknown exciting problem to be challenged and allows various attempts. The beginning of the study of inertia effects can be traced back to the works developed by Galileo (Drake, 1978) and Newton (Newton, 1687). Certainly, more than four centuries passed since the famous far-reaching discovery of Galileo (in 1602-1604) that all bodies fall at the same rate (Drake, 1978) - an apparent enigmatic equality of inertial and passive gravitational mass, which led to an early empirical version of the suggestion that the gravity and inertia may somehow result from a single mechanism. Besides describing these early gravitational experiments, Newton in *Principia Mathematica* (Newton, 1687) has proposed a comprehensive approach to studying the relation between the gravitational and inertial masses of a body. Newton describes his precise pendulum experiments with "gold, silver, lead, glass, sand, common salt, wood, water and wheat" testing WPE - equality of inertial and passive gravitational mass.

Einstein's biographer Leopold Infeld wrote in 1950 (Infeld, 1950). "No one in our century, with the exception of Einstein, wondered about this law any longer", These efforts led to Einstein's extension in 1907 of WPE to all of physics (Beck & Havas, 1989): "...We consider two systems Σ_1 and Σ_2 in motion. Let Σ_1 be accelerated in the direction of its X-axis, and let γ be the (temporally constant) magnitude of that acceleration. Σ_2 shall be at rest, but it shall be located in a homogeneous gravitational field that imparts to all objects an acceleration -γ in the direction of the X-axis". And then he formulate his principle of equivalence (EPE): "At our present state of experience we have thus no reason to assume that the systems Σ_1 and Σ_2 differ from each other in any respect, and in the discussion that follows, we shall therefore assume the complete physical equivalence of a gravitational field and a corresponding acceleration of the reference system". This involved *relative* acceleration in an attempt to introduce ideas of Ernst Mach into his theory. These ideas gave the theory its name. This did not prove to be a happy idea since this notion makes mathematical sense only for bodies having the same 4-velocity and from a physical point of view accelerations are *absolute*.

Ever since, there is an ongoing quest to understand the reason for the universality of the gravity and inertia, attributing to the WPE, which establishes the independence of free-fall trajectories of the internal composition and structure of bodies. At present, the variety of consequences of the precision experiments from astrophysical observations makes it possible to probe this fundamental issue more deeply by imposing the constraints of various analyzes. Currently, the observations performed in the Earth-Moon-Sun system (Everitt & et al., 2009, 2011, Faller & et al., 1990, Gabriel & Haugan, 1990, Gillies, 1997, Haugan & Kauffmann, 1995, Hayasaka & Takeuchi, 1989, Heifetz & et al., 2009, Imanishi & et al., 1991, Keiser & et al., 2009, Luo & et al., 2002, Muhlfelder & et al., 2009, Ni, 2011, Nitschke & Wilmarth, 1990, Quinn & Picard, 1990, Silbergleit & et al., 2009, Turyshev, 2008, Will, 2006, Zhou & et al., 2002), or at galactic and cosmological scales (Haugan & Lämmerzahl, 2001, Lämmerzahl & Bordé, 2001, Ni, 2005a,b,c, 2008), probe more deeply both WPE and strong EPE. The intensive efforts have been made, for example, to clear up whether the rotation state would affect the trajectory of test particle. Shortly after the development of the work by Hayasaka & Takeuchi (1989), in which is reported that, in weighing gyros, it would be a violation of WPE, by Faller & et al. (1990), Imanishi & et al. (1991), Nitschke & Wilmarth (1990), Quinn & Picard (1990) performed careful weighing experiments on gyros with improved precision, but found only null results which are in disagreement with the report of (Hayasaka & Takeuchi, 1989). The interferometric free-fall experiments by Luo & et al. (2002) and Zhou & et al. (2002) again found null results in disagreement with (Hayasaka & Takeuchi, 1989). For rotating bodies, the ultraprecise Gravity Probe B experiment (Everitt & et al., 2009, 2011, Heifetz & et al., 2009, Keiser & et al., 2009, Muhlfelder & et al., 2009, Silbergleit & et al., 2009), which measured the frame-dragging effect and geodetic precession on four quartz gyros, has the best accuracy. GP-B serves as a starting point for the measurement of the gyrogravitational factor of particles. Whereas, the gravitomagnetic field, which is locally equivalent to a *Coriolis field* and generated

doi: https://doi.org/10.52526/25792776-23.70.2-212

by the absolute rotation of a body, has been measured too. This, with its superb accuracy, verifies WPE for unpolarized bodies to an ultimate precision - a four-order improvement on the noninfluence of rotation on the trajectory, and ultraprecision on the rotational equivalence (Ni, 2011). Moreover, the theoretical models may indicate cosmic polarization rotations which are being looked for and tested in the CMB experiments (Ni, 2008). To look into the future, measurement of the gyrogravitational ratio of particle would be a further step, see (Ni, 2005c) and references therein, towards probing the microscopic origin of gravity. Also, the inertia effects in fact are of vital interest for the phenomenological aspects of the problem of neutrino oscillations, see e.g. (Atwood & et al., 1984, Bonse & Wroblewski, 1983, Capozziello & Lambiase, 2000, Cardall & Fuller, 1997, Colella et al., 1975, Gasperini, 1988, Halprin & Leung, 1991, Pantaleone et al., 1993, Piniz et al., 1997, de Sabbata & Gasperini, 1981). All these have evoked the study of the inertial effects in an accelerated and rotated frame. In doing this, it is a long-established practice in physics to use the hypothesis of locality for extension of the Lorentz invariance to accelerated observers in Minkowski spacetime (Misner et al., 1973, Synge, 1960). This in effect replaces the accelerated observer by a continuous infinity of hypothetical momentarily comoving inertial observers along its wordline. This assumption, as well as its restricted version, so-called, clock hypothesis, which is a hypothesis of locality only concerned about the measurement of time, are reasonable only if the curvature of the wordline could be ignored. As long as all relevant length scales in feasible experiments are very small in relation to the huge acceleration lengths of the tiny accelerations we usually experience, the curvature of the wordline could be ignored and that the differences between observations by accelerated and comoving inertial observers will also be very small. In this line, in 1990, Hehl and Ni proposed a framework to study the relativistic inertial effects of a Dirac particle (Hehl & Ni, 1990), in agreement with (Li & Ni, 1979, Ni, 1977, Ni & Zimmermann, 1978). Ever since this question has become a major preoccupation of physicists, see e.g. (Bakke & Furtado, 2010, Bini et al., 2004, Hehl et al., 1991, Maluf & Faria, 2008, Maluf et al., 2007, Marzlin, 1996, Mashhoon, 2002, 2011, Pan & Ren, 2011, Silenko & Teryaev, 2007). Even this works out, still, it seems quite clear that such an approach is a work in progress, and that it will have to be extended to describe physics for arbitrary accelerated observers. Beyond the WPE, there is nothing convincing in the basic postulates of physics for the origin and nature of inertia to decide on the issue. Despite our best efforts, all attempts to obtain a true knowledge of the geometry related to the noninertial reference frames of an arbitrary observer seem doomed, unless we find *a physical principle the inertia might refer to*, and that a working alternative *relativistic theory of inertia* is formulated. Otherwise one wanders in a darkness.

In particular, the concept of a uniformly accelerated, gravitation-free reference system without the use of special relativity is the problem (Schucking, 2009, Schucking & Surowitz, 2012). In Newton's theory the acceleration, γ, could be a vector in the x-direction constant in space and time independent of the velocity of a body moving in the x-direction. Not so in Minkowski spacetime. There the acceleration vector has to be orthogonal to the 4-velocity and it would appear that homogeneity of the acceleration field in spacetime could no longer be achieved. That is, the notion of relative acceleration exists only for particles whose four-velocities agree. Interpreting the gravitational acceleration of a falling object as minus the acceleration of the reference system had to be restricted to objects at rest. It was a letter from Max Planck that had alerted Einstein to this fact, which was acknowledged by Einstein in the Erratum (1908, p. 317) to Ref. (Beck & Havas, 1989): "A letter by Mr. Planck induced me to add the following supplementary remark so as to prevent a misunderstanding that could arise easily. ...A reference system at rest situated in a temporally constant, homogeneous gravitational field is treated as physically equivalent to a uniformly accelerated, gravitation-free reference system. The concept 'uniformly accelerated' needs further clarification". Einstein then pointed out that "the equivalence was to be restricted to a body with zero velocity in the accelerated system. In a linear approximation, he concluded, this was sufficient because only linear terms had to be taken into account". Einstein's retreat raises the question whether it is impossible to find a homogeneous uniformly accelerated reference system, or, assuming exact validity of his principle of equivalence, a homogeneous gravitational field. But, as it is pointed out by Schucking & Surowitz (2012), a homogeneous gravitational field in Minkowski spacetime can be constructed if the reference frames in gravitational theory are understood as spaces with a flat connection and torsion defined through teleparallelism. In 1907 Einstein did not show the equivalence of acceleration and gravitation described by spacetime curvature. He did not show either the equivalence of geodesics and non-geodesics or the equivalence of rotating and non-rotating systems. What he did, we now can see more clearly, was the introduction of accelerated reference systems exhibiting torsion through distant parallelism. This kind of torsion was first introduced by Einstein in 1928. There were physical consequences that needed to be checked for these systems, like the constancy of the speed of light independent of acceleration, no influence

doi: https://doi.org/10.52526/25792776-23.70.2-212

of acceleration on the rate of clocks and the length of standards. As far as these assumptions have been tested, they appear to be in order.

Various attempts at the resolution of difficulties that are encountered in linking Mach's principle with Einstein's theory of gravitation have led to many interesting investigations. For example, by Mashhoon & Wesson (2012) is shown that the GR can be locally embedded in a Ricci-flat 5D manifold such that every solution of GR in 4D can be locally embedded in a Ricci-flat 5D manifold, and that the resulting inertial mass of a test particle varies in space-time.

However, the inertial forces are not of gravitational origin as it was proposed by EPE, because there are many controversies to question the validity of such a description. Synge confesses in his monograph (Synge (1960), in introduction) ". . . I have never been able to understand this Principle. ...Does it mean that the effects of a gravitational field are indistinguishable from the effects of an observer's acceleration? If so, it is false. In Einstein's theory, either there is a gravitational field or there is none, according as the Riemann tensor does or does not vanish. This is an absolute property; it has nothing to do with any observer's worldline. Space-time is either flat or curved, and in several places of the book I have been at considerable pains to separate truly gravitational effects due to curvature of space-time from those due to curvature of the observer's worldline (in most ordinary cases the latter predominate)..."

The difficulty is brought into sharper focus by considering the laws of inertia, including their quantitative aspects. That is, Mach principle and its modifications do not provide a quantitative means for computing the inertial forces. Brans's thorough analysis (Brans, 1977) has shown that no extra inertia is induced in a body as a result of the presence of other bodies. If the matter distribution is not isotropic, and if the inertia is due to gravitational interactions, then one of the consequences of Mach's principle could be conceivable that the concentration of matter near the centre of our galaxy may result in an anisotropy of inertia at the earth which could be detected experimentally. Testing this question, the experiments by Cocconi & Salpeter (1960), Drever (1961), Hughes et al. (1960) do not found such anisotropy of inertial mass. The experiment suggested by Cocconi and Salpeter was to observe the Zeeman splitting in the excited nuclear state of Fe^{57} by use of the Mössbauer effect. The effect of some anisotropy of inertia is then very similar to that for the atomic Zeeman effect, except that one is now dealing with the motion of the nucleon in the Fe^{57} responsible for the γ-ray transition (at least on a shell-model picture) instead of the motion of an electron. They found that the variation Δm of mass with direction, if it exists, should satisfy $\frac{\Delta m}{m} \leq 10^{-9}$. The most sensitive test is obtained in (Hughes et al., 1960) from a nuclear magnetic resonance experiment with a Li^7 nucleus of spin $I = 3/2$. This method gives a sensitivity some factor of 10^6 greater than could be achieved in the experiment suggested by Cocconi and Salpeter using the Mössbauer effect. The magnetic field was of about 4700 gauss was stabilized against the proton resonance frequency with the Atomichron as a frequency standard. Only a single line was observed. The increase in sensitivity over that which one could obtain from the Mössbauer effect is due to the far narrower line width obtainable for a transition with a nucleus in its ground state as compared with a nucleus in an excited state. The south direction in the horizontal plane points within 22 degrees towards the center of our galaxy, and 12 hour later this same direction along the earth's horizontal plane points 104 degrees away from the galactic center. If the nuclear structure of Li^7 is treated as a single $P_{3/2}$ proton in a central nuclear potential, the variation Δm of mass with direction, if it exists, was found to satisfy $\frac{\Delta m}{m} \leq 10^{-20}$. This is by now very strong evidence that there is no anisotropy of mass which is due to the effects of mass in our galaxy. Hence it seems that within the framework of the Mach theory as discussed by Cocconi and Salpeter one should conclude that there is no anisotropy of mass of the type which varies as $P_2(cos\theta)$ associated with effects of mass in our galaxy. Here $P_2(cos\theta)$ is the Legendre polynomial of order 2, and θ is the angle between the direction of acceleration of the particle (determined by the direction of an external magnetic field H and by the magnetic quantum state) and the direction to the galactic center. In the same time, Dicke (1961) and Ni (1983) have pointed out that when anisotropic effects on both kinetic and potential energies are considered, the null results are to be expected provided that the anisotropy couples in the same way to both forms of energy. It is concluded that the extremely accurate null result of the experiment of (Hughes et al., 1960) seemed does not cast doubt upon the validity of Mach's principle. They stated that, on the contrary, this important experiment shows, with great precision, that inertial anisotropy effects are universal, the same for all particles. These experiments can thus be regarded as a test of the universal coupling of gravity to all forms of mass-energy. Anyway, the subsequent experimental test along this line (Prestage & et al., 1985), using nuclear-spin-polarized $^9Be^+$ ions, also gives null result on spatial anisotropy and thus supporting local Lorentz invariance. In this experiment the frequency of a nuclear spin-flip transition in $^9Be^+$ has been compared to the frequency of a hydrogen maser transition to

doi: https://doi.org/10.52526/25792776-23.70.2-212

see if the relative frequencies depend on the orientation of the $^9Be^+$ ions in space. Obtained null result represents a decrease in the limits set by (Hughes et al., 1960) and (Drever, 1961) on a spatial anisotropy by a factor of about 300.

Our idea is that the *universality* of gravitation and inertia attribute to the single mechanism of origin from geometry but having a different nature. We have ascribed, therefore, the inertia effects (second part of inertia) to the geometry itself but as having a nature other than 4D Riemannian space (Ter-Kazarian, 2012). The key to our construction procedure of the toy model is an assignment to each and every particle individually a new fundamental constituent of hypothetical 2D, so-called, *master-space* (MS_p), subject to certain rules. The MS_p, embedded in the background 4D-space, is an *unmanifested* indispensable individual companion to the particle of interest. Within this scheme, the MS_p was presumably allowed to govern the motion of individual particle in the background 4D-space. The particle has to live with MS_p-companion as an intrinsic property devoid of any external influence. This together with the idea that the inertia effects arise as a deformation/(distortion of local internal properties) of MS_p, are the highlights of the alternative *relativistic theory of inertia* (RTI) (Ter-Kazarian, 2012). The crucial point is to observe that, in spite of totally different and independent physical sources of gravity and inertia, the RTI furnishes justification for the introduction of the PE. However, this investigation obviously is incomplete unless it has conceptual problems for further motivation and justification of introducing the fundamental concept of MS_p. The way we assigned such a property to the MS_p is completely *ad hoc* and there are some obscure aspects of this hypothesis. Moreover, this theory will certainly be incomplete without revealing the physical processes that underly the *inertial uniform motion* of a particle in flat space.

Since in (Ter-Kazarian, 2023), we already have solved these questions in the framework of *global* MS_p-SUSY theory, then on these premises, in the present paper we develop the *local* $\widetilde{MS}_p$-SUSY theory in order to address the *accelerated motion and inertia effects*. A curvature of $\widetilde{MS}_p$ arises entirely due to the inertial properties of the Lorentz-rotated frame of interest, i.e. a *fictitious gravitation*, which can be globally removed by appropriate coordinate transformations. Whereas, in order to become on the same footing with the distorted space $\widetilde{MS}_p$, the space $\widetilde{M}_4$ refers only to the accelerated proper reference frame of a particle.

With this perspective in sight, we will proceed according to the following structure. To start with, in Section 2 we revisit the global `double space´- or MS_p-SUSY as a guiding principle to make the rest of paper understandable. We give a glance at MS_p, and outline the key points of the proposed symmetry. More about the accelerated motion is said in Section 3, but this time in the framework of local $\widetilde{MS}_p$-SUSY. In Section 4, we turn to non-trivial linear representation of the $\widetilde{MS}_p$-SUSY algebra. In Section 5 we briefly discuss the inertia effects. In Section 6, we turn to model building in the 4D background Minkowski space-time On these premises, we discuss the theory beyond the hypothesis of locality in Section 7. In this, we compute the improved metric and other relevant geometrical structures in noninertial system of arbitrary accelerating and rotating observer in Minkowski space-time. The case of semi-Riemann background space V_4 is studied in Section 8, whereas we give justification for the introduction of the *weak* principle of equivalence (WPE) on the theoretical basis, which establishes the independence of free-fall trajectories of the internal composition and structure of bodies. The implications of the inertial effects for the more general post-Riemannian geometry are briefly discussed in Section 9. Concluding remarks are presented in Section 10. For brevity, whenever possible undotted and dotted spinor indices often can be ruthlessly suppressed without ambiguity. Unless indicated otherwise, we take natural units, $h = c = 1$.

2. Probing SR behind the MS_p-SUSY, revisited

For a benefit of the reader, as a guiding principle to make the rest of paper understandable, in this section we necessarily recount some of the highlights behind of *global* MS_p-SUSY (Ter-Kazarian, 2023, 2024), on which the *local* $\widetilde{MS}_p$-SUSY is based. The latter is the only framework in use throughout the paper.

The flat MS_p is the 2D composite space

$$MS_p \equiv \underline{M}_2 = \underline{R}^1_{(+)} \oplus \underline{R}^1_{(-)}, \tag{1}$$

with Lorentz metric. The ingredient 1D-space $\underline{R}^1_{\underline{m}}$ is spanned by the coordinates $\underline{\eta}^{\underline{m}}$. The following notational conventions are used throughout this paper: all quantities related to the space $\underline{M}_2$ will be underlined. In particular, the underlined lower case Latin letters $\underline{m}, \underline{n}, ... = (\pm)$ denote the world indices related to $\underline{M}_2$.

Suppose the position of the particle is specified by the coordinates $x^m(s)$ $(x^0 = t)$ in the basis e_m (m=0,1,2,3) at given point in the background M_4 space. Consider a smooth (injective and continuous)

doi: https://doi.org/10.52526/25792776-23.70.2-212

embedding $\underline{M}_2 \hookrightarrow M_4$. That is, a smooth map $f: \underline{M}_2 \longrightarrow M_4$ is defined to be an immersion (the embedding which is a function that is a homeomorphism onto its image):

$$\underline{e}_0 = e_0, \quad \underline{x}^0 = x^0, \quad \underline{e}_1 = \vec{n}, \quad \underline{x}^1 = |\vec{x}|, \tag{2}$$

where $\vec{x} = e_i x^i = \vec{n}|\vec{x}|$ $(i = 1,2,3)$. Given the inertial frames $S_{(4)}, S'_{(4)}, S''_{(4)}, ...$ in unaccelerated uniform motion in M_4, we may define the corresponding inertial frames $\underline{S}_{(2)}$, $\underline{S}'_{(2)}$, $\underline{S}''_{(2)}, ...$ in $\underline{M}_2$, which are used by the non-accelerated observers for the positions $\underline{x}^r, \underline{x}'^r, \underline{x}''^r, ...$ of a free particle in flat $\underline{M}_2$. According to (2), the time axes of the two systems $\underline{S}_{(2)}$ and $S_{(4)}$ coincide in direction, and the time coordinates are taken the same. For the case at hand,

$$\underline{v}^{(\pm)} = \frac{d\eta^{(\pm)}}{d\underline{x}^0} = \frac{1}{\sqrt{2}}(\underline{v}^0 \pm \underline{v}^1), \quad \underline{v}^1 = \frac{d\underline{x}^1}{d\underline{x}^0} = |\vec{v}| = |\frac{d\vec{x}}{dx^0}|, \tag{3}$$

and that

$$\underline{u} = \underline{e}_m \underline{v}^m = (\underline{\vec{v}}_0, \underline{\vec{v}}_1), \quad \underline{\vec{v}}_0 = \underline{e}_0 \underline{v}^0, \quad \underline{\vec{v}}_1 = \underline{e}_1 \underline{v}^1 = \vec{n}|\vec{v}| = \vec{v}, \tag{4}$$

therefore, $\underline{u} = u = (e_0, \vec{v})$. To explain why MS$_p$ is two dimensional, we note that only 2D real *null vectors* are allowed as the basis at given point in MS$_p$, which is embedded in M_4. Literally speaking, the $\underline{M}_2$ can be viewed as 2D space living on the 4D world sheet.

The elementary act of particle motion at each time step (t_i) through the infinitely small spatial interval $\triangle x_i = (x_{i+1} - x_i)$ in M_4 during the time interval $\triangle t_i = (t_{i+1} - t_i) = \varepsilon$ is probably the most fascinating challenge for physical research. Since this is beyond our perception, it appears legitimate to consider extension to the infinitesimal Schwinger transformation function, $F_{ext}(x_{i+1}, t_{i+1}; x_i, t_i)$, in fundamentally different aspect. We hypothesize that

in the limit $n \to \infty (\varepsilon \to 0)$, the elementary act of motion consists of an `annihilation´ of a particle at point $(x_i, t_i) \in M_4$, which can be thought of as the transition from initial state $|x_i, t_i >$ into unmanifested intermediate state, so-called, `motion´ state, $|\underline{x}_i, \underline{t}_i >$, and of subsequent `creation´ of a particle at infinitely close final point $(x_{i+1}, t_{i+1}) \in M_4$, which means the transition from `motion´ state, $|\underline{x}_i, \underline{t}_i >$, into final state, $|x_{i+1}, t_{i+1} >$. The motion state, $|\underline{x}_i, \underline{t}_i) >$, should be defined on unmanifested `master´ space, $\underline{M}_2$, which includes the points of all the atomic elements, $(\underline{x}_i, \underline{t}_i) \in \underline{M}_2$ $(i = 1, 2, ...)$.

This furnishes justification for an introduction of *unmanifested master space*, $\underline{M}_2$.

The fields of spin-zero $(\vec{S} = \vec{K} = 0)$ scalar field $A(x)$ and spin-one $A^n(x)$, corresponding to the $(1/2, 1/2)$ representation, transform under a general Lorentz transformation as follows:

$$\begin{array}{ll} \underline{A}(\underline{\eta}) \equiv A(x), & (\text{spin} \quad 0); \\ \underline{A}^{\underline{m}}(\underline{\eta}) = \Lambda^{\underline{m}}{}_n A^n(x), & (\text{spin} \quad 1). \end{array} \tag{5}$$

The map from $SL(2,C)$ to the Lorentz group is established through the $\vec{\sigma}$-Pauli spin matrices, $\sigma^m = (\sigma^0, \sigma^1, \sigma^2, \sigma^3) \equiv (I_2, \vec{\sigma})$, $\bar{\sigma}^m \equiv (I_2, -\vec{\sigma})$, where I_2 is the identity two-by-two matrix.

According to embedding map (2), the $\underline{\sigma}$-matrices are

$$\sigma^{\underline{m}} = \sigma^{(\pm)} = \frac{1}{\sqrt{2}}(\sigma^{\underline{0}} \pm \sigma^{\underline{1}}) = \frac{1}{\sqrt{2}}(\sigma^0 \pm \sigma^3). \tag{6}$$

The matrices $\sigma^{\underline{m}}$ form a basis for two-by-two complex matrices $\underline{P}$:

$$\underline{P} = (p_{\underline{m}}\sigma^{\underline{m}}) = (p_{(\pm)}\sigma^{(\pm)}) = (p_{\underline{0}}\sigma^{\underline{0}} + p_{\underline{1}}\sigma^{\underline{1}}), \tag{7}$$

provided $p_{(\pm)} = i\partial_{\underline{\eta}^{(\pm)}}$, $p_{\underline{0}} = i\partial_{\underline{x}^0}$ and $p_{\underline{1}} = i\partial_{\underline{x}^1}$. The real coefficients $p'_{\underline{m}}$ and $p_{\underline{m}}$, like p'_m and p_m, are related by a Lorentz transformation $p'_{\underline{m}} = \Lambda^{\underline{n}}_{\underline{m}} p_{\underline{n}}$, because the relations $det(\sigma^{\underline{m}} p_{\underline{m}}) = p_{\underline{0}}^2 - p_{\underline{1}}^2$ and $det\, M = 1$ yield $p'^2_{\underline{0}} - p'^2_{\underline{1}} = p_{\underline{0}}^2 - p_{\underline{1}}^2$. Correspondence of $p_{\underline{m}}$ and $\underline{P}$ is uniquely: $p_{\underline{m}} = \frac{1}{2}Tr(\sigma^{\underline{m}}\underline{P})$, which combined with (9) yields

$$\Lambda^{\underline{m}}_{\underline{n}}(M) = \frac{1}{2}\, Tr\left(\sigma^{\underline{m}} M \sigma^{\underline{n}} M^{\dagger}\right). \tag{8}$$

Thus, both hermitian matrices P and P' or $\underline{P}$ and $\underline{P}'$ have expansions, respectively, in σ or $\underline{\sigma}$:

$$(\sigma^m\, p'_m) = M(\sigma^m\, p_m)M^{\dagger}, \quad (\sigma^{\underline{m}} p'_{\underline{m}}) = M(\sigma^{\underline{m}} p_{\underline{m}})M^{\dagger}, \tag{9}$$

where $M(M \in SL(2,C))$ is unimodular two-by-two matrix. Meanwhile $(\underline{\chi}\, \sigma^{\underline{m}}\, \bar{\underline{\zeta}})\, \underline{A}_{\underline{m}}$ is a Lorentz scalar if the following condition is satisfied:

$$\Lambda^{\underline{m}}_{\underline{n}}(M)\sigma^{\underline{n}}_{\alpha\dot{\alpha}} = (M^{-1})_{\alpha}{}^{\beta}\sigma^{\underline{m}}_{\beta\dot{\beta}}(M^{-1})^{\dagger\dot{\beta}}{}_{\dot{\alpha}}. \tag{10}$$

doi: https://doi.org/10.52526/25792776-23.70.2-212

A two-component $(1/2,0)$ Weyl fermion, $\chi_\beta(x)$, therefore, transforms under Lorentz transformation to yield $\underline{\chi}_\alpha(\underline{\eta})$:

$$\chi_\beta(x) \longrightarrow \underline{\chi}_\alpha(\underline{\eta}) = (M_R)_\alpha{}^\beta\, \chi_\beta(x), \quad \alpha,\beta = 1,2, \tag{11}$$

where the orthochronous Lorentz transformation, corresponding to a rotation by the angles ϑ_3 and ϑ_2 about, respectively, the axes n_3 and n_2, is given by rotation matrix

$$M_R = e^{i\frac{1}{2}\sigma_2\vartheta_2} e^{i\frac{1}{2}\sigma_3\vartheta_3}. \tag{12}$$

There with the rotation of an hermitian matrix P is

$$p_{\underline{m}}\sigma^{\underline{m}} = M_R\, p_m\sigma^m\, M_R^\dagger, \tag{13}$$

where p_m and $p_{\underline{m}}$ denote the momenta $p_m \equiv m(ch\beta,\, sh\beta\sin\vartheta_2\cos\vartheta_3,\, sh\beta\sin\vartheta_2\sin\vartheta_3,$ $sh\beta\cos\vartheta_2)$, and $p_{\underline{m}} \equiv m(ch\underline{\beta},\, 0,\, 0,\, sh\underline{\beta})$.

A two-component $(0,1/2)$ Weyl spinor field is denoted by $\bar{\chi}^{\dot\beta}(x)$, and transforms as

$$\bar{\chi}^{\dot\beta}(x) \longrightarrow \underline{\bar{\chi}}^{\dot\alpha}(\underline{\eta}) = (M_R^{-1})^{\dagger\dot\alpha}{}_{\dot\beta}\, \bar{\chi}^{\dot\beta}(x), \quad \dot\alpha,\dot\beta = 1,2. \tag{14}$$

The so-called `dotted´ indices have been introduced to distinguish the $(0,1/2)$ representation from the $(1/2,0)$ representation. The `bar´ over the spinor is a convention that this is the $(0,1/2)$-representation. We used the Van der Waerden notations for the Weyl two-component formalism: $(\underline{\bar{\chi}}_{\dot\alpha})^* = \underline{\chi}_\alpha$ and $\underline{\bar{\chi}}_{\dot\alpha} = (\underline{\chi}_\alpha)^*$.

The odd part of the supersymmetry algebra is composed entirely of the spin-1/2 operators $Q_\alpha{}^i,\ Q_\beta{}^j$. In order to trace a maximal resemblance in outward appearance to the standard SUSY theories, here we set one notation $\hat{m} = (m \quad \text{if} \quad Q = q, \text{ or } \underline{m} \quad \text{if} \quad Q = \underline{q})$, and as before the indices α and $\dot\alpha$ run over 1 and 2.

If that is the case as above, a *creation* of a particle in $\underline{M}_2$ means its transition from initial state defined on M_4 into intermediate state defined on $\underline{M}_2$, while an *annihilation* of a particle in $\underline{M}_2$ means vice versa. The same interpretation holds for the *creation* and *annihilation* processes in M_4. All the fermionic and bosonic states taken together form a basis in the Hilbert space. The basis vectors in the Hilbert space composed of $H_B \otimes H_F$ is given by

$$\{|\underline{n}_b > \otimes|0>_f,\ |\underline{n}_b > \otimes f^\dagger\,|0>_f\},$$

or

$$\{|n_b > \otimes|\underline{0}>_f,\ |n_b > \otimes \underline{f}^\dagger\,|\underline{0}>_f\},$$

where we consider two pairs of creation and annihilation operators $(b^\dagger,\, b)$ and $(f^\dagger,\, f)$ for bosons and fermions, respectively, referred to the background space M_4, as well as $(\underline{b}^\dagger,\, \underline{b})$ and $(\underline{f}^\dagger,\, \underline{f})$ for bosons and fermions, respectively, as to background master space $\underline{M}_2$. Accordingly, we construct the quantum operators, $(q^\dagger,\, \underline{q}^\dagger)$ and $(q,\, \underline{q})$, which replace bosons by fermions and vice versa:

$$\begin{array}{l} q\,|\underline{n}_b,\, n_f >= q_0\sqrt{\underline{n}_b}\,|\underline{n}_b - 1,\, n_f + 1>, \\ q^\dagger\,|\underline{n}_b,\, n_f >= q_0\sqrt{\underline{n}_b + 1}\,|\underline{n}_b + 1,\, n_f - 1>, \end{array} \tag{15}$$

and that

$$\begin{array}{l} \underline{q}\,|n_b,\, \underline{n}_f >= q_0\sqrt{n_b}\,|n_b - 1,\, \underline{n}_f + 1>, \\ \underline{q}^\dagger\,|n_b,\, \underline{n}_f > q_0\sqrt{n_b + 1}\,|n_b + 1,\, \underline{n}_f - 1>. \end{array} \tag{16}$$

This framework combines bosonic and fermionic states on the same footing, rotating them into each other under the action of operators q and $\underline{q}$. So, we may refer the action of the supercharge operators q and $q^\dagger$ to the background space M_4, having applied in the chain transformations of fermion χ (accompanied with the auxiliary field F as it will be seen later on) to boson $\underline{A}$, defined on $\underline{M}_2$:

$$\longrightarrow \chi^{(F)} \longrightarrow \underline{A} \longrightarrow \chi^{(F)} \longrightarrow \underline{A} \longrightarrow \chi^{(F)} \longrightarrow. \tag{17}$$

Respectively, we may refer the action of the supercharge operators $\underline{q}$ and $\underline{q}^\dagger$ to the $\underline{M}_2$, having applied in the chain transformations of fermion $\underline{\chi}$ (accompanied with the auxiliary field $\underline{F}$) to boson A, defined on the background space M_4:

$$\longrightarrow \underline{\chi}^{(\underline{F})} \longrightarrow A \longrightarrow \underline{\chi}^{(\underline{F})} \longrightarrow A \longrightarrow \underline{\chi}^{(\underline{F})} \longrightarrow. \tag{18}$$

doi: https://doi.org/10.52526/25792776-23.70.2-212

The successive atomic double transitions of a particle $M_4 \rightleftharpoons \underline{M}_2$ is investigated within MS$_p$-SUSY, wherein all the particles are living on M_4, their superpartners can be viewed as living on MS$_p$. The underlying algebraic structure of MS$_p$-SUSY generators closes with the algebra of *translations* on the original space M_4 in a way that it can then be summarized as a non-trivial extension of the Poincaré group algebra those of the commutation relations of the bosonic generators of four momenta and six Lorentz generators referred to M_4. Moreover, if there are several spinor generators $Q_\alpha{}^i$ with $i = 1, ..., N$ - theory with $N-$extended supersymmetry, can be written as a graded Lie algebra of SUSY field theories, with commuting and anticommuting generators:

$$\begin{array}{l} \{Q_\alpha{}^i,\, \bar{Q}^j{}_{\dot\alpha}\} = 2\delta^{ij}\,\sigma^{\hat m}_{\alpha\dot\alpha}\,p_{\hat m}; \\ \{Q_\alpha{}^i,\, Q_\beta{}^j\} = \{\bar{Q}^i{}_{\dot\alpha},\, \bar{Q}^j{}_{\dot\beta}\} = 0; \quad [p_{\hat m},\, Q_\alpha{}^i] = [p_{\hat m},\, \bar{Q}^j{}_{\dot\alpha}] = 0, \quad [p_{\hat m},\, p_{\hat n}] = 0. \end{array} \tag{19}$$

The anticommuting (Grassmann) parameters $\epsilon^\alpha(\xi^\alpha,\, \underline{\xi}^\alpha)$ and $\bar\epsilon^\alpha(\bar\xi^\alpha,\, \underline{\bar\xi}^\alpha)$:

$$\{\epsilon^\alpha,\, \epsilon^\beta\} = \{\bar\epsilon^\alpha,\, \bar\epsilon^\beta\} = \{\epsilon^\alpha,\, \bar\epsilon^\beta\} = 0, \quad \{\epsilon^\alpha,\, Q_\beta\} = \cdots = [p_{\hat m},\, \epsilon^\alpha] = 0, \tag{20}$$

allow us to write the algebra (19) for $(N = 1)$ entirely in terms of commutators:

$$[\epsilon Q,\, \bar{Q}\bar\epsilon] = 2\epsilon\sigma^{\hat m}\bar\epsilon p_{\hat m}, \quad [\epsilon Q,\, \epsilon Q] = [\bar{Q}\bar\epsilon,\, \bar{Q}\bar\epsilon] = [p^{\hat m},\, \epsilon Q] = [p^{\hat m},\, \bar{Q}\bar\epsilon] = 0. \tag{21}$$

For brevity, here the indices $\epsilon Q = \epsilon^\alpha Q_\alpha$ and $\bar\epsilon\bar{Q} = \bar\epsilon_{\dot\alpha}\bar{Q}^{\dot\alpha}$ will be suppressed unless indicated otherwise. This supersymmetry transformation maps tensor fields $\mathcal{A}(A,\, \underline{A})$ into spinor fields $\psi(\chi,\, \underline{\chi})$ and vice versa. From the algebra (21) we see that Q has mass dimension 1/2. Therefore, as usual, fields of dimension ℓ transform into fields of dimension $\ell + 1/2$ or into derivatives of fields of lower dimension. It can be checked that the supersymmetry transformations close supersymmetry algebra:

$$(\delta_{\xi_1}\delta_{\xi_2} - \delta_{\xi_2}\delta_{\xi_1})\underline{A} = -2i(\xi_1\sigma^m\bar\xi_2 - \xi_2\sigma^m\bar\xi_1)(\delta^0_m\underline{\partial}_0 + \tfrac{1}{|\vec x|}x^i\delta_{im}\underline{\partial}_1)\underline{A}. \tag{22}$$

The guiding principle of MS$_p$-SUSY resides in constructing the superspace which is a 14D-extension of a direct sum of background spaces $M_4 \oplus \underline{M}_2$ (spanned by the 6D-coordinates $X^{\hat m} = (x^m,\, \underline{\eta}^{\underline{m}})$ by the inclusion of additional 8D-fermionic coordinates $\Theta^\alpha = (\theta^\alpha,\, \underline{\theta}^\alpha)$ and $\bar\Theta_{\dot\alpha} = (\bar\theta_{\dot\alpha},\, \underline{\bar\theta}_{\dot\alpha})$, as to $(q,\, \underline{q})$, respectively. Therewith thanks to the embedding $\underline{M}_2 \hookrightarrow M_4$, the spinors $(\underline{\theta}, \underline{\bar\theta})$, in turn, induce the spinors $\theta(\underline{\theta}, \underline{\bar\theta})$ and $\bar\theta(\underline{\theta}, \underline{\bar\theta})$, as to M_4. These spinors satisfy the following relations:

$$\begin{array}{l} \{\Theta^\alpha,\, \Theta^\beta\} = \{\bar\Theta_{\dot\alpha},\, \bar\Theta_{\dot\beta}\} = \{\Theta^\alpha,\, \bar\Theta_{\dot\beta}\} = 0, \\ [x^m,\, \theta^\alpha] = [x^m,\, \bar\theta_{\dot\alpha}] = 0, \quad [\underline{\eta}^{\underline{m}},\, \underline{\theta}^\alpha] = [\underline{\eta}^{\underline{m}},\, \underline{\bar\theta}_{\dot\alpha}] = 0. \end{array} \tag{23}$$

and $\Theta^{\alpha *} = \bar\Theta^{\dot\alpha}$. Points in superspace are identified by the generalized coordinates

$$z^{(M)} = (X^{\hat m},\, \Theta^\alpha,\, \bar\Theta_{\dot\alpha}) = (x^m,\, \theta^\alpha,\, \bar\theta_{\dot\alpha}) \oplus (\underline{\eta}^{\underline{m}}, \underline{\theta}^\alpha,\, \underline{\bar\theta}_{\dot\alpha}).$$

We have then the one most commonly used `real´ or `symmetric´ superspace parametrized by

$$\Omega(X,\, \Theta,\, \bar\Theta) = e^{i(-X^{\hat m}p_{\hat m} + \Theta^\alpha Q_\alpha + \bar\Theta_{\dot\alpha}\bar{Q}^{\dot\alpha})} = \Omega_q(x,\, \theta,\, \bar\theta) \times \Omega_{\underline{q}}(\underline{\eta},\, \underline{\theta},\, \underline{\bar\theta}), \tag{24}$$

where we now imply a summation over $\hat m = (m, \underline{m})$. To study the effect of supersymmetry transformations, we consider

$$g(0,\, \epsilon,\, \bar\epsilon)\,\Omega(X,\, \Theta,\, \bar\Theta) = e^{i(\epsilon^\alpha Q_\alpha + \bar\epsilon_{\dot\alpha}\bar{Q}^{\dot\alpha})}\, e^{i(-X^{\hat m}p_{\hat m} + \Theta^\alpha Q_\alpha + \bar\Theta_{\dot\alpha}\bar{Q}^{\dot\alpha})}. \tag{25}$$

the transformation (25) induces the motion:

$$g(0,\, \epsilon,\, \bar\epsilon)\,\Omega(X^{\hat m},\, \Theta,\, \bar\Theta) \;\to (X^{\hat m} + i\,\Theta\,\sigma^{\hat m}\,\bar\epsilon - i\,\epsilon\,\sigma^{\hat m}\,\bar\Theta,\; \Theta + \epsilon,\, \bar\Theta + \bar\epsilon), \tag{26}$$

namely,

$$\begin{array}{l} g_q(0,\, \xi,\, \bar\xi)\,\Omega_q(x,\, \theta,\, \bar\theta) \;\to (x^m + i\,\theta\,\sigma^m\,\bar\xi - i\,\xi\,\sigma^m\,\bar\theta,\; \theta + \xi,\, \bar\theta + \bar\xi), \\ g_{\underline{q}}(0,\, \underline{\xi},\, \underline{\bar\xi})\,\Omega_{\underline{q}}(\underline{\eta},\, \underline{\theta},\, \underline{\bar\theta}) \;\to (\underline{\eta}^{\underline{m}} + i\,\underline{\theta}\,\sigma^{\underline{m}}\,\underline{\bar\xi} - i\,\underline{\xi}\,\sigma^{\underline{m}}\,\underline{\bar\theta},\; \underline{\theta} + \underline{\xi},\, \underline{\bar\theta} + \underline{\bar\xi}). \end{array} \tag{27}$$

The spinors $\theta(\underline{\theta}, \underline{\bar\theta})$ and $\bar\theta(\underline{\theta}, \underline{\bar\theta})$ satisfy the embedding relations $\Delta\underline{x}^0 = \Delta x^0$ and $\Delta\underline{x}^2 = (\Delta\vec x)^2$, so from (27) we obtain

$$\underline{\theta}\,\sigma^0\,\underline{\bar\xi} - \underline{\xi}\,\sigma^0\,\underline{\bar\theta} = \theta\,\sigma^0\,\bar\xi - \xi\,\sigma^0\,\bar\theta, \quad (\underline{\theta}\,\sigma^3\,\underline{\bar\xi} - \underline{\xi}\,\sigma^3\,\underline{\bar\theta})^2 = (\theta\,\vec\sigma\,\bar\xi - \xi\,\vec\sigma\,\bar\theta)^2. \tag{28}$$

doi: https://doi.org/10.52526/25792776-23.70.2-212

The *atomic displacement* caused by double transition of a particle $M_4 \rightleftharpoons \underline{M}_2$ reads

$$\Delta\underline{\eta}_{(a)} = \underline{e}_m \Delta\underline{\eta}^m_{(a)} = \underline{u}\tau, \tag{29}$$

where the components $\Delta\underline{\eta}^m_{(a)}$ are written

$$\Delta\underline{\eta}^m_{(a)} = (\underline{\theta}\,\sigma^m\,\underline{\bar\theta})\tau. \tag{30}$$

In Van der Warden notations for the Weyl two-component formalism $\underline{\bar\theta}_{\dot\alpha} = (\underline{\theta}_\alpha)^*$, the (29) can be recast into the form

$$\Delta\underline{\eta}^2_{(a)} = \tfrac{1}{2}\left[(\Delta\underline{x}^0_{(a)}q)^2 - (\Delta\underline{x}^1_{(a)})^2\right], \tag{31}$$

where $\Delta\underline{x}^0_{(a)} = \underline{v}^0\tau$, $\Delta\underline{x}^1_{(a)} = \underline{v}^1\tau$, and $\underline{v}^{(\pm)} = \frac{1}{\sqrt{2}}(\underline{v}^0 \pm \underline{v}^1)$. Hence the velocities of light in vacuum, $\underline{v}^0 = c$, and of a particle ,$\underline{\vec v}_1 = \underline{e}_1\underline{v}^1 = \vec n|\vec v| = \vec v$ ($|\vec v| \leq c$), are

$$\begin{aligned}\underline{v}^0 &= \underline{\theta}\,\sigma^0\,\underline{\bar\theta} = (\underline{\theta}_1\,\underline{\bar\theta}_1 + \underline{\theta}_2\,\underline{\bar\theta}_2) = \underline{\theta}\,\underline{\bar\theta},\\ \underline{v}^1 &= \underline{\theta}\,\sigma^1\,\underline{\bar\theta} = (\underline{\theta}_1\,\underline{\bar\theta}_1 - \underline{\theta}_2\,\underline{\bar\theta}_2),\end{aligned} \tag{32}$$

where

$$\begin{aligned}\theta_1(\underline{\theta},\,\underline{\bar\theta}) &= \tfrac{1}{2}\left[\left(\underline{v}^0 + \sqrt{\tfrac{2}{3}}\underline{v}^1\right)^{1/2} + \left(\underline{v}^0 - \sqrt{\tfrac{2}{3}}\underline{v}^1\right)^{1/2}\right],\\ \theta_2(\underline{\theta},\,\underline{\bar\theta}) &= \tfrac{1}{2}\left[\left(\underline{v}^0 + \sqrt{\tfrac{2}{3}}\underline{v}^1\right)^{1/2} - \left(\underline{v}^0 - \sqrt{\tfrac{2}{3}}\underline{v}^1\right)^{1/2}\right].\end{aligned} \tag{33}$$

Thus we derive the first founding property (i) that *the atomic displacement* $\Delta\underline{\eta}_{(a)}$, caused by double transition of a particle $M_4 \rightleftharpoons \underline{M}_2$, is an invariant:

$$\text{(i)}\quad \Delta\underline{\eta}_{(a)} = \Delta\underline{\eta}'_{(a)} = \cdots = inv. \tag{34}$$

The (32) gives the second (ii) founding property that the bilinear combination $\underline{\theta}\,\underline{\bar\theta}$ is a constant:

$$\text{(ii)}\quad c = \underline{\theta}\,\underline{\bar\theta} = \underline{\theta}'\,\underline{\bar\theta}' = \cdots = const. \tag{35}$$

The latter yields a second postulate of SR (Einstein's postulate) - *the velocity of light, c, in free space appears the same to all observers regardless the relative motion of the source of light and the observer.* The c is the maximum attainable velocity (32) for uniform motion of a particle in Minkowski background space, M_4. Equally noteworthy is the fact that (34) and (35) combined yield *invariance of the element of interval between two events* $\Delta x = k\Delta\underline{\eta}_{(a)}$ *(for given integer number k) with respect to the Lorentz transformation*:

$$\begin{aligned}&k^2\Delta\underline{\eta}^2_{(a)} = (c^2 - \underline{v}_1^2)\Delta t^2 = (c^2 - \vec v^{\,2})\Delta t^2 = (\Delta x^0)^2 - (\Delta\vec x)^2 \equiv (\Delta s)^2 = (\Delta x'^0)^2 -\\ &(\Delta\vec x)'^2 \equiv (\Delta s')^2 = \cdots = inv.,\end{aligned} \tag{36}$$

where $x^0 = ct, \quad x^{0'} = ct', \ldots.$ We have here introduced a notion of physical relative finite *time intervals* between two events $\Delta t = k\tau/\sqrt{2}$, $\Delta t' = k\tau'/\sqrt{2}, \ldots.$

3. Accelerated motion and local $\widetilde{MS}_p$-SUSY

On the premises of Section 2, in what follows, we address the *accelerated motion and inertia effects* in the framework of *local* $\widetilde{MS}_p$-SUSY.

In case of an accelerated ($a = |\vec a| \neq 0$) motion of a particle in M_4, according to (27), we have then

$$\begin{aligned}&\tfrac{i}{\sqrt{2}}\left(\underline{\theta}\,\sigma^3\tfrac{d^2\bar\xi}{dt^2} - \tfrac{d^2\xi}{dt^2}\sigma^3\underline{\bar\theta}\right) = \tfrac{d^2q}{dt^2} = a = \tfrac{1}{\sqrt{2}}\left(\tfrac{d^2\eta^{(+)}}{dt^2} - \tfrac{d^2\eta^{(-)}}{dt^2}\right) =\\ &\tfrac{1}{\sqrt{2}}\left(a^{(+)} - a^{(-)}\right), \quad a^{(\pm)} = \tfrac{dv^{(\pm)}}{dt}.\end{aligned} \tag{37}$$

So, we may relax the condition $\partial_{\hat m}\epsilon = 0$ and promote this symmetry to a local supersymmetry in which the parameter $\epsilon = \epsilon(X^{\hat m})$ depends explicitly on $X^{\hat m} = (\widetilde{x}^m,\, \widetilde{\underline{\eta}}^m)$, where $\widetilde{x}^m \in \widetilde{M}_4$ and $\widetilde{\underline{\eta}}^m \in \widetilde{\underline{M}}_2$. The

doi: https://doi.org/10.52526/25792776-23.70.2-212

mathematical structure of the local $\widetilde{MS}_p$-SUSY theory has much in common with those used in the geometrical framework of standard supergravity theories. Such a local SUSY can already be read off from the algebra (21) in the form

$$[\epsilon(X)Q,\, \bar{Q}\bar{\epsilon}(X)] = 2\epsilon(X)\sigma^{\hat{m}}\bar{\epsilon}(X)\widetilde{p}_{\hat{m}}, \tag{38}$$

which says that the product of two supersymmetry transformations corresponds to a translation in space-time of which the four momentum $\widetilde{p}_{\hat{m}}$ is the generator. In accord, the transformation (22) is expected to be somewhat of the form

$$[\delta_{\epsilon_1(X)},\, \delta_{\epsilon_2(X)}]V \sim \epsilon_1(X)\sigma^{\hat{m}}\bar{\epsilon}_2(X)\,\partial_{\hat{m}}V, \tag{39}$$

that differ from point to point, namely this is the notion of a general coordinate transformation. Whereupon we see that for the local $\widetilde{MS}_p$-SUSY to exist it requires the background spaces $(\widetilde{M}_4,\, \widetilde{\underline{M}}_2)$ to be curved. Thereby, the space $\widetilde{M}_4$, in order to become on the same footing with the distorted space $\widetilde{\underline{M}}_2$, refers to the accelerated proper reference frame of a particle, without relation to other matter fields. A useful guide in the construction of local superspace is that it should admit rigid superspace as a limit. The reverse is also expected, since if one starts with a constant parameter ϵ (20) and performs a local Lorentz transformation, then this parameter will in general become space-time dependent as a result of this Lorentz transformation.

Supergravity theories have been successfully formulated in terms of differential forms in superspace. We may introduce supergravity in a way which is manifestly covariant under such coordinate transformations. This leads us to extend the concept of differential forms to superspace. Coordinates of curved superspace are denoted

$$z^M = (X^{\hat{m}},\, \Theta,\, \bar{\Theta}) = z^{(\widetilde{M}_4)} \oplus z^{(\widetilde{\underline{M}}_2)} = (\widetilde{x}^m,\, \theta,\, \bar{\theta}) \oplus (\widetilde{\eta}^{\underline{m}},\, \underline{\theta},\, \bar{\underline{\theta}}), \tag{40}$$

and differential elements

$$dz^M = (dX^{\hat{m}},\, d\Theta,\, d\bar{\Theta}) = dz^{(\widetilde{M}_4)} \oplus dz^{(\widetilde{\underline{M}}_2)} = (d\widetilde{x}^m,\, d\theta,\, d\bar{\theta}) \oplus (d\widetilde{\eta}^{\underline{m}},\, d\underline{\theta},\, d\bar{\underline{\theta}}), \tag{41}$$

where $M \equiv (\hat{m}, \hat{\mu}, \hat{\dot{\mu}})$, $\hat{m} \equiv (m, \underline{m})$, $\Theta^{\hat{\mu}} \equiv (\theta^{\mu}, \underline{\theta}^{\underline{\mu}})$ and $\bar{\Theta}_{\hat{\dot{\mu}}} \equiv (\bar{\theta}_{\dot{\mu}}, \bar{\underline{\theta}}_{\underline{\dot{\mu}}})$. The $\hat{\mu}$ are all upper indices, while $\hat{\dot{\mu}}$ is a lower index. Elements of superspace obey the following multiplication law:

$$z^M z^N = (-1)^{nm} z^N z^M. \tag{42}$$

Here n is a function of N and m is a function of M. These functions take the values zero or one, depending on whether N and M are vector or spinor indices. Exterior products in superspace are defined in complete analogy to ordinary space:

$$\begin{aligned} &dz^M \wedge z^N = -(-1)^{nm} dz^N \wedge dz^M, \\ &dz^M z^N = (-1)^{nm} dz^N \wedge z^M. \end{aligned} \tag{43}$$

With this definition, differential forms have a standard extension to superspace. The differentials are written to the left of the coefficient function and the indices are labeled in such a way that there is always an even number of indices between those being summed. We shall, as usual, drop the symbol $\wedge$ for exterior multiplication. Functions of the superspace variable z are called zero-forms. Having defined superspace forms, we must also introduce exterior derivatives. Exterior derivatives map zero-forms into one-forms. Equations written in terms of differential forms and exterior derivatives are covariant under coordinate changes. Objects which transform linearly under a representation of the structure group are called tensors. Note that exterior derivatives do not map tensors into tensors. Connections are Lie algebra valued one-forms. The curvature tensor is a Lie algebra valued two-form. The curvature form and the covariant derivative of a tensor are, in general, the only tensorial quantities which may be constructed by taking derivatives. Higher derivatives lead to identities (and not to new tensors) because of the fact that $dd = 0$. These identities are called Bianchi identities. Bianchi identities of the first type are found from the covariant derivative. Bianchi identities of the second type are found from the curvature form. Here we shall forbear to write the details out as the standard theory is so well known. Together with other details of the theory, they can be seen in the textbooks, e.g. (Wess & Bagger, 1983, West, 1987).

Similar to (26), the multiplication of two local successive supersymmetric transformations induces the motion

$$\begin{aligned} &g(0,\, \epsilon(X),\, \bar{\epsilon}(X))\,\Omega(X^{\hat{m}},\, \Theta,\, \bar{\Theta}) \longrightarrow \\ &(X^{\hat{m}} + i\,\Theta\,\sigma^{\hat{m}}\,\bar{\epsilon}(X) - i\,\epsilon(X)\,\sigma^{\hat{m}}\,\bar{\Theta},\, \Theta + \epsilon(X),\, \bar{\Theta} + \bar{\epsilon}(X)). \end{aligned} \tag{44}$$

In its simplest version, supergravity was conceived as a quantum field theory whose action included the gravitation field term, where the graviton coexists with a fermionic field called gravitino, described by the

doi: https://doi.org/10.52526/25792776-23.70.2-212

Rarita-Scwinger kinetic term. The two fields differ in their spin: 2 for the graviton, 3/2 for the gravitino. The different 4D $N=1$ supergravity multiplets all contain the graviton and the gravitino, but differ by their systems of auxiliary fields. For a detailed discussion we refer to the papers by (Binetruy et al., 2001, Fayet & Ferrara, 1977, Jacob, 1987, Nilles, 1984, Wess & Bagger, 1983, West, 1987, van Nieuwenhuizen, 1981, van Nieuwenhuizen et al., 1976). These fields would transform into each other under local supersymmetry. We may use the usual language which is almost identical to the vierbien formulation of GR with some additional input. In this framework supersymmetry and general coordinate transformations are described in a unified way as certain diffeomorphisms. The motion (44) generates certain coordinate transformations:

$$z^M \longrightarrow z'^M = z^M - \zeta^M(z), \tag{45}$$

where $\zeta^M(z)$ arc arbitrary functions of z. The dynamical variables of superspace formulation are the frame field $E^A(z)$ and connection Ω. Using the analogue of Cartan's local frame, the superspace $(z^M,\,\Theta,\,\bar\Theta)$ has at each point a tangent superspace spanned by the frame field defined as a 1-form over superspace

$$E^A(z) = dz^M E_M^A(z), \tag{46}$$

with coefficient superfields, generalizing the usual frame, namely supervierbien $E_M^A(z)$. Here, we use the first half of capital Latin alphabet $A, B, \ldots$ to denote the anholonomic indices related to the tangent superspace structure group, which is taken to be just the Lorentz group. The inverse vielbein $E_A{}^M(z)$ is defined by the relations

$$E_M^A(z) E_A{}^N(z) = \delta_M^N, \quad E_A{}^M(z) E_M^B(z) = \delta_A{}^B, \tag{47}$$

where

$$\delta_M^N = \begin{pmatrix} \delta_{\hat m}^{\hat n} & 0 & 0 \\ 0 & \delta_{\hat\mu}{}^{\hat\nu} & 0 \\ 0 & 0 & \delta_{\dot{\hat\mu}}{}^{\dot{\hat\nu}} \end{pmatrix}, \tag{48}$$

The formulation of supergravity in superspace provides a unified description of the vierbein and the Rarita-Schwinger fields, which are identified in a common geometric object, the local frame $E^A(z)$ of superspace. They are manifestly coordinate independent. The upper index A is reserved for the structure group, for which we take the Lorentz group. This is because we would like to recover supersymmetric flat space as a solution to our dynamical theory. With this choice, the reference frame defined by the vielbein is locally Lorentz covariant.

$$\delta E^A = E^B L_B^A(z), \quad \delta E_M^A = E_M^B L_B^A(z). \tag{49}$$

The indices transforming under the structure group will be called Lorentz indices. The Lorentz generators $L_B^A(z)$ have three irreducible components: $L_{\hat b}{}^{\hat a}, L_\beta{}^\alpha$ and $L^{\dot\beta}{}_{\dot\alpha}$. The vielbein forms $E^{\hat a} = dz^M E_M^{\hat a}$, $E^{\hat\alpha} = dz^M E_M^{\hat\alpha}$, and $E_{\dot{\hat\alpha}} = dz^M E_{M\dot{\hat\alpha}}$ are coordinate-independent irreducible Lorentz tensors.

To formulate covariant derivatives one must introduce a connection form

$$\phi = dz^M \phi_M, \quad \phi_M = \phi_{MA}^B, \tag{50}$$

transforming as follows under the structure group:

$$\delta\phi = \phi L - L\phi - dL. \tag{51}$$

Connections are Lie algebra valued one-forms

$$\phi = dz^M \phi_M^r(z) i T^r, \tag{52}$$

with the following transformation law:

$$\phi' = X^{-1}\phi X - X^{-1} dX, \tag{53}$$

where r runs over the dimension of the algebra. The connection is the second dynamical variable in this theory. The ϕ_{MA}^B is Lie algebra valued in its two Lorentz indices:

$$\phi_{MAB} = -(-1)^{ab}\phi_{MBA}. \tag{54}$$

doi: https://doi.org/10.52526/25792776-23.70.2-212

The covariant derivative of the vielbein is called torsion:

$$T^A = dE^A + E^B\phi_B{}^A. \tag{55}$$

In flat space it is possible to transform the vielbein into the global reference frame: $E^A = e^A$. It is defined up to rigid Lorentz transformations. In this frame the connection vanishes: $\phi = 0$. The torsion, however, is non-zero because of the following non-zero components:

$$T_{\hat{\alpha}\hat{\dot{\beta}}}{}^{\hat{c}} = T_{\hat{\dot{\beta}}\hat{\alpha}}{}^{\hat{c}} = 2i\sigma_{\hat{\alpha}\hat{\dot{\beta}}}{}^{\hat{c}}. \tag{56}$$

The curvature tensor is defined in terms of the connection:

$$R = d\phi + \phi\phi. \tag{57}$$

It is a Lie algebra valued two-form:

$$R_A{}^B = \tfrac{1}{2}dz^M dz^N R_{NMA}{}^B. \tag{58}$$

Covariant derivatives with respect to local Lorentz transformations are constructed by means of the spin connection Ω, which is a 1-form in superspace. Supergauge transformations are constructed from the general coordinate and structure group transformations of superspace:

$$L_B{}^A = -\zeta^C\phi_{CB}{}^A. \tag{59}$$

They amount to a convenient reparametrization of these transformations. Supergauge transformations map Lorentz tensors into Lorentz tensors and reduce to supersymmetry transformations in the limit of flat space. The parameter ζ characterizes infinitesimal changes in coordinates. Whereas, either ζ^A or ζ^M may be chosen as the field-independent transformation parameter. Its companion then depends on the fields through the vielbein. Since we would like Lorentz tensors to transform into Lorentz tensors, we shall choose ζ^A to be field-independent. Supergauge transformations consist of a general coordinate transformation with field-independent parameter ζ^A followed by a structure group Lorentz transformation with field-dependent parameter (68). It is among this restricted class of transformations that we shall find the gauged supersymmetry transformations.

The super-vielbein $E_M{}^A$ and spin-connection Ω contain many degrees of freedom. Although some of these are removed by the tangent space and supergeneral coordinate transformations, there still remain many degrees of freedom. There is no general prescription for deducing necessary covariant constraints which if imposed upon the superfields of super-vielbein and spin-connection will eliminate the component fields. However, some usual constraints can be found using tangent space and supergeneral coordinate transformations of the torsion and curvature covariant tensors, given in appropriate super-gauge. The transformation parameters ζ^A and $L_{\hat{a}\hat{b}}$ are functions of superspace. Their lowest components characterize general coordinate transformations in six-dimensional X-space $[\zeta^{\hat{a}}(X^{\hat{m}})]$, gauged supersymmetry transformations $[\zeta^{\hat{\alpha}}(X)], \zeta_{\hat{\dot{\alpha}}}(X)]$, and local Lorentz transformations $L_{\hat{a}\hat{b}}(X)$. We will use their higher components to transform away certain $\Theta = \bar{\Theta} = 0$ components of the vielbein and the connection. Let us consider the vielbein. Its transformation law may be written as a super-gauge transformation together with an additional Lorentz transformation $L_B{}^A$:

$$\delta_\zeta E_M{}^A = -\mathcal{D}_M\zeta^A - \zeta^B T_{BM}{}^A + E_M{}^B L_B{}^A. \tag{60}$$

The lowest component of this equation gives the transformation property of $E_M{}^A|_{\Theta=\bar{\Theta}=0}$. Higher components of ζ^A enter $\delta E_M{}^A|$ through the covariant derivatives $\mathcal{D}_{\hat{\mu}}\zeta^A$ and $\bar{\mathcal{D}}^{\hat{\dot{\mu}}}\zeta^A$. One may use these higher components to transform super-vielbein to the final form, see e.g. (Wess & Bagger, 1983), where the minimum number of independent component fields are the graviton, $e_{\hat{m}}{}^{\hat{a}}(X)$, and the gravitino, $\psi_{\hat{m}}{}^{\hat{\alpha}}(X), \bar{\psi}_{\hat{m}\hat{\dot{\alpha}}}(X)$. Since

$$E_A{}^M(z)\big|_{\Theta=\bar{\Theta}=0} = E_{\underline{a}}{}^{\underline{m}}(z^{(\widetilde{\underline{M}}_2)})\Big|_{\underline{\theta}=\bar{\underline{\theta}}=0} \oplus E_a{}^m(z^{(\widetilde{M}_4)})\Big|_{\theta=\bar{\theta}=0}, \tag{61}$$

doi: https://doi.org/10.52526/25792776-23.70.2-212

accordingly, we find

$$E_{\underline{a}}{}^{\underline{m}}(z^{(\underline{\widetilde{M}}_2)})\Big|_{\underline{\theta}=\underline{\bar{\theta}}=0} = \begin{pmatrix} e_{\underline{m}}{}^{\underline{a}}(\widetilde{\eta}) & \frac{1}{2}\psi_{\underline{m}}{}^{\underline{\alpha}}(\widetilde{\eta}) & \frac{1}{2}\bar{\psi}_{\underline{m}\,\underline{\dot{\alpha}}}(\widetilde{\eta}) \\ 0 & \delta_{\underline{\mu}}{}^{\underline{\alpha}} & 0 \\ 0 & 0 & \delta^{\underline{\dot{\mu}}}{}_{\underline{\dot{\alpha}}} \end{pmatrix},$$

$$E_a{}^m(z^{(\widetilde{M}_4)})\Big|_{\theta=\bar{\theta}=0} = \begin{pmatrix} e_m{}^a(x) & \frac{1}{2}\psi_m{}^\alpha(x) & \frac{1}{2}\bar{\psi}_{m\dot{\alpha}}(x) \\ 0 & \delta_\mu{}^\alpha & 0 \\ 0 & 0 & \delta^{\dot{\mu}}{}_{\dot{\alpha}} \end{pmatrix}. \tag{62}$$

The fields of graviton and gravitino cannot be gauged away. Provided, we have

$$e_{\hat{a}}{}^{\hat{m}}e_{\hat{m}}{}^{\hat{b}} = \delta_{\hat{a}}^{\hat{b}}, \quad \psi_{\hat{a}}{}^{\hat{\mu}} = e_{\hat{a}}{}^{\hat{m}}\psi_{\hat{m}}{}^{\hat{\alpha}}\delta_{\hat{\alpha}}^{\hat{\mu}}, \quad \bar{\psi}_{\hat{a}\hat{\dot{\mu}}} = e_{\hat{a}}{}^{\hat{m}}\bar{\psi}_{\hat{m}\hat{\dot{\alpha}}}\delta^{\hat{\dot{\mu}}}{}_{\hat{\dot{\alpha}}}. \tag{63}$$

The tetrad field

$$e_{\hat{m}}^{\hat{a}}(X) = (e_{\underline{m}}^{\underline{a}}(\widetilde{\eta}), e_m{}^a(x))$$

plays the role of a gauge field associated with local transformations. The Majorana type field

$$\frac{1}{2}\psi_{\hat{m}}{}^{\hat{\alpha}} = \frac{1}{2}(\psi_{\underline{m}}{}^{\underline{\alpha}}(\widetilde{\eta}), \psi_m{}^\alpha(x))$$

is the gauge field related to local supersymmetry. These two fields belong to the same supergravity multiplet which also accommodates auxiliary fields so that the local supersymmetry algebra closes. Under infinitesimal transformations of local supersymmetry, they transformed as

$$\begin{aligned} \delta e_{\hat{m}}^{\hat{a}} &= i(\psi_{\hat{m}}\sigma^{\hat{a}}\zeta - \zeta\sigma^{\hat{a}}\bar{\psi}_{\hat{m}}), \\ \delta\psi_{\hat{m}} &= -2\mathcal{D}_{\hat{m}}\zeta^{\hat{\alpha}} + ie_{\hat{m}}^{\hat{c}}\{\tfrac{1}{3}M(\varepsilon\sigma_{\hat{c}}\bar{\zeta})^{\hat{\alpha}} + b_{\hat{c}}\zeta^{\hat{\alpha}} + \tfrac{1}{3}b^{\hat{d}}(\zeta\sigma_{\hat{d}}\bar{\sigma}_{\hat{c}})\}, \end{aligned} \tag{64}$$

etc., where $M(X) = -6R(z)|_{\Theta=\bar{\Theta}=0}$ and $b_{\hat{a}}(X) = -3G(z)|_{\Theta=\bar{\Theta}=0}$ are the auxiliary fields, and

$$\begin{aligned} &\zeta^{\hat{\alpha}}(z) = \zeta^{\hat{\alpha}}(X), \quad \bar{\zeta}^{\hat{\alpha}}(z) = \bar{\zeta}^{\hat{\alpha}}(X), \\ &\zeta^{\bar{a}}(z) = 2i[\Theta\sigma^{\hat{a}}\bar{\zeta}(X) - \zeta(X)\sigma^{\hat{a}}\bar{\Theta}]. \end{aligned} \tag{65}$$

These auxiliary fields are not restricted by any differential equations in X-space.

4. Non-trivial linear representation of the $\widetilde{MS}_p$-SUSY algebra

With these guidelines to follow, we start by considering the simplest example of a supersymmetric theory in six dimensional background curved spaces $\widetilde{M}_4 \oplus \underline{\widetilde{M}}_2$ as the $\widetilde{MS}_p$-generalization of flat space MS$_p$-SUSY model. The chiral superfields are defined as $\bar{\mathcal{D}}_{\hat{\dot{\alpha}}}\Phi = 0$, which reduces to $\bar{D}_{\hat{\dot{\alpha}}}\Phi = 0$ in flat space. To obtain a feeling for this model we may consider first example of non-trivial linear representation $(\widehat{\chi}, \mathcal{A}, \mathcal{F})$, of the $\widetilde{MS}_p$-SUSY algebra. This has $N = 1$ and $s_0 = 0$, and contains two Weyl spinor states of a massive Majorana spinor $\widehat{\chi}(\chi,\, \underline{\chi})$, two complex scalar fields $\mathcal{A}(A,\, \underline{A})$, and two more real scalar degrees of freedom in the complex auxiliary fields $\mathcal{F}(F,\, \underline{F})$, which provide in supersymmetry theory the fermionic and bosonic degrees of freedom to be equal off-shell as well as on-shell, and are eliminated when one goes on-shell. The component multiplets, $(\widehat{\chi}, \mathcal{A}, \mathcal{F})$, are called the chiral or scalar multiplets. We could define the component fields as the coefficient functions of a power series expansion in Θ and $\bar{\Theta}$. This decomposition, however, is coordinate-dependent. It is, therefore, more convenient to define them as

$$\mathcal{A} = \Phi|_{\Theta=\bar{\Theta}=0}\,, \quad \widehat{\chi}_{\hat{\alpha}} = \tfrac{1}{\sqrt{2}}\mathcal{D}_{\hat{\alpha}}\,\Phi|_{\Theta=\bar{\Theta}=0}\,, \quad \mathcal{F} = -\tfrac{1}{4}\mathcal{D}^{\hat{\alpha}}\mathcal{D}_{\hat{\alpha}}\,\Phi|_{\Theta=\bar{\Theta}=0}\,, \tag{66}$$

which carry Lorentz indices. They are related to the Θ and $\bar{\Theta}$ expansion coefficients through a transformation which depends on the supergravity multiplet. The transformation laws of the component fields are found from the transformation law of the superfield Φ:

$$\delta\Phi = -\zeta^A\mathcal{D}_A\Phi, \tag{67}$$

doi: https://doi.org/10.52526/25792776-23.70.2-212

provided, the parameters ζ^A are specified as (65). Under infinitesimal transformations of local supersymmetry, the transformation law of the chiral multiplet (see e.g. Wess & Bagger (1983),), incorporating with embedding map $\underline{\widetilde{M}}_2 \hookrightarrow \widetilde{M}_4$, which is the map (2) rewritten for curved spaces $\underline{\widetilde{M}}_2$ and $\widetilde{M}_4$, and the transformation law $\underline{A}(\widetilde{\eta}) = A(\widetilde{x}$ (5) for spin-zero scalar field, give

$$
\begin{aligned}
&\delta \underline{A} = -\sqrt{2}\zeta^\alpha \chi_\alpha, \\
&\delta \chi_\alpha = -\sqrt{2}\zeta_\alpha F - i\sqrt{2}\sigma_{\alpha\dot\beta}{}^{a}\bar\zeta^{\dot\beta}\widehat{D}_a \underline{A}, \\
&\delta F = -\frac{\sqrt{2}}{3} M^* \zeta^\alpha \chi_\alpha + \bar\zeta^{\dot\alpha}\left(\frac{1}{6}\sqrt{2} b_{\alpha\dot\alpha}\chi^\alpha - i\sqrt{2}\widehat{D}_{\alpha\dot\alpha}\chi^\alpha\right),
\end{aligned}
\tag{68}
$$

where

$$
\begin{aligned}
&\widehat{D}_a \underline{A} \equiv e_a{}^m \left[\left(\frac{\partial \widetilde{x}^0}{\partial \widetilde{x}^m}\right)\widetilde{\partial}_{\underline{0}}\,\underline{A} + \left(\frac{\partial |\vec{\widetilde{x}}|}{\partial \widetilde{x}^m}\right)\widetilde{\partial}_{\underline{1}}\,\underline{A} - \frac{1}{\sqrt{2}}\psi_m{}^\mu \chi_\mu\right], \\
&\widehat{D}_a \chi_\alpha = e_a{}^m\left(\mathcal{D}_m \chi_\alpha - \frac{1}{\sqrt{2}}\psi_{m\alpha}F - \frac{i}{\sqrt{2}}\bar\psi_m{}^{\dot\beta}\widehat{D}_{\alpha\dot\beta}\underline{A}\right).
\end{aligned}
\tag{69}
$$

In the same way, we should define the spinor $\underline{\chi}$ as the field into which $A(x)$ transforms. In this case, the infinitesimal supersymmetry transformations for $Q = \underline{q}$ read

$$
\begin{aligned}
&\delta A = -\sqrt{2}\underline{\zeta}^{\underline{\alpha}}\underline{\chi}_{\underline{\alpha}}, \\
&\delta \underline{\chi}_{\underline{\alpha}} = -\sqrt{2}\underline{\zeta}_{\underline{\alpha}}\underline{F} - i\sqrt{2}\sigma_{\underline{\alpha}\underline{\dot\beta}}{}^{\underline{a}}\underline{\bar\zeta}^{\underline{\dot\beta}}\widehat{D}_{\underline{a}}A, \\
&\delta \underline{F} = -\frac{\sqrt{2}}{3}\underline{M}^*\underline{\zeta}^{\underline{\alpha}}\underline{\chi}_{\underline{\alpha}} + \underline{\bar\zeta}^{\underline{\dot\alpha}}\left(\frac{1}{6}\sqrt{2}\underline{b}_{\underline{\alpha}\underline{\dot\alpha}}\underline{\chi}^{\underline{\alpha}} - i\sqrt{2}\widehat{D}_{\underline{\alpha}\underline{\dot\alpha}}\underline{\chi}^{\underline{\alpha}}\right),
\end{aligned}
\tag{70}
$$

where

$$
\begin{aligned}
&\widehat{D}_{\underline{a}} A \equiv \underline{e}_{\underline{a}}{}^{\underline{m}}\left[\left(\frac{\partial \widetilde{x}^0}{\partial \underline{\widetilde{x}}^{\underline{m}}}\right)\widetilde{\partial}_0\, A + \left(\frac{\partial \widetilde{x}^i}{\partial \underline{\widetilde{x}}^{\underline{m}}}\right)\widetilde{\partial}_i\, A - \frac{1}{\sqrt{2}}\underline{\psi}_{\underline{m}}{}^{\underline{\mu}}\underline{\chi}_{\underline{\mu}}\right], \\
&\widehat{D}_{\underline{a}}\chi_{\underline{\alpha}} = \underline{e}_{\underline{a}}{}^{\underline{m}}\left(\mathcal{D}_{\underline{m}}\underline{\chi}_{\underline{\alpha}} - \frac{1}{\sqrt{2}}\underline{\psi}_{\underline{m}\,\underline{\alpha}}\underline{F} - \frac{i}{\sqrt{2}}\underline{\bar\psi}_{\underline{m}}{}^{\underline{\dot\beta}}\widehat{D}_{\underline{\alpha}\underline{\dot\beta}}A\right).
\end{aligned}
\tag{71}
$$

The graviton and the gravitino form thus the basic multiplet of local $\widetilde{MS}_p$-SUSY, and one expects the simplest locally supersymmetric model to contain just this multiplet. The spin 3/2 contact term in total Lagrangian arises from equations of motion for the torsion tensor, and that the original Lagrangian itself takes the simpler interpretation of a minimally coupled spin (2, 3/2) theory.

5. Inertial effects

We would like to place the emphasis on the essential difference arisen between the standard supergravity theories and some rather unusual properties of local $\widetilde{MS}_p$-SUSY theory. In the framework of the standard supergravity theories, as in GR, a curvature of the space-time acts on all the matter fields. The source of graviton is the energy-momentum tensor of matter fields, while the source of gravitino is the spin-vector current of supergravity. In the local $\widetilde{MS}_p$-SUSY theory, unlike the supergravity, instead we argue that a deformation/(distortion of local internal properties) of MS_p, is the origin of the *absolute acceleration* ($\vec{a}_{abs} \neq 0$) and inertia effects (*fictitious graviton*). This refers to the particle of interest itself, without relation to other matter fields, so that this can be globally removed by appropriate coordinate transformations. A next member of the basic multiplet of local $\widetilde{MS}_p$-SUSY -*fictitious gravitino*, will be arisen under infinitesimal transformations of local supersymmetry, because the $\widetilde{MS}_p$-SUSY is so constructed as to make these two particles just as being the two bosonic and fermionic states in the curved background spaces $\widetilde{M}_4$ and $\underline{\widetilde{M}}_2$, respectively, or vice versa. Whereas, in order to become on the same footing with the distorted space $\underline{\widetilde{M}}_2$, the space $\widetilde{M}_4$ refers only to the accelerated proper reference frame of a particle. With these physical requirements, a standard Lagrangian consisted of the gravitation field Lagrangian plus a part which contains the Rarita-Schwinger field, and coupling of supergravity with matter superfields evidently no longer holds. Instead we are now looking for an alternative way of implications of local $\widetilde{MS}_p$-SUSY for the model of accelerated motion and inertial effects. For example, we may with equal justice start from the reverse, which as we mentioned before is also expected. If one starts with a constant parameter ϵ (20) and performs a local Lorentz transformation, which can only be implemented if MS and space-time are curved (deformed/distorted) ($\widetilde{M}_2$, $\widetilde{M}_4$), then this parameter will in general become space-time dependent as a result of this Lorentz transformation, which readily implies *local* $\widetilde{MS}_p$-SUSY. In going into practical details of the realistic local $\widetilde{MS}_p$-SUSY model, it remains to derive the explicit form of the

doi: https://doi.org/10.52526/25792776-23.70.2-212

vierbien $e_{\hat{m}}^{\;\hat{a}}(\varrho) \equiv (e_m^{\;a}(\varrho),\, e_{\underline{m}}^{\;\underline{a}}(\varrho))$, which describes *fictitious graviton* as a function of *local rate* $\varrho(\eta, m, f)$ of instantaneously change of the velocity $v^{(\pm)}$ of massive (m) test particle under the unbalanced net force (f). We, of course, does not profess to give any clear-cut answers to all the problems addressed, the complete picture of which, of course, is largely beyond the scope of present paper. In particular, the latter does not allows us to offer here a straightforward recipe for deducing the vierbien $e_{\hat{m}}^{\;\hat{a}}(\varrho)$ in the framework of quantum field theory of $\widetilde{MS}_p$-supergravity, where the accelerated frame has to be described as the frame that has torsion. This will be a separate topic for research in a subsequent paper. Therefore, cutting short where our analysis is leading to, instead we now turn to recently derived by Ter-Kazarian (2012) the vierbien $e_{\hat{m}}^{\;\hat{a}}(\varrho)$ in the framework of classical physics. Together with other usual aspects of the theory, the latter illustrates a possible solution to the problems of inertia behind spacetime deformations. It was argued that a deformation/(distortion of local internal properties) of $\underline{M}_2$ is the origin of inertia effects that can be observed by us. Consequently, the next member of the basic multiplet of local $\widetilde{MS}_p$-SUSY -*fictitious gravitino*, $\psi_{\hat{m}}^{\;\alpha}(\varrho)$, will be arisen under infinitesimal transformations of local supersymmetry (64), provided by the local parameters $\zeta^M(a)$ (45).

For brevity reason, we shall forbear here review of certain essential theoretical aspects of a general *distortion of local internal properties of MS_p*, formulated in the framework of classical physics by Ter-Kazarian (2012). But for the self-contained arguments, the interested reader is invited to consult the original paper.

6. Model building in the 4D background Minkowski space-time

In this section, we briefly discuss the RTI in particular case when the relativistic test particle accelerated in the background flat M_4 space under an unbalanced net force other than gravitational, but we refer to the original paper for more details. To make the remainder of our discussion a bit more concrete, it proves necessary to provide, further, a constitutive ansatz of simple, yet tentative, linear *distortion transformations* of the basis $\underline{e}_{\underline{m}}$ at the point of interest in flat space $\underline{M}_2$, which can be written in terms of *local rate* $\varrho(\eta, m, f)$ of instantaneously change of the measure $\underline{v}^{\underline{m}}$ of massive test particle under the unbalanced net force (f) (Ter-Kazarian, 2012):

$$\begin{aligned} e_{(\tilde{+})}(\varrho) &= D_{(\tilde{+})}^{\;\underline{m}}(\varrho)\, \underline{e}_{\underline{m}} = \underline{e}_{(+)} - \varrho(\eta, m, f)\, \underline{v}^{(-)}\, \underline{e}_{(-)}, \\ e_{(\tilde{-})}(\varrho) &= D_{(\tilde{-})}^{\;\underline{m}}(\varrho)\, \underline{e}_{\underline{m}} = \underline{e}_{(-)} + \varrho(\eta, m, f)\, \underline{v}^{(+)}\, \underline{e}_{(+)}, \end{aligned} \tag{72}$$

Clearly, these transformations imply a violation of relation $e^2_{\underline{\mu}}(\varrho) \neq 0$ for the null vectors $\underline{e}_{\underline{m}}$. The norm in the resulting general deformed/distorted space $\widetilde{\mathcal{M}}_2$ now can be rewritten in terms of space-time variables as

$$id = e\,\vartheta \equiv d\widetilde{\widetilde{q}} = \widetilde{e}_0 \otimes d\widetilde{t} + \widetilde{e}_q \otimes d\widetilde{q}, \tag{73}$$

where $\widetilde{e}_0$ and $\widetilde{e}_q$ are, respectively, the temporal and spatial basis vectors in $\widetilde{\mathcal{M}}_2$:

$$\widetilde{e}_0(\varrho) = \tfrac{1}{\sqrt{2}}\left[e_{(\tilde{+})}(\varrho) + e_{(\tilde{-})}(\varrho)\right], \quad \widetilde{e}_q(\varrho) = \tfrac{1}{\sqrt{2}}\left[e_{(\tilde{+})}(\varrho) - e_{(\tilde{-})}(\varrho)\right]. \tag{74}$$

Hence, in the framework of the space-time deformation/distortion theory (Ter-Kazarian, 2012), we can compute the general metric $\widetilde{g}$ as

$$\widetilde{g} = g_{\tilde{r}\tilde{s}}\, d\widetilde{q}^{\tilde{r}} \otimes d\widetilde{q}^{\tilde{s}}, \tag{75}$$

provided

$$g_{\tilde{0}\tilde{0}} = (1 + \tfrac{\varrho v_q}{\sqrt{2}})^2 - \tfrac{\varrho^2}{2}, \quad g_{\tilde{1}\tilde{1}} = -(1 - \tfrac{\varrho v_q}{\sqrt{2}})^2 + \tfrac{\varrho^2}{2}, \quad g_{\tilde{1}\tilde{0}} = g_{\tilde{0}\tilde{1}} = -\sqrt{2}\varrho. \tag{76}$$

We suppose that a second observer, who makes measurements using a frame of reference $\widetilde{S}_{(2)}$ which is held stationary in curved (deformed/distorted) master space $\widetilde{\mathcal{M}}_2$, uses for the test particle the corresponding space-time coordinates $\widetilde{q}^{\tilde{r}}\left((\widetilde{q}^{\tilde{0}},\, \widetilde{q}^{\tilde{1}}) \equiv (\widetilde{t},\, \widetilde{q})\right)$. The very concept of the local *absolute acceleration* (in Newton's terminology) is introduced by Ter-Kazarian (2012), brought about via the Fermi-Walker transported frames as

$$\vec{a}_{abs} \equiv \vec{e}_q\, \tfrac{d(\varrho)}{\sqrt{2}ds_q} = \vec{e}_q \, |\tfrac{de_{\hat{0}}}{ds}| = \vec{e}_q\, |\mathbf{a}|. \tag{77}$$

doi: https://doi.org/10.52526/25792776-23.70.2-212

Here we choose the system $S_{(2)}$ in such a way as the axis $\vec{e}_q$ lies along the net 3-acceleration $(\vec{e}_q\,||\,\vec{e}_a)$, $(\vec{e}_a = \vec{a}_{net}/|\vec{a}_{net}|)$, $\vec{a}_{net}$ is the local net 3-acceleration of an arbitrary observer with proper linear 3-acceleration, $\vec{a}$, and proper 3-angular velocity, $\vec{\omega}$, measured in the rest frame: $\vec{a}_{net} = \frac{d\vec{u}}{ds} = \vec{a} \wedge \vec{u} + \vec{\omega} \times \vec{u}$, where $\mathbf{u}$ is the 4-velocity. A magnitude of $\vec{a}_{net}$ can be computed as the simple invariant of the absolute value $|\frac{d\mathbf{u}}{ds}|$ as measured in rest frame:

$$|\mathbf{a}| = |\tfrac{d\mathbf{u}}{ds}| = \left(\tfrac{du^l}{ds},\ \tfrac{du_l}{ds}\right)^{1/2}. \tag{78}$$

Following Misner et al. (1973), Synge (1960), we also define the orthonormal frame, $e_{\underline{a}}$, carried by an accelerated observer, who moves with proper linear 3-acceleration, $\vec{a}(s)$, and proper 3-rotation, $\vec{\omega}(s)$. Particular frame components are $e_{\underline{a}}$, where $\underline{a} = \hat{0}, \hat{1}$, etc. Let the zeroth leg of the frame $e_{\hat{0}}$ be 4-velocity $\mathbf{u}$ of the observer that is tangent to the worldline at a given event $x^l(s)$ and we parameterize the remaining spatial triad frame vectors $e_{\hat{i}}$, orthogonal to $e_{\hat{0}}$, also by (s). The spatial triad $e_{\hat{i}}$ rotates with proper 3-rotation $\vec{\omega}(s)$. The 4-velocity vector naturally undergoes Fermi-Walker transport along the curve C, which guarantees that $e_{\hat{0}}(s)$ will always be tangent to C determined by $x^l = x^l(s)$:

$$\frac{de_{\underline{a}}}{ds} = -\Phi\, e_{\underline{a}} \tag{79}$$

where the antisymmetric rotation tensor Φ splits into a Fermi-Walker transport part Φ_{FW} and a spatial rotation part Φ_{SR}:

$$\Phi^{lk}_{FW} = a^l u^k - a^k u^l, \quad \Phi^{lk}_{SR} = u_m \omega_n \varepsilon^{mnlk}. \tag{80}$$

The 4-vector of rotation ω^l is orthogonal to 4-velocity u^l, therefore, in the rest frame it becomes $\omega^l(0, \vec{\omega})$, and ε^{mnlk} is the Levi-Civita tensor with $\varepsilon^{0123} = -1$. So, the resulting metric (75) is reduced to

$$d\tilde{s}^2_q = \Omega^2(\overline{\varrho})\, ds^2_q, \quad \Omega(\overline{\varrho}) = 1 + \overline{\varrho}^2,\ \overline{\varrho}^2 = v^2\varrho^2, \quad \underline{v}^2 = \underline{v}^{(+)}\underline{v}^{(-)}, \quad \varrho = \sqrt{2}\int_0^{s_q} |\mathbf{a}| ds'_q. \tag{81}$$

Combining (37) and (77), we obtain

$$\varrho = \frac{i}{\gamma_q^2}\left|\left(\underline{\theta}\,\sigma^3 \frac{d\bar{\xi}}{ds_q} - \frac{d\xi}{ds_q}\sigma^3\underline{\bar{\theta}}\right)\right|, \tag{82}$$

where $\gamma_q = (1 - v_q^2)^{-1/2}$. The resulting *inertial force* $\vec{f}_{(in)}$ has computed by Ter-Kazarian (2012) as

$$\vec{f}_{(in)} = -m\,\Gamma^1_{\tilde{r}\tilde{s}}(\varrho)\frac{d\tilde{q}^{\tilde{r}}}{d\tilde{s}_q}\frac{d\tilde{q}^{\tilde{s}}}{d\tilde{s}_q} = -\frac{m\vec{a}_{abs}}{\Omega^2(\overline{\varrho})\,\gamma_q}, \tag{83}$$

Whereupon, in case of absence of rotation, the relativistic inertial force reads

$$\vec{f}_{(in)} = -\frac{1}{\Omega^2(\overline{\varrho})\,\gamma_q\gamma}[\vec{F} + (\gamma - 1)\frac{\vec{v}(\vec{v}\cdot\vec{F})}{|\vec{v}|^2}]. \tag{84}$$

Note that the inertial force arises due to *nonlinear* process of deformation of MS_p, resulting after all to *linear* relation (84). So, this also ultimately requires that MS_p should be two dimensional, because in this case we may reconcile the alluded *nonlinear* and *linear* processes by choosing the system $S_{(2)}$ in only allowed way mentioned above. At low velocities $v_q \simeq |\vec{v}| \simeq 0$ and tiny accelerations we usually experience, one has $\Omega(\overline{\varrho}) \simeq 1$, therefore the (84) reduces to the conventional non-relativistic law of inertia

$$\vec{f}_{(in)} = -m\vec{a}_{abs} = -\vec{F}. \tag{85}$$

At high velocities $v_q \simeq |\vec{v}| \simeq 1$ $(\Omega(\overline{\varrho}) \simeq 1)$, if $(\vec{v}\cdot\vec{F}) \neq 0$, the inertial force (84) becomes

$$\vec{f}_{(in)} \simeq -\frac{1}{\gamma}\vec{e}_v(\vec{e}_v\cdot\vec{F}), \tag{86}$$

and it vanishes in the limit of the photon $(|\vec{v}| = 1, m = 0)$. Thus, it takes force to disturb an inertia state, i.e. to make the *absolute acceleration* $(\vec{a}_{abs} \neq 0)$. The *absolute acceleration* is due to the real deformation/distortion of the space $\underline{M}_2$. The *relative* $(d(\tau_2\varrho)/ds_q = 0)$ acceleration (in Newton's terminology) (both magnitude and direction), to the contrary, has nothing to do with the deformation/distortion of the space $\underline{M}_2$ and, thus, it cannot produce an inertia effects.

doi: https://doi.org/10.52526/25792776-23.70.2-212

7. Beyond the hypothesis of locality

In SR an assumption is required to relate the ideal inertial observers to actual observers that are all noninertial, i.e., accelerated. Therefore, it is a long-established practice in physics to use the hypothesis of locality (Hehl & Ni, 1990, Hehl et al., 1991, Li & Ni, 1979, Mashhoon, 2002, 2011, Misner et al., 1973, Ni, 1977, Ni & Zimmermann, 1978), for extension of the Lorentz invariance to accelerated observers in Minkowski space-time. The standard geometrical structures, referred to a noninertial coordinate frame of accelerating and rotating observer in Minkowski space-time, were computed on the base of the assumption that an accelerated observer is pointwise inertial, which in effect replaces an accelerated observer at each instant with a momentarily comoving inertial observer along its wordline. This assumption is known to be an approximation limited to motions with sufficiently low accelerations, which works out because all relevant length scales in feasible experiments are very small in relation to the huge acceleration lengths of the tiny accelerations we usually experience, therefore, the curvature of the wordline could be ignored and that the differences between observations by accelerated and comoving inertial observers will also be very small. However, it seems quite clear that such an approach is a work in progress, which reminds us of a puzzling underlying reality of inertia, and that it will have to be extended to describe physics for arbitrary accelerated observers. Ever since this question has become a major preoccupation of physicists, see e.g. (Hehl et al., 1991, Maluf & Faria, 2008, Maluf et al., 2007, Marzlin, 1996, Mashhoon, 95, 1988, 1990a,b, 2002, 2011) and references therein. The hypothesis of locality represents strict restrictions, because in other words, it approximately replaces a noninertial frame of reference $\widetilde{S}_{(2)}$, which is held stationary in the deformed/distorted space $\widetilde{\mathcal{M}}_2 \equiv \underline{V}_2^{(\varrho)}\,(\varrho \neq 0)$, where $\underline{V}_2$ is the 2D semi-Riemann space, with a continuous infinity set of the inertial frames $\{S_{(2)},\, S'_{(2)},\, S''_{(2)}, ...\}$ given in the flat $\underline{M}_2\,(\varrho = 0)$. In this situation the use of the hypothesis of locality is physically unjustifiable. Therefore, it is worthwhile to go beyond the hypothesis of locality with special emphasis on distortion of $\underline{M}_2$ ($\underline{M}_2 \longrightarrow \underline{V}_2^{(\varrho)}$), which we might expect will essentially improve the standard results. Here, following (Mashhoon, 2002, Misner et al., 1973), we introduced a geodesic coordinate system - the coordinates relative to the accelerated observer (the laboratory coordinates), in the neighborhood of the accelerated path. We choose the zeroth leg of the frame, $\breve{e}_{\hat{0}}$, as before, to be the unit vector $\mathbf{u}$ that is tangent to the worldline at a given event $x^\mu(s)$, where (s) is a proper time measured along the accelerated path by the standard (static inertial) observers in the underlying global inertial frame. Following (Maluf & Faria, 2008, Maluf et al., 2007, Marzlin, 1996, Mashhoon, 95, 1988, 1990a,b, 2002, 2011), in analogy with the Faraday tensor, one can identify the antisymmetric acceleration tensor $\Phi_{ab} \longrightarrow (-\mathbf{a},\, \omega)$, with $\mathbf{a}(s)$ as the translational acceleration $\Phi_{0i} = -a_i$, and $\omega(s)$ as the frequency of rotation of the local spatial frame with respect to a nonrotating (Fermi- Walker transported) frame $\Phi_{ij} = -\varepsilon_{ijk}\,\omega^k$. The invariants constructed out of Φ_{ab} establish the acceleration scales and lengths. The hypothesis of locality holds for huge proper acceleration lengths $|I|^{-1/2} \gg 1$ and $|I^*|^{-1/2} \gg 1$, where the scalar invariants are given by $I = (1/2)\,\Phi_{ab}\,\Phi^{ab} = -\vec{a}^2 + \vec{\omega}^2$ and $I^* = (1/4)\,\Phi^*_{ab}\,\Phi^{ab} = -\vec{a}\cdot\vec{\omega}$ $(\Phi^*_{ab} = \varepsilon_{abcd}\,\Phi^{cd})$ (Mashhoon, 95, 1988, 1990a,b, 2002, 2011). Suppose the displacement vector $z^\mu(s)$ represents the position of the accelerated observer. According to the hypothesis of locality, at any time (s) along the accelerated worldline the hypersurface orthogonal to the worldline is Euclidean space and we usually describe some event on this hypersurface ("local coordinate system") at x^μ to be at $\widetilde{x}^\mu$, where x^μ and $\widetilde{x}^\mu$ are connected via $\widetilde{x}^0 = s$ and

$$x^\mu = z^\mu(s) + \widetilde{x}^i\,\bar{e}^{\,\mu}_{\,\hat{i}}(s). \tag{87}$$

Consequently, the standard metric of semi-Riemannian 4D background space $V_4^{(0)}$ in noninertial system of the accelerating and rotating observer, computed on the base of hypothesis of locality (see also Mashhoon (95, 1988, 1990a,b, 2002, 2011)), is:

$$\begin{aligned}&\widetilde{g} = \eta_{\mu\nu}\,dx^\mu \otimes dx^\nu = \left[(1+\vec{a}\cdot\vec{\widetilde{x}})^2 + (\vec{\omega}\cdot\vec{\widetilde{x}})^2 - (\vec{\omega}\cdot\vec{\omega})(\vec{\widetilde{x}}\cdot\vec{\widetilde{x}})\right] d\widetilde{x}^0 \otimes d\widetilde{x}^0 - \\ &2\,(\vec{\omega}\wedge\vec{\widetilde{x}})\cdot d\vec{\widetilde{x}} \otimes d\widetilde{x}^0 - d\vec{\widetilde{x}} \otimes d\vec{\widetilde{x}},\end{aligned} \tag{88}$$

We see that the hypothesis of locality leads to the 2D semi-Riemannian space, $V_{\underline{2}}^{(0)}$, with the incomplete metric $\widetilde{g}\quad(\varrho = 0)$:

$$\widetilde{g} = \left[(1+\widetilde{q}^{\,1}\widetilde{\varphi}_0)^2 - (\widetilde{q}^{\,1}\widetilde{\varphi}_1)^2\right] d\widetilde{q}^{\,0} \otimes d\widetilde{q}^{\,0} - 2\,(\widetilde{q}^{\,1}\widetilde{\varphi}_1)\,d\widetilde{q}^{\,1} \otimes d\widetilde{q}^{\,0} - d\widetilde{q}^{\,1} \otimes d\widetilde{q}^{\,1}, \tag{89}$$

provided,

$$\widetilde{q}^{\,1}\widetilde{\varphi}_0 = \widetilde{x}^i\,\Phi^0_i, \quad \widetilde{q}^{\,1}\widetilde{\varphi}_1 = \widetilde{x}^i\,\Phi^j_i\,\widetilde{e}^{\,-1}_j. \tag{90}$$

doi: https://doi.org/10.52526/25792776-23.70.2-212

Therefore, our strategy now is to deform the metric (89) by carrying out an additional deformation of semi-Riemannian 4D background space $V_4^{(0)} \longrightarrow \widetilde{M}_4 \equiv V_4^{(\varrho)}$, in order it becomes on the same footing with the complete metric $\widetilde{g} \quad (\varrho \neq 0)$ (75) of the distorted space $\widetilde{\underline{\mathcal{M}}}_2 \equiv \underline{V}_2^{(\varrho)}$. Let the Latin letters $\hat{r}, \hat{s}, ... = 0, 1$ be the anholonomic indices referred to the anholonomic frame $e_{\hat{r}} = e^{\tilde{s}}{}_{\hat{r}}\,\partial_{\tilde{s}}$, defined on the $\underline{V}_2^{(\varrho)}$, with $\partial_{\tilde{s}} = \partial/\partial\,\widetilde{q}^{\tilde{s}}$ as the vectors tangent to the coordinate lines. So, a smooth differential 2D-manifold $\underline{V}_2^{(\varrho)}$ has at each point $\widetilde{q}^{s}$ a tangent space $\widetilde{T}_{\widetilde{q}}\underline{V}_2^{(\varrho)}$, spanned by the frame, $\{e_{\hat{r}}\}$, and the coframe members $\vartheta^{\hat{r}} = e_{s}{}^{\hat{r}}\, d\widetilde{q}^{\tilde{s}}$, which constitute a basis of the covector space $\widetilde{T}^{\star}_{\widetilde{q}}\underline{V}_2^{(\varrho)}$. All this nomenclature can be given for $\underline{V}_2^{(0)}$ too. Then, we may compute corresponding vierbein fields $\widetilde{e}_{r}{}^{\hat{s}}$ and $e_{r}{}^{\hat{s}}$ from the equations

$$g_{\tilde{r}\tilde{s}} = \widetilde{e}_{\tilde{r}}{}^{\hat{r}'}\,\widetilde{e}_{\tilde{s}}{}^{\hat{s}'}\,o_{\hat{r}'\hat{s}'}, \quad g_{\tilde{r}\tilde{s}}(\varrho) = e_{\tilde{r}}{}^{\hat{r}'}(\varrho)\,e_{\tilde{s}}{}^{\hat{s}'}(\varrho)\,o_{\hat{r}'\hat{s}'}, \tag{91}$$

with $\widetilde{g}_{rs}$ (89) and $g_{\tilde{r}\tilde{s}}(\varrho)$ (76). Hence

$$\begin{array}{l} \widetilde{e}_{\tilde{0}}{}^{\hat{0}} = 1 + \vec{a}\cdot\vec{\widetilde{x}}, \quad \widetilde{e}_{\tilde{0}}{}^{\hat{1}} = \vec{\omega}\wedge\vec{\widetilde{x}}, \quad \widetilde{e}_{\tilde{1}}{}^{\hat{0}} = 0, \quad \widetilde{e}_{\tilde{1}}{}^{\hat{1}} = 1, \\ e_{\tilde{0}}{}^{\hat{0}}(\varrho) = 1 + \frac{\varrho v_q}{\sqrt{2}}, \quad e_{\tilde{0}}{}^{\hat{1}}(\varrho) = \frac{\varrho}{\sqrt{2}}, \quad e_{\tilde{1}}{}^{\hat{0}}(\varrho) = -\frac{\varrho}{\sqrt{2}}, \quad e_{\tilde{1}}{}^{\hat{1}}(\varrho) = 1 - \frac{\varrho v_q}{\sqrt{2}}. \end{array} \tag{92}$$

A deformation $V_4^{(0)} \longrightarrow V_4^{(\varrho)}$ is equivalent to a straightforward generalization of (87) as

$$x^{\mu} \longrightarrow x^{\mu}_{(\varrho)} = z^{\mu}_{(\varrho)}(s) + \widetilde{x}^{i}\, e^{\mu}{}_{\hat{i}}(s), \tag{93}$$

provided, as before, $\widetilde{x}^{\mu}$ denotes the coordinates relative to the accelerated observer in 4D background space $V_4^{(\varrho)}$. A displacement vector from the origin is then $dz^{\mu}_{\varrho}(s) = e^{\mu}{}_{\hat{0}}(\varrho)\,d\widetilde{x}^{0}$, Inverting $e_{r}{}^{\hat{s}}(\varrho)$ (92), we obtain $e^{\mu}{}_{\hat{a}}(\varrho) = \pi_{\hat{a}}{}^{\hat{b}}(\varrho)\,\overline{e}^{\mu}{}_{\hat{b}}$, where

$$\begin{array}{l} \pi^{\hat{0}}_{\hat{0}}(\varrho) \equiv (1 + \frac{\varrho^2}{2\gamma_q^2})^{-1}(1 - \frac{\varrho v_q}{\sqrt{2}})\,(1 + \vec{a}\cdot\vec{\widetilde{x}}), \quad \pi^{\hat{i}}_{\hat{0}}(\varrho) \equiv -(1 + \frac{\varrho^2}{2\gamma_q^2})^{-1}\frac{\varrho}{\sqrt{2}}\,\widetilde{e}^{i}\,(1 + \vec{a}\cdot\vec{\widetilde{x}}), \\ \pi^{\hat{0}}_{\hat{i}}(\varrho) \equiv (1 + \frac{\varrho^2}{2\gamma_q^2})^{-1}\left[(\vec{\omega}\wedge\vec{\widetilde{x}})(1 - \frac{\varrho v_q}{\sqrt{2}}) - \frac{\varrho}{\sqrt{2}}\right]\widetilde{e}_{i}^{-1}, \quad \pi^{\hat{j}}_{\hat{i}}(\varrho) = \delta^{j}_{i}\,\pi(\varrho), \\ \pi(\varrho) \equiv (1 + \frac{\varrho^2}{2\gamma_q^2})^{-1}\left[(\vec{\omega}\wedge\vec{\widetilde{x}})\,\frac{\varrho}{\sqrt{2}} + 1 + \frac{\varrho v_q}{\sqrt{2}}\right]. \end{array} \tag{94}$$

Thus,

$$dx^{\mu}_{\varrho} = dz^{\mu}_{\varrho}(s) + d\widetilde{x}^{i}\,e^{\mu}{}_{\hat{i}} + \widetilde{x}^{i}\,de^{\mu}{}_{\hat{i}}(s) = (\tau^{\hat{b}}\,d\widetilde{x}^{0} + \pi^{\hat{b}}_{\hat{i}}\,d\widetilde{x}^{i})\,\overline{e}^{\mu}{}_{\hat{b}}, \tag{95}$$

where

$$\tau^{\hat{b}} \equiv \pi^{\hat{b}}_{\hat{0}} + \widetilde{x}^{i}\left(\pi^{\hat{a}}_{\hat{i}}\Phi^{b}_{a} + \frac{d\pi^{\hat{b}}_{\hat{i}}}{ds}\right). \tag{96}$$

Hence, in general, the metric in noninertial frame of arbitrary accelerating and rotating observer in Minkowski space-time is

$$\widetilde{g}(\varrho) = \eta_{\mu\nu}\,dx^{\mu}_{\varrho}\otimes dx^{\nu}_{\varrho} = W_{\mu\nu}(\varrho)\,d\widetilde{x}^{\mu}\otimes d\widetilde{x}^{\nu}, \tag{97}$$

which can be conveniently decomposed according to

$$\begin{array}{l} W_{00}(\varrho) = \pi^2\left[(1 + \vec{a}\cdot\vec{\widetilde{x}})^2 + (\vec{\omega}\cdot\vec{\widetilde{x}})^2 - (\vec{\omega}\cdot\vec{\omega})(\vec{\widetilde{x}}\cdot\vec{\widetilde{x}})\right] + \gamma_{00}(\varrho), \\ W_{0i}(\varrho) = -\pi^2\,(\vec{\omega}\wedge\vec{\widetilde{x}})^{i} + \gamma_{0i}(\varrho), \quad W_{ij}(\varrho) = -\pi^2\,\delta_{ij} + \gamma_{ij}(\varrho), \end{array} \tag{98}$$

and that

$$\begin{array}{l} \gamma_{00}(\varrho) = \pi\,\left[(1 + \vec{a}\cdot\vec{\widetilde{x}})\zeta^{0} - (\vec{\omega}\wedge\vec{\widetilde{x}})\cdot\vec{\zeta}\right] + (\zeta^{0})^2 - (\vec{\zeta})^2, \quad \gamma_{0i}(\varrho) = -\pi\,\zeta^{i} + \tau^{\hat{0}}\,\pi^{\hat{0}}_{\hat{i}}, \\ \gamma_{ij}(\varrho) = \pi^{\hat{0}}_{\hat{i}}\,\pi^{\hat{0}}_{\hat{j}}, \quad \zeta^{0} = \pi\,\left(\tau^{\hat{0}} - 1 - \vec{a}\cdot\vec{\widetilde{x}}\right), \quad \vec{\zeta} = \pi\,\left(\vec{\tau} - \vec{\omega}\wedge\vec{\widetilde{x}}\right). \end{array} \tag{99}$$

As we expected, according to (97)- (99), the matric $\widetilde{g}(\varrho)$ is decomposed in the following form:

$$g(\varrho) = \pi^2(\varrho)\,\widetilde{g} + \gamma(\varrho), \tag{100}$$

where $\gamma(\varrho) = \gamma_{\mu\nu}(\varrho)\,d\widetilde{x}^{\mu}\otimes d\widetilde{x}^{\nu}$ and $\Upsilon(\varrho) = \pi^{\hat{a}}_{\hat{a}}(\varrho) = \pi(\varrho)$. In general, the geodesic coordinates are admissible as long as

$$\left(1 + \vec{a}\cdot\vec{\widetilde{x}} + \frac{\zeta^{0}}{\pi}\right)^2 > \left(\vec{\omega}\wedge\vec{\widetilde{x}} + \frac{\vec{\zeta}}{\pi}\right)^2. \tag{101}$$

doi: https://doi.org/10.52526/25792776-23.70.2-212

The equations (88) and (97) say that the vierbein fields, with entries $\eta_{\mu\nu}\,\overline{e}^{\,\mu}_{\ \hat{a}}\,\overline{e}^{\,\nu}_{\ \hat{b}} = o_{\hat{a}\hat{b}}$ and $\eta_{\mu\nu}\,e^{\,\mu}_{\ \hat{a}}\,e^{\,\nu}_{\ \hat{b}} = \gamma_{\hat{a}\hat{b}}$ lead to the relations

$$\widetilde{g} = o_{\hat{a}\hat{b}}\,\widetilde{\vartheta}^{\hat{a}} \otimes \widetilde{\vartheta}^{\hat{b}}, \quad g = o_{\hat{a}\hat{b}}\,\vartheta^{\hat{a}} \otimes \vartheta^{\hat{b}} = \gamma_{\hat{a}\hat{b}}\,\widetilde{\vartheta}^{\hat{a}} \otimes \widetilde{\vartheta}^{\hat{b}}, \tag{102}$$

which readily leads to the coframe fields:

$$\begin{array}{l} \widetilde{\vartheta}^{\hat{b}} = \overline{e}_{\ \mu}^{\ \hat{b}}\,dx^{\mu} = \widetilde{e}^{\hat{b}}_{\ \mu}\,d\widetilde{x}^{\mu}, \quad \widetilde{e}^{\hat{b}}_{\ 0} = N^{b}_{0}, \quad \widetilde{e}^{\hat{b}}_{\ i} = N^{b}_{i}, \\ \vartheta^{\hat{b}} = \overline{e}_{\ \mu}^{\ \hat{b}}\,dx^{\mu}_{\varrho} = e^{\hat{b}}_{\ \mu}\,d\widetilde{x}^{\mu} = \pi^{\hat{b}}_{\ \hat{a}}\,\widetilde{\vartheta}^{\hat{a}}, \quad e^{\hat{b}}_{\ 0} = \tau^{\hat{b}}, \quad e^{\hat{b}}_{\ i} = \pi^{\hat{b}}_{\ \hat{i}}. \end{array} \tag{103}$$

Here $N^0_0 = N \equiv \left(1 + \vec{a}\cdot\vec{\widetilde{x}}\right)$, $\quad N^0_i = 0$, $\quad N^i_0 = N^i \equiv \left(\vec{\omega}\cdot\vec{\widetilde{x}}\right)^i$, $\quad N^j_i = \delta^j_i$. In the standard $(3+1)$-decomposition of space-time, N and N^i are known as *lapse function* and *shift vector*, respectively (Gronwald & Hehl, 1996). Hence, we may easily recover the frame field $e_{\hat{a}} = e^{\mu}_{\ \hat{a}}\,\widetilde{e}_{\mu} = \pi_{\hat{a}}^{\ \hat{b}}\,\widetilde{e}_{\hat{b}}$ by inverting (103):

$$\begin{array}{l} e_{\hat{0}}(\varrho) = \frac{\pi(\varrho)}{\pi(\varrho)\,\tau^{\hat{0}}(\varrho) - \pi^{\hat{0}}_{\hat{k}}(\varrho)\,\tau^{\hat{k}}(\varrho)}\,\widetilde{e}_0 - \frac{\tau^{\hat{i}}(\varrho)}{\pi(\varrho)\,\tau^{\hat{0}}(\varrho) - \pi^{\hat{0}}_{\hat{k}}(\varrho)\,\tau^{\hat{k}}(\varrho)}\,\widetilde{e}_i, \\ e_{\hat{i}}(\varrho) = -\frac{\pi^{\hat{0}}_{\hat{i}}(\varrho)}{\pi(\varrho)\,\tau^{\hat{0}}(\varrho) - \pi^{\hat{0}}_{\hat{k}}(\varrho)\,\tau^{\hat{k}}(\varrho)}\,\widetilde{e}_0 + \pi^{-1}(\varrho)\left[\delta^j_i + \frac{\tau^j(\varrho)\,\pi^{\hat{0}}_{\hat{i}}(\varrho)}{\pi(\varrho)\,\tau^{\hat{0}}(\varrho) - \pi^{\hat{0}}_{\hat{k}}(\varrho)\,\tau^{\hat{k}}(\varrho)}\right]\widetilde{e}_j. \end{array} \tag{104}$$

A *generalized transport* for deformed frame $e_{\hat{a}}$, which includes both the Fermi-Walker transport and distortion of $\underline{M}_2$, can be written in the form

$$\frac{de^{\,\mu}_{\ \hat{a}}}{ds} = \widetilde{\Phi}_a^{\ b}\,e^{\mu}_{\ \hat{b}}, \tag{105}$$

where a *deformed acceleration tensor* $\widetilde{\Phi}_a^{\ b}$ concisely is given by

$$\widetilde{\Phi} = \frac{d\,\ln\pi}{ds} + \pi\,\Phi\,\pi^{-1}. \tag{106}$$

Thus, we derive the tetrad fields $e_r^{\ \hat{s}}(\varrho)$ (92) and $e^{\mu}_{\ \hat{a}}(\varrho)$ (104) as a function of *local rate* ϱ of instantaneously change of a constant velocity (both magnitude and direction) of a massive particle in M_4 under the unbalanced net force, describing corresponding *fictitious graviton*. Then, the *fictitious gravitino*, $\psi_{\hat{m}}^{\ \alpha}(\varrho)$, will be arisen under infinitesimal transformations of local supersymmetry (64), provided by the local parameters $\zeta^M(a)$ (45).

8. Involving the background semi-Riemann space V_4; Justification for the introduction of the WPE

We can always choose *natural coordinates* $X^{\alpha}(T,X,Y,Z) = (T,\,\vec{X})$ with respect to the axes of the local free-fall coordinate frame $S_4^{(l)}$ in an immediate neighbourhood of any space-time point $(\widetilde{x}_p) \in V_4$ in question of the background semi- Riemann space, V_4, over a differential region taken small enough so that we can neglect the spatial and temporal variations of gravity for the range involved. The values of the metric tensor $\widetilde{g}_{\mu\nu}$ and the affine connection $\widetilde{\Gamma}^{\lambda}_{\mu\nu}$ at the point $(\widetilde{x}_p)$ are necessarily sufficient information for determination of the natural coordinates $X^{\alpha}(\widetilde{x}^{\mu})$ in the small region of the neighbourhood of the selected point (Weinberg, 1972). Then the whole scheme outlined in the previous subsections (a) and (b) will be held in the frame $S_4^{(l)}$. The general *inertial force* computed by Ter-Kazarian (2012) reads

$$\widetilde{\vec{f}}_{(in)} = -\frac{m\vec{a}_{abs}}{\Omega^2(\overline{\varrho})\,\gamma_q} = -\frac{\vec{e}_f}{\Omega^2(\overline{\varrho})\,\gamma_q}|f^{\alpha}_{(l)} - m\frac{\partial X^{\alpha}}{\partial\widetilde{x}^{\sigma}}\Gamma^{\sigma}_{\mu\nu}\frac{d\widetilde{x}^{\mu}}{dS}\frac{d\widetilde{x}^{\nu}}{dS}|. \tag{107}$$

Whereas, as before, the two systems S_2 and $S_4^{(l)}$ can be chosen in such a way as the axis $\vec{e}_q$ of $S_{(2)}$ lies $(\vec{e}_q = \vec{e}_f)$ along the acting net force $\vec{f} = \vec{f}_{(l)} + \vec{f}_{g(l)}$, while the time coordinates in the two systems are taken the same, $q^0 = t = X^0 = T$. Here $\vec{f}_{(l)}$ is the SR value of the unbalanced relativistic force other than gravitational and $\vec{f}_{g(l)}$ is the gravitational force given in the frame $S_4^{(l)}$. Despite of totally different and independent sources of gravitation and inertia, at $f^{\alpha}_{(l)} = 0$, the (107) establishes the independence of free-fall $(v_q = 0)$ trajectories of the mass, internal composition and structure of bodies. This furnishes a justification for the introduction of the WPE. A remarkable feature is that, although the inertial force has a nature different than the gravitational force, nevertheless both are due to a distortion of the local inertial properties of, respectively, 2D $\underline{M}_2$ and 4D-background space.

doi: https://doi.org/10.52526/25792776-23.70.2-212

9. The inertial effects in the background post Riemannian geometry

If the nonmetricity tensor $N_{\lambda\mu\nu} = -\mathcal{D}_\lambda\, g_{\mu\nu} \equiv -g_{\mu\nu\,;\lambda}$ does not vanish, the general formula for the affine connection written in the space-time components is (Poplawski, 2009)

$$\Gamma^\rho{}_{\mu\,\nu} = \overset{\circ}{\Gamma}{}^\rho{}_{\mu\,\nu} + K^\rho{}_{\mu\nu} - N^\rho{}_{\mu\nu} + \tfrac{1}{2} N_{(\mu}{}^\rho{}_{\nu)}, \tag{108}$$

where the metric alone determines the torsion-free Levi-Civita connection $\overset{\circ}{\Gamma}{}^\rho{}_{\mu\nu}$, $K^\rho{}_{\mu\nu} : \; = 2Q_{(\mu\nu)}{}^\rho + Q^\rho{}_{\mu\nu}$ is the non-Riemann part - the affine *contortion tensor*. The torsion, $Q^\rho{}_{\mu\nu} = \frac{1}{2} T^\rho{}_{\mu\nu} = \Gamma^\rho{}_{[\mu\,\nu]}$ given with respect to a holonomic frame, $d\,\vartheta^\rho = 0$, is a third-rank tensor, antisymmetric in the first two indices, with 24 independent components. We now compute the relativistic inertial force for the motion of the matter, which is distributed over a small region in the U_4 space and consists of points with the coordinates x^μ, forming an extended body whose motion in the space, U_4, is represented by a world tube in space-time. Suppose the motion of the body as a whole is represented by an arbitrary timelike world line γ inside the world tube, which consists of points with the coordinates $\tilde{X}^\mu(\tau)$, where τ is the proper time on γ. Define

$$\delta x^\mu = x^\mu - \tilde{X}^\mu, \;\; \delta x^0 = 0, \;\; u^\mu = \tfrac{d\,\tilde{X}^\mu}{d\,s}. \tag{109}$$

The *Papapetrou equation of motion for the modified momentum* (Bergmann & Thompson, 1953, Møller, 1958, Papapetrou, 1974, Poplawski, 2009) is

$$\tfrac{\overset{\circ}{\mathcal{D}}\,\Theta^\nu}{\mathcal{D}\,s} = -\tfrac{1}{2}\; \overset{\circ}{R}{}^\nu{}_{\mu\sigma\rho}\, u^\mu\, J^{\sigma\rho} - \tfrac{1}{2}\, N_{\mu\rho\lambda}\, K^{\mu\rho\lambda:\,\nu}, \tag{110}$$

where $K^\mu_{\nu\lambda}$ is the contortion tensor,

$$\Theta^\nu = P^\nu + \tfrac{1}{u^0}\; \overset{\circ}{\Gamma}{}^\nu_{\mu\,\rho}\,(u^\mu\, J^{\rho 0} + N^{0\mu\rho}) - \tfrac{1}{2u^0}\, K_{\mu\rho}{}^\nu\, N^{\mu\rho 0} \tag{111}$$

is referred to as the *modified 4-momentum*, $P^\lambda = \int \tau^{\lambda 0}\, d\,\Omega$ is the ordinary 4-momentum, $d\,\Omega := d\,x^4$, and the following integrals are defined:

$$\begin{array}{l} M^{\mu\rho} = u^0 \int \tau^{\mu\rho}\, d\,\Omega, \quad M^{\mu\nu\rho} = -u^0 \int \delta x^\mu\, \tau^{\nu\rho}\, d\,\Omega, \quad N^{\mu\nu\rho} = u^0 \int s^{\mu\nu\rho}\, d\,\Omega, \\ J^{\mu\rho} = \int(\delta x^\mu\, \tau^{\rho 0} - \delta x^\rho\, \tau^{\mu 0} + s^{\mu\rho 0})\, d\,\Omega = \frac{1}{u^0}(-M^{\mu\rho 0} + M^{\rho\mu 0} + N^{\mu\rho 0}), \end{array} \tag{112}$$

where $\tau^{\mu\rho}$ is the energy-momentum tensor for particles, $s^{\mu\nu\rho}$ is the spin density. The quantity $J^{\mu\rho}$ is equal to $\int(\delta x^\mu\, \tau^{kl} - \delta x^\rho\, \tau^{\mu\lambda} + s^{\mu\rho\lambda})\, d\,S_\lambda$ taken for the volume hypersurface, so it is a tensor, which is called the *total spin tensor*. The quantity $N^{\mu\nu\rho}$ is also a tensor. The relation $\delta x^0 = 0$ gives $M^{0\nu\rho} = 0$. It was assumed that the dimensions of the body are small, so integrals with two or more factors δx^μ multiplying $\tau^{\nu\rho}$ and integrals with one or more factors δx^μ multiplying $s^{\nu\rho\lambda}$ can be neglected. The *Papapetrou equations of motion for the spin* (Bergmann & Thompson, 1953, Møller, 1958, Papapetrou, 1974, Poplawski, 2009) is

$$\tfrac{\overset{\circ}{\mathcal{D}}}{\mathcal{D}s}\, J^{\lambda\nu} = u^\nu\, \Theta^\lambda - u^\lambda\, \Theta^\nu + K^\lambda{}_{\mu\rho}\, N^{\nu\mu\rho} + \tfrac{1}{2}\, K_{\mu\rho}{}^\lambda\, N^{\mu\nu\rho} - K^\nu{}_{\mu\rho}\, N^{\lambda\mu\rho} - \tfrac{1}{2}\, K_{\mu\rho}{}^\nu\, N^{\mu\rho\lambda}. \tag{113}$$

Computing from (110), in general, the relativistic inertial force, exerted on the extended spinning body moving in the RC space U_4, can be found to be

$$\begin{array}{l} \vec{f}_{(in)}(x) = -\frac{m\vec{a}_{abs}(x)}{\Omega^2(\varrho)\,\gamma_q} = -m\, \frac{\vec{e}_f}{\Omega^2(\varrho)\,\gamma_q} \left| \frac{1}{m}\, f^\alpha_{(l)} - \frac{\partial X^\alpha}{\partial x^\mu} \left[\overset{\circ}{\Gamma}{}^\mu_{\nu\lambda}\, u^\nu\, u^\lambda + \right.\right. \\ \left.\left. \frac{1}{u^0}\; \overset{\circ}{\Gamma}{}^\mu_{\nu\rho}\,(u^\nu\, J^{\rho 0} + N^{0\nu\rho}) - \frac{1}{2u^0}\, K_{\nu\rho}{}^\mu\, N^{\nu\rho 0} + \frac{1}{2}\; \overset{\circ}{R}{}^\mu{}_{\nu\sigma\rho}\, u^\nu\, J^{\sigma\rho} + \frac{1}{2}\, N_{\nu\rho\lambda}\, K^{\nu\rho\lambda:\,\mu} \right] \right|. \end{array} \tag{114}$$

10. Concluding remarks

In the framework of local $\widetilde{MS}_p$-SUSY, we address the inertial effects. The local $\widetilde{MS}_p$-SUSY can only be implemented if $\underline{\widetilde{M}}_2$ and $\widetilde{M}_4$ are curved (deformed). Whereas the space $\widetilde{M}_4$, in order to become on the same footing with the distorted space $\underline{\widetilde{M}}_2$, refers to the accelerated reference frame of a particle, without relation to other matter fields. Thus, unlike gravitation, a curvature of space-time arises entirely due to the inertial properties of the Lorentz-rotated frame of interest, i.e. a *fictitious gravitation* which can be globally removed by appropriate coordinate transformations. The superspace $(z^M,\, \Theta,\, \bar{\Theta})$ is a direct sum extension of

doi: https://doi.org/10.52526/25792776-23.70.2-212

background double spaces $\widetilde{M}_4 \oplus \widetilde{\underline{M}}_2$, with an inclusion of additional fermionic coordinates $(\Theta(\underline{\theta}, \theta),\ \bar{\Theta}(\bar{\underline{\theta}}, \bar{\theta}))$ induced by the spinors $(\underline{\theta}, \bar{\underline{\theta}})$, which refer to $\widetilde{\underline{M}}_2$. Thereby thanks to the embedding $\widetilde{\underline{M}}_2 \hookrightarrow \widetilde{M}_4$, the spinors $(\underline{\theta}, \bar{\underline{\theta}})$, in turn, induce the spinors $\theta(\underline{\theta}, \bar{\underline{\theta}})$ and $\bar{\theta}(\underline{\theta}, \bar{\underline{\theta}})$, as to $\widetilde{M}_4$. The $\widetilde{MS}_p$-SUSY was conceived as a quantum field theory whose action included the Einstein-Hilbert term, where the graviton coexists with a fermionic field called gravitino, described by the Rarita-Scwinger kinetic term. The two fields differ in their spin: 2 for the graviton, 3/2 for the gravitino. The spin 3/2 contact term in total Lagrangian arises from equations of motion for the torsion tensor, and that the original Lagrangian itself takes the simpler interpretation of a minimally coupled spin (2, 3/2) theory. The only source of graviton and gravitino is the acceleration of a particle, because the $\widetilde{MS}_p$-SUSY is so constructed as to make these two particles just as being the two bosonic and fermionic states of a particle of interest in the background spaces M_4 and $\underline{M}_2$, respectively, or vice versa. The different 4D $N = 1$ supergravity multiplets all contain the graviton and the gravitino, but differ by their systems of auxiliary fields. In this framework supersymmetry and general coordinate transformations are described in a unified way as certain diffeomorphisms. The dynamical variables of superspace formulation are the frame field $E^A(z)$ and spin-connection Ω. The superspace has at each point a tangent superspace spanned by the frame field $E^A(z) = dz^M E_M^{\ A}(z)$, defined as a 1-form over superspace, with coefficient superfields, generalizing the usual frame, namely supervierbien $E_M^{\ A}(z)$. Covariant derivatives with respect to local Lorentz transformations are constructed by means of the spin connection, which is a 1-form in superspace as well. There is no general prescription for deducing necessary covariant constraints which if imposed upon the superfields of super-vielbein and spin-connection will eliminate the component fields. However, some usual constraints are found using tangent space and supergeneral coordinate transformations of the torsion and curvature covariant tensors, given in appropriate super-gauge. A coupling of supergravity with matter superfields evidently no longer holds in resulting theory. Instead, we argue that a deformation/(distortion of local internal properties) of MS$_p$ is the origin of inertia effects that can be observed by us. In going into practical details of the realistic local $\widetilde{MS}_p$-SUSY model, we briefly review of certain aspects of a general distortion of local internal properties of MS$_p$ and derive the explicit form of the vierbien $e_{\hat{m}}^{\ \underline{a}}(\varrho) \equiv (e_m^{\ a}(\varrho),\, e_{\underline{m}}^{\ \underline{a}}(\varrho))$, which describes *fictitious graviton* as a function of *local rate* $\varrho(\eta, m, f)$ of instantaneously change of the velocity $v^{(\pm)}$ of massive (m) test particle under the unbalanced net force (f). We discuss the inertia effects by going beyond the hypothesis of locality. This allows to improve essentially the relevant geometrical structures referred to the noninertial frame in Minkowski space-time for an arbitrary velocities and characteristic acceleration lengths. Despite the totally different and independent physical sources of gravitation and inertia, this approach furnishes justification for the introduction of the WPE. Consequently, we relate the inertia effects to the more general post-Riemannian geometry. We derive a general expression of the relativistic inertial force exerted on the extended spinning body moving in the Rieman-Cartan space.

References

Atwood D., et al. 1984, Phys. Rev. Lett., 52, 1673

Bakke K., Furtado C., 2010, Phys. Rev. D, 82, 084025

Beck A., Havas P., 1989, The Collected Papers of Albert Einstein. Princeton University Press, Princeton, NJ, vol. 2; pp. 252–311. The quote is on p. 302.

Bergmann P., Thompson R., 1953, Phys. Rev., 89, 400

Binetruy P., Girardi G., Rrimm R., 2001, Physics Reports, 343, 255

Bini D., Cherubini C., Mashhoon B., 2004, Class. and Quant. Gr., 21, 3893

Bonse U., Wroblewski T., 1983, Phys. Rev. Lett., 51, 1401

Brans C., 1977, Phys. Rev. Lett., 39, 856

Capozziello S., Lambiase G., 2000, Eur. Phys. J C, 16, 155

Cardall C., Fuller G., 1997, Phys. Rev. D, 55, 7960

Cocconi G., Salpeter E., 1960, Phys. Rev. Lett., 4, 176

Colella R., Overhauser A., Werner S., 1975, Phys. Rev. Lett., 34, 1472

Dicke R., 1961, Phys. Rev. Lett., 7, 359

Drake S., 1978, Galileo at work. Chicago, University of Chicago Press

doi: https://doi.org/10.52526/25792776-23.70.2-212

Drever R., 1961, Phil. Mag., 6, 683

Everitt C. W. F., et al. 2009, Space Sci. Rev., 148, 53

Everitt C. W. F., et al. 2011, Phys. Rev. Lett., 106, 221101

Faller J., et al. 1990, Phys. Rev. Lett., 64, 825

Fayet P., Ferrara S., 1977, Physics Reports, 32, 249

Gabriel M., Haugan M., 1990, Phys. Rev. D, 41, 2943

Gasperini M., 1988, Phys. Rev. D, 38, 2635

Gillies G., 1997, Rep. Prog. Phys., 60, 151

Gronwald F., Hehl F., 1996, On the Gauge Aspects of Gravity. Proc. of the 14th Course of the School of Cosmology and Gravitation on Quantum Gravity, held at Erice, Italy. Eds. Bergmann P G, de Sabbata V, and Treder H.-J., World Scientific, Singapore

Halprin A., Leung C., 1991, Phys. Rev. Lett., 67, 1833

Haugan M., Kauffmann T., 1995, Phys. Rev. D, 52, 3168

Haugan M., Lämmerzahl C., 2001, in Gyrod, Clocks, Interferometers...: Testing Relativistic Gravity in Space. C. Lämmerzahl, C.W.F. Everitt, F.W. Hehl (eds.): Springer–Velag, p.195

Hayasaka H., Takeuchi S., 1989, Phys. Rev. Lett., 63, 2701

Hehl F., Ni W.-T., 1990, Phys. Rev. D, 42, 2045

Hehl F., Lemke J., Mielke E., 1991, Two lectures on fermions and gravity. In: Geometry and Theoretical Physics, Debrus J and Hirshfeld A C (eds.) (Springer, Berlin) p.56

Heifetz M., et al. 2009, Space Sci. Rev., 148, 411

Hughes V. W., Robinson H. G., Beltran-Lopez V., 1960, Phys. Rev. Lett., 4, 342

Imanishi A., et al. 1991, J. Phys. Soc. Jpn., 60, 1150

Infeld L., 1950, Albert Einstein. Charles Scribner's Sons , New York, p. 47

Jacob M., 1987, Supersymmetry and Supergravity. North Holland, Amsterdam

Keiser G., et al. 2009, Space Sci. Rev., 148, 383

Lämmerzahl C., Bordé C., 2001, in Gyrod, Clocks, Interferometers...: Testing Relativistic Gravity in Space. C. Lämmerzahl, C.W.F. Everitt, F.W. Hehl (eds.): Springer–Velag, p.466

Li W.-Q., Ni W.-T., 1979, Chin. J. Phys, 16, 214

Luo J., et al. 2002, Phys. Rev. D, 65, 042005

Maluf J., Faria F., 2008, Ann. der Physik, 520, 326

Maluf J., Faria F., Ulhoa S., 2007, Class. Quantum Grav., 24, 2743

Marzlin K.-P., 1996, Phys. Lett. A, 215, 1

Mashhoon B., 95, Phys. Rev. Lett., 198, 9

Mashhoon B., 1988, Phys. Rev. Lett., 61, 2639

Mashhoon B., 1990a, Phys. Lett. A, 143, 176

Mashhoon B., 1990b, Phys. Lett. A, 145, 147

Mashhoon B., 2002, Ann. der Physik, 514, 532

Mashhoon B., 2011, Ann. der Physik, 523, 226

Mashhoon B., Wesson P., 2012, Annalen Phys., 524, 63

Misner C., Thorne K., Wheeler J., 1973, Gravitation. Freeman, San Francisco

Møller C., 1958, Ann. Phys. (NY), 4, 347

Muhlfelder B., et al. 2009, Space Sci. Rev., 148, 429

Newton I., 1687, Philosophiae Naturalis Principia Mathematica. http://plato.stanford.edu/entries/newton-principia

Ni W.-T., 1977, Chinese J. Phys., 15, 51

Ni W.-T., 1983, Precision Measurement and Gravitational Experiments. (National Tsing Hua University, Taiwan, China

doi: https://doi.org/10.52526/25792776-23.70.2-212

Ni W.-T., 2005a, Int. J. Mod. Phys. D, 14, 901

Ni W.-T., 2005b, Chin. Phys. Lett., 22, 33

Ni W.-T., 2005c, Chin. Phys. Lett., 22, 33

Ni W.-T., 2008, Prog. Theor. Phys. Suppl., 172, 49

Ni W.-T., 2011, Phys. Rev. Lett., 107, 051103

Ni W.-T., Zimmermann M., 1978, Phys. Rev. D, 17, 1473

Nilles H., 1984, Physics Reports, 110, 1

Nitschke J., Wilmarth P., 1990, Phys. Rev. Lett., 64, 2115

Pan Y., Ren J., 2011, Int. J Theor. Phys., 50, 724

Pantaleone J., Halprin A., Leung C., 1993, Phys. Rev. D, 47, R4199(R)

Papapetrou A., 1974, Lectures on general relativity. (Reidel D)(ISBN 9027705402)

Piniz D., Roy M., Wudka J., 1997, Phys. Rev. D, 56, 2403

Poplawski N., 2009, Spacetime and fields. arXiv[gr-qc/0911.0334]

Prestage J., et al. 1985, Phys. Rev. Lett., 54, 2387

Quinn T., Picard A., 1990, Nature, 343, 732

Schucking E., 2009, arXiv:0903.3768[physics.hist-ph]

Schucking E., Surowitz E., 2012, arXiv:gr-qc/0703149

Silbergleit A., et al. 2009, Space Sci. Rev., 148, 397

Silenko A., Teryaev O., 2007, Phys. Rev. D, 76, 061101(R)

Synge J., 1960, Relativity: The General Theory. North-Holland, Amsterdam

Ter-Kazarian G., 2012, Advances in Mathematical Physics, 2012, Article ID 692030, 41 pages,doi:10.1155/2012/692030, Hindawi Publ. Corporation

Ter-Kazarian G., 2023, Communications of BAO, 70, ??

Ter-Kazarian G., 2024, To appear in Grav. Cosmol., 30, No 1

Turyshev S., 2008, Annu. Rev. Nucl. Part. Sci., 58, 207

Weinberg S., 1972, Gravitation and Cosmology. J. W. and Sons, New York

Wess J., Bagger J., 1983, Supersymmetry and Supergravity. Princeton University Press, Princeton, New Jersey

West P., 1987, Introduction to Supersymmetry and Supergravity. World Scientific, Singapure

Will C., 2006, Living Rev. Relativity, 9, 3

Zhou Z., et al. 2002, Phys. Rev. D, 66, 022002

de Sabbata V., Gasperini M., 1981, Nuovo Cimento A, 66, 479

van Nieuwenhuizen P., 1981, Physics Reports, 68, 189

van Nieuwenhuizen P., Freedman D., Ferrara S., 1976, Phys. Rev. D, 13, 3214

doi: https://doi.org/10.52526/25792776-23.70.2-212

Communications of BAO, Vol. 70, Issue 2, 2023, pp. 235-241

Reflection of Radiation from a Plane-Parallel Half-Space in the Case of Redistribution of Radiation by Frequencies and Directions

H. V. Pikichyan

Byurakan Astrophysical Observatory, 378433, Aragatsotn Region, Armenia

Abstract

The method introduced in the author's two previous works is used to solve the problem of diffuse reflection from a semi-infinite plane-parallel scattering-absorbing medium in the general case of redistribution of radiation by frequencies and directions in an elementary act of scattering. A system of functional equations was obtained to determine the unknown eigenfunctions and eigenvalues. The initial problem of the six explanatory variables is explicitly expressed in terms of these eigenfunctions that depend only on three independent variables (dimensionless frequency, zenith angle, and azimuth).

Keywords: *radiative transfer, diffuse reflection problem, Ambartsumian's nonlinear functional equation, redistribution over frequencies and directions, multidimensional eigenfunctions and eigenvalues problem*

1. TIntroduction and purpose of the study

In the author's last two works (Pikichyan, 2023a,b), a new approach was developed to solve the problem of diffuse reflection from a semi-infinite medium. In the first work, two particular cases were considered: a one-dimensional medium with a general law of radiation redistribution by frequencies and anisotropic monochromatic scattering in a plane-parallel semi-infinite medium. In the second work, the case of isotropic scattering with redistribution of radiation by frequencies in a semi-infinite scattering-absorbing medium with plane-parallel symmetry was analyzed. In these three cases of multiple scattering problems, the separation of the independent variables was achieved without decomposition or any special representation of the characteristics of the elementary act of scattering.

In order to solve the initial problem of multiple scatterings in a scattering-absorbing medium, it is traditionally accepted (the relevant references are given in Pikichyan (2023a,b) to first solve some auxiliary problem of representing the characteristics of a single act of scattering (i.e., the function of redistribution of radiation by frequencies or the indicatrix of scattering) in the form of a special decomposition, where "separation of variables" would take place. Then, in the course of solving the initial problem of multiple scatterings, this skillfully introduced quality of "variable separation" is automatically transferred to the final characteristics of the radiation field, i.e., to the solution of the problem of diffuse reflection of radiation from the medium. The new approach proposed in the above-mentioned works compares favorably with the traditional one because in solving the initial problem of diffuse reflection in order to achieve the final property of "variable separation", there is no need to introduce any auxiliary problem.

In more general terms, it can be argued that the solution of the problem of diffuse reflection is traditionally analytically approximated through some degenerate kernel. If, in the cases of both incoherent and anisotropic scattering, this is traditionally achieved by preliminarily posing the solution of some auxiliary problem on the mathematical description of a unit act of scattering in the form of a degenerate kernel, then in the new approach there is no need to consider any auxiliary problem on the decomposition of the characteristics of a single act of scattering. Here it is possible to express the solution of the initial problem of multiple scattering directly through some specially constructed form of the degenerate kernel, without affecting the form of the single act of scattering. The problem of radiative transfer in the general case of redistribution of radiation by frequencies and directions was considered in Engibaryan & Nikogosyan (1972a,b), where the function of redistribution by frequencies and directions was previously presented in the form of a special decomposition.

doi: https://doi.org/10.52526/25792776-23.70.2-235

The purpose of this study is to apply a new approach introduced in Pikichyan (2023a,b) to solve the problem of diffuse reflection in the general case of redistribution of radiation by frequencies and directions. It will be shown below that the diffuse reflection function, which formally depends on six independent variables, is explicitly expressed in terms of some specially constructed eigenfunctions that depend on only three independent variables. There is no need for any decomposition or special representation of the redistribution function by frequencies and directions.

2. Statement and solution of the problem

In the problem of diffuse reflection of radiation from a plane-parallel semi-infinite scattering-absorbing medium in the case of the general law of radiation redistribution by frequencies and directions, the nonlinear Ambartsumian's functional equation has the form (see also Engibaryan & Nikogosyan, 1972b)(see also Engibaryan, Nikogosyan 1972b)

$$\frac{4\pi}{\lambda}\mu'\left(\frac{\alpha(x)}{\mu}+\frac{\alpha(x')}{\mu'}\right)\rho\left(x,\mu;x'\mu';\varphi-\varphi'\right)=r\left(x,\mu;x'-\mu';\varphi-\varphi'\right)+$$

$$\mu'\int_{-\infty}^{+\infty}\int_0^{2\pi}\int_0^1 r\left(x,\mu;x''',\mu''';\varphi-\varphi'''\right)\rho\left(x',\mu';x''',\mu''';\varphi'-\varphi'''\right)\frac{d\mu''}{\mu''}d\varphi''dx''+$$

$$\int_{-\infty}^{+\infty}\int_0^{2\pi}\int_0^1 \rho\left(x,\mu;x''',\mu''';\varphi-\varphi'''\right)r\left(x''',-\mu''';x',-\mu';\varphi'''-\varphi'\right)d\mu'''d\varphi'''dx'''+$$

$$\mu'\int_{-\infty}^{+\infty}\int_0^{2\pi}\int_0^1\int_{-\infty}^{+\infty}\int_0^{2\pi}\int_0^1 \rho\left(x,\mu;x''',\mu''';\varphi-\varphi'''\right)r\left(x''',-\mu''';x'',\mu'';\varphi'''-\varphi''\right)\cdot$$

$$\rho\left(x',\mu';x''\mu'';\varphi'-\varphi''\right)\frac{d\mu''}{\mu''}d\varphi''dx''d\mu'''d\varphi'''dx'''. \tag{1}$$

Here: $\rho\left(x,\mu;x'\mu';\varphi-\varphi'\right)$ is a diffuse reflection function in a probabilistic representation, i.e., the density of the conditional probability of quantum, which one leaving a semi-infinite medium (generally speaking after multiple scatterings) with parameters (x,μ,φ) if the latter had values (x',μ',φ') at the entrance to the medium, and $r\left(x,\mu;x',\mu';\varphi-\varphi'\right)$ is the redistribution function of radiation by frequencies and directions, i. e., is a similar probability density, describing a single act of scattering. At the same time, the values x and x' are the dimensionless frequencies of the quanta leaving the medium and falling on it, respectively. The values μ, φ and μ', φ' are directions correspond to them (in relation to the external normal to the boundary of the medium), μ, μ' are cosines of zenith angles, φ, φ' are the azimuths corresponding to them. is the probability of the "survival" of the quantum in the elementary act of scattering (also called the albedo of single scattering). It should be noted that there are correlations:

$$r\left(x,x';\gamma\right)=r\left(x,\mu;x',\mu';\varphi-\varphi'\right),\gamma=\overrightarrow{n}\cdot\overrightarrow{n}',\overrightarrow{n}\equiv(\mu,\varphi),\mu\in[0,1],\varphi\in[0,2\pi], \tag{2}$$

and the expressions are also valid:

$$r\left(x,-\mu;x',-\mu';\varphi-\varphi'\right)=r\left(x,+\mu;x',+\mu';\varphi-\varphi'\right),$$

$$r\left(x,+\mu;x',-\mu';\varphi-\varphi'\right)=r\left(x',+\mu';x,-\mu;\varphi'-\varphi\right)),$$

$$\rho\left(x,\mu;x'\mu';\varphi-\varphi'\right)\mu'=\rho\left(x'\mu';x,\mu;\varphi'-\varphi\right)\mu. \tag{3}$$

With (3), the functional equation (1) is rewritten as

$$\frac{4\pi}{\lambda}\mu'\left(\frac{\alpha(x)}{\mu}+\frac{\alpha(x')}{\mu'}\right)\rho\left(x,\mu;x'\mu';\varphi-\varphi'\right)=r\left(x,\mu;x'-\mu';\varphi-\varphi'\right)+$$

$$\int_{-\infty}^{+\infty}\int_0^{2\pi}\int_0^1 r\left(x,\mu;x''',\mu''';\varphi-\varphi'''\right)\rho\left(x',\mu';x''',\mu''';\varphi'-\varphi'''\right)d\mu'''d\varphi'''dx'''+$$

doi: https://doi.org/10.52526/25792776-23.70.2-235

$$\int_{-\infty}^{+\infty}\int_0^{2\pi}\int_0^1 \rho\left(x,\mu;x'',\mu'';\varphi-\varphi''\right) r\left(x'',\mu'';x',\mu';\varphi''-\varphi'\right) d\mu'' d\varphi'' dx''+$$

$$\int_{-\infty}^{+\infty}\int_0^{2\pi}\int_0^1\int_{-\infty}^{+\infty}\int_0^{2\pi}\int_0^1 \rho\left(x,\mu;x''',\mu''';\varphi-\varphi'''\right) r\left(x''',-\mu''';x'',\mu'';\varphi'''-\varphi''\right)\cdot$$

$$\cdot\rho\left(x',\mu';x''\mu'';\varphi'-\varphi''\ \right) d\mu'' d\varphi'' dx'' d\mu''' d\varphi''' dx'''. \tag{4}$$

Let's enter the value

$$K\left(x,\mu;x',\mu';\varphi-\varphi'\right)\equiv \mu'\left(\frac{\alpha\left(x\right)}{\mu}+\frac{\alpha\left(x'\right)}{\mu'}\right)\rho\left(x,\mu;x'\mu';\varphi-\varphi'\right). \tag{5}$$

Obviously, $K\left(x,\mu;x',\mu';\varphi-\varphi'\right)$ is a symmetrical, positive, and continuous function

$$K\left(x,\mu;x',\mu';\varphi-\varphi'\right)=K\left(x',\mu';x,\mu;\varphi-\varphi'\right), \tag{6}$$

its knowledge uniquely determines the initial value $\rho\left(x,\mu;x'\mu';\varphi-\varphi'\right)$.
Our goal is to construct the newly introduced value $K\left(x,\mu;x',\mu';\varphi-\varphi'\right)$ and by (5) finding $\rho\left(x,\mu;x'\mu';\varphi-\varphi'\right)$. Given the notation (5), equation (4) will take the form

$$\frac{4\pi}{\lambda}K\left(x,\mu;x',\mu';\varphi-\varphi'\right)=r\left(x,\mu;x'-\mu';\varphi-\varphi'\right)+$$

$$\int_{-\infty}^{+\infty}\int_0^{2\pi}\int_0^1 r\left(x,\mu;x''',\mu''';\varphi-\varphi'''\right)\frac{K\left(x',\mu';x''',\mu''';\varphi'-\varphi'''\right)}{\frac{\alpha(x')}{\mu'}+\frac{\alpha(x''')}{\mu'''}}\frac{d\mu'''}{\mu'''}d\varphi''' dx'''+$$

$$\int_{-\infty}^{+\infty}\int_0^{2\pi}\int_0^1 \frac{K\left(x,\mu;x'',\mu'';\varphi-\varphi''\right)}{\frac{\alpha(x)}{\mu}+\frac{\alpha(x'')}{\mu''}} r\left(x'',\mu'';x',\mu';\varphi''-\varphi'\right)\frac{d\mu''}{\mu''}d\varphi'' dx''\ +$$

$$\int_{-\infty}^{+\infty}\int_0^{2\pi}\int_0^1\int_{-\infty}^{+\infty}\int_0^{2\pi}\int_0^1 \frac{K\left(x,\mu;x''',\mu''';\varphi-\varphi'''\right)}{\frac{\alpha(x)}{\mu}+\frac{\alpha(x''')}{\mu'''}} r\left(x''',-\mu''';x'',\mu'';\varphi'''-\varphi''\right)\cdot$$

$$\frac{K\left(x',\mu';x''\mu'';\varphi'-\varphi''\right)}{\frac{\alpha(x')}{\mu'}+\frac{\alpha(x'')}{\mu''}}\frac{d\mu''}{\mu''}d\varphi'' dx''\frac{d\mu'''}{\mu'''}d\varphi''' dx'''. \tag{7}$$

Thus, we need to build the desired kernel $K\left(x,\mu;x',\mu';\varphi-\varphi'\right)$ given by a nonlinear multidimensional functional integral equation (7). For the introduced symmetric kernel $K\left(x,\mu;x',\mu';\varphi-\varphi'\right)$ substitute the multivariate problem for the eigenvalues ν_i and the eigenfunctions $\beta_i\left(x,\mu,\varphi\right)$

$$\nu_i\beta_i\left(x,\mu,\varphi\right)=\int_{-\infty}^{+\infty}\int_0^{2\pi}\int_0^1 K\left(x,\mu;x'\mu';\varphi-\varphi'\right)\beta_i\left(x',\mu',\varphi'\right)d\mu' d\varphi' dx', \tag{8}$$

with the orthonormalization condition

$$\int_{-\infty}^{+\infty}\int_0^{2\pi}\int_0^1 \beta_i\left(x,\mu,\varphi\right)\beta_j\left(x,\mu,\varphi\right)d\mu d\varphi dx=\delta_{ij}. \tag{9}$$

From (7) and (8) with regard to (9) it is not difficult to obtain the expression

$$\frac{4\pi}{\lambda}\nu_i\beta_i\left(x,\mu,\varphi\right)=Z_i\left(x,\mu,\varphi\right)+\int_{-\infty}^{+\infty}\int_0^{2\pi}\int_0^1 r\left(x,\mu;x'',\mu'';\varphi-\varphi''\right)Q_i\left(x'',\mu'',\varphi''\right)\frac{d\mu''}{\mu''}d\varphi'' dx''+$$

$$\int_{-\infty}^{+\infty}\int_0^{2\pi}\int_0^1 \frac{K\left(x,\mu;x'',\mu'';\varphi-\varphi''\right)}{\frac{\alpha(x)}{\mu}+\frac{\alpha(x'')}{\mu''}}U_i\left(x'',\mu'',\varphi''\right)\frac{d\mu''}{\mu''}d\varphi'' dx''+$$

doi: https://doi.org/10.52526/25792776-23.70.2-235

$$\int_{-\infty}^{+\infty}\int_{0}^{2\pi}\int_{0}^{1}\int_{-\infty}^{+\infty}\int_{0}^{2\pi}\int_{0}^{1}\frac{K\left(x,\mu;x''',\mu''';\varphi-\varphi'''\right)}{\frac{\alpha(x)}{\mu}+\frac{\alpha(x''')}{\mu'''}}r\left(x''',-\mu''';x'',\mu'';\varphi'''-\varphi''\right)\cdot$$
$$\cdot\, Q_i\left(x'',\mu'',\varphi''\right)\frac{d\mu''}{\mu''}d\varphi''dx''\frac{d\mu'''}{\mu'''}d\varphi'''dx'''. \tag{10}$$

The following designations were adopted here:

$$Z_i\left(x,\mu,\varphi\right)\equiv\int_{-\infty}^{+\infty}\int_{0}^{2\pi}\int_{0}^{1}r\left(x,\mu;x',-\mu';\varphi-\varphi'\right)\beta_i\left(x',\mu',\varphi'\right)d\mu'd\varphi'dx', \tag{11}$$

$$Q_i\left(x'',\mu'',\varphi''\right)\equiv\int_{-\infty}^{+\infty}\int_{0}^{2\pi}\int_{0}^{1}\frac{K\left(x',\mu';x'',\mu'';\varphi'-\varphi''\right)}{\frac{\alpha(x')}{\mu'}+\frac{\alpha(x'')}{\mu''}}\beta_i\left(x',\mu',\varphi'\right)d\mu'd\varphi'dx', \tag{12}$$

$$U_i\left(x'',\mu'',\varphi''\right)\equiv\int_{-\infty}^{+\infty}\int_{0}^{2\pi}\int_{0}^{1}r\left(x'',\mu'';x'\mu';\varphi''-\varphi'\right)\beta_i\left(x',\mu',\varphi'\right)d\mu'd\varphi'dx'. \tag{13}$$

Symmetrical, positive, and continuous kernel $K\left(x,\mu;x',\mu';\varphi-\varphi'\right)$ can be approximated by a bilinear series

$$K\left(x,\mu;x',\mu';\varphi-\varphi'\right)\sim K_N\left(x,\mu;x',\mu';\varphi-\varphi'\right)=\sum_{m=1}^{N}\nu_m\beta_m\left(x,\mu,\varphi\right)\beta_m\left(x',\mu',\varphi'\right). \tag{14}$$

Using the decomposition (14), the ratio (10) can be rewritten as

$$\frac{4\pi}{\lambda}\nu_i\beta_i\left(x,\mu,\varphi\right)=Z_i\left(x,\mu,\varphi\right)+\int_{-\infty}^{+\infty}\int_{0}^{2\pi}\int_{0}^{1}r\left(x,\mu;x'',\mu'';\varphi-\varphi''\right)Q_i\left(x'',\mu'',\varphi''\right)\frac{d\mu''}{\mu''}d\varphi''dx''+$$
$$\sum_{m=1}^{N}\nu_m\beta_m\left(x,\mu,\varphi\right)\int_{-\infty}^{+\infty}\int_{0}^{2\pi}\int_{0}^{1}\frac{\beta_m\left(x'',\mu'',\varphi''\right)}{\frac{\alpha(x)}{\mu}+\frac{\alpha(x'')}{\mu''}}U_i\left(x'',\mu'',\varphi''\right)\frac{d\mu''}{\mu''}d\varphi''dx''+$$
$$\sum_{m=1}^{N}\nu_m\beta_m\left(x,\mu,\varphi\right)\int_{-\infty}^{+\infty}\int_{0}^{2\pi}\int_{0}^{1}\int_{-\infty}^{+\infty}\int_{0}^{2\pi}\int_{0}^{1}\frac{\beta_m\left(x''',\mu''',\varphi'''\right)}{\frac{\alpha(x)}{\mu}+\frac{\alpha(x''')}{\mu'''}}r\left(x''',-\mu''';x'',\mu'';\varphi'''-\varphi''\right)\cdot$$
$$\cdot\, Q_i\left(x'',\mu'',\varphi''\right)\frac{d\mu''}{\mu''}d\varphi''dx''\frac{d\mu'''}{\mu'''}d\varphi'''dx''' \,. \tag{15}$$

Accounting (14) to (12) gives

$$Q_i\left(x'',\mu'',\varphi''\right)\equiv\sum_{m=1}^{N}\nu_m\beta_m\left(x'',\mu'',\varphi''\right)\int_{-\infty}^{+\infty}\int_{0}^{2\pi}\int_{0}^{1}\frac{\beta_m\left(x',\mu',\varphi'\right)}{\frac{\alpha(x')}{\mu'}+\frac{\alpha(x'')}{\mu''}}\beta_i\left(x',\mu',\varphi'\right)d\mu'd\varphi'dx'. \tag{16}$$

Substitution (16) to (15) leads to the equation

$$\frac{4\pi}{\lambda}\nu_i\beta_i\left(x,\mu,\varphi\right)=Z_i\left(x,\mu,\varphi\right)+\sum_{m=1}^{N}\nu_m\int_{-\infty}^{+\infty}\int_{0}^{2\pi}\int_{0}^{1}r\left(x,\mu;x'',\mu'';\varphi-\varphi''\right)\beta_m\left(x'',\mu'',\varphi''\right)\cdot$$
$$\int_{-\infty}^{+\infty}\int_{0}^{2\pi}\int_{0}^{1}\frac{\beta_m\left(x,\mu',\varphi'\right)}{\frac{\alpha(x')}{\mu'}+\frac{\alpha(x'')}{\mu''}}\beta_i\left(x',\mu',\varphi'\right)d\mu'd\varphi'dx'\frac{d\mu''}{\mu''}d\varphi''dx''+$$
$$\sum_{m=1}^{N}\nu_m\beta_m\left(x,\mu,\varphi\right)\int_{-\infty}^{+\infty}\int_{0}^{2\pi}\int_{0}^{1}\frac{\beta_m\left(x'',\mu'',\varphi''\right)}{\frac{\alpha(x)}{\mu}+\frac{\alpha(x'')}{\mu''}}U_i\left(x'',\mu'',\varphi''\right)\frac{d\mu''}{\mu''}d\varphi''dx''+$$

doi: https://doi.org/10.52526/25792776-23.70.2-235

$$\sum_{m=1}^{N}\sum_{n=1}^{N}\nu_m\nu_n\beta_m\left(x,\mu,\varphi\right)\int_{-\infty}^{+\infty}\int_{0}^{2\pi}\int_{0}^{1}\int_{-\infty}^{+\infty}\int_{0}^{2\pi}\int_{0}^{1}\frac{\beta_m\left(x''',\mu''',\varphi'''\right)}{\frac{\alpha(x)}{\mu}+\frac{\alpha(x''')}{\mu'''}}r\left(x''',-\mu''';x'',\mu'';\varphi'''-\varphi''\right)\beta_n\left(x'',\mu'',\varphi''\right)\cdot$$

$$\int_{-\infty}^{+\infty}\int_{0}^{2\pi}\int_{0}^{1}\frac{\beta_n\left(x',\mu',\varphi'\right)}{\frac{\alpha(x')}{\mu'}+\frac{\alpha(x'')}{\mu''}}\beta_i\left(x',\mu',\varphi'\right)d\mu'd\varphi'dx'\frac{d\mu''}{\mu''}d\varphi''dx''\frac{d\mu'''}{\mu'''}d\varphi'''dx'''. \tag{17}$$

Let's introduce the notations:

$$w_{ni}\left(x'',\mu'',\varphi''\right)\equiv\beta_n\left(x'',\mu'',\varphi''\right)\int_{-\infty}^{+\infty}\int_{0}^{2\pi}\int_{0}^{1}\frac{\beta_n\left(x',\mu',\varphi'\right)}{\frac{\alpha(x')}{\mu'}+\frac{\alpha(x'')}{\mu''}}\beta_i\left(x',\mu',\varphi'\right)d\mu'd\varphi'dx',$$

$$D_{mi}\left(x,\mu,\varphi\right)\equiv\int_{-\infty}^{+\infty}\int_{0}^{2\pi}\int_{0}^{1}r\left(x,\mu;x'',\mu'';\varphi-\varphi''\right)w_{mi}\left(x'',\mu'',\varphi''\right)\frac{d\mu''}{\mu''}d\varphi''dx''+\beta_m\left(x,\mu,\varphi\right)\cdot$$

$$\int_{-\infty}^{+\infty}\int_{0}^{2\pi}\int_{0}^{1}\frac{\beta_m\left(x'',\mu'',\varphi''\right)}{\frac{\alpha(x)}{\mu}+\frac{\alpha(x'')}{\mu''}}\frac{d\mu''}{\mu''}d\varphi''dx''\int_{-\infty}^{+\infty}\int_{0}^{2\pi}\int_{0}^{1}r\left(x'',\mu'';x'\mu';\varphi''-\varphi'\right)\beta_i\left(x',\mu',\varphi'\right)d\mu'd\varphi'dx',$$

$$V_{mni}\left(x,\mu,\varphi\right)\equiv\beta_m\left(x,\mu,\varphi\right)\int_{-\infty}^{+\infty}\int_{0}^{2\pi}\int_{0}^{1}\int_{-\infty}^{+\infty}\int_{0}^{2\pi}\int_{0}^{1}\frac{\beta_m\left(x''',\mu''',\varphi'''\right)}{\frac{\alpha(x)}{\mu}+\frac{\alpha(x''')}{\mu'''}}r\left(x''',-\mu''';x'',\mu'';\varphi'''-\varphi''\right)\cdot$$

$$\cdot\, w_{ni}\left(x'',\mu'',\varphi''\right)\frac{d\mu''}{\mu''}d\varphi''dx''\frac{d\mu'''}{\mu'''}d\varphi'''dx'''. \tag{18}$$

Then equation (17) for finding eigenfunctions $\beta_i\left(x,\mu,\varphi\right)$ will finally be written in the form

$$\frac{4\pi}{\lambda}\nu_i\beta_i\left(x,\mu,\varphi\right)=Z_i\left(x,\mu,\varphi\right)+\sum_{m=1}^{N}\nu_mD_{mi}\left(x,\mu,\varphi\right)+\sum_{m=1}^{N}\sum_{n=1}^{N}\nu_m\nu_nV_{mni}\left(x,\mu,\varphi\right). \tag{19}$$

With the help of the orthonormalization condition (9), it is not difficult to derive from the system (19) a nonlinear system of algebraic equations for finding the eigenvalues ν_i ,

$$\frac{4\pi}{\lambda}\nu_i=b_i+\sum_{m=1}^{N}\nu_mc_{mi}+\sum_{m=1}^{N}\sum_{n=1}^{N}\nu_m\nu_nf_{mni}\ , \tag{20}$$

where the notations are entered:

$$b_i\equiv\int_{-\infty}^{+\infty}\int_{0}^{2\pi}\int_{0}^{1}Z_i\left(x,\mu,\varphi\right)\beta_i\left(x,\mu,\varphi\right)d\mu d\varphi dx, \tag{21}$$

$$c_{mi}\equiv\int_{-\infty}^{+\infty}\int_{0}^{2\pi}\int_{0}^{1}D_{mi}\left(x,\mu,\varphi\right)\beta_i\left(x,\mu,\varphi\right)d\mu d\varphi dx, \tag{22}$$

$$f_{mni}\equiv\int_{-\infty}^{+\infty}\int_{0}^{2\pi}\int_{0}^{1}V_{mni}\left(x,\mu,\varphi\right)\beta_i\left(x,\mu,\varphi\right)d\mu d\varphi dx. \tag{23}$$

Taking into account the ratios (11) and (8) in the notations (21)-(23) gives them the form:

$$b_i\equiv\int_{-\infty}^{+\infty}\int_{0}^{2\pi}\int_{0}^{1}\int_{-\infty}^{+\infty}\int_{0}^{2\pi}\int_{0}^{1}\beta_i\left(x,\mu,\varphi\right)r\left(x,\mu;x',-\mu';\varphi-\varphi'\right)\beta_i\left(x',\mu',\varphi'\right)d\mu'd\varphi'dx'd\mu d\varphi dx \tag{24}$$

$$c_{mi}\equiv\int_{-\infty}^{+\infty}\int_{0}^{2\pi}\int_{0}^{1}\left[\int_{-\infty}^{+\infty}\int_{0}^{2\pi}\int_{0}^{1}r\left(x,\mu;x'',\mu'';\varphi-\varphi''\right)w_{mi}\left(x'',\mu'',\varphi''\right)\frac{d\mu''}{\mu''}d\varphi''dx''+\right.$$

doi: https://doi.org/10.52526/25792776-23.70.2-235

$$\beta_m(x,\mu,\varphi)\int_{-\infty}^{+\infty}\int_0^{2\pi}\int_0^1 \frac{\beta_m(x'',\mu'',\varphi'')}{\frac{\alpha(x)}{\mu}+\frac{\alpha(x'')}{\mu''}}\frac{d\mu''}{\mu''}d\varphi''dx''\cdot$$

$$\int_{-\infty}^{+\infty}\int_0^{2\pi}\int_0^1 r\left(x'',\mu'';x'\mu';\varphi''-\varphi'\right)\beta_i\left(x',\mu',\varphi'\right)d\mu'd\varphi'dx'\beta_i(x,\mu,\varphi)\,d\mu d\varphi dx\ , \tag{25}$$

$$f_{mni}\equiv\int_{-\infty}^{+\infty}\int_0^{2\pi}\int_0^1\int_{-\infty}^{+\infty}\int_0^{2\pi}\int_0^1 w_{mi}\left(x'',\mu'',\varphi''\right)r\left(x''',-\mu''';x'',\mu'';\varphi'''-\varphi''\right)w_{ni}\left(x'',\mu'',\varphi''\right)\frac{d\mu''}{\mu''}d\varphi''dx''\frac{d\mu'''}{\mu'''}d\varphi''' \tag{26}$$

By opening the square brackets and taking into account the first notation of (18), the ratio (2) is given a simpler shape

$$c_{mi}\equiv 2\int_{-\infty}^{+\infty}\int_0^{2\pi}\int_0^1\int_{-\infty}^{+\infty}\int_0^{2\pi}\int_0^1 \beta_i(x,\mu,\varphi)\,r\left(x,\mu;x'',\mu'';\varphi-\varphi''\right)w_{mi}\left(x'',\mu'',\varphi''\right)\frac{d\mu''}{\mu''}d\varphi''dx''d\mu dx d\varphi. \tag{27}$$

Thus, it follows from (5) and (14) that the explicit solution of the problem of diffuse reflection in the general case of redistribution of radiation in frequencies and directions is given by the expression

$$\rho\left(x,\mu;x'\mu';\varphi-\varphi'\right)=\frac{\sum_{m=1}^{N}\nu_m\beta_m(x,\mu,\varphi)\,\beta_m(x',\mu',\varphi')}{\mu'\left(\frac{\alpha(x)}{\mu}+\frac{\alpha(x')}{\mu'}\right)}\ , \tag{28}$$

where the values of $\beta_m(x,\mu,\varphi)$ satisfy the system of nonlinear functional integral equations (19) taking into account the notations (18), and the values ν_m satisfy the system of nonlinear algebraic equations (20) taking into account the notations (24), (26), (27).

The general scheme of the organization of the joint calculation of systems (19) and (20) does not differ from those described in the two previous works (Pikichyan 2023a, b). There is also no difference in the general line of calculations for obtaining an analytical two-way relationship between the solutions of the traditional and developed approaches, so we will not dwell on them here, in order to avoid unnecessary cumbersomeness.

3. Conclusion

In this paper, using the approach introduced in the author's two previous works (Pikichyan 2023a, b), conventionally called the method of "decomposition of the resultant field (DRF)", it is shown that the desired diffuse reflection function $\rho(x,\mu;x'\mu';\varphi-\varphi')$ formally dependent on six independent quantities, is expressed in terms of some specially constructed eigenfunctions $\beta_m(x,\mu,\varphi)$ dependent on only three variables. To compute the desired eigenfunctions and their corresponding eigenvalues, a system consisting of nonlinear functional integral and nonlinear algebraic equations was obtained. The physical basis for the effectiveness of the developed approach lies in the fact that in the process of multiple scattering of the quantum, with each subsequent act of scattering, the field becomes more and more "smooth", due to a certain mathematical procedure of its integration with the characteristics of previous scatterings. As a result, it is easier to represent the "smoothed" characteristics of the multiple scattering field by decomposition into a series according to some specially constructed self-consistent system of orthonormalized functions than to use the same procedure for the characteristics of the primary "unsmoothed" field of a single scattering act.

Acknowledgements

I would like to express my sincere gratitude to Professor Levon Gurgen Arabadzhyan for numerous discussions and valuable mathematical consultations during the implementation of this work.

References

Engibaryan N. B., Nikogosyan A. G., 1972a, Astrophysics, 8, 39

Engibaryan N. B., Nikogosyan A. G., 1972b, Akademiia Nauk Armianskoi SSR Doklady, 54, 91

doi: https://doi.org/10.52526/25792776-23.70.2-235

Pikichyan H. V., 2023a, Communications of the Byurakan Astrophysical Observatory, 70, 143

Pikichyan H. V., 2023b, Communications of the Byurakan Astrophysical Observatory, 70, 204

doi: https://doi.org/10.52526/25792776-23.70.2-235

Communications of BAO, Vol. 70, Issue 2, 2023, pp. 242-248

The Pleiades flare stars in the Gaia era

V. Hambaryan[1,2*], S. Ghazaryan[2†], L. ambardzumyan[2,3‡], R. Neuhaeuser[1§], A. Mirzoyan[4¶], K.P. Tsvetkova[5‖ 1]

[1]Astrophysical Institute and University Observatory of Friedrich-Schiller-University Jena, Germany
[2]Byurakan Astrophysical Observatory after V.A. Ambartsumian, Armenia
[3]Astrophysical Research Laboratory of Physics Institute, Yerevan State University, Armenia
[4]Center for Asptroparticle Physics, YSU, Armenia
[5]Institute of Astronomy with NAO, Bulgarian Academy of Sciences, Sofia, Bulgaria

Abstract

We study the six dimensional arrangement of flare stars in the Pleiades cluster region using the third release of the *Gaia*–mission (*Gaia* DR3) and we provide preliminary, a new, original view of the spatial configuration of the flare "star-members" of the cluster.

1. Introduction

Historically, star clusters have always been cornerstones for our knowledge of stellar evolution. The Pleiades is the best studied northern cluster and qualifies as a benchmark region (see, e.g. Lodieu et al., 2019). Numerous multi-wavelength surveys have been conducted in the region to study in depth the stellar and sub-stellar members. Pleiades members share a significant common proper motion compared to neighboring stars with $(\mu_\alpha \cos\delta,\, \mu_\delta) \sim (19.5,\, -45.5)$ mas/yr (Jones, 1981, van Leeuwen, 2009). This large mean motion, high galactic latitude ($b \sim 24°$), and low reddening along the line of sight of the cluster ($\mathrm{E}(B-V) = 0.03$ mag) makes it one of the best targets for comprehensive astrometric and photometric study. The cluster is also nearby, with the Hipparcos distance placing the Pleiades at 120.2 ± 1.9 pc (van Leeuwen, 2009) while other works suggest a mean distance of 134 pc with an uncertainty of 5 pc (Gatewood et al., 2000, Johnson & Mitchell, 1958, Pinfield et al., 2000, Southworth et al., 2005). The age of the cluster has also been debated in the literature, ranging from 70–130±20 Myr.

In 1954, Ambartsumian (1954), while analyzing the problem of the nature of continuous emission in the spectra of T Tauri type stars, called attention to the unusual observational fact that during the brief flares of UV Cet type stars, continuous emission also arises in their spectra. At the same time Haro (1954, 1956) suggested that the flare stars (FSs) in the vicinity of the Sun and the FSs in stellar associations belong to the same physical class of variables and might have a similar origin, i.e., that they represent different evolutionary stages of the common predecessors, namely, T Tauri or T Tauri–like stars.

Of decisive significance in the confirmation of this fundamentally new idea was the accidental discovery by Johnson & Mitchell (1958) of the first flare star in the Pleiades cluster. This discovery encouraged photographic observations which led to the detection of a several dozen FSs.

Ambartsumian (1969) developed a simple statistical method that makes it possible to estimate the total number of unknown FSs in any stellar system by the numbers of FSs to have flared up once and twice. By application of this method to the data of the Pleiades 68 FSs, known in that time, a conclusion was reached:

- All or almost all faint stars in the Pleiades cluster are FSs;
- The stage of flare activity is a regular stage in the evolution of red dwarf stars, through which all stars of this class must pass.

*Valeri.Hambaryan@uni-jena.de, Corresponding author
†satenikghazarjan@yahoo.de
‡hambardzumyanlian@gmail.com
§Ralph.Neuhaeuser@uni-jena.de
¶arikinna2014@gmail.com
‖katya.tsvetkova09@gmail.com

doi: https://doi.org/10.52526/25792776-23.70.2-242

These results were so important for the evolution of red dwarfs that they initiated a campaign of wide-field photographic observations at the many observatories which led to discovery and study FSs in the regions of different ages stellar clusters and associations. In particular, in the Pleiades cluster region were detected ~ 500 new FSs (HCG catalog, Haro et al., 1982, the catalog presents the data of 519 FSs). The list of FSs in the Pleiades region was completed by discovery of a new FSs after publication of the HCG catalog and contains the data of 547 FSs (hereafter the HCG+ catalog, Mirzoyan, 1993, 1495 flares during effective observational time of ~ 3200 hours) and the estimated total number of FSs is ~ 1000 (Akopian, 2021). The regular photographic observations with wide–angle telescopes of FSs of stellar groups stopped in the early 80th of the 20th century because of cardinal changes of types of detectors for astronomical observations.

Recently, in the literature reported studies of randomly flashing objects obtained with the Kepler orbital observatory. In particular, Ilin et al. (2021) for the Pleiades region inspected 741 light curves (provided by Kepler spacecraft 2009-2018 Koch et al. (2010) based on mission K2 "Second Light" Howell et al. (2014)) and detected 1583 flares of 487 stars, with the probability of membership $p > 0.8$ (Cantat-Gaudin et al., 2018, Olivares et al., 2018b, Rebull et al., 2016). Note that average flare frequency is much higher with Kepler observations in comparison to the above mentioned photographic ones (further analysis of the Kepler FSs data beyond the scope of this paper and will be published elsewhere).

Naturally, a question was raised: *Whether all FSs observed in the Pleiades region are members of the cluster, i.e. have common motion and are located in the same volume in the space?*

2. The Pleiades FSs *before* the Gaia mission

The first part of the question, i.e. common proper motion, was addressed using the catalog of members based on the extensive studies of astrometric, photometric, and spectroscopic observations of the Pleiades (e.g. Hambly et al., 1993, Haro et al., 1982, Hertzsprung, 1947, Jones, 1981, Schilbach et al., 1995, Stauffer, 1982, 1984, Stauffer et al., 1991, among others).

Naturally, apart from the Pleiades FSs members, several non–member FSs of the cluster have been found. Some of the latter belong to the Hyades, others to the solar vicinity (i.e., foreground stars), probably others to some yet unidentified stellar system, or simply to the general Galactic field (background stars).

The question is: *What is the percentage of non–members among observed FSs in the Pleiades cluster region?*

For computing cluster membership, above mentioned various authors (e.g., Hambly et al., 1993, Schilbach et al., 1995, Stauffer et al., 1991), used a method (e.g., Sanders, 1971, Vasilevskis et al., 1958) which proposes to fit the sum of two bi–dimensional Gaussians or a combination of a Gaussian and a linear model to the proper motion distribution. For selecting reliable members of the cluster, a photometric criterion also was used. This approach assumes a common nature of motions of all members and did not yield realistic results (e.g., Schilbach et al., 1995). It excludes the possibility of the existence of different moving groups within the same stellar system arising from non–coeval star formation, or does not take into account the orbital motion of double and chaotic motion of multiple stars, which distorts the general picture of the established distribution of motions.

The first indication that flare activity could be possibly used as a reliable criterion for determining the membership of stars in stellar systems was obtained from the discussion of the distribution of FSs in the Pleiades cluster region. Namely, the space distribution of FSs in the Pleiades cluster showed (e.g., Chavushian, 1979, Chavushian et al., 1999, 2004, Hambaryan, 1998, Mirzoyan, 1976, 1983, Mirzoyan et al., 1993) that the concentration of FSs around the center of the Pleiades cluster is the same, i.e. the surface density of FSs decreases upon distance from the center of cluster, irrespective their proper motion or membership probability.

Nevertheless, these studies showed that significant number of FSs in the Pleiades region can be considered as *non–members* (52% and 35%, Hambly et al., 1993, Jones, 1981, accordingly).

An alternative estimate of the expected number of classical FSs (UV Cet type) to be detected by photographic multi-exposure method of observations of the Pleiades cluster region and belonging to the general Galactic star field, under assumption that UV Cet type stars distributed uniformly, is ~ 170, (i.e., not exceeding 20% Hambaryan, 1998, Mirzoyan et al., 1988).

doi: https://doi.org/10.52526/25792776-23.70.2-242

3. The Pleiades FSs with *Gaia* DR3

Given the unprecedent precise astrometric and kinematic parameters of stars provided by *Gaia* DR3 release a numerous surveys of distinct sizes and depths have looked at the Pleiades (see, e.g., Heyl et al., 2022, Hunt & Reffert, 2023, Lodieu et al., 2019, Olivares et al., 2018a,b, Qin et al., 2023, see their references). Most of them provided also member list of the Pleiades (1100-1300 member stars) and characteristic parameters, such as core and tidal radii (r_{core} = 2.5-3.5pc and r_{tidal} = 10-18pc), of the cluster.

We have identified FSs from HCG+ catalog in the Pleiades region with *Gaia* DR3 sources and verified it by using identification charts. In addition we identified them also with most recent Pleiades member star list (Qin et al., 2023) also based on the *Gaia* DR3 data. In Fig. 1 are presented results of this identification and some analysis of them depending on the observed distances of the FSs in the Pleiades cluster region. It also suggests that $\sim$ 30% of the observed FSs can be considered as *non–members* of the Pleiades cluster from the point of view of the common proper motion and allocation in the same volume in the space.

A catalog and identification charts of the Pleiades flare stars (519 FSs),
Haro, G.; Chavira, E.; Gonzalez, G. 1982, (completed, i.e. HCG+)

HCG+ catalogue of the Pleiades Flare Stars: → 547

With Gaia DR3 Ids

Number of the Pleiades FSs with 2 parameters solution → 503
Number of the Pleiades FSs with 5 parameters solution → 492
Number of the Pleiades FSs with 5 parameters solution +
Radial velocities → 211 (320 with Simbad database)

$$\frac{Plx}{e\_Plx} \geq 5 \;\&\; RUWE < 1.4 \qquad R_{tidal} = 11.3\,pc; \quad d_{Pleiades} = 135.15pc$$

RUWE -> a renormalized unit weight error

$$N_{FS} = \begin{cases} 15, & d \leq 100pc \\ 326, & 100 < d < 170 \\ 151, & d \geq 170\,pc \end{cases}$$

$$N_{FS} = \begin{cases} 15, & d \leq 100pc \\ 336, & 100 < d < 200 \\ 141, & d \geq 170\,pc \end{cases}$$

Percentage of „non-members“ ≈ 30%

Figure 1. Identification of the Pleiades FSs (HCG+) with *Gaia* DR3.

Moreover, the distribution of parallaxes and proper motions also show double–peaked shape of all FSs stars observed in the Pleiades cluster region and having *Gaia* DR3 ID numbers (see, Fig. 2).

In contrary, distribution of radial velocities is uni-modal (Fig.2) and angular distribution of the FSs around the center of the Pleiades cluster does not show any significant asymmetry (Fig.3).

These results can be interpreted with a number of statements:

- Two groups of flare stars with different flare activity levels;
- Coeval/Non-coeval star formation;
- Another distant star cluster in the background of the Pleiades;

doi: https://doi.org/10.52526/25792776-23.70.2-242

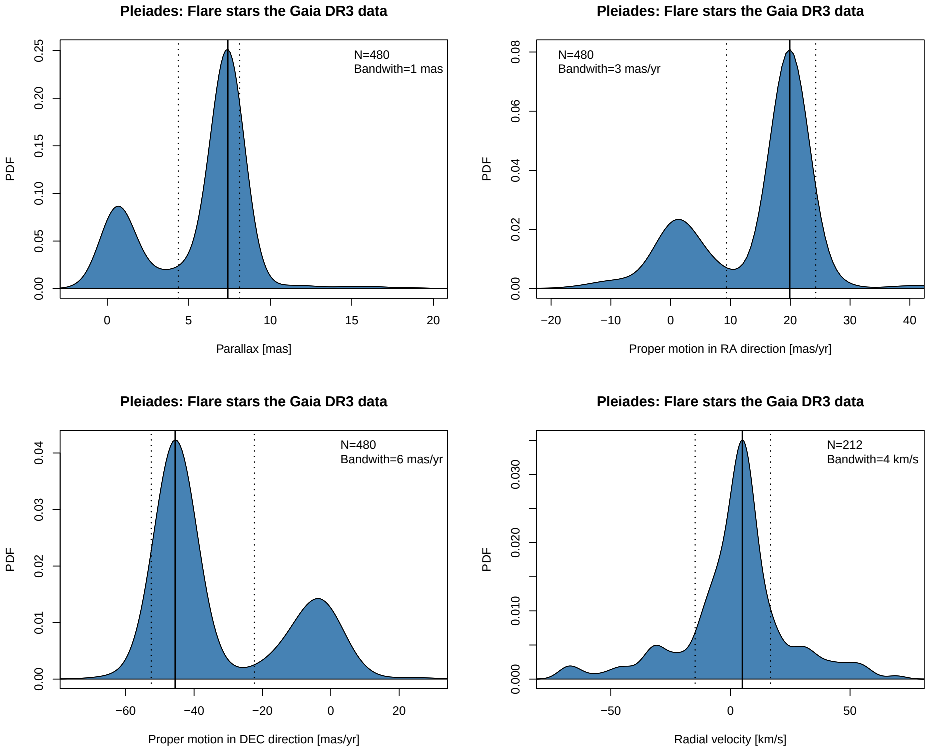

Figure 2. Distribution of the Pleiades FSs astrometric and kinematic parameters based on the data of *Gaia* DR3

- Owing to the dynamical evolution of the Pleiades open cluster some number of stars have already escaped it, and currently are in the same evolutionary stage, i.e. showing similar flaring activity as member stars of the same mass.

The last possibility was not considered in the previous studies of FSs observed in the Pleiades cluster region. Most recently, Heyl et al. (2022) reconstructed the Pleiades with *Gaia* EDR3 by selecting all objects within 100 pc of the Sun and all sources within 200 pc of the Sun that lie within 45° of the Pleiades on the sky and divided into two groups, i.e. member stars and escapees (i.e., evaporated stars owing to the dynamical evolution of a stellar cluster). Namely, to find the center-of-mass motion and position for the Pleiades, the proper, motions of all stars within one degree on the sky from the center of the cluster was determined and by using those stars within the sample that have radial velocities measured with *Gaia* DR2, the reconstruction for the others was performed, and the mean velocity of the stars of the Pleiades cluster relative to the Sun was estimated: $v_{cluster} = (-7.1 \pm 0.4; -28.3 \pm 0.1; -144 \pm 0.2)\ km/s$. Using all the stars within the sample, the mean displacement of the cluster relative to the Sun was calculated: $d_{cluster} = (-120.99 \pm 0.20; 28.96 \pm 0.06; -54.23 \pm 0.10)\ pc$. To find the escapees, the evaporated velocity was computed assuming that the $v_{evaporated} \approx \sqrt{2} * v_\sigma$. $v_\sigma \approx 2.4\ km * s^{-1}$, so $v_{evaporated} \approx 3.4\ km * s^{-1}$. We have revisited these lists and completed with the data (mainly radial velocities) of *Gaia* DR3 and *Simbad astronomical database*. In the Fig. 4 are shown distribution of the member and evaporated stars around of the center–of–mass of the Pleiades cluster and in the inner panels of the figures (see, Fig.4) are given kinematic characteristics of them using 3D positions and velocities. Obviously, evaporated stars are distributed over much greater distances from the center–of–mass, showing also greater velocities in comparison to the member ones.

doi: https://doi.org/10.52526/25792776-23.70.2-242

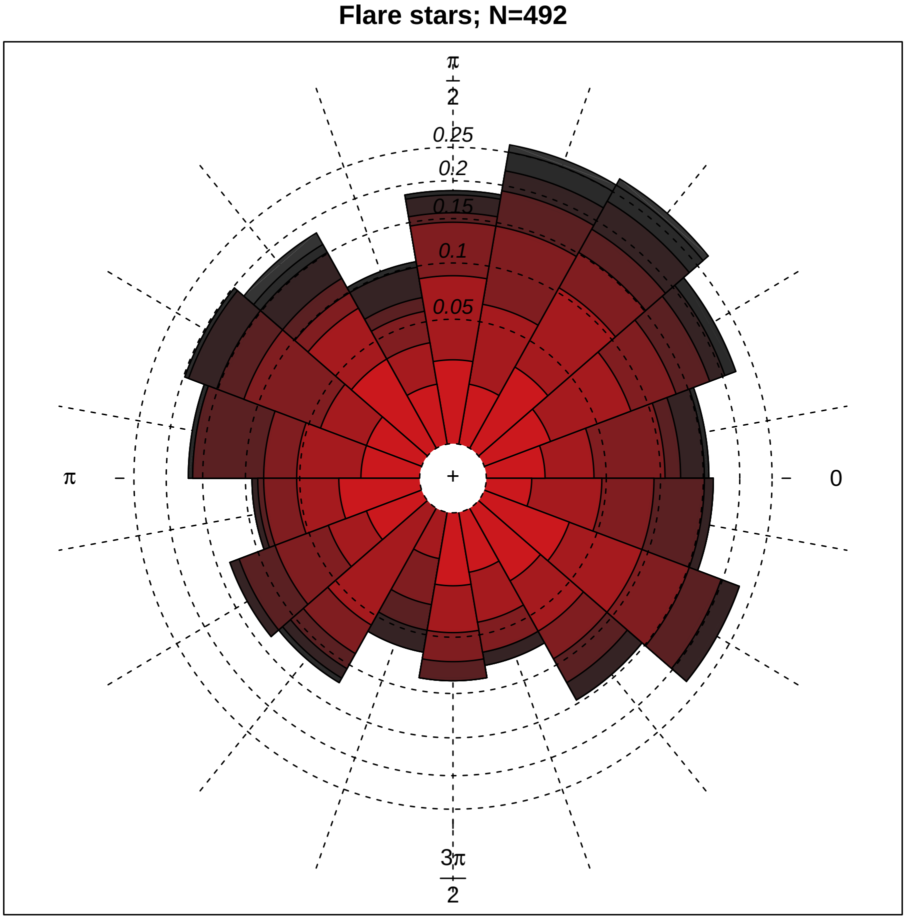

Figure 3. A succinct view of the angular distances and directions of 492 FSs relative to the center of the Pleiades cluster based on the data of *Gaia* DR3.

Despite to the slightly different occupied regions on the sky, we have compared and cross-matched lists of Pleiades member stars presented in the three catalogs (HCG+, Ilin et al. (2021) and Heyl et al. (2022)). It is noticeable that Heyle's 24 escapee stars are included in Ilin's catalogue of flare stars. Also 289 Heyl escape stars and 492 HCG+ member stars have 8 overlaps.

Next, we identified FSs (HCG+ catalog) observed in the Pleiades cluster region with Heyl et al. (2022) lists and performed trace-back motion analysis (see, e.g. Hambaryan et al., 2022, Neuhäuser et al., 2020) of FSs–escapees. It showed, that out of 109 non–member FSs 69 (63%), most probably, were within the tidal radius (11.3 pc) of the Pleiades cluster in the past $\sim$ 3-8 Myr ago.

4. Concluding remarks

Despite significant number of FSs observed in the Pleiades cluster region can be considered as "non–members", i.e. do not show common proper motion and not located in the same volume in the space, nevertheless, they must be considered as members of the Pleiades cluster from the evolutionary point of view, i.e. they are in the same, flare activity stage of red dwarf stars.

Thus, depending on the astrophysical problem:

1) To study present day mass function or distribution FSs around to the center of the cluster:
   - classical membership is preferable.
2) For statistical estimators of flare frequencies:
   - flybys and escapees must be taken into account.

doi: https://doi.org/10.52526/25792776-23.70.2-242

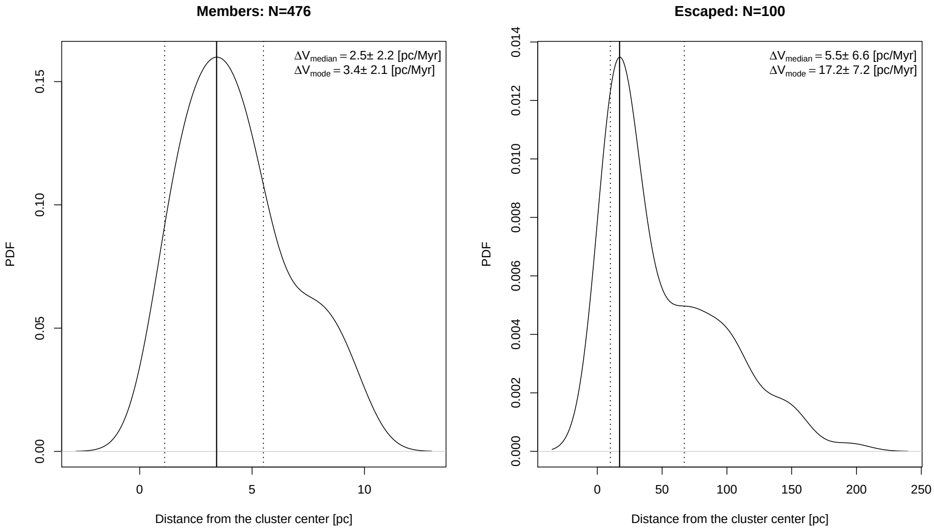

Figure 4. Distribution of member and escaped stars of the Pleiades cluster using 3D positions and velocities based on the *Gaia* DR3 data.

Acknowledgments

This work was supported by the Science Committee of RA (Adjunct Research Professorship Program (Remote Laboratory) project No 22RL-039). It is also presented during 15th Joint Byurakan-Abastumani Colloquium held on 1-5 May 2023 in Byurakan and dedicated to Lyudwik Mirzoyan's 100th anniversary.

References

Akopian A. A., 2021, Communications of the Byurakan Astrophysical Observatory, 68, 150

Ambartsumian V. A., 1954, Communications of the Byurakan Astrophysical Observatory, 13, 3

Ambartsumian V., 1969, Publ. House Acad. Sci. Armenian SSR. Yerevan, p. 283

Bouy H., et al., 2015, Astron. Astrophys. , 577, A148

Cantat-Gaudin T., et al., 2018, Astron. Astrophys. , 618, A93

Chavushian H., 1979, PhD thesis, Byurakan Astrophysical Observatory, p. 283

Chavushian H. S., Oskanian A. V., Broutian G. H., 1999, Astrophysics, 42, 404

Chavushian H. S., Pikichian H. V., Oskanian A. V., Broutian G. H., 2004, Astrophysics, 47, 313

Feigelson E. D., Babu G. J., 2012, Modern Statistical Methods for Astronomy. Cambridge University Press

Gaia Collaboration et al., 2018, Astron. Astrophys. , 616, A10

Gatewood G., de Jonge J. K., Han I., 2000, Astrophys. J. , 533, 938

Hambaryan V. V., 1998, in Donahue R. A., Bookbinder J. A., eds, Astronomical Society of the Pacific Conference Series Vol. 154, Cool Stars, Stellar Systems, and the Sun. p. 1492

Hambaryan V., et al., 2022, Mon. Not. R. Astron. Soc. , 511, 4123

Hambly N. C., Hawkins M. R. S., Jameson R. F., 1993, Astron. and Astrophys. Suppl. Ser. , 100, 607

Haro G., 1954, Boletin de los Observatorios Tonantzintla y Tacubaya, 2, 11

Haro G., 1956, Boletin de los Observatorios Tonantzintla y Tacubaya, 2, 8

Haro G., Chavira E., Gonzalez G., 1982, Boletin del Instituto de Tonantzintla, 3, 3

Hertzsprung E., 1947, Annalen van de Sterrewacht te Leiden, 19, A1

Heyl J., Caiazzo I., Richer H. B., 2022, Astrophys. J. , 926, 132

Howell S. B., et al., 2014, Publications of the Astronomical Society of the Pacific, 126, 398

Hunt E. L., Reffert S., 2023, Astron. Astrophys. , 673, A114

Ilin E., Schmidt S. J., Poppenhäger K., Davenport J. R. A., Kristiansen M. H., Omohundro M., 2021, Astron. Astrophys. , 645, A42

doi: https://doi.org/10.52526/25792776-23.70.2-242

Johnson H. L., Mitchell R. I., 1958, Astrophys. J. , 128, 31

Jones B. F., 1981, Astron. J. , 86, 290

Koch D. G., et al., 2010, The Astrophysical Journal Letters, 713, L79

Lodieu N., Pérez-Garrido A., Smart R. L., Silvotti R., 2019, Astron. Astrophys. , 628, A66

Mirzoyan L. V., 1976, in Kharadze E. K., ed., Stars and Galaxies from Observational Points of View. pp 121–127

Mirzoyan A. L., 1983, Astrofizika, 19, 588

Mirzoyan L. V., 1993, Astrofizika, 36, 277

Mirzoyan L. V., Ambaryan V. V., Garibdzhanyan A. T., Mirzoyan A. L., 1988, Astrofizika, 29, 531

Mirzoyan L. V., Hambarian V. V., Mirzoyan A. L., 1993, Astrofizika, 36, 395

Neuhäuser R., Gießler F., Hambaryan V. V., 2020, Mon. Not. R. Astron. Soc. , 498, 899

Olivares J., et al., 2018a, Astron. Astrophys. , 612, A70

Olivares J., et al., 2018b, Astron. Astrophys. , 617, A15

Pinfield D. J., Hodgkin S. T., Jameson R. F., Cossburn M. R., Hambly N. C., Devereux N., 2000, Mon. Not. R. Astron. Soc. , 313, 347

Qin S., Zhong J., Tang T., Chen L., 2023, Astrophys. J. Suppl. Ser. , 265, 12

Rebull L. M., et al., 2016, The Astronomical Journal, 152, 113

Sanders W. L., 1971, Astron. Astrophys. , 14, 226

Sarro L. M., et al., 2014, Astron. Astrophys. , 563, A45

Schilbach E., Robichon N., Souchay J., Guibert J., 1995, Astron. Astrophys. , 299, 696

Southworth J., Maxted P. F. L., Smalley B., 2005, Astron. Astrophys. , 429, 645

Stauffer J. R., 1982, Astron. J. , 87, 1507

Stauffer J. R., 1984, Astrophys. J. , 280, 189

Stauffer J., Klemola A., Prosser C., Probst R., 1991, Astron. J. , 101, 980

Stauffer J. R., Schultz G., Kirkpatrick J. D., 1998, Astrophys. J. Lett. , 499, L199

Vasilevskis S., Klemola A., Preston G., 1958, Astron. J. , 63, 387

van Leeuwen F., 2009, Astron. Astrophys. , 497, 209

doi: https://doi.org/10.52526/25792776-23.70.2-242

On The Astronomical Context of Fish-shaped Vishap Stone Stelae

H.A. Malkhasyan *

NAS RA V. Ambartsumian Byurakan Astrophysical Observatory (BAO), Armenia

Abstract

The work discusses the problems related to the celestial parallels of Fish-shaped Vishap (dragon) stone stelae. In particular, it is shown that these monuments are the material manifestations of the cult of the constellation Pisces Austrinus (the Southern Fish) and relate to the modern Pisces of zodiac only indirectly. At the same time, the well-known result of their dating by astronomical methods does not change qualitatively, but is more clarified, by placing about 18800 BC. Here, the coincidence of the heliacal rising of Fomalhaut (α Piscis Austrini) and the ancient Armenian Navasard holiday (beginning of the year, 4 days before summer solstice) is taken as the basis of the calculation.

Keywords: *Fish-shaped Vishap Stone Stelae, Piscis Austrinus, Archaeoastronomy, Megalithic Monuments, Armenian Calendar History, Cultural Astronomy*

1. Introduction

Archaeology, especially in the last decade, has touched a lot on the importance of the study of the Vishap stones of the Armenian Highlands (Bobokhyan et al., 2012, 2015, Gilibert et al., 2012, 2013, Petrosyan & Bobokhyan, 2015). The most up-to-date comprehensive information of them is especially reflected in the last publications (Bobokhyan et al., 2020, Gilibert, 2020, Hnila et al., 2019, 2023). However, the works on their astronomical essence are unique. For the first time, the astronomical significance of the Bullheaded and Fish-shaped Vishap stones is hinted, that they may correspond to the Taurus and Pisces constellations of the zodiac, respectively (Khnkikyan, 1997). Astronomer Grigor Broutian made a more meaningful reference to this consideration later. In the mentioned work (Broutian, 2020), according to their astronomical context Vishap stones are classified into 5 main types, which are matched to 5 adjacent constellations of the zodiac (Table 1) (Broutian, 2020). Considering this pattern, the author tried to calculate the approximate date of their creation. In particular, it was based on the fact that, according to the Armenian calendar tradition, the main event of the year is the Navasard holiday and it was celebrated 8 days before the summer solstice[1] in ancient times. With this logic, **the time when the Sun was in the range of the constellation corresponding to Vishap stone on the day of Navasard was calculated** (Table 1).

It is clear, and the author himself states (Broutian, 2020), that such a calculation is very approximate, because in order to make an accurate calculation, it is necessary to specify at which particular point of the constellation the position of the Sun was on the specified day. It should also be noted that the start point of calculation in the mentioned work was the time when the Sun passed from one constellation to another (for example, from Aries to Pisces), and the beginning of the Salvation Era (1 AD) was taken as a time of such transition when the Sun passed from Aries to Pisces at the vernal equinox (Broutian, 2020). However, in the conditions of the mentioned antiquity, such rough[2]

*malkhasyan.hayk84@gmail.com

[1] About the Navasard fast see section 5.

[2] In the mentioned work of Grigor Broutian, 25766 years are taken as the duration of one whole precession, but its more adjusted duration is 25776 years. Such a small difference does not qualitatively affect the obtained results in any way, but in our calculations we took the number 25776 as a basis.

Table 1. Classification and astronomical dating of Vishap stones by Grigor Broutian

Type of Vishap	Corresponding constellation	Date (BC)
Donkeyheaded	Cancer	28487.4
Whit the pair of birds	Gemini	26331.4
Bullheaded	Taurus	24184.4
Ramheaded	Aries	22037.4
Fish-shaped	Pisces	19890.4

calculation is completely acceptable. However, **it should be specially emphasized that if we take as the starting point of the calculation, not the transition from Aries to Pisces, but the conventional midpoint of the section of the Ecliptic "crossing the constellation domain", then the x error will be approximately[3] 1074 years**.

$$x = \frac{25776(precession)}{12 \times 2} = 1074$$

Taking into account such deviations, it is completely acceptable and logical to subtract 2148 years from the dates given in Table 1. In other words, such a calculation allows us to take an interval of 2148 years for the time of the corresponding Vishap stone, accepting the date obtained by Grigor Brutean as its early limit. For example, **it is more correct for Fish-shaped Vishap stones to take period 19897-17749 BC, and the midpoint will be 18823 BC**.

2. The problems in the astronomical interpretation of Fish-shaped Vishap stones.

However convincing such results are (Broutian, 2020), apart from being highly approximate, they are also problematic in several other fundamental issues. Some of these are particularly relevant to the astronomical context of Fish-shaped Vishap stones. Of course, in the analysis of other types of Vishap stones, some questions also have not been addressed yet. One of such problems is the fact that the pair of birds are depicted on the upper part of some Vishap stones, at the same time on the others they are located lower. However, we will not address these problems here and will discuss only some questions related to the astronomical interpretation of Fish-shaped Vishap stones. In particular:

2.1. The Pisces constellation known to us in the zodiac is not odd in number, and Fish-shaped Vishap stones are clearly "statues" of one fish (Figure 1).

The point is that, for example, the idea of a pair of storks depicted on some Vishap stones is clearly connected with the Gemini constellation (Broutian, 2020), which we deal upon in another context, when discussing the Zorats Qarer monument (Malkhasyan, 2022a). In other words, we have the canonical iconography of a pair of birds and the corresponding Gemini constellation (with a idea of pair) in the sky. The same is to be expected in the case of the Pisces constellation, but here an inconsistency arises. Some explanations can be given to this (for example, that in very ancient times, perhaps, this constellation was perceived as *fish and not fishes*, especially since in the Armenian map of Middle Age ("Hamatarats Ashkharacoyc") (Vanandeci, 1695) it is indicated as a *fish instead of fishes* (Tumanyan (1985) p. 12), but such assumptions are extremely flawed and unfounded. In the oldest Sumerian astrolabs known to us, the Pisces of the zodiac are known as "Tails" (^{mul}QUNI.MEŠ), where MEŠ is a indicator of plural (Davtyan (2004) pp. 40-42). Moreover, in modern literature it is customary to consider one of these Tails to be the Swallow's and the other of the Fish (Hoffmann (2021) pp. 127-129) (Figure 2).

[3] The domain of a constellation is a well-defined concept today and was fixed in 1922 by a decision of the International Astronomical Union. However, we do not know any data about these in ancient times. Therefore, the equal part of the year for the 12 constellations of the zodiac are conventionally assigned to. That is, one whole precession time is divided into 12 equal parts (25776/12=2148). Therefore, the center of that period will differ from its borders by 1074 years (2148/2=1074).

Figure 1. The Fish-shaped Vishap stone from Geghama mountains (Imirzek 2) (Petrosyan & Bobokhyan (2015) p. 347)

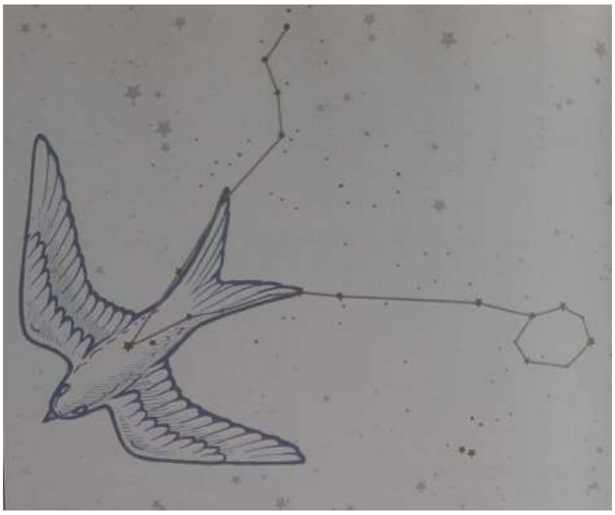

a

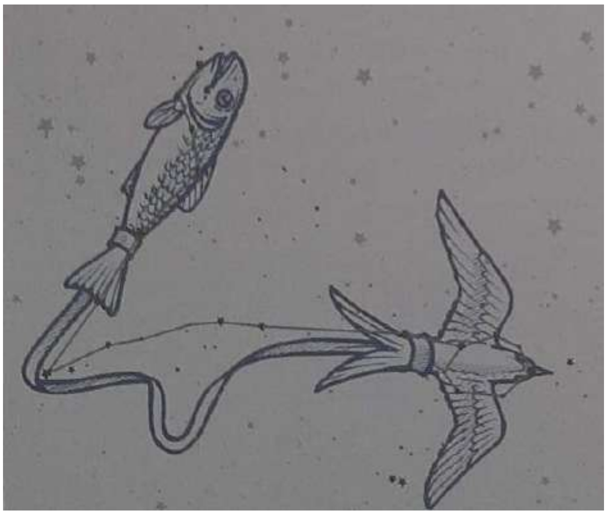

b

Figure 2. Depicting of Pisces stars in Mesopotamia according to Hoffmann S.M.. (a) Position of the Great Swallow (V-shaped Tails) constellation in Mesopotamian imagery. (b) Fish and bird tied with ribbon from the Uruk city, later times.

Later Egyptian sources already depict the pair of fishes in this part of the sky (Lull & Belmonte (2009) fig. 6.25, p. 192). It is particularly noteworthy that we are not aware of any bifurcated fish tailed Vishap stones. Moreover, they are compared to the so called "Loko" fish species (Broutian, 2020, Petrosyan, 2015), whose tail is also not bifurcated, so this question remains open.

2.2. Sumerian astrolabs also describe the constellation known as the "Great Swallow" (mul.ŠIM.MAH) in the modern zone of Pisces.

Such a placement of the Great Swallow constellation is substantiated by the studies of several authors (Hoffmann, 2021, Hunger & Pingree, 1999, Van der Waerden, 1974). At the same time, it is also known that the "Tsitsarn" (the Swallow) constellation is present in Armenian sources (Acharian, 1926), which cannot be considered clearly identified in the sky yet, but it is noted that this is most likely identical to the the constellation of Great Swallow from Sumerian list (Davtyan (2004) pp. 19-20). If the Armenian "Tsitsarn" constellation corresponds to the Mesopotamian The Great Swallow, which in turn is directly related to the modern Pisces or is a part of it, and there is no other valid argument to the contrary, then the logical question arises. How can the Swallow be related to the Fish-shaped Vishap stones, as it has not found any visible expression on their?

2.3. There are no obvious bright stars in the modern Pisces constellation.

The brightest stars in this constellation are 4-5th apparent magnitude and barely visible to the human eye. At the same time, if we are talking about observing the position of the Sun in the range of the constellation, it should be noted that it is highly unlikely to see the mentioned stars with the naked eye under the conditions of such illumination of the sky. In other words, in order to observe their heliacal rising, the Sun must at least pass from Pisces to Aries, and in this case, already, the logic of the above-discussed calculation (Broutian, 2020) becomes, to put it mildly, unclear. On the other hand, if this constellation was associated with the main event of the year and was the main object of worship, it is hard to imagine that in the sky it was expressed whit barely visible or a few stars. This hypothesis is also supported by the fact that the main stars in the ancient Armenian calendars were chosen to be quite bright (1st apparent magnitude) (α Virginis (m=$0^m.95$) in the Protohaykian calendar (9000 AD) (Broutian, 2016, 2017), α Orionis (m=$0^m.45$) in the Haykian calendar (2341 BC) (Broutian, 1985b, 1997). Another main star change was revealed in 5800 BC: α Canis Majoris (m= $-1^m.45$) (Broutian & Malkhasyan, 2021, Malkhasyan, 2021b, 2023a). So the question of the brightness of the stars also remains open.

Thus, it is obvious that the above-mentioned questions (subsections 2.1, 2.2 and 2.3) require clear answers, which is the main problem of this work. It is also clear that in the case of such antiquity, the material we have is very scarce. So, it is especially important for the facts of the starting point of the study to be highly reliable. Only written evidence can have such reliability, the most reliable of which, as mentioned above, are the Sumerian cuneiform MUL.APIN lists. Therefore, it is necessary to first look there for the answers to the questions that concern us.

3. The Fish in MUL.APIN.

As mentioned above, the modern Pisces (^{mul}QUNI.MEŠ) is attested in Mesopotamian sources as "Tails" and spelled with the plural indicator MEŠ (Davtyan (2004) pp. 40-46). At the same time, we also see some positional commonalities of the constellations Tails and Swallow, which, as mentioned (see subsections 2.1 and 2.2), are problematic in terms of the conjunction of this domain of the sky with Fish-shaped Vishap stones. Let us also add to this that the author himself on another occasion (Broutian, 2021b) takes the northern part of the Pisces as a manifestation of the Mother Goddess, citing again the famous *A-nu-ni-tu* constellation from Mesopotamian sources (Van der Waerden, 1974), comparing it with the Armenian Mother Goddess Anahit (with the "Artater Parav" of the epic "Sasnay Tsrer") (Broutian, 2021b). Armen Davtyan also tried to explain this identification to some extent, noting, however, that **such "confusion" is the result of some distortions in later sources**[4] (Davtyan (2004) pp. 126-129). We have thoroughly discussed the celestial parallel of the cult of Mother Anahit ("Artater Parav") on another occasion (Malkhasyan, 2021a), identifying it with the modern constellation of Cassiopeia, so we will not go into the details here. Taking such data into account, it becomes clear that **to equate the astronomical content of Fish-shaped Vishap stones with Pisces constellation is questionable, to say the least, and the connection must be sought elsewhere**.

Here we should mention that another constellation is known to us from Mesopotamia, which is called Fish and is written with the ideogram ^{mul}KU$_6$. The latter is identical with the Piscis Austrinus constellation (the Southern Fish) and especially its brightest star **Fomalhaut (α Piscis Austrini)** (Hunger & Pingree, 1999, Van der Waerden, 1974). Now, since in the same cuneiform sources there is also the Fish constellation (star), let's see how well it corresponds to the Fish-shaped Vishap stones in

[4]Translated from Armenian and highlighted by us.

its content. To this end, let's take some considerations about the Piscis Austrinus constellation point by point and see how far they answer the questions 2.1, 2.2 and 2.3 stated above.

1) First of all, it is obvious that **the Piscis Austrinus constellation is not expressed by any plural feature**, which immediately leaves the first point (2.1) out of the questions.

2) **In Mesopotamia, this constellation was given great importance from a mythological point of view**. First, as mentioned, for the Southern Fish, the ideographic inscription **(a fish image is drawn)** was chosen (Davtyan (2004) pp. 41-42), which is more reliable, because in the case of Vishap stones, we also have **a fish-shaped cult monument**. On the other hand, this constellation is strongly associated with the main deity of the pantheon **Haya**, who is the embodiment of the Father God (Davtyan (2004) pp. 109-110, Hoffmann (2021) pp. 93-95). This constellation is also associated with the Mesopotamian God Ohannes (fishman) (Allen (1963) pp. 344-347, Davtyan (2004) p. 42), who is depicted with a "fish-shaped helmet" and is considered the Creator God (Broutian, 2021a). It is clear that, contrary to the mythological and pictographic vagueness of the Zodiac Pisces, here we have strictly canonical ideas. Accordingly, the question mentioned in second point (2.2) can be answered by examining this constellation.

3) **The main star of the constellation, Fomalhaut, is not comparable to any star of the Pisces with its great apparent magnitude (m=1^m.15).** As mentioned in the previous subsection (2.3), the brightness of a star is an important factor in observations of its heliacal rising. In addition, it is more likely that the star heralding a major calendar event is chosen from among the brightest stars. In this sense, the main deity discussed in the previous point, the fact that the Fish-shaped Vishap stones are the main cult monuments (Broutian, 2020) and the great brightness of the star Fomalhaut are completely in harmony with each other. Let's also remember here that the rising of the constellation corresponding to the main deity (The Father God, Haykn (Orion) constellation) was determined the beginning of the year in the Armenian Haykian calendar in 2341 BC (Broutian, 1985a,b, 1997). Since the Mesopotamian Fish has a direct connection or is identified with the idea of the Father God, then it is here that one can also look for answers to the problems mentioned in point 2.3. Now let's take a closer look at the content of the Piscis Austinus (Southern Fish) constellation.

4. The description of the Piscis Austrinus constellation.

First, the name of the main star of this constellation, Fomalhaut (*Fum al Ḥūt*), translated from Arabic, means "mouth of the fish - lat. *os piscis*" (in other sources, it is also sometimes mentioned as "the eye of the fish") (Allen (1963) pp. 344-347). Notably, Fish-shaped Vishap stones also have well-defined mouth and eyes, and it is often difficult to distinguish parts other than the head on these monuments (sometimes the gills, fins and zigzag symbols are prominent (Harutyunyan, 2015)). It is also noted that the Pscis Austrinus **drinks the whole stream of water** and this notion goes back to more ancient times (Allen (1963) pp. 344-347). The latter description is more than in harmony with the mythological context of the dragon-fish (as well as Fish-shaped Vishap stones) (Harutyunyan, 2015), which sometimes **drains the springs**. On the other hand, in same context, the stars of the constellation are associated or attributed to Aquarius in some sources (Allen (1963) pp. 344-347). This is especially important because many star maps depict the constellations of Aquarius and Piscis Austrinus as a single entity. For example, in the Egyptian Zodiac, Aquarius is also depicted with a fish at his feet (Lull & Belmonte (2009) fig. 6.25, p. 192). Parallel to this, Aratos writes: *"One large and bright by both the Pourer's feet"* (Allen (1963) pp. 344-347). This connection is also evident from the medieval Armenian map (Vanandeci, 1695). Here the water from the Aquarius pitcher flows completely into the mouth of the Piscis Austrinus (Figure 3). In other words, the above-mentioned ideas were preserved in Armenian sources until the later Middle Ages.

As we can see, there is no obstacle to accepting that the Fish-shaped Vishap stones are a monumental manifestation of the worship of the Sumerian Fish (^{mul}KU$_6$) (modern

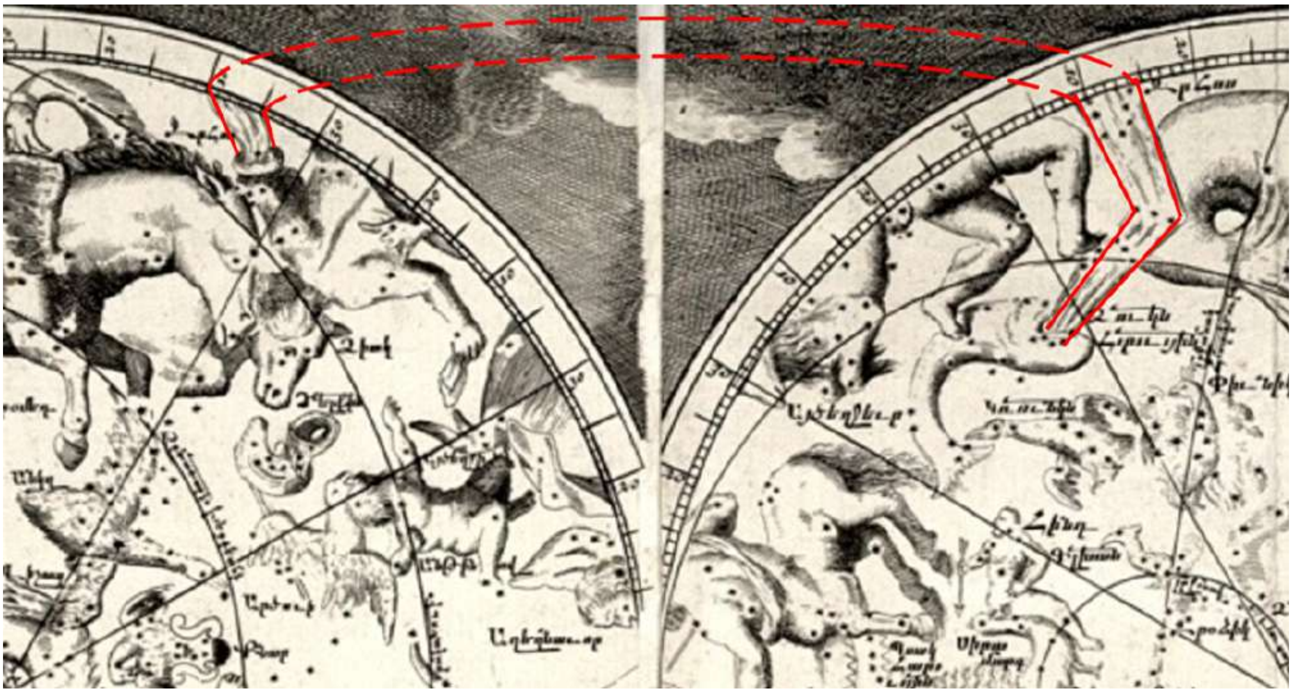

Figure 3. Fragment from the map "Hamatarats Ashkharhacoyc" published by Ghukas Vanandeci in 1695 (Amsterdam). The markings in red are according by us and show the flow of water from Aquarius's [*Djrhos*] pitcher to the mouth of the Southern Fish [*Dzukn Harawayin*].

Piscis Austinus) constellation and especially its main star Fomalhaut[5] **(α Piscis Austrini)**. It remains to calculate in which epoch the heliacal rising of this star took place on the first day of the year. For this purpose, let's first answer an important question. What day should be taken as the beginning of the year?

5. About the beginning of the year in ancient Armenian tradition.

The following was known to us about the main event of the ancient Armenian calendars, the beginning of the year (Navasard holiday), before the recent studies of the megalithic "observatory" Zorats Qarer.

- At the beginning of the Haykian calendar (2341 BC) Navasard was marked by the heliacal rising of the star α Orionis, 7-8 days before the summer solstice (Broutian, 1985b, 1997). *However, modern accurate calculation methods*[6] *show that in 2341 BC, the heliacal rising of the α Orionis at 5° horizon from 39.5° latitude north has been visible 20 days before the summer solstice. It is obvious that there is a need to clarify this issue*[7]*, especially since there are serious, even historical, justifications in favor of date 2341 BC* (Broutian (1997) pp. 211-246, 363-373).
- The beginning of the Protohaykian calendar (9000 BC) was marked by the heliacal rising of the star α Virginis, 8 days before the summer solstice (Broutian, 2016, 2017). *At the same time, the mentioned calculation methods show that in 9000 BC, from 39.5° latitude north, the heliacal rising of the star α Virginis has been visible on the 5° above the horizon 16 days before the summer solstice.*

At the same time, the last results of the studies of the Zorats Karer monument indicate that the apparent disappearance of the α Virginis in 9000 BC, it was observable on the summer solstice in the

[5] The other stars in the modern Piscis Austrinus constellation are significantly fainter in brightness (5^{th} apparent magnitude), so we will leave them out of consideration.

[6] All calculation data given in the article are according to Stellarium v0.20.4, www.stellarium.org

[7] We will not address this issue here, as it is beyond the scope of this article.

direction of the observational angle of the stone No. 198, at an elevation of about 20° (Broutian & Malkhasyan, 2021, Malkhasyan, 2022b). Studies show that in the mentioned year, the 7-8 day Navasard holidays covered the summer solstice, started 4 days before and ended 3 days after it (Malkhasyan, 2024). The beginning of the holiday corresponds in its content to the autumn grain harvest, and the summer solstice to the offering of "bread" (Malkhasyan, 2022b). If we draw a parallel between grain harvest and fishing (see in detail (Malkhasyan, 2023b)), then we should consider the heliacal rising of the Fomalhaut as an event heralding the beginning of fishing. Therefore, it is more correct to take the results obtained by studying the Zorats Qarer monument as the beginning of the year **(4 days before the summer solstice)** (Malkhasyan, 2024), especially since they are the oldest data known to us so far. At the same time, we will also give the results that will be obtained by calculating for the summer solstice and 8 days before it (Table 2). So, what kind of data can be taken as a starting point in calculating the heliacal rising time of a star?

6. About the calculation conditions.

To calculate the heliacal rising of any star, one must first select a latitude. Let's take into account several important circumstances.

- Taking into account several fundamental considerations 39.5° latitude north was taken into account for calculating the beginning date of the Haykian and Protohaykian calendars and the solar ascension of the main stars of those calendars (Broutian, 1985b, 2016).
- Later, the possible observation of the main star of the Protohaykian calendar was revealed in the Zorats Qarer megalithic monument of Syunik province (Armenia), which is located at 39.55° latitude north (Broutian & Malkhasyan, 2021, Malkhasyan, 2022b).
- Vishap stones are located in high mountain plains (2000-3000m above sea level). Recently, archaeologists discovered dozens of examples of Fish-shaped Vishap stones in the place called "Tirin Katar" of Aragats Mountain, and some of them were buried (Bobokhyan et al., 2015). According to archaeological methods, they are dated no later than in the 6^{th}-5^{th} millennia BC (Hnila et al., 2019). At the same time, **there is no scientific data on the earliest limit of their made yet** (Gilibert, 2020). This circumstance is important because the Fish-shaped Vishap stones unearthed here are the oldest dated by archaeological methods so far. "Tirin Katar" is located approximately 40.2° latitude north. In addition, the Geghama Mountains, known for their large accumulations of Vishap Stones (Bobokhyan et al., 2015), are located at approximately the same (39.8°) latitude.

Considering the above circumstances, it is acceptable to take 40° latitude north in the calculation. We should also consider the fact that the actual angular elevation of the horizon at the supposed observing location is unknown. However, in mountainous conditions, the elevation of the real horizon generally does not exceed 5°. The justification for this is actually available from the data of the real horizon seen from the Zorats Qarer monument (Malkhasyan, 2022b). **So let's see in which millennium the heliacal rising of the Fomalhaut has been observable 4 days before the summer solstice at 40° latitude north and 5° above mathematical horizon.**

7. Results and discussion.

The examination reveals Fomalhaut's heliacal rising occurred 4 days before the summer solstice in 18800 BC[8] under the above mentioned conditions (Table 2) (Figure 4). It should be noted that the declination of the star in the mentioned year is very close to the declination of the Sun on the equinox (Table 2), that is, the star rose very close to the East.

[8] Of course, this date can be deviated from between 18850 and 18750 BC, taking into account the observer's visual acuity, real horizon elevation, parallax, refraction, etc. However, the 50-year error can be ignored in such problems.

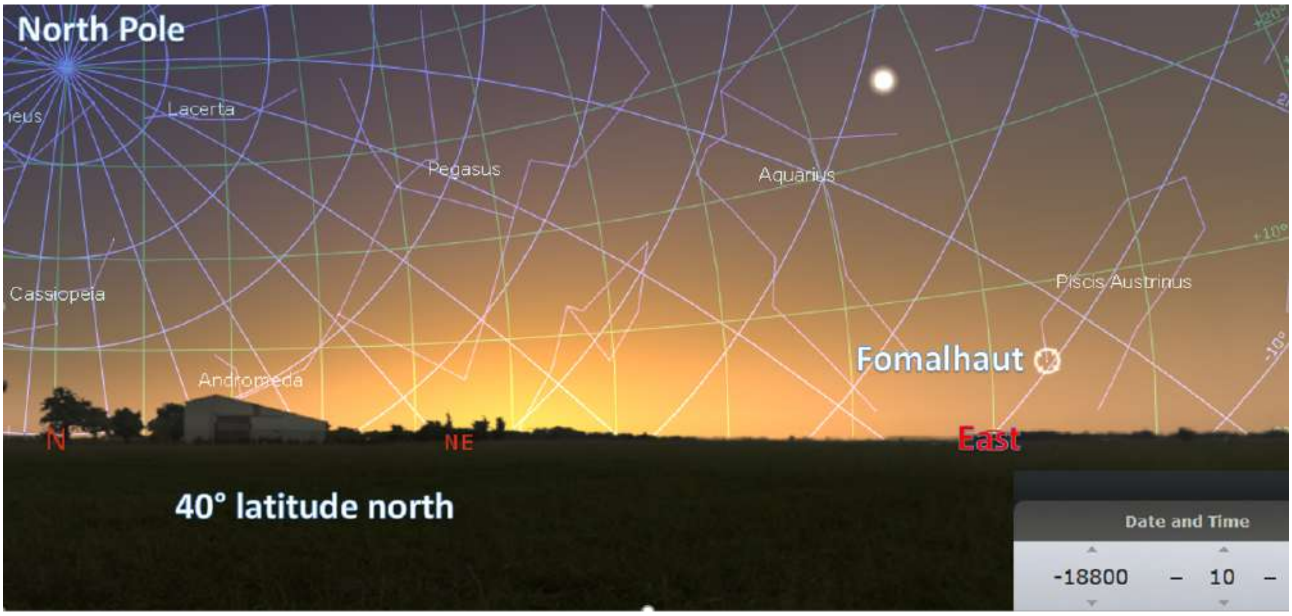

Figure 4. Sky veiw 18800 BC, 4 days before summer solstice at Fomalhaut's heliacal rising. Reconstructed in *Stellarium v0.20.4* software www.stellarium.org, added some notes.

Table 2. Data for the Fomalhaut by years and heliacal rising days. Azimuths from the South point calculated for the 5° elevation and 40° latitude north are given. All calculation data given in the table are according to *Stellarium v0.20.4*. www.stellarium.org

Fomalhaut (α Piscis Austrini)	**18400 BC**	**18800 BC**	**19200 BC**
Declination (δ)	$+1°42'$	$+0°21'$	$-1°08'$
Right ascension (α)	3^h35^m	3^h14^m	2^h53^m
Rising Azimuth (A)	$271°50'$	$273°36'$	$275°34'$
The day of heliacal rising	Summer solstice (SS)	4 days before SS	8 days before SS

It is clear that the received date (18800 BC) coincides with the midpoint of the period (19897-17749 BC; see section 1) when the sunrise has been in the domain of modern Pisces (Figure 4) 8 days before the summer solstice. In other words, **the result we obtained not only does not contradict, but coincides with the dating obtained previously** (Broutian, 2020). **It turns out that the qualitative result of the calculation is the same in both cases, but here, the problems 2.1, 2.2 and 2.3, listed above and not discussed before, have already been solved.** Moreover, Fomalhaut's direct connection with the Fish-shaped Vishap stones can be the basis for having some, however vague, ideas about the calendar (even if the primitive, simple calendar elements) of times of such antiquity. With these considerations, it is worth studying those examples of Armenian mythology and folklore that especially refer to the **dragon-fish**. We have already touched on one of them, which tells **about the dragon-fish and the bear** (Bense (1972) p. 48). A partial astronomical examination of that legend revealed that, along with religious ideas, it also contains information about the celestial motions of the **Piscis Austrinus** and the **Ursae Majoris** constellations, which refers to 22000-10000 BC (Malkhasyan, 2023b). As we can see, this result does not contradict, but in some sense complements the dating obtained above. Of course, Armenian mythology (folklore) can contain much more extensive information about the dragon-fish at the period of its worship. Therefore, such studies can shed light on calendar conceptions of time immemorial.

It should be noted that calendar elements are already expressed. In particular, if the main star of any calendar is known and its heliacal rising is taken as a main event of the year (the beginning of the year), then it is perfectly acceptable to also consider the day of the heliacal setting of that star in order to derive calendar structures. The heliacal setting of Fomalhaut in 18800 BC, at 40° latitude north and 5° above the mathematical horizon, it would have been observable 24 days after the vernal

Table 3. The main stars of the pre-christian Armenian calendars are given on chronology

Calendar	Constellation	Main star	Date	Interval
The period of Dragon-fish worship	Piscis Austrinus	Fomalhaut	18800 BC	
				3300 years
?	?	?	*15500 BC*	+
				3250 years
?	?	?	*12250 BC*	+
				3250 years
Protohaykian calendar	Virgo	Spica	9000 BC	
				3200 years
The change of the main star	Canis Majoris	Sirius	5800 BC	
				3459 years
Haykian calendar	Orion	Betelgeuse	2341 BC	

equinox. That is, **Fomalhaut has not been visible for 65 days**[9] **in the mentioned millennium at 40° latitude north**. This is completely in harmony with the basic structure of the Protohaykian calendar (Broutian (1997) pp. 416-430). In other words, **the period of Fomalhaut's absence corresponds to the "extra-annual" part (65-70 days) of the Protohaykian calendar, and the period when it has been visible corresponds to the time of the "main year" (295-300 days)**. However, such considerations require a separate, more detailed analysis.

One more important circumstance should be mentioned here. In fact, in the tradition of the ancient Armenian calendars, we fixed another calendar main star as well (Fomalhaut α Piscis Austrini), that refers to the 18800 BC. Therefore, it is worth considering all the main stars[10] chronologically (Table 3). If we pay attention to the Table 3, we will notice that there is a certain pattern[11] in the intervals of the dates. It gives the impression that the main star has changed every 3250 years (this is approximately 1/8 of the duration of one full precession (25776/8=3222)). **Such a regularity allows us to assume that two more changes took place about 15500 and 12250 BC** (Table 3). It is noteworthy that the dating of an episode of the Armenian "Sasnay Tsrer" epic was obtained in 15500 BC in a completely different way (Broutian, 2021c). However, such considerations only create a wide field for further detailed studies of the history of Armenian calendars.

Summary

Contrary to the opinions (Broutian, 2020, Khnkikyan, 1997) that the celestial parallel of the Fish-shaped Vishap stones is the modern Pisces constellation, some questions are put forward. To answer them, reference is made to the data deciphered from the cuneiform records of Mesopotamia. Based on them it becomes clear that as a **most likely celestial parallel of the Fish-shaped Vishap Stones should be fixed the modern Piscis Austrinus constellation.** Moreover, since the **Fomalhaut** of this constellation is significantly brighter than the others, it is also **fixed as the main one**.

Then, taking into account the date (4 days before the summer solstice) of the heliacal rising of the main stars in the ancient Armenian calendars, the time of the heliacal rising of the Fomalhaut is calculated. **The resulting age of 18800 BC is fully consistent with the previous result** (Broutian, 2020) **of an astronomical dating of Fish-shaped Vishap stones**. At the same time, all the mentioned problematic questions are already answered.

The obtained results take one small step forward in the astronomical studies of Vishap stones, at the same time, they are some foundation for revealing the long-standing layers of the history of Armenian astronomy.

[9] 93 days (from vernal equinox (VE) to summer solstice (SS) - 4 days (heliacal rising 4 days before SS) - 24 days (heliacal setting 24 days after VE) = 65 days.

[10] See subsection 2.3.

[11] This pattern was noticeable even before the emergence of Fomalhaut (Broutian & Malkhasyan (2021) f.(31), p. 124).

References

Acharian H., 1926, 2, 456

Allen R., 1963, Star Names Their Lore and Meaning. Dover Edition, New York

Bense 1972, Armenian Ethnography and Folklore, (Collected by Sahak Movsisyan (Bense), compiled by his son Soghomon Taronetsi). NAS ASSR Institute of Archeology and Ethnography, 3, Yerevan

Bobokhyan A., Gilibert A., Hnila P., 2012, "Aramazd", Armenian Journal of Near Eastern Studies, VII, 2, 7

Bobokhyan A., Gilibert A., Hnila P., 2015, The Vishap Stone Stelae, Edited by Petrosyan A. and Bobokhyan A., "Gitutyun" publ., 269

Bobokhyan A., Gilibert A., Hnila P., 2020, in Proceedings of the 11th International Congress on the Archaeology of the Ancient Near East. pp 17–30

Broutian G., 1985a, Etchmiadzin, 1, 51

Broutian G., 1985b, Etchmiadzin, 2-3, 72

Broutian G., 1997, The Armenian Calendar. Mother See of Holy Etchmiadzin

Broutian G., 2016, Bazmavep, 3-4, 11

Broutian G., 2017, in Non-stable Universe: Energetic Resources, Activity Phenomena, and Evolutionary Processes, Proceedings of an International Symposium dedicated to the 70th anniversary of the Byurakan Astrophysical Observatory held at NAS RA, Yerevan and Byurakan, Armenia 19-23 September 2016, Edited by A. Mickaelian, Astronomical Society of the Pacific, Conference Series, volume 511, San Francisco. , pp 296–302

Broutian G., 2020, Etchmiadzin, 4, 44

Broutian G., 2021a, Etchmiadzin, 10, 63

Broutian G., 2021b, Etchmiadzin, 12, 72

Broutian G., 2021c, Communications of BAO, 68(1), 105

Broutian G., Malkhasyan H., 2021, Bazmavep, 3-4, 107

Davtyan A., 2004, Armenian Stellar Mithology. "Tigran Metz", Yerevan

Gilibert A., 2020, L'arte armena. Storia critica e nuove prospettive, pp 151–165

Gilibert A., Bobokhyan A., Hnila P., 2012, Mitteilungen der Deutschen Orient-Gesselschaft zu Berlin, 144, 93

Gilibert A., Bobokhyan A., Hnila P., 2013, Veröffentlichungen des Landesamtes für Denkmalpflege und Archäologie Sachsen Anhalt - Landesmuseum für Vorgeschichte, Halle, 67, 195

Harutyunyan S., 2015, The Vishap Stone Stelae, Edited by Petrosyan A. and Bobokhyan A., "Gitutyun" publ., 53

Hnila P., Gilibert A., Bobokhyan A., 2019, in , Natur und Kult in Anatolien. Ege Yayınları, pp 283–302

Hnila P., Gilibert A., Bobokhyan A., 2023, in , Systemizing the Past, edited by Yervand H. Grekyan and Arsen A. Bobokhyan. Archaeopress Archaeology, pp 162–171

Hoffmann S., 2021, Wie Der Löwe An Den Himmel Kam (Auf Den Spuren Der Sternbilder). Kosmos, Stuttgart, Germany

Hunger H., Pingree D., 1999, Astral Sciences in Mesopotamia. Brill, Leiden, Boston, Köln

Khnkikyan O., 1997, Newsletter of social sciences, 3, 148

Lull J., Belmonte J., 2009, Supreme Council of Antiquities Press, Cairo, Chapter 6, 155

Malkhasyan H., 2021a, Bazmavep, 3-4, 149

Malkhasyan H., 2021b, Communications of BAO, 68(2), 407

Malkhasyan H., 2022a, Communications of BAO, 69(1), 100

Malkhasyan H., 2022b, Communications of BAO, 69(2), 324

Malkhasyan H., 2023a, Bazmavep, 1-2, 125

Malkhasyan H., 2023b, Proceedings of International Scientific-practical Conference: "Armenology in the Context of Languages and Cultures", Moscow, April 18

Malkhasyan H., 2024, Bazmavep, 1-2, (accepted)

Petrosyan A., 2015, The Vishap Stone Stelae, Edited by Petrosyan A. and Bobokhyan A., “Gitutyun” publ., 13

Petrosyan A., Bobokhyan A., 2015, The Vishap Stone Stelae. NAS RA Institute of Archaeology and Ethnography, “Gitutyun” publ., 419p., Yerevan

Tumanyan B., 1985, On the History of Armenian Astronomy. YSU, Yerevan

Van der Waerden B., 1974, Science Awakening II: The Birth of Astronomy. Oxford University Press, First Edition

Vanandeci G., 1695, Hamatarats Ashkharhacoyc. (map), Amsterdam

Communications of BAO, Vol. 70, Issue 2, 2023, p. 260

Introduction

Editorial board *

NAS RA V. Ambartsumian Byurakan Astrophysical Observatory (BAO)

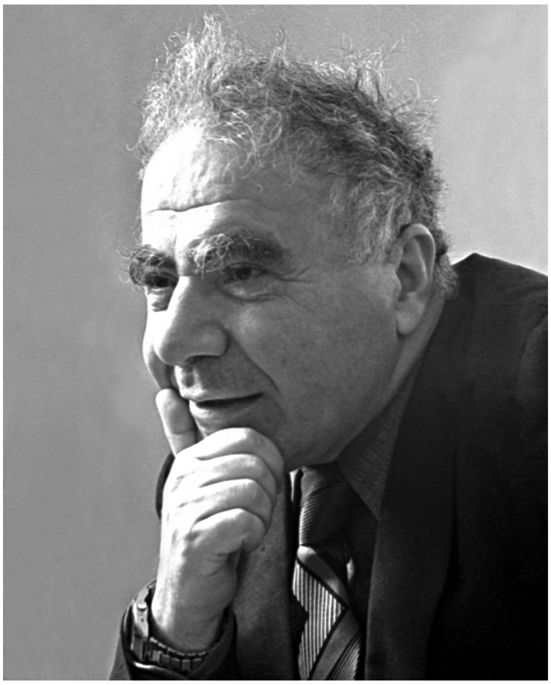

Viktor Ambartsumian (1908-1996)

Viktor A. Ambartsumian was one of the greatest astronomers and scientists of the 20th century, he revolutionized our views on the evolution and dynamics of the Universe. Our perception and further investigation of the non-stable phenomena in the Universe is due to Ambartsumian's efforts and contribution in science that is why the anniversary meeting is entitled "Non-Stable Phenomena in the Universe". Ambartsumian carried out basic research in Astronomy and Cosmogony. It covered Astrophysics, Theoretical Physics and Mathematical Physics, and mostly focused on the physics of nebulae, star systems, and extragalactic astronomy. He particularly developed the theory of the Planetary Nebulae. He is best known for having discovered the Stellar Associations and predicted Activity of Galactic Nuclei, which became the most important topic of the extragalactic astronomy. Ambartsumian introduced important Statistical Methods to predict the total number of eruptive stars in stellar aggregates. In his later career, Ambartsumian held views in contradiction to the consequences of the general relativity, such as rejecting the existence of black holes and suggesting Superdense Matter that conditions the activity of stars and galaxies.

The scientific heritage of *V. A. Ambartsumyan* still largely determines the directions of scientific research not only by the staff of the Byurakan Astrophysical Observatory (BAO), but by scientists from other countries. On September 18-21, 2023, the International conference *"Non-Stable Phenomena in the Universe"* was organized in BAO. It was dedicated to V. A. Ambartsumyan's 110th anniversary. About 50 astrophysicists from various countries took part in the conference. Works covering a wide range of astrophysical issues were presented at the colloquium:

- Active Sun and the Solar System;
- Instability phenomena in the world of stars and nebulae;
- Active Galactic Nuclei and Starburst galaxies;
- Groups and clusters of galaxies;
- Observational and Theoretical Cosmology;
- Astrochemistry, Astrobiology and Exoplanets;
- Theoretical interpretation of non-stable phenomena in the Universe.

Active scientific discussion of the presented tasks will undoubtedly serve as a guarantee for further fruitful cooperation.

This issue of "Communications of BAO" includes the proceedings presented on the the International conference *"Non-Stable Phenomena in the Universe"*. All the papers passed relevant peer-review.

*combao@bao.am

Communications of BAO, Vol. 70, Issue 2, 2023, pp. 261-276

Astronomical Surveys and Active Galaxies

A. M. Mickaelian,[*] H. V. Abrahamyan,[†] G. M. Paronyan,[‡] G. A. Mikayelyan,[§] R.R.Andreasyan ,[¶] A. G. Sukiasyan,[‖] L. A. Hambardzumyan,[**] V. K. Mkrtchyan,[††] and A. A. Gasparyan[‡‡]

NAS RA V. Ambartsumian Byurakan Astrophysical Observatory (BAO), Armenia

Abstract

Astronomical Surveys are the main source for discoveries in astronomy. We are giving the most important parameters the significance of the surveys, their main products: images, photometric, spectroscopic and other data. Among the surveys, namely extragalactic ones, most important are those for Active Galaxies (both Active Galactic Nuclei (AGN) and Starburst (SB) Galaxies), and particularly the AGN. These objects reveal many spatial and physical characteristics helping understanding the Universe. We give a brief review of our searches and studies for Active Galaxies.

Keywords: *Multiwavelength Astronomy – Astronomical Surveys – Big Data in Astronomy – Active Galaxies – Active Galactic Nuclei – Starburst Galaxies*

1. Astronomical Surveys

Most of astronomical discoveries in old times happened by chance. Having relatively narrow fields of view, astronomers, planning their observations could not make pre-selections among the vast number of objects. The invention of the wide-field telescope by Bernd Schmidt in 1930 led to construction of Schmidt telescopes with Field of Views (FoV) of several degrees (the area covering a few dozens of degrees) and systematic study of large fields, Astronomical Surveys. 8 big Schmidt telescopes were built in 1940s-1970s, and 4 modern ones were built in recent decades. The Byurakan Astrophysical Observatory (BAO) installed a 1m Schmidt telescope which was operational in 1960-1991 with its 3 objective prisms, the largest at the time. It was re-operated in 2015 with a new equipment for multi-band photometry and digital receiver.

The Importance of Astronomical Surveys is very high. Here are the main arguments and justifications:

- Discovery of new cosmic objects
- Distinguishing types of cosmic objects and their abundance in the Universe
- Spatial distribution: Stellar (Galactic) Astronomy and Extragalactic Astronomy (including Cosmology); as well as kinematics and dynamics
- The geometry of Space
- Luminosity functions of Cosmic objects, their evolution
- The development of Multiwavelength and Multimessenger Astronomy
- Statistics of different objects and their properties

[*] aregmick@yahoo.com, Corresponding author
[†] abrahamyanhayk@gmail.com
[‡] paronyan_gurgen@yahoo.com
[§] gormick@mail.ru
[¶] randreasyan@gmail.com
[‖] andranik.suqiasyan.1995@mail.ru
[**] hambardzumyanlian@gmail.com
[††] varduhi.mkrtchyan.99@bk.ru
[‡‡] gasparyananna1997@mail.ru

doi: https://doi.org/10.52526/25792776-23.70.2-261

- Revelation of astrophysical laws and regularities based on large statistics

The main parameters of Astronomical Surveys are:

- Method (photometric, multiband, multiwavelength, spectroscopic: objective prism, polarimetric), methodology
- Sky area: location and coverage (all-sky, large area, deep surveys in small areas)
- Wavelength range (otherwise, given in energies – for high-energy range, or frequencies – mostly for radio)
- Spatial and spectral resolution, spectral dispersion
- Sensitivity (in fluxes, energies, etc.) / limiting magnitude
- Completeness (detection limit, classification limit)

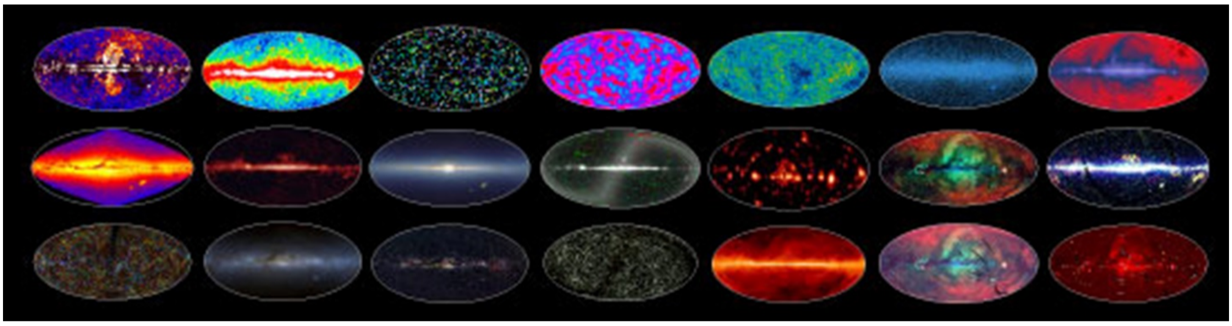

2. Wide Field Plate Data Base (WFPDB)

In the WFPDB (www.skyarchive.org), there are 414 archives, 2,204,725 plates from 125 observatories, obtained between 1879 and 2002 (the digital observations started in early 1990s and now they are active in all modern telescopes). They include 2,128,330 direct and 64,095 objective prism plates. Among the biggest plate collections there are: Harvard (USA) – 600,000 plates; Sonnenberg (Germany) – 270,000; Italy (all Italian archives) – 87,000; Kyiv (Ukraine) – 85,000; SAI (Moscow, Russia) – 50,000; etc. BAO archive has a collection of 37,500 plates.

Among the wide field observations and all-sky and/or large area astronomical surveys, one should mention the Palomar Observatory Sky Surveys (POSS), namely POSS1 and POSS2. Based on these observations, a number of catalogs and databases were built (APM, MAPS, USNO, GSC, etc.).

3. Multiwavelength Astronomy

3.1. Gamma-ray Astronomy and cosmic gamma-ray sources

Among gamma-ray observatories, one should mention the CGRO – Cosmic Gamma Ray Observatory, 1990 that provided ∼1300 discrete gamma-ray sources; and its 2704 BATSE detected gamma-ray bursts.

Later on, GLAST (Fermi, 1873 sources), INTEGRAL (723 sources), Swift (9387 sources), BeppoSAX (1087 sources) and some others were launched and provided more gamma-ray sources. Many of them are still unknown.

3.2. X-ray Astronomy and cosmic X-ray sources

ROSAT is among the most important X-ray telescopes and X-ray surveys, especially if considering the importance of all-sky surveys. ROSAT made an all-sky X-ray survey in 0.1-2.4 keV energy range and resulted in these catalogs:

- ROSAT All-Sky Survey Bright Source Catalogue (ROSAT BSC). 18,806 sources (Voges et al. 1999)

doi: https://doi.org/10.52526/25792776-23.70.2-261

- ROSAT All-Sky Survey Faint Source Catalogue (ROSAT FSC). 105,924 sources (Voges et al. 2000)

In Table 1, we give the most important X-ray surveys and projects, mostly the all-sky and large area ones.

Telescope	Country	Years	Energy (keV	Results	Number of sources
Uhuru (SAS-1)	USA	1970-1973	2 - 20	Sky survey	339
HEAO-1	USA	1977-1979	0.25 - 10 000	Sky survey	842
Einstein (HEAO-2)	USA	1978-1981	0.2 - 20	Pointed deep observations	1435
EXOSAT	ESA	1983-1986	0.04 - 80	Sky survey	1210
Granat	France, Russia	1989-1999	2 - 100 000	Pointed deep observations, Sky survey	1551
ROSAT	Germany	1990-1999	0.07 - 2.4	Sky survey	124 730
ASCA (Astro-D)	Japan	1993-2001	0.4 - 10	Sky survey, spectral observations	1190
Rossi XTE (RXTE)	USA	1995-2012	2 - 250	Sky survey	321
BeppoSAX	Italy	1996-2002	0.1 - 300	Gamma bursts, broad-band spectroscopy	253
Chandra (CXO)	USA	1999-pres.	0.07 - 10	Pointed deep observations	380 000
XMM-Newton	ESA	1999-pres.	0.25 - 12	Pointed deep observations	372 728
INTEGRAL	ESA	2002-pres.	15 - 10 000	Pointed deep observations	1126
Swift	USA	2004-2008	0.2 - 150	Sky survey, gamma bursts	1256

Table 1. The list of the most important X-ray surveys and projects.

The list of known types of cosmic X-ray sources is the following:

- Solar System bodies
- bright stars
- stellar hot coronae
- late-type (M) dwarfs
- white dwarfs (WD) and hot subdwarfs
- X-ray binaries
- intermediate mass X-ray binaries
- cataclysmic variables (CV)
- magnetars
- Supernovae remnants (SNR)
- bright galaxies
- Active Galactic Nuclei (AGN)
- blazars
- clusters of galaxies

3.3. UV Astronomy and cosmic UV sources

In Ultraviolet (UV), less surveys have been carried out, however, the NASA Galaxy Evolution Explorer (GALEX) was rather efficient and productive; it observed the sky in two wavelength bands; Far-UV (FUV) and Near-UV (NUV) and provided the catalogs AIS (All-sky Imaging Survey) and MIS (Medium-depth Imaging Survey), totaling in 82,992,086 UV sources (Bianchi et al. 2017). The immediate neighboring to optical short UV wavelength range was observed by Hubble Space Telescope (HST), however no systematic all-sky survey was made.

doi: https://doi.org/10.52526/25792776-23.70.2-261

3.4. IR Astronomy and cosmic IR sources

Among the most important ones are:

- Two Micron All Sky Survey (2MASS) (Cutri et al. 2003). J(1.25), H(1.65), and K_s(2.17), brighter than 1mJy sources (to a 3 sigma limiting sensitivity of 17.1, 16.4 and 15.3 mag in the three bands, respectively), resolution 2", 470,992,970 sources, including ~300,000,000 stars and 1,650,000 galaxies
- IRAS Point Source Catalog (PSC): all-sky, 12, 25, 60, 100 μm (0.4, 0.5, 06, 1.0 Jy sensitivity limit), 245,889 sources (IRAS Catalog of Point Sources, 1986)
- IRAS Faint Source Catalog (FSC): high galactic latitudes, 180,000 sources (Moshir et al. 1990)
- AKARI (ASTRO-F or IRIS – InfraRed Imaging Surveyor, Feb 2006), 68.5 cm telescope, wavelength range 2-180 μm, 13 bands.
- Infrared Camera (IRC), 9 and 18 μm, sensitivity $\sim$ 50 and 120 mJy. Spatial resolution is about 9.4", 877,091 sources (851,189 observed at 9 μm and 195,893 at 18 μm)
- Far-Infrared Surveyor (FIS), 65, 90, 140, and 160 μm, ~430,000 sources
- Wide-Field Infrared Survey Explorer (WISE). NASA, 14.12.2009. 40 cm (16 inch), Four infrared wavelength bands at 3.4, 4.6, 12 and 22μm. The FoV is 47 arcmin wide. 747,634,026 sources

We give in Table 2 the list of the most important IR surveys and projects and in Table 3, the IR ranges and their characteristics, as well as cosmic objects that radiate in the given wavelength range.

Telescope or project	**Countries**	**Years**	$\lambda(\mu)$	**Results**	**Number of sources**
IRAS	USA	1983	8-120	sky survey	405 769
ISO	Europe	1996	2.5-240	IR spectra	~30 000
Spitzer	USA	2003	3-180	IR deep images and spectra	4 261 028
AKARI	Japan	2006	7-180	sky survey	1 298 044
Herschel	Europe	2009	55-672	far IR	
WISE	USA	2010	3-28	sky survey	563 921 584
DENIS	Europe	1996	0.82, 1.24, 2.16	Southern sky survey	355 220 325
2MASS	USA	2003	1.24, 1.66, 2.16	sky survey	470 992 970

Table 2. The list of the most important IR surveys and projects.

Spectral range	$\lambda(\mu)$	**T (K)**	**Studied cosmic objects**
Near IR	(0.76-1) - 5	740 - (3000-5200)	cold red stars, stellar envelopes,planetary nebulae
Mid IR	5 - (25-40)	(92.5-140) - 740	planets, comets and asteroids, stellar radiation heated dust, protoplanetary disks, gas-dust nebulae
Far IR	(25-40) - (200-350)	(10.6-18.5) - (92.5-140)	cold gas radiation, central regions of galaxies, very cold molecular clouds

Table 3. IR ranges and their characteristics, as well as cosmic objects that radiate in the given wavelength range.

3.5. Radio Astronomy and cosmic radio sources

Radio astronomy has been mainly done from ground-based observations. Here are the most important radio all-sky surveys:

- **GB6:** 6cm (4.85GHz), 0<DEC<75, S⩾18mJy, 75,162 sources

doi: https://doi.org/10.52526/25792776-23.70.2-261

- **87GB:** (Gregory et al. 1991), also 6cm (4.85GHz), 54,579 sources
- **Westerborck Northern Sky Survey (WENSS, WN):** (de Bruyn et al. 1998), 92cm (330MHz), 229,420 sources
- **NVSS:** (Condon et al. 1998): all-sky at 21cm (1.4GHz), S>2.5mJy, 1-7 arcsec (>15mJy-2.5mJy), 1,773,484 sources
- **FIRST:** 10,000 sq.deg., 21cm (1.4GHz), S>1mJy, 5 arcsec, high galactic latitudes (>30deg), 811,117 sources (White et al. 1998)
- **8C:** A deep 38-MHz radio survey of the area declination >+60 deg (Rees 1990)

At present astronomers distinguish the *sub/mm* and *mm* wavelength range between IR and radio. A few telescopes worked in this range (ex. James Clerk Maxwell Telescope (JCMT) in Hawaii, 15m diameter) and later on a few large facilities were built, most important among them – ALMA (Atacama Large Millimeter/submillimeter Array, ESO) in Chile, an interferometer array of 54×12.0m and 12×7.0m antennas.

4. The overall picture of the astronomical surveys

In Figure 1 we give the distribution of astronomical surveys by number of objects and limiting magnitude. Gaia has provided a catalog with the largest number of objects, 1.8 billion objects. A few others also have more than 1 billion objects (ex. USNO-B1.0). They provide objects till 22-23 magnitude. On the other hand, we have deep surveys (HDF, HUDF, SDF, FDF, GOODS, COSMOS) providing smaller number of objects but with limiting magnitudes up to 30 and fainter.

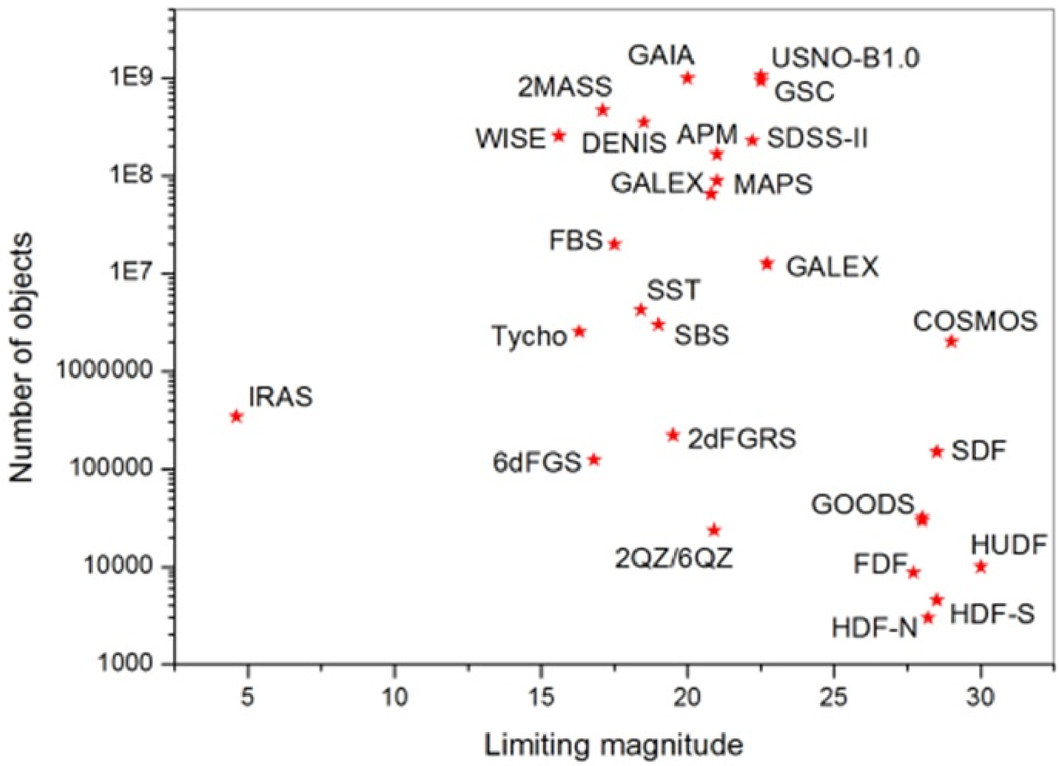

Figure 1. The distribution of astronomical surveys by number of objects and limiting magnitude.

Table 4 gives the list of all-sky and large-area astronomical catalogs in increasing wavelength range from gamma-rays to radio built on the basis of surveys (both ground-based and Space) and their main parameters: name, years, spectral range, sky area covered, sensitivity (limiting magnitude) and the number of sources. Though 44 catalogs are listed, the list is still not complete.

We give in Table 5 and Figure 2 the numbers of catalogued astronomical objects at different wavelength ranges and their distribution. Though the figure is in logarithmic scale, however the numbers are so different that some ranges are not even seen. But not only the number of objects is important and not only the

doi: https://doi.org/10.52526/25792776-23.70.2-261

numbers of objects make up Big Data in astronomy. Very often, we obtain hundreds, thousands, and millions of data units from one single astronomical object, ex. when we obtain its high-resolution spectrum or make a decomposition analysis of the spectral lines, where hundreds of profiles are checked and analysed for each solution (Figures 3 and 4).

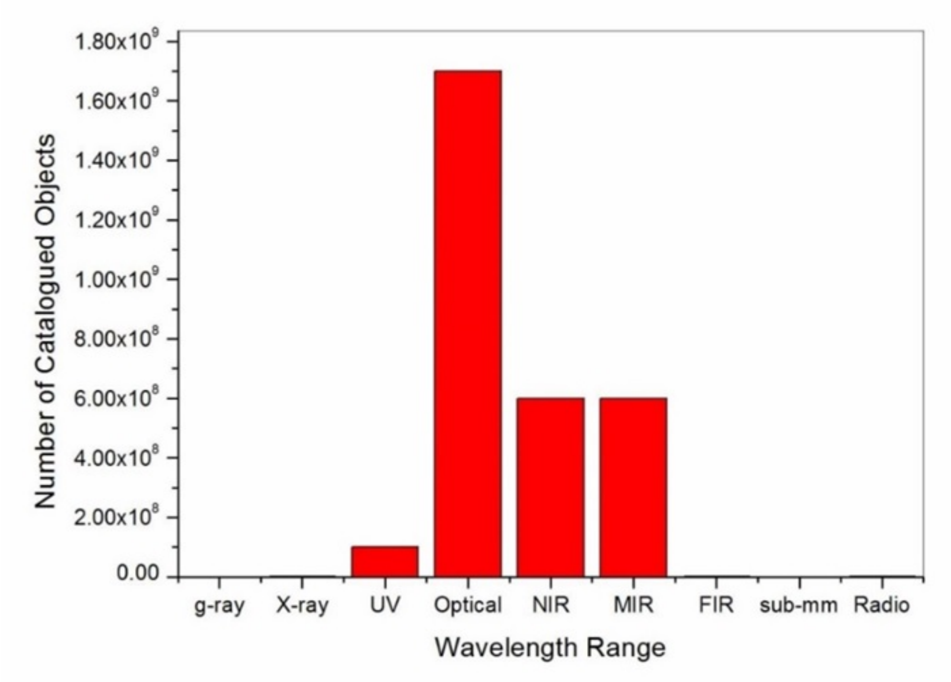

Figure 2. The distribution of the numbers of catalogued astronomical objects at different wavelength ranges.

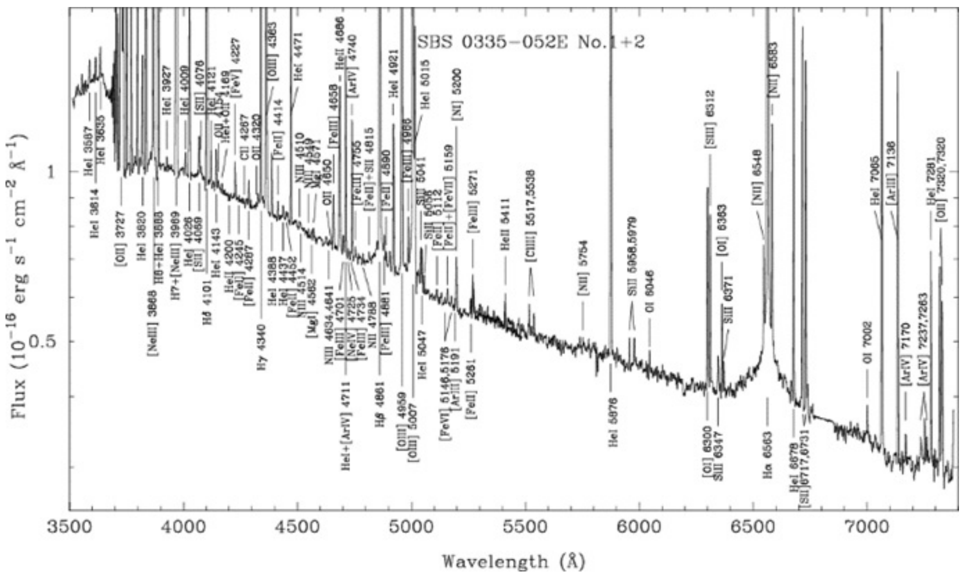

Figure 3. . The high-resolution spectrum of the BCDG SBS 0335-052E, where hundreds of spectral lines can be distinguished and measured.

5. Big Data in Astronomy

Volume – the quantity of generated and stored data. The size of the data determines the value and potential insight, whether it can be considered big data or not.
Variety - the type and nature of the data. This helps people who analyze it to effectively use the resulting insight. Big data draws from text, images, audio, video; plus, it completes missing pieces through data fusion.

Velocity - in this context, the speed at which the data is generated and processed to meet the demands and challenges that lie in the path of growth and development. Big data is often available in real-time.

doi: https://doi.org/10.52526/25792776-23.70.2-261

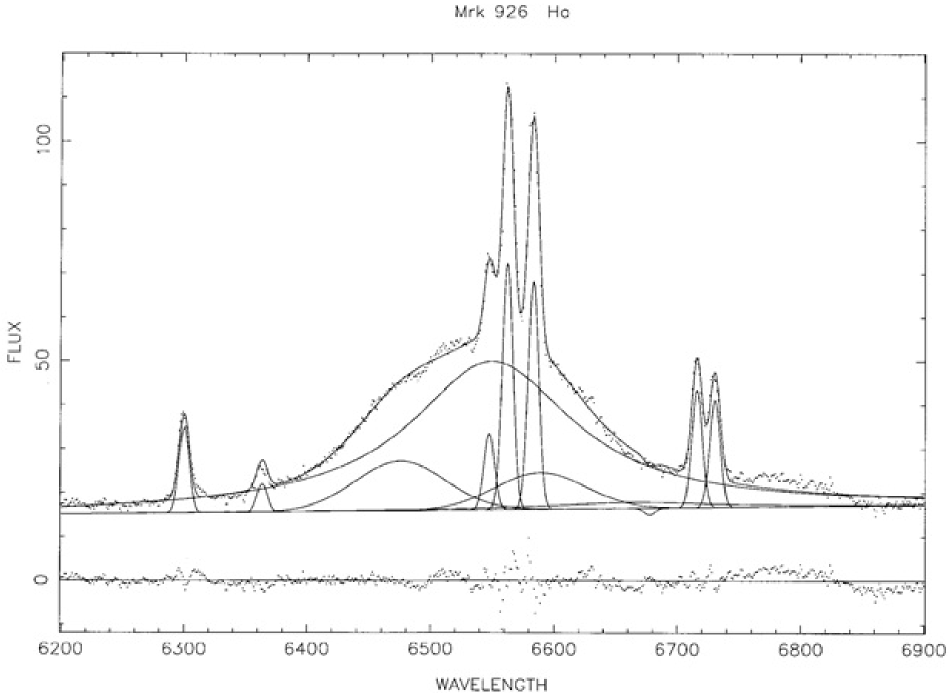

Figure 4. Decomposition analysis of the spectral lines for Mrk 926 H-alpha region with one of the solutions, where H-alpha summarizing profile is presented as having 3 broad line components and 1 narrow line.

Veracity - the data quality of captured data can vary greatly, affecting the accurate analysis.

In Astronomy, all these criteria are well met; we have the largest amount of data coming from the Universe, there is a wide variety of them, the velocity of accumulation is rather high as well and the veracity is maintained by astronomical standards, Virtual Observatory (VO) methods, etc. To give an understanding of data volumes in Astronomy, we give in the Table 6 a number of important astronomical projects with their information volumes.

6. Active Galaxies

Most of the surveys given above have tight relation to Active Galaxies, especially the non-optical ones, as many Active Galaxies strongly radiate in gamma-ray, X-ray, UV, IR and radio.

We can substantiate the importance of Active Galaxies as follows:

- The origin and evolution of galaxies
- Morphology
- Interacting and Merging galaxies
- Star Formation in galaxies
- Luminosity function of galaxies
- Radiation mechanisms
- Radiation mechanisms
- Presence of relativistic jets
- The theory of Super-Massive Black Holes (SMBH)

doi: https://doi.org/10.52526/25792776-23.70.2-261

- Energetic resources
- The cosmological role of active galaxies

7. Recent Results related to Studies of Active Galaxies in Byurakan

Studies for Active Galaxies have been for many years one of the main research topic in Byurakan. Since 1990s, we have introduced the multiwavelength approach to these studies and many new interesting results appeared. In Table 7, we give the list of all our group works related to multiwavelength search and studies of active galaxies. The consecutive columns present: years of the projects, authors involved, survey name or description and its short name, objectives and number of objects discovered/revealed or studied.

These studies reveal many important characteristics of AGN and SB, as well as allow revealing outliers at different distributions and diagrams, which very often appear to be unique or rare objects.

Acknowledgements

This work was partially supported by the Republic of Armenia Ministry of Education and Science (RA MES) State Committee of Science, in the frames of the research projects No. 15T-1C257 and 21AG-1C053 (2021-2026). This work was made possible in part by research grants from the Armenian National Science and Education Fund (ANSEF) based in New York, USA (PS-astroex-2597, 2022-2023).

References

Abdollahi S., et al., 2020, Astrophys. J. Suppl. Ser. , 247, 33

Abrahamian H. V., Mickaelian A. M., 1993, Astrophysics, 36, 306

Abrahamian H. V., Mickaelian A. M., 1994a, Astrophysics, 37, 27

Abrahamian H. V., Mickaelian A. M., 1994b, Astrophysics, 37, 117

Abrahamian H. V., Mickaelian A. M., 1996, Astrophysics, 39, 315

Abrahamyan H. V., Mickaelian A. M., 2016a, in Mickaelian A. M., Khosroshahi H. G., Harutyunian H. A. E. ., eds, Proceedings of Armenian-Iranian Astronomical Workshop (AIAW). pp 208–212

Abrahamyan H. V., Mickaelian A. M., 2016b, in Mickaelian A., Lawrence A., Magakian T., eds, Astronomical Society of the Pacific Conference Series Vol. 505, Astronomical Surveys and Big Data. p. 193

Abrahamyan H. V., Mickaelian A. M., Knyazyan A. V., 2015, Astronomy and Computing, 10, 99

Abrahamyan H. V., Mickaelian A. M., Paronyan G. M., Mikayelyan G. A., Gyulzadyan M. V., 2018a, Astronomy and Computing, 25, 176

Abrahamyan H. V., Mickaelian A. M., Mikayelyan G. A., Paronyan G. M., 2018b, Communications of the Byurakan Astrophysical Observatory, 65, 1

Abrahamyan H. V., Mickaelian A. M., Paronyan G. M., Mikayelyan G. A., 2018c, Izvestiya Glavnoj Astronomicheskoj Observatorii v Pulkove, 222, 5

Abrahamyan H. V., Mickaelian A. M., Paronyan G. M., Mikayelyan G. A., Gyulzadyan M. V., 2019a, Communications of the Byurakan Astrophysical Observatory, 66, 1

Abrahamyan H. V., Mickaelian A. M., Paronyan G. M., Mikayelyan G. A., 2019b, Astronomische Nachrichten, 340, 437

Abrahamyan H. V., Mickaelian A. M., Paronyan G. M., Mikayelyan G. A., Gyulzadyan M. V., 2019c, VizieR Online Data Catalog (other), 0620, J/other/A+C/25

Abrahamyan H. V., Mickaelian A. M., Paronyan G. M., Mikayelyan G. A., 2020a, Astrophysics, 63, 322

Abrahamyan H. V., Mickaelian A. M., Paronyan G. M., Mikayelyan G. A., 2020b, VizieR Online Data Catalog (other), 0160, J/other/Ap/63

Abrahamyan H. V., Mickaelian A. M., Paronyan G. M., Mikayelyan G. A., Sukiasyan A. G., 2021, Communications of the Byurakan Astrophysical Observatory, 68, 441

Abrahamyan H. V., Mickaelian A. M., Paronyan G. M., Mikayelyan G. A., 2022, Communications of the Byurakan Astrophysical Observatory, 69, 340

Abrahamyan H. V., Mickaelian A. M., Paronyan G. M., Mikayelyan G. A., Sukiasyan A. G., 2023a, Astrophysics, 66, 11

Abrahamyan H. V., Mickaelian A. M., Mikayelyan G. A., Paronyan G. M., Sukiasyan A. G., Mkrtchyan V. K., Hambardzumyan L. A., 2023b, Communications of the Byurakan Astrophysical Observatory, 70, 83

Abramyan G. V., Mickaelian A. M., 1993a, Astrophysics, 35, 363

Abramyan G. B., Mickaelian A. M., 1993b, Astrophysics, 36, 62

doi: https://doi.org/10.52526/25792776-23.70.2-261

Abramyan G. B., Mickaelian A. M., 1994, Astrophysics, 37, 224

Abramyan G. V., Lipovetskii V. A., Mickaelian A. M., Stepanyan D. A., 1990a, Astrophysics, 33, 418

Abramyan G. V., Lipovetskii V. A., Mickaelian A. M., Stepanyan D. A., 1990b, Astrophysics, 33, 493

Abramyan G. V., Lipovetskii V. A., Mickaelian A. M., Stepanyan D. A., 1991, Astrophysics, 34, 7

Almeida A., et al., 2023, Astrophys. J. Suppl. Ser. , 267, 44

Ambartsumian V. A., 1958, in La structure et l'évolution de l'universe. pp 241–249

Ambartsumian V. A., 1961, Astron. J. , 66, 536

Arakelian M. A., 1975, ComBAO, 47, 3

Baier F. W., Petrosyan M. B., Tiersch H., Shakhbazyan R. K., 1974, Ap, 10, 327

Balaian S. K., Akopian S. A., Mickaelian A. M., Burenkov A. N., 2001, Astronomy Letters, 27, 284

Baumgartner W. H., Tueller J., Markwardt C. B., Skinner G. K., Barthelmy S., Mushotzky R. F., Evans P. A., Gehrels N., 2013, Astrophys. J. Suppl. Ser. , 207, 19

Bennett C. L., et al., 2013, Astrophys. J. Suppl. Ser. , 208, 20

Bianchi L., Herald J., Efremova B., Girardi L., Zabot A., Marigo P., Conti A., Shiao B., 2011, Astrophys. Space. Sci. , 335, 161

Bird A. J., et al., 2010, ApJS, 186, 1

Bottacini E., Ajello M., Greiner J., 2012, Astrophys. J. Suppl. Ser. , 201, 34

Cirimele G., et al., 2008, in , Digitized First Byurakan Survey. pp 19–37

Condon J. J., Cotton W. D., Greisen E. W., Yin Q. F., Perley R. A., Taylor G. B., Broderick J. J., 1998, Astron. J. , 115, 1693

Cutri R. M., et al., 2003, VizieR Online Data Catalog, p. II/246

Cutri R. M., et al., 2013, Explanatory Supplement to the AllWISE Data Release Products, Explanatory Supplement to the AllWISE Data Release Products, by R. M. Cutri et al.

Ebisawa K., Bourban G., Bodaghee A., Mowlavi N., Courvoisier T. J. L., 2003, Astron. Astrophys. , 411, L59

Erastova L. K., Mickaelian A. M., 2016, in Mickaelian A., Lawrence A., Magakian T., eds, Astronomical Society of the Pacific Conference Series Vol. 505, Astronomical Surveys and Big Data. p. 242

Erastova L. K., Mickaelian A. M., 2017, Astronomical and Astrophysical Transactions, 30, 261

Eritsyan M. A., Mickaelian A. M., 1993, Astrophysics, 36, 126

Evans I. N., et al., 2010, Astrophys. J. Suppl. Ser. , 189, 37

Fischer J. U., Hasinger G., Schwope A. D., Brunner H., Boller T., Trümper J., Voges W., Neizvestnyj S., 1998, Astronomische Nachrichten, 319, 347

Forman W., Jones C., Cominsky L., Julien P., Murray S., Peters G., Tananbaum H., Giacconi R., 1978, Astrophys. J. Suppl. Ser. , 38, 357

Gaia Collaboration 2022, VizieR Online Data Catalog, p. I/356

Geach J. E., et al., 2017, Mon. Not. R. Astron. Soc. , 465, 1789

Gigoyan K. S., Mickaelian A. M., 1999, Astrophysics, 42, 37

Gregory P. C., Condon J. J., 1991, Astrophys. J. Suppl. Ser. , 75, 1011

Gregory P. C., Scott W. K., Douglas K., Condon J. J., 1996, Astrophys. J. Suppl. Ser. , 103, 427

Gyulzadyan M. V., Mickaelian A. M., Abrahamyan H. V., Paronyan G. M., 2016a, in Mickaelian A. M., Khosroshahi H. G., Harutyunian H. A. E. ., eds, Proceedings of Armenian-Iranian Astronomical Workshop (AIAW). pp 227–229

Gyulzadyan M. V., Mickaelian A. M., Abrahamyan H. V., Paronyan G. M., 2016b, in Mickaelian A., Lawrence A., Magakian T., eds, Astronomical Society of the Pacific Conference Series Vol. 505, Astronomical Surveys and Big Data. p. 162

Gyulzadyan M. V., Mickaelian A. M., Abrahamyan H. V., Paronyan G. M., Mikayelyan G. A., 2017, in Mickaelian A. M., Harutyunian H. A., Nikoghosyan E. H., eds, Astronomical Society of the Pacific Conference Series Vol. 511, Non-Stable Universe: Energetic Resources, Activity Phenomena, and Evolutionary Processes. p. 192

Gyulzadyan M. V., Mickaelian A. M., Abrahamyan H. V., Mikayelyan G. A., Paronyan G. M., 2018, Communications of the Byurakan Astrophysical Observatory, 65, 392

Hales S. E. G., Riley J. M., Waldram E. M., Warner P. J., Baldwin J. E., 2007, Mon. Not. R. Astron. Soc. , 382, 1639

Heckman T. M., 1980, A&A, 87, 152

doi: https://doi.org/10.52526/25792776-23.70.2-261

Helfand D. J., White R. L., Becker R. H., 2015, Astrophys. J. , 801, 26

Herschel Point Source Catalogue Working Group et al., 2020, VizieR Online Data Catalog, p. VIII/106

Hoffmeister C., 1929, AN, 236, 233

Hovhannisyan A., Sargsyan L. A., Mickaelian A. M., Weedman D. W., 2011, Astrophysics, 54, 147

IRAS 1986, Joint IRAS Science W.G., IRAS Catalog of Point Sources, Version 2.0

Ishihara D., et al., 2010, Astron. Astrophys. , 514, A1

Kazarian M. A., Mickaelian A. M., 2007, Ap, 50, 127

Kazarian M. A., Adibekyan V. Z., McLean B., Allen R. J., Petrosian A. R., 2010, Ap, 53, 57

Khachikian E. Y., Weedman D. W., 1974, ApJ, 192, 581

Lasker B. M., et al., 2008, Astron. J. , 136, 735

Lyke B. W., et al., 2020, Astrophys. J. Suppl. Ser. , 250, 8

Markarian B. E., Stepanian J. A., Erastova L. K., 1987, IAU S121, p. 25

Markarian B. E., Lipovetsky V. A., Stepanian J. A., Erastova L. K., Shapovalova A. I., 1989, Soobshcheniya Spetsial'noj Astrofizicheskoj Observatorii, 62, 5

Massaro E., Mickaelian A. M., Nesci R., Weedman D., 2008, The Digitized First Byurakan Survey

Massaro E., Maselli A., Leto C., Marchegiani P., Perri M., Giommi P., Piranomonte S., 2015, Ap&SS, 357, 75

Mauch T., Murphy T., Buttery H. J., Curran J., Hunstead R. W., Piestrzynski B., Robertson J. G., Sadler E. M., 2003, Mon. Not. R. Astron. Soc. , 342, 1117

Mazzarella J. M., Balzano V. A., 1986, ApJS, 62, 751

McMahon R. G., Irwin M. J., Maddox S. J., 2000, VizieR Online Data Catalog, p. I/267

Mickaelian A. M., 1995, Astrophysics, 38, 349

Mickaelian A. M., 2000a, Astronomical and Astrophysical Transactions, 18, 557

Mickaelian A. M., 2000b, Astrophysics, 43, 309

Mickaelian A. M., 2001a, Astrophysics, 44, 33

Mickaelian A. M., 2001b, Astrophysics, 44, 185

Mickaelian A. M., 2002, Astrophysics, 45, 288

Mickaelian A. M., 2003a, in IAU General Assembly. p. E1

Mickaelian A. M., 2003b, Astronomical and Astrophysical Transactions, 22, 753

Mickaelian A. M., 2003c, in Proceedings of JENAM-2002. pp 76–80

Mickaelian A. M., 2004a, Baltic Astronomy, 13, 655

Mickaelian A. M., 2004b, Astrophysics, 47, 361

Mickaelian A. M., 2004c, Astron. Astrophys. , 426, 367

Mickaelian A. M., 2008, Astron. J. , 136, 946

Mickaelian A. M., 2012, Baltic Astronomy, 21, 331

Mickaelian A. M., 2015, Iranian Journal of Astronomy and Astrophysics, 2, 1

Mickaelian A. M., 2016a, Baltic Astronomy, 25, 75

Mickaelian A. M., 2016b, Astronomy Reports, 60, 857

Mickaelian A. M., 2016c, in Mickaelian A., Lawrence A., Magakian T., eds, Astronomical Society of the Pacific Conference Series Vol. 505, Astronomical Surveys and Big Data. p. 117

Mickaelian A. M., 2016d, in Mickaelian A., Lawrence A., Magakian T., eds, Astronomical Society of the Pacific Conference Series Vol. 505, Astronomical Surveys and Big Data. p. 203

Mickaelian A. M., 2017, Communications of the Byurakan Astrophysical Observatory, 64, 15

Mickaelian A. M., 2020, Communications of the Byurakan Astrophysical Observatory, 67, 159

Mickaelian A. M., 2021a, in Mickaelian A. M., ed., , Byurakan Astrophysical Observatory - 75 years of outstanding achievements. p. 116

doi: https://doi.org/10.52526/25792776-23.70.2-261

Mickaelian A. M., 2021b, Communications of the Byurakan Astrophysical Observatory, 68, 174

Mickaelian A. M., Gigoyan K. S., 1998a, Astrophysics, 41, 161

Mickaelian A. M., Gigoyan K. S., 1998b, Astrophysics, 41, 232

Mickaelian A. M., Sargsyan L. A., 2004a, Astrophysics, 47, 91

Mickaelian A. M., Sargsyan L. A., 2004b, Astrophysics, 47, 213

Mickaelian A. M., Sargsyan L. A., 2010, Astrophysics, 53, 483

Mickaelian A. M., Sinamyan P. K., 2010, Mon. Not. R. Astron. Soc. , 407, 681

Mickaelian A. M., Eritsyan M. A., Abramyan G. V., 1991, Astrophysics, 34, 186

Mickaelian A. M., Gigoyan K. S., Russeil D., 1997, Astrophysics, 40, 379

Mickaelian A. M., Akopian S. A., Balaian S. K., Burenkov A. N., 1998, Astronomy Letters, 24, 635

Mickaelian A. M., Gonçales A. C., Véron-Cetty M. P., Véron P., 1999, Astrophysics, 42, 1

Mickaelian A. M., Balayan S. K., Hakopian S. A., 2001a, Astronomical and Astrophysical Transactions, 20, 315

Mickaelian A. M., Gonçalves A. C., Véron-Cetty M. P., Véron P., 2001b, Astrophysics, 44, 14

Mickaelian A. M., Hakopian S. A., Balayan S. K., Dodonov S. N., Afanasiev V. L., Burenkov A. N., Moiseev A. V., 2002a, Bulletin of the Special Astrophysics Observatory, 53, 144

Mickaelian A. M., Balayan S. K., Hakopian S. A., 2002b, in Green R. F., Khachikian E. Y., Sanders D. B., eds, Astronomical Society of the Pacific Conference Series Vol. 284, IAU Colloq. 184: AGN Surveys. p. 217

Mickaelian A. M., Hakopian S. A., Balayan S. K., 2002c, in Green R. F., Khachikian E. Y., Sanders D. B., eds, Astronomical Society of the Pacific Conference Series Vol. 284, IAU Colloq. 184: AGN Surveys. p. 220

Mickaelian A. M., Hovhannisyan L. R., Sargsyan L. A., 2003, Astrophysics, 46, 177

Mickaelian A. M., Hovhannisyan L. R., Engels D., Hagen H. J., Voges W., 2006, Astron. Astrophys. , 449, 425

Mickaelian A. M., et al., 2007, Astron. Astrophys. , 464, 1177

Mickaelian A. M., Mikayelyan G. A., Sinamyan P. K., 2011, Mon. Not. R. Astron. Soc. , 415, 1061

Mickaelian A. M., Abrahamyan H. V., Paronyan G. M., Harutyunyan G. S., 2013, Astronomische Nachrichten, 334, 887

Mickaelian A. M., Paronyan G. M., Abrahamyan H. V., Gyulzadyan M. V., Mikayelyan G. A., 2016a, in Mickaelian A. M., Khosroshahi H. G., Harutyunian H. A. E. ., eds, Proceedings of Armenian-Iranian Astronomical Workshop (AIAW). pp 170–177

Mickaelian A. M., Paronyan G. M., Harutyunyan G. S., Abrahamyan H. V., Gyulzadyan M. V., 2016b, Astronomical and Astrophysical Transactions, 29, 333

Mickaelian A. M., Paronyan G. M., Abrahamyan H. V., Gigoyan K. S., Gyulzadyan M. V., Kostandyan G. R., 2016c, Astronomical and Astrophysical Transactions, 29, 451

Mickaelian A., Paronyan G., Abrahamyan H., 2016d, IAU Focus Meeting, 29B, 91

Mickaelian A. M., Astsatryan H. V., Knyazyan A. V., Mikayelyan G. A., 2017a, BAOJ Physics, 2, 8

Mickaelian A. M., et al., 2017b, Communications of the Byurakan Astrophysical Observatory, 64, 102

Mickaelian A. M., Gyulzadyan M. V., Abrahamyan H. V., Paronyan G. M., Mikayelyan G. A., 2017c, in Mickaelian A. M., Harutyunian H. A., Nikoghosyan E. H., eds, Astronomical Society of the Pacific Conference Series Vol. 511, Non-Stable Universe: Energetic Resources, Activity Phenomena, and Evolutionary Processes. p. 149

Mickaelian A. M., Harutyunyan G. S., Sarkissian A., 2018a, Astronomy Letters, 44, 351

Mickaelian A. M., Abrahamyan H. V., Gyulzadyan M. V., Paronyan G. M., Mikayelyan G. A., 2018b, Astrophys. Space. Sci. , 363, 237

Mickaelian A. M., Abrahamyan H. V., Paronyan G. M., Mikayelyan G. A., Gyulzadyan M. V., 2019, Communications of the Byurakan Astrophysical Observatory, 66, 173

Mickaelian A. M., Abrahamyan H. V., Paronyan G. M., Mikayelyan G. A., Gyulzadyan M. V., 2020, Communications of the Byurakan Astrophysical Observatory, 67, 149

Mickaelian A. M., Abrahamyan H. V., Paronyan G. M., Mikayelyan G. A., 2021a, in Mickaelian A. M., ed., , Byurakan Astrophysical Observatory - 75 years of outstanding achievements. p. 133

Mickaelian A. M., Abrahamyan H. V., Paronyan G. M., Mikayelyan G. A., 2021b, Frontiers in Astronomy and Space Sciences, 7, 82

Mickaelian A. M., Andreasyan R. R., Abrahamyan H. V., Paronyan G. M., Mikayelyan G. A., Sukiasyan A. G., Mkrtchyan V. K., 2021c, Astronomical and Astrophysical Transactions, 32, 331

doi: https://doi.org/10.52526/25792776-23.70.2-261

Mickaelian A. M., Mikayelyan G. A., Abrahamyan H. V., Paronyan G. M., 2021d, Communications of the Byurakan Astrophysical Observatory, 68, 163

Mickaelian A. M., Abrahamyan H. V., Paronyan G. M., Mikayelyan G. A., 2022a, Communications of the Byurakan Astrophysical Observatory, 69, 179

Mickaelian A. M., Abrahamyan H. V., Mikayelyan G. A., Paronyan G. M., 2022b, Communications of the Byurakan Astrophysical Observatory, 69, 10

Mickaelian A. M., Abrahamyan H. V., Paronyan G. M., Mikayelyan G. A., Andreasyan R. R., Sukiasyan A. G., Hambardzumyan L. A., Mkrtchyan V. K., 2023, Communications of the Byurakan Astrophysical Observatory, 70, 68

Mikayelyan G. A., Mickaelian A. M., Abrahamyan H. V., Paronyan G. M., 2018, Communications of the Byurakan Astrophysical Observatory, 65, 13

Mikayelyan G. A., Mickaelian A. M., Abrahamyan H. V., Paronyan G. M., Gyulzadyan M. V., 2019a, Astrophysics, 62, 452

Mikayelyan G. A., Mickaelian A. M., Abrahamyan H. V., Paronyan G. M., Gyulzadyan M. V., 2019b, Communications of the Byurakan Astrophysical Observatory, 66, 31

Monet D., Canzian B., Harris H., Reid N., Rhodes A., Sell S., 1998, VizieR Online Data Catalog, p. I/243

Monet D. G., et al., 2003, Astron. J. , 125, 984

Moshir M., et al. 1990, IRAS Faint Source Catalogue, p. 0

Oke J. B., Gunn J. E., 1974, ApJL, 189, L5

Osterbrock D. E., 1981, ApJ, 249, 462

Osterbrock D. E., Pogge R. W., 1985, ApJ, 297, 166

Paronyan G. M., Mickaelian A. M., 2015, Izvestiya Glavnoj Astronomicheskoj Observatorii v Pulkove, 222, 77

Paronyan G. M., Mickaelian A. M., Abrahamyan H. V., 2016, in Mickaelian A., Lawrence A., Magakian T., eds, Astronomical Society of the Pacific Conference Series Vol. 505, Astronomical Surveys and Big Data. p. 189

Paronyan G. M., Mickaelian A. M., Abrahamyan H. V., Mikayelyan G. A., 2018a, Communications of the Byurakan Astrophysical Observatory, 65, 412

Paronyan G. M., Mickaelian A. M., Abrahamyan H. V., Mikayelyan G. A., 2018b, Izvestiya Glavnoj Astronomicheskoj Observatorii v Pulkove, 226, 52

Paronyan G. M., Mickaelian A. M., Harutyunyan G. S., Abrahamyan H. V., Mikayelyan G. A., 2019, Astrophysics, 62, 147

Paronyan G. M., Mickaelian A. M., Abrahamyan H. V., Mikayelyan G. A., 2020, Astrophysics, 63, 166

Paronyan G. M., Mickaelian A. M., Abrahamyan H. V., Mikayelyan G. A., 2021a, Astrophysics, 64, 277

Paronyan G. M., Mickaelian A. M., Abrahamyan H. V., Mikayelyan G. A., Sukiasyan A. G., 2021b, Communications of the Byurakan Astrophysical Observatory, 68, 528

Paronyan G. M., Mickaelian A. M., Abrahamyan H. V., Mikayelyan G. A., Sukiasyan A. G., Hambardzumyan L. A., Mkrtchyan V. K., 2023, Communications of the Byurakan Astrophysical Observatory, 70, 88

Paturel G., Petit C., Rousseau J., Vauglin I., 2003, Astron. Astrophys. , 405, 1

Planck Collaboration et al., 2016, Astron. Astrophys. , 594, A26

Rees N., 1990, Mon. Not. R. Astron. Soc. , 244, 233

Revnivtsev M., Sazonov S., Jahoda K., Gilfanov M., 2004, Astron. Astrophys. , 418, 927

Sabzali V., Davoudifar P., Mickaelian A. M., 2016, in Mickaelian A. M., Khosroshahi H. G., Harutyunian H. A. E. ., eds, Proceedings of Armenian-Iranian Astronomical Workshop (AIAW). pp 233–238

Sanders D. B., Mirabel I. F., 1996, Ann. Rev. Astron. Astrophys. , 34, 749

Sargsyan L. A., Mickaelian A. M., 2006, Astrophysics, 49, 19

Sargsyan L. A., Mickaelian A. M., Weedman D., Houck J., 2007, in JENAM-2007, "Our Non-Stable Universe". pp 50–50

Sargsyan L., Mickaelian A., Weedman D., Houck J., 2008, Astrophys. J. , 683, 114

Sargsyan L. A., Mickaelian A. M., Weedman D. W., Houck J. R., 2010, in Harutyunian H. A., Mickaelian A. M., Terzian Y., eds, Evolution of Cosmic Objects through their Physical Activity. pp 231–237

Sargsyan L., Weedman D., Lebouteiller V., Houck J., Barry D., Hovhannisyan A., Mickaelian A., 2011, Astrophys. J. , 730, 19

Schmidt M., 1963, Nature, 197, 1040

Schmitt J. L., 1968, Nature, 218, 663

doi: https://doi.org/10.52526/25792776-23.70.2-261

Seyfert C. K., 1943, ApJ, 97, 28

Sinamian P. K., Mickaelian A. M., 2006, Astrophysics, 49, 333

Sinamyan P. K., Mickaelian A. M., 2008a, Astrophysics, 51, 37

Sinamyan P. K., Mickaelian A. M., 2008b, Astrophysics, 51, 226

Sinamyan P. K., Mickaelian A. M., 2009, Astrophysics, 52, 76

Sinamyan P. K., Sargsyan L. A., Mickaelian A. M., Massaro E., Nesci R., Rossi C., Gaudenzi S., Cirimele G., 2007, in JENAM-2007, "Our Non-Stable Universe". pp 82–82

Strittmatter P. A., Serkowski K., Carswell R., Stein W. A., Merrill K. M., Burbidge E. M., 1972, ApJ, 175, L7

Talezade Lari M. H., Davoudifar P., Mickaelian A. M., 2016, in Mickaelian A. M., Khosroshahi H. G., Harutyunian H. A. E. ., eds, Proceedings of Armenian-Iranian Astronomical Workshop (AIAW). pp 213–217

Terlevich R., 1997, RMAA, 6, 1

Terlevich R., 2000, In: Advanced Lectures on the Starburst-AGN Connection, Eds. Aretxaga, I.; Mújica, R.; Kunth, D., World Scientific, p. 279

Thuan T. X., Martin G. E., 1981, ApJ, 247, 823

Véron-Cetty M. P., Véron P., 2010, A&A, 518, A10

Véron-Cetty M. P., et al., 2004a, A&A, 414, 487

Véron-Cetty M. P., et al., 2004b, Astron. Astrophys. , 414, 487

Véron P., Gonçales A. C., Véron-Cetty M. P., 1997, A&A, 319, 52

Verrecchia F., in't Zand J. J. M., Giommi P., Santolamazza P., Granata S., Schuurmans J. J., Antonelli L. A., 2007, Astron. Astrophys. , 472, 705

Voges W., et al., 1999, Astron. Astrophys. , 349, 389

Voges W., et al., 2000, IAU Circ., 7432, 3

Webb N. A., et al., 2020, Astron. Astrophys. , 641, A136

Weedman D. W., 1977, Vistas in Astronomy, 21, 55

Wood K. S., et al., 1984, Astrophys. J. Suppl. Ser. , 56, 507

Yamamura I., Makiuti S., Ikeda N., Fukuda Y., Oyabu S., Koga T., White G. J., 2010, VizieR Online Data Catalog, p. II/298

Zickgraf F. J., Engels D., Hagen H. J., Reimers D., Voges W., 2003, A&A, 406, 535

doi: https://doi.org/10.52526/25792776-23.70.2-261

Survey, Catalogue	**Years**	**Spectral range**	**Sky area** (deg^2)	**Sensitivity (mag/mJy)**	**Number of sources**
Fermi-GLAST	2008-2014	10MeV-100GeV	Alll-sky		3,033
CGRO	1991-1999	20keV-30GeV	All-sky		1,300
INTEGRAL	2002-2014	15keV-10MeV	All-sky		1,126
Swift	2004-2008	14-150keV	All-sky		84,979
XMM-Newton	1999-2014	0.25-12keV	Pointed		372,728
Chandra	1999-2014	0.07-10keV	Pointed		380,000
ROSAT BSC	1990-1999	0.07-2.4keV	All-sky		18,806
ROSAT FSC	1990-1999	0.07-2.4keV	All-sky		105,924
GALEX AIS	2003-2012	1344-2831A	21435	20.8”	65,266,291
GALBX MIS	2003-2012	1344-2831A	1,579	22.7”	12,597,912
APM	2000	opt b, r	20,964	21.0”	166,466,987
MAPS	2003	opt O, E	20,964	21.0”	89,234,404
USNO-A2.0	1998	opt B, R	All-sky	21.0”	526,280,881
USNO-B1.0	2003	opt B, R, I	All-sky	22.5”	1,045,913,669
SuperCOSMOS	2001	opt B, R, I	All-sky	22.5”	1,900,000,000
GSC 2.3.2	2008	opt j, V, F, N	All-sky	22,5”	945,592,683
FBS	1965-1980	3400-6900A	17,056	17,5”	20,000,000
SBS	1978-1991	3400-6950A	965	19.0”	3,000,000
HQS	1985-1997	3400-5300A	14,000	19,0”	16,000,000
HES	1990-1996	3400-5300A	9,000	18,0”	5,000,000
Tycho-2	1989-1993	opt BT, VT	All-sky	16,3”	2,539,913
SDSS photo	2000-2015	opt u, g, r, i, z	14,555	22.2”	932,891,133
SDSS spectro	2000-2015	3000-10800A	14,555	17.7”	4,355,200
DENIS	1996-2001	0.8-2.4μm	16,700	18.5”	355,220,325
2MASS PSC	1997-2001	1.1-2.4μm	All-sky	17.1”	470,992,970
2MASS ESC	1997-2001	1.1-2.4μm	All-sky	17”1	1,647,599
WISE	2009-2013	3-22μm	All-sky	15.6”	747,634,026
AKARI IRC	2006-2008	7-26μm	38,778	50my	870,973
Spitzer	2003-2009	3-180μm	Pointed	0.6μJy	4,261,028
IRAS PSC	1983	8-120μm	39,603	400mJy	245,889
IRAS FSC	1983	8-120μm	34,090	400mJy	173,044
IRAS SSSC	1983	8-120μm	39,603	400mJy	16,740
AKARI FIS	2006-2008	50-180μm	40,428	550mJy	427,071
Herschel	2009-2013	55-672μm	Pointed	6mJy	340,968
ALMA	2011-2014	0.3-9.6mm	Pointed	50μJy	
Planck	2009-2011	0.35-10mm	All-sky	183mJy	33,566
WMAP	2001-2011	3-14mm	All-sky	500mJy	471
GB6	1986-1987	6cm	20,320	18mJy	75,162
NVSS	1998	21cm	33,827	2.5mJy	1,773,484
FIRST	1999-2015	21cm	10,000	1mJy	946,432
SUMSS	2003-2012	36cm	8,000	1mJy	211,080
WENSS	1998	49/92cm	9,950	18mJy	229,420
7C	2007	198cm	2,388	40mJy	43,683
VLA LFSS	2007	406cm	All-sky	700mJy	92,963

Table 4. The list of all-sky and large-area astronomical catalogs in increasing wavelength range from gamma-rays to radio and their main parameters.

doi: https://doi.org/10.52526/25792776-23.70.2-261

Wavelength range	Number of objects
Gamma-ray	10 000
X-ray	1 500 000
UV	100 000 000
Optical	2 400 000 000
NIR	600 000 000
MIR	600 000 000
FIR	500 000
Sub-mm/mm	100 000
Radio	2 000 000

Table 5. The numbers of catalogued astronomical objects at different wavelength ranges.

Surveys, Projects	Short	Range	Information Volume
Digitized First Byurakan Survey	DFBS	opt	400 GB
Digital Palomar Observatory Sky Survey	DPOSS	opt	3 TB
Two Micron All-Sky Survey	2MASS	NIR	10 TB
Green Bank Telescope	GBT	radio	20 TB
Galaxy Evolution Explorer	GALEX	UV	30 TB
Sloan Digital Sky Survey	SDSS	opt	140 TB
SkyMapper Southern Sky Survey			500 TB
Panoramic Survey Telescope and Rapid Response System, expected	PanSTARRS	opt	40 PB
Large Synoptic Survey Telescope, expected	LSST	opt	200 PB
Square Kilometer Array, expected	SKA	radio	4.6 EB

Table 6. Data volumes in big astronomical projects.

doi: https://doi.org/10.52526/25792776-23.70.2-261

Years	Authors	Survey	Short	Objectives	Number
1986-2001	H. Abrahamian, A. Mickaelian	First Byurakan Survey, 2nd Part	FBS BSOs	QSOs and Seyferts	1103
1994-2010	A. Mickaelian et al.	Byurakan-IRAS Galaxies	BIG	IRAS galaxies	1278
2001-pres.	A. Mickaelian	Bright AGN	AGN	Statistical studies of bright AGN	10 000
2002-2006	A. Mickaelian et al.	Byurakan-Hamburg-ROSAT Catalogue BHRC	BHRC	ROSAT sources	2791
2003-2010	A. Mickaelian et al.	Spitzer ULIRGs	Spitzer	ULIRGs	32
2010-pres.	A. Mickaelian et al.	Markarian galaxies	Mrk	Markarian galaxies	1544
2010-pres.	G. Paronyan, A. Mickaelian, et al.	HRC/BHRC AGN content	X-ray AGN	X-ray AGN	4253
2015-pres.	H. Abrahamyan, G. Mikayelyan, A. Mickaelian	IRAS PSC/FSC Combined Catalog extragalactic sources	IRAS	IRAS galaxies	145 902
2013-2018	H. Abrahamyan, A. Mickaelian et al.	Variable radio sources at 1400 MHz	NVSS/FIRST	Variable radio sources	6301
2013-pres.	A. Mickaelian, G. Paronyan, et al.	Search for X-ray/ radio AGN	ROSAT/NVSS	X-ray/ radio AGN	9193
2014-pres.	H. Abrahamyan, A. Mickaelian et al.	MW study of Blazars	BZCAT	Blazars	3561
2018-pres.	G. Mikayelyan, A. Mickaelian et al.	IRAS PSC/FSC Combined Catalogue ULIRG/HLIRG	ULIRG/ HLIRG	High luminosity IR galaxies	114
2001-2007	A. Mickaelian, et al.	Fine analysis of AGN spectra	Bright AGN	Physical properties of AGN	90
2002-pres.	A. Mickaelian, et al.	Search for new AGN in DFBS	DFBS AGN	New bright active galaxies	10 000
2006-pres.	A. Mickaelian, et al.	Fine classification of active galaxies	Mickaelian classification	Active galaxies accurate types/subtypes	10 000

Table 7. The list of BAO "Astronomical Surveys" research department projects related to multiwavelength search and studies of active galaxies.

Observational evidence of instability phenomena related to open star clusters based on Gaia data

D. A. Kovaleva *

Institute of Astronomy, Russian Acad. Sci., Moscow, 48 Pyatnitskaya st., Russia

Abstract

The vast amount of high-quality astrometric and photometric data from Gaia space mission opened new prospects in the investigation of the population of galactic star clusters. In particular, a number of observational evidence have emerged in relation to the phenomena of instability that previously were mainly predicted by dynamical simulations. These are signs of former violent relaxation, ongoing tidal disruption, interaction between the clusters and results of disruption of the clusters. We discuss methods of discovery of such evidence along with some interesting examples.

Keywords: *open star clusters, Gaia, tidal tails, disruption of star clusters*

1. Introduction

The importance of process of disruption of stellar systems in the evolution of Galaxy was stressed by V. A. Ambartsumyan in his pioneering analytical works on dynamical evolution of stellar systems / statistical mechanics (Ambartsumian, 1955, 1985). In these papers, starting from at least 1938, he suggested reliable estimates for the lifetime of open star clusters and a description of the process of their disruption.

Afterwards, especially with raise of N-body modelling, different aspects of dynamical evolution of open star clusters have been explored since 1970s (e.g., Aarseth et al., 1974, Tutukov, 1978). Let us provide a few examples to illustrate the problems explored. In the paper by Moyano Loyola & Hurley (2013) authors quantitatively analyze the mechanisms that produced the cluster escapers, such as evaporation through weak two-body encounters, energetic close encounters, or stellar evolution events. Chumak & Rastorguev (2006) have numerically simulated the formation, structure, and dynamical evolution of the population of stars that escaped from open clusters via tidal tails. Shukirgaliyev et al. (2017, 2019) explored the open cluster survivability after instantaneous gas expulsion, in the process of violent relaxation.

However, though basically the scheme of “Birth, Evolution and Death” (Kroupa, 2001) of star clusters seemed to be understood by the beginning of this century, lack of observational information prevented numerous models to lean on well defined boundary conditions. Only the approach based on broad statistics could provide some very general quantitative clues for the evolution of open clusters (Just et al., 2023, Piskunov et al., 2018). As for the fine details, in the era before Gaia the situation was as follows. Although models predicted open clusters to have extended low surface density features like tidal tails (Chumak et al., 2010, Ernst et al., 2011, Küpper et al., 2010), or halo (Danilov et al., 2014) which may serve as evidence of cluster dynamical evolution, observational signs were very modest (Röser et al., 2011) or nonexistent. The true extent and scale of these features could have not been assessed. The known massive stellar streams were mainly products of evolution of globular clusters (see, e.g., Koposov et al., 2010).

After the start of the Gaia space mission Gaia Collaboration et al. (2016), its data releases, especially DR2 (Gaia Collaboration et al., 2018) and EDR3 (Gaia Collaboration et al., 2021) became table-turners in many aspects of star cluster investigation. This involved drastic improvement in the selection of cluster membership, as well as development of methods involving the use of clustering algorithms to search for new clusters and related aggregates (see a review in Hunt & Reffert, 2021). These data also provided numerous chances to obtain and interpret signatures of processes of instability during the cluster evolution. For them, however, the methods of search and discovery should be specifically adjusted.

*dana@inasan.ru

doi: https://doi.org/10.52526/25792776-23.70.2-277

In this paper, we provide a review of the methods and some results (including ours) of search and discovery of low-surface-density extended stellar groups signifying evidence of processes of instability. We follow the natural course of events. Section 2 is dedicated to the remnants of the star formation process. Section 3 deals with search of the expended features in the vicinity of known clusters. Section 4 describes the approach of automatic blind search in the multiparameter space for the search of moving groups and low-mass stellar streams originating from disrupted open clusters. Section 5 summarizes the main ideas of this review.

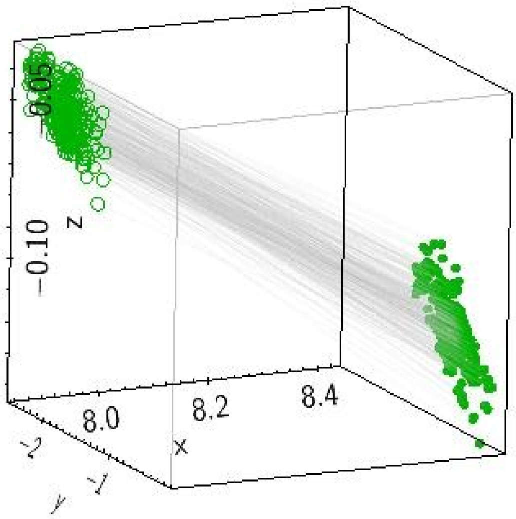

Figure 1. The location of the probable members of Group V in heliocentric carthesian galactic coordinates: present day – filled circles, 16 Myr backwards – empty circles. Thin grey lines connect positions of the same stars.

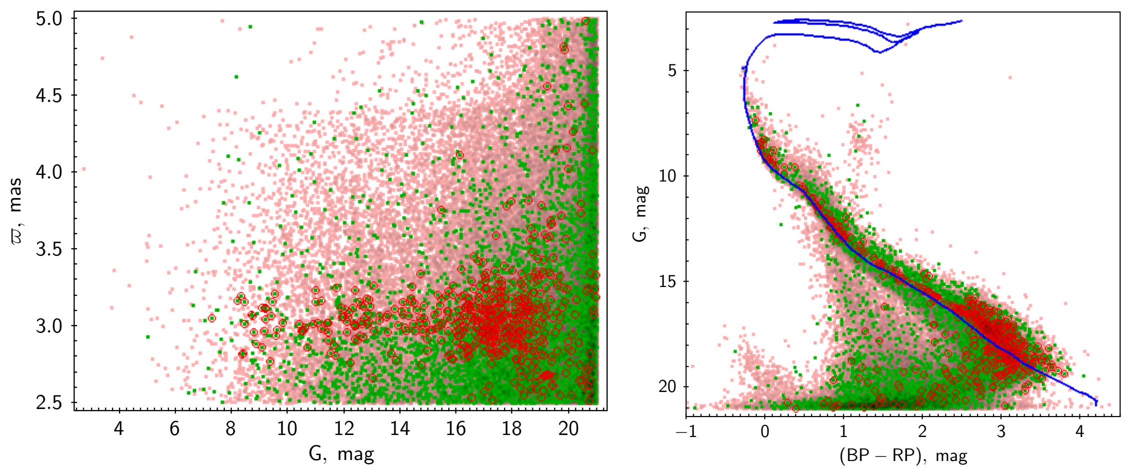

Figure 2. Probable members of [BBJ2018] 6 over parallax vs Gaia G magnitude (left panel) and in the color-magnitude diagram. Rose dots – background stars, green dots — probable stars of spatial vicinity of the group, open red circles – probable members of the stream. On the right panel, blue isochrone from Padova webserver CMD3.3 http://stev.oapd.inaf.it/cmd is for age of 50 Myr, similarly to age defined for Cr 135 and UBC 7 (Kovaleva et al., 2020).

2. Star formation remnants

A consensus converges to star formation taking place within molecular clouds containing embedded star clusters, filaments, fibers (e.g. André, 2017, André et al., 2010, Lada & Lada, 2003, Portegies Zwart et al.,

doi: https://doi.org/10.52526/25792776-23.70.2-277

2010). On the way from protocluster to open cluster, it should survive the violent relaxation (dynamical response to the expulsion of the residual star-forming gas). It is known that young star clusters tend to form groups, especially in the regions where star formation is going on (Casado, 2022, Conrad et al., 2017, Vaher et al., 2023). However, it was a newly discovered fact that one may detect a groupings of stars of extent up to hundreds of parsec, following past complex gaseous filamentary structures between the protoclusters and remaining after the gas expulsion from the region. The imprints of such structures have been discovered in star forming regions in Vela (Beccari et al., 2020) and in Orion (Jerabkova et al., 2019). We have independently identified similar group named Group V of extent of 60 to 70 pc hosting 150 to 300 members in Orion A (Vereshchagin et al., 2023) which most probably refers to the structure previously investigated by Jerabkova et al. (2019) and by Getman et al. (2019). In all described cases, the relict structures were noticed in the course of investigation kinematical and spatial structure of stellar population of a certain region, and probable members of these structures selected using statistical methods. The procedures used by Vereshchagin et al. (2023) involve a combination of approaches using suggestions on distribution of spatial velocities of probable members and a clustering algorithm DBSCAN applied to specially prepared dataset of probable pairs (for further details, see Sapozhnikov & Kovaleva, 2021). The backward integration of the orbits of the elements of the group in the gravitational potential of the Galaxy with *galpy* (Bovy, 2015) demonstrates its slow spread in the course of past 16 to 17 Myr which is the approximate age of the group (see Fig. 1). The calculation demonstrated at the figure lays on the dispersion of tangential velocities and neglects dispersion of radial velocities. The calculation for the groupings of members based on their mean 3D spacial velocities and their dispersion indicates that its extension approximately doubled during past 16 Myr.

3. Search in the vicinity of known clusters: tidal tails, halo

In the clusters that have survived violent relaxation, the period of two-body relaxation starts which tends to form their structure consisting of approximately spherical core and outskirts. These outskirts are primarily subjected to disintegration processes such as tidal disruption, disk crossing, differential rotation, providing runaway population. It may form tidal tails and an extended halo (also known as a corona) around the cluster. Such structures are sometimes discovered simply by selection of probable members of a cluster and making an analysis of their spatial and kinematical distribution. However, to discover their full extent, which, with Gaia data, happened to be much larger than we could expect, one may need to use a dynamic model of a structure, as it was done by Jerabkova et al. (2021). In this work, the tidal tails of Hyades were followed up to 800 pc, and their internal structural characteristics were revealed. Such a detailed investigations promises new fundamental results concerning testing of the theory of gravitation (Kroupa et al., 2022), dynamical evolution (Pflamm-Altenburg et al., 2023) and ages of clusters (Dinnbier et al., 2022).

Methods of recovery of expected but missing structures intrinsically related to the known clusters may use a search with clustering algorithms using known characteristics of the clusters. To discover the tidal tails of Coma Ber, Tang et al. (2019) applied cuts in proper motion to decrease the number of sources, and then used a method based on the self-organizing map to identify relevant structures. Using two methods, Clusterix and UPMASK, Carrera et al. (2019) discover an extended halo of NGC 2628 which radius, 50 pc, exceeds preliminary estimates more than twice. On the other hand, we discovered an extended halo of the binary cluster Cr 135 and UBC 7 (Kovaleva et al., 2020) by selection of cluster's members based on kinematical and photometrical probabilities.

4. Stellar streams and moving groups. Methods of discovery

The dissolution of star clusters may occur at different stages of their evolution. As a result of gas expulsion, the cluster may be destroyed and one or several moving groups may remain, in addition to runaway stars. Otherwise, the open cluster may be destroyed by the Galaxy disk passage, encounters giant molecular clouds, or just dissolved via the tidal tails to become a stellar stream (see, e.g., Tutukov et al., 2020). Unlike star clusters, the detection and classification of extended groups and streams where stars are not concentrated in space but just keep similar movement, in large surveys such as Gaia may be challenging. Usually it is successful for the main streams (Alvey et al., 2023, Ibata et al., 2023), or in dedicated searches in a limited multi-parameter region.

doi: https://doi.org/10.52526/25792776-23.70.2-277

So, a search in the Solar vicinity led to the discovery of a massive stellar stream originating, supposedly, from the destruction of an open cluster very similar to Pleiades independently by the two groups of authors (Ratzenböck et al., 2020, Röser & Schilbach, 2020). Fürnkranz et al. (2019) at first discovered overdensities in velocity space with wavelet decomposition method, applied filters, and then used DBSCAN to a primary selection of the data. They independently discovered the tidal tails of Coma Ber and a moving group, previously unknown and unrelated to Coma Ber. We used a DBSCAN applied to the preliminarily prepared catalog of stellar pairs to discover the full extent of these stellar structures (Sapozhnikov & Kovaleva, 2021).

Further analysis of the vicinity of a binary cluster Cr 135 and UBC 7 (Kovaleva et al., 2020) in Vela-Puppis region led us to the discovery of a stellar stream with kinematical properties and age very similar to those of Cr 135. This is why it reveals itself if one considers probabilities of membership to this cluster. This stream may be be connected to this structure was previously described as loosely spread cluster [BBJ2018] 6 by Beccari et al. (2018), however, its full extent is a way larger than it has been supposed initially. At Fig. 1 the probable members of the stream are compared with the background and with the stars of spatial vicinity in the Vela-Puppis region. One sees them clustering over parallax and along the same isochrone.

5. Conclusions

The results of Gaia mission have provided a valuable opportunity for researchers to discover and investigate observational evidence of processes of dynamical evolution of open clusters. These are remnants of processes of formation of stars, remnants of processes of their quick and slow disruption in the course of violent relaxation or two-body relaxation, encounters with the giant molecular clouds or passage through the disk of Galaxy. These structures may be discovered in dedicated systematic searches or in connection with the investigation of some clusters or other objects. Even solar vicinity revealed to be abundant with unknown previously moving groups, clusters with tidal tails, stellar streams. Many known star clusters at close investigation revealed their extended halos. The scale and extent of these stellar structures is usually much larger than was expected before. This provides us with the clues to fundamental problems of dynamical history and evolution of our Galaxy.

Acknowledgements

This work has made use of data from the European Space Agency (ESA) mission *Gaia* (`https://www.cosmos.esa.int/gaia`), processed by the *Gaia* Data Processing and Analysis Consortium (DPAC, `https://www.cosmos.esa.int/web/gaia/dpac/consortium`). Funding for the DPAC has been provided by national institutions, in particular the institutions participating in the *Gaia* Multilateral Agreement. The use of TOPCAT, an interactive graphical viewer and editor for tabular data (Taylor, 2005), is acknowledged.

References

Aarseth S. J., Henon M., Wielen R., 1974, Astron. Astrophys. , 37, 183

Alvey J., Gerdes M., Weniger C., 2023, Mon. Not. R. Astron. Soc. , 525, 3662

Ambartsumian V. A., 1955, The Observatory, 75, 72

Ambartsumian V. A., 1985, in Goodman J., Hut P., eds, Vol. 113, Dynamics of Star Clusters. p. 521

André P., 2017, Comptes Rendus Geoscience, 349, 187

André P., et al., 2010, Astron. Astrophys. , 518, L102

Beccari G., Boffin H. M. J., Jerabkova T., Wright N. J., Kalari V. M., Carraro G., De Marchi G., de Wit W.-J., 2018, Mon. Not. R. Astron. Soc. , 481, L11

Beccari G., Boffin H. M. J., Jerabkova T., 2020, Mon. Not. R. Astron. Soc. , 491, 2205

Bovy J., 2015, Astrophys. J. Suppl. Ser. , 216, 29

Carrera R., et al., 2019, Astron. Astrophys. , 627, A119

Casado J., 2022, Universe, 8, 113

Chumak Y. O., Rastorguev A. S., 2006, Astronomy Letters, 32, 157

Chumak Y. O., Platais I., McLaughlin D. E., Rastorguev A. S., Chumak O. V., 2010, Mon. Not. R. Astron. Soc. , 402, 1841

Conrad C., et al., 2017, Astron. Astrophys. , 600, A106

Danilov V. M., Putkov S. I., Seleznev A. F., 2014, Astronomy Reports, 58, 906

doi: `https://doi.org/10.52526/25792776-23.70.2-277`

Dinnbier F., Kroupa P., Šubr L., Jeřábková T., 2022, Astrophys. J. , 925, 214

Ernst A., Just A., Berczik P., Olczak C., 2011, Astron. Astrophys. , 536, A64

Fürnkranz V., Meingast S., Alves J., 2019, Astron.~Astrophys, 624, L11

Gaia Collaboration et al., 2016, Astron. Astrophys. , 595, A1

Gaia Collaboration et al., 2018, Astron. Astrophys. , 616, A1

Gaia Collaboration et al., 2021, Astron. Astrophys. , 649, A1

Getman K. V., Feigelson E. D., Kuhn M. A., Garmire G. P., 2019, Mon. Not. R. Astron. Soc. , 487, 2977

Hunt E. L., Reffert S., 2021, Astron. Astrophys. , 646, A104

Ibata R., et al., 2023, arXiv e-prints, p. arXiv:2311.17202

Jerabkova T., Boffin H. M. J., Beccari G., Anderson R. I., 2019, Mon. Not. R. Astron. Soc. , 489, 4418

Jerabkova T., Boffin H. M. J., Beccari G., de Marchi G., de Bruijne J. H. J., Prusti T., 2021, Astron. Astrophys. , 647, A137

Just A., Piskunov A. E., Klos J. H., Kovaleva D. A., Polyachenko E. V., 2023, Astron. Astrophys. , 672, A187

Koposov S. E., Rix H.-W., Hogg D. W., 2010, Astrophys. J. , 712, 260

Kovaleva D. A., et al., 2020, Astron. Astrophys. , 642, L4

Kroupa P., 2001, in Montmerle T., André P., eds, Astronomical Society of the Pacific Conference Series Vol. 243, From Darkness to Light: Origin and Evolution of Young Stellar Clusters. p. 387 (`arXiv:astro-ph/0010405`), doi:10.48550/arXiv.astro-ph/0010405

Kroupa P., et al., 2022, Mon. Not. R. Astron. Soc. , 517, 3613

Küpper A. H. W., Kroupa P., Baumgardt H., Heggie D. C., 2010, Mon. Not. R. Astron. Soc. , 401, 105

Lada C. J., Lada E. A., 2003, Ann. Rev. Astron. Astrophys. , 41, 57

Moyano Loyola G. R. I., Hurley J. R., 2013, Mon. Not. R. Astron. Soc. , 434, 2509

Pflamm-Altenburg J., Kroupa P., Thies I., Jerabkova T., Beccari G., Prusti T., Boffin H. M. J., 2023, Astron. Astrophys. , 671, A88

Piskunov A. E., Just A., Kharchenko N. V., Berczik P., Scholz R. D., Reffert S., Yen S. X., 2018, Astron. Astrophys. , 614, A22

Portegies Zwart S. F., McMillan S. L. W., Gieles M., 2010, Ann. Rev. Astron. Astrophys. , 48, 431

Ratzenböck S., Meingast S., Alves J., Möller T., Bomze I., 2020, Astron. Astrophys. , 639, A64

Röser S., Schilbach E., 2020, Astron. Astrophys. , 638, A9

Röser S., Schilbach E., Piskunov A. E., Kharchenko N. V., Scholz R. D., 2011, Astron. Astrophys. , 531, A92

Sapozhnikov S., Kovaleva D., 2021, Open Astronomy, 30, 191

Shukirgaliyev B., Parmentier G., Berczik P., Just A., 2017, Astron. Astrophys. , 605, A119

Shukirgaliyev B., Parmentier G., Berczik P., Just A., 2019, Mon. Not. R. Astron. Soc. , 486, 1045

Tang S.-Y., et al., 2019, Astrophys.~J., 877, 12

Taylor M. B., 2005, in Shopbell P., Britton M., Ebert R., eds, Astronomical Society of the Pacific Conference Series Vol. 347, Astronomical Data Analysis Software and Systems XIV. p. 29

Tutukov A. V., 1978, Astron. Astrophys. , 70, 57

Tutukov A. V., Sizova M. D., Vereshchagin S. V., 2020, Astronomy Reports, 64, 827

Vaher E., Hobbs D., McMillan P., Prusti T., 2023, Astron. Astrophys. , 679, A105

Vereshchagin S., Chupina N., Lyzenko K., Kalinkin A., Kondratev N., Kovaleva D., Sapozhnikov S., 2023, Galaxies, 11, 99

doi: `https://doi.org/10.52526/25792776-23.70.2-277`

Role of galactic disc thickness in magnetic field generation

E.A. Mikhailov *[1, 2] and M.V. Frolova†[2]

[1]P.N. Lebedev Physical Institute, Moscow, 119991, Russia
[2]M.V. Lomonosov Moscow State University, Moscow, 119991, Russia

Abstract

A large variety of galaxies have magnetic structures of lengthscales comparable with their radius. Theoretically, their existence is based on the dynamo mechanism. It is based on alpha-effect characterizing helicity of the turbulent motions and differential rotation which is connected with changing angular velocity. The field can be destroyed by turbulent diffusion, so the mechanism is threshold and can be realized only for the case when first and second effect are more intensive than the third one. Equations of magnetohydrodynamics that are used to describe the dynamo mechanism, are too difficult to be solved. So, usually different approximation taking into account details of astrophysical objects are used. As for galaxies, a thin disc approximation has been developed. It works properly for galactic objects with small half-thickness. However, as for thick discs we should take a model which uses more complicated structure of the field. Here we find the threshold for the field generation for thick astrophysical discs.

Keywords: *magnetic fields, galaxies, eigenvalue problem*

1. Introduction

Lots of galaxies have regular magnetic fields (Arshakian et al., 2009). First arguments for it were obtained while studying cosmic rays. Simple models predicted that the rays should concentrate in the equatorial plane. However, their spatial distribution is quite uniform, so something should change their trajectories. This is caused by the magnetic field, and Enrico Fermi in his pioneer work estimated its value which is quite close to the modern observations (about 1 microgauus) (Fermi, 1949). A large number of observational proofs were connected with synchrotron emission studies (Ginzburg, 1959). Today most of the observational measurements are based on Farady rotation (Andreasyan & Makarov, 1989, Beck et al., 1996, Manchester, 1972). As for Milky Way, usually pulsars are taken (now there are 10^3 ones (Andreasyan et al., 2020). As for another galaxies, the extragalactic sources are taken to find the magnetic fields (Oppermann et al., 2011).

From the theoretical point of view, the process of the magnetic field generation seems to contain three stages. First of all, initial fields are connected with Biermann battery mechanism (Biermann & Schlüter, 1951). It is connected with fluxes of protons and electrons. They have principally different masses, and interact with the moving particles according to different laws. So there are circular currents which produce vertical magnetic fields (Mikhailov & Andreasyan, 2021).

After that, the field is enlarged by the turbulent dynamo. It is connected with properties of small-scale motions, and it can produce magnetic fields which have the strength of order of microgauss. The problem is that such field is associated with small turbulent cells, and it has random directions (Arshakian et al., 2009).

Then the large-scale dynamo begins its action. The average magnetic field is non-zero because the number of turbulent cells is finite. So, the field can be enlarged by the large-scale dynamo (Arshakian et al., 2009). It is based on two basic effects. Firstly, it is the differential rotation which characterizes non-solid rotation of the galactic disc. This process it connected with transition of the radial component of the field to the angular one. Secondly, the dynamo contains alpha-effect which is connected with helicity of the turbulent motions (curl of the turbulent velocity has a projection on the velocity itself, and if we average it, the corresponding coefficient should be included to the equations). Alpha-effect helps to make radial

*ea.mikhajlov@physics.msu.ru, Corresponding author
†pashentceva.mv17@physics.msu.ru

doi: https://doi.org/10.52526/25792776-23.70.2-282

magnetic field from the angular one. These two effect work jointly and enlarge the solution. However, they should compete with the turbulent diffusivity, which tries to destroy structures of the magnetic field. So the magnetic field generation is connected with the treshold effect, and it is possible only if first two processes are more effective than the turbulent dissipation. Usually it is described by the so-called dynamo number, which includes vertical scaleheight of the disc, angular velocity and typical velocity of the turbulent motions (Beck et al., 1996). If it is larger than some critical value, we can say that the magnetic field in the galaxy can grow, else it decays.

The field growth can be studied using Steenbeck – Krause – Raedler equation (also called mean field dynamo equation) which is three-dimensional (Krause & Raedler, 1980). It is quite difficult both for the analytical and numerical solution, so different approximations are used. The approximations usually take into account symmetry properties of the object, and usually the equations are reduced to a pair of formulaes.

As for the galaxies, usually the thin disc approximation is used. It was developed by Moss (1995), Subramanian & Mestel (1993), and it considered half-thickness of the disc as a small parameter. The field component which is perpendicular to the disc can be neglected, and its partial derivative can be taken from the non-divergence condition. The z-structure of the field is assumed according to the cosine law, so the z-derivatives can be calculated algebraically. Also the coefficients which characterize averaged characteristics of the motion of the medium.

The evolution equations describe the magnetic field growth according to an exponential law (Mikhailov & Pashentseva (Frolova), 2022b). If we assume such law, we can obtain an eigenvalue problem for the magnetic field. As for the thin disc model in the axisymmetric case, the eigenvalues and the eigenfunctions can be found exactly (Mikhailov, 2020). The eigenvalue characterizes the possibility of the magnetic field growth. Also, positive values characterize if the field can principally grow. It is important that the magnetic field growth rate includes the dynamo number.

However, this model is not applicable for discs, where the half-thickness can be comparable with the radius of the disc. The vertical structure can differ from the simple cosine model, and the vertical flows can occur and change the magnetic field. So we should take the models which describe z-dependence in more detail (Mikhailov & Pashentseva (Frolova), 2022a).

As for this case, the eigenvalue problem is much more complicated. It can be solved only approximately using perturbation theory. As for the non-perturbed case we can take the results which have been obtained for thin disc model.

Here we give a review of results connected with the study of the magnetic field in thin and thick galactic discs (Mikhailov & Pashentseva (Frolova), 2022a,b). After that we show the numerical tests of the magnetic field growth for different parameters.

2. Thin disc approximation

In the case of thin disc, we can describe the magnetic field in the equatorial plane using two components depending on distance from the center r: the angular one B_φ and the radial one B_r. We will assume that components of the field are proportional to $\cos\left(\frac{\pi z}{2h}\right)$, where z is the distance from the equatorial plane, and h is the half-thickness of the disc. Using the dimensional variables and measuring the lengths in units of the radius of the galaxy, and times in the units of $\frac{h^2}{\eta}$, we will obtain the following system of equations (Moss 1995; Mikhailov 2020):

$$\frac{\partial B_r}{\partial t} = -R_\alpha B_\varphi - \frac{\pi^2 B_r}{4} + \lambda^2 \left(\frac{\partial^2 B_r}{\partial r^2} + \frac{1}{r}\frac{\partial B_r}{\partial r} - \frac{B}{r^2} + \frac{1}{r^2}\frac{\partial^2 B_r}{\partial \varphi^2}\right);$$

$$\frac{\partial B_\varphi}{\partial t} = -R_\omega B_r - \frac{\pi^2 B_\varphi}{4} + \lambda^2 \left(\frac{\partial^2 B_\varphi}{\partial r^2} + \frac{1}{r}\frac{\partial B_\varphi}{\partial r} - \frac{B_\varphi}{r^2} + \frac{1}{r^2}\frac{\partial^2 B_\varphi}{\partial \varphi^2}\right);$$

with boundary conditions:

$$B_r|_{r=0} = B_r|_{r=1} = B_\varphi|_{r=0} = B_\varphi|_{r=1} = 0.$$

Here R_α characterizes the alpha-effect, R_ω shows differential rotation and $\lambda = \frac{h}{R}$ is the dissipation parameter (Moss 1995).

Taking into account that the magnetic field is proportional to $\exp \gamma t$, we can rewrite the problem in eigenvalue form (Mikhailov 2020):

$$\gamma B_r = -R_\alpha B_\varphi - \frac{\pi^2 B_r}{4} + \lambda^2 \left(\frac{\partial^2 B_r}{\partial r^2} + \frac{1}{r}\frac{\partial B_r}{\partial r} - \frac{B}{r^2} + \frac{1}{r^2}\frac{\partial^2 B_r}{\partial \varphi^2}\right);$$

doi: https://doi.org/10.52526/25792776-23.70.2-282

$$\gamma B_\varphi = -R_\omega B_r - \frac{\pi^2 B_\varphi}{4} + \lambda^2 \left(\frac{\partial^2 B_\varphi}{\partial r^2} + \frac{1}{r}\frac{\partial B_\varphi}{\partial r} - \frac{B_\varphi}{r^2} + \frac{1}{r^2}\frac{\partial^2 B_\varphi}{\partial \varphi^2} \right).$$

The eigenvalue will be:

$$\gamma_n^{\pm} = -\frac{\pi^2}{4} \pm \sqrt{D} - \lambda^2 \mu_{1,n}^2.$$

Corresponding eigenfunctions are (Mikhailov 2020):

$$B_r^+ = \sqrt{R_\alpha} J_1(\mu_{1,n} r);$$

$$B_\varphi^+ = -\sqrt{R_\omega} J_1(\mu_{1,n} r);$$

$$B_r^- = \sqrt{R_\alpha} J_1(\mu_{1,n} r);$$

$$B_\varphi^- = \sqrt{R_\omega} J_1(\mu_{1,n} r).$$

Here J_1 is the Bessel function and $\mu_{1,n}$ is the zero of this function ($J_1(\mu_{1,n}) = 0$). $D = R_\alpha R_\omega$ is the dynamo number. It can be obtained as $D = 9\frac{h^2\Omega^2}{u^2}$ where u is the turbulent velocity.

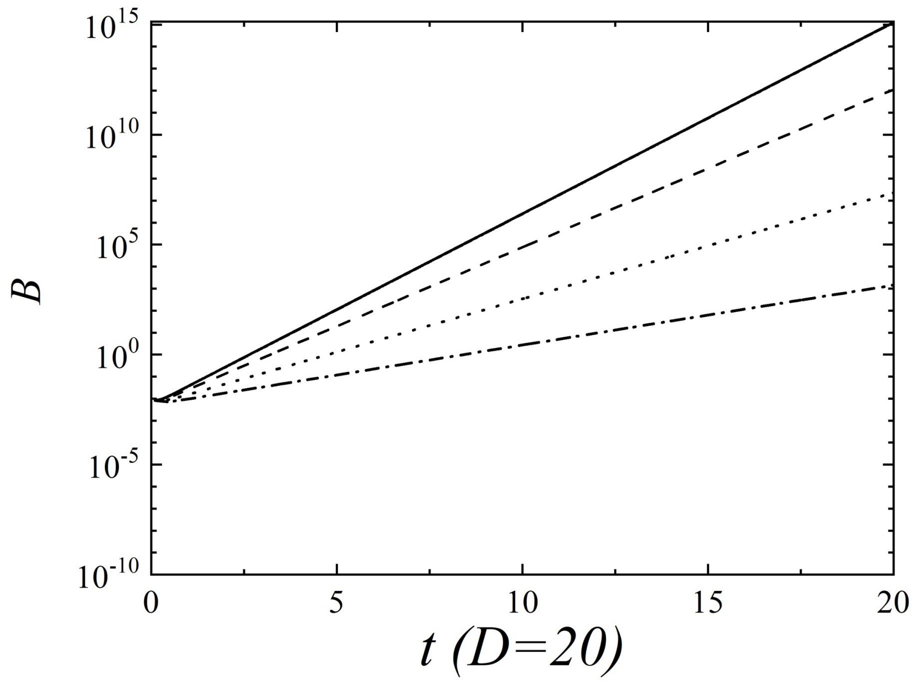

Figure 1. Magnetic field evolution for $D = 20$. Solid line shows $\chi = 1$, dashed line – $\chi = 0.7$, dotted line – $\chi = 0.3$, dot-dashed line – $\chi = 0$,

3. Thick disc model

As for the thick disc, the field will also depend on the distance from the equatorial plane, and the equation will be (Mikhailov & Pashentseva (Frolova), 2022a):

$$\frac{\partial B_r}{\partial t} = -R_\alpha B_\varphi - \chi R_\alpha z \frac{\partial B}{\partial z} + \lambda^2 \left(\frac{\partial^2 B_r}{\partial z^2} + \frac{\partial^2 B_r}{\partial r^2} + \frac{1}{r}\frac{\partial B_r}{\partial r} - \frac{B}{r^2} + \frac{1}{r^2}\frac{\partial^2 B_r}{\partial \varphi^2} \right);$$

$$\frac{\partial B_\varphi}{\partial t} = -R_\omega B_r + \lambda^2 \left(\frac{\partial^2 B_r}{\partial z^2} + \frac{\partial^2 B_\varphi}{\partial r^2} + \frac{1}{r}\frac{\partial B_\varphi}{\partial r} - \frac{B_\varphi}{r^2} + \frac{1}{r^2}\frac{\partial^2 B_\varphi}{\partial \varphi^2} \right);$$

with boundary conditions:

$$B_r|_{r=0} = B_r|_{r=1} = B_\varphi|_{r=0} = B_\varphi|_{r=1} = 0;$$

doi: https://doi.org/10.52526/25792776-23.70.2-282

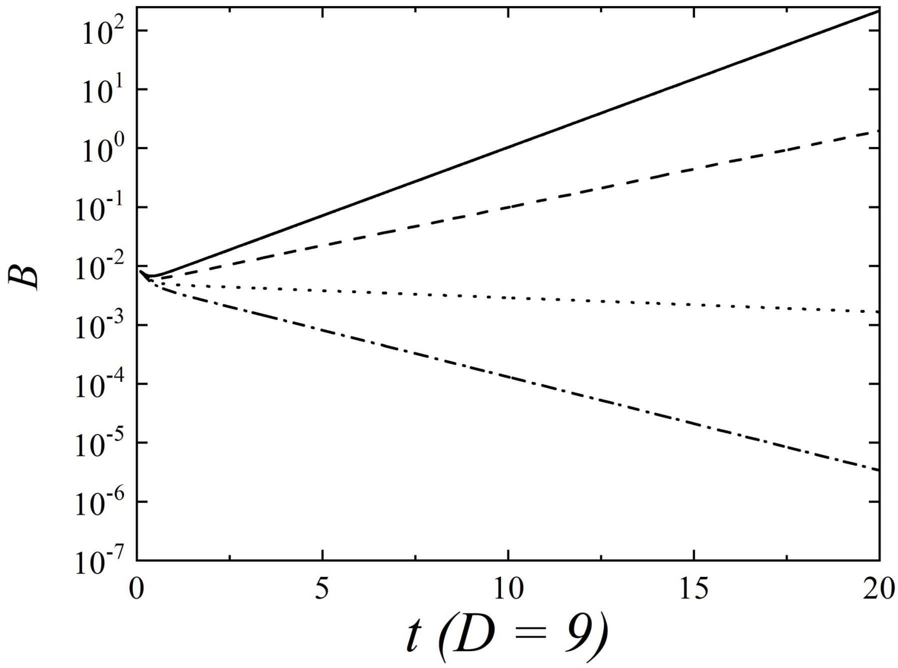

Figure 2. Magnetic field evolution for $D = 9$. Solid line shows $\chi = 1$, dashed line – $\chi = 0.7$, dotted line – $\chi = 0.3$, dot-dashed line – $\chi = 0$,

$$B_r|_{z=-\lambda} = B_r|_{z=\lambda} = B_\varphi|_{z=-\lambda} = B_\varphi|_{z=\lambda} = 0.$$

Here χ characterizes the role of vertical flows. The problem in the eigenvalue form is (Mikhailov & Pashentseva 2023):

$$\gamma B_r = -R_\alpha B_\varphi - \chi R_\alpha z \frac{\partial B}{\partial z} + \lambda^2 \left(\frac{\partial^2 B_r}{\partial z^2} + \frac{\partial^2 B_r}{\partial r^2} + \frac{1}{r}\frac{\partial B_r}{\partial r} - \frac{B}{r^2} + \frac{1}{r^2}\frac{\partial^2 B_r}{\partial \varphi^2} \right);$$

$$\gamma B_\varphi = -R_\omega B_r + \lambda^2 \left(\frac{\partial^2 B_r}{\partial z^2} + \frac{\partial^2 B_\varphi}{\partial r^2} + \frac{1}{r}\frac{\partial B_\varphi}{\partial r} - \frac{B_\varphi}{r^2} + \frac{1}{r^2}\frac{\partial^2 B_\varphi}{\partial \varphi^2} \right);$$

Approximate value of the eigenvalue is (Mikhailov & Pashentseva (Frolova), 2022a):

$$\gamma^{\pm}_{nm} = \pm\sqrt{D} - \frac{\chi}{4}\sqrt{D} - \lambda^2 \mu^2_{1,n} - \frac{\pi m^2}{4}$$

Eigenfunctions are the following:

$$B^+_{r\ nm} = \sqrt{R_\alpha} J_1(\mu_n r) \sin\left(\frac{\pi m(z-\lambda)}{2\lambda} \right);$$

$$B^+_{\varphi\ nm} = -\sqrt{R_\omega} J_1(\mu_n r) \sin\left(\frac{\pi m(z-\lambda)}{2\lambda} \right);$$

$$B^-_{r\ nm} = \sqrt{R_\alpha} J_1(\mu_n r) \sin\left(\frac{\pi m(z-\lambda)}{2\lambda} \right);$$

$$B^-_{\varphi\ nm} = \sqrt{R_\omega} J_1(\mu_n r) \sin\left(\frac{\pi m(z-\lambda)}{2\lambda} \right).$$

doi: https://doi.org/10.52526/25792776-23.70.2-282

4. Magnetic field growth and critical value

As it can be seen, the main effect is connected with the role of the parameter χ. The critical dynamo number will be:

$$D_{cr} = \frac{4}{4-\chi}\left(\frac{\pi^2}{4} + \lambda^2\mu_{1,n}^2\right).$$

The field can grow if $D > D_{cr}$, when $\gamma_{nm}^{\pm} > 0$.

As for the growing magnetic field, we can check the approximate values numerically. The results are shown on figure 1.

5. Conclusion

We have studied the magnetic field growth for different models of the field growth in galactic discs. It has been shown that for thin and thick discs the results are different (Mikhailov & Pashentseva (Frolova), 2022a). We have checked the approximate analytical results using numerical modelling. It is shown that larger values of parameter χ makes the field growth rate larger. Also, the critical dynamo number becomes smaller.

References

Andreasyan R. R., Makarov A. N., 1989, Astrophysics, 30, 101

Andreasyan R. R., Mikhailov E. A., Andreasyan H. R., 2020, Astronomy Reports, 64, 189

Arshakian T. G., Beck R., Krause M., Sokoloff D., 2009, Astron. Astrophys. , 494, 21

Beck R., Brandenburg A., Moss D., Shukurov A., Sokoloff D., 1996, Ann. Rev. Astron. Astrophys. , 34, 155

Biermann L., Schlüter A., 1951, Physical Review, 82, 863

Fermi E., 1949, Physical Review, 75, 1169

Ginzburg V. L., 1959, in Bracewell R. N., ed., Vol. 9, URSI Symp. 1: Paris Symposium on Radio Astronomy. p. 589

Krause F., Raedler K. H., 1980, Mean-field magnetohydrodynamics and dynamo theory

Manchester R. N., 1972, Astrophys. J. , 172, 43

Mikhailov E. A., 2020, Moscow University Physics Bulletin, 75, 420

Mikhailov E. A., Andreasyan R. R., 2021, Astronomy Reports, 65, 715

Mikhailov E. A., Pashentseva (Frolova) M. V., 2022a, Mathematics, 11, 3106

Mikhailov E. A., Pashentseva (Frolova) M. V., 2022b, Moscow University Physics Bulletin, 77, 741

Moss D., 1995, Mon. Not. R. Astron. Soc. , 275, 191

Oppermann N., Junklewitz H., Robbers G., Enßlin T. A., 2011, Astron. Astrophys. , 530, A89

Subramanian K., Mestel L., 1993, Mon. Not. R. Astron. Soc. , 265, 649

doi: https://doi.org/10.52526/25792776-23.70.2-282

Communications of BAO, Vol. 70, Issue 2, 2023, pp. 287-291

Activity phenomena in the baryonic universe as a result of interaction between baryonic objects and the carrier of dark energy

Harutyunian H.A. *

Byurakan Astrophysical Observatory, Armenia

Abstract

Non-stable phenomena are under consideration for rather long time. Mostly two issues seem to be very essential in connection with non-stability, namely, their role in the evolution of cosmic objects and the sources providing energy for non-stability manifestations. We argue here that the energy exchange with the dark energy carrier may be the main mechanism of energy providing. Backed by the contemporary ideas about the dark energy, we accept that this new-found energy homogeneously fills all space at all scales and interacts with cosmic objects belonging to all hierarchical levels. We argue that baryons mass is changeable quantity depending on the environmental physical conditions and therefore it is a subject of evolution as the objects of other hierarchical classes. Moreover, we argue in favour of new paradigm to be used for the further development of cosmology and cosmogony, which is not based on the a priory hypothesis by Kant and Laplace.

Keywords: *dark energy, baryon matter, interaction, energy exchange; activity phenomena, energetic resources.*

1. Introduction

After Ambartsumian moved to Armenia in 1943 and began working at the Byurakan Observatory in 1946, the direction of his scientific research changed noticeably. Instead of theoretical works of the Leningrad period, in which he skillfully applied his extensive mathematical knowledge, in Byurakan research of a more physical nature came to the fore. However, in many papers of that period he again have been using some of the results obtained in the first period of his career. This applies to all scientific directions that he began at the Byurakan Observatory, both the study of stellar associations and flare stars, and work on the activity of galactic nuclei.

It was in Byurakan that he formulated in its final form the concept of the importance of active or unstable phenomena in the process of formation and evolution of cosmic objects. Despite the fact that he had previously studied various types of non-stationary processes, namely the dynamics of planetary nebulae, the disintegration of stellar systems, etc., nevertheless, undoubtedly, he began to understand in more detail the role of these phenomena in cosmogonic processes, when he formulated, the so-called Byurakan concept. In this concept, instability is cosmic objects is considered an internal feature of an object, independent of the physical state of the environment, much like in the case of radioactivity of atomic nuclei.

To be more precise, two main trends can be noted in his papers of the Byurakan period. The first thing we talked about was repeatedly emphasizing the leading role of activity or instability phenomena in the process of formation of cosmic objects. But there was a second innovation, which is the introduction of the idea of the formation of cosmic objects through the decay of denser/superdense matter, as opposed to the dominant Kant-Laplace hypothesis.

At present there is no doubt that any active phenomenon in the baryonic world is associated with the release of a certain amount of excess energy. The issue of where this energy comes from has always been one of the liveliest discussions. Over time, many different mechanisms have been proposed. However, mainstream science eventually settled on the nuclear fusion and accretion mechanisms, second one as the

*hhayk@bao.sci.am

doi: https://doi.org/10.52526/25792776-23.70.2-287

most efficient source of energy on all scales. Despite this, it can now be easily argued that after the discovery of dark energy, the situation has changed dramatically and again there is a need for new mechanisms. Here we consider a completely different mechanism that pumps portions of dark energy into baryonic objects, which sooner or later turns them into an unstable or active stat, since no any object can survive possessing huge internal energy.

2. Activity phenomena and the problem of energetic sources

Unstable phenomena are observed almost everywhere. The variety of active processes is clearly visible at all hierarchical levels of the Universe. Everywhere in our baryonic Universe one can find a huge variety of active processes, ranging from elementary particles and atomic nuclei to clusters of galaxies and the Universe as a whole. Indeed, our baryonic Universe at present is in a active expansion process as well.

The two most important issues to be clarified are the origin of the released during the activity stage energy, and the physical mechanism of moving the object into stage of instability. In fact, these two issues are likely related closely. In general, the issue of energy release is always extremely complex. Various sources of energy generation in cosmic objects have been used, and, as we mentioned in the Introduction, for the most powerful cases the accretion mechanism is chosen always as the most effective one. This approach drastically differs from one suggested by Ambartsumian. However, here is one essential issue, Ambartsumian knew about all proposed energy generation mechanism before suggesting a new one.

It is not difficult to see that the accretion mechanism is nothing more than the conversion of the potential energy of matter obtained as a result of a hypothetical grand explosion into other forms of energy. In other words, in this case, the energy of the initial grandiose explosion, called the big bang, is used as a source of energy released during instability phenomena, while Ambartsumian insisted on a mechanism for producing energy inside the unstable objects. Then a very essential question arises: which mechanism is correct and where could be found fingerprints of the main mechanism?

Ambartsumian proposed the above ideas when he was already a world-famous scientist. The results he obtained in many areas of physics and astrophysics had already changed some prevailing ideas. And this was thanks to his new, mostly alternative thinking and new approach to the long-lasting problems. Of course, nothing ever went without obstacles. Nevertheless, each time he managed to find all the necessary and sufficient arguments to prove that he was right. But the problems associated with the latest research were much more complex. The laws of modern physics deny the possibility of existing very massive clumps of superdense matter.

To clarify this situation, two possibilities should be considered. The first is what the scientific mainstream states continuously. This approach argues that Ambartsumian is wrong in this particular case, and the energy sources are indeed located outside of unstable objects and most likely coincide with sources associated with the accretion of surrounding matter onto objects. The nuclear fusion, merging of cosmic objects are the links of one chain.

The second possible version, on the contrary, proceeds from the fact that the analysis of observational data made by Ambartsumian, coupled with his physical intuition, led to the correct conclusion. But then everything rests on the fact that the physical laws that are used to calculate some massive configurations of gravitational objects do not describe the physical nature of existing patterns quite adequately. Simply, these laws do not back his "strange" suggestion. And therefore, the situation remains approximately the same as it was, say, in the case of the geocentric model of the world - to fit the observational data with the dominating hypothesis one needs to add many new free parameters.

What's the catch? What did Ambartsumian not take into account? Is there today some essential effect which was not taken into account several decades ago and which can change the situation? The only major effect unknown in Ambartsumian epoch, when he was proposing his "strange" ideas, is the introduction of dark energy into usage (Perlmutter et al. (1999), Riess et al. (1998)). Dark energy, which contains (according the accepted estimates) around 70 percents of all mass/energy, was not known and never could be used by him. This is the hugest energy store which never was taken into account, since even a quarter century ago nobody did know about it. But the amazing thing is that even now when the physical picture of dark energy is more or less known and estimates of its amount exist, nobody considers it as a real source of energy which can be transferred to the baryonic objects.

Let's look at this situation in more detail. Such consideration should begin from the very beginning of the discovery of this new type of energy. Indeed, it was discovered (presumed) when the acceleration of the

doi: https://doi.org/10.52526/25792776-23.70.2-287

expansion of the baryonic Universe was discovered, while the scientific community was trying to estimate the expected (as a consequence of the simple Big Bang model) deceleration of the expansion of the Universe. The argument in favour of attracting an unknown type of energy is very transparent and justified, since in order to accelerate galaxies, a certain amount of energy should be transferred to them. This means that the very discovery of dark energy already implies its injection into the ordinary baryonic matter. Therefore, no any doubt may be about the intensive interaction between the carrier of dark energy, whatever it is, and baryonic objects.

So, first conclusion that we arrive at using only observational data states that the carrier of dark energy, whatever it appears to be, certainly interacts with the baryonic matter. This unknown carrier of energy, interacting with the baryonic objects, possesses at least 70 percents of all mass/energy, while all our baryonic universe contains less than 5 percents. In this case, a not very strange question arises: could dark energy serve as a storehouse of energy resources for all the unstable phenomena that we observe everywhere? After all, the energy required for all observed instability phenomena is only a tiny fraction of the dark energy reserves.

For further analysis of the physical picture of what is happening, we will proceed from the following issues. The interaction between different systems takes place according to the known laws of thermodynamics. Then one can apply the second law of thermodynamics, which determines the direction of energy flow when substances with different energies interact. It states that energy flows from a system with a higher energy level to another with less energy.

On the other hand, it is known that all baryonic objects and their systems possess of negative energy, which means that their existence is provided namely due to the lack of the energy necessary for their disintegration. Therefore, there is no doubt that as a result of interaction between the baryonic world and the carrier of dark energy baryonic objects constantly gain portions of energy. Moreover, if the contemporary idea that dark energy homogeneously fills all spatial volumes is correct, then energy accumulation cosmic objects goes on at all hierarchical levels of baryonic universe.

Thus, the observational facts and known physical laws do not deny the possibility of dark energy transfer to the baryonic objects. This is very essential issue in searching of an energy source for the various instability phenomena, since this mechanism of energy transfer and accumulation has a universal nature and could be applied for all cosmic objects at all hierarchical levels.

3. The level of atomic nuclei and elementary particles

It is known that atomic nuclei exist as an integral objects of our world solely due to their unique feature - the mass defect. This is the lack of mass in a nucleus compared to the same number of protons and neutrons in a free state, and evidently this is one of the most important properties of baryon matter, which is observed only in the microcosm. One might call it the universal mechanism of conversing the mass into energy and vise versa. The second manifestation of this property is that the mass defect calculated for one baryon changes when we consider different atomic nuclei. It is not a trivial issue even if we have accepted the existence of such a feature as mass defect. Its real meaning is much dipper. This means that baryons can have different masses depending on the physical conditions under which they are found, they can fit to the physical conditions if they change under various reasons.

The energy equivalent to the mass defect is known as the binding energy of the nucleus. It is the amount of energy, which can split nucleus into individual baryons, if somehow is injected into the nucleus and absorbed by it completely. So, one of natural ways of energy injection can serve the interaction mechanism between the atomic nuclei and the dark energy carrier. When interacting with a carrier of dark energy, some tiny amount of this energy is constantly injected into the nucleus, as a result of which the nuclear binding energy and the nuclear mass defect very slowly decrease. We mentioned previously that this process inevitably destabilizes the atomic nuclei, since gradually grows its mass and decreases the keeping its integrity binding energy. If we accept the fact of the existence of dark energy, which can partially be transferred to baryon objects, then it inevitably indicates a secular destabilization of all objects, including atomic nuclei and baryons themselves, changing the entire physical picture that we knew.

We are accustomed to thinking that atomic nuclei, heavier than hydrogen and helium, are formed in the depths of stars due to nuclear fusion (the nuclear analogue of merging and accretion). It is also well known that, for energy reasons, such reactions are possible only up to the iron nucleus. After iron, the specific binding energy decreases, and the formation of heavier nuclei in the same way becomes energetically

doi: https://doi.org/10.52526/25792776-23.70.2-287

unfavorable. The existence of heavy radioactive nuclei seems even more strange if they were also formed by an ingenious way of capturing neutrons. Nature would hardly go to great lengths to create nuclei that are destined to decay one way or another. In the paradigm under consideration, all processes go in one direction - gradual destabilization, and radioactive nuclei are those nuclei that have already moved from the rank of stable to the rank of unstable.

So, the final effect of gradual destabilization of the nucleus may be the transition of this stable nucleus to the radioactive category. Radioactivity is actually some form of activity where an atomic nucleus disintegrates or releases a particle/energy due to excess internal energy. Physicists have always known this. Here we only add our vision of where this excess energy comes from and believe that this is the result of the interaction of atomic nuclei with the carrier of dark energy.

In any large cosmic object (star, galactic core), consisting of a huge number of atoms, all atomic nuclei are in one way or another subject to the changes described above. At any given time, some portion of atomic nuclei is radioactive and releases absorbed dark energy in the form of both kinetic and radiative energy. Moreover, this process is more intense the deeper we look, since, as we have noticed above, multi-baryon nuclei should be preserved in deeper layers where the physical conditions are still favourable for their stable existence.

4. Systems of cosmic objects

Currently, the mainstream of cosmology and cosmogony continues to adhere to the Kant-Laplace hypothesis about the formation of cosmic objects as a result of gravitational compression of rarefied matter. Since it is believed that the initially contracting clouds had a negative total energy, the idea that the final result of such compression could be an expanding system is not allowed. Both the solar system and galaxy clusters are good examples. That is why in the solar system, for example, they try to explain clearly observed expansions, say, by tidal effects and the transfer of angular momentum of the central object to the outgoing one. And to compensate for the very large dispersion of galaxies in a cluster, the concept of dark mass was introduced.

It seems very strange that even after the discovery of dark energy, the mainstream continues to obey the dictates of the above-mentioned hypothesis. Unlike dark mass, introduced to reconcile observational data with an a priori accepted hypothesis, the introduction of dark energy is a transparent statement of observational data. Therefore, there is no doubt that if there is a need to choose between these two dark substances, then the second has a clear advantage.

If our reasoning about the interaction of baryonic matter with the dark energy carrier and the transfer of energy to baryonic objects is correct, we will inevitably come to the conclusion that the total energy of all cosmic objects and their systems gradually increases over time. In this case, it doesn't even matter what the rate of energy transfer is. The important thing is that energy is transferred in one direction - from the dark energy carrier to baryon objects. Since energy has the property of being cumulative, over time it accumulates in these objects and their systems. This means that there is a change in the energy balance, and sooner or later they will need to release the accumulated energy. This occurs through the expansion of any systems of gravitational objects, the release of energy in the form of clumps of matter or excess radiation. It is these phenomena that we call manifestations of activity or instability.

Moreover, this is an evolutionary stage of any object, and, apparently, it should have recurrent behavior. Indeed, if an object manages to accumulate so much energy over a certain time that it already threatens its existence, then it should already release this energy. It is then that the activity phenomena discussed here occur. Liberation from accumulated energy is a more fleeting process than its accumulation. As soon as the amount of accumulated energy ceases to be a threat to the integral existence of a given object, the emission processes stop. However, the accumulation process continues, and after some time the activity stage may repeat.

We would like to recall some well-known examples of unstable phenomena. Let us first remember the active volcanoes on Earth. They fade away for a while, which can last for decades, centuries and even millennia, and wake up again spewing out enormous amounts of energy. Flare stars exhibit flares that are randomly distributed in time and interspersed with periods of relative quiet. Repeat novae are good examples of this series. It is also interesting that the amplitude of the latter increases the longer their resting period lasts. In all these cases, periods of rest can be considered the necessary time for energy accumulation.

doi: https://doi.org/10.52526/25792776-23.70.2-287

5. Concluding remarks.

Obviously, in the process of interaction between baryonic matter and the dark energy carrier, the latter transfers some of its energy to baryonic objects. We already have mentioned that originally the revealing of dark energy happened exceptionally thanks to this energy transfer and acceleration of the Universe expansion. On the other hand, it is this interaction that may be the desired mechanism for providing energy to all the diversity of active or unstable phenomena. It is also clear that if this mechanism is actually implemented, then the amount of energy released during active processes can be considered insignificant compared to the total supply of dark energy.

Within the framework of the considered paradigm, most known instability phenomena can be easily explained using only this energy conversion mechanism. If this mechanism is applied, then the inconsistency of the ideas of a black hole and dark matter introduced into science becomes obvious. These hypothetical object and substance, in our opinion, entered science and settled there only because some central scenarios of cosmology and cosmogony built at once on base of some hypotheses, actually had nothing to do with reality. This is reminiscent of the use of the geocentric system in the Middle Ages.

This approach and the mechanism of energy transfer to baryon objects based on it seem more transparent and realistic. You can even think carefully and implement a method for solving the inverse problem, in which the amount of energy released during unstable phenomena is used as input data to determine the rate of energy transfer to various objects. It is clear that this is by no means a trivial task. However, on the other hand, it does not seem completely hopeless and can lead to interesting results.

References

Perlmutter S., et al., 1999, Astrophys. J. , 517, 565

Riess A. G., et al., 1998, Astron. J. , 116, 1009

doi: https://doi.org/10.52526/25792776-23.70.2-287

Communications of BAO, Vol. 70, Issue 2, 2023, pp. 292-296

The role of environment on the formation of different FR type extragalactic radio sources

R. R. Andreasyan *[1], G. M. Paronyan†[1], and A. G. Sukiasyan‡[1]

[1]NAS RA V. Ambartsumian Byurakan Astrophysical Observatory (BAO)

Abstract

We study the environment of nearby extragalactic radio sources of different morphological type from our sample. We chose 30 3C radio galaxies of different FR class for which we have several observational dates on wavelength from radio to X ray. For the study we select the regions with radius of 500 pc around of the parent galaxy of radio sources. We bring the optical maps of these regions that are overlaid on the radio maps and maps in all available wavelength. The preliminary review show that there are some differences in the neighboring regions around radio galaxies of different FR classes.

Keywords: *radio sources, FR, 3C radio galaxies*

1. Introduction.

The study of active galaxies is one of traditional direction of Byurakan observatory. In this paper we present some of our results in this direction, the study of different physical and morphological properties of extragalactic radio sources.

Extragalactic radio sources mainly are divided on two groups: compact and extended radio sources. One of the well-known classifications of extended radio galaxies is the (FR) classification of Fanaroff and Riley (Fanaroff & Riley, 1974), which is based on the radio brightness distribution over the radio image. Radio galaxies with relatively lower radio luminosity, in which the radio brightness decreases from the center to the edges, are classified as I class radio galaxies (FRI), and radio galaxies with higher radio luminosity, in which the radio brightness increases from the center to the edges of the II class (FR II). Figure 1 shows examples of extragalactic radio sources of FRI and FRII types.

At present, the Fanaroff-Riley dichotomy has been studied quite well and many other differences in physical and morphological features have been found for different classes of radio galaxies. Partly in our early studies a correlation was found between the optical and radio axes of nearby FRII radio galaxies and no correlation for FRI radio galaxies (Andreasyan & Sol, 1999) (Fig.2 left); a correlation of the average radio polarization angles with the radio axes for nearby FRII radio galaxies and no correlation for FRI radio galaxies (Andreasyan et al., 2002) (Fig.2 right); a correlation of the ellipticity of parent optical galaxies associated with radio galaxies of different classes (Andreasyan & Sol, 2000) (Fig 3), etc. For the study we use data of nearby extragalactic radio sources from our samples (Andreasyan & Abrahamyan, 2021). In these samples we have data for 267 nearby radio galaxies identified with elliptical galaxies brighter than 18^{th} magnitude (sample1) and 280 extragalactic radio sources with known position angles between the integrated intrinsic radio polarization and radio axes (sample 2). For these radio galaxies we bring the following data: Radio Sours Name, oPA - the position angle of the major axis of optical galaxy, rPA - the position angle of radio axis, dPA - the relative position angle between optical and radio axes, E - the ellipticity of the optical galaxy identified with radio sources, FR - the Fanaroff Riley class, M - the optical magnitude, SI - the spectral index, z - the redshift, logP - the radio luminosity, K - the ratio of major to minor axis of radio image, Ref. for the radio maps and FR classes.

Here are some results from our above-mentioned papers.

*randreasyan@gmail.com, Corresponding author
†paronyan_gurgen@yahoo.com
‡andranik.suqiasyan.1995@mail.ru

doi: https://doi.org/10.52526/25792776-23.70.2-292

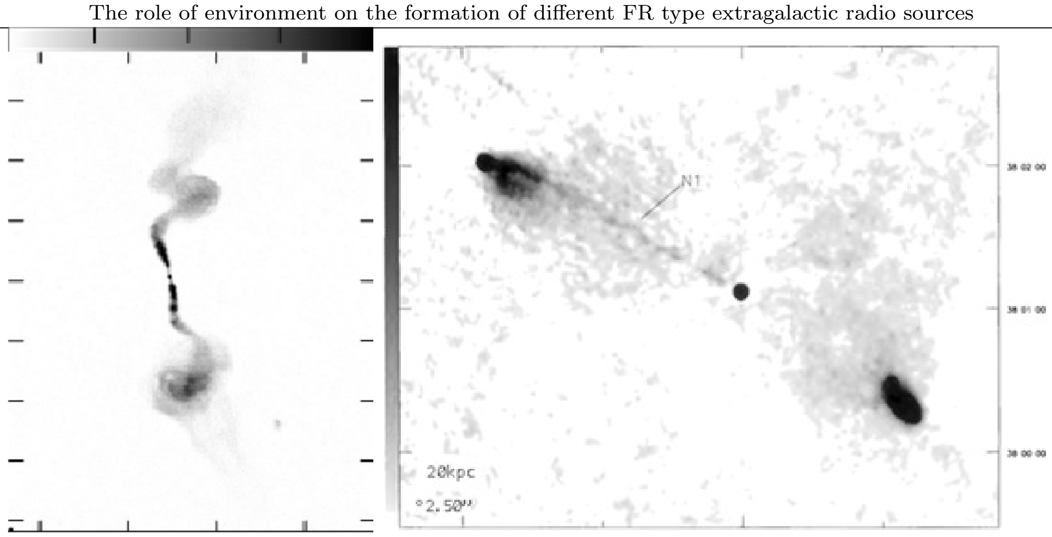

Figure 1. Extragalactic radio sources of FRI type 3C449 (left) and FRII type 3C111 (right).

.

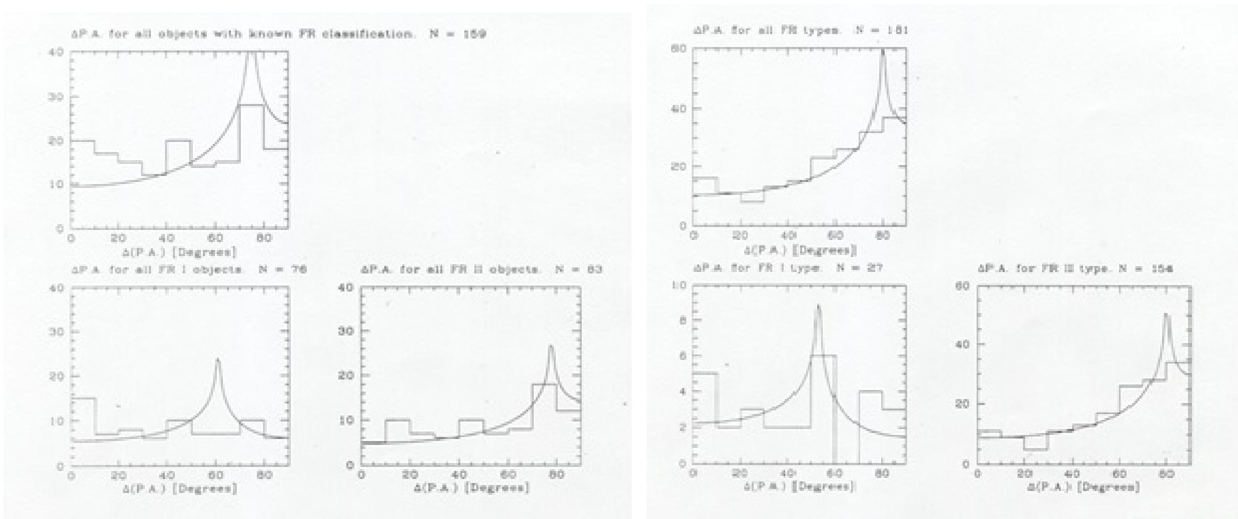

Figure 2. The distribution of angles between the optical and radio axes (left) and angles between average radio polarization and radio axes (right).

.

The ellipticity of parent optical galaxies of FRII type radio galaxies is larger than the ellipticity of parent optical galaxies of FRI type objects.

These large differences in morphology and physical properties of different classes of extragalactic radio sources can be due to differences in parent optical galaxies or in differences of the extragalactic medium around the radio source in which the radio source is expanding.

In order to reveal the influence of the environment on extragalactic radio source, we study the close proximity (regions with radius of 500 pc around of the central radio galaxies) of the well-known Giant radio sources 3C31, 3C449, NGC315, NGC6251 from our sample of about 30 nearby 3C radio galaxies of different FR types chosen from (Andreasyan & Abrahamyan, 2021).

2. The study of the neighborhood of radio galaxies.

For the study we construct the maps of optical galaxies that are overlaid on the radio map of 3C radio source. We use also the maps of these regions in all available wavelength. Here we present more detail analyses and new results for the radio galaxy of FRI type 3C31.

The 3C 31 class FRI radio source has been identified with the NGC 383 parent galaxy, which is the central object of the group of galaxies, which in turn is a member of the Perseus-Pisces supercluster (Sakai et al., 1994) and has been studied quite well. Numerous results and useful data have now been obtained

doi: https://doi.org/10.52526/25792776-23.70.2-292

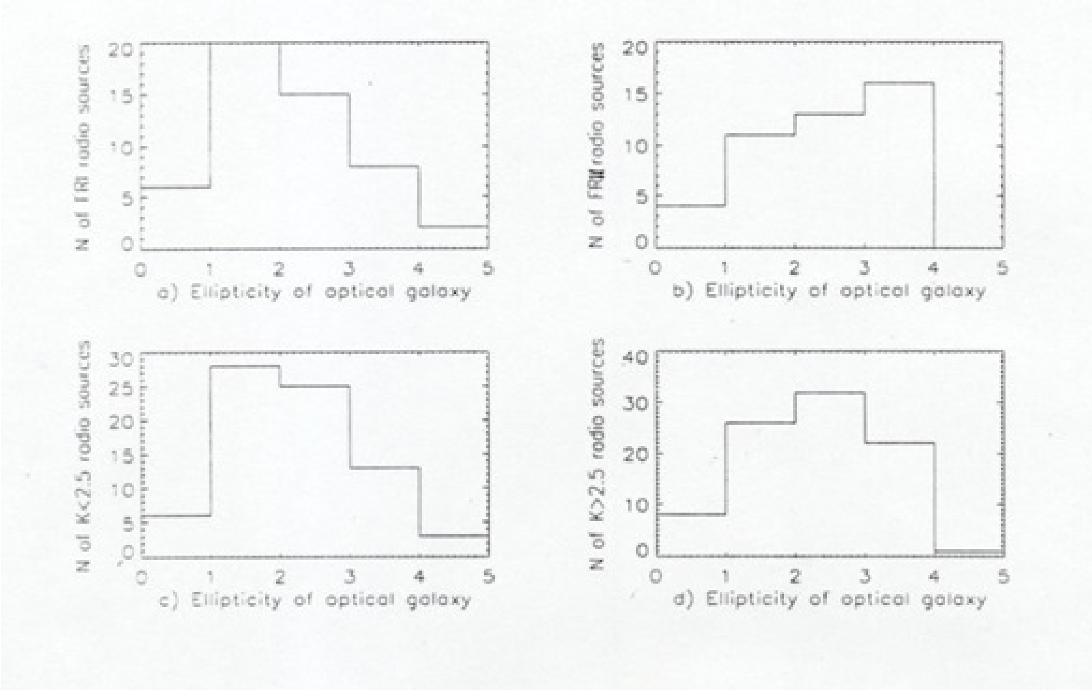

Figure 3. The ellipticity of optical parent galaxies for different FR types and for different classes of K classification.

.

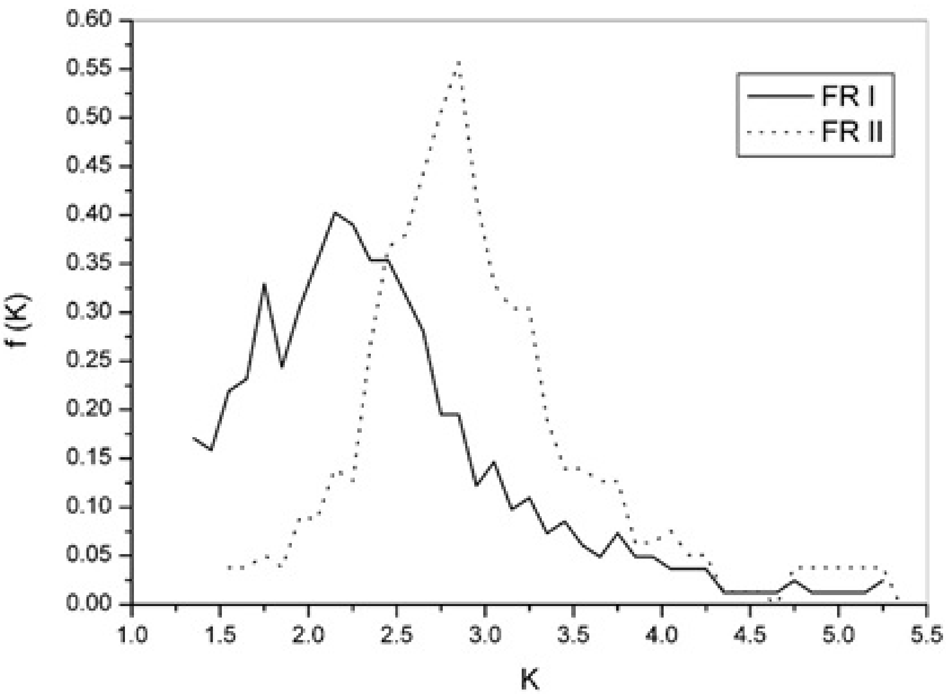

Figure 4. The distribution function from elongation parameter K for FRI and FRII class radio galaxies.

.

doi: https://doi.org/10.52526/25792776-23.70.2-292

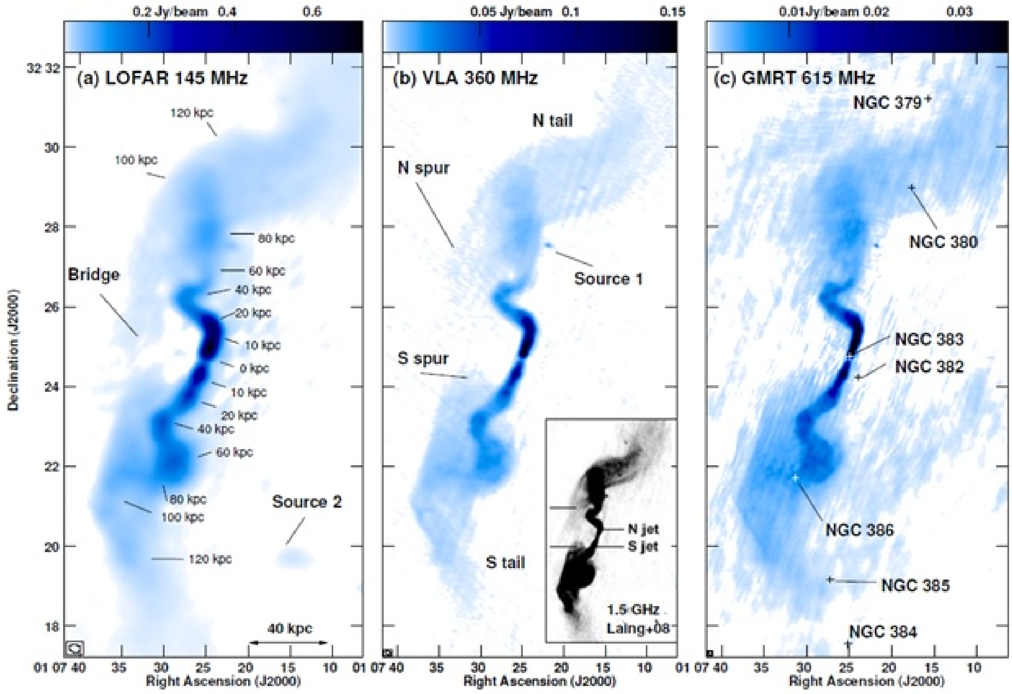

Figure 5. Radio image maps of the FRI class radio galaxy 3C 31 at three different frequencies (Heesen et al., 2018)

.

for these objects (Croston & Hardcastle, 2014, Hardcastle et al., 2002, Laing & Bridle, 2002, Martel et al., 1999, Parma et al., 1999, Strom et al., 1983). Of these, here we highlight some of the data of interest to us, which can be used in the present work. On figure 5 we bring the radio map of 3C31 at frequency of 1400 MHz (corresponding to FIRST observations) with the overlaid optical region with the central galaxy NGC 383. As it is seen a group of galaxies in the form of a chain has the direction of the radio image. It is more obvious on the figure 6 of same region from the paper (Heesen et al., 2018) at different frequencies, 145, 360 and 615 MHz corresponding to LOFAR, VLA and GMRT observations, respectively.

From figures we see that the elliptical galaxies NGC 380 and NGC 386 are located respectively in the northern and southern parts of the 3C31 radio image. These galaxies, together with the central SA0 type galaxy of the group NGC 383 are on the same line, the direction of which coincides with the direction of central part of radio image with great accuracy.

Radio jet simulations (Laing & Bridle, 2002) have shown that the direction of the central jet is approximately 52^o with the line of sight. Moreover, the northern part of the jet approaches the observer, while the southern part moves away. On the other hand, the analysis of the redshifts of the mentioned optical galaxies shows that the relative line of sight velocity of the northern galaxy NGC 380 compared to the central galaxy NGC 383 is directed towards the observer as for the northern jet, and the relative velocity of the southern galaxy NGC 386 is directed away from the observer as for the southern jet. This probably suggests that the direction of the spatial velocities of these galaxies also coincides with the direction of the velocities of the radio jets and, therefore, galaxies NGC 380 and NGC 386 move away from the central galaxy NGC 383 in opposite directions coincide with the direction of the radio jets.

We calculated the time of removal of galaxies from the central galaxy. The calculation results are shown in Table 1. Δz is difference of redshifts from the central galaxy NGC 383, ΔV and ΔV_0 – the relative line of sight and spatial velocities respectively, d and d_o -the projected on the sky and spatial distances, T- the time of removal of galaxies.

Table 1. Results of Calculations.

Galaxies	Δz	ΔV	ΔV_0	**d**	d_0	**T**
NGC380	-0.00224	-672	1092	97.07	123.2	110
NGC386	+0.00153	+459	745.5	70.64	89.64	118

The table shows that the galaxies NGC 380 and NGC 386 were near the galaxy NGC 383 about 110

doi: https://doi.org/10.52526/25792776-23.70.2-292

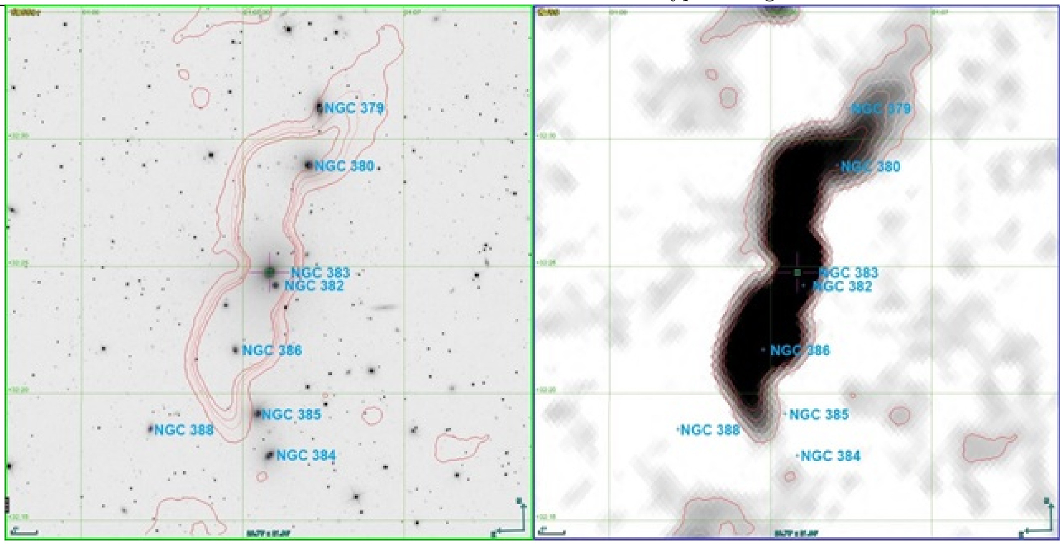

Figure 6. The region of a group of galaxies with the central object NGC 383 and radio source 3C31 of the FRI class at a frequency of 1400 MHz.

.

million years ago. A very close passage of these three galaxies then probably occurred, after which the recession of the galaxies NGC 380 and NGC 386 from the more massive central galaxy NGC383 began. A natural question arises whether such a close passage can be the cause (trigger) of the beginning of radioactivity of the central galaxy. As a reliable argument for such assumption can be the result of the modeling of the spectral characteristics of the radio emission of the central part of the radio galaxy 3C31 that gives an estimate of the age of the central jet of about 100 million years (Heesen et al., 2018).

References

Andreasyan R. R., Abrahamyan H. V., 2021, Communications of the Byurakan Astrophysical Observatory, 68, 75

Andreasyan R. R., Sol H., 1999, Astrophysics, 42, 275

Andreasyan R. R., Sol H., 2000, Astrophysics, 43, 413

Andreasyan R. R., Appl S., Sol H., 2002, Astrophysics, 45, 198

Croston J. H., Hardcastle M. J., 2014, Mon. Not. R. Astron. Soc. , 438, 3310

Fanaroff B. L., Riley J. M., 1974, Mon. Not. R. Astron. Soc. , 167, 31P

Hardcastle M. J., Worrall D. M., Birkinshaw M., Laing R. A., Bridle A. H., 2002, Mon. Not. R. Astron. Soc. , 334, 182

Heesen V., et al., 2018, Mon. Not. R. Astron. Soc. , 474, 5049

Laing R. A., Bridle A. H., 2002, Mon. Not. R. Astron. Soc. , 336, 328

Martel A. R., et al., 1999, Astrophys. J. Suppl. Ser. , 122, 81

Parma P., Murgia M., Morganti R., Capetti A., de Ruiter H. R., Fanti R., 1999, Astron. Astrophys. , 344, 7

Sakai S., Giovanelli R., Wegner G., 1994, Astron. J. , 108, 33

Strom R. G., Fanti R., Parma P., Ekers R. D., 1983, Astron. Astrophys. , 122, 305

doi: https://doi.org/10.52526/25792776-23.70.2-292

Infrared surveys to search for high proper motion stars

E.D. Malik*[1,2] and O.Yu. Malkov†[2]

[1]Physics Faculty, Moscow State University, Moscow, Russia
[2]Institute of Astronomy RAS, Moscow, Russia

Abstract

There are restrictions on the nature and characteristics of nearby brown dwarfs (including hypothetical component of the Sun), imposed by the current results of the work of the Gaia space observatory. In particular, even close brown dwarfs of spectral type Y3 and colder will go unnoticed by the Gaia observatory, although they may well be already included in infrared survey catalogues. Here we present information on modern infrared surveys, which can be used for a search for such objects.

Keywords: *brown dwarfs, infrared photometric surveys*

1. Introduction

Results of the work of the Gaia space observatory (Gaia Collaboration et al., 2016, 2022) impose certain restrictions on the nature and location of nearby brown dwarfs (including hypothetical component of the Sun). The fact that the companion is not registered by the observatory leaves the following marginal possibilities: a cool brown dwarf (Y3 and later) in an orbit inside the Oort cloud, or an L/T brown dwarf in a higher orbit (from 10^5 AU). At the same time, the companion is quite likely cataloged in the 2MASS, WISE or other infrared surveys. In particular, it was shown (Malkov, 2023) that such an object should demonstrate a noticeable proper motion – units or tens of arc seconds per year. In the next Section we present information on modern infrared surveys, which can be used for a search for such objects. The last Section contains conclusions.

2. Infrared Missions

2.1. Two Micron All Sky Survey

2MASS (Cutri & et al, 2003) was held between 1997 - 2001 using two telescopes in order to cover both Northern and Southern hemispheres, resulting in the All-Sky Data Release. It's products include a Point Source Catalog, containing positions and photometry for more then 4.7 billion objects. The sky was observed in bands J (1.24 μm), H (1.66 μm), and K_S (2.16 μm) with limits of 15.8^m, 15.1^m, 14.3^m respectively.

2.2. Wide-field Infrared Survey Explorer

WISE (Cutri & et al, 2014) is an imaging survey in the W1 (3.4 μm), W2 (4.6 μm), W3 (12 μm) and W4 (22 μm) mid-infrared bands. The WISE All-Sky Data Release includes data taken in 2010 and covers >99 percent of the sky with total of ~0.56 billion sources detected. Limiting magnitudes are W1: 17.30^m, W2: 15.84^m, W3: 11.59^m, W4: 8.0^m.

2.3. Deep Near-Infrared Survey

DENIS project (DENIS Consortium, 2005) surveyed all-southern sky in three wavelength bands: Gunn-i (0.82 μm), J (1.25 μm), and K_S (2.15 μm) with limiting magnitudes 18.5^m, 16.5^m and 14.0^m, respectively. Observations were carried out between 1995 and 2001 and the third release of DENIS data consists of 355,220,325 point sources.

*malik.ed20@physics.msu.ru
†malkov@inasan.ru, Corresponding author

doi: https://doi.org/10.52526/25792776-23.70.2-297

2.4. Infrared Astronomical Satellite mission

IRAS (Neugebauer et al., 1984) was launched in space in 1983 and was the pioneering mission produced the first maps of the entire sky (95 percent) at four infrared wavelengths: 12 μm, 25 μm, 60 μm and 100 μm. IRAS Catalog of Point Sources contains about 250000 well-confirmed objects.

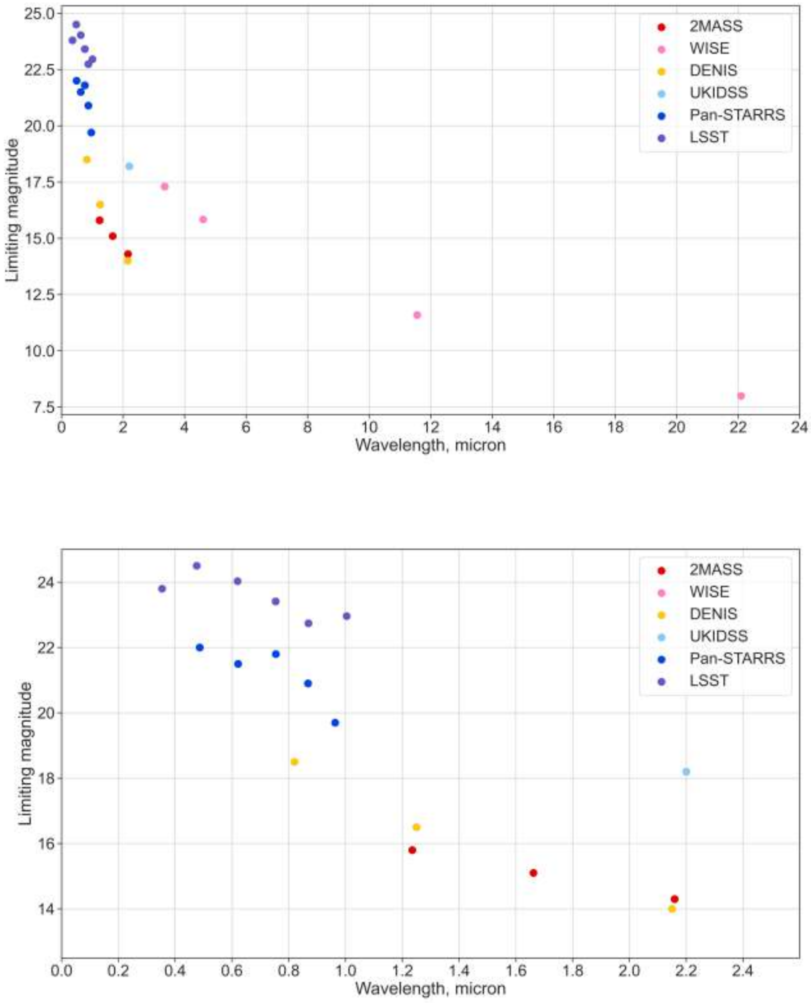

Figure 1. Limiting magnitudes for surveys' bandpasses. Every dot responds to a center of band in micrometers. The bottom picture highlights the left part of the top figure.

2.5. UKIRT Infrared Deep Sky Survey

UKIDSS (Lawrence & et al, 2007) is a set of surveys conducted on the United Kingdom Infra-red Telescope (UKIRT) which began in 2005. Covering 7500 square degrees of the Northern sky, UKIDSS Release 9 contains around 140 million sources. Survey utilizes four bands: Y (1.0 μm) J (1.2 μm) H (1.6 μm) and K (2.2 μm) with limit of K = 18.4^m.

2.6. The Panoramic Survey Telescope & Rapid Response System

Pan-STARRS (Chambers & et al, 2016) is a system for wide-field sky imaging in five bands: g (0.4866 μm), r (0.6215 μm), i (0.7545 μm), z (0.8679 μm), y (0.9633 μm) with depths of 23.3, 23.2, 23.1, 22.3 and 21.3 respectively. The Pan-STARRS release 1 (PS1) covers 30000 square degrees, containing more than 1.9 billion sources.

doi: https://doi.org/10.52526/25792776-23.70.2-297

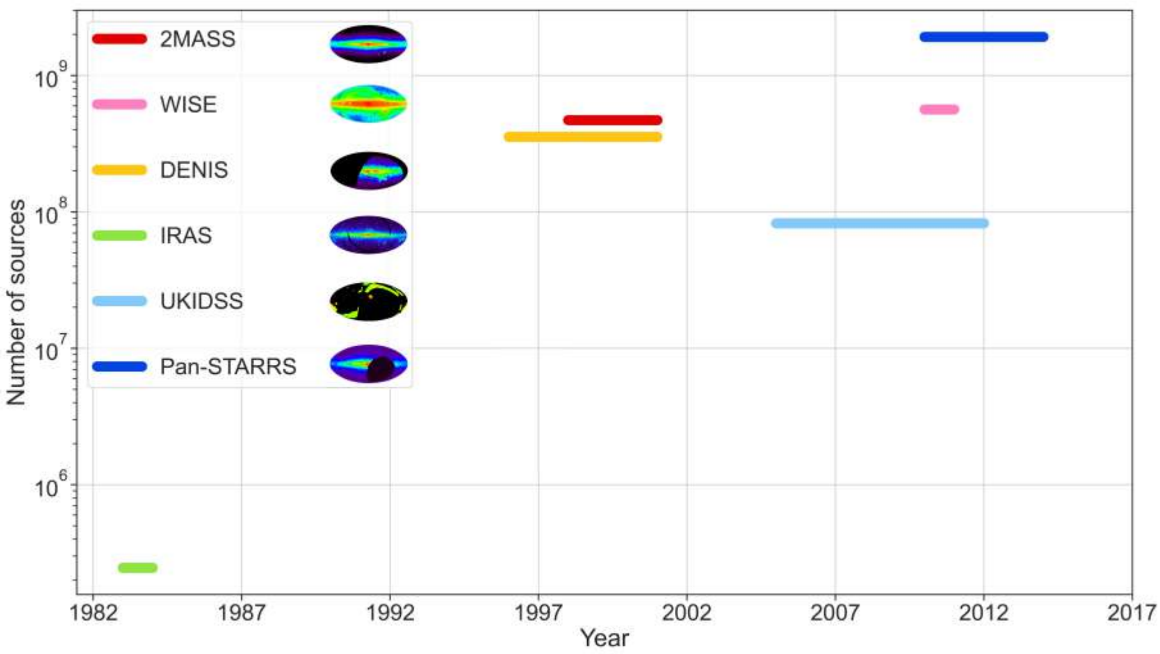

Figure 2. Number of detected sources for completed missions.

2.7. Large Synoptic Survey Telescope

LSST (Ivezić et al., 2019) is upcoming survey. It will observe 18000 square degrees area, resulting in about 32 trillion observations of 20 billion galaxies and stars. Observations will be carried out in six bands: u (0.3539 μm), g (0.47595 μm), r (0.6197 μm), i (0.75385 μm), z (0.86925 μm), y (1.00375 μm). Limiting magnitudes are u: 23.8^m, g: 24.5^m, r: 24.03^m, i: 23.41^m, z: 22.74^m, y: 22.96^m.

doi: https://doi.org/10.52526/25792776-23.70.2-297

doi: https://doi.org/10.52526/25792776-23.70.2-297

Table 1. Surveys description

Survey	Number of sources	Sky coverage	Epoch
			years
2MASS	470992970	95%	1998-2001
WISE	563921584	>99%	2010
DENIS	355220325	~16700 sq. degs	1996-2001
IRAS	245889	>96%	1983
UKIDSS	82655526	4000 sq. degs	2005-2012
Pan-STARRS	1919106885	30000 sq. degs	2010-2014
LSST	-	18000 sq. degs	2022-2032

Table 2. Surveys description: photometry

Survey	Passbands wavelengths	Limit magnitude
	μm	mag
2MASS	J: 1.235, H: 1.662, K_s: 2.159	J: 15.8, H: 15.1, K_s: 14.3
WISE	W1: 3.35, W2: 4.60, W3: 11.56, W4: 22.09	W1: 17.30, W2: 15.84, W3: 11.59, W4: 8.0
DENIS	Gunn-i: 0.82, J: 1.25, K_s: 2.15	Gunn-i: 18.5, J: 16.5, K_s: 14.0
IRAS	12, 25, 60, 100	
UKIDSS	Y: 1.02, J: 1.25, H: 1.63, K: 2.20, H2: 2.12	K: 18.2
Pan-STARRS	g: 0.4866, r: 0.6215, i: 0.7545, z: 0.8679, y: 0.9633	g: 22.0, r: 21.8, i: 21.5, z: 20.9, y: 19.7
LSST	u: 0.3539, g: 0.47595, r: 0.6197, i: 0.75385, z: 0.86925, y: 1.00375	u: 23.8, g: 24.5, r: 24.03, i: 23.41, z: 22.74, y: 22.96

3. Conclusion

This paper presents information on modern photometric infrared surveys (2MASS, WISE, DENIS, IRAS, UKIDSS, Pan-STARRS, LSST) that can be used to find high proper motion stars. Here we give information about the number of objects in the surveys, sky coverage, epoch of observations and photometric bands.

Acknowledgements

We would like to thank Dana Kovaleva whose constructive comments greatly helped us to improve the paper. This research has made use of NASA's Astrophysics Data System, and use of the VizieR catalogue access tool, CDS, Strasbourg, France.

References

Chambers K. C., et al 2016, arXiv e-prints,

Cutri R. M., et al 2003, VizieR Online Data Catalog, 2246

Cutri R. M., et al 2014, VizieR Online Data Catalog, 2328

DENIS Consortium 2005, VizieR Online Data Catalog, 1

Gaia Collaboration et al., 2016, Astron. Astrophys. , 595, A1

Gaia Collaboration et al., 2022, arXiv e-prints, p. arXiv:2208.00211

Ivezić Ž., et al., 2019, Astrophys. J. , 873, 111

Lawrence A., et al 2007, Mon. Not. R. Astron. Soc. , 379, 1599

Malkov O. Y., 2023, Astronomy Reports, 67, 288

Neugebauer G., et al., 1984, Astrophys. J. Lett. , 278, L1

doi: https://doi.org/10.52526/25792776-23.70.2-297

Terrestrial complex for receiving information from small spacecrafts

S. B. Makarov *[1], S. V. Zavjalov[1], S. V. Volvenko[1], I. Lavrenyuk[1], M. Ya. Vinnichenko[1], A. K. Aharonyan[2], and V. H. Avetisyan[2]

[1]Peter the Great St. Petersburg Polytechnic University, St. Petersburg, Russia
[2]Russian-Armenian University, Erevan, Armenia

Abstract

The work is devoted to the development of a terrestrial complex for receive and process information from small spacescrafts. The main requirement for these stations is their simplicity and maximum availability both in terms of cost and operating capabilities. Such stations provide a two-way exchange of information with spacecrafts in the frequency range 435-438 MHz, receive and process data transmitted in the VHF band by amateur and student satellites, and receive communications from the international space station crew and radio amateurs on Earth.

Keywords: *CubeSat, AIS, space receiver, marine communication systems*

1. Introduction

The Russian project "Space-Pi" is being implemented from 2022 to 2025. This project is designed to attract schoolchildren and student from universities to scientific and technical activities and popularize space research and technology among them. It is also acceptable to use software and hardware sets in the educational environment (cubesat designers, virtual twins of satellites and a test base) for work in schools, universities and development centers.

The scientific component of the project is to obtain new knowledge and its practical application in the creation of cubesats and payloads for them. It is supposed to test scientific hypotheses, develop directions for data processing due to cheaper methods of obtaining data collected by grouping cubesats, as well as increasing the reliability and miniaturization of their on-board systems.

An important part of the "Space-Pi" project is the creation of network of terrestrial stations for receiving information from small spacecrafts (Selva & Krejci (2012), Klofas et al. (2008)). The main requirement for these stations is their simplicity and maximum availability both in terms of cost and operating capabilities. Such stations provide a two-way exchange of information with spacecrafts in the frequency range 435-438 MHz, receive and process data transmitted in the VHF band by amateur and student satellites, and receive communications from the international space station crew and radio amateurs on Earth.

2. Terrestrial stations for receiving information from small spacecrafts

In the "Space-Pi" project terrestrial stations for receiving information from small spacecrafts provides:

- reception of telemetric information coming during communication sessions with the spacecraft via the radio link channel, its transmission to digital form to a long-term storage system;
- processing and temporary storage of information, its transfer in digital form to analysis;
- forecasting the movement of spacecraft in orbit,
- calculation of conditions of communication sessions,

*makarov@cee.spbstu.ru, corresponding author

doi: https://doi.org/10.52526/25792776-23.70.2-302

- display on the map of the trajectories of the spacecraft, the location and radio visibility zone of the antenna,
- diagnostics and software control of the antenna,
- scheduling communication sessions.

The station can provide processing telemetry information from amateur and student satellites to evaluate:

- parameters of the power supply system;
- temperature regime of onboard systems;
- communication system parameters;
- the impact of the satellite being in the shadow or illuminated part of the orbit;
- trends in the state of on-board systems.

The station is equipped with a directional VHF antenna located on a turntable, a low-noise amplifier (LNA) with an injector that provides its power, a transceiver electronics unit, an anti-vandal heating and processing block, a feeder line. The turntable provides possibility to point the antenna at a spacecraft flying in the radio visibility zone. The station is also equipped with a set of software necessary for control and management of space sensors, as well as for processing the received information. Fig. 1 shows the block diagram of the station.

In this project, we propose to use multi-frequency signals for organizing communications in the subpolar regions of the Earth. We consider Orthogonal frequency-division multiplexing (OFDM) signals as a general form of multi-frequency signals. Simulation model for formation and reception of OFDM signals and corresponding amplitude limiter are shown on fig. 2.

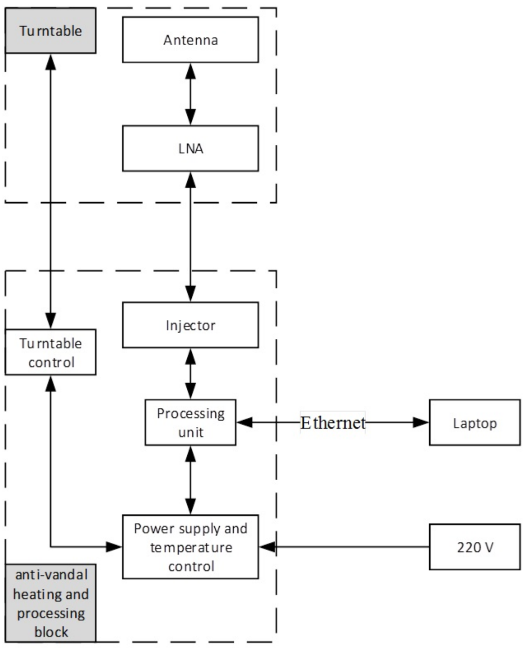

Figure 1. Meteor trails.

Fig. 2 shows the view of the antenna. The main characteristics of this antenna are as follows:

- Frequency range: 435 – 438 MHz,
- Gain: 6-8 dBi,
- Low requirements for placement,
- Easy installation, low windage, light construction, low maintenance,

doi: https://doi.org/10.52526/25792776-23.70.2-302

Figure 2. Antenna device.

- Wide beam pattern.

The receiver is based on the SDR platform and has the following characteristics:

- Frequency range: 500 kHz to 1.7 GHz,
- Bandwidth: 3.2MHz,
- Types of modulation: NFM/AM/LSB/USB/WFM/DSB and others.
- Thermally compensated reference oscillator.

A low-noise amplifier is also necessary to improve the quality of signal reception from spacecraft. Its appearance is shown on Figure 3. Operating frequency ranges: from 136 to 148 MHz (Band 1), from 435 to 438 MHz (Band 2).

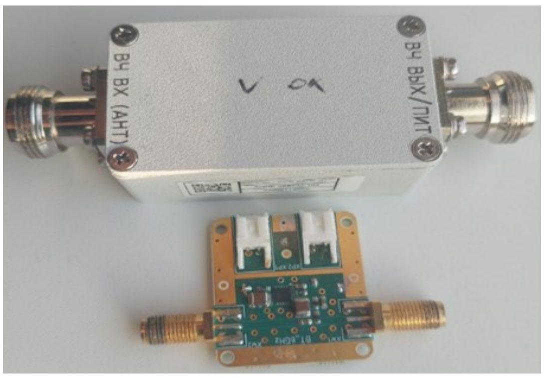

Figure 3. Low noise amplifier.

3. Conclusion

For full-fledged work with the station, it is required to obtain an amateur radio call sign and register the frequency of the ground station. The station provides possibility to work and control spacecraft in the VHF band, analyzing the received target information and the technical condition of the satellites.

doi: https://doi.org/10.52526/25792776-23.70.2-302

Acknowledgements

This work was supported by Ministry of Science and Higher Education of the Russian Federation (state assignment).

References

Klofas B., Anderson J., Leveque K., 2008, CubeSat Developers Conference San Louis Obispo, 1, 1

Selva D., Krejci D., 2012, Acta Astronautica, 74, 55

doi: https://doi.org/10.52526/25792776-23.70.2-302

Unraveling the Origins and Development of the Galactic Disk through Metal-Poor Stars

Maria Rah *[1,2], Manolya Yatman[3], Ali Taani[4], Ahmad A. Abushattal[5], and Mohammad K. Mardini[6]

[1]Byurakan Astrophysical Observatory, Armenia; R-PhD Student at BAO
[2]National Astronomical Observatory, Chinese Academy of Sciences, China; The Silk Road Project at NAOC
[3]Physics Department, Bryn Mawr College, 19010, Philadelphia, USA
[4]Physics Department, Faculty of Science, Al Balqa Applied University,19117, Salt, Jordan
[5]Department of Physics, Al-Hussein Bin Talal University, P.O. Box 20, 71111, Ma'an, Jordan
[6]Department of Physics, Zarqa University, Zarqa 13110, Jordan

Abstract

The Milky Way is a spiral galaxy comprising three main components: the Bulge, the Disk, and the Halo. Of particular interest is the Galactic disk, which holds a significant portion of the baryonic matter angular momentum and harbors at least two primary stellar populations: the thin and thick disks. Understanding the formation and evolution of the Galactic disk is crucial for comprehending the origins and development of our Galaxy. Stellar archaeology offers a means to probe the disk's evolution by listening to the cosmological narratives of its oldest and most pristine stars, specifically the metal-poor stars. In this study, we employed accurate photometric metallicity estimates and Gaia Early Data Release 3 astrometry to curate a pure sample of the oldest Galactic stars. This proceeding presents a summary of our primary findings.

Keywords: *Early universe — Galaxy: dynamics — Galaxy: disc*

1. Introduction

The pioneering research carried out by Gilmore & Reid (1983) centered on investigating the stellar populations present in our Milky Way galaxy. The study extensively examined the motion and distribution of metals among stars, yielding valuable insights into the structure and evolution of our galaxy. An important discovery stemming from this research was the identification of distinct stellar groups, categorized according to their motion characteristics. These stars were divided into two main clusters: a thin disk population characterized by low velocity dispersion, and a thick disk population exhibiting higher velocity dispersion. This finding implies that diverse dynamic processes contributed to the formation and development of these two components. Furthermore, as stated by Gilmore & Reid (1983), both the thin and thick disk populations exhibited various metallicities; however, younger stars within the thin disk component generally displayed a preference for higher metallicity levels. This supports theories that suggest star formation in the Milky Way took place over a long period of time, and that subsequent generations of stars showed higher levels of enrichment with heavy elements. We have collected the key characteristics of these two distinct populations, as reported in literature and listed in Table 1.

More recently, Carollo et al. (2019) identified two distinct modes of the Galactic thick-disk: "in-situ" and "ex-situ". The in-situ population refers to the formation of stars within the Galactic disk, while the ex-situ population involves stars that were formed elsewhere and later accreted onto the our Galaxy. This component is referred to as the Metal-Weak Thick Disk. In this context, Mardini et al. (2022b) investigated the nature of this component by employing accurate photometric metallicity estimates and Gaia Early Data Release 3 astrometry (Gaia Collaboration et al., 2023). Furthermore, during the Gaia era, numerous studies have utilized these astrometry to yield essential constraints regarding the formation and evolution of our galaxy, the Milky Way (Abu-Dhaim et al., 2022, Chiti et al., 2021a,b, Hong et al., 2023, Mardini et al., 2022a, 2023, Placco et al., 2023, Zepeda et al., 2023). In a nutshell, the study by Mardini et al. (2022a) offers

*E-mail: mariarah.astro@gmail.com, Corresponding author

doi: https://doi.org/10.52526/25792776-23.70.2-306

Table 1. Orbital properties of the Galactic thin disk, thick disk, and inner halo

Parameter	unit	Thin disk	Thick disk	Inner halo	Atari disk
h_R	(kpc)	2.6 - 3.00	2.0 - 3.0	...	2.48 $\pm$ 0.05
h_Z	(kpc)	0.14 - 0.36	0.5 - 1.1	...	$1.68^{+0.19}_{-0.15}$
$< V_\phi >$	(km s^{-1})	208	182	0	154 $\pm$ 1
Z_{max}	(kpc)	< 0.8	0.8 - 3.0	> 3.0	< 3.0
e	....	< 0.14	0.3 - 0.5	> 0.7	0.30 - 0.7

See Mardini et al. (2022b); and references therein.

significant insights into the formation and evolution of our Galaxy by emphasizing the spatial, kinematic, and chemical characteristics of this component, which suggest that multiple mechanisms contribute to Galactic disk growth.

2. Method and Analysis

We have developed two separate techniques, namely velocity and action space analysis, to initially select a pure sample of stars with [Fe/H] ≤ -0.8 form the APOGEE-2/SDSS-IV dataset (Blanton et al., 2017). By displaying kinematics that are characteristic of the thick disk, our resulting sample consists of 90,000 stars with high-quality measurements of [Fe/H] and astrometry. We then calculated the positions of our stars using the equations described in Equations 1. The velocity calculations were carried out according to Equation 2. In order to categorize our sample into the main Galactic components (i.e., Halo, thin disk, and thick disk), we defined velocity distributions as explained in Equation 3. The relative probabilities for the ratios between thick-disk-to-thin-disk (TD/D) and thick-disk-to-halo (TD/H) were determined using Equation 4. Each thick disk star was assigned with a membership probability of TD/D > 2.0, while stars with TD/D < 0.5 were classified as thin disk stars. Moreover, we excluded stars with TD/H < 10.0 to minimize potential contamination from the Galactic halo.

The above-mentioned method efficiently identifies stars exhibiting disk-like kinematics. Nonetheless, it is crucial to acknowledge that this approach might erroneously categorize halo stars, which have nearly-circular orbits and low orbital eccentricities, as disk-like stars (e.g., Brauer et al., 2022, Mardini et al., 2019a,b, 2020, Placco et al., 2020). To minimize the risk of contamination from the Galactic Halo, we have developed an alternative method that relies on stellar actions, as described by Equation 5. Furthermore, we utilized a spherically symmetric ad hoc approximation to evaluate the three distribution functions (DFs) individually, as outlined in Equation 6. The figure depicting the relative density distribution of each Galactic component, along with the dark matter profile, can be found in Figure 1. It is worth mentioning that the potential demonstrates a primarily isotropic characteristic (see Almusleh et al., 2021, Mardini et al., 2019c, Taani et al., 2019a,b,c, 2020, 2022). This yielded a sample of my 87075 stars, which spans a wide metallicity range.

3. Results and Conclusions

The average rotational velocity of our sample shows a 30 km s^{-1} lag compared to the well-known thick disk. To understand the origins of our sample stars, we analyze derived gradients, the shape of the eccentricity distribution, and theoretical scenarios for thick disk formation (Abdusalam et al., 2020, Al-Tawalbeh et al., 2021, Al-Wardat et al., 2021, Masda et al., 2019). We also calculate the scale height and scale length of our sample using Equations 7, 8, 9, and 10. In terms of size, our sample is similar to the Galactic thick disk in the radial direction but has greater vertical extension. Furthermore, the distribution of orbital eccentricities in our sample bridges between those typically observed in the thick disk and halo populations. Our investigation into orbital eccentricities also reveals a significant number of stars with high eccentricities. These findings, combined with theoretical predictions, suggest that this population was introduced to our Galaxy through an early merger event involving the proto-Milky Way.

doi: https://doi.org/10.52526/25792776-23.70.2-306

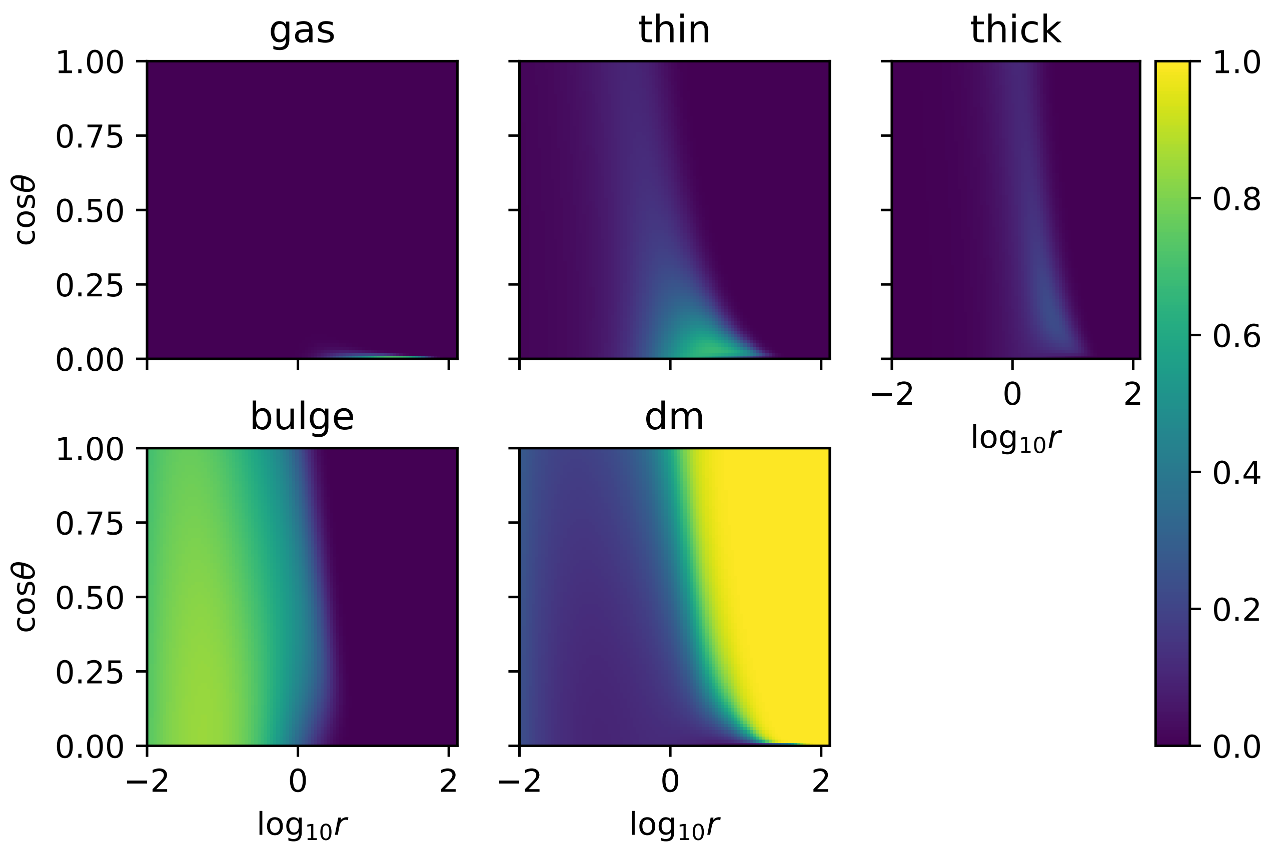

Figure 1. The relative density of each of the components.

$$\begin{aligned} X &= R_{\odot} - d\cos(l)\cos(b) \\ Y &= -d\sin(l)\cos(b) \\ Z &= d\sin(b) \end{aligned} \tag{1}$$

$$\begin{aligned} V_R &= U\cos\phi + (V + V_{rot})\sin\phi \\ V_\phi &= (V + V_{rot})\cos\phi - U\sin\phi \\ V_z &= W \end{aligned} \tag{2}$$

$$\begin{aligned} f(U,V,W) = k \cdot \exp(&- \frac{(V_{\mathrm{LSR}} - V_{\mathrm{asym}})^2}{2\sigma_V^2} \\ &- \frac{W_{\mathrm{LSR}}^2}{2\sigma_W^2} - \frac{U_{\mathrm{LSR}}^2}{2\sigma_U^2}) \end{aligned} \tag{3}$$

$$\begin{aligned} TD/D &= \frac{X_{TD}.f_{TD}}{X_D.f_D} \\ TD/H &= \frac{X_{TD}.f_{TD}}{X_H.f_H} \end{aligned} \tag{4}$$

$$f_{halo}(J_r, J_z, L_z) = f_0 \left[1 + \frac{J_r + J_z + |L_z|}{J_0}\right]^{\beta_*} \tag{5}$$

$$\Phi_{\mathrm{approx}}(r) = -\Phi_{0,\mathrm{fit}} \frac{r_{\mathrm{fit}}}{r} \left[1 - \frac{1}{(1 + r/r_{\mathrm{fit}})^{\beta_{\mathrm{fit}} - 3}}\right] \tag{6}$$

doi: https://doi.org/10.52526/25792776-23.70.2-306

$$\frac{\partial f}{\partial t} + v_R \frac{\partial f}{\partial R} + \frac{v_\phi}{R^2}\frac{\partial f}{\partial \phi} + v_z \frac{\partial f}{\partial z} - \left(\frac{\partial \Phi}{\partial R} - \frac{v_\phi^2}{R^3}\right)\frac{\partial f}{\partial v_R} - \frac{\partial \Phi}{\partial \phi}\frac{\partial f}{\partial v_\phi} - \frac{\partial \Phi}{\partial z}\frac{\partial f}{\partial v_z} = 0, \tag{7}$$

$$\rho K_Z = \frac{\partial(\rho\sigma_{V_Z}^2)}{\partial Z} + \frac{1}{R}\frac{\partial(R\rho\sigma_{V_{R,Z}}^2)}{\partial R} \tag{8}$$

$$\frac{\sigma_{V_\phi}^2}{\sigma_{V_R}^2} - 2 + \frac{2R}{h_R} - \frac{V_c^2 - \bar{V_\phi}^2}{\sigma_{V_R}^2} + \frac{\sigma_{V_Z}^2}{\sigma_{V_R}^2} = 0 \tag{9}$$

$$\frac{\partial \ln \sigma_{V_Z}^2}{\partial Z} - \frac{1}{h_Z} + \frac{K_Z}{\sigma_{V_Z}^2} = 0 \tag{10}$$

References

Abdusalam K., Ablimit I., Hashim P., Lü G. L., Mardini M. K., Wang Z. J., 2020, Astrophys. J. , 902, 125

Abu-Dhaim A., Taani A., Tanineah D., Tamimi N., Mardini M., Al-Wardat M., 2022, Acta Astronomica. , 72, 171

Al-Tawalbeh Y. M., et al., 2021, Astrophysical Bulletin, 76, 71

Al-Wardat M. A., et al., 2021, Research in Astronomy and Astrophysics, 21, 161

Almusleh N. A., Taani A., Özdemir S., Rah M., Al-Wardat M. A., Zhao G., Mardini M. K., 2021, Astronomische Nachrichten, 342, 625

Blanton M. R., et al., 2017, Astron. J. , 154, 28

Brauer K., Andales H. D., Ji A. P., Frebel A., Mardini M. K., Gómez F. A., O'Shea B. W., 2022, Astrophys. J. , 937, 14

Carollo D., et al., 2019, Astrophys. J. , 887, 22

Chiti A., Frebel A., Mardini M. K., Daniel T. W., Ou X., Uvarova A. V., 2021a, Astrophys. J. Suppl. Ser. , 254, 31

Chiti A., Mardini M. K., Frebel A., Daniel T., 2021b, Astrophys. J. Lett. , 911, L23

Chiti A., et al., 2023, Astron. J. , 165, 55

Gaia Collaboration et al., 2023, Astron. Astrophys. , 674, A1

Gilmore G., Reid N., 1983, mnras, 202, 1025

Hong J., et al., 2023, arXiv e-prints, p. arXiv:2311.02297

Mardini M. K., et al., 2019a, The Astrophysical Journal, 875, 89

Mardini M. K., Placco V. M., Taani A., Li H., Zhao G., 2019b, The Astrophysical Journal, 882, 27

Mardini M. K., Ershiadat N., Al-Wardat M. A., Taani A. A., Özdemir S., Al-Naimiy H., Khasawneh A., 2019c, in Journal of Physics Conference Series. p. 012024 (arXiv:1904.09608), doi:10.1088/1742-6596/1258/1/012024

Mardini M. K., et al., 2020, The Astrophysical Journal, 903, 88

Mardini M. K., et al., 2022a, Mon. Not. R. Astron. Soc. , 517, 3993

Mardini M. K., Frebel A., Chiti A., Meiron Y., Brauer K. V., Ou X., 2022b, Astrophys. J. , 936, 78

Mardini M. K., Frebel A., Betre L., Jacobson H., Norris J. E., Christlieb N., 2023, arXiv e-prints, p. arXiv:2305.05363

Masda S. G., Docobo J. A., Hussein A. M., Mardini M. K., Al-Ameryeen H. A., Campo P. P., Khan A. R., Pathan J. M., 2019, Astrophysical Bulletin, 74, 464

Placco V. M., et al., 2020, Astrophys. J. , 897, 78

Placco V. M., et al., 2023, arXiv e-prints, p. arXiv:2310.17024

Taani A., Karino S., Song L., Al-Wardat M., Khasawneh A., Mardini M. K., 2019a, Research in Astronomy and Astrophysics, 19, 012

Taani A., Abushattal A., Mardini M. K., 2019b, Astronomische Nachrichten, 340, 847

Taani A., Karino S., Song L., Mardini M., Al-Wardat M., Abushattal A., Khasawneh A., Al-Naimiy H., 2019c, in Journal of Physics Conference Series. p. 012029, doi:10.1088/1742-6596/1258/1/012029

Taani A., Khasawneh A., Mardini M., Abushattal A., Al-Wardat M., 2020, arXiv e-prints, p. arXiv:2002.03011

Taani A., Vallejo J. C., Abu-Saleem M., 2022, Journal of High Energy Astrophysics, 35, 83

Zepeda J., et al., 2023, Astrophys. J. , 947, 23

doi: https://doi.org/10.52526/25792776-23.70.2-306

Communications of BAO, Vol. 70, Issue 2, 2023, pp. 310-315

Identification of birth places of high-velocity stars: CepOB2 association

S. Ghazaryan[1] *, L. Hambardzumyan[1,3] †, A. Grigoryan[1] ‡, K. Gigoyan[1] §, K.-U. Michel[2] ¶, V. Hambaryan[1,2] ‖, R. Neuhaeuser[2] **1

[1]Byurakan Astrophysical Observatory, Byurakan 0213, Aragatsotn Province,Armenia
[2]Astrophysikalisches Institut und Universitaets-Sternwarte Jena, Schillergaesschen 2-3, 07745 Jena, Germany
[3]Astrophysical Research Laboratory of Physics Institute, Yerevan State University, Armenia

Abstract

We have searched high-velocity stars (runaway, walk-away, pulsars, HMXBs and LMXBs), which could have, most probably, originated in the complex CepOB2 association, i.e. in the cores (small clusters or multiple stellar systems) of it. With the trace-back motion study of them we found at least two pairs consisting of a runaway star and pulsar, which were within stellar groups in the Cep OB2 association $\sim$ 1.5-5.5 Myr ago.

1. Introduction

Ambartsumian (1947, 1955) provided the first evidence that formation of single, double and multiple stars still ongoing in the Galaxy in an extended gravitationally unbound stellar associations. Their dimensions can range from a few to a few hundred pc with space densities <0.1 $\mathcal{M}_\odot$ pc^{-3} (for recent review see, e.g., Wright, 2020).

On the other hand, stars are also formed in compact (up to a few dozens pc) groups in gravitationally bound clusters with a relatively higher space densities >1 $\mathcal{M}_\odot$ pc^{-3} (Lada & Lada, 2003).

However, there are also a significant number (10–30%, see, e.g., Renzo et al., 2019, Stone, 1979) of young massive stars which are observed in the Galactic general field and called "Runaway stars", a term first introduced by Blaauw (1961). Runaway stars are thought to have formed in the stellar associations and have been ejected into the general Galactic field by two proposed mechanisms: dynamical ejection or binary supernova. The first mechanism, proposed by Ambartsumian (1954) in a Trapezium type (non-hierarchical) young multiple, dynamically non-stable systems, was further developed by Poveda et al. (1967). In contrary, the binary ejection mechanism was first proposed by Blaauw (1961) to explain the ejection of runaway O and B stars out of galactic plane. In this scenario the secondary star of a close binary becomes unbound when the primary explodes as a supernova (SN).

On the other hand, depending on separation and component masses prior to the explosion (i.e. phase of mass transfer before the SN, and the subsequent inversion of the mass ratio) and the amount of asymmetry involved (i.e. the magnitude of the kick velocity imparted to the neutron star during the explosion), the binary will either get unbound (ejecting a single runaway star and neutron star) or it will remain bound (see, e.g., Tauris & Takens, 1998). In case of the latter, its center of gravity will be accelerated and one could expect to observe a binary system, either as a member of a stellar association or runaway close binary nearby to a parental stellar group, comprised by a neutron star and a normal star as High- or Low-Mass X-ray Binary (HMXB or LMXB, respectively), if the separation is sufficiently small for accretion to occur.

*satenikghazarjan@yahoo.de, Corresponding author
†hambardzumyanlian@gmail.com
‡argrig2001@gmail.com
§k9gig@tutanota.de
¶kai-uwe.michel@uni-jena.de
‖Valeri.Hambaryan@uni-jena.de
**Ralph.Neuhaeuser@uni-jena.de

doi: https://doi.org/10.52526/25792776-23.70.2-310

Note that the magnitude of the kick velocity also depends on the evolutionary status of the pre-explosion close binary system (dynamical stability of mass transfer to the secondary, see, e.g., Hainich et al., 2020).

Note, also, on the possibility of the so-called two-step-ejection scenario, i.e. massive binary ejection from star clusters and a second acceleration of a massive star during a subsequent supernova explosion (Dorigo Jones et al., 2020, Pflamm-Altenburg & Kroupa, 2010).

Thanks to the unprecedent highly precise *Gaia* data, we can now trace back the motion of runaway stars in 3D. With the newly available *Gaia DR3* data, we can expect a large step forward in the understanding of the origin of runaway stars, SNe in binaries, and their dynamics.

It is worth to note that recent systematic search and identification of stellar clusters (Hunt & Reffert, 2023) based on the *Gaia DR3* data revealed a number of groups, sometimes, including also previously known members of extended stellar associations (see, e.g. Melnik & Dambis, 2020b).

In this context, it is very interesting to identify the parent stellar group of high-velocity stars (runaway, walk-away, pulsars, HMXBs and LMXBs), which could have, most probably, originated in these stellar groups, i.e. cores of an extended star forming region.

In this work, we concentrate on the search, identification and kinematic study of high velocity stars, former members of the stellar groups of the complex and extended CepOB2 association (Szilágyi et al., 2023).

2. Selection of runaway targets and parental stellar groups

To find candidates for runaway stars around CepOB2 association, the average center of the CepOB2 association with 30 degree radius has been taken and the runaway candidates from our list of known runaway stars (Hoogerwerf et al., 2001, Maíz Apellániz et al., 2018, Mdzinarishvili, 2004, Mdzinarishvili & Chargeishvili, 2005, Tetzlaff et al., 2011a,b, Tetzlaff et al., 2012, Tetzlaff et al., 2013, 2014) were filtered. As a result, from 392 known runaway stars 67 runaway candidates were filtered. Later on, we chose among them the ones, which are in up to 2000 pc distance and got 52 candidates. For each of the 13 stellar groups the mean velocity was calculated. In order to understand the directions of motion of stars and stellar groups, we calculated for each of 52 runaway candidates and 13 stellar groups the ratio of the difference of their distances to the difference of their velocities. Finally, 20 runaway candidates were chosen. The cross-match with Melnik's field stars (Melnik & Dambis, 2020a) has been done and as a result we got 26 runaway candidates. Eight of them had bow shocks.

To search for runaway pulsars, High Mass X-ray binaries (HMXB) and Low Mass X-ray binaries (LMXB), from ATNF 1.70 catalogue (Manchester et al., 2005), which consists from 3389 pulsars, 398 pulsars were chosen, which transverse velocities were given. Among them, 64 candidates were chosen with 60 degree radius and 4000 pc distance criteria assumption, and finally 15 candidates were selected. For HMXB's Fortin's catalogue (Fortin et al., 2023) was used and by the same criteria 14 HMXBs were chosen. For LMXB's Liu's catalogue (Liu et al., 2001) was used and again by the same criteria two runaway LMXBs were chosen.

3. Trace-back motion study

In order to identify former members of young stellar groups within extended stellar association Cep OB2 we performed trace-back motion study of probable candidates of runaway stars and pulsars (see previous sections). For this purpose using the present-day positions and velocities of them we trace back and compared with the positions of the known young stellar groups in the past. With the distribution of times corresponding to the minimum separation of a pair of runaway star and pulsar within stellar group one may determine significance/probability that the triple were "in the same place at the same time".

To study the Galactocentric motion of selected candidates we use the code described in Neuhäuser et al. (2020), which computes the orbits by a numerical integration of their equations of motion as defined by the Galaxy gravitational potential consisting of a three component (bulge, disc, and halo) axisymmetric model (Model III from Bajkova & Bobylev, 2017). In addition, the Galaxy gravitational potential is supplemented with the more realistic, non-axisymmetric, and time-dependent terms, which take into account the influence of the central bar and the spiral density wave (Bajkova & Bobylev, 2019, Fernández et al., 2008, Palous et al., 1993).

doi: https://doi.org/10.52526/25792776-23.70.2-310

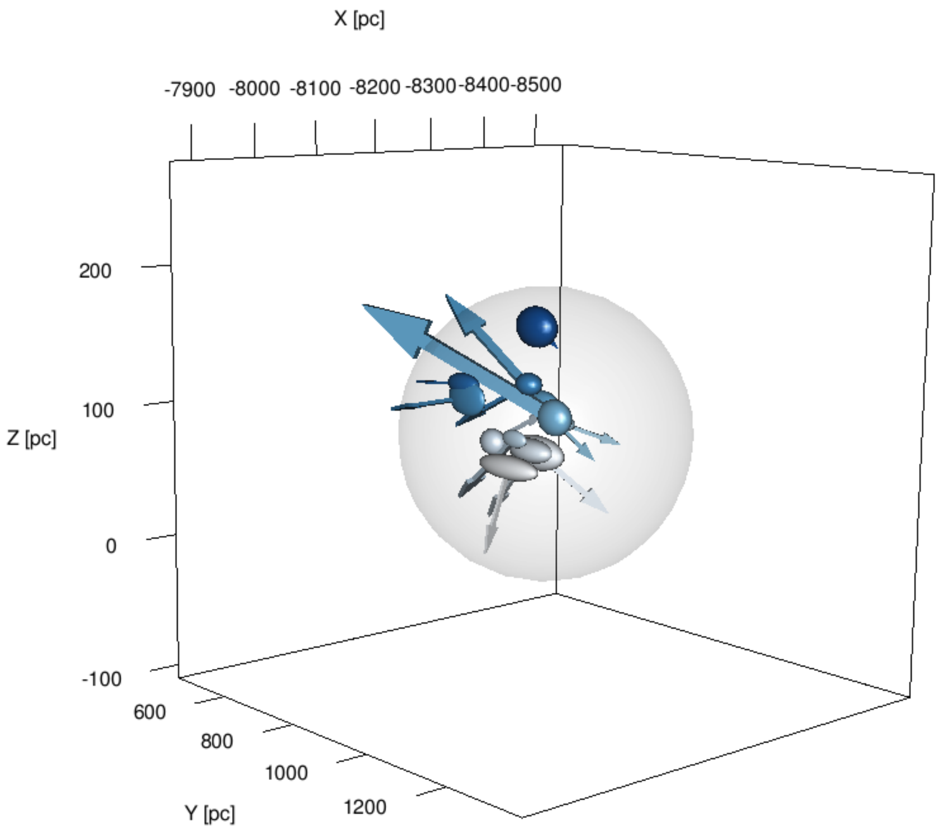

Figure 1. Galactocentric cartesian coordinates of the centers of Cep OB2 extended association (grey ellipsoid,see Table 1 Melnik & Dambis, 2020b) and stellar groups (Szilágyi et al., 2023) within it based on the astrometric and kinematic parameters of their members according to the *Gaia DR3*. Arrows length are corresponding to the expected positions after 15 Myr and the color of each stellar group are coded according to their ages (see, Szilágyi et al., 2023, 2-15 Myr), the darker is younger one.

In order to take account of the uncertainties in the astrometric parameters of the star and associations, each one was replaced by large number of clones, each with astrometric parameters drawn from a multivariate normal distribution. This is done using the covariance matrix of astrometric parameters from *Gaia DR3* (Gaia Collaboration 2018) for the runaway star, for pulsars five astrometric parameters from the catalog of pulsars (Manchester et al., 2005, radial velocities were drawn from the Maxwell's distribution taking into account transverse velocities) and for the stellar groups with the parameters determined by us (see Table 1). Such a procedure is superior to the individual, independent random drawing of each parameter that ignores their mutual dependence.

An application of this procedure to the selected candidates of runaway star, pulsar and young stellar groups lead to the results presented in the Table 2 (see also Fig. 2).

4. Conclusions and outlook

Thus, for the most probable birth place of two runaway stars (*Gaia DR3* 2179226690440773888 and 2203102516722685184) and three pulsars (B0011+47, J2053+4650 and J1431-4715) can be considered Cep OB2 extended association, i.e. within five young stellar groups (see, Table 2). All these runaway star and pulsar pairs with close approve show significant number of orbits (column Nsuc in the Table 2 out of 3 Giga simulations) within a certain young stellar group in the past. Indeed, the probabilities that such a triple

doi: https://doi.org/10.52526/25792776-23.70.2-310

Table 1. Galactocentric cartesian coordinates of the centers of Cep OB2 extended association (Melnik & Dambis, 2020b) and stellar groups (Szilágyi et al., 2023) within it based on the astrometric and kinematic parameters of their members according to the *Gaia DR3*.

Name		X [pc]	Y [pc]	Z [pc]	U [pc/Myr]	W [pc/Myr]	W [pc/Myr]
Cep OB2	median	-8211.27	916.36	82.13	32.50	240.84	2.16
	mad	68.92	91.82	38.50	4.30	7.93	5.74
Group 1	median	-8235.12	855.58	156.32	30.34	241.48	0.99
	mad	7.14	16.59	5.52	8.09	18.18	5.47
Group 2	median	-8125.07	831.75	118.77	32.71	232.67	1.86
	mad	3.89	14.11	2.88	1.99	12.80	1.92
Group 3	median	-8198.78	890.17	117.84	33.05	228.69	-0.57
	mad	5.32	9.83	2.98	4.54	21.79	3.12
Group 4	median	-8123.05	843.65	109.66	33.67	228.85	0.96
	mad	3.21	16.52	4.75	5.90	39.63	5.08
Group 5	median	-8221.91	889.62	102.52	34.47	226.51	6.91
	mad	4.45	14.46	3.39	3.98	13.78	3.74
Group 6	median	-8212.18	937.48	94.91	38.34	215.09	6.80
	mad	6.31	13.20	4.83	3.82	22.76	1.99
Group 7	median	-8235.97	895.66	91.23	27.77	241.71	-0.31
	mad	4.24	10.34	4.10	6.08	20.42	2.88
Group 8	median	-8263.45	883.77	84.08	27.09	243.46	0.91
	mad	5.34	9.49	2.21	13.24	42.33	3.80
Group 9	median	-8158.97	913.60	81.40	30.81	228.44	-1.69
	mad	2.48	10.60	2.34	6.45	38.30	3.71
Group 10	median	-8171.07	839.36	73.81	26.66	241.63	3.36
	mad	5.04	9.78	3.52	4.18	21.94	1.86
Group 11	median	-8222.75	862.91	65.15	31.47	231.74	-1.87
	mad	6.30	18.68	3.26	5.76	23.04	2.03
Group 12	median	-8235.46	859.03	62.40	26.00	244.40	-1.20
	mad	7.03	23.76	4.68	8.90	31.18	2.90
Group 13	median	-8150.05	912.29	61.05	35.12	240.87	-1.86
	mad	5.77	25.81	3.19	4.83	23.31	2.37

(stellar group, runaway star and pulsar) might be by a chance (owing to the uncertainties of the astrometric parameters) are lower by several orders of the magnitude in comparison to the observed probabilities and if they, in reality, were at that time in the same place.

Whether they originated in a binary or multiple stellar system needs further study and performing this type of an analysis is out of the scope of this presentation. In order to study the possibility of different ejection mechanisms of stars from a stellar system we have prepared (still in development) a simulation code in C++. The code takes into account the gravitational forces between the stars, gravitational potential of the Galaxy and the star cluster, and the evolution of the a star (including mass loss over time and potentially asymmetrical supernova explosion). The code uses Yoshida 4 numerical integration method (Yoshida, 1990) to numerically solve the differential equations of motion, and it adjusts the integration timestep using regularization methods. Among the output results we get the exact parameters of supernova explosions that happened (the time, direction and magnitude of the kick velocity), as well as the escape parameters of the stars.

doi: https://doi.org/10.52526/25792776-23.70.2-310

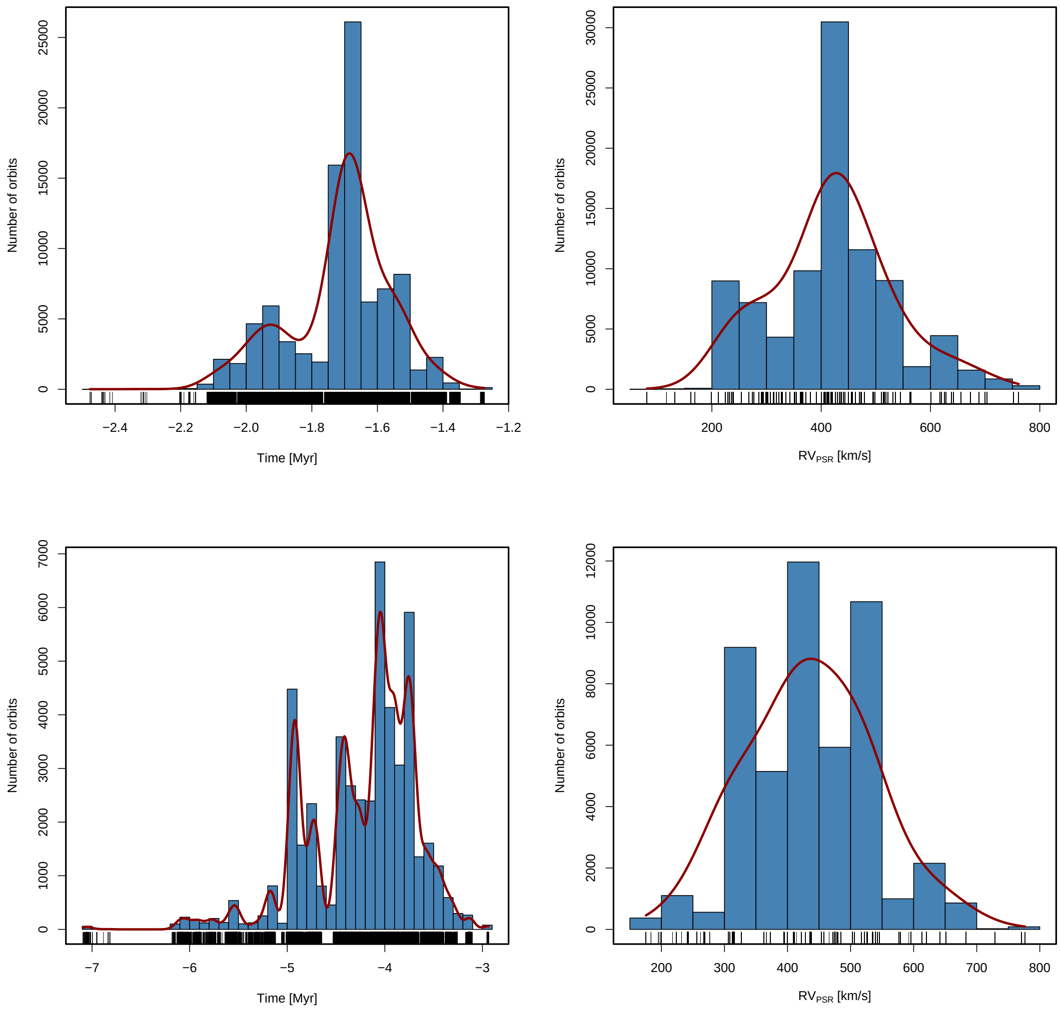

Figure 2. *Left panels:* flight times between pairs of runaway star *Gaia DR3* 2179226690440773888, PSR B0011+47 and *Gaia DR3* 2179226690440773888, PSR J2053+4650 and stellar groups No. 10 and 11 (Szilágyi et al., 2023) peaking at -1.7 and -4.4 Myr, respectively and having minimum separation less than 3pc. *Right panels:* Distributions of radial velocities of pulsars drawn from the Maxwell's distribution (see, Table 2).

Table 2. Most probable birth places of a stellar pairs consisting of a runaway star and pulsar in the Cep OB2 extended association (Melnik & Dambis, 2020b) and stellar groups (Szilágyi et al., 2023).

Group #	Gaia DR3	PSR	Nsuc	Tmin [Myr]	RVpsr [km/s]
10	2179226690440773888	B0011+47	90644	$-1.69^{-0.06}_{+0.17}$	$427.9^{-105.6}_{+94.5}$
11	2203102516722685184	B0011+47	76252	$-1.79^{-0.13}_{+0.27}$	$335.4^{-163.8}_{+21.4}$
5	2203102516722685184	J2053+4650	55922	$-3.40^{-0.39}_{+0.01}$	$673.2^{-143.3}_{+4.1}$
11	2203102516722685184	J2053+4650	36899	$-4.04^{-0.47}_{+0.47}$	$436.4^{-63.2}_{+106.5}$
12	2179226690440773888	J2053+4650	44210	$-3.43^{-0.62}_{+0.03}$	$505.7^{-78.4}_{+30.7}$
11	2179226690440773888	J2053+4650	42560	$-4.40^{-0.08}_{+0.31}$	$482.9^{-24.2}_{+47.4}$
12	2179226690440773888	J1431-4715	14513	$-4.51^{-0.33}_{+0.95}$	$384.9^{-105.9}_{+166.0}$
12	2203102516722685184	J2053+4650	11907	$-4.23^{-0.71}_{+0.06}$	$416.4^{-114.0}_{+24.7}$

doi: https://doi.org/10.52526/25792776-23.70.2-310

Acknowledgments

This work was supported by the Science Committee of RA (Adjunct Research Professorship Program (Remote Laboratory) project No 22RL-039).

References

Ambartsumian V. A., 1947, The evolution of stars and astrophysics

Ambartsumian V. A., 1954, Communications of the Byurakan Astrophysical Observatory, 15, 3

Ambartsumian V. A., 1955, The Observatory, 75, 72

Bajkova A., Bobylev V., 2017, Open Astronomy, 26, 72

Bajkova A. T., Bobylev V. V., 2019, Mon. Not. R. Astron. Soc. , 488, 3474

Baumgardt H., Kroupa P., 2007, Mon. Not. R. Astron. Soc. , 380, 1589

Blaauw A., 1961, Bull. Astron. Inst. Neth. , 15, 265

Dorigo Jones J., Oey M. S., Paggeot K., Castro N., Moe M., 2020, Astrophys. J. , 903, 43

Fernández D., Figueras F., Torra J., 2008, Astron. Astrophys. , 480, 735

Fortin F., García F., Simaz Bunzel A., Chaty S., 2023, Astron. Astrophys. , 671, A149

Goodwin S. P., Bastian N., 2006, Mon. Not. R. Astron. Soc. , 373, 752

Hainich R., et al., 2020, Astron. Astrophys. , 634, A49

Hoogerwerf R., de Bruijne J. H. J., de Zeeuw P. T., 2001, Astron. Astrophys. , 365, 49

Hunt E. L., Reffert S., 2023, Astron. Astrophys. , 673, A114

Lada C. J., Lada E. A., 2003, Ann. Rev. Astron. Astrophys. , 41, 57

Liu Q. Z., van Paradijs J., van den Heuvel E. P. J., 2001, Astron. Astrophys. , 368, 1021

Maíz Apellániz J., Pantaleoni González M., Barbá R. H., Simón-Díaz S., Negueruela I., Lennon D. J., Sota A., Trigueros Páez E., 2018, Astron. Astrophys. , 616, A149

Manchester R. N., Hobbs G. B., Teoh A., Hobbs M., 2005, Astron. J. , 129, 1993

Mdzinarishvili T. G., 2004, Astrophysics, 47, 155

Mdzinarishvili T. G., Chargeishvili K. B., 2005, Astron. Astrophys. , 431, L1

Melnik A. M., Dambis A. K., 2020a, Astrophys. Space. Sci. , 365, 112

Melnik A. M., Dambis A. K., 2020b, Mon. Not. R. Astron. Soc. , 493, 2339

Neuhäuser R., Gießler F., Hambaryan V. V., 2020, Mon. Not. R. Astron. Soc. , 498, 899

Palous J., Jungwiert B., Kopecky J., 1993, Astron. Astrophys. , 274, 189

Pflamm-Altenburg J., Kroupa P., 2010, Mon. Not. R. Astron. Soc. , 404, 1564

Poveda A., Ruiz J., Allen C., 1967, Boletin de los Observatorios Tonantzintla y Tacubaya, 4, 86

Renzo M., et al., 2019, Astron. Astrophys. , 624, A66

Stone R. C., 1979, Astrophys. J. , 232, 520

Szilágyi M., Kun M., Ábrahám P., Marton G., 2023, Mon. Not. R. Astron. Soc. , 520, 1390

Tauris T. M., Takens R. J., 1998, Astron. Astrophys. , 330, 1047

Tetzlaff N., Neuhäuser R., Hohle M. M., 2011a, Mon. Not. R. Astron. Soc. , 410, 190

Tetzlaff N., Eisenbeiss T., Neuhäuser R., Hohle M. M., 2011b, Mon. Not. R. Astron. Soc. , 417, 617

Tetzlaff N., Schmidt J. G., Hohle M. M., Neuhäuser R., 2012, Publications of the Astronomical Society of Australia, 29, 98–108

Tetzlaff N., Torres G., Neuhäuser R., Hohle M. M., 2013, Mon. Not. R. Astron. Soc. , 435, 879

Tetzlaff N., Dinçel B., Neuhäuser R., Kovtyukh V. V., 2014, Mon. Not. R. Astron. Soc. , 438, 3587

Ward J. L., Kruijssen J. M. D., Rix H.-W., 2020, Mon. Not. R. Astron. Soc. , 495, 663

Wright N. J., 2020, , 90, 101549

Yoshida H., 1990, Physics Letters A, 150, 262

Communications of BAO, Vol. 70, Issue 2, 2023, pp. 316-320

The influence of environmental effects on Type Ia Supernovae Standardization

A. Yu. Baluta *[1], M. V. Pruzhinskaya†[2], P. Rosnet[2], and N. Pauna[2]

[1]Faculty of Physics, Lomonosov Moscow State University, Moscow, Russia
[2]Laboratoire de Physique de Clermont, Université Clermont Auvergne, IN2P3/CNRS, France

Abstract

Type Ia Supernovae (SNe Ia) are used as reliable cosmic distance indicators and their standardization is necessary for a more accurate measurement of the cosmological parameters of the Universe using the Hubble diagram. However, the Hubble diagram still shows intrinsic dispersion, potentially influenced by the supernova's environment. In this study, we reproduce Hubble fit diagrams for the Pantheon supernovae data, and also investigate the possibility of introducing various standardization equations for supernovae that exploded in early- and late-type galaxies. We analyze 330 SNe Ia from the Pantheon cosmological sample to study how host galaxy morphology affects SN Ia standardization. We find that SNe Ia hosted by early-type galaxies have different standardization parameters compared to those hosted by late-type galaxies. We conclude that correcting for host galaxy morphology significantly impacts the accuracy of the Hubble diagram fit.

Keywords: *supernovae: general; cosmology: observations, cosmological parameters, distance scale*

1. Introduction

Type Ia supernovae (SNe Ia) are known as standard candles or indicators of cosmological distances. In 2011, Saul Perlmutter, Brian Schmidt and Adam Riess received the Nobel Prize in Physics "for the discovery of the accelerating expansion of the Universe through observations of distant supernovae" (Perlmutter et al., 1999, Riess et al., 1998). In fact, it would be more correct to call SNe Ia standardizable objects. As observational data accumulated, Baade (1938) discovered the universality of their light curves: they show a rapid increase to the maximum in 2-3 days and then a drop of $\sim 3^m$ for every $25-30$ days.

In the 1970s, B. W. Rust and Yu. P. Pskovskii independently revealed an empirical relationship linking the supernova luminosity with its light curve parameters (Pskovskii, 1977, Rust, 1974). After that, many models of standardization of Type Ia supernovae were proposed using various parameters of the light curve. In our work, we use one of such models called the SALT2 standardization model (Guy et al., 2007) with two light-curve parameters: the color, $c = (B-V)_{MAX} - \langle B-V \rangle$, and the stretch, x_1, of the supernova's light curve. The observed distance modulus μ taking into account the standardization equation is presented as follows:

$$\mu = m_B - M_B + \alpha x_1 - \beta c, \tag{1}$$

where m_B is the apparent magnitude at maximum in B-band, α, β, M_B are the parameters of the standardization equation. In the recent cosmological analysis (Scolnic et al., 2018), host stellar mass correction (Δ_M) and correction for distance biases due to intrinsic scatter and selection effects (Δ_B), are taken into account.

These corrections are suitable yet not ideal as they do not completely get rid of the distance modulus dispersion on the Hubble diagram. There is an intrinsic supernova luminosity dispersion left, which for one of the most recent cosmological analyses is $\sim 0.1^m$ (Brout et al., 2022). We believe this spread may be related to environmental effects.

The goal of this work is to reproduce the Hubble diagram (supernova's distance modulus vs. redshift) for the Pantheon SN sample (Scolnic et al., 2018), as well as to improve the standardization equation taking

*nast0307@mail.ru, corresponding author
†pruzhinskaya@gmail.com

doi: https://doi.org/10.52526/25792776-23.70.2-316

into account the supernova environment. We investigate the possibility of using different standardization equations for two populations of supernovae: those that exploded in galaxies of early (E-S0/a) and late (Sa-Sd, Ir) morphological types.

2. Data and methodology

Our research is based on a comprehensive dataset from the Pantheon sample (Scolnic et al., 2018). This sample consists of 1048 SNe Ia in the range of $0.01 < z < 2.3$ discovered by various surveys including Pan-STARRS1 (PS1; Rest et al. 2014, Scolnic et al. 2014), Sloan Digital Sky Survey (SDSS; Kollmeier et al. 2019, Supernova Legacy Survey (SNLS; Conley et al. 2011, Sullivan et al. 2011) and Hubble Space Telescope surveys (HST; Riess et al. 2007, Suzuki et al. 2012). To ensure transparency and reproducibility, we sourced the data from GitHub[1] and collected coordinates, redshift ($z_{\rm CMB}$, $z_{\rm HD}$), host galaxy mass, stretch and color parameters, distance modulus, and associated errors for each supernova. We adopt the morphological classification of host galaxies for 330 supernovae from Pruzhinskaya et al. 2020. All morphological types of hosts are divided into two general groups: early-type galaxies and late-type galaxies. Thus, 91 SNe Ia from Pantheon sample exploded in early-type galaxies and 240 SNe have late-type hosts.

It is known from the literature (Audcent-Ross et al., 2020, Lampeitl et al., 2010, Pruzhinskaya et al., 2020, Roman et al., 2018, Sullivan et al., 2003, 2006, 2010) that supernova luminosity depends on the host galaxy parameters (for example, metallicity, stellar mass, star formation rate, local color, galactocentric distance, etc.). In our work we study the influence of host galaxy morphology on the cosmological analysis.

3. Hubble diagram

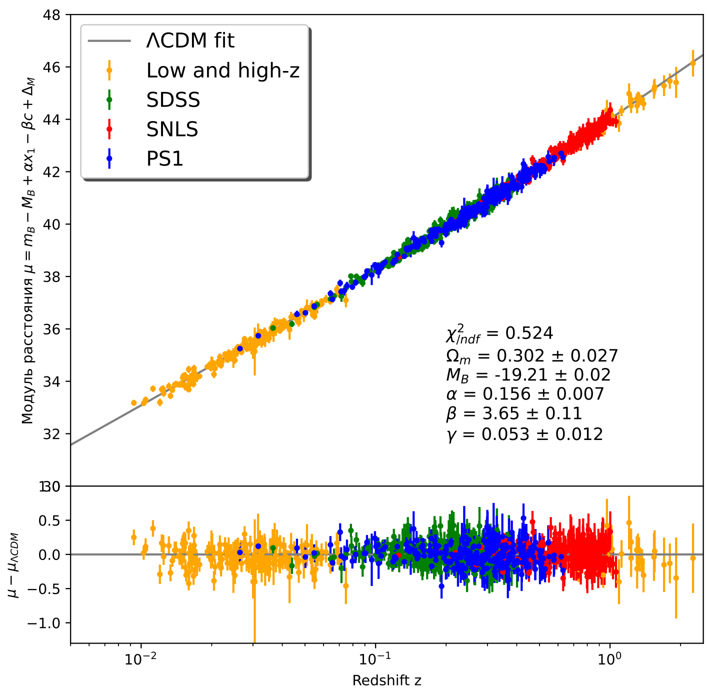

Figure 1. Hubble diagram plotted with all Pantheon supernovae.

To begin with, it is necessary to reproduce the Pantheon Hubble diagram (see Fig. 1). Assuming the flat ΛCDM cosmology, we found standardization parameters of supernovae (α, β, M_B) and cosmological parameter (Ω_m) by minimizing the Hubble residuals. The value of the Hubble constant corresponds to the one recently measured by Riess et al. (2022): $H_0 = 73.04$ km s^{-1} Mpc^{-1}.

[1] https://github.com/dscolnic/Pantheon

doi: https://doi.org/10.52526/25792776-23.70.2-316

Table 1. Comparison of the obtained values of the free parameters of the Hubble fit diagram with the work Scolnic et al. (2018) for $H_0 = 73.04$ km s^{-1} Mpc^{-1}.

Parameter	This work	Scolnic et al. (2018)
Ω_M	0.302 ± 0.028	0.298 ± 0.022
M_B	-19.204 ± 0.016	—
α	0.155 ± 0.007	0.157 ± 0.005
β	3.687 ± 0.109	3.689 ± 0.089
γ	0.055 ± 0.012	0.054 ± 0.009

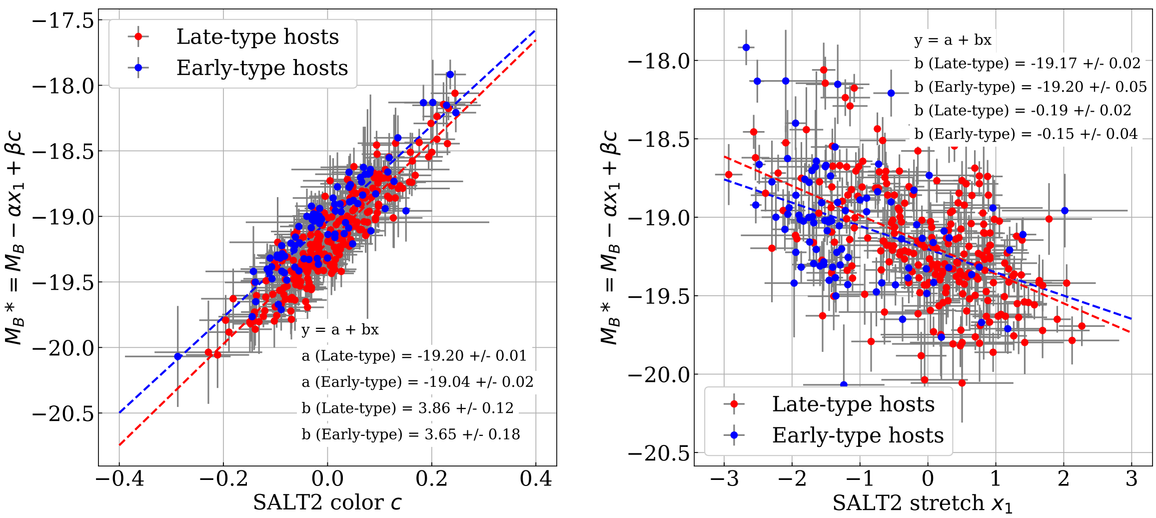

Figure 2. $M_B{}^\star$ vs. SALT2 parameters. SNe in late-type galaxies are shown with red colour and blue colour represents SNe in early-type galaxies.

The results of the fit are presented in the Table 1 and are in a good agreement with original work of Scolnic et al. (2018).

4. Hypothesis of different standardization equations

Pruzhinskaya et al. (2020) found a dependency between the stretch parameter x_1 and the morphological type of the host galaxy of supernova. It was concluded that supernovae in early-type galaxies were characterized by lower values of the stretch parameter compared to supernovae in late-type galaxies.

It is interesting to see whether the inclination angles of the dependence of $M_B^\star$ (see Eq. 2) – the standardized absolute magnitude – on the color and stretch parameters for the two supernova populations are different. In case of observing a characteristic fracture on the graph, we can conclude that it is worth to introduce various standardization equations for supernovae in various types of galaxies:

$$M_B^\star = M_B - \alpha_1 x_{1,PA} - \alpha_2 x_{1,SF} + \beta_1 c_{PA} + \beta_2 c_{SF}\,, \tag{2}$$

where $\alpha_1 x_{1,PA}$ and $\beta_1 c_{PA}$ are related to early-type galaxies, and $\alpha_2 x_{1,SF}$ and $\beta_2 c_{SF}$ to the late-type ones.

We plotted 330 SNe Ia with known host morphological types on the Fig. 2 of the dependence of $M_B^\star$ on the parameters of color and stretch. The α and β values were taken from the Table 1. The hypothesis is it might be possible to present two different standardization equations for these groups of supernovae and thus we performed linear approximation for them. We do not observe significant differences in the mean values of the slope angle for these two supernova populations. However, on the left subplot we see a shift in magnitudes between two host environments. On the right subplot we do not observe a shift but we can distinguish two clusters, indicating that SNe with smaller x_1 are mainly hosted by early-type galaxies.

doi: https://doi.org/10.52526/25792776-23.70.2-316

5. Supernovae standardization for different groups

Since we are investigating the features of the supernova environment, we separately approximate the Hubble diagrams for supernovae which exploded in early-type galaxies and for ones exploded in late-type galaxies. We perform a Hubble diagram fit for these two subsamples of supernovae without any environmental correction. The cosmological parameter Ω_m is fixed to the value given in the Table 1.

The results in the form of joint confidence contour plots containing correlations of the standardization parameters within 1-σ are presented on the left panel of Fig. 3. The blue color indicates the results of approximation for supernovae in old and passive environment, and red color states for supernovae in young and active environment. Green stars represent standardization parameters obtained for the entire sample of 1048 Pantheon supernovae. At the same time, for two populations, we observe obvious discrepancies in the values of absolute magnitudes M_B depending on color and stretch parameters of the supernovae light curves.

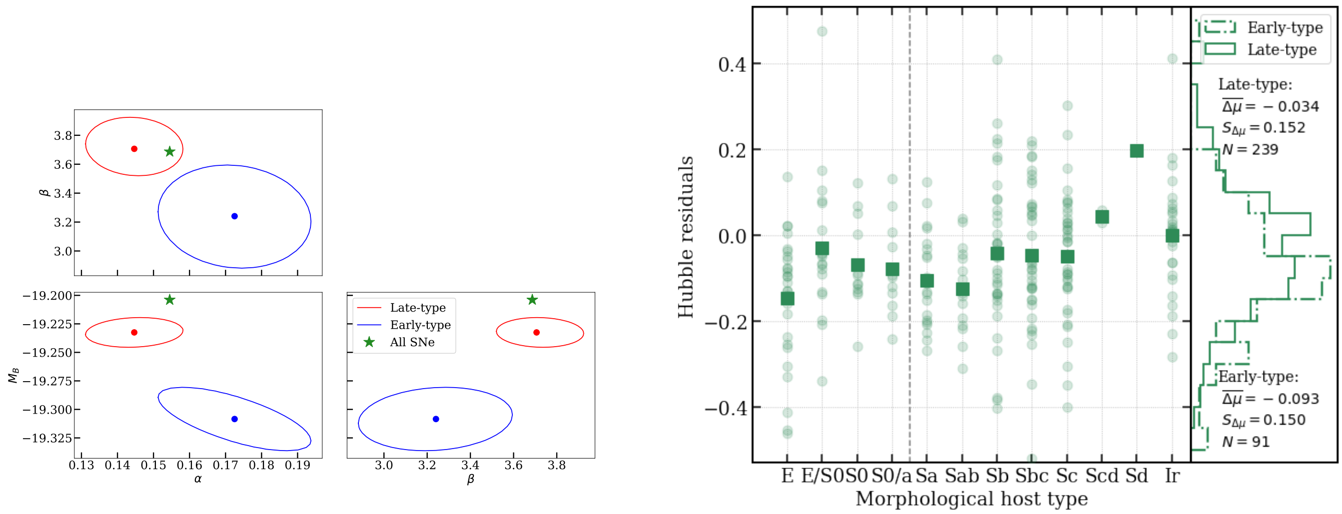

Figure 3. *Left panel:* Joint confidence contours (1-σ) in three-parameter plots of α, β, M_B for fits where the supernovae are split according to the host galaxy morphology. Red ellipses represent SNe in star-forming environment and blue ellipses represent SNe in passive environment. Dots are the central values for each subsample and green stars represent values for the whole Pantheon fit. The density of matter is fixed to the value $\Omega_m = 0.302$ for the full Pantheon fit ($N_{SNe} = 1048$).
Right panel: Hubble residuals for 330 SNe with known host morphology types from Pantheon SNe Ia sample. The squares denote the mean values $\overline{\Delta\mu}$ in each morphological bin. The right subplot is the normalised histogram of $\Delta\mu$ distribution for early-type and late-type morphological supernovae groups.

Thus, we state that without any additional environmental correction the standardization procedure is incomplete. This can also be seen on the Hubble residuals plot. On the right panel of Figure 3 we show the dependence between the Hubble diagram residuals $\Delta\mu = \mu - \mu_{\text{model}}$ and host morphology. SNe in early-type galaxies (old environment) possess slightly smaller values of $\overline{\Delta\mu}$ compared to SNe in late-type galaxies (star-forming environment), which indicates that environmental effects need to be taken into account to fulfil the intrinsic dispersion.

6. Discussion and conclusions

In the course of our study, we successfully approximated the Hubble diagram for the Pantheon sample of 1048 Type Ia supernovae. This was done both for the entire sample as a whole and for individual groups of supernovae, depending on the type of environment – star-forming or passive.

However, the question of introducing various standardization parameters that take into account supernovae environment remains open. The figures showed that the average absolute value of the luminosity of supernovae at the maximum differ depending on the host galaxy type. In particular, supernovae in late-type galaxies have large values of the stretch parameter compared to supernovae in the passive environment. This leads to a shift depending on the color (see Fig. 2). In the future, we plan to continue exploring the possibility of introducing various standardization equations for different populations of supernovae: not only

doi: https://doi.org/10.52526/25792776-23.70.2-316

the host galaxy morphological type, but also the galactocentric distance can be considered as a criterion for attribution to a particular population.

We confirm that environmental correction should be introduced in order to minimize the luminosity dispersion on the Hubble diagram.

The code to perform the described analysis is availavle at `GitHub`[2].

References

Audcent-Ross F. M., Meurer G. R., Audcent J. R., Ryder S. D., Wong O. I., Phan J., Williamson A., Kim J. H., 2020, Mon. Not. R. Astron. Soc. , 492, 848

Baade W., 1938, Astrophys. J. , 88, 285

Brout D., et al., 2022, Astrophys. J. , 938, 110

Conley A., et al., 2011, Astrophys. J. Suppl. Ser. , 192, 1

Guy J., et al., 2007, Astron. Astrophys. , 466, 11

Guy J., et al., 2010, Astron. Astrophys. , 523, A7

Kollmeier J., et al., 2019, in Bulletin of the American Astronomical Society. p. 274

Lampeitl H., et al., 2010, Astrophys. J. , 722, 566

Perlmutter S., et al., 1999, Astrophys. J. , 517, 565

Pruzhinskaya M. V., Novinskaya A. K., Pauna N., Rosnet P., 2020, Mon. Not. R. Astron. Soc. , 499, 5121

Pskovskii I. P., 1977, , 21, 675

Rest A., et al., 2014, Astrophys. J. , 795, 44

Riess A. G., et al., 1998, Astron. J. , 116, 1009

Riess A. G., et al., 2007, Astrophys. J. , 659, 98

Riess A. G., et al., 2022, Astrophys. J. Lett. , 934, L7

Roman M., et al., 2018, Astron. Astrophys. , 615, A68

Rust B. W., 1974, PhD thesis, Oak Ridge National Laboratory, Tennessee

Scolnic D., et al., 2014, Astrophys. J. , 795, 45

Scolnic D. M., et al., 2018, Astrophys. J. , 859, 101

Sullivan M., et al., 2003, Mon. Not. R. Astron. Soc. , 340, 1057

Sullivan M., et al., 2006, Astrophys. J. , 648, 868

Sullivan M., et al., 2010, Mon. Not. R. Astron. Soc. , 406, 782

Sullivan M., et al., 2011, Astrophys. J. , 737, 102

Suzuki N., et al., 2012, Astrophys. J. , 746, 85

[2] https://github.com/pruzhinskaya/SN_environment

doi: https://doi.org/10.52526/25792776-23.70.2-316

Communications of BAO, Vol. 70, Issue 2, 2023, pp. 321-327

Building the Largest Sample of IR Galaxies. Preliminary Results

G. A. Mikayelyan *, A. M. Mickaelian, H. V. Abrahamyan, and G. M. Paronyan

NAS RA V. Ambartsumian Byurakan Astrophysical Observatory (BAO), Byurakan 0213, Aragatzotn Province, Armenia

Abstract

To build the IRAS full extragalactic sample (including both point-like sources - QSOs, and extended ones - galaxies), we have applied several approaches. Cross-correlation of IRAS PSC/FSC Combined Catalogue with optical catalogues of already known galaxies, quasars and blazars such as The NGC 2000.0 Catalog, Third Reference Catalogue of Bright Galaxies, The Roma BZCAT, Astrometric Catalogue 5 and many others. Cross-correlation of IRAS PSC/FSC Combined Catalogue with optical catalogues giving data, which can be used to determine galaxy candidates, for example Sloan Digital Sky Survey (SDSS, contains data about point like and extended objects), The APM North Catalogue (contains data about ellipticity of objects), etc. Cross-correlation of IRAS PSC/FSC Combined Catalogue with GAIA DR3, which gives data about proper motions of objects (we can consider the objects having real proper motions as stars and exclude them from the sample). If all data show the same type of object, then we give it as a genuine one, and if there is an ambiguity, we give the most probable type with a flag. All this will lead to construction of a confident sample of optical counterparts of extragalactic objects of IRAS PSC/FSC: galaxies and quasars. We also will study IR/opt flux ratios, which may serve as one more characteristic to reveal galaxies with very high SFR. We will carry out calculation of IR luminosities for all IR galaxies. We expect revelation of many new ULIRGs and HLIRGs and building their largest samples.

Keywords: *IR - IR Galaxies - ULIRG - Catalogues - Galaxies - AGN - Starburst*

1. Introduction

Astronomy is now in its multiwavelength era, however most interesting results are being obtained in the infrared (IR), especially Far-IR (FIR), and especially considering the recent ground-based surveys and space missions. Astronomical IR sources contain a number of interesting cosmic objects: quasars and other Active Galactic Nuclei (AGN), late-type stars, planetary nebulae (PN), variables, etc. Infrared galaxies (galaxies of this type were discovered in 1983 by the InfraRed Astronomical Satellite, IRAS) appear to be single, gas rich spirals whose infrared luminosity is created largely by the formation of stars within them. However, some galaxies' luminosity come from an AGN. These AGNs reside in compact regions at the centers of galaxies and have higher than normal luminosity. In addition, many IR galaxies appeared to be interacting/merging systems.

The Activity of Galaxies as predicted by Ambartsumian (1958, 1961) and further developed by many other authors, may be nuclear and starburst. The first one relates to the nuclei of galaxies and these objects are called AGN. It is revealed by the non-thermal emission, which is present from γ-ray to radio. The accretion on Super-Massive Black Hole (SMBH) at the central part of the galaxy is considered as the original source of energy. Starburst activity is related to high Star Formation Rates (SFR) at short periods of evolution. Typical SFR is a few $M_\odot$ yr^{-1}, but may reach up to 103 $M_\odot$ yr^{-1}. Thus, high-luminosity galaxies may be fed also by fast burst of star formation (Starburst, SB). It is established that interrelationship between these two types is important for formation and evolution of galaxies, star-formation and metal enrichment history of the Universe. Still, there are significant controversies around the question whether there is a physical relation between SB and AGN and which of these two causes the other one.

There are some especially powerful IR galaxies, called Luminous InfraRed Galaxies (LIRG); their luminosity may come from starburst, and also an AGN. These galaxies contain more energy in the IR portion of the spectrum. The energy given off by LIRGs is comparable to that of a quasar, which before were

*gormick@mail.ru, Corresponding author

doi: https://doi.org/10.52526/25792776-23.70.2-321

known as the most energetic objects in the Universe. LIRGs are galaxies with luminosities above 10^{11} $L_\odot$ (100 billion times that of our Sun; Sanders & Mirabel 1996). LIRGs are more abundant than starburst galaxies, Seyfert galaxies and quasars at comparable luminosity. IR galaxies emit more energy in the IR than at all other wavelengths combined. Galaxies with luminosities above 10^{12} $L_\odot$, are Ultra-Luminous Infrared Galaxies (ULIRG's). Many of the LIRG's and ULIRG's are showing interactions and disruptions. In many of these types of galaxies the SFR is about 100 per year as compared to Our Galaxy which has SFR only 1 star per year; this creates the high level of luminosity. More luminous than ULIRGs are the HLIRG, Hyper-Luminous Infrared Galaxies ($>10^{13}$ $L_\odot$). The most luminous class is the ELIRG, Extremely Luminous Infrared Galaxies.

Optical identifications of the IRAS sources from both IRAS Point Source Catalogue (PSC, IRAS 1986) and Faint Source Catalogue (FSC, Moshir et al. 1990) are rather complicated and uncertain due to the positional errors and many doubtful detections. IRAS PSC and IRAS FSC provide photometric information of fluxes at wavelength bands centered at 12, 25, 60 and 100 μm. IRAS PSC contains 245,889 sources from the whole sky and IRAS FSC contains 173,044 sources at galactic latitudes $|b| > 10°$. Abrahamyan et al. (2015) cross-matched these two catalogues and created IRAS PSC/FSC Combined Catalogue. In frame of the Armenian Virtual Observatory (ArVO), they created a software through which they made cross-correlations (Knyazyan et al., 2011). IRAS PSC/FSC Combined Catalogue contains 345,163 sources. To obtain accurate positions and fluxes in other IR bands the authors carried out cross-correlations with recent catalogues: AKARI IRC (Ishihara et al., 2010), AKARI FIS (Yamamura et al., 2010) and AllWISE (Cutri et al., 2013) also having J, H, and K data from 2MASS (Cutri et al., 2003). We give in Table 1 the main characteristics of the catalogues IRAS PSC, IRAS FSC, AKARI IRC, AKARI FIS and AllWISE.

Table 1. Main characteristics of IRAS PSC, IRAS FSC, AKARI IRC, AKARI FIS and AllWISE catalogues.

Catalogues	**IRAS-PSC**	**IRAS-FSC**	**AKARI-IRC**	**AKARI-FIS**	**AllWISE**
Year	1986	1989	2010	2010	2013
Wavebands (μm)	12, 25, 60, 100	12, 25, 60, 100	9, 18	65, 90, 140, 160	3.4, 4.6, 11.6, 22.6, 1.25, 1.65, 2.17
Wavelengths coverage (μm)	8-120	8-120	6.7-25.6	50-180	1.2-2.2, 2.6-28
Resolution (")	40	20	0.3	0.8	0.5
Sensitivity (Jy)	0.25, 0.25, 0.4, 1.0	0.1-0.5	0.05, 0.12	~0.55	0.00008-0.006
Sky area	All-sky	$\|b\| > 10°$	All-sky	All-sky	All-sky
Sky coverage (%)	96	83	94	98	99
Number of sources	245,889	173,044	870,973	427,071	747,634,026
Reference	IRAS (1986)	Moshir et al. (1990)	Ishihara et al. (2010)	Yamamura et al. (2010)	Cutri et al. (2013)

There have been a number of studies on identifications of IRAS galaxies since the release of IRAS catalogs: IRAS Revised Bright Galaxy Sample (Sanders et al., 2003); Far-InfraRed (FIR) sources (Bertin et al., 1997); IRAS galaxies towards the Boötes void (Strauss & Huchra, 1988); IRAS point sources in the area of Fornax, Hydra I and Coma clusters (Wang et al., 1991); IRAS 1.2 μm survey (Fisher et al., 1995); IRAS galaxies in Virgo cluster area (Yuan et al., 1996); and some others.

Since 1995, a project of optical identifications has been carried out in the Byurakan Astrophysical Observatory (Mickaelian, 1995), in order to detect new galaxies with bursts of star formation in their central regions (SB, or Starburst galaxies) (Weedman et al., 1981), galaxies with active nuclei (AGN, active galactic nuclei) (Ambartsumian, 1958), interacting pairs, and galaxies with high IR luminosity (ULIRG, Ultra-Luminous IR Galaxies), which resulted in revealing 1178 galaxies and 399 stars, named Byurakan-IRAS Galaxies (BIG) (Mickaelian & Sargsyan, 2004) and Byurakan-IRAS Stars (BIS) (Mickaelian & Gigoyan, 2006), respectively. Identifications using low-dispersion spectra of the First Byurakan Survey (FBS or Markarian survey) (Markarian et al., 1989) and its digitized version, DFBS (Massaro et al., 2008, Mickaelian et al., 2007) guaranteed better selection of optical counterparts compared to other identification works.

BIG objects have been studied spectroscopically using BAO 2.6 m (Mickaelian et al., 2003, Sargsyan & Mickaelian, 2006), Special Astrophysical Observatory (SAO, Russia) 6 m (Balayan et al., 2001, Mickaelian et al., 1998), Observatoire de Haute-Provence (OHP, France) 1.93 m (Mickaelian, 2004) telescopes and the Sloan Digital Sky Survey (Abolfathi et al., 2018) (Mickaelian et al., 2018). Altogether 255 BIG objects have been studied and classified. The spectroscopic studies of BIG objects facilitate the concurrent solution of

doi: https://doi.org/10.52526/25792776-23.70.2-321

several problems. These problems range from confirming the extragalactic nature of objects and determining their redshifts to detailed analyses of the objects' structure, which proved to be of greatest interest, such as galaxies with enhanced IR luminosities and/or with nuclear or starburst activity.

Until now IRAS remains the only all-sky survey giving data in Far-IR (namely 60 and 100 mum). There also is AKARI FIS catalog, however there are doubts in the correctness of its flux calibration. In IRAS PSC/FSC Combined Catalogue, out of 345,163 sources, there are 145,902 (42.3 %) candidate galaxies to be checked by cross-correlations with optical catalogues. In this project we investigate this sample to create a large list of genuine IRAS-selected galaxies. Having the largest sample, we can achieve the best understanding of many properties of IR galaxies.

2. Research methods

To build the IRAS full extragalactic sample, we have applied several approaches. First of all we have cross-correlated the IRAS PSC/FSC Combined Catalogue with optical catalogues of already known galaxies, quasars and blazars. The search radius was taken differently for each catalogue, depending on its own positional errors. After cross-correlation only the single matches in given search radius were taken as genuine ones. Below in Table 2 are the catalogues with their refrences and object quantities, search radii and the numbers of single matches after cross-correlations:

Table 2. Optical catalogues of already known galaxies, quasars, blazars and cross-correlation results with IRAS PSC/FSC Combined Catalogue.

Catalogues and references	**Number of objects**	**Search radius**	**Associations with IRAS PSC/FSC**
Catalogued Galaxies and Quasars observed in the IRAS Survey, Version 2 (Fullmer & Lonsdale, 1989)	11,444	10 arcsecs	5,377
NGC 2000.0, The Complete New General Catalogue and Index Catalogue of Nebulae and Star Clusters by J.L.E. Dreyer (Sinnott, 1988)	13,226	2 arcmins	4,006
Third Reference Catalogue of Bright Galaxies (RC3, de Vaucouleurs et al., 1995)	23,011	2 arcmins	7,956
A catalogue of quasars and active nuclei 13th edition (Véron-Cetty & Véron, 2010)	168,940	10 arcsecs	1,271
The Roma BZCAT - 5th edition (Massaro et al., 2015)	3,561	10 arcsecs	40
Astrometric Catalogue 5, LQAC-5 (Souchay et al., 2019)	592,809	3 arcsecs	1,364
SDSS quasar catalog, sixteenth data release (DR16Q, Lyke et al., 2020)	750,414	3 arcsecs	111
QSOs selection from SDSS and WISE (Richards et al., 2015)	1,604,577	3 arcsecs	180

The next step was cross-correlating the IRAS PSC/FSC Combined catalogue with catalogues giving data, which can be used to determine galaxy candidates, for example data about point like and extended objects, ellipticity of objects, etc. Below are the catalogues with their object quantities, data which was used to determine galaxy candidates, search radii and the numbers of single matches after cross-correlations:

- Sloan Digital Sky Surveys (SDSS), Release 16 (DR16, Ahumada et al., 2020) containing 1,231,051,050 objects. SDSS marks all extended objects as galaxies, so we take them as galaxy candidates. The search radius was taken 3 arcsecs; 46,396 single matches were found.
- HYPERLEDA. I. Catalog of galaxies (Paturel et al., 2003) containing 983,261 objects. This catalogue is the new Principal Galaxies Catalogue (PGC2003), which contains candidates of galaxies. The search radius was taken 1 arcmins; 33,309 single matches were found.
- The APM-North Catalogue (McMahon et al., 2000) containing 166,466,987 objects. APM gives the data about ellipticity of objects (1-a/b, where "a" is the minor axis diameter and "b" is the major

doi: https://doi.org/10.52526/25792776-23.70.2-321

axis diameter). When the ellipticity is bigger than 0.5, we consider them as galaxy candidates. The search radius was taken 3 arcsecs; 37,232 single matches were found.

- Gaia DR3 Part 2. Extra-galactic (Gaia Collaboration, 2022) containing 11,491,504 objects. In this catalogue all extended objects have been separated from Gaia DR3. The search radius was taken 3 arcsecs; 21,599 single matches were found.

In addition we have cross-correlated our catalogue with radio catalogues, considering that sources having strong radio emission are most likely extragalactic. Below are cross-correlation results with radio catalogues:

- 1.4GHz NRAO VLA Sky Survey (NVSS, Condon et al., 1998) containing 1,773,484 sources. The search radius was taken 75 arcsecs; 42,072 single matches were found.

- The FIRST Survey Catalog (Helfand et al., 2015) containing 946,432 sources. The search radius was taken 15 arcsecs; 6,640 single matches were found.

The last step was the cross-correlation of IRAS PSC/FSC Combined Catalogue with GAIA DR3, which gives data about proper motions of objects, so that we can consider the objects having real proper motions as stars and exclude them from the sample:

- Gaia DR3 Part 1. Main source (Gaia Collaboration, 2022) containing 1,811,709,771 objects. The search radius was taken 3 arcsecs; 217,385 single matches were found.

If all data show the same type of object, then we give it as a genuine one, and if there is an ambiguity, we give the most probable type with a flag. The order of the catalogs by their priority is the following: 1. Catalogued Galaxies and Quasars observed in the IRAS Survey, Version 2; NGC 2000.0; RC3; A catalogue of quasars and active nuclei 13th edition; The Roma BZCAT - 5th edition; Astrometric Catalogue 5, LQAC-5; SDSS quasar catalog, sixteenth data release; QSOs selection from SDSS and WISE; 2. SDSS DR16; 3. Gaia DR3 Part 2. Extra-galactic; 4. The APM-North Catalogue; 5. HYPERLEDA. I. Catalog of galaxies; 6. NVSS; FIRST.

3. Preliminary results

In Figure 1 we show our preliminary results after cross-correlations. The first column shows 183,168 star candidates for which Gaia DR3 gives proper motions with the ratio of proper motion and its error bigger than 3. In the second column there are 80,998 unknown sources that have no matches after all cross-correlations (most probably, these sources may appear either faint galaxies or false sources, ex. cirruses). In the third column we have 68,940 galaxy candidates and the last column shows 12,057 confirmed or genuine galaxies or QSOs.

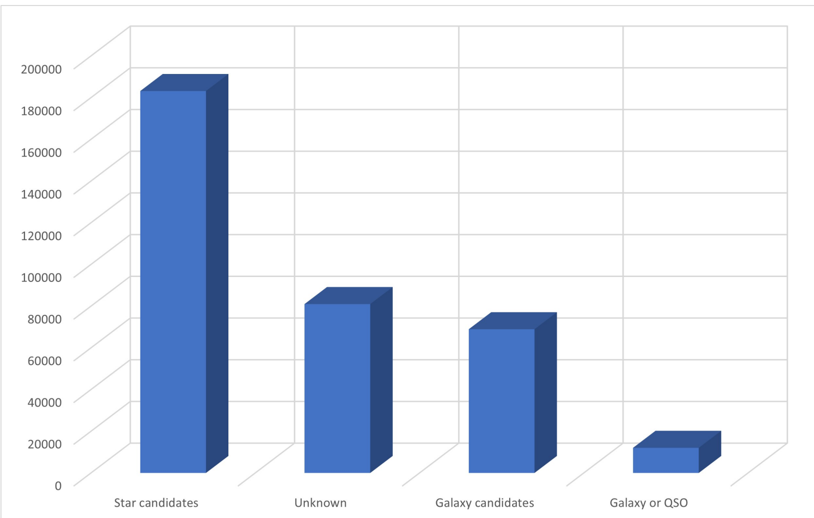

Figure 1. The distribution of the number of objects by type

doi: https://doi.org/10.52526/25792776-23.70.2-321

Our next step is to finalize the results of the cross-correlations and decide with the nature of objects: star, galaxy, quasar, unknown (which may also include nebulae, ex. planetary nebulae). We will publish the Extragalactic Sample of IRAS.

4. Future studies

High Luminosity Infrared Galaxies. Using the IRAS PSC/FSC Combined Catalogue containing 345,162 sources with improved astrometric data and SDSS spectroscopy for redshifts and luminosities, we have found 114 very high luminosity IRAS galaxies; HLIRGs and ULIRGs (Mikayelyan et al., 2018). Having the confirmed extragalactic sample, we will carry out calculation of IR luminosities for all IR galaxies. We expect revelation of many new ULIRGs and HLIRGs and building their largest samples. Figure 2 shows an analysis of their IR luminosities *vs.* redshifts. A few objects show obvious deviation from the standard sequence for most of the objects and have much higher luminosities. We will search for such objects to see if this is a rule or exception; in both cases we will find either a sample of such objects or extremely unique ones.

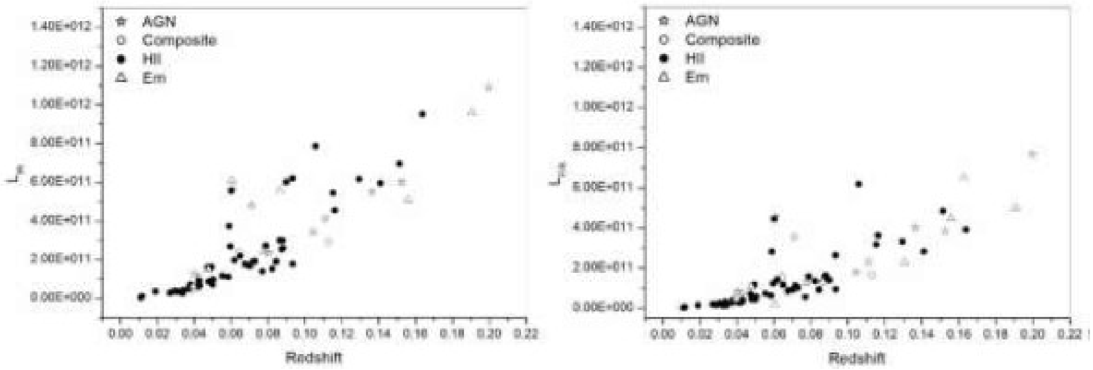

Figure 2. IR luminosities against redshifts for 70 IR galaxies showing a few of them outlying the standard sequence for most of galaxies. These are probably ULIRGs.

Another issue is the study of the highest IR luminosity of a single galaxy, as most of high luminosity IR galaxies show interaction and merging features. The preliminary studies show that this limit is near 10^{12} Solar luminosities.

Study of IR/optical flux ratios. The IR luminosity alone is not the only relevant parameter to reveal interesting IR galaxies. The IR/optical flux ratio may serve as an additional characteristic to reveal galaxies with very high SFR. We aim at the revelation of very high IR/opt flux ratio objects among the IRAS PSC/FSC Combined Catalogue involving objects with detected Far-IR (IRAS 60 and 100 μm). Among the goals of this study may be the revelation of objects with very high IR/opt flux ratio, so called IR-excess galaxies and the distribution of IR/opt flux ratios to reveal the possible limit between the normal and IR galaxies, as well as the detailed study of IR/opt for different types of AGN and Starburst galaxies.

Morphological study of IR galaxies. SDSS images are reliable for morphological study of the images of IR galaxies; to carry out morphological classification and to reveal interacting pairs/multiples and mergers. IR galaxies at higher luminosities show strong features of interactions and merging. For our sample it will be rather important to have statistics between single galaxies and pairs/multiples, as well as mergers. We give in Figure 3 examples of SDSS images of interacting/merging IR galaxies.

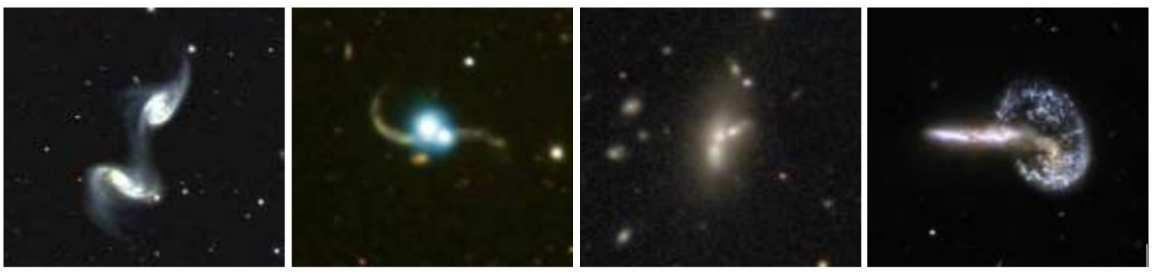

Figure 3. SDSS images showing interacting/merging IR galaxies

doi: https://doi.org/10.52526/25792776-23.70.2-321

5. Summary

We have cross-correlated IRAS PSC/FSC Combined catalogue with optical catalogues of already known galaxies, quasars and blazars (Catalogued Galaxies and Quasars observed in the IRAS Survey, Version 2; NGC 2000.0, The Complete New General Catalogue and Index Catalogue of Nebulae and Star Clusters by J.L.E. Dreyer; Third Reference Catalogue of Bright Galaxies; A catalogue of quasars and active nuclei 13th edition; The Roma BZCAT - 5th edition; Astrometric Catalogue 5, LQAC-5; SDSS quasar catalog, sixteenth data release; QSOs selection from SDSS and WISE), catalogues giving data, which can be used to determine galaxy candidates (Sloan Digital Sky Surveys DR16; HYPERLEDA. I. Catalog of galaxies; The APM-North Catalogue; Gaia DR3 Part 2. Extra-galactic), radio catalogues (1.4GHz NRAO VLA Sky Survey; The FIRST Survey Catalog) and GAIA DR3. After cross-correlation out of 345,163 IR sources we have revealed 12,057 galaxies, quasars or blazars and 68,940 galaxy candidates. Due to cross-correlation with GAIA DR3 we have revealed 183,168 stars. However, 80,998 IRAS sources still remain unknown.

Acknowledgements

This research was partly accomplished by the Republic of Armenia Science Committee for the Advanced Research Grant 21AG-1C053 Revelation of Early Stages of Galaxy Evolution by Means of MW Study of Active Galaxies (2021-2026).

References

Abolfathi B., Aguado D., Aguilar G., et al. 2018, The Astrophysical Journal Supplement Series, 235, issue 2, article id. 42, p. 19

Abrahamyan H. V., Mickaelian A. M., Knyazyan A. V., 2015, Astronomy and Computing, 10, 99

Ahumada R., et al., 2020, Astrophys. J. Suppl. Ser. , 249, 3

Ambartsumian V. A., 1958, in La structure et l'évolution de l'universe. pp 241–249

Ambartsumian V. A., 1961, Astron. J. , 66, 536

Balayan S., Akopyan S., Mickaelian A., Burenkov A., 2001, Pis'ma v Astron. zh. 27, 330

Bertin E., Dennefeld M., Moshir M., 1997, Astron. Astrophys. 323, 685

Condon J. J., Cotton W. D., Greisen E. W., Yin Q. F., Perley R. A., Taylor G. B., Broderick J. J., 1998, Astron. J. , 115, 1693

Cutri R. M., et al., 2003, VizieR Online Data Catalog, p. II/246

Cutri R. M., et al., 2013, Explanatory Supplement to the AllWISE Data Release Products, Explanatory Supplement to the AllWISE Data Release Products, by R. M. Cutri et al.

Fisher K., Huchra J., Strauss M., Davis M., Yahil A., Schlegel D., 1995, Astrophys. J. Suppl. Ser. 100, 69

Fullmer L., Lonsdale C. J., 1989, JPL D-1932, p. 0

Gaia Collaboration 2022, VizieR Online Data Catalog, p. I/356

Helfand D. J., White R. L., Becker R. H., 2015, Astrophys. J. , 801, 26

IRAS 1986, Joint IRAS Science W.G., IRAS Catalog of Point Sources, Version 2.0

Ishihara D., et al., 2010, Astron. Astrophys. , 514, A1

Knyazyan A., Mickaelian A., Astsatryan H., 2011, International Journal "Information Theories and Applications, 18, 243

Lyke B. W., et al., 2020, Astrophys. J. Suppl. Ser. , 250, 8

Markarian B., Lipovetsky V., Stepanian J., Erastova L., Shapovalova A., 1989, Comm. SAO 62, 5

Massaro E., Mickaelian A., Nesci R., Weedman D., 2008, The Digitized First Byurakan Survey (Roma, Italy)

Massaro E., Maselli A., Leto C., Marchegiani P., Perri M., Giommi P., Piranomonte S., 2015, Astrophys. Space. Sci. , 357, 75

McMahon R. G., Irwin M. J., Maddox S. J., 2000, VizieR Online Data Catalog, p. I/267

Mickaelian A., 1995, Astrophysics 38, 625

Mickaelian A., 2004, Astrofizika 47, 425

Mickaelian A., Gigoyan K., 2006, Astron. Astrophys. 455, 765. Catalog No. III/237a in Vizier, CDS, Strasbourg

Mickaelian A., Sargsyan L., 2004, Astrofizika 47, 109

Mickaelian A., Akopyan S., Balayan S., Burenkov A., 1998, Pis'ma v Astron. zh. 24, 736

doi: https://doi.org/10.52526/25792776-23.70.2-321

Mickaelian A., Oganesyan L., Sargsyan L., 2003, Astrofizika 46, 221

Mickaelian A., et al., 2007, Astron. Astrophys. 464, 1177

Mickaelian A., Harutyunyan G., Sarkissian A., 2018, Astronomy Letters, Volume 44, Issue 6, pp.351-361

Mikayelyan G. A., Mickaelian A. M., Abrahamyan H. V., Paronyan G. M., 2018, Communications of the Byurakan Astrophysical Observatory, 65, 13

Moshir M., et al., 1990, in Bulletin of the American Astronomical Society. p. 1325

Paturel G., Petit C., Prugniel P., Theureau G., Rousseau J., Brouty M., Dubois P., Cambrésy L., 2003, Astron. Astrophys. , 412, 45

Richards G. T., et al., 2015, Astrophys. J. Suppl. Ser. , 219, 39

Sanders D. B., Mirabel I. F., 1996, Ann. Rev. Astron. Astrophys. , 34, 749

Sanders D., Mazzarella J., Kim D.-C., Surace J., Soifer B. T., 2003, Astron. J. 126, 1607

Sargsyan L., Mickaelian A., 2006, Astrofizika 49, 19

Sinnott R. W., 1988, NGC 2000.0: The Complete New General Catalogue and Index Catalogues of Nebulae and Star Clusters by J. L. E. Dreyer

Souchay J., et al., 2019, Astron. Astrophys. , 624, A145

Strauss M., Huchra J., 1988, Astron. J. 95, 1602

Véron-Cetty M. P., Véron P., 2010, Astron. Astrophys. , 518, A10

Wang G., Leggett S., Clowes R., MacGillivray H., Savage A., 1991, MNRAS 248, 112

Weedman D., Feldman F., Balzano V., et al. 1981, Astrophys. J. 248, 105

Yamamura I., Makiuti S., Ikeda N., Fukuda Y., Oyabu S., Koga T., White G. J., 2010, VizieR Online Data Catalog, p. II/298

Yuan Q., Zhu Z., Yang Z., He X., 1996, Astron. Astrophys. Suppl. Ser. 115, 267

de Vaucouleurs G., de Vaucouleurs A., Corwin H. G., Buta R. J., Paturel G., Fouque P., 1995, VizieR Online Data Catalog, p. VII/155

doi: https://doi.org/10.52526/25792776-23.70.2-321

Communications of BAO, Vol. 70, Issue 2, 2023, pp.328-334

BL Lacertae: Recovering intrinsic trajectory of a quasi-stationary jet feature on subparsec-scales

L.A. Hambardzumyan *[1,2], T.G. Arshakian †[1,3], and A.B. Pushkarev ‡[4]

[1]Byurakan Astrophysical Observatory after V.A. Ambartsumian, Armenia
[2]Astrophysical Research Laboratory of Physics Institute, Yerevan State University, Armenia
[3]I. Physikalisches Institut, Universität zu Köln, Zülpicher Strasse 77, Köln, Germany
[4]Crimean Astrophysical Observatory, Nauchny, Crimea

Abstract

Very Long Baseline Array (VLBA) observations allow us to investigate the fine structure and dynamics of the inner part of the BL Lacertae jet. Long-term VLBA monitoring at 15 GHz has revealed the existence of a quasi-stationary component (QSC) in the jet interior, located about 0.26 mas from the radio core, followed by superluminal moving radio components. The study of the QSC motion is important in order to shed light on the dynamics of the inner part of the relativistic jet on spatial scales of milliparsecs. The latter is problematic due to measurement errors on such scales. In addition, the apparent QSC motion is a combination of the intrinsic motion of the QSC and the radio core, which predominantly occurs in the direction of the jet axis. Careful error analyses and apparent trajectory smoothing techniques are important to reveal the QSC intrinsic motion. We use 164 epochs of VLBA monitoring of the jet in BL Lacertae, available as part of the MOJAVE program, to study the QSC motion. We apply a moving average method to filter out the core contribution, which allows the detection of QSC intrinsic motion and develop an algorithm to clean up the smoothed trajectory using QSC positioning errors. We find that the QSC intrinsic trajectory is a combination of irregular reversals occurring on scales from about 0.15 yr to 0.5 yr. An analysis of the estimates of the reversal characteristics is presented for smoothed and cleaned trajectories.

Keywords: *BL Lacertae objects: individual: BL Lacertae, galaxies: active, radio continuum: galaxies, galaxies: jets.*

1. Introduction

Blazars belonging to the class of radio-loud active galactic nuclei (AGN) are characterised by the presence of relativistic jets oriented at small angles with respect to the observer's line of sight. We focus on the study of the interior of the jet of the BL Lacertae object on sub-parsec scale using the Very Long Baseline Array (VLBA) observations. The observations on interferometric radio telescopes allow us to investigate the structure and dynamics of the jet on scales of milliarcseconds. Monitoring of BL Lacertae with the VLBA at 15 GHz has revealed a jet structure consisting of a bright radio core (apparent origin of the jet at which the optical depth of synchrotron radiation $\tau_\nu \approx 1$) and a quasi-stationary component (QSC) located at 0.26 mas and referred to as C7 and that moving superluminal components appear downstream the C7 component (Arshakian et al., 2020, Cohen et al., 2014, 2015). According to Cohen et al. (2015), the dynamics of the quasi-stationary C7 component has the potential to influence the outer jet behaviour, extending over distances of several hundred parsecs.

Using VLBA data of 116 observational epochs (1999–2016) available from the MOJAVE (Monitoring Of Jets in Active galactic nuclei with VLBA Experiments) program (Lister et al., 2018), Arshakian et al. (2020) showed that C7 exhibits predominantly superluminal velocities ($\sim 2c$) with an asymmetric brightness distribution on the sky both along and across the jet axis. They confirmed the connection between large C7 amplitudes of displacement vectors and the excitation of relativistic transverse waves during the active and

*hambardzumyanlian@gmail.com, Corresponding author
†t.arshakian@gmail.com
‡pushkarev.alexander@gmail.com

doi: https://doi.org/10.52526/25792776-23.70.2-328

stable phases of the jet. They found that the observed (apparent) C7 motion is a combination of the C7 proper motion and the core displacement, which typically occurs in the direction of the jet axis and due to resolution-dependent core bias and/or changes in particle density or magnetic field amplitude, and developed a method to estimate the statistical characteristics of the C7 intrinsic motion and the radio core motion. They showed that the contribution of both motions to the apparent motion of C7 is comparable. In order to perform a comprehensive analysis of the intrinsic trajectory of C7, we need to minimise the effect of the core displacement and treat carefully the C7 positioning errors. Here, we use data from 164 VLBA observations at 15 GHz within a period of 1999–2020 and apply a moving average filter to the apparent C7 trajectory to smooth out the core displacement effect and analyse the positional errors using a cleaning algorithm. The advantages and disadvantages of smoothing and cleaning the C7 trajectory and characteristics of C7 reversal motion are discussed.

BL Lacertae has a redshift $z = 0.0686$ (Vermeulen et al., 1995), which corresponds to a scale factor of 1.3 pc mas^{-1}, assuming $H_0 = 71$ km s^{-1} Mpc^{-1} , $\Omega_\lambda = 0.73$ and $\Omega_m = 0.27$ (Komatsu et al., 2009).

2. Observed trajectory of quasi-stationary component

Analysis of radio maps of VLBA observations over a 20-year period (1999–2020) revealed a radio core, a quasi-stationary component, and moving radio components (Lister et al., 2021). Figure 1 illustrates the separation of the radio components from the radio core with epoch. It is noticeable that the C7 component (marked in yellow) is 0.26 mas away from the radio core, and 37 components appear to emerge from C7. The slope of a linear fit of the moving components determines the apparent radial velocity. The components have a wide range of apparent speeds distributed between $3c$ and $10c$ expressed in units of the speed of light. Cohen et al. (2014) reported the highest apparent speed of $9.2c$ for moving features from 1996 to 2013. Similar maximum apparent speed $(10 \pm 1)c$ is estimated for the component number C52 (ejected in 2013.4) during the time period between 2013 and 2020.

Methods for data reduction, model construction and error estimation are given in Lister et al. (2009), Cohen et al. (2014, 2015) and Arshakian et al. (2020). To analyse the motion of C7, we use the displacement

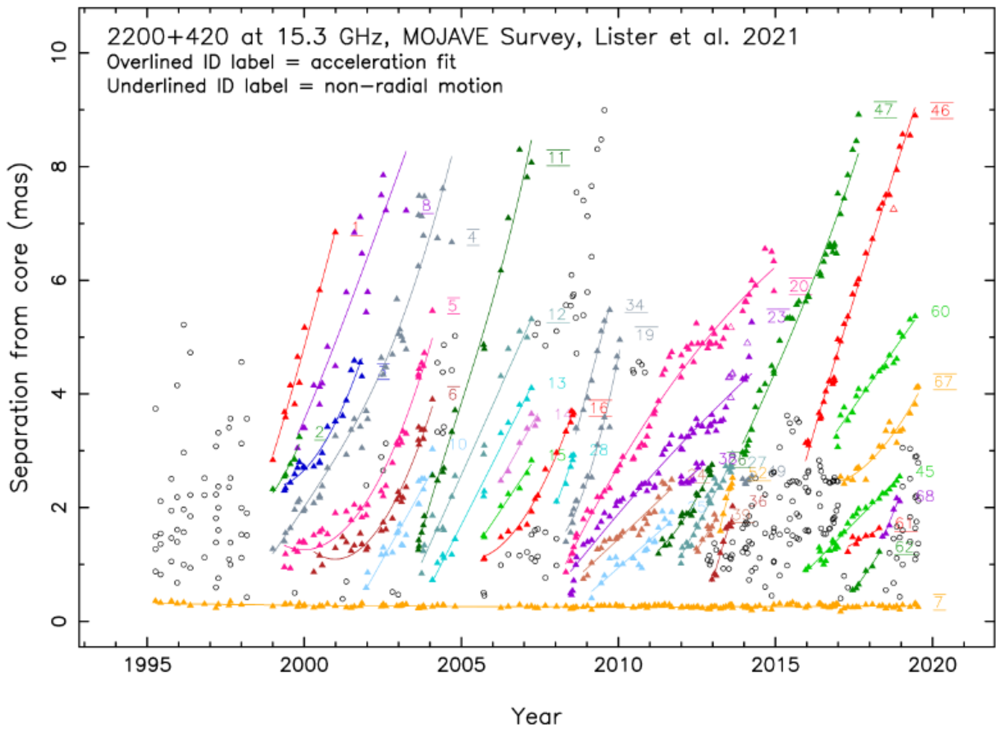

Figure 1: Separation of the components from the radio core[1]. Quasi-stationary C7 component (yellow triangles) is located at 0.26 mas from the core, moving components have superluminal speeds between $\approx (3 - 10)c$ (colored symbols).

[1]The plot is sourced from the MOJAVE web page.

doi: https://doi.org/10.52526/25792776-23.70.2-328

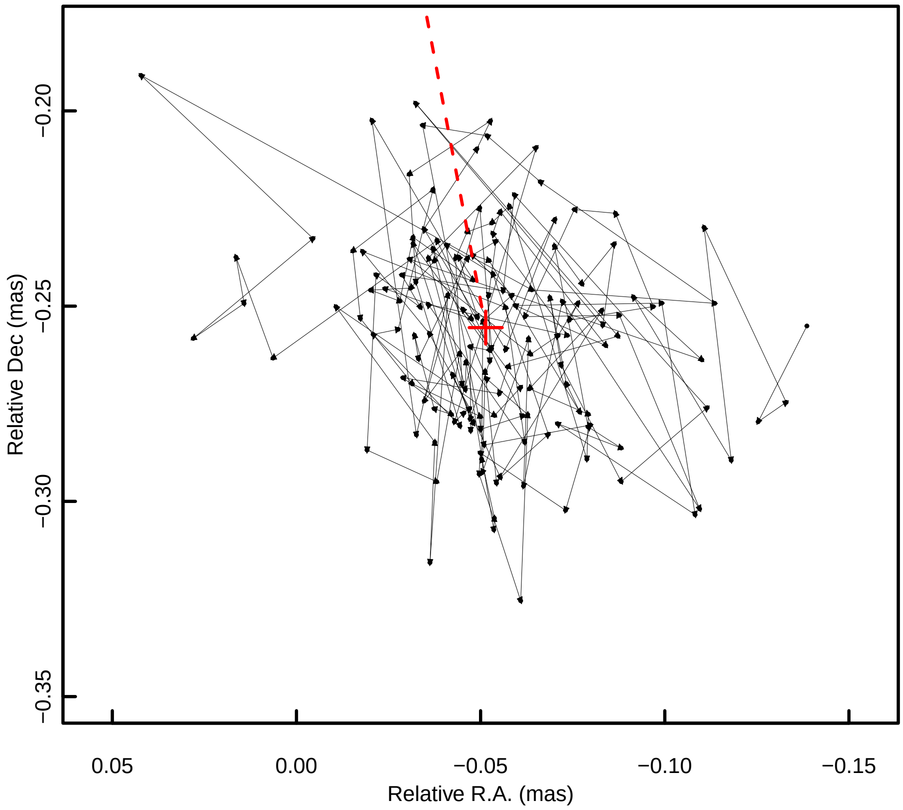

Figure 2: Observed trajectory of C7 in the RA–Dec plane. The central axis of the jet (red dashed line) connects the median position of C7 (red plus sign) and the radio core located at (0,0).

vector, which delineates the trajectory of C7 between two consecutive epochs of observations and indicates the direction of motion. The time intervals Δt between observations varied from a few days to several months with a median value of ≈ 30 days. The average C7 position uncertainties along and across the jet were estimated by Arshakian et al. (2020) to be 5 μas and 2 μas, respectively. They considered these values as lower limits, while real errors can exceed these estimates by a factor of 1.5–2.

Figure 2 shows the observed trajectory of C7 for a time period 1999.37–2019.97. The median center is at position $\mathrm{RA}_{\mathrm{med}} = -0.051$ mas and $\mathrm{Dec}_{\mathrm{med}} = -0.255$ mas. The dashed line connecting the radio core and the median center of C7 is the central axis of the jet, at the positional angle PA $= -169°$. The observed trajectory of C7 appears complex and zigzagging mainly due to significant displacements of the radio core along the jet axis.

3. Smoothing and cleaning the trajectory of C7

As we discussed above, to recover the C7 intrinsic motion it is essential to smooth out the wobbling of the core which happens primarily along the jet direction. For this we apply the moving average filter with a sliding window of four positions to smooth the observed trajectory on scales of ~ 0.05 mas. The size of the sliding window seems to be optimal for preserving the C7 intrinsic trajectory (Hambardzumyan et al., 2023), which is shown in Figure 3. Certain structural patterns such as oscillatory and reverse motions on various spatial scales are visible. Visual inspection of the smoothed trajectory is described in Hambardzumyan et al. (2023).

In addition to the core displacements, the observed C7 trajectory is affected by large positional uncertainties. Asymmetric 1σ positional errors of the C7 location overlap when the displacement is relatively small (Figure 4, left panel). This can lead to unreliable measurements of displacement vectors. To eliminate such non-robust displacements we propose a trajectory refinement algorithm. The algorithm works as follows: the length of the displacement vector (r) between two consecutive positions, and the positioning errors along the displacement vector (σ_1 and σ_2) are calculated. If r is greater than or equal to $\sigma_1 + \sigma_2$ (the ellipses do not intersect), the two positions are considered distinct; if r is less than $\sigma_1 + \sigma_2$ (the ellipses intersect), the algorithm discards the position with the larger error. This iterative process is applied to each pair of

doi: https://doi.org/10.52526/25792776-23.70.2-328

positions. The resulting refined trajectory is shown in Figure 4 (right panel) for the time period between 1999 and 2005. A detailed look at Figure 4 shows that some trajectory patterns have undergone changes after the refinement of the smoothed trajectory. In the left panel of Figure 4, the loop-like pattern positioned at about $(-0.07, -0.24)$ and having the counterclockwise motion turned into a clockwise sharp reversal (right panel). Transformation occurs also for the loop-like motions located at around $(-0.058, -0.277)$ and $(-0.047, -0.24)$ (see Figure 4, left panel). A total of five loop-like structures and seven reversed trajectories with a spatial scale of less than 0.01 mas (corresponding to a time scale of about 0.45 yr) transformed or flattened during the 20-year time period after the refinement procedure. Three of these trajectories changed their direction from anti-clockwise to clockwise. The full refined C7 trajectory for the time period from 1999 to 2020 is shown in Figure 5.

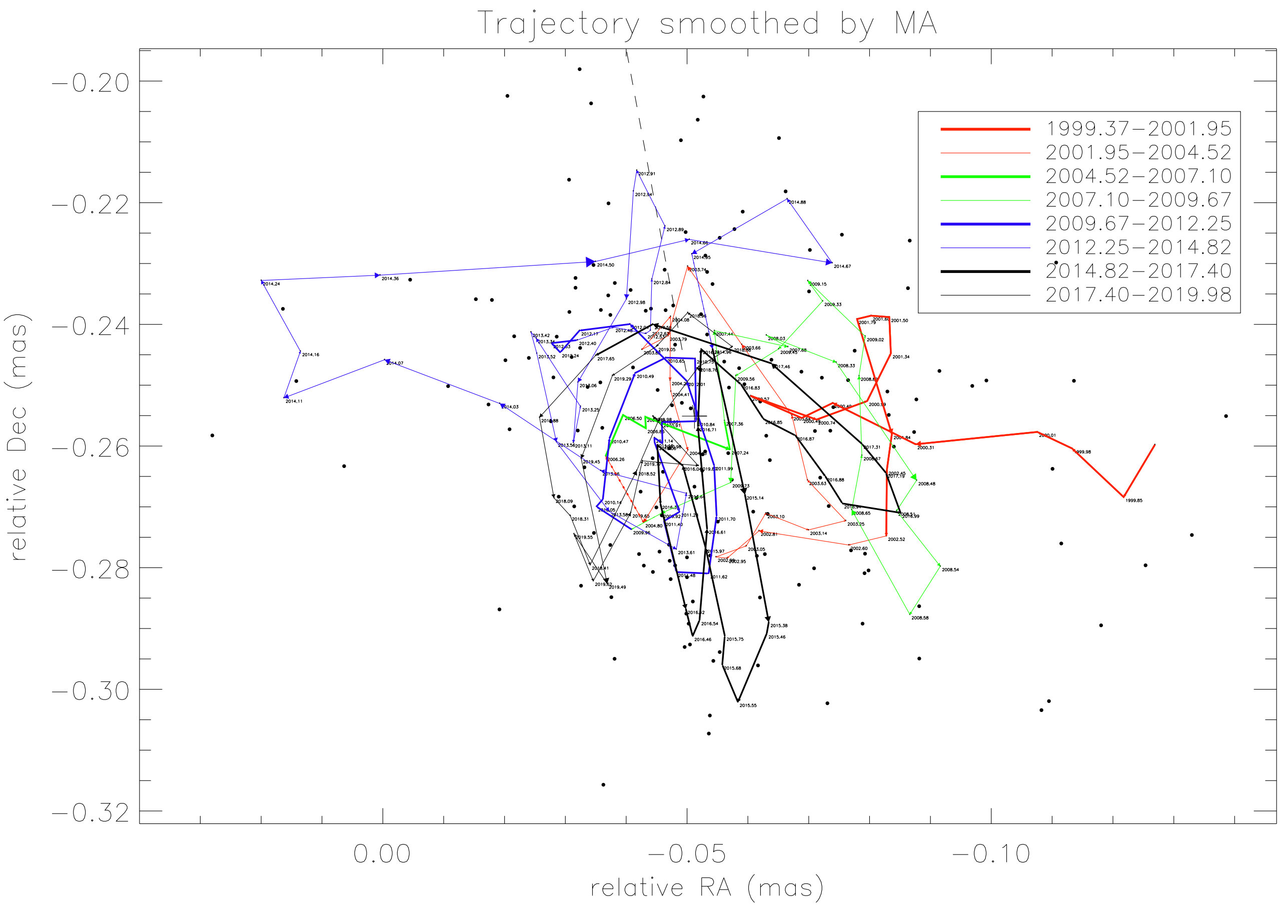

Figure 3: The apparent trajectory of C7 smoothed by moving average method with a sliding window of length $m = 4$. The numbers along the smoothed trajectory are the observation epochs in years (yr). The observed positions of C7 component are marked by dots. The radio core is at $(0, 0)$ position, which is connected with the median position of C7 (plus sign) by the jet central axis (dashed line). Thick and thin colored lines represent the time intervals of 2.95 yr. Arrows indicate the direction of movement.

doi: https://doi.org/10.52526/25792776-23.70.2-328

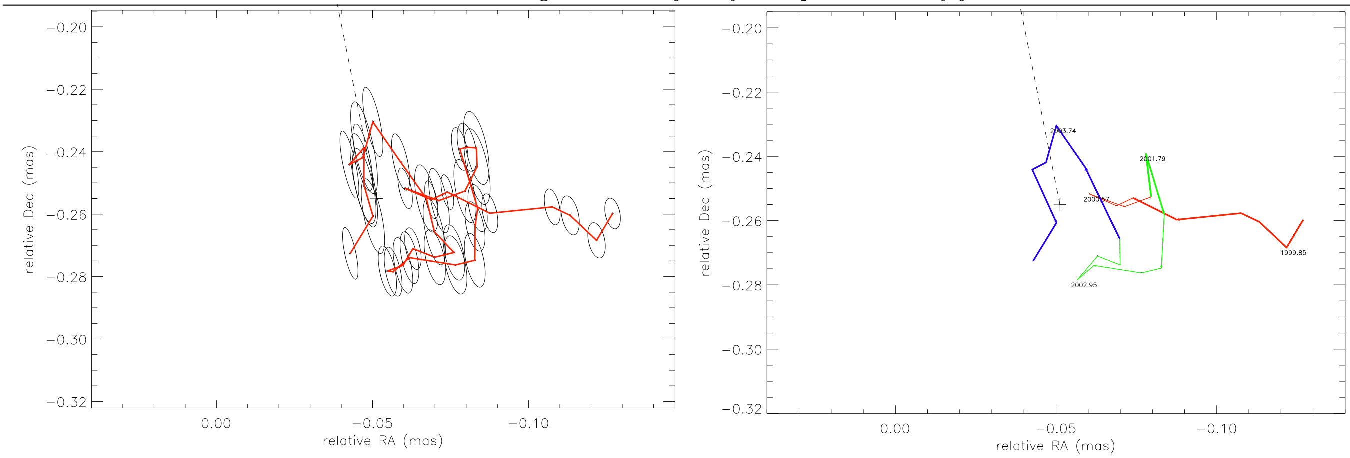

Figure 4: The smoothed C7 trajectory (left panel) and its refined version (right panel) are shown for the time interval 1999-2005. In the left panel, the asymmetric positioning errors are represented as ellipses where large and small radii correspond to the positioning errors along and across the jet axis, respectively. In the right panel, the turning points of the reversals are labelled by the epoch of observations.

Approximately 27% of positions are discarded by the cleaning algorithm, effectively eliminating trajectories on spatial scales $\lesssim 0.01$ mas (or 0.013 pc). The refined trajectory is further used for detailed investigation and classification. Upon visual examination of the trajectory, we observe both quasi-regular and irregular reverse motions. Reversible trajectories are either straight or curved and are accompanied by the occurrence of arc-shaped, loop-shaped, and W-shaped configurations as a turning point, although the latter are less common. The quasi-regular motion of C7 has a characteristic period of about 1.4 yr.

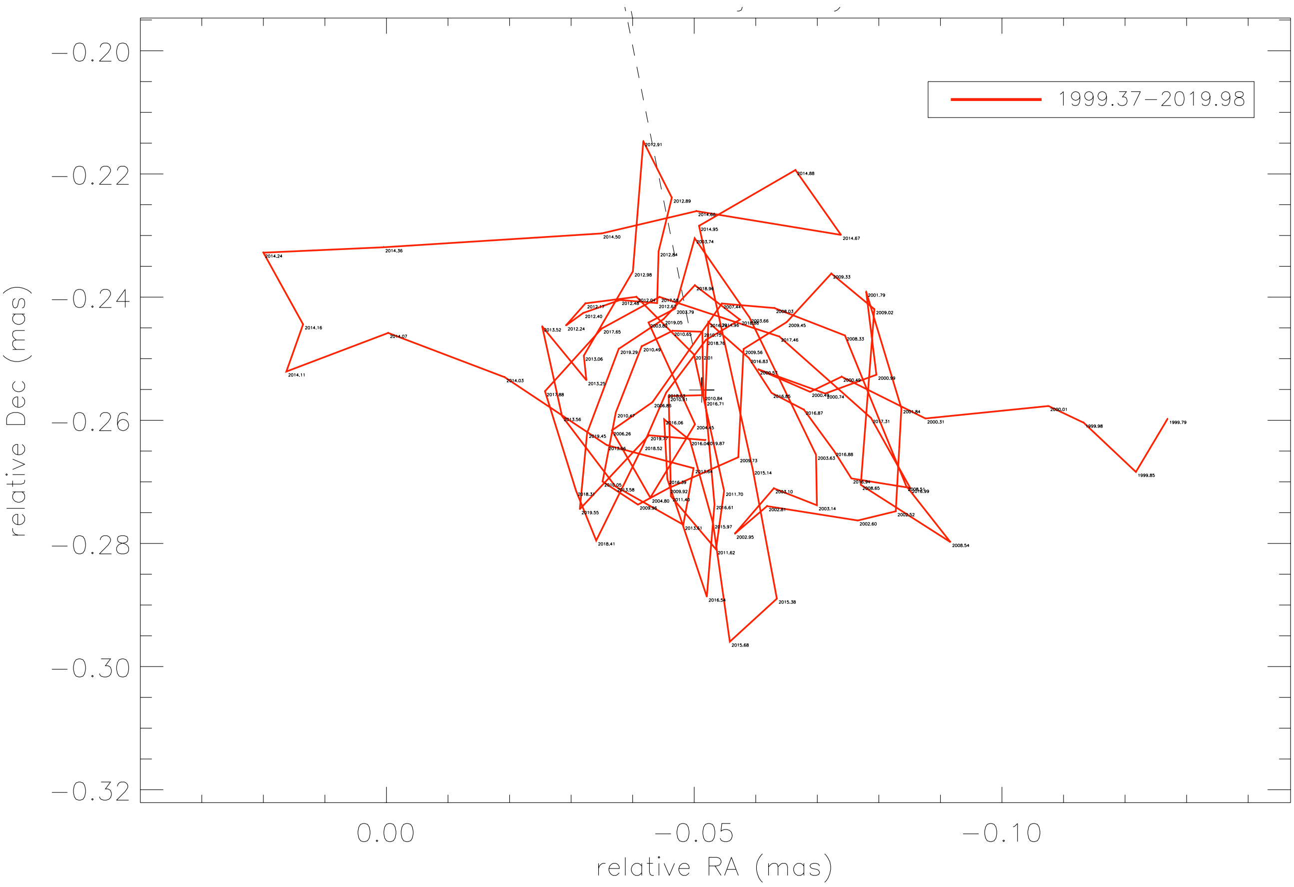

Figure 5: Refined trajectory of the smoothed C7 apparent trajectory. The radio core is at $(0,0)$ position, which is connected with the median position of C7 (plus sign) by the jet central axis (dashed line). The numbers along the trajectory are the epochs of observations in years from which the direction of motion can be determined.

doi: https://doi.org/10.52526/25792776-23.70.2-328

4. Characteristics of reversals

The refinement procedure eliminates scales smaller than 0.01 mas and improves the reliability of displacement vector measurements. The latter allows us to define a reversal as a trajectory in which two consecutive displacement vectors have an angle less than 90° at the turning point. A total of 24 reversals are identified, which are further classified as U-turns (angles $< 45°$), V-turns (angles $> 45°$ and $< 90°$), and loop-like reversals. The distribution of 22 distances between turning points of the reversals is shown in the Figure 6 (the distance between 2004.8 and 2006.4 is excluded from the calculations because of the large gap between observations). The distribution is not uniform, it appears to have two peaks at ~ 0.05 mas and ~ 0.11 mas. The mean value of the distances between turning points is 0.062 mas, and the standard deviation is 0.029 mas.

We now compare the reversal characteristics of the smoothed trajectory (Hambardzumyan et al., 2023) and the refined trajectory. We measure these characteristics in the same way as described in Hambardzumyan et al. (2023). After trajectory refinement, the time intervals between successive reversals typically range from 0.1 yr to 1.4 yr, excluding the two outliers. The typical reversal period is about 0.65 ± 0.08 yr. Prior to trajectory refinement, the median time interval is 0.50 ± 0.09 yr. The azimuthal angle, which is the angle between the jet axis and the line connecting the median centre and the turning point, has a uniform distribution for both smoothed and refined trajectory reversals. The distributions of radial distances from the median centre of the scattered positions to the turning points of the reversals have clustering around 0.029 ± 0.003 mas and 0.032 ± 0.004 mas for the smoothed and refined trajectories, respectively. In general, the estimates of the statistical characteristics of the reversals for these two trajectories coincide within the errors.

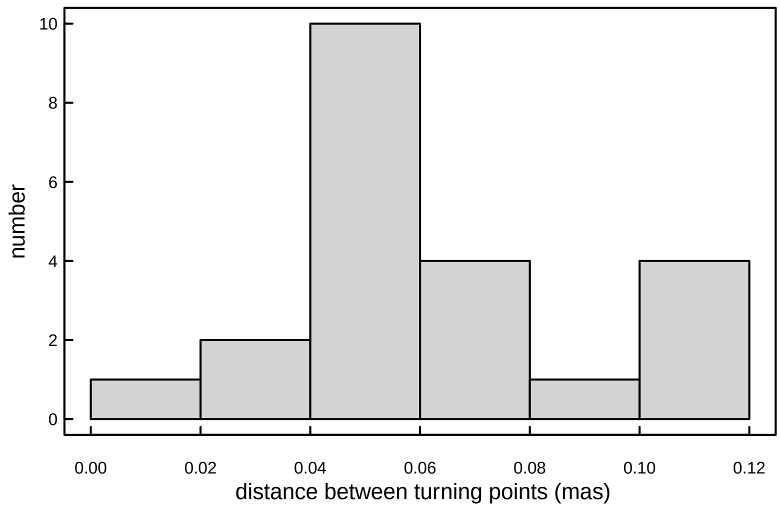

Figure 6: The distribution of distances between turning points of 22 reversals.

Acknowledgements

The VLBA is a facility of the National Radio Astronomy Observatory, a facility of the National Science Foundation that is operated under cooperative agreement with Associated Universities, Inc. This research has made use of data from the MOJAVE database that is maintained by the MOJAVE team (Lister et al., 2018).

References

Arshakian T. G., Pushkarev A. B., Lister M. L., Savolainen T., 2020, Astron. Astrophys. , 640, A62

Cohen M. H., et al., 2014, Astrophys. J. , 787, 151

Cohen M. H., et al., 2015, Astrophys. J. , 803, 3

Hambardzumyan L. A., Arshakian T. G., Pushkarev A. B., 2023, Communications of the Byurakan Astrophysical Observatory, 70, 94

doi: https://doi.org/10.52526/25792776-23.70.2-328

Komatsu E., et al., 2009, Astrophys. J. Suppl. Ser. , 180, 330

Lister M. L., et al., 2009, Astron. J. , 138, 1874

Lister M. L., Aller M. F., Aller H. D., Hodge M. A., Homan D. C., Kovalev Y. Y., Pushkarev A. B., Savolainen T., 2018, Astrophys. J. Suppl. Ser. , 234, 12

Lister M. L., Homan D. C., Kellermann K. I., Kovalev Y. Y., Pushkarev A. B., Ros E., Savolainen T., 2021, Astrophys. J. , 923, 30

Vermeulen R. C., Ogle P. M., Tran H. D., Browne I. W. A., Cohen M. H., Readhead A. C. S., Taylor G. B., Goodrich R. W., 1995, Astrophys. J. Lett. , 452, L5

doi: https://doi.org/10.52526/25792776-23.70.2-328

Application of small spacecraft for automatic identification of vessels

S.B. Makarov *[1], S.V. Zavjalov[1], S.V. Volvenko[1], I. Lavrenyuk[1], I.N. Gorbunov[1], M.Ya. Vinnichenko[1], A.K. Aharonyan[2], and V.H. Avetisyan[2]

[1]Peter the Great St. Petersburg Polytechnic University, St. Petersburg, Russia
[2]Russian-Armenian University, Erevan, Armenia

Abstract

The work is devoted to the development of a specialized complex based on a CubeSat 3U nanosatellite for receiving and processing signals from the AIS system. With the help of such system, it is planned to form a domestic AIS space constellation. The urgency is connected with the current absence of the Russian Federation's own satellite means of obtaining AIS data for monitoring the movement of ships in the world's oceans and in its own water area. Access to this data is becoming critical in connection with the development of the Northern Sea Route and the development of shipping in the Azov, Black Seas and the Far East.

Keywords: *CubeSat, AIS, space receiver, marine communication systems*

1. Introduction

The AIS system is a set of transceivers located both on ships and at coastal base stations (Chen & Wu (2023), Putra et al. (222)). These devices are capable of exchanging information about ships - location, course, speed, and other technical data. AIS also allows the exchange of additional information, which is provided by the standards, including broadcast and address messages (Spadon et al. (2023), Oumimoun et al. (2022)). Since the AIS operates in the VHF band and the installation height of the transceivers is limited by the height of the vessel, the communication range is on average about 50-70 km (about 30 nautical miles). This determines the size of the zone in which the ships can exchange all the information provided. The AIS uses a self-organizing multiple access system, which guarantees the ability to receive and transmit messages without conflicts with other transceivers within the same zone.

If the ship is far from the coast, it is not possible to exchange information with the base station, which raises the problem of monitoring remote ships. To solve this problem, spacecraft are used. A nanosatellite platform is used as such a device - a simple, reliable and proven solution with low cost and the possibility of mass production.

2. Satellite AIS receivers

On August 9, 2022, on the "Soyuz-2.1B" launch vehicle, several CubeSat 3U spacecrafts were launched into orbit, carrying a payload - on-board space receivers of AIS signals. Since 2023, AIS data collected by these vehicles from orbit has already been used for monitoring and safety of the movement of fishing vessels. The spacecraft themselves were developed by Sputnix in collaboration with leading Russian universities (Fig. 1). These nanosatellites have been launched into Earth orbit and are still active and functioning.

The onboard AIS receiver is a hardware and software system designed specifically for installation in a CubeSat satellite (Fig. 2). The device was developed and tested at Peter the Great St. Petersburg Polytechnic University. The receiver receives and processes AIS signals transmitted on 161.975 MHz and 162.025 MHz channels from transmitters of both class A and class B (with reduced power). The receiver has one antenna input. The sensitivity of the receiver allows it to confidently receive signals with a power of 2 W at distances of more than 2500 km. All processing and decoding is done directly in the on-board receiver.

doi: https://doi.org/10.52526/25792776-23.70.2-335

Figure 1. Left: spacecraft CubeSat 3U SXC3-214-MIET-AIS, on which the onboard receiver of AIS signals is installed. Right: spacecraft CubeSX-HSE-2, on which the onboard receiver of AIS signals is installed.)

.

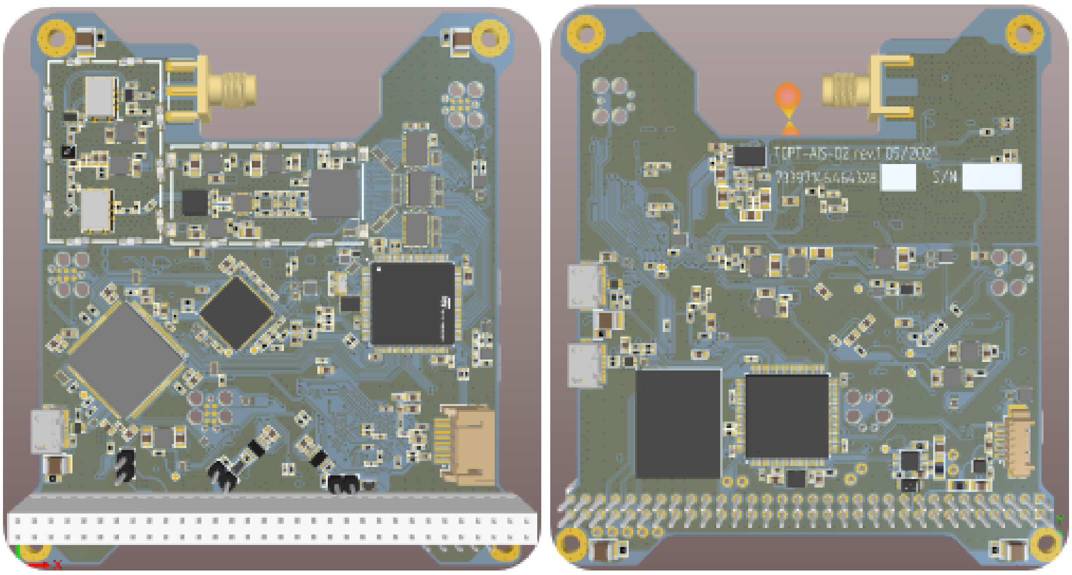

Figure 2. External view of the model of onboard AIS receiver.)

.

The device transmits the received information to the onboard computer of the spacecraft, then the collected information is dumped from the spacecraft to the Earth using a network of ground stations. The stations receive telemetry from vehicles, transmit control commands and receive information from the payload. Since the launch of the spacecraft, a number of tests have also been carried out, during which the correct functioning of the vehicles and the payload was assessed.

3. AIS information from space.

The result of processing information from the onboard AIS receiver is data on sea and river vessels, coast stations, buoys and other devices equipped with AIS transmitters. After processing using specialized software, you can display the location of ships on the map (Fig. 3), as well as build tracks for their movement. Fig. 4 shows accepted sea vessels on the Northern Sea Route, the Far East, as well as river vessels of the Russian Federation.

*makarov@cee.spbstu.ru, corresponding author

doi: https://doi.org/10.52526/25792776-23.70.2-335

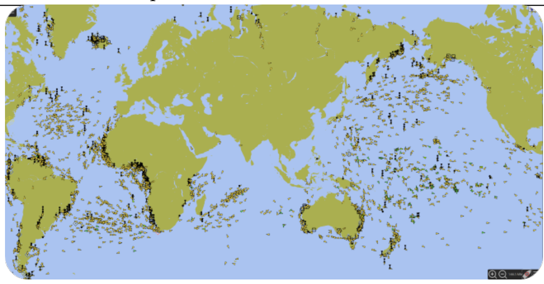

Figure 3. Visualization of information received from the onboard receiver.

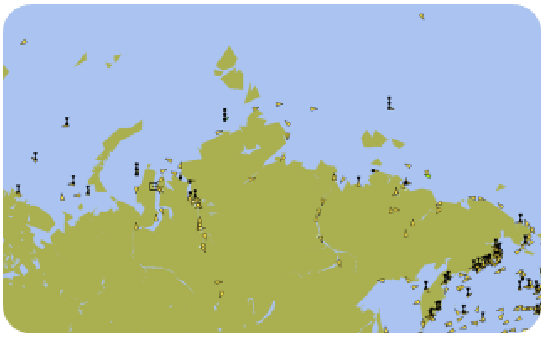

Figure 4. Display of sea and river vessels in the waters of the Russian Federation.

4. Conclusion

The launch of CubeSat format spacecraft carrying on-board AIS receivers as a payload was carried out. These devices were developed at Peter the Great St. Petersburg Polytechnic University. Spacecraft receive information for monitoring navigation: the name and ownership of the vessel, type and status, IMO number (number in the International Maritime Organization (International Maritime Organization)), location, course and speed of the vessel, date, and port of destination. The work was done under the Space-Pi program.

Acknowledgements

This work was supported by Ministry of Science and Higher Education of the Russian Federation (state assignment).

References

Chen M. Y., Wu H. T., 2023, IEEE Transactions on Industrial Informatics, 19, 870

Oumimoun B., Nahiri H., Idmouida A. e. a., 2022, IEEE Asia Pacific Conference on Wireless and Mobile (APWiMob), 11, 1

Putra W., Sumarudin A., Suheryadi A., Hidayat R., 222, 2022 International Conference on Electrical Engineering, Computer and Information Technology (ICEECIT), Jember, Indonesia, p. 95

Spadon G., Ferreira M., Soares A., Matwin S., 2023, IEEE Access, 11, 18821

doi: https://doi.org/10.52526/25792776-23.70.2-335

Communications of BAO, Vol. 70, Issue 2, 2023, pp.338-343

Kinematic structure of the stellar population of the solar neighborhood by Gaia DR3

E.S. Postnikova [*], S.V. Vereshchagin, N.V. Chupina, and D.A. Mosunova

Institute of Astronomy, Russian Academy of Science, Moscow, Russia

Abstract

The data of modern catalogs allow us to consider in detail the issue of the spatial velocity distribution. The stars in the solar vicinity make it possible to avoid errors and draw detailed conclusions about their kinematics. For a corrected study, we took a sample of stars from the Gaia DR3 within 300 pc. This area contains a number of star clusters and streams. It was found that in the circumscribed vicinity the direction of the stars is divided into several vast concentrations, the apex of motion of which lies in the direction of the motion of the Sun and in the direction of motion of the Ursa Major group, which in turn is divided into two separate groups in direction in space. In addition, a group of stars is considered, which, according to their kinematic characteristics, most likely belong to a halo or bulge. High-velocity stars are also considered under the assumption of their nature.

Keywords: *stellar kinematics, galaxy, stars*

1. Introduction

The vicinity of the Sun in the region of 300 pc is a fairly close region and here observations are not interfered with gas clouds, which makes it possible to select stars with the most reliable parameters in 6D phase space. Investigation of the solar vicinity are an important part of studying the structure of the Galaxy. In this region, low-luminosity stars are also available for study, the observation of which at large distances from the Sun is extremely limited.

It is believed that representatives of all galactic subsystems are located in the vicinity of the Sun. Such data is very important for stellar statistics. If the dependence of any parameters on the galactocentric distance are known, it is possible to obtain a quantitative estimate of this value for the Galaxy as a whole. An example of such a parameter is the spatial density of stars in the circumsolar environment. The calculated distribution of the parameters of stars belonging to the solar vicinity are also quite reliable.

Gaia DR3 (2022) star data allows to select stars with the most reliable phase space determinations. Residual velocities and chemical composition carry information about the chemical and dynamic evolution of the Galaxy and the formation of its subsystems. An effective tool for extracting this information is complex statistical studies of the indicated characteristics of stars in the galactic field and star clusters.

In this paper, the putative stars of the galaxy halo in the vicinity of the sun have been considered, their percentage have been estimated, high-velocity stars have been considered, proposals have been made about their origin, as well as large-scale kinematic structures in the selected vicinity have identified using the AD-diagram method.

2. Data selection

The sample of stars located at a distance from the Sun up to 300 pc was taken from the Gaia DR3 (ref) catalog. The stars were selected according to the following criteria: $RUWE < 1.4$, $\sigma_\varpi/\varpi \leq 10\%$, $\sigma_{\mu\alpha}/\mu_\alpha \leq 10\%$ and $\sigma_{\mu\delta}/\mu_\delta \leq 10\%$.

Stars with available G and RV values were taken. No restrictions on radial velocity error were applied in order to obtain the most complete sample of stars. Thus, 1,412,752 stars were selected.

[*] esp@inasan.ru

doi: https://doi.org/10.52526/25792776-23.70.2-338

The chemical and astrometric data used to obtain the characteristics of the selected stars are obtained from APOGEE DR17(Abdurro'uf et al. (2022)), GALAH 3 (Buder et al. (2021)), LAMOST DR8 (Wang et al. (2023)) and Gaia DR3 (2022) catalogues, respectively.

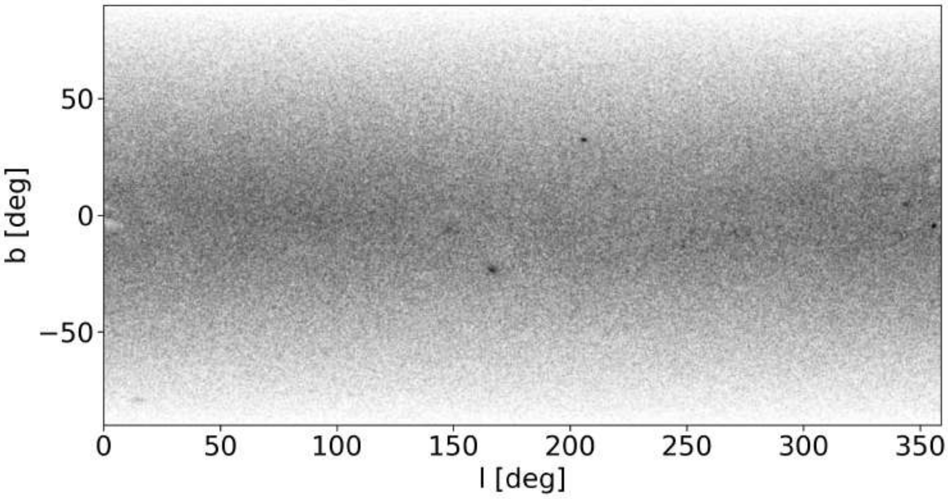

Figure 1. Distribution of stars in the galactic coordinate system (l, b), n=1,412,752

For all selected stars, a kinematic and spatial distribution was constructed. The position of stars in the sky is generally uniform, although the graph shows small clumps that are star clusters (Fig. 1).

The distribution of stars in the Galactic velocity components (UVW) calculation was considered according to the formulae and matrix equations presented in Johnson & Soderblom (1987). Here, we adopt a local standard of rest velocity V_{LSR} = 220 km/s Tian et al. (2015), and the solar peculiar motion $(U, V, W)_{Sun}$ = (-8.5, 13.38, 6.49) Coşkunoğlu et al. (2011). We use this $6D$ phase space information to study the kinematics of our sample stars in the Galaxy.

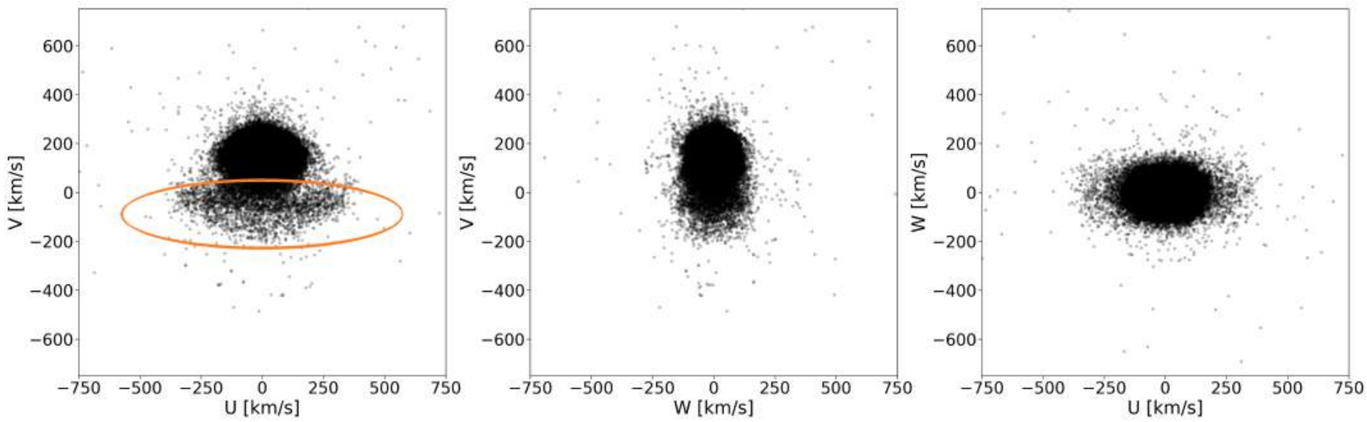

Figure 2. Distribution of velocity components relative to the Galaxy center (GC) of the entire sample. The supposed halo population is highlighted in an orange oval.

Figure 2 shows the distribution of velocities of stars in our sample. As you can see, it is predominantly approximately elliptical. The isolated parts and inhomogeneities are visible on the VU and VW planes. In Gaia Collaboration et al. (2018), this is explained by the fact that in the solar vicinity there are a number of moving groups and dynamical streams and the existence in this region of under-density of stars, as well as stars of other substructures of the Galaxy. If we look at the UW plane, we see that the bottom part of the diagram differs from the central part. In the Fig. 2 this area is circled with an oval. We assume that these are possible halo stars, the population of which also penetrates to the disk. Halo stars are characterized by the fact that they move in highly elongated orbits. In addition, the plots show a small number of stars with high velocities, lying far beyond the main clump. These can be high-velocity stars of various origins, such as, for example, disintegrated close binaries stars or it can be accelerated by a massive galactic nucleus, or those that came to us from other galaxies.

To separate the populations of the disk and other parts of the galaxy, the Toomre diagram (Fig. 3) was

doi: https://doi.org/10.52526/25792776-23.70.2-338

used, which is often used to distinguish stars by their kinematic properties. The abscissa axis shows the galactocentric velocity V_{LSR}, that is, the velocity of the object in the direction of rotation of the Galaxy. The orthogonal components of velocity $\sqrt{U^2_{LSR} + W^2_{LSR}}$ are plotted along the ordinate axis.

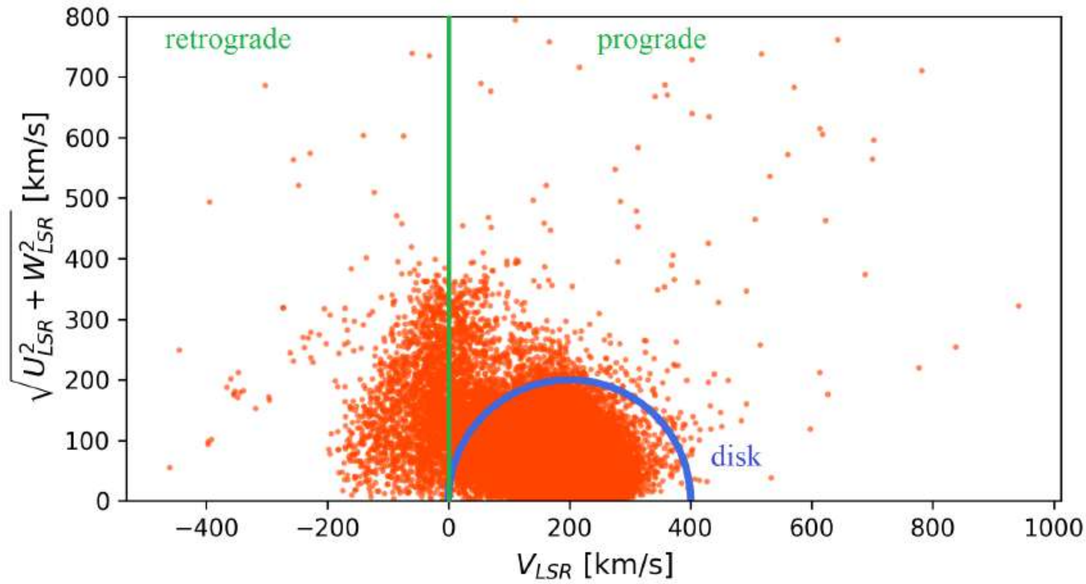

Figure 3. Toomre diagram of stars in the solar neighborhood. The blue semicircle line divide disk/non-disk Galaxy star population components. Green line divide retrograde and prograde stars.

Velocities that is, the velocity of the object in the direction of rotation of the Galaxy are plotted along the abscissa axis.

A semicircle in Fig. 3 separates the components of the disk and other populations, where the stars of the disk are chosen so that $|V - V_{LSR}| < 220$ km/s where $V_{LSR} = 220$ km/s. Here we use the definition of a halo, following Bonaca et al. (2017). It can be seen that many sources are concentrated precisely in the disk region. In addition, a more dispersed population with a greater spread of speeds is clearly visible. Thus, 3818 stars were selected, which will be further discussed in this paper.

3. Non-disk stars

The stars selected above were analyzed using metallicity from APOGEE DR17, GALAH3, LAMOST DR8 catalogs. For our sample, 170 stars were found in APOGEE, 67 stars in GALAH, and 58 stars in LAMOST. The distribution of stars by metallicity based on these catalogs is shown in Fig. 4. We also matched star in catalogs: GALAX and APOGEE - 3 matches, LAMOST and APOGEE - 9 matches, GALAX and LAMOST - 1 match. Metallicity value are mostly consistent with each other, however, the values for metallicity in LAMOST are slightly biased towards lower estimates regarding GALAX and APOGEE. Various authors give different estimates of what metallicity value “halo stars” start at, but on average it is -1 or -1.2 dex. As you can see (Fig. 4, left panel), there are quite a lot of such stars here, at least half. Previously, Carollo et al. (2007), based on SDSS data, revived the idea that the halo could be represented by two widely overlapping components. The inner halo peaks at $[Fe/H] \sim$ -1.6 dex, while the outer halo peaks around $[Fe/H] \sim$ -2.2 dex. In that idea our sample, for the most part, there are stars of the inner halo with $[Fe/H] \approx$ -1.2 $\pm$ 0.7 and very small traces of the outer halo around $[Fe/H] \sim$ -2.2, Fig. 4.

It is noticeable (Fig. 4) that our sample also contains a sufficient number of stars with disk metallicity ($[Fe/H]$ <-1.2). Some metal-rich stars are in retrograde orbits, some of them also have high velocities, not all stars with disk metallicity are in the disk region. Bonaca et al. (2017) obtained a similar result in their study. The existence of metal-rich stars in kinematically defined halo stars means that metallicity is not the best marker for separating galaxy populations. In other case the region is contaminated by stars from an extragalactic streams that has similar metallicity to that of the disk.

doi: https://doi.org/10.52526/25792776-23.70.2-338

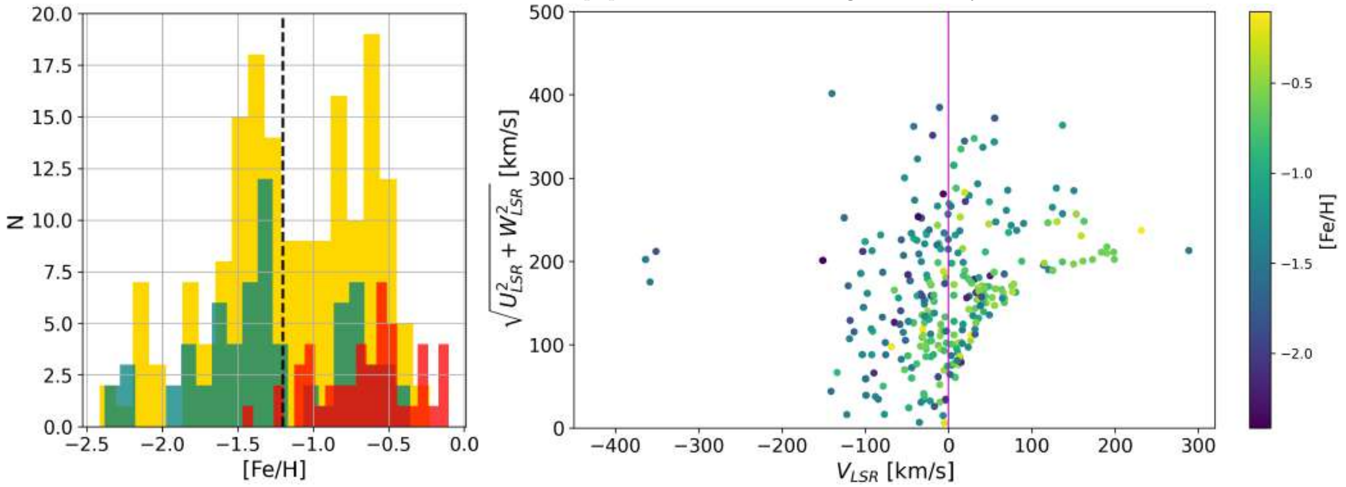

Figure 4. Left panel: distribution stars of our sample by metallicity on GALAX (green), LAMOST (red) and APOGEE (yellow) data. Black dashed line divide metallicity of disk and halo population. Right panel: Toomre diagram for non-disk population with metallicity grade. Violet line divided prograde and retrograde stars.

4. High-velocity stars

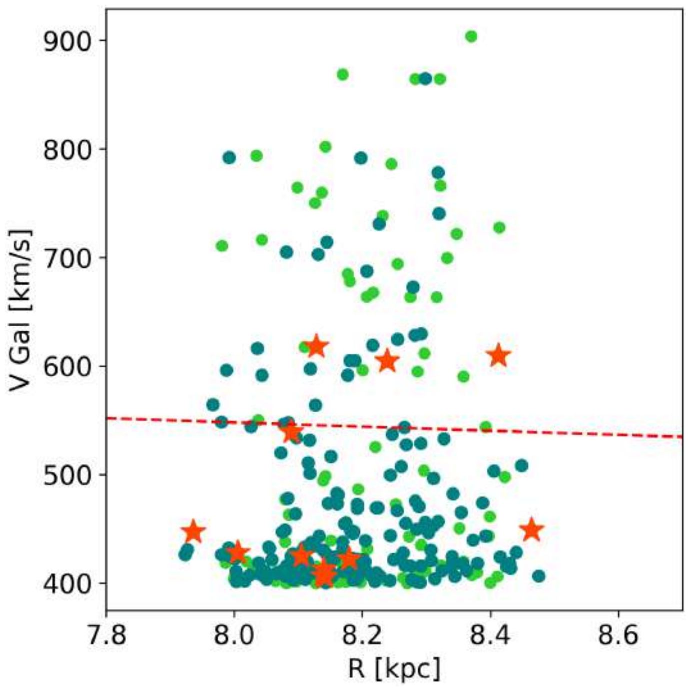

Figure 5. Total velocity in the Galactic rest-frame V_{Gal} as a function of the Galactocentric distance, R, for 286 hight-velocity stars with retrograde motion (dark-green dots) and prograde motion (light-green dots). Stars wit $[Fe/H]$ <-1.2 marked by asterisk. Red dashed curve is escape velocity for Galaxy potential from galpy (Bovy, 2022)

According to Du et al. (2019), stars whose spatial speed relative to the Galactic center is more than 400 km/s called high-velocity. There are 286 such stars in our sample. The place of their birth can be located both in the disk and in the bulge, and some originated from dwarf galaxies. Such stars in the Galaxy is associated with various mechanisms. The of origin of high-velocity stars may be due to the decay of close binary system as a result of supernova explosions, dynamic collisions between stars in dense star systems such as young star clusters, collisions between a single star and a double massive black hole in a GC. Halo stars can also reach high speeds when they are part of the debris of satellite galaxies destroyed by tidal interaction. Some stars formed in the disk and were then ejected into the halo.

doi: https://doi.org/10.52526/25792776-23.70.2-338

Marchetti et al. (2019). However, this work not provide an analysis of these mechanisms for all selected stars. Fig. 5 shows our sample of high-velocity stars plotted with respect the velocity of escape from the Galaxy and position relative to the center of the galaxy. As can be seen, some of these stars are located beyond the curve indicating the escape velocity at a given radius. It means that some of the stars in the sample have a potential to leave the Galaxy.

Our sample was also compared with other catalogs based on Gaia data. Unfortunately, most studies of high-velocity stars are for stars at large distances. A recent extensive study of 591 HVS Li et al. (2021) has only 1 such star within 300 pc - $GaiaDR2$ 2874966759081257728. According to LAMOST, its radial velocity RV = 233 km/s, but by Gaia DR3 used in this work, the speed is RV = -109.08±36.37 km/s, which, in correspondence with other data, excludes it from the list of high-velocity stars in our paper. Because it is spectroscopy binary star, this could lead to errors in determining its velocity. In Du et al. (2018) also contains high-velocity stars within 300 pc, but only HiVel 13 and HiVel 6 were included in our sample (HiVel 8 and 10 was rejected by $RUWE$ >1.4), the rest of the stars Li et al. (2021) did not meet our velocity criterion.

5. Large-scale structures by AD-diagram

To study of large-scale kinematics the method of AD-diagrams or the diagram of individual apexes of stars is used. We call the individual apex of a star a point on the celestial sphere with coordinates (A, D) in the equatorial coordinate system (A - right ascension, D - declination) that the star's spatial velocity vector points to when placed at the center. Below we consider not apexes, but antiapexes. On the celestial sphere, antiapexes and apexes are located at diametrically opposite points, the coordinates of which in longitude have a difference of 180°, and in latitude they differ in sign. A description of the method, diagramming techniques, and formulas for determining error ellipses can be found in Chupina et al. (2001).

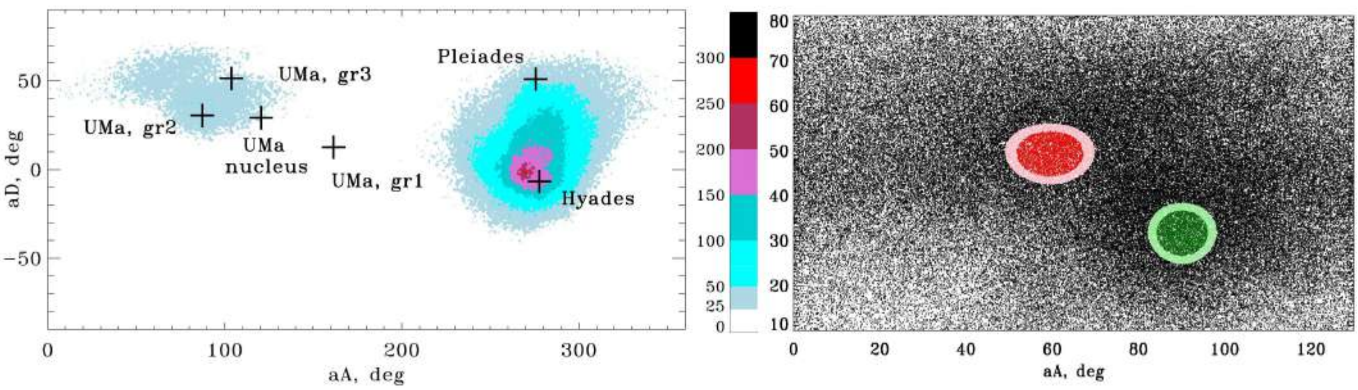

Figure 6. Left panel: antiapexes of stars and antiapexes of centers of star clusters and streams in the solar vicinity. Colorbar displays the number of stars per square pixel. On the right panel shown a sample of stars belonging to large-scale structures in UMa direction. Saturated red and saturated green areas are stars with probability of belonging $P \geq 60\%$ pale green and pale red $40\% \geq P < 60\%$.

In Fig. 6, the left panel shows a diagram of the density of our sample stars apexes. It is clear that there are pronounced overdensites in some clumps. Clumps on the right side at left panel, reflects the movement of the Sun in this region of the galactic disk with a centroid in the direction $(l, b) \sim$ (45°, 20°) (or $(ra, dec) \sim$ (265°, 21°)). The scattering relative to the centroid is associated with the spread of stellar velocities. The antiapexes of the two closest, richest clusters are clearly visible - the Pleiades (apex position by Elsanhoury et al. (2018)) and the Hyades (apex position by Postnikova et al. (2018)).

At the left panel concentration region on Fig. 6 we see the centroid coincides with good accuracy in the direction to the anticenter of the Galaxy. Possible that picture reflects the radial component of the movement of the Sun relative to nearby stars towards the center of the Milky Way at a speed of about 10 km/s. Near this concentration region are the apexes of various parts of the Ursa Major flow Vereshchagin et al. (2018), but is not part of the Ursa Major flow by their parameters. We identified concentration peaks and selected the most likely members of this structure. Within concentration peak 1 (red region, Fig. 6, right) contains 6051 stars with probability $P > 60$, and concentration peak 2 (green region) contains 5451 stars, respectively. The concentrations peaks equatorial coordinates of peak 1: (aA, aD) = (59.47±11.20° ,

doi: https://doi.org/10.52526/25792776-23.70.2-338

49.24±6.81°) and of peak 2 - $(aA, aD) = (90.16\pm5.71°$, $31.61\pm13.83°$).

As mentioned above, it is possible that this overdensity in velocity space is a consequence of the motion of the Sun, but it is also possible that the structure is a part of a larger galactic structure, more extensive than a star cluster or stellar streams, but much smaller than the galaxy arms. It is possible that the presence of such structures was described by Gaia Collaboration et al. (2018), who divides the velocity field in the solar vicinity into several regions.

6. Results

The kinematics of the stellar population in the solar neighborhood within 300 pc has been analyzed. The sample of stars was taken from the Gaia DR3 catalog. The sample is divided into two categories - stars belonging to and not belonging to the galactic disk. The latter may belong to a thick disk, halo, bulge and, possibly, other galaxies that are satellites of the Galaxy. There was insufficient data on the chemical composition and other data to most accurately analyze the origin of stars that kinematically do not belong to the disk. 286 high-velocity stars were discovered, including some that may eventually leave the galaxy. In the apex diagram, it was possible to identify three areas of concentration in the direction of motion of the stars using the apex positions: one large area on the right (associated mainly with the Hyades stream) and two areas of concentration of points on the left (associated with the Ursa Major stream) in Fig. 6.

Acknowledgements

This work used data from the European Space Agency (ESA) Gaia mission (https://www.cosmos.esa.int/gaia) processed by the Gaia Data Processing and Analysis Consortium (DPAC, https://www.cosmos.esa. int/web/gaia/dpac/consortium). Funding for DPAC was provided by national institutions, in particular those participating in the Gaia Multilateral Agreement. Gaia mission website: https://www.cosmos.esa.int/gaia. Gaia Archives website: https://archives.esac.esa.int/gaia. This study used the SIMBAD database (http://cds.u-strasbg.fr) operated by CDS, Strasbourg, France.

References

Abdurro'uf Accetta K., Aerts C., Silva Aguirre et al. 2022, Astrophys. J. Suppl. Ser. , 259, 35

Bonaca A., Conroy C., Wetzel A., Hopkins P. F., Kereš D., 2017, Astrophys. J. , 845, 101

Bovy J., 2022, galpy: Galactic dynamics package, Astrophysics Source Code Library, record ascl:1411.008

Buder S., Sharma S., Kos J., Amarsi et al. 2021, Mon. Not. R. Astron. Soc. , 506, 101

Carollo D., Beers T. C., Lee Y. S., Chiba et al. 2007, Nature. , 450, 1020

Chupina N. V., Reva V. G., Vereshchagin S. V., 2001, Astron. Astrophys. , 371, 115

Coşkunoğlu B., Ak S., Bilir S., Karaali S., Yaz et al. 2011, Mon. Not. R. Astron. Soc. , 412, 1237

Du C., Li H., Liu S., Donlon T., Newberg H. J., 2018, Astrophys. J. , 863, 87

Du C., Li H., Yan Y., Newberg H. J., Shi et al. 2019, Astrophys. J. Suppl. Ser. , 244, 4

Elsanhoury W. H., Postnikova E. S., Chupina N. V., Vereshchagin S. V., et al. 2018, Astrophys. Space. Sci. , 363, 58

Gaia Collaboration Katz D., Antoja T., Romero-Gómez M., et al. 2018, Astron. Astrophys. , 616, A11

Gaia DR3 2022, VizieR Online Data Catalog, p. I/355

Johnson D. R. H., Soderblom D. R., 1987, Astron. J. , 93, 864

Li Y.-B., Luo A.-L., Lu Y.-J., Zhang X.-S., Li J., Wang R., et al. 2021, Astrophys. J. Suppl. Ser. , 252, 3

Marchetti T., Rossi E. M., Brown A. G. A., 2019, Mon. Not. R. Astron. Soc. , 490, 157

Postnikova E. S., Vereshchagin S. V., Chupina N. V., 2018, in Stars and Satellites, Proceedings of the Memorial Conference Devoted to A.G. Masevich 100th Anniversary. Publisher, pp 228–234

Tian H.-J., Liu C., Carlin J. L., Zhao Y.-H., et al. 2015, Astrophys. J. , 809, 145

Vereshchagin S. V., Chupina N. V., Postnikova E. S., 2018, Astronomy Reports, 62, 502

Wang R., Luo A. L., Zhang S., Ting Y.-S., O'Briain T., Lamost Mrs Collaboration 2023, Astrophys. J. Suppl. Ser. , 226, 40

doi: https://doi.org/10.52526/25792776-23.70.2-338

Mid-infrared detectors for space electronics based on InAs-core/InP-shell nanowires

M.Ya. Vinnichenko *[1], R.V. Ustimenko†[1], D.A. Karaulov[1], D.A. Firsov[1], V.V. Fedorov[2], A.M. Mozharov[2], D.A. Kirilenko[3,4], I.S. Mukhin[1,2], H.A. Sarkisyan[5], D.B. Hayrapetyan[5], and E.M. Kazaryan[5]

[1]Peter the Great St. Petersburg Polytechnic University, Saint Petersburg, Russia
[2]Alferov University, Saint Petersburg, Russia
[3]ITMO University, Saint Petersburg, Russia
[4]Ioffe Institute, Saint Petersburg, Russia
[5]Russian-Armenian University, Erevan, Armenia

Abstract

The Mid-Infrared (MIR) spectral range is most important for free-space communications and astronomy. It contains radiation emitted by astrophysical objects during evolution of the planets, stars, galaxies and in particular by prebiosignature molecules on exoplanets. Nanowires (NWs) are expected to improve various optoelectronic devices, including IR photodetector technology. The bandgap of the catalystless InAs NWs can be tuned by introducing mechanical strain due to lattice mismatches in the core/shell NWs structures. Passivation with wider bandgap InP shell provide highly tunable functionality for future electronic devices. Temperature dependence of photoluminescence (PL) spectra of NWs InAs and InAs-core/InP-shell was acquired using Fourier-spectrometer. The position of the high-energy PL peak between calculated values of Eg for wurtzite and sphalerite structures confirms the formation of NWs into a combined polytype. Low energy PL peak is connected with parasitic bulk islands. Surface passivation successfully eliminates surface states and provides nontrivial temperature dependence of high-energy PL peak due to tensile and compressive strain in InAs core. Thus, detectors based on NWs InAs and InAs-core/InP-shell structures can operate in the MIR range of the spectrum with a wavelength from 2 to 5 μm.

Keywords: *nanowires, passivation, detectors, radiation sources, photoluminescence*

1. Introduction

The infrared (IR) spectral range is one of the richest windows of the electromagnetic spectrum emitted by astrophysical objects during the evolution of planets, stars and galaxies. The Mid-IR (MIR) region is most important for free-space communications and astronomy, since the high transparency of the atmosphere at 3–5 μm and 8–12 μm allows transmission without significant atmospheric absorption (Tan & Mohseni (2018)). So it allows to trace star and planet formation, allows to study the first phases of galaxy evolution through stars and accreting black holes. Moreover, searching for biosignatures lying in MIR spectral range on exoplanets can reveal evidence of active biological processes on worlds beyond the Solar System. Studying molecules in exoplanet atmospheres associated with life (biosignatures) and its origins (prebiosignatures) such as, hydrogen cyanide (HCN), hydrogen sulfide (H_2S), cyanoacetylene (HCN), carbon monoxide (CO), methane (CH_4), acetylene (C_2H_2), ammonia (NH), nitric oxide (NO), and formaldehyde (CH_2O), can give us insight into the geochemical and physical processes occurring on terrestrial exoplanets (Claringbold et al. (2023)).

Semiconductor nanowires (NWs) have great prospects as a platform for electronic devices. NWs are expected to improve various optoelectronic devices (Zhang et al. (2015)). This is possible thanks to their significant advantages over thin films, quantum wells, and bulk materials due to their small size and small area of contact with the substrate. NWs can be easily synthesized on lattice-mismatched substrates such

*mvin@spbstu.ru, corresponding author
†ratmirustimenko@yandex.ru

doi: https://doi.org/10.52526/25792776-23.70.2-344

as Si, cheap glass, and even plastics (Khayrudinov et al. (2020)). Semiconductor NWs are highly flexible due to submicrometer diameters. Thus, this is possible to improve properties in particular IR photodetector technology which has various applications such as: infrared astronomy, free space optical communications, search and rescue, surveillance, missile tracking, night vision, navigation, weather monitoring, pollution measurement and so on.

The narrow bandgap of the InAs NWs attracts wide attention as a building base of future IR photodetectors and radiation sources. It can be tuned by introducing mechanical strain due to lattice mismatches in the core/shell NWs, providing highly tunable functionality for future devices (Rota et al. (2016)). Surface passivation with a wider-gap semiconductor improves optical properties by removing the influence of surface states, which have a significant effect due to the large surface-to-volume ratio of NWs (Treu et al. (2013)).

Detectors based on InAs NWs operate in the MIR spectral range with a wavelength of 2 to 5 μm, like Near-IR spectrograph on the James Webb Space Telescope, which covers 0.6–5.3 μm wavelength range (Jakobsen et al. (2022)).

2. Samples and experimental setup

Catalystless pristine InAs NWs and an InAs-core/InP-shell NWs with a coherent shell, were grown by molecular beam epitaxy on Si(111). Scanning electron microscopy (SEM) images of the samples reveal a bottom up structure of array InAs NWs with some amount of parasitic three-dimensional islands (see Fig. 1). The average diameter of one NW was about 200 μm. A high-resolution transmission electron microscopy (HRTEM) study of single NWs reveals that all synthesized NW heterostructures have a random hexagonal close-packed (RHCP) structure consisting of a random sequence of cubic and hexagonal stacking.

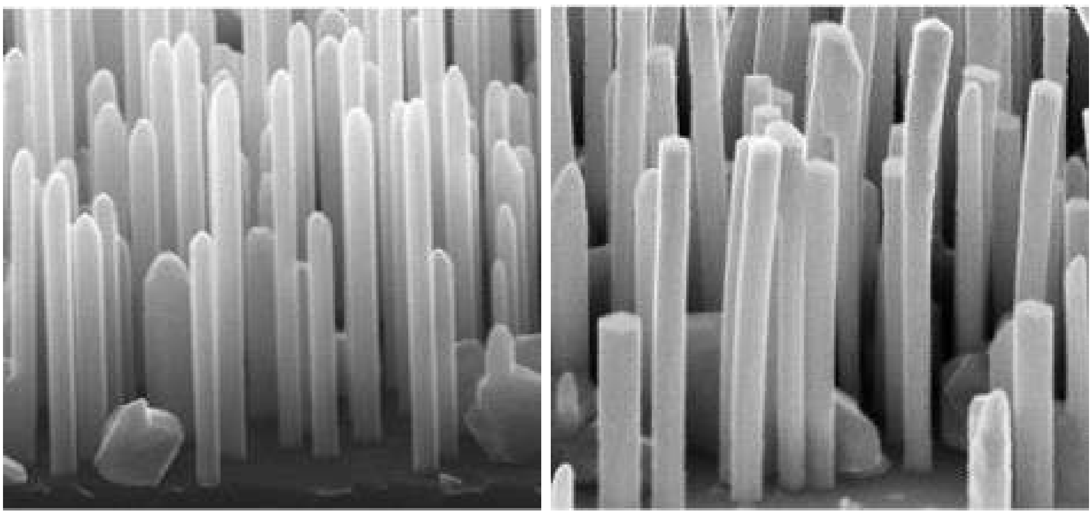

Figure 1. SEM images of pristine (on the left) and core/shell (on the right) InAs NWs.

.

The energy-dispersive X-ray (EDX) map in the vicinity of NW tip shows that a significant volume of InP is formed at tapered NW tip, while the thickness of the InP shell grown on the NW side walls varies between opposite NW side facets and tends to decrease to the base of NW. Also TEM, XRD, and Raman results show the mechanical strain in the studied InAs-core/InP-shell NWs.

Photoluminescence spectra were obtained with a vacuum Fourier-spectrometer (Bruker Vertex 80v) working in the step-scan mode, with a KBr beam splitter and a Ge entrance window on the liquid nitrogen-cooled indium antimonide (InSb) photodetector. The sample was mounted into a closed-cycle cryostat (Janis PTCM-4-7) covered with a mid-IR light transparent ZnSe window. Optical pumping of the samples was provided by using a continuous wave diode pumped solid-state Nd/YAG laser (with photon energy about 1.16 eV) with an optical chopper (340 Hz). A photoluminescence signal from InSb photodetector was demodulated using a SR830 digital lock-in amplifier.

doi: https://doi.org/10.52526/25792776-23.70.2-344

3. Experimental results

During investigation, cryogenic PL spectra of pristine InAs NWs (see Fig. 2) and heterostructured InAs-core/InP-shell NWs (see Fig. 3) at different temperature and different optical pumping power were obtained. Two PL peaks are visible in all spectra. The low-energy peak corresponds to PL from parasitic islands of the bulk InAs sphalerite phase, and the high-energy peak corresponds to PL from NWs . Position of the high-energy PL peak is between the calculated values for Eg of wurtzite (481 meV) and sphalerite (411 meV), which confirms the formation of NWs into a combined polytype. No significant effect of optical pump power on the shape of the spectra was found.

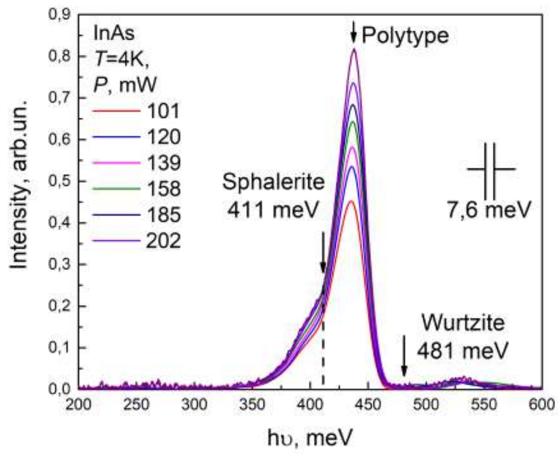

Figure 2. PL spectra of pristine NWs InAs at different levels optical pumping at 4 K.

With increasing temperature, the right PL peak of pristine InAs NWs behaves like Warshni low of Eg and moves to the low energy with the increase of temperature. Photoluminescence spectra of two different heterostructured InAs-core/InP-shell NWs with shell growth times of 10 minutes and 30 minutes demonstrate a nontrivial dependence on temperature of the position of the right PL peak. The PL signal level increases as the passivation layer increases, which indicates the successful elimination of surface states.

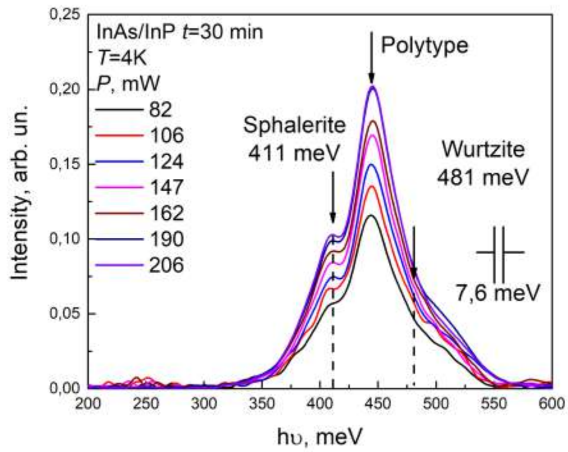

Figure 3. PL spectra of NWs InAs-core/InP-shell large shell at different levels optical pumping at 4 K.

On comparison of the PL spectra from three samples at same temperature and optical pumping, it can be seen that the PL spectra from passivated samples are shifted to higher energies, which indicates the presence of stresses exerted by the shell. The thicker the shell layer, the greater the compression and the greater the displacement.

doi: https://doi.org/10.52526/25792776-23.70.2-344

4. Conclusion

Thus, PL spectra of NWs pristine InAs and heterostructured InAs-core/InP-shell with different shell thickness were investigated. The bandgap of the InAs NWs can be adjusted by introducing mechanical strain due to lattice mismatche in the core/shell structure. Surface passivation with a wider-gap InP improves optical properties by removing the influence of surface states. So, it provides highly tunable functionality for future electronic devices in particular in IR photodetectors based on semiconductor InAs nanowires, wich can operate in the MIR range of the spectrum with a wavelength 2–5 μm, like Near-IR spectrograph on the James Webb Space Telescope, which covers 0.6–5.3 μm wavelength range.

Acknowledgements

This work was supported by the Russian Scientific Foundation (RSF project 22-19-00494) and Ministry of Science and Higher Education of the Russian Federation (state assignment).

References

Claringbold A. B., Rimmer P. B., Rugheimer S., et al. 2023, Astron. J., 166, 21

Jakobsen P., Ferruit P., Alves de Oliveira c., et al. 2022, A&A, 661, A80

Khayrudinov V., Remennyi M., Raj V., et al. 2020, ACS Nano, 14, 7484

Rota M. B., Ameruddin A. S., Fonseka H. A., et al. 2016, Nano Lett., 16, 5197–5203

Tan C. L., Mohseni H., 2018, Nanophotonics, 7, 169

Treu J., Bormann M., Schmeiduch H., et al. 2013, Nano Lett., 13, 6070–6077

Zhang Y., Wu J., Aagesen M., et al. 2015, J. Phys. D: Appl. Phys., 48, 29

doi: https://doi.org/10.52526/25792776-23.70.2-344

The Concept of the Massive Photon and its Astrophysical Implications

G.A. Saiyan *

Kelly Serrvices Incorporation, Educational Staffing, Missouri, USA

Abstract

We discuss the concept of the massive photon with its possible implications in astrophysics. We use the term "mass equivalent" instead of relativistic or effective mass. We also analyzed modified Planck's law and estimated (mean mass/rest mass) ratio in connection to the temperature of blackbody radiation of the massive photons. This ratio diverges at high temperatures and approaches unity at low temperatures.The "mass equivalent" for the CMB radiation was estimated to be equal to 0.0468% of the total mass of the Universe. We have discussed importance of the Breit-Wheeler process of particle – antiparticle production in the early Universe. We have evaluated the upper limit of the rest mass of the photon using gravitational and cosmological redshifts. A correlation was found between estimated masses of the photon and the lowest/highest frequencies of the spectral bands used for estimation of the mass.

Keywords: *the rest mass of the photon, optical dispersion in vacuum; modified Planck's law, gravitational and cosmological red shifts, linear regression*

1. Introduction

The question of whether photons have non-zero rest mass has been a subject of debates for many years. Being out of mainstream physical studies,this hypothesis is, nevertheless, of great interest in physics and astrophysics, and may have serious implications for field theories and cosmology as well as the theory of radiation transfer and physics of active astrophysical sources. The most rigorous mathematical foundation for findings pertaining to the massive photon hypothesis is the Proca equation (Poenaru et al., 2006, Tu et al., 2004), which can be reduced to the Klein-Gordon equation - the quantized version of the energy-momentum relation (also relativistic dispersion equation). Making use of these equations one can obtain an expression for optical dispersion in vacuum – frequency - dependent speed of light in free space. This term appears in the modified Planck's law (Torres-Hernanadez J., 1985), time dispersion (or frequency - dependent electromagnetic signal time arrival formula) and can be used to estimate relative speed of light variations at different frequencies from astrophysical sources (Biller S.D., 1999, Shaefer, 1999). In the last paragraphs we estimate the mass of the photon by making use of uncertainties in gravitational and cosmological redshifts and show the correlation between the rest mass of the photon and the lowest/highest frequencies of spectral bands used for estimation of the mass. (Breit G., 1934)

2. Energy-momentum relation

This relation is also known as the relativistic dispersion equation and is written in the form $E^2 = (pc)^2 + (\mu_\gamma c^2)^2$. Here E is the energy of a particle with the rest (invariant) mass μ_γ moving with the speed v, c is the invariant speed of light (included in Lorentz transformations) and $\vec{p} = \frac{E\vec{v}}{c^2}$ is its momentum. If we write $E = h\nu$, where h is the Plank constant ($h = 6.626x10^{-34}Js$), then we can derive the formula for the optical dispersion in vacuum (or "inherent dispersion" relation):

$$v = c\sqrt{1 - \frac{\nu_0^2}{\nu^2}} \tag{1}$$

Here $\nu_0 = \frac{\mu_\gamma c^2}{h}$ "rest frequency" (not to be understood literally). For $\nu_0 \ll \nu$ (1) can be reduced to $v = csqrt\left(1 - \frac{\nu_0 2}{2\nu^2}\right)$. These results be derived from the Proca equation (Tu et al., 2004).

*grigori$_s aiyan@hotmail.com$

doi: https://doi.org/10.52526/25792776-23.70.2-348

Table 1. Mass ratio vs. parameter b

b	0.01	0.1	1	5	10	20	70
$\frac{m}{m_\gamma}$	270.32	17.067	3.048	1.360	1.166	1.079	1.021

3. The mass equivalent

The relation (1) can be obtained from the formula for the "relativistic mass" (m) of the photon $m = \frac{m_\nu}{\sqrt{1-\frac{v^2}{c^2}}}$ the term that was a subject of multiple criticism by different authors (see Okun, 1989, Taylor E.F., 1992). We can rewrite this formula as follows $m = \frac{c}{\sqrt{1-\frac{m_\gamma^2}{m^2}}}$. It makes visible the fact that the invariant mass is zero if $v = c$. In the meantime, its "relativistic mass" (m) could be an arbitrary number. Although the double limit (when v approaches c and $_\gamma$ approaches zero) leads to the mathematical uncertainty $\frac{0}{0}$, the physical limit of the "relativistic mass" still does exist and equals to $m = \frac{h\nu}{c^2}$. The ratio on the right side has a dimension of mass and will be interpreted as "mass equivalent".

4. The photon mean mass equivalent for Planck spectrum

The mean energy of photons in Planck spectrum is $\langle\varepsilon\rangle \approx 2.701\,kT$ (R., 1978). Thus, the mean mass (equivalent) of the photon is $m = \frac{2.701kT}{c^2} = 4.148 \times 10^{-40}Tkg$. If we take $T = 10000K$ for a typical A-star, we obtain $\langle m\rangle = 4.148 \times 10^{-36}kg$. Comparing it with the mass of the electron $m_e = 9.109 \times 10^{-31}$ kg we see that the mean mass equivalent of the photon from A- stars is approximately $10^{-5} - 10^{-4}$ times lighter. Photons become heavier with increase in temperature. For CMB radiation $\langle m\rangle = 1.132 \times 10^{-39}kg$.

5. Modified Planck's law (MPL)

The blackbody radiation of massive photons can be derived from the partition function and for the spectral energy density takes the form (Torres-Hernanadez J., 1985):

$$\rho(\nu, \mu_\gamma, T) = \rho_0(\nu, T)\sqrt{1 - (\frac{m_\gamma c^2}{h\nu})^2}\;; \quad \rho(\nu, T) = \frac{8\pi h\nu^3}{c^3}\frac{1}{e^{h\nu}kT - 1}, \tag{2}$$

where $\rho_0(\nu, T)$ is the standard Planck,s law (PL). Graph of MPL is shown on Fig. 1. and is compared with PL for two different temperatures.

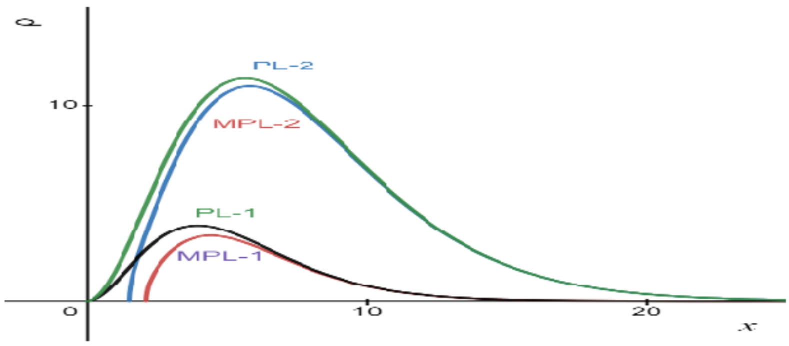

Figure 1. Modified (MPL) and regular (PL) Planck's laws.

The function 2 was used to calculate the mass ratio $\frac{\langle m\rangle}{\mu_\gamma}$ for different values of the parameter $b = \frac{m_\gamma c^2}{kT}$.

For high temperatures ($m_\gamma c^2 \ll kT$) $b \ll 1$ and MPL approaches PL, and the mass ratio tends to infinity. For low temperatures ($kT \ll m_\gamma c^2$) $b \gg 1$ and $m_\gamma \rightarrow < m >$. We can say that the upper limit of the invariant mass of the photon does not exceed the mean mass equivalent of the photon of the modified Planck spectrum. These calculations will be shown in more detail in a separate paper.

doi: https://doi.org/10.52526/25792776-23.70.2-348

6. The mass equivalent of the CMB radiation

CMB radiation is considered to be an example of the perfect blackbody radiation with temperature $T = 2.728\,K$. With its energy density $u = 4.17367 \times 10^{-14} J/m^3$ and the density of the mass equivalent $\rho = \frac{u}{c^2} = 4.6374 \times 10^{-30} kg/m^3$ in the volume of the Universe within the Standard Cosmological Model $V = 3.568 \times 10^{80} m^3$ (based on measured cosmological parameters, Bennet, 2013, Hinshaw G., et al, 2013, NASA/WMAP & Science team, 2011, Planck Collaboration et al., 2021) the mass of the CMB radiation is $M_C MB = \rho V = 1.655 \times 10^{51} kg$ or 4.6842×10^{-4} of the total mass of the Universe with the energy density (in mass units) $9.9 \times 10^{-27} kg/m^3$.

7. Breit-Wheeler process of particle-antiparticle pair production

As it may seem from the above, the mass of the photon tends to infinity with increase in temperature. However, the increased radiation density will result in $e^- e^+$ pair production from collisions of two photons (Breit G., 1934), which may prevent their mass growth. This (BW) process is found to have a very low probability $\sim 10^{-7} - 10^{-4}$ (Ribeyre & et al., 2016) with the cross section $\sim r_e^2, r_e \sim 2.8179 \times 10^{-15} m$ -classical electron radius. It was confirmed experimentally (Adam et al., 2021) when about 200 GeV energy level was achieved. The equivalent temperature for this energy is $\sim (10^{14} - 10^{15})\,K$, typical for and soon after the electroweak epoch of the Universe. How massive photons with finite Compton wavelengths may affect duration of the pre-combination epoch of the Universe is a question that, as far as we know, has not been discussed yet.

8. Gravitational redshift corrected for the optical dispersion in vacuum

The optical dispersion in vacuum discussed above results in additional redshift in spectra of astrophysical objects. Indeed, the gravitational redshift in the standard scenario is defined as

$$\frac{\Delta\nu}{\nu'} = \frac{r_g}{2r} \quad \Delta\nu = \nu - \nu' \quad (\nu > \nu') \tag{3}$$

where ν is the emitted frequency, ν' - observed frequency, r_g - gravitational radius, r is the distance from the center of gravity at which the redshift is measured. This equation can be rewritten in the following way, if we account for the optical dispersion effect in vacuum:

$$z = \frac{\Delta\nu'}{\nu'} = \frac{r_y}{2r}(1 + \frac{\nu_0^2}{\nu^2}) \tag{4}$$

This relationship shows that the gravitational redshift becomes more reddish with decrease in frequency and remains close to standard values when the frequency increases. If we denote ν" an observed frequency of radiation in the modified gravitational shift scenario and put $z' = \frac{\delta\nu''}{\nu"} = \frac{\nu' - \nu"}{\nu"}$, then the difference $\Delta z = z' - z$ can be interpreted in terms of uncertainties in measured redshifts. Using the existing accuracy of measurements $\sim 10^{-9} - 10^{-5}$ (Mueller H., 2010) one can find the upper limit of the mass of the photon by applying formula $\mu_\gamma = 7.362 \times 10^{-51} \nu \times \sqrt{\frac{\delta z}{z}}$ if δz and z are known. For the pulsar PSR J0348+0432 z=0.2226 (Xian-Feng & Huan-Yu, 2014). If $\Delta z = 7.5 \times 10^{-5}$ and $\nu = 10^1 5 Hz$, then $m_\gamma \sim 1.305 \times 10^{-39} kg$.

9. Modified cosmological redshift

Similar conclusions are true for the cosmological redshift as well. In non-relativistic standard scenario $V \ll c, z = \frac{V}{c}$, V is the recession velocity of a galaxy. If we denote $z' = \frac{V}{v}$, ν is the frequency-dependent speed of light, then $z^= z(1 + \frac{\nu_0^2}{2\nu^2})$ – modified redshift with optical dispersion in vacuum. Decrease in frequency makes redshift more reddish. Decrease in frequency makes redshift more reddish. If we assign the difference $\Delta z = z' - z$ to uncertainties in measured redshifts $\sim 10^{-4}$ (Rosseli & et al., 2022), then we find for the upper limit of the rest mass of the photon: $m_\gamma \leq \frac{h}{c^2} sqrt \frac{2}{z} \times 10^{-2} \times \nu$. For the galaxy Mrk 421 with the spectral band at $\nu = 10^{15}$ Hz, $\mu_\gamma \leq 5.933 \times 10^{-37}$ kg against the published one $2.1 \times 10^(-31)$ kg in γ-band with $\nu \sim 10^{26}$ Hz (Biller S.D., 1999, Shaefer, 1999). One can notice that both redshift-based estimates of the photon mass are linked to a frequency like many others.

doi: https://doi.org/10.52526/25792776-23.70.2-348

10. The correlation "Estimated mass of the photon vs frequency"

The mass of the photon in the Proca equation is a constant. But estimates of its upper limit can depend on the radiating energy generation mechanisms and its interactions with matter in space as well as experimental and observational factors. We have analyzed published data on estimates on upper limits of the mass of the photon (see Shaefer, 1999, Tu et al., 2004) and multiple refewrences therein) and have found the correlation between the mass (in grams) and the lowest/highest requency (in Hz) in specific spectral bands picked to evaluate the upperr limit of the mass in logarithmic scale $x = log(\nu), y = log(m_\gamma)$.The line of the best fit based on 29 points was found in the case of lowest frequency with the coefficient $R \approx 0.7709$ (for highest and midpoint frequencies $R \approx 0.513$ and 0.524, correspondingly). The linear regression is described by the equation $y = 0.59632x - 46.596$ and shown on Fig. 2. The standard deviation of differences between published and our recalculated mass logarithms $\sigma = 2.034$. Two examples are Mrk 421 galaxy with $m_\gamma \sim 1.061 \times 10^{-31}$ g against $2.1 \times 10^(- 28)$ g published and Gamma Ray Burst GRB 930131 with $m_\gamma \sim 1.073 \times 10^{-37}$ g against 7.4×10^{38} g (frequency 7.2×10^{18} Hz, Shaefer, 1999).

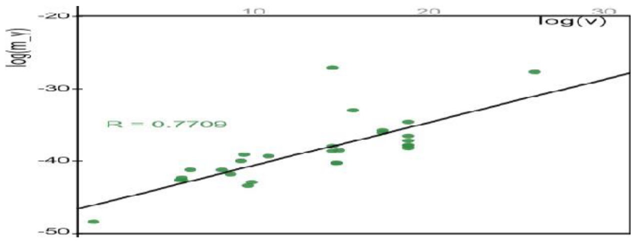

Figure 2. Estimated mass of the photon vs. frequency.

A few values of the mass associated with specific frequencies have been included in the statistics as well. The main conclusion is that the lower is the frequency used for measurements the lower is the estimated mass of the photon. These results will be discussed in more detail in a separate publication.

11. Conclusions

The hypothesis about the non-zero mass of the photon was discussed in connection with some astrophysical implications. We coin the term "mass equivalent" instead of traditionally used relativistic/effective mass. It is shown that the rest (invariant) mass of the photon can not exceed the mean value of the mass equivalent for Planck photons. The mean mass equivalent of the photon is proportional to the temperature of a blackbody radiation. The mass of the CMB radiation was found to be equal to 0.0468% of the total mass of the Universe. Corrections to the gravitational and cosmological redshifts, caused by the frequency - dependent speed of light, show that both redshifts are more reddish compared with their standard scenarios. A statistical study of published data shows that the lower is the frequency of radiation used to estimate the mass of the photon the lower is the value of the obtained mass.

Acknowledgements

The author is grateful to Dr. V. Airapetian from NASA for discussions and criticism as well as for the assistance in finding some archived materials.

References

Adam J., et al., 2021, Phys. Rev. Lett., 127, 052302

Bennet C.L. e. a., 2013, Astrophys. J. Suppl, 208, 20

Biller S.D. e. a., 1999, in Proceedings of 26th International Cosmic Ray Conference, August 17-25, 1999, Salt Lake City, Utah, USA. AIP Conf.Proc. 516 (2000),New York, p. 6

Breit G. W. G., 1934,] https://doi.org/10.1103/PhysRev.46.1087, 46

Hinshaw G., et al 2013, Astroph.J.Suppl.Ser., 208

Lowenthal D., 1973, Phys.Rev. D, 8

doi: https://doi.org/10.52526/25792776-23.70.2-348

Mueller H. Peters A. C. S., 2010, Nature, 463

NASA/WMAP Science team 2011, NASA's Wilkinson Microwave Anisotropy Probe, 24

Okun L. B., 1989, Physics Today, 42, 31

Planck Collaboration et al., 2021, Astron. Astrophys. , 652, C4

Poenaru D. N., Gherghescu R. A., Greiner W., 2006, in Exotic Nuclei and Nuclear/Particle Astrophysics. pp 152–159

R. F., 1978, Statistical Mechanics. Mir, Moscow,Russia in Russian

Ribeyre X., et al. 2016, Phys.Rev, E93, 013201

Rosseli H., et al. 2022, arXiv.2206,053313v.2,

Shaefer B., 1999, Phys.Rev.Lett., 82, 4964

Taylor E.F. Wheeler J., 1992, Spacetime Physics. 2nd edition. Freeman and Company, New York, USA

Torres-Hernanadez J. 1985, Phys. Rev. A., 32, 623

Tu L.-C., Luo J., Gillis G. T., 2004, Rep.Prog. Phys., 68, 77

Xian-Feng Z., Huan-Yu J., 2014, Rev. Mex. Astron. Astrofis., 50, 204

doi: https://doi.org/10.52526/25792776-23.70.2-348

Discovery of new red stars with digitized plates of the μ Cephei ragion

E. L. Karapetyan*[1], K. S. Gigoyan †[2], and G. R. Kostandyan ‡[2]

[1]Yerevan State University, Astronomy Department, 0025, Alex Manoogian 1, Yerevan, Armenia
[2]INAS RA V. Ambartsumian Byurakan Astrophysical Observatory (BAO), Byurakan 0213, Aragatzotn Province, Armenia

Abstract

The results of the spectral classification of 357 red stars observed in the Cepheus region are presented. 257 of the featured stars are included in the KP2001 catalogue. We found the remaining 100 red stars as a result of digitizing plates used in compiling the KP2001 catalog. All star data is taken from the *GAIA* DR3 database. These stars are most likely giants and supergiants. None of them were included in the catalog of variable stars. It has been suggested that further research may reveal variability in many of these.

Keywords: *red stars: variability*

1. Introduction

Stars M and C type or red stars play an important role in stellar evolution. They can be in various subsystems in the Galaxy. Studies of red stars are of great importance to interpret the stages of stellar development, as well as to understand the physics of the main sequence transitions - giant-supergiant-dwarf, as well as the detection of evolved stars of the late spectral class and their spectral studies. The observation material was obtained in 1970 with the 1-m Schmidt telescope of the Byurakan Observatory with $1^0.5$ and 4^0 prisms, covering the range $\alpha = 23^h32^m.7$, $\delta = +67^0$.

2. Discovery of new red stars with digitized plates

We detected the red stars on the digitized plates using standard image analysis software (FITS VIEW, SAO IMAGE ds9 and Aladin v11.0). The spectral classification of red stars was carried out primarily using spectra obtained using a 4° objective prism. To determine the subtypes of stars, we used the TiO $\lambda\lambda$ 7054, 7589, 8300, 8432 Å and VO $\lambda\lambda$ 7400, 7900 Å absorption bands wich are the main classification criterion. Figure 1 shows examples of low-resolution spectral shapes for the newly discovered objects on the digitized Plate which are red stars.

*e.karapetyan@ysu.am, Corresponding author
†kgigoyan@bao.sci.am
‡kostandyan@bao.sci.am

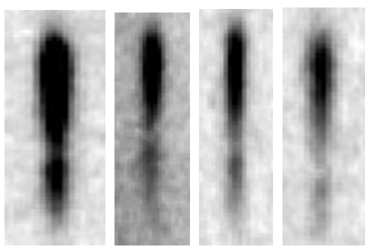

Figure 1. Low-resolution spectral shapes for the newly discovered 4 objects on BAO Plate Archive.

doi: https://doi.org/10.52526/25792776-23.70.2-353

Table 1. Gaia DR3 and 2MASS photometric data for the 10 new confermed red stars

RAJ2000 "h:m:s"	RAJ2000 "d:m:s"	2MASS	J mag	H mag	K mag	G mag	BP-RP mag
23 11 30.16	+66 30 19.13	23113015+6630191	8.06	6.96	6.44	11.95	3.532
23 12 29.20	+66 05 13.08	23122918+6605130	9.27	8.12	7.71	13.10	3.623
23 12 48.20	+68 13 56.12	23124820+6813561	9.08	7.93	7.51	12.94	3.689
23 12 50.47	+66 48 13.95	23125043+6648139	8.87	7.65	7.22	12.87	3.743
23 13 23.45	+67 43 42.82	23132344+6743429	8.76	7.35	6.66	13.36	3.909
23 14 09.44	+66 30 19.54	23140942+6630195	8.92	7.69	7.22	13.11	4.252
23 14 38.67	+66 40 54.40	23143866+6640544	8.73	7.55	7.17	12.38	3.091
23 14 53.85	+67 25 00.47	23145385+6725004	7.73	6.58	6.24	11.29	3.085
23 14 55.93	+68 17 02.82	23113015+6630191	8.06	6.96	6.44	11.95	3.532
23 15 06.16	+67 38 30.71	23122918+6605130	9.27	8.12	7.71	13.10	3.623

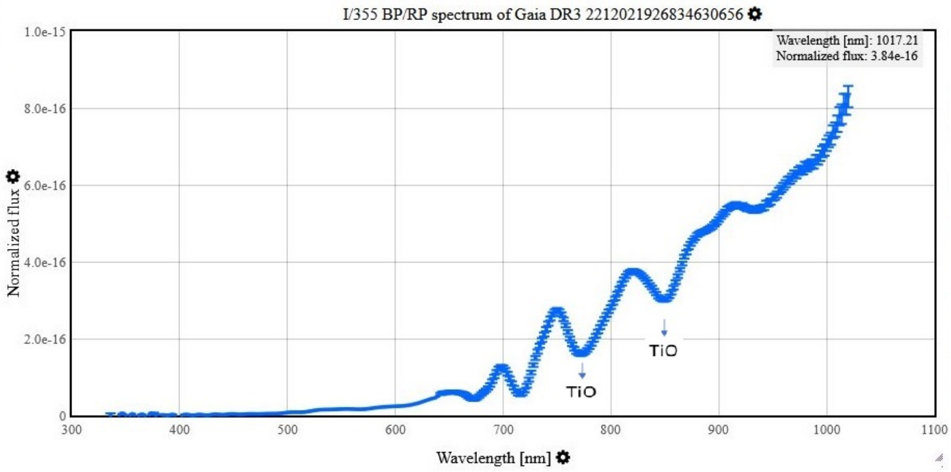

Figure 2. Gaia DR3 spectrum of the object Gaia DR3 2212021926834630656.

3. Gaia DR3 and 2MASS photometry

Table 1 presents the Gaia DR3 and 2MASS (Two Micron All-Sky Survey) JHKs photometric data for the 10 new red stars. We also used traditional color-color plots (J-H, H-K) to distinguish between the luminosity class of dwarfs and giants. The diagram clearly shows that most of the new objects are red giants and supergiants.

4. Gaia DR3 spectroscopy

All new objects were cross-matched with Gaia DR3 catalogue (CDS VizieR Catalogue I/355/gaiadr3) sources. Figure 2 presents Gaia DR3 low-resolution spectrum of the object Gaia DR3 2212021926834630656. Gaia low-resolution spectra are available at CDS ViziR data basa - I/355/spectra.

5. Summary

In the present work we found 100 red stars in a region of Cepheus with an area of about 17 deg^2 . We determined their spectral subtypes, which range from M0 to M10.

References

Bessell M. S., Brett J. M., 1988, pasp, 100, 1134

Brown et al., 2021, Astron. Astrophys. , 650, C3

Kazarian M. A., Petrosian G. V., 2001, Astrophysics, 44, 335

Nassau J. J., Stephenson C. B., Caprioli G., 1964, Astrophys. J. , 139, 864

doi: https://doi.org/10.52526/25792776-23.70.2-353

New M-type stars found in the BAO Plate Archive centered at $\alpha = +\ 15^h\ \delta = +58^0$

G. R. Kostandyan *and K. S. Gigoyan †

INAS RA V. Ambartsumian Byurakan Astrophysical Observatory (BAO), Byurakan 0213, Aragatzotn Province, Armenia

Abstract

The BAO Plate Archive low-resolution spectral plate centered at $\alpha = +\ 15^h\ \delta = +58^0$ is analyzed to find new late-type stars. 23 new late-type stars have been detected. New objects were cross-correlated with *GAIA* DR3, 2MASS, AllWISE, TESS and SDSS catalogues. For the detected objects, we present luminosity classes estimated from Gaia DR3 and 2MASS photometry and available proper motions. The majority of the objects are M dwarfs. Two objects are M giants.

Keywords: *late-type -stars: M dwarfs*

1. Introduction

Byurakan Astrophysical Observatory (BAO) Plate Archive is one of the largest astronomical archives in the world. BAO archive holds some 37.000 astronomical plates, films or other carriers of observational data. A project on Digitization of BAO Plate Archive and creation of BAO Interactive Astronomical Database (shortly BAO Plate Archive project, BAO PAP) was aimed at preservation of BAO valuable observational material accumulated during 1947-1991(Mikayelyan et al., 2021).

The BAO Plate Archive low-resolution spectral plate centered at $\alpha = +\ 15^h\ \delta = +58^0$ were obtained at the Byurakan Astrophysical Observatory on 14/15 April 1983 with the 1m Schmidt telescope, equipped with a 4^0 prism.

2. New BAO Plate Archive late-type stars

Low-resolution spectral plate was analyzed with the help of standard image analysis software (FITSVIEW and SAOImage ds9) and Aladin v11.0. This visualization allows us to detect red and faint candidate stars. M-type stars are easily distinguished owing to the absorption bands of molecular TiO at wavelengths of $\lambda\lambda$ 4584, 4762, 4954, 5167, 5500, 6200, 7054, 7589, 8300, 8432 Å(Gahm, 1970, Nassau et al., 1964). Figure 1 shows examples of of two-dimensional, low-resolution spectral shapes for the newly detected 2 objects on BAO Plate Archive which are M dwarfs.

3. Gaia EDR3 data

All new objects were cross-matched with Gaia DR3 catalogue (CDS VizieR Catalogue I/355/gaiadr3) sources. The low-resolution spectra for two objects are not available in the Gaia DR3 data base. Gaia DR3 data (Brown et al., 2021) allows an independent verification of our classification, and the O-rich nature are confirmed for the new objects. Figure 2 presents Gaia DR3 low-resolution spectrum for the object Gaia DR3 1617231147460075776.

*kostandyan@bao.sci.am, Corresponding author

†kgigoyan@bao.sci.am

doi: https://doi.org/10.52526/25792776-23.70.2-355

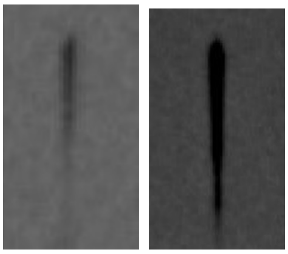

Figure 1. Low-resolution spectral shapes for the newly detected 2 objects on BAO Plate Archive.

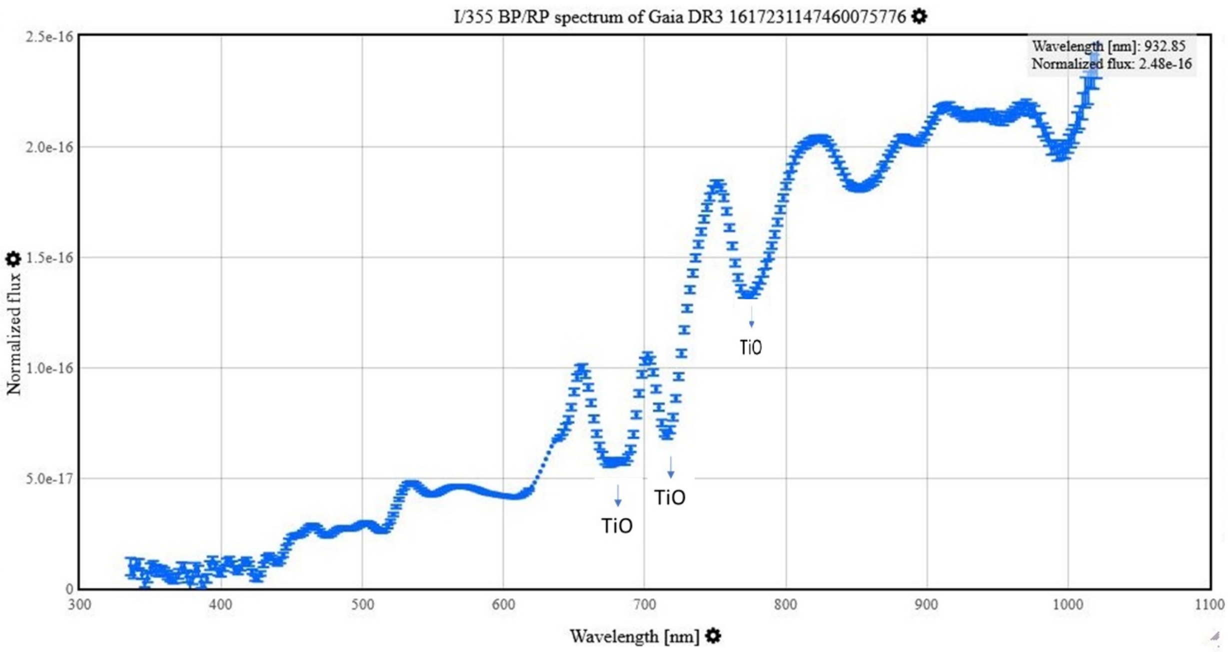

Figure 2. Gaia DR3 low-resolution spectrum for the object Gaia DR3 1617231147460075776..

doi: https://doi.org/10.52526/25792776-23.70.2-355

4. Summary

23 new M-type stars have been found in the BAO Plate Archive. In order to gain more information on the M dwarfs identified in the BAO Plate Archive, GaiaEDR3 high-accuracy astrometric and photometric data and Transiting Exoplanet Survey Satellite data are used to characterize these M-type stars. We present luminosity classes estimated from Gaia DR3, 2MASS, TESS photometry and available proper motions. Gaia DR3 data allows an independent verification of our classification, and the O-rich nature are confirmed for the new objects. The majority of the objects are M dwarfs. Two objects are M giants.

Acknowledgements

This research has made use of results from the SAO/NASA Astrophysics Data System Bibliographic Services, as well as the SIMBAD and VizieR databases, operated at CDS, Strasbourg, France, and Two Micron All Sky Survey, which is a joint project of the University of Massachusetts and the Infrared Processing and Analysis Center, funded by NASA and NSF.

References

Brown et al., 2021, Astron. Astrophys. , 650, C3

Gahm G. F., 1970, Astron. Astrophys. , 4, 268

Mikayelyan G. A., et al., 2021, Communications of the Byurakan Astrophysical Observatory, 68, 97

Nassau J. J., Stephenson C. B., Caprioli G., 1964, Astrophys. J. , 139, 864

doi: https://doi.org/10.52526/25792776-23.70.2-355

Morphological Study of Active Galaxies based on SDSS Images. Preliminary Results

V.K. Mkrtchyan [*], A.M. Mickaelian[†], H.V. Abrahamyan[‡], G.A. Mikayelyan[§] and G.M. Paronyan[¶]

NAS RA V. Ambartsumian Byurakan Astrophysical Observatory (BAO)

Abstract

Activity in galaxies has mainly two major forms: Active Galactic Nuclei (AGN) and Starburst (SB). Moreover, different types of AGN have different morphology. However, this question has not yet been properly investigated and due to old low-quality images, the morphology of many galaxies is not well described. SDSS images give a good possibility to homogeneously classify galaxies and investigate differences by the activity types. The concentration of the central part and the ratio between the central bulge and the total flux is a subject for detailed study. We use SDSS images to classify different types of active galaxies (both AGN and Starburst) and understand differences between QSOs, Seyferts 1 and 2, LINERS and Composites, as well as Starburst galaxies. The best expectation from our study will be the preliminary classification of active galaxies into activity types based on the images and before having their spectral types.

Keywords: *galaxies, active galactic nuclei, starburst galaxies, morphology*

Introduction

An Active Galactic Nucleus (AGN) is a compact and highly energetic region at the center of a galaxy, characterized by a high luminosity across the electromagnetic spectrum. AGNs are powered by the accretion of mass onto a Super Massive Black Hole (SMBH) located at the center of the galaxy. The intense radiation emitted from the AGN can outshine the combined light from the stars in the host galaxy.

Quasars are the most luminous objects in the Universe. Their luminosities can be thousands of times greater than that of an entire galaxy, making them visible across vast cosmic distances. Quasars exhibit high redshifts in their spectra, indicating that they are located at large distances from Earth. The high redshift is a result of the expansion of the universe and provides information about the quasar's age and the early stages of galaxy formation. Seyfert galaxies are a subtype of active galaxies, which have nuclei that emit much higher-than-expected energy levels. The activity is attributed to the presence of a supermassive black hole in the galactic center. Seyfert galaxies are more luminous than typical galaxies, but they are less luminous than quasars. The active nucleus contributes significantly to the total luminosity of the galaxy. Seyfert galaxies exhibit emission lines in their spectra. These lines arise from the ionized gas in the vicinity of the supermassive black hole. The emission lines in Seyfert galaxies are typically narrower than those observed in quasars.

Seyfert galaxies are classified into two main types based on the width of their emission lines:

Seyferts 1: These galaxies have broad emission lines, indicating high-velocity gas in the accretion disk around the central black hole.

Seyferts 2: These galaxies have narrower emission lines, suggesting that the line-emitting regions are more extended.

[*]varduhi.mkrtchyan.99@bk.ru, Corresponding author
[†]aregmick@yahoo.com
[‡]abrahamyanhayk@gmail.com
[§]gormick@mail.ru
[¶]paronyan_gurgen@yahoo.com

doi: https://doi.org/10.52526/25792776-23.70.2-358

Studied data

We selected 20 objects from Sy1 and 20 objects from Sy2 from the Catalogue of Quasars and Active Galactic Nuclei (VCV-13) and made up the isodenses for these objects using the "Aladin Sky Atlas[1]" software. We measured the ratio of the diameters of the images bounded by the largest and smallest isodenses and then calculated the average value of the obtained results.

Preliminary Results

The preliminary results show that most of the AGN have a strong concentration into their central parts; bulges or just the centre, whatever the central image is. There is a strict boundary between the central formation and the whole image, while for normal galaxies the transition is much smoother (gradual) and very often it is not easy to define the core at all. For the preliminary study, we used 20 Sy1 and 20 Sy2 type galaxies and obtained the average centre/total ratio around 0.12 and 0.13, respectively. We have tried to make a parallel study between the corresponding images and spectra where the core and stellar contribution is well defined (synchrotron continuum and emission lines on one hand and thermal continuum and absorption lines on the other). Further studies will involve much more statistics and will reveal the real morphological differences between different types of activity.

Summary

Active Galactic Nuclei (AGN) have different morphology. SDSS images give a good possibility to homogeneously classify galaxies and investigate differences by the activity types. The concentration of the central part is a subject for detailed study.

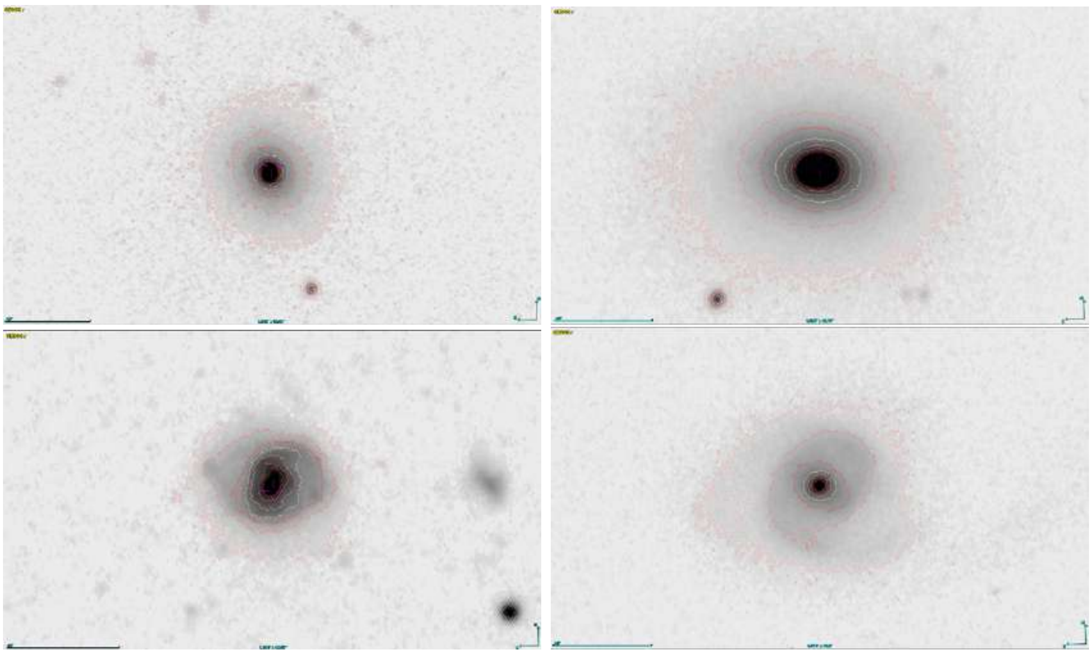

Figure 1. Isodenses for 4 Seyferts 1 galaxies using "Aladin Sky Atlas" software.

.

We use SDSS images to classify different types of active galaxies (both AGN and Starburst) and understand differences between QSOs, Seyferts 1 and 2, LINERS and Composites, as well as Starburst galaxies. For that used "Aladin Sky Atlas" software. The best expectation from our study will be the preliminary classification of active galaxies into activity types based on the images and before having their spectral types.

[1] https://aladin.cds.unistra.fr/

doi: https://doi.org/10.52526/25792776-23.70.2-358

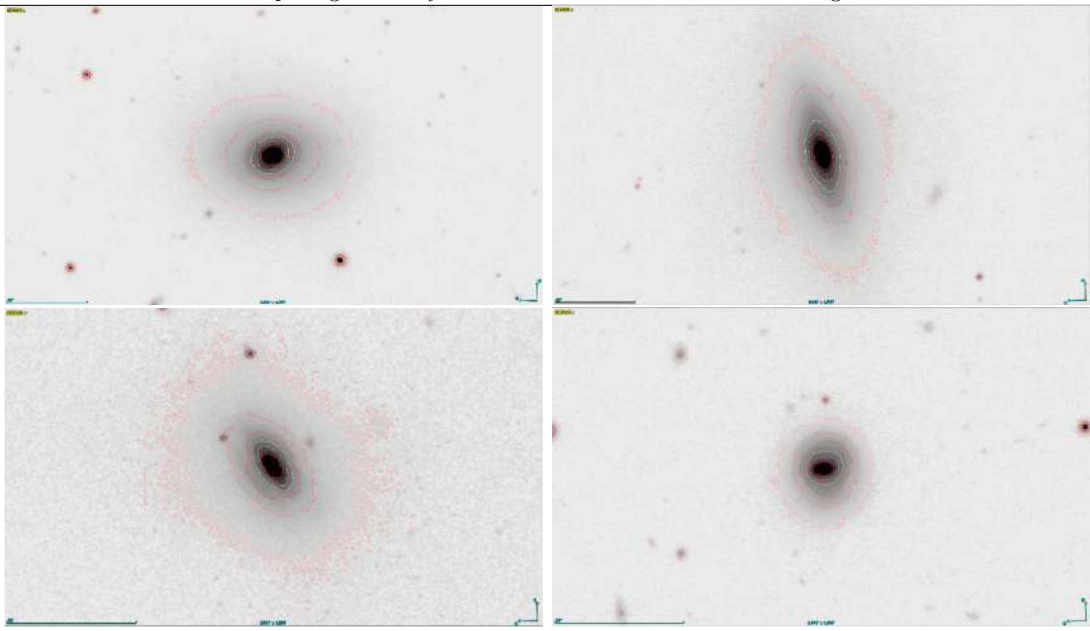

Figure 2. Isodenses for 4 Seyferts 2 galaxies using "Aladin Sky Atlas" software.

.

References

Abdurro'uf et al., 2022, Astrophys. J. Suppl. Ser. , 259, 35

Abrahamyan H. V., Mickaelian A. M., Mikayelyan G. A., Paronyan G. M., 2018, Communications of the Byurakan Astrophysical Observatory, 65, 1

Abrahamyan H. V., Mickaelian A. M., Paronyan G. M., Mikayelyan G. A., Gyulzadyan M. V., 2019, Communications of the Byurakan Astrophysical Observatory, 66, 1

Abrahamyan H. V., Mickaelian A. M., Paronyan G. M., Mikayelyan G. A., 2020, Astrophysics, 63, 322

Mickaelian A. M., 2015, Iranian Journal of Astronomy and Astrophysics, 2, 1

Mickaelian A. M., Abrahamyan H. V., Gyulzadyan M. V., Paronyan G. M., Mikayelyan G. A., 2018, Astrophys. Space. Sci. , 363, 237

Mickaelian A. M., Abrahamyan H. V., Paronyan G. M., Mikayelyan G. A., 2021, Frontiers in Astronomy and Space Sciences, 7, 82

Mickaelian A. M., Abrahamyan H. V., Mikayelyan G. A., Paronyan G. M., 2022, Communications of the Byurakan Astrophysical Observatory, 69, 10

Paronyan G. M., Mickaelian A. M., Harutyunyan G. S., Abrahamyan H. V., Mikayelyan G. A., 2019, Astrophysics, 62, 147

Paronyan G. M., Mickaelian A. M., Abrahamyan H. V., Mikayelyan G. A., 2020, Astrophysics, 63, 166

Véron-Cetty M. P., Véron P., 2000, Astron. Astrophys. Rev. , 10, 81

Véron-Cetty M. P., Véron P., 2010, Astron. Astrophys. , 518, A10

doi: https://doi.org/10.52526/25792776-23.70.2-358

Communications of BAO, Vol. 70, Issue 2, 2023, pp. 361-365

Analysis of the short wavelength range of QSOs

A. G. Sukiasyan,[*] A. M. Mickaelian,[†] H. V. Abrahamyan,[‡] G. M. Paronyan,[§] and G. A. Mikayelyan[¶]

NAS RA V. Ambartsumian Byurakan Astrophysical Observatory (BAO), Armenia

Abstract

In this work we try to classify objects using the MgII 2798 Å line from optical spectra. For that, we use BZQ type objects from BZCAT catalogue. From SDSS catalogues we have 618 BZQ objects which have optical spectra and only in 139 objects there are MgII and H_β lines simultaneously (z=0.3345-1.0915). By the shape of MgII lines, we grouped these spectra into 3 categories: Broad & Narrow, Broad+Narrow, and Broad.

Keywords: *QSO, MgII line, blazars, spectral classification*

1. Introduction

Among the Active Galactic Nuclei (AGN) the most interesting are blazars in combinations of two subtypes: a) BL Lac (BLL) objects and special types of quasars (QSO): Optically Violently Variables (OVV) and b) Highly Polarized Quasars (HPQ). A blazar is characterized as a very compact quasar, associated with a presumed Super Massive Black Hole (SMBH) at the center of an active giant elliptical galaxy. Blazars are the most energetic objects in the Universe. The object BL Lac was originally discovered by Hoffmeister as a variable star, and later it was identified by Schmitt as an extragalactic radio source. In Massaro et al. (2015) it was presented the blazar catalog BZCAT v.5, where the objects are distributed into 4 types: BZB (Lacertides, BL Lac or BLL), BZQ (Quasars), BZG (Galaxies), and BZU (Undetermined class).

2. Studied data

In this work, using BZQ sources from BZCAT catalogue, we compare their H_β line profiles with MgII ones. For the spectral data, we cross-corelated BZQ sources with SDSS catalogue. As a result, we have 618 objects which have optical spectra from SDSS catalogue. In the next step we choose objects which have H_β and MgII lines in the optical spectral range (3500-10500 Å). It made it possible to distinguish 139 objects which have both of lines in spectra. Using the shape of MgII line, we grouped these spectra in 3 categories: Broad & Narrow (broad line profile with clearly separated narrow line), Broad+Narrow (a broad component overlapped with narrow line), Broad (simple broad line without any details). In figures 2, 2, and 2 we give these categories.

3. Preliminary Results

In Table 3 (for 12 objects), we give the preliminary results of this work.

In Table 3, we give the shape of MgII line by the activity type for all 139 objects having SDSS spectrum with the presence of both MgII and H_β. A similar distribution is given in Figure 4. Some very preliminary distribution is observed; e. g. some subtypes have only some definite MgII shape (all NLQ1.0 are Broad & Narrow, all Narrow Line QSOs do not have MgII shape "Broad").

[*]andranik.suqiasyan.1995@mail.ru, Corresponding author

[†]aregmick@yahoo.com

[‡]abrahamyanhayk@gmail.com

[§]paronyan_gurgen@yahoo.com

[¶]gormick@mail.ru

doi: https://doi.org/10.52526/25792776-23.70.2-361

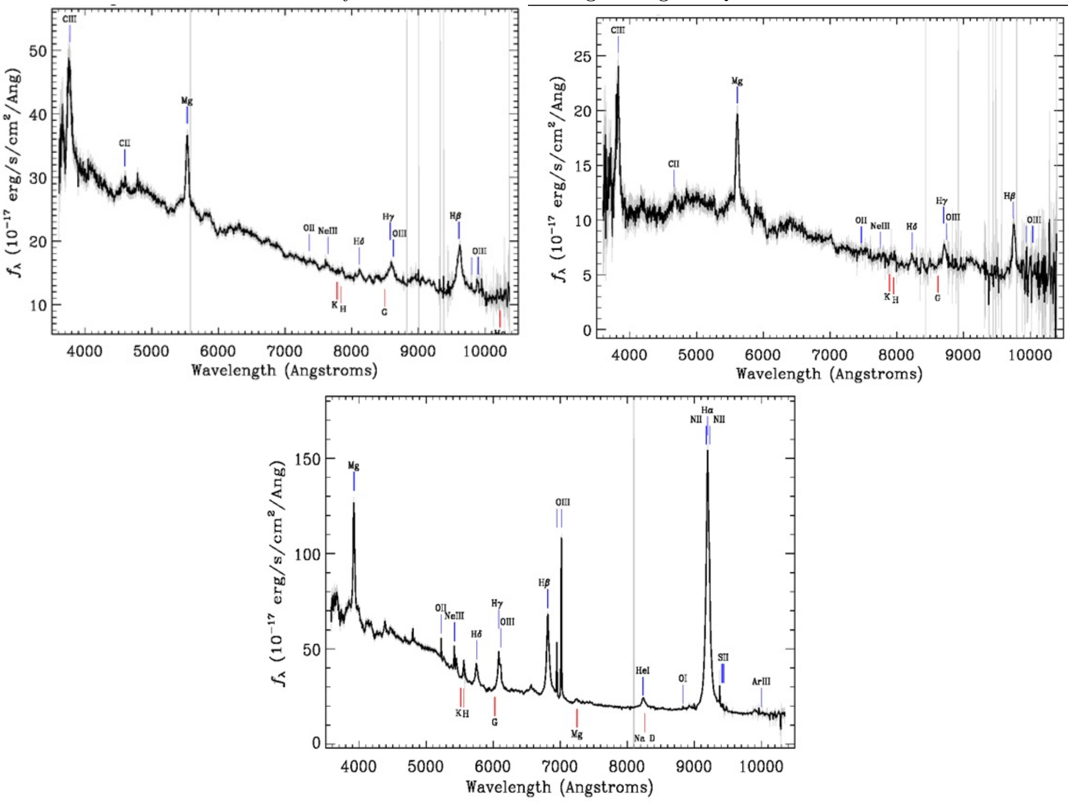

Figure 1. Spectra with MgII line "Broad & Narrow" (broad line profile with clearly separated narrow line).
.

4. Summary

To understand the behavior of the MgII 2798Å emission line in QSOs spectra and to possibly also use it for the classification (especially for high-redshift objects not showing H_α and H_β in the optical range), we have selected QSOs having both H_β and MgII simultaneously in the SDSS spectral range (3500-10500 Å). These are objects with redshifts between 0.3345-1.0915. 139 objects have been selected and investigated. We have classified their MgII line shape into 3 categories: "Broad", "Broad & Narrow" and "Broad + Narrow". The preliminary results show that this number of objects is still small to have enough statistics and to distinguish any regularity. However, some selected distribution has been found, e. g. some subtypes have definite MgII shape (all NLQ1.0 are Broad & Narrow, all Narrow Line QSOs do not have MgII shape "Broad", etc.). In the following studies, we will continue to investigate the short wavelength range of the QSOs to reveal features that may substitute Balmer lines for their classification by activity types.

References

Abdurro'uf et al., 2022, Astrophys. J. Suppl. Ser. , 259, 35

Abrahamyan H. V., 2020, Astronomische Nachrichten, 341, 703

Abrahamyan H. V., Mickaelian A. M., Mikayelyan G. A., Paronyan G. M., 2018, Communications of the Byurakan Astrophysical Observatory, 65, 1

Abrahamyan H. V., Mickaelian A. M., Paronyan G. M., Mikayelyan G. A., Gyulzadyan M. V., 2019, Communications of the Byurakan Astrophysical Observatory, 66, 1

Abrahamyan H. V., Mickaelian A. M., Paronyan G. M., Mikayelyan G. A., 2020, Astrophysics, 63, 322

Massaro E., Maselli A., Leto C., Marchegiani P., Perri M., Giommi P., Piranomonte S., 2015, Astrophys. Space. Sci. , 357, 75

Mickaelian A. M., 2015, Iranian Journal of Astronomy and Astrophysics, 2, 1

Mickaelian A. M., 2021, in Mickaelian A. M., ed., , Byurakan Astrophysical Observatory - 75 years of outstanding achievements. p. 116

Mickaelian A. M., Harutyunyan G. S., Sarkissian A., 2018a, Astronomy Letters, 44, 351

Mickaelian A. M., Abrahamyan H. V., Gyulzadyan M. V., Paronyan G. M., Mikayelyan G. A., 2018b, Astrophys. Space. Sci. , 363, 237

doi: https://doi.org/10.52526/25792776-23.70.2-361

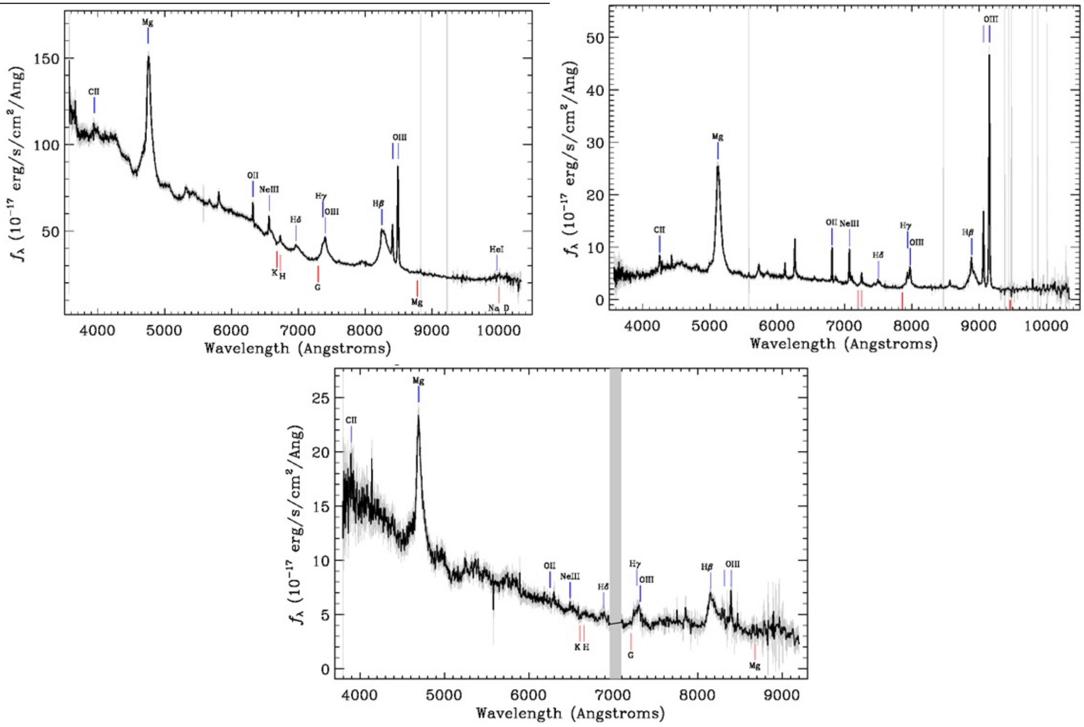

Figure 2. Spectra with MgII line "Broad+Narrow" (a broad component overlapped with narrow line).
.

Mickaelian A. M., Abrahamyan H. V., Paronyan G. M., Mikayelyan G. A., 2021, Frontiers in Astronomy and Space Sciences, 7, 82

Mickaelian A. M., Abrahamyan H. V., Mikayelyan G. A., Paronyan G. M., 2022, Communications of the Byurakan Astrophysical Observatory, 69, 10

Mikayelyan G. A., Mickaelian A. M., Abrahamyan H. V., Paronyan G. M., Gyulzadyan M. V., 2019, Astrophysics, 62, 452

Osterbrock D. E., 1980, in Ninth Texas Symposium on Relativistic Astrophysics. pp 22–38, doi:10.1111/j.1749-6632.1980.tb15916.x

Osterbrock D. E., 1981, Astrophys. J. , 249, 462

Paronyan G. M., Mickaelian A. M., Harutyunyan G. S., Abrahamyan H. V., Mikayelyan G. A., 2019, Astrophysics, 62, 147

Paronyan G. M., Mickaelian A. M., Abrahamyan H. V., Mikayelyan G. A., 2020, Astrophysics, 63, 166

Reines A. E., Greene J. E., Geha M., 2013, Astrophys. J. , 775, 116

Riess A. G., et al., 2004, Astrophys. J. , 607, 665

Véron-Cetty M. P., Véron P., 2000, Astron. Astrophys. Rev. , 10, 81

Véron-Cetty M. P., Véron P., 2010, Astron. Astrophys. , 518, A10

doi: https://doi.org/10.52526/25792776-23.70.2-361

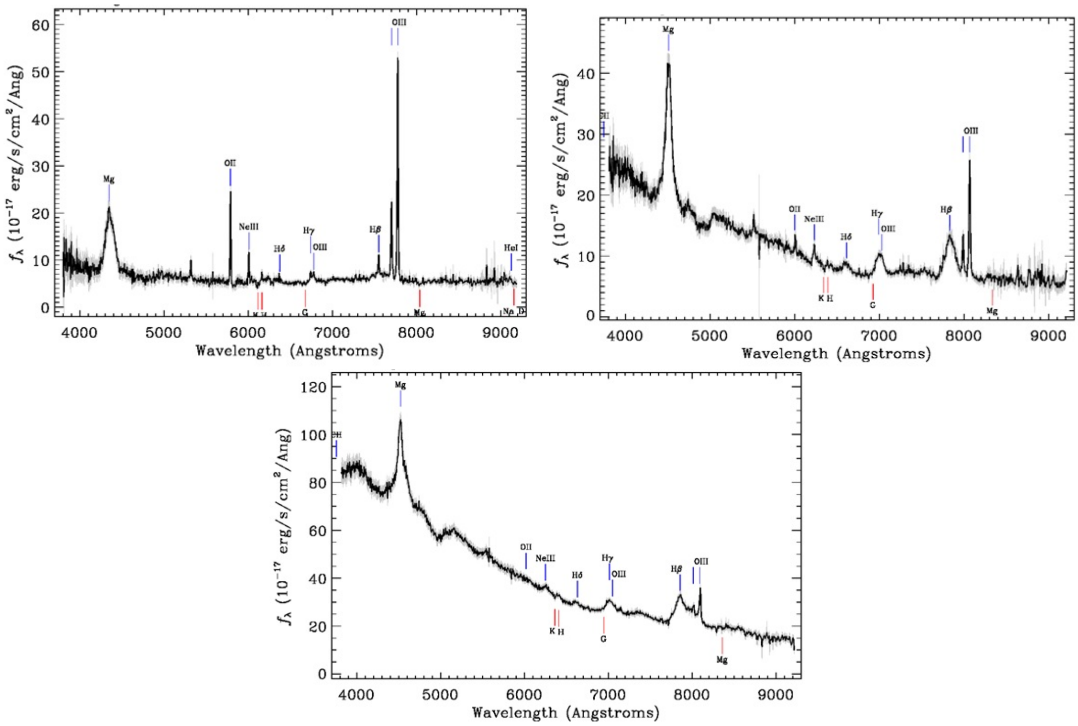

Figure 3. Spectra with MgII line “Broad” (simple broad line without any details).

.

Table 1. Preliminary results of this work

Name	**MgII shape category**	**OIII/ H_β**	**Optical class**
5BZQ J0039-1111	Broad	>3	QSO1.8/LINER
5BZQ J0121+1149	Broad	>3	QSO1.8/LINER
5BZQ J0123+2615	Broad	>2	QSO1.5
5BZQ J0745+3313	Broad	>2	QSO1.0
5BZQ J0010+2047	Broad & Narrow	>3	QSO1.5
5BZQ J0106-1034	Broad & Narrow	>2	QSO1.2
5BZQ J0113+1324	Broad & Narrow	>2	QSO1.2
5BZQ J0122-0935	Broad & Narrow	1	QSO1.2
5BZQ J0059+0006	Broad + Narrow	>2	QSO1.2
5BZQ J0112+2020	Broad + Narrow	1	NLQ1.2
5BZQ J0121+0422	Broad + Narrow	>2	QSO1.5
5BZQ J0124+2805	Broad + Narrow	>3	S1.8

doi: https://doi.org/10.52526/25792776-23.70.2-361

Table 2. Shape of MgII line by the activity type

Activity Type	MgII shape category			**Total**
	Broad	Broad & Narrow	Broad + Narrow	
Sy 1.5		2		2
Sy 1.8			2	2
NLS 1.5		1		1
NLQ 1.0		4		4
NLQ 1.2		11	5	16
NLQ 1.5		1	3	4
NLQ 1.0/LINER		1		1
NLQ 1.2/LINER		1		1
QSO	1	1		2
QSO 1.0	5	6	16	27
QSO 1.2	6	20	24	50
QSO 1.5	3	7	7	17
QSO 1.8		2	5	7
QSO 1.9			1	1
QSO 1.0/LINER		1		1
QSO 1.5/LINER	1			1
QSO 1.8/LINER	2			2
Total	18	58	63	139

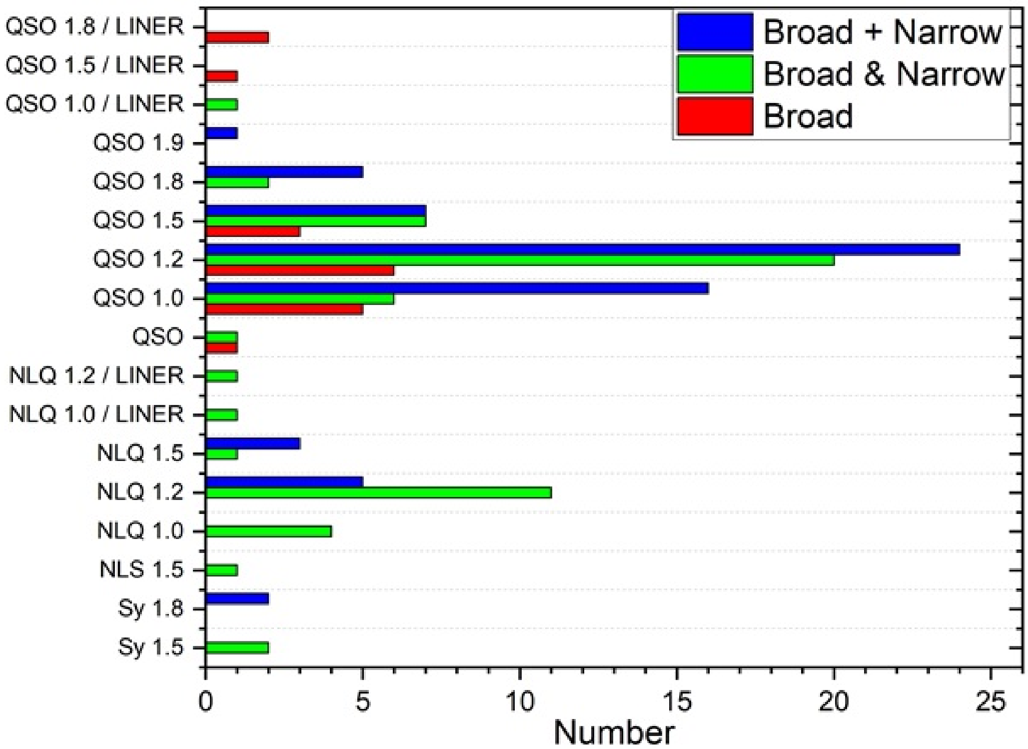

Figure 4. Distribution of shape of MgII line by the activity type.

.

doi: https://doi.org/10.52526/25792776-23.70.2-361